IMPACT OF TEMPORAL LANDCOVER CHANGES IN SOUTHEASTERN IDAHO RANGELANDS

EXECUTIVE SUMMARY
SIGNIFICANT FINDINGS AND ACHIEVEMENTS

- Wildfires are commonplace in the West and managing post-fire recovery is important relative to the sustainability of rangeland natural resources and much of the economy of Idaho and the Intermountain West. A key to effective post-fire recovery is the understanding of where high-severity fires have occurred as these areas are most impacted ecologically and most susceptible to erosion and invasion by non-native plants such as Cheatgrass. As a result, high-severity fire areas experience a state of degraded rangeland health that can affect the site for several years.

  To aid land managers and decision-makers we developed accurate and reliable fire severity modeling techniques for semi-arid rangelands which perform better than other techniques commonly applied today (e.g., the normalized burn ratio which was developed for forested ecosystems and later applied to rangelands). This technique uses classification tree analysis and yields overall accuracies exceeding 85% (cf. chapter 9).

  Further research into fire severity modeling demonstrates that the models can be produced using field observations and post-fire imagery only with little loss in accuracy compared to using pre- and post-fire imagery. This greatly reduces the time and costs associated with the production of fire severity models (cf. chapter 10).

- Fire severity investigations using hyperspectral imagery indicate that fire severity can be accurately determined (>70%) for all fire severity classes in shrub-dominated areas. Distinguishing between moderate- and high-severity fires in shrub-dominated areas was challenging. However, moderate-severity fires could not be accurately distinguished in grass-dominated areas (cf. chapter 7).

- Field and hyperspectral remote sensing investigations confirmed that the majority of water repellent soils were found in areas of moderate and high severity fires but that a level of "background" soil repellency was also found within unburned areas as well. Hyperspectral image processing results indicate that water repellent soils could be detected only when using fire severity as a surrogate/proxy (cf. chapter 7).

- Much emphasis has been placed on the use of various vegetation indices derived from remote sensing imagery. Our research demonstrates that proper application and interpretation of vegetation indices relative to *in situ* field conditions is not as straightforward as commonly accepted. Indeed, the relationship between any pair of simple band ratios shows high correlation ($R^2 \geq 0.88$) regardless of the bands involved in the analysis. This suggests the need to further investigate the use, application, and practicality of vegetation indices in general (cf. chapter 13).

- A new technique was discovered using the quotient of two simple band ratios to effectively identify the most photosynthetically active vegetation in an area. This process uses the simple band ratios of the shortwave infrared-green / shortwave infrared-near infrared bands (cf. chapter 13).

- Comparisons of post-fire vegetation indices reveal fundamentally different responses of mountain big sagebrush compared to Wyoming big sagebrush. Changes in the greenness of rangelands are more pronounced and enduring following fire in Wyoming sagebrush compared to mountain sagebrush (cf. chapter 14).

- Understanding and reporting error and bias is critical to the proper and ethical use of geospatial technologies as a decision support tool. We investigated bootstrap resampling as a means to arrive at an accuracy statement with high confidence (i.e., 95%). Our research indicates that numerous iterations (>80) are frequently required to achieve confidence in classification validation (cf. chapter 15).

- Recent research in western rangelands suggests that greater soil loss can occur through wind rather than water erosion. In our previous NASA-funded research, we found little evidence of wind erosion in mountain big sagebrush communities and results presented here (cf. chapter 21) indicates that although substantial soil erosion occurs in the first few months following summer fires in Wyoming sagebrush communities, the re-colonization of burn areas following the first winter is likely adequate to stabilize soils. One of the most extensive and intensive land treatments in southern Idaho is post-fire reseeding for emergency stabilization of soils. In light of our research, the effectiveness of this management practice requires further consideration. We have obtained additional DOD funding to further examine wind erosion and addition funding from the USDI-BLM to investigate vegetation effects on wind erosion.

- Fire, post-fire rehabilitation methods, and some grazing regimes tend to promote grasses at the loss of sagebrush and other native perennial forbs. These changes likely confer benefits to exotic forbs such as leafy spurge. (cf. chapter 20) and these findings support the idea that maintaining an assemblage of functionally diverse native species can minimize weed invasions. Additional funding has been obtained from the USDA to continue this research.

- Several hundred people participated in formal public outreach events sponsored by this study (the annual Geospatial Range Sciences Conference and World GIS Day events) and broadened their knowledge of GIS and remote sensing applications to solve real-world problems. Countless others have benefited from this study, its research results and data sharing as users who have visited the study's website, http://giscenter.isu.edu/research/techpg/nasa_tlcc/template.htm

- As a direct result of knowledge gained at a Geospatial Range Sciences Conference, Massacre Rocks State Park (Idaho) has proposed a change in their land management practices to implement the use of livestock as a management tool instead of using prescribed fire, chemical herbicide/pesticides, and/or passive total rest. This progressive move by the park demonstrates the ability of geospatial technologies and the promulgation of geospatial research to benefit society.

- Three students (Finley, Goh, and Norton) completed their Master of Science degrees with support from this grant and mentoring by its investigators (cf. chapters 6-8 and chapters 17-19). In addition, numerous other graduate and undergraduate students were involved in this study and partially funded to pursue their degree programs while being mentored in geographic information science

- Four papers have been published in peer-reviewed journals, three MS theses have been completed, and six manuscripts are currently in preparation and/or review.

Range Vegetation Assessment in the Big Desert, Upper Snake River Plain, Idaho 2005

Jed Gregory, Idaho State University, GIS Training and Research Center, 921 S. 8th Ave., Stop 8104, Pocatello, Idaho 83209-8104

Luke Sander, Idaho State University, GIS Training and Research Center, 921 S. 8th Ave., Stop 8104, Pocatello, Idaho 83209-8104

Keith T. Weber, GISP, Idaho State University, GIS Training and Research Center, 921 S. 8th Ave., Stop 8104, Pocatello, Idaho 83209-8104 (webekeit@isu.edu)

ABSTRACT
Vegetation data was collected at 305 randomly located sample points between June 1 and July 15, 2005 (206 in the USDI BLM Big Desert Region and 99 in the O'Neal Study area located 3 miles north of McCammon, Idaho). We collected data describing percent cover of grasses and shrubs, dominant weed and shrub species, fuel load, sagebrush age, GAP vegetation class, presence of microbial crust, litter type, forage availability, and photo points. Sample points were stratified by fire, grazing, and rest treatments. A high amount of cheatgrass was found as well as a high amount of bare ground. However, in 2005 forage availability increased from previous years, probably due to increased rainfall.

KEYWORDS: vegetation, sampling, GIS, remote sensing, GPS.

INTRODUCTION

Many factors influence land cover changes. Wildfire has been, and will always be, a primary source of broad scale land cover change. After a wildfire occurs a change in both plant community composition and plant structure results. In a completely unaltered system, there are plants and shrubs that establish themselves very quickly. In some systems, native plants are in competition with non-native vegetation that is more aggressive. The increase of non-native vegetation can directly result in the reduction of livestock and wildlife carrying capacities. Fire frequency may also increase. An example of non-native vegetation that out competes native vegetation and increases fire frequency is cheatgrass (*Bromus tectorum*). The Big Desert study area is approximately 71 km northwest of Pocatello and the center of the study area is approximately 113º 4' 18.68" W and 43º 14' 27.88" N. (Figure 1)

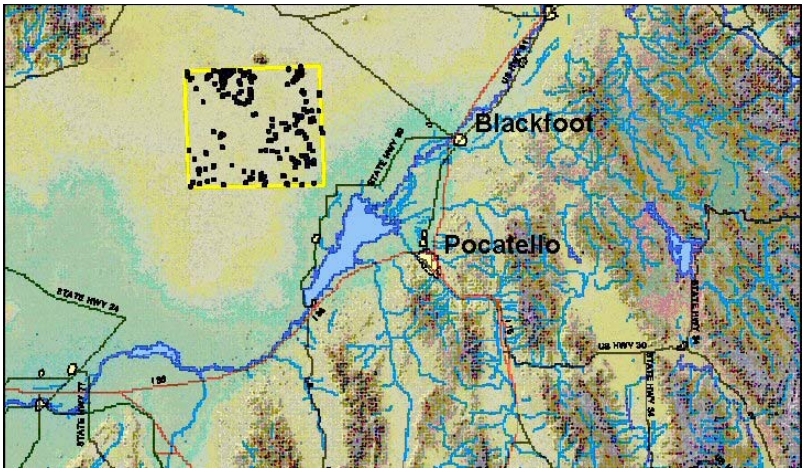

Figure 1. Southeastern Idaho and this study's Area of Concern (bounded in yellow rectangle) .

We assessed research in all possible areas; fire, no fire, grazing and no grazing. After comparing various traits in each of these areas we can create generalizations and these generalizations can then shed light on relationships between these variables and may aid range managers in making decisions about prescribed fire and grazing management.

METHODS

Two hundred twenty-five sample points were randomly generated across the study area. Each point met the following criteria;

1) >70 meters from an edge (road, trail, or fence line)
2) <750 meters from a road.

The sample points were stratified by treatment: 1) fire (within the past 10 years) 2) grazing and 3) rest. In 2005 50 points were created in each of these strata. Twenty-five addition points were generated within the boundaries of the 2001 burn area. The location of each point was recorded using a Trimble GeoXT GPS receiver (+/-1m with a 95% CI) using native latitude-longitude (WGS 84)(Serr et al., 2005)Points were occupied until a minimum of 120 positions were acquired and WAAS was used whenever available. All points were post-process differentially corrected using Idaho State University's GPS community base station. The sample points were then projected into Idaho Transverse Mercator NAD 83 using Trimble's Pathfinder office for datum transformation and ESRI's ArcGIS for projection.

Ground Cover Estimation
Visual estimates were made of percent cover for the following; bare ground, litter and duff, grass, shrub, and dominant weed. Cover was classified into one of nine classes (1) None, 2) 1-5%, 3) 6-15%, 4) 16-25%, 5) 26-35%, 6) 36-50%, 7) 51-75%, 8) 76-95%, and 9) >95%).

Observations were assessed by viewing the vegetation while viewing the ground perpendicular to its surfce as technicians walked each site. This was done to emulate what a "satellite sees". In other words the vegetation was viewed from nadir (90 degree angle) as much as possible.

Fuel Load Estimation
Based upon field vegetation training techniques provided by the BLM office in Shoshone Idaho, fuel load was estimated at each sample point. Visual observations of an area equivalent to a Landsat pixel, (28.5mpp or approximately 812 m^2), centered over the sample point were used to estimate fuel load (table 1).

Table 1. Fuel Load Classes and associated tonnage of fuels.

Fuel Load Classes (Tons/Acre)	
1	0.74
2	1.00
3	2.00
4	4.00
5	>6.00

These categories were derived from Anderson (1982).

Forage Measurement
Available forage was measured using a plastic coated cable hoop 93 inches in circumference, or 0.44 m². The hoop was randomly tossed into each of four quadrants (NW, NE, SE, and SW) centered over the sample point. All vegetation within the hoop that was considered adequate forage for cattle, sheep, and wild ungulates was clipped and weighed (+/-1g) using a Pesola scale tared to the weight of an ordinary paper bag. All grass species (except cheatgrass (*Bromus tectorum*)) were considered forage. The measurements were then used to estimate forage amount in AUM's, pounds per acre, and kilograms per hectare (Sheley, Saunders, Henry 1995)

Microbiotic Crust Presence
Microbiotic crusts (Johnston 1997) are formed by living organisms and their by-products, creating a surface crust of soil particles bound together by organic materials. The presence of microbiotic crust was evaluated at each sample point and recorded as either present or absent. Any trace of a microbiotic crust was defined as "presence".

GAP Analysis
Vegetation cover was described using a list of vegetation cover types from the GAP project (Jennings 1997). The GAP vegetation description that most closely described the sample point was selected and recorded.

Litter Type
Litter was defined as any biotic material that is no longer living. Litter decomposes and creates nutrients for new growth. For the litter to decompose it needs to be in contact with the soil in order for the microbes in the soil to break down the dead substance. If the litter is suspended in the air it turns a gray color and takes an immense amount of time to decompose through chemical oxidation. If it is on the ground it is a brownish color and decomposes biologically at a much faster rate. The type of litter present was recorded by color: either gray (oxidizing) or brown litter (decaying).

Big Sagebrush (Artemisia tridentata spp.) Age Estimation

Maximum stem diameter of Big sagebrush plants was measured using calipers (+/-1cm) to approximate the age of each plant (Perryman, Olson 2000) A maximum of four samples were taken at each sample point, one within each quadrant (NW, NE, SE, and SW). The sagebrush plant nearest the plot center within each quadrant was measured using calipers (+/-1cm) and converted to millimeters. The age of each big sagebrush plant was then estimated using the following equation (AGE = 6.1003 + 0.5769 [diameter in mm]).

Photo Points
Digital photos were taken in each of 4 cardinal directions (N, E, S, and W) from the sample point.

RESULTS
Percent Cover Bare Ground, Grass, and Microbiotic Crust
Fifty-six percent of all 2005 field samples (n = 305) had >50% exposed bare ground. The dominant weed --if any were present-- was always cheatgrass. Cheatgrass was present at 71% of points sampled. Thirty percent of the sample points had >5% cheatgrass cover. Eighty-six percent of the samples had <16% grass cover. Microbiotic crust was present at 56 of the 305 points sampled.

Big Sagebrush Age Estimation
The mean age of sagebrush plants was 39.76 yrs (n = 215). The minimum age was 9 yrs and the maximum age was 121 yrs (Figure 2). Twenty-seven sample points fell within the boundary of the 2001 fire. Nineteen of those had no sagebrush plants growing. Of the eight points that had sagebrush present 2 had an average age > 65 and 6 had an average age ≤ 20.

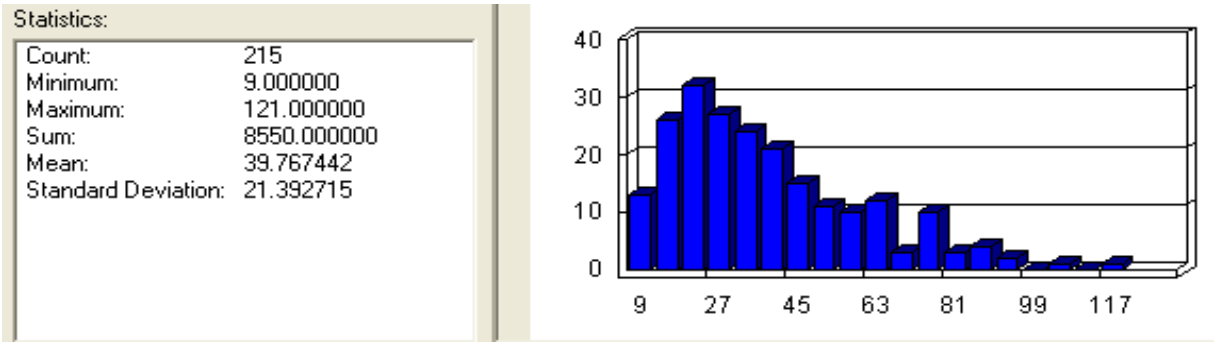

Figure 2. Age distribution of Big Sagebrush in the study area 2005

Forage Measurements
Using AUM Analyzer software (Sheley, Saunders, Henry 1995), forage amount and available Animal Units were calculated for all sample points. Mean forage available was 488.12kg/ha. The minimum forage available was 23 kg/ha and the maximum forage available was 4147 kg/ha.

"Microbial crust is formed by living organisms and their by-products, creating a surface crust of soil particles bound together by organic materials" (Johnston 1997). These are common in very poor rangelands and they are sometimes one of the last things left alive. They can retain water very well even against an osmotic pull. In 2004 only four sample points recorded microbial crust presence, while in 2005 fifty-six of 305 sample points had microbial crust present.

CONCLUSIONS
The available forage present on the range in 2005 varied from what was found in previous years. The calculated pounds per acre and Kilograms per hectare, in sampled areas almost doubled from 2004 to 2005. In 2005 there was a higher amount of precipitation during the month of May than in 2004, which allowed the vegetation to have more moisture available during the peak of the growth cycle (May and early June). Bare ground exposure

estimates varied in 2005, appearing to be lower than either of the two previous years. Variations occurred in all five cover types from 2004 to 2005 as illustrated below (figure 3). Variation in percent shrub cover from 2004 to 2005 is probably attributable to the fact that a higher proportion of samples were taken in areas that had burned in the last 10 years in 2005 than in 2004. Recently burned areas (having burned within the last 10 years) are less likely to have developed high shrub cover. Variations in forage, percent bare ground, percent grass, and percent cheat grass may be due to a greater amount of spring moisture during the last two years (Table 2).

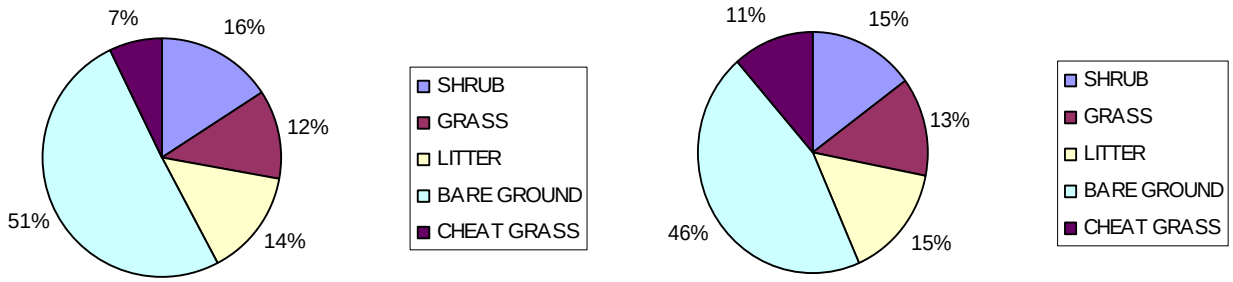

Figure 3.Variations from 2004 (left) and 2005 (right) in the mean percent cover of five cover types observed in the field.

Table 2. Recent annual precipitation (inches)

Month	2003	2004	2005
May	0.53	1.91	2.75
June	0.14	0.56	0.47
July	0.00	1.09	0.14

ACKNOWLEDGEMENTS

This study was made possible by a grant from the National Aeronautics and Space Administration Goddard Space Flight Center. ISU would also like to acknowledge the Idaho Delegation for their assistance in obtaining this grant.

LITERATURE CITED

Anderson, Hal E. 1982. Aids to Determining Fuel Models For Estimating Fire Behavior. USDA For. Serv. Gen. Tech. Rep. INT-122. Ogden, Utah

Jennings, Michael. 1997. "Gap Analysis Program". USGS URL: http://www.gap.uidaho.edu

Johnston, Roxanna. 1997. Introduction to Microbiotic Crusts. USDA NRCS Gen. Tech. Rep.

Montana State University. "AUM Analyzer" Sheley, Roger. Saunders Steve. Henry, Charles. Reprinted May 2003 URL: http://www.montana.edu/wwwpb/pubs/mteb133.pdf

Perryman, B. L., and R. A. Olson, 2000. Age-stem diameter relationships of big sagebrush and their management implications. J Range Management. 53: 342-346.

Heitschmidt, R.K., Klement, K.D., and M.R. Haferkamp, 2005, Interactive Effects of Drought and Grazing on Northern Great Plains Rangelands: Rangeland Ecology & Management, v. 58, p. 11-19.

Serr, K., Windholz, T., and Weber, K., 2006, Comparing GPS Receivers: A Field Study. Journal of the Urban and Regional Information Systems Association Volume 18 No. 2. p19-23.

Range Vegetation Assessment in the Upper Snake River Plain, Idaho 2006

Jamen Underwood, Idaho State University, GIS Training and Research Center, 921 S. 8th Ave., Stop 8104, Pocatello, Idaho 83209-8104

Jacob Tibbits, Idaho State University, GIS Training and Research Center, 921 S. 8th Ave., Stop 8104, Pocatello, Idaho 83209-8104

Keith T. Weber, Idaho State University, GIS Training and Research Center, 921 S. 8th Ave., Stop 8104, Pocatello, Idaho 83209-8104 (webekeit@isu.edu)

ABSTRACT

Vegetation data was collected at randomly located sample points between June 5 and September 1, 2006 (n=100 in the USDI BLM Big Desert Region, n=233 in the Hitching Post pasture of the United States Sheep Experiment Station, and n=145 in the ISU O'Neal Ecological Reserve). Data was collected describing the 1) percent cover of grasses and shrubs, 2) dominant weed and shrub species, 3) fuel load, 4) sagebrush age, 5) GAP land cover class, 6) presence of microbial crust, 7) litter type, 8) forage availability, and 9) photo points. Sample points were stratified by fire, grazing, and total rest treatments. The three study areas had variations in the ground cover perhaps due to the different treatments.

KEYWORDS: vegetation, sampling, GIS, remote sensing, GPS.

INTRODUCTION

Many factors influence land cover changes. Wildfire has been, and will always be, a primary source of broad scale land cover change. After a wildfire occurs a change in both plant community composition and plant structure results. In a completely unaltered system, there are plants and shrubs that establish themselves very quickly. In some systems, native plants are in competition with non-native vegetation that is more aggressive. The increase of non-native vegetation can directly result in the reduction of livestock and wildlife carrying capacities. Fire frequency may also increase. An example of non-native vegetation that out competes native vegetation and increases fire frequency is cheatgrass (*Bromus tectorum*). The approximate location of the three study areas are shown below (Figure 1).

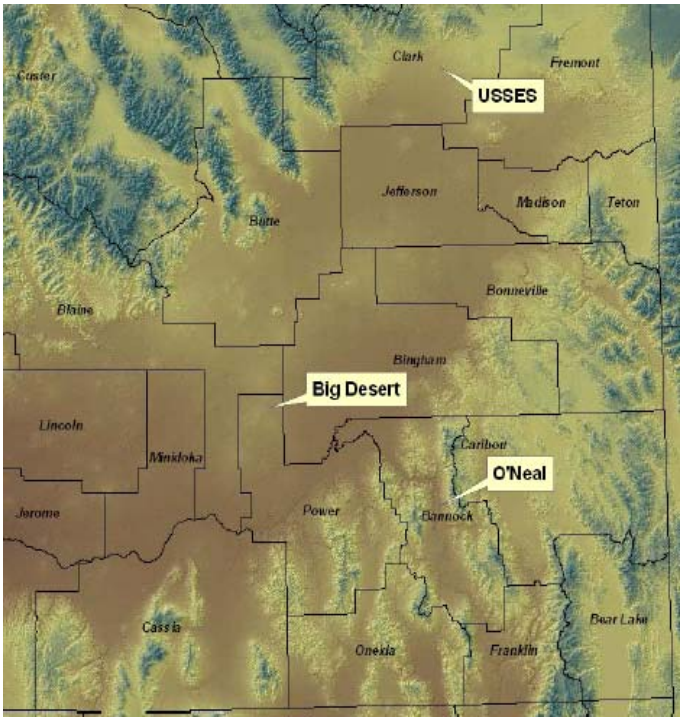

Figure 1. Southeastern Idaho and the study's Area of Concern.

We assessed research in all possible areas; fire, no fire, grazing and no grazing. After comparing various traits in each of these areas we can create generalizations and these generalizations can then shed light on relationships between these variables and may aid range managers in making decisions about prescribed fire and grazing management.

METHODS

Sample points were randomly generated across the study area. Each point met the following criteria;

1) >70 meters from an edge (road, trail, or fence line)
2) <750 meters from a road.

The sample points were stratified by treatment: 1) fire (within the past 10 years) 2) grazing and 3) rest (Table 1). The treatments differed at each study area. The Big Desert covered a much larger geographical location than the other two areas and had a mix of only grazing and fire treatments. The Hitching Post pasture at the USSES had a prescribed burn in September 2005. Most of the points (75%) there were within the fire boundary. The sample points at the O'Neal Ecological Reserve were evenly distributed among three grazing treatment types: total rest, rest rotation, and high intensity/short duration.

Table 1. Treatment summary for each study area.

	Treatment					
Study Area	**Fire**	**Grazing**	**Fire and Grazing**	**Rest**	**Rest and Fire**	**Sum**
Big Desert	0	51	46	0	3	100
USSES	0	0	0	57	176	233
O'Neal	0	96	0	50	0	146
Sum	0	147	46	107	179	479

The location of each point was recorded using a Trimble GeoXT GPS receiver (+/-0.9 m with a 95% CI) using native latitude-longitude (WGS 84)(Serr et al., 2006)Points were occupied until a minimum of 60 positions were acquired and WAAS was used whenever available. All points were post-process differentially corrected using Idaho State University's GPS community base station. The sample points were then projected into Idaho Transverse Mercator NAD 83 using Trimble's Pathfinder office for datum transformation and ESRI's ArcGIS for projection (Gneiting, et al., 2005).

Ground Cover Estimation

Visual estimates were made of percent cover for the following; bare ground, litter and duff, grass, shrub, and dominant weed. Cover was classified into one of 9 classes (1) None, 2) 1-5%, 3) 6-15%, 4) 16-25%, 5) 26-35%, 6) 36-50%, 7) 51-75%, 8) 76-95%, and 9) >95%).

Observations were assessed by viewing the vegetation perpendicular to the earth's surface as technicians walked each site. This was done to emulate what a "satellite sees". In other words the vegetation was viewed from nadir (90 degree angle) as much as possible.

Fuel Load Estimation

Based upon field vegetation training techniques provided by the BLM office in Shoshone Idaho, fuel load was estimated at each sample point. Visual observations of an area equivalent to a SPOT pixel, (10 mpp or approximately 100 m^2), centered over the sample point were used to estimate fuel load (Table 2).

Table 2. Fuel Load Classes and associated tonnage of fuels.

Fuel Load Class	(Tons/Acre)
1	0.74
2	1.00
3	2.00
4	4.00
5	>6.0

These categories were derived from Anderson (1982).

Forage Measurement

Available forage was measured using a plastic coated cable hoop 93 inches in circumference, or 0.44 m^2. The hoop was randomly tossed into each of four quadrants (NW, NE, SE, and SW) centered over the sample point. All vegetation within the hoop that was considered adequate forage for cattle, sheep, and wild ungulates was clipped and weighed (+/-1g) using a Pesola scale tared to the weight of an ordinary paper bag. All grass species were considered forage. The measurements were then used to estimate forage amount in AUM's, pounds per acre, and kilograms per hectare (Sheley et al. 1995). Forage measurements were not made at the USSES.

Microbiotic Crust Presence

Microbiotic crusts (Johnston 1997) are formed by living organisms and their by-products, creating a surface crust of soil particles bound together by organic materials. The presence of microbiotic crust was evaluated at each sample point and recorded as either present or absent. Any trace of a microbiotic crust was defined as "presence".

GAP Analysis
Land cover was described using a list of vegetation cover types from the GAP project (Jennings 1997). The GAP vegetation description that most closely described the sample point was selected and recorded.

Litter Type
Litter was defined as any biotic material that is no longer living. Litter decomposes and creates nutrients for new growth. For the litter to decompose it needs to be in contact with the soil in order for the microbes in the soil to break down the dead substance. If the litter is suspended in the air it turns a gray color and takes an immense amount of time to decompose through chemical oxidation. If it is on the ground it is a brownish color and decomposes biologically at a much faster rate. The type of litter present was recorded by color: either gray (oxidizing) or brown litter (decaying).

Big Sagebrush (Artemisia tridentata spp.) Age Estimation
Maximum stem diameter of Big sagebrush plants was measured using calipers (+/-1cm) to approximate the age of each plant (Perryman and Olson 2000) A maximum of four samples were taken at each sample point, one within each quadrant (NW, NE, SE, and SW). The sagebrush plant nearest the plot center within each quadrant was measured using calipers (+/-1cm) and converted to millimeters. The age of each big sagebrush plant was then estimated using the following equation (AGE = 6.1003 + 0.5769 [diameter in mm]). Sage measurements were not taken at the USSES.

Photo Points
Digital photos were taken in each of 4 cardinal directions (N, E, S, and W) from the sample point.

RESULTS
Percent Cover Bare Ground, Grass, and Microbiotic Crust
Fifteen percent of all 2006 field samples (*n* = 479) had >50% exposed bare ground. The dominant weed --if any were present-- was usually cheatgrass. At the USSES the dominant weed was "other" (usually Canada Thistle (Cirsium arvense) at eighty-six percent of the sample points. Cheatgrass was present at 60% of all points sampled. Twenty percent of the sample points had >5% cheatgrass cover. Sixty percent of the samples had <16% grass cover. All the sample points at the O'Neal Reserve had <16% grass cover. Microbiotic crust was present at 184 of the 478 points sampled.

Big Sagebrush Age Estimation
The mean age of sagebrush plants was 24.27 years (*n* = 181). The minimum age was 10 yrs and the maximum age was 55 yrs (Figure 2).

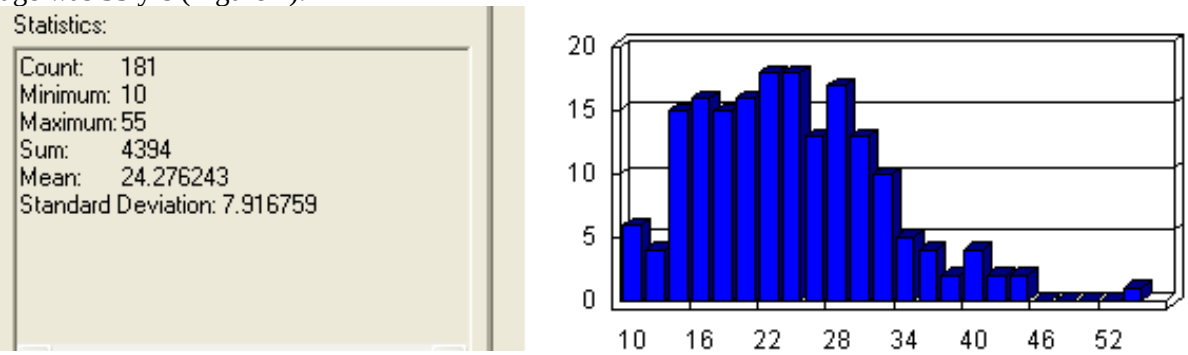

Figure 2. Sagebrush age distribution as sampled during the 2006 field season.

Forage Measurements
Using AUM Analyzer software (Sheley, Saunders, Henry 1995), forage amount and available Animal Units were calculated for the Big Desert and O'Neal sample points. Mean forage available was 226.8 kg/ha. The minimum forage available was 6 kg/ha and the maximum forage available was 1666 kg/ha.

"Microbial crust is formed by living organisms and their by-products, creating a surface crust of soil particles bound together by organic materials" (Johnston 1997). These are common in very poor rangelands and they are sometimes one of the last things left alive. They can retain water very well even against an osmotic pull. In 2005, fifty-six of 305 (18.4%) sample points had microbial crust present, while in 2006 184 of 478 (38.5%) sample points had microbial crust present.

CONCLUSIONS
The differences between the three study areas were interesting. Figures 3-6 are histograms of ground cover estimates for the three study areas and the 2005 data (2005 includes the Big Desert and the O'Neal Reserve). The Big Desert had less bare ground than the other two areas. This area may have benefited from two good rain years, resulting in the lower bare ground. There may have also been some observational bias. The histograms for the USSES and the O'Neal areas match their respective 2005 histograms better than does the Big Desert. These differences may have been caused by different treatments in each of the areas. The Big Desert has a variety of treatments over a large area, the Hitching Post pasture at the USSES burned in 2005 and the O'Neal Study area currently has three different grazing treatments being applied: total rest, rest rotation, and high intensity short duration grazing. The high intensity short duration pasture had very little grass and higher amounts of litter due to the intensity of grazing and little recover time before the vegetation data was collected. O'Neal data was also collected later in the season (August 7, 2006 to September 1, 2006)

One factor affecting ground cover at the USSES was the presence of a large amount of forbs, primarily lupine. Lupine species are known to flourish after a fire. Ninety six of 233 points had forb coverage between 16-25 percent. The fire also affected the grass and shrub cover as there were lower percent shrub and higher percent grass recorded than at the other two study areas. This may be due to the fact that this site is a higher elevation site with a slightly higher moisture regime and a different grazing history.

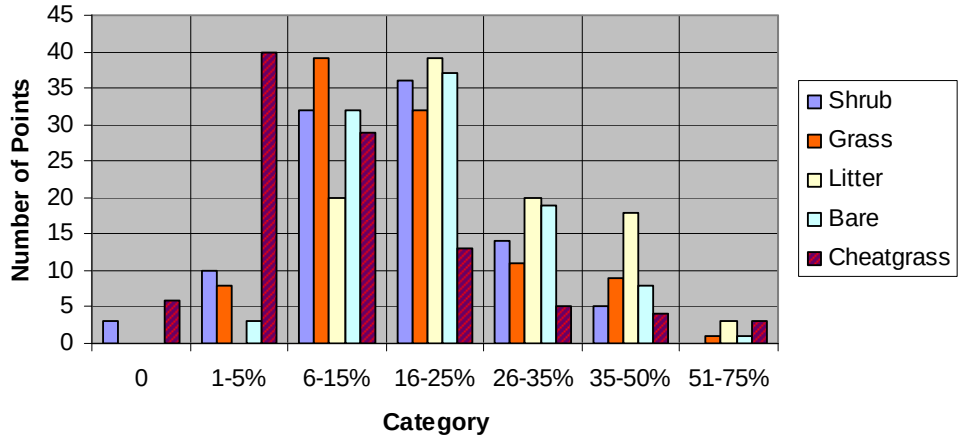

Figure 3. 2006 USDI BLM Big Desert ground cover

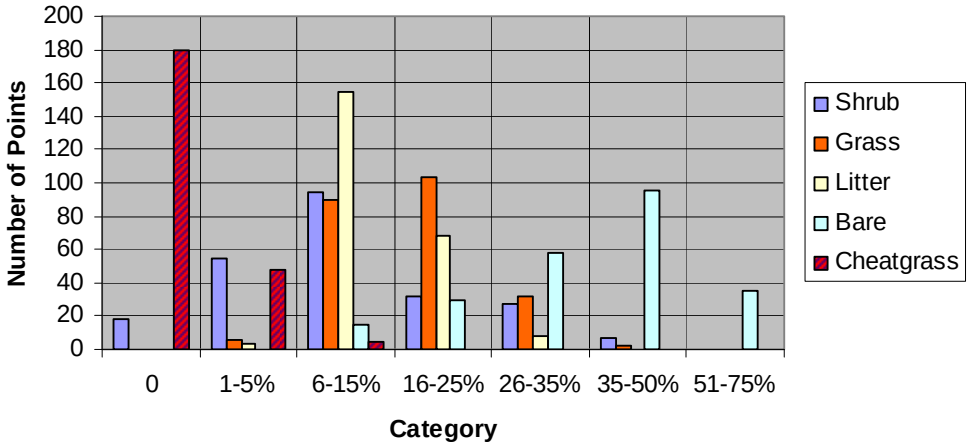

Figure 4. 2006 US Sheep Experiment Station ground cover

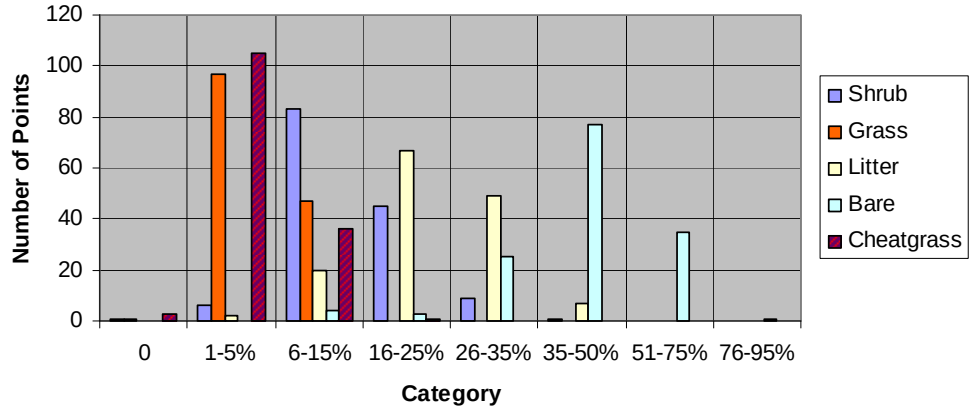

Figure 5. 2006 O'Neal Ecological Reserve ground cover

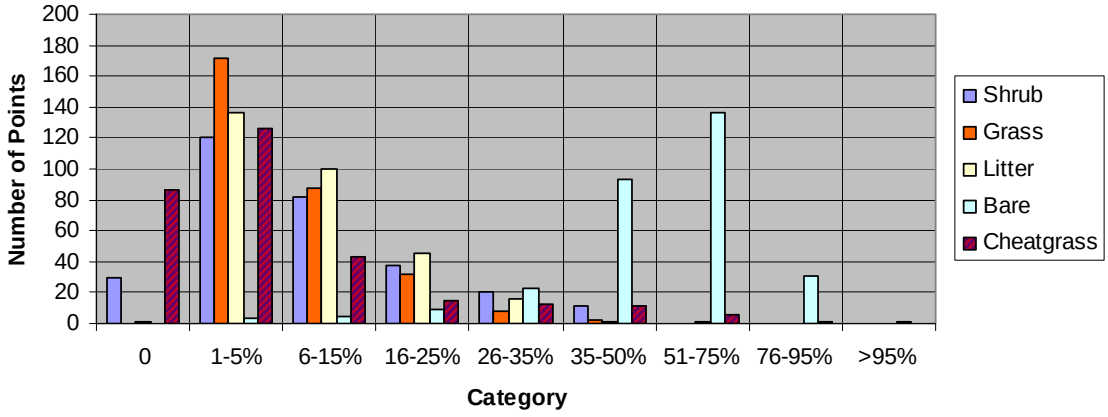

Figure 6. Ground cover at the USDI BLM Big Desert based upon 2005 field sampling.

ACKNOWLEDGEMENTS

This study was made possible by a grant from the National Aeronautics and Space Administration Goddard Space Flight Center. ISU would also like to acknowledge the Idaho Delegation for their assistance in obtaining this grant.

LITERATURE CITED

Anderson, Hal E. 1982. Aids to Determining Fuel Models For Estimating Fire Behavior. USDA For. Serv. Gen. Tech. Rep. INT-122. Ogden, Utah

Gnieting, P., Gregory, J., and Weber, K., 2005, Datum Transforms Involving WGS84. URL visited February 2007. URL: http://giscenter.isu.edu/research/techpg/nasa_tlcc/template.htm

Jennings, Michael. 1997. "Gap Analysis Program". USGS URL: http://www.gap.uidaho.edu

Johnston, Roxanna. 1997. Introduction to Microbiotic Crusts. USDA NRCS Gen. Tech. Rep.

Montana State University. "AUM Analyzer" Sheley, Roger. Saunders Steve. Henry, Charles. Reprinted May 2003 URL: http://www.montana.edu/wwwpb/pubs/mteb133.pdf

Perryman, B. L., and R. A. Olson, 2000. Age-stem diameter relationships of big sagebrush and their management implications. J Range Management. 53: 342-346.

Serr, K., Windholz, T., and Weber, K., 2006, Comparing GPS Receivers: A Field Study. *Journal of the Urban and Regional Information Systems Association Volume 18 No. 2*. p19-23.

[THIS PAGE LEFT BLANK INTENTIONALLY]

Range Vegetation Assessment in the Big Desert, Upper Snake River Plain, Idaho 2007

Jamey Anderson, Idaho State University, GIS Training and Research Center, 921 S. 8th Ave., Stop 8104, Pocatello, Idaho 83209-8104

Jacob Tibbitts, Idaho State University, GIS Training and Research Center, 921 S. 8th Ave., Stop 8104, Pocatello, Idaho 83209-8104

Keith T. Weber, GISP, Idaho State University, GIS Training and Research Center, 921 S. 8th Ave., Stop 8104, Pocatello, Idaho 83209-8104 (webekeit@isu.edu)

ABSTRACT

Vegetation data was collected at 101 randomly located sample points between May 29 and June 13, 2007 in the US Department of Interior, Bureau of Land Management Big Desert Region. Data was collected describing the 1) percent cover of grasses, shrubs, litter, and bare ground, 2) dominant weed and shrub species, 3) fuel load, 4) sagebrush age, 5) GAP land cover classification, 6) presence of microbial crust, 7) litter type, 8) forage availability, and 9) photo points. Sample points were stratified by fire and grazing treatments. Analysis showed a decrease in shrub and litter cover, and an increase in bare ground cover following the 2006 Crystal Fire.

KEYWORDS: sampling, GIS, remote sensing, GPS

INTRODUCTION

Many factors influence land cover changes. Wildfire has been, and will continue to be, a primary source of broad scale land cover change. After a fire occurs, changes in both plant community composition and plant structure often result. In a completely unaltered system, native plants and shrubs reestablish themselves in a burned area very quickly, while in altered systems, such as the Big Desert, native plants compete with non-native vegetation. An increase in non-native vegetation and a resulting decrease in usable forage can reduce livestock and wildlife carrying capacities. Variability of fire frequency and fire intensity also plays a critical role in the composition and cover density of vegetative communities, native or otherwise. Cheatgrass (*Bromus tectorum*) is an example of a non-native grass species that is very competitive with native vegetation and also increases fire frequency.

Following the 2006 field season, a fire occurred in the Big Desert study area that burned approximately 89,000 ha. The 2007 field season was designed to assess post-fire recovery by comparing burned sites to immediately adjacent unburned sites.

Data from the 2006 field season was compared to data from the 2007 field season, in an attempt to find trends in shrub, litter, bare ground, and grass cover due both to fire and long term changes. These same ground cover data will also be analyzed within the context of the 220,000 acre Crystal Fire (Figure 1). Started on August 15, the Crystal Fire spread over the Big Desert field site, affecting 17% of points sampled during the previous month, 2006, and 52 % of subsequent sample points from the 2007 season.

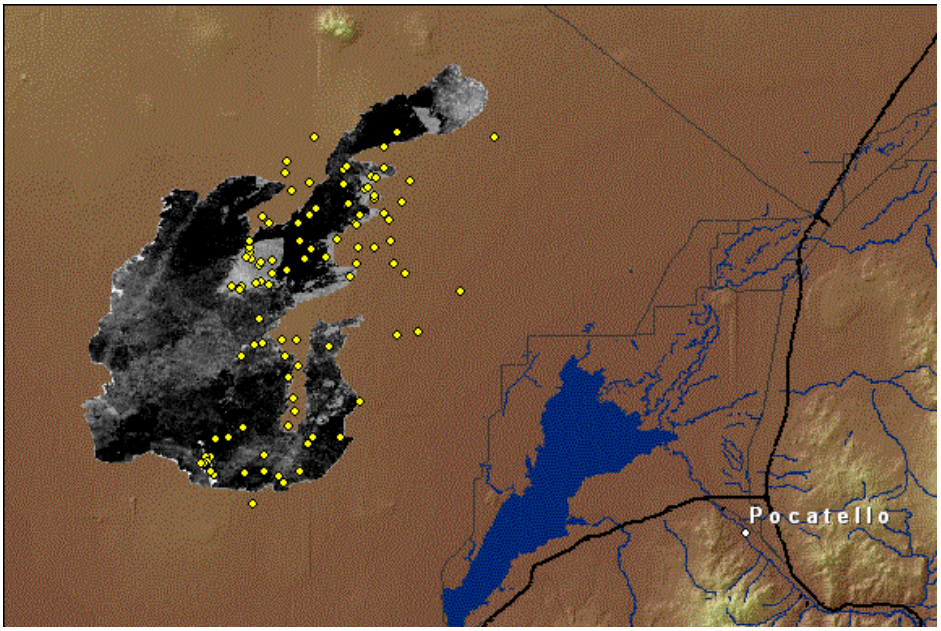

Figure 1. Big Desert sample points overlaying the 2006 Crystal Fire.

METHODS

The study area, known as the Big Desert, lies in southeastern Idaho, approximately 71 km northwest of Pocatello. The center of the study area is located at 113º 4’ 18.68” W and 43º 14’ 27.88” N (Figure 1). This area is managed by the Bureau of Land Management (BLM) and exhibits a large variety of native species as well as invasive species. The area is a sagebrush-steppe semi-desert which is bordered by

geologically young lava formations to the south and west. Irrigated agricultural lands border the study area to its north, south and east. The area has a history of livestock grazing and wildfire occurrence.

Sample points (n=101) were randomly generated across the study area (Figure 1). Each point met the following criteria;

1) >70 meters from an edge (road, trail, or fence line)
2) <750 meters from a road.

Sample points were stratified by treatment: 1) fire and 2) grazing. The location of each point was recorded using a Trimble GeoXH GPS receiver using latitude-longitude (WGS 84). Points were occupied until a minimum of 60 positions were acquired and Wide Area Augmentation System (WAAS) was used whenever available. All points were post-process differentially corrected (+/-0.20 m with a 95% CI) using an array of southeastern Idaho continuously operation reference stations (CORS) each located <80 km of the study area. All sample points were projected into Idaho Transverse Mercator NAD 83, using ESRI's ArcGIS (Gneiting, et al., 2005).

Ground Cover Estimation

Visual estimates were made of percent cover for the following; bare ground, litter and duff, grass, shrub, and dominant weed. Cover was classified into one of nine classes (None, 1-5%, 6-15%, 16-25%, 26-35%, 36-50%, 51-75%, 76-95%, and >95%).

Observations were assessed by viewing the vegetation perpendicular to the earth's surface. This was done to emulate what a "satellite sees". In other words the vegetation was viewed from nadir (directly overhead) as much as possible.

Fuel Load Estimation

Fuel load was estimated at each sample point. Visual observations of an area equivalent to a single SPOT5 pixel, (10 mpp or approximately 100 m^2), centered over the sample point were used to estimate fuel load (Table 1).

Table 1. Fuel load classes and associated tonnage of fuels from Anderson (1982).

Fuel Load Class	(Tons/Acre)
1	0.74
2	1.00
3	2.00
4	4.00
5	>6.00

Forage Measurement

Available forage was measured using a plastic coated cable hoop 2.36 meters in circumference, or 0.44 m^2. The hoop was randomly tossed into each of four quadrants (NW, NE, SE, and SW) centered over the sample point. All grass species within the hoop considered forage for cattle, sheep, and wild ungulates were clipped and weighed (+/-1g) using a Pesola scale tared to the weight of an ordinary paper bag. The measurements were then used to estimate forage amount in AUM's, pounds per acre, and kilograms per hectare (Sheley et al. 1995).

Microbiotic Crust Presence
Microbiotic crusts (Johnston 1997) are formed by living organisms and their by-products, creating a surface crust of soil particles bound together by organic materials. These are common in very poor rangelands and are often one of the last organisms left alive during drought conditions. The presence of microbiotic crust was evaluated at each sample point and recorded as either present or absent. Any trace of a microbiotic crust was defined as "presence"

GAP Analysis
Land cover was described using a list of vegetation cover types from the GAP project (Jennings 1997). The GAP vegetation description that most closely described the sample point was selected and recorded.

Litter Type
Litter was defined as any biotic material that is no longer living. Litter decomposes and creates nutrients for new growth. For the litter to decompose it needs to be in contact with the soil in order for the microbes in the soil to break down the dead substance. If the litter is suspended in the air it turns a gray color and takes an immense amount of time to decompose through chemical oxidation. If it is on the ground it is a brownish color and decomposes biologically at a much faster rate. The type of litter present was recorded by color: either gray (oxidizing) or brown litter (decaying).

Big Sagebrush (Artemisia tridentata spp.) Age Estimation
Maximum stem diameter of Big sagebrush plants were used to approximate the age of each plant (Perryman and Olson 2000). A maximum of four samples were taken at each sample point, one within each quadrant (NW, NE, SE, and SW) centered over the sample point. The sagebrush plant nearest the plot center within each quadrant was measured using calipers (+/-1cm) and estimated to millimeters. The age of each big sagebrush plant was then estimated using the following equation (AGE = 6.1003 + 0.5769 [diameter in mm]).

Photo Points
Digital photos were taken in each of 4 cardinal directions (N, E, S, and W) from the sample point.

RESULTS
Percent Cover Bare Ground, Weed, Grass, and Microbiotic Crust
Twenty eight percent of all 2007 Big Desert field samples (n = 101) had >50% exposed bare ground. The dominant weed (if a weed was recorded) was always cheatgrass. Cheatgrass was present at 81% of all points sampled. Thirty-three percent of the sample points had >5% cheatgrass cover. Fifty one percent of the samples had <16% grass cover. Microbiotic crust was present at 10% of the points sampled.

Big Sagebrush Age Estimation
The mean age of sagebrush was 23.8 years (n = 68). The minimum age was 8 yrs and the maximum age was 89 years (Figure 2).

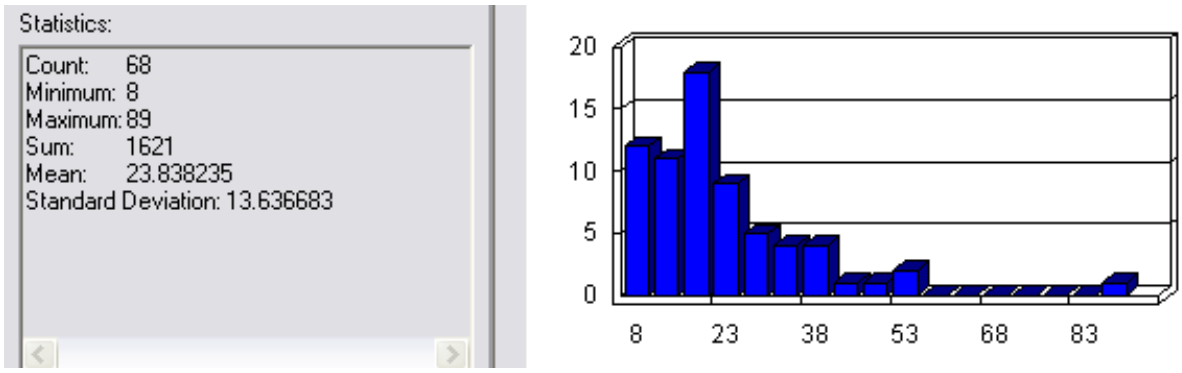

Figure 2. Sagebrush age distribution as sampled during the 2007 field season.

Forage Measurements

Using AUM Analyzer software (Sheley, Saunders, Henry 1995), forage amount and available Animal Units were calculated for the Big Desert sample points. Mean forage available was 361.97 kg/ha, which was lower than the 2006 mean of 460 kg/ha. The minimum forage available was 0 kg/ha and the maximum forage available was 1302 kg/ha (Figure 3).

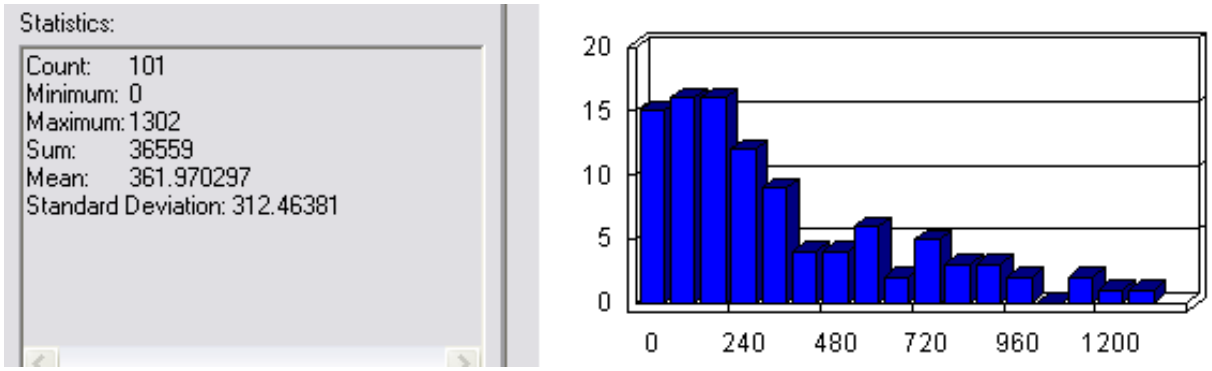

Figure 3. Forage estimates (kg/ha) as sampled during the 2007 field season.

Cover Class Trends and Fire

Simple comparisons between the 2006 and 2007 Big Desert sampling data show very interesting trends in the bare ground, shrub, grass, and litter cover classes (Figures 4 and 5). These trends include: an increase in bare ground cover (Figure 6), a decrease in litter cover (Figure 7), and a decrease in shrub cover (Figure 8). The Crystal Fire (Figure 1) spread over the Big Desert field site, affecting 17% of points sampled during 2006 field season, and 52 % of sample points from the 2007 season. There were fourteen 2006 (pre-burn) sample sites found within the boundary of the Crystal fire, these were compared to a random selection of fourteen 2007 post-burn sample sites. A pre- and post- fire comparison of litter, shrub, grass, and bare ground changes at these samples sites (Figures 9, 10, and 11) shows distinct changes in litter, shrub, and bare ground cover percentages. This comparison combined with a similar comparison of non-burn sample sites, confirms the effects of the fire on shrub, bare ground, and litter cover percentages in burned sample sites (Figures 12, 13, and 14). Weed cover showed little discernable change between the 2006 and 2007 samplings.

CONCLUSIONS

A portion of the trend in bare ground, litter, and shrub cover can be attributed to several sample points located on unvegetated lava; however, the pre- and post-fire comparison of select sites show that the decrease in litter and shrub cover, and the increase in bare ground, is most likely the result of the large range fire that occurred after the 2006 field season. Also, grass cover change anomalies might be attributed to the widespread Crested Wheatgrass (Agropyrron spicatum) plantings during post fire recovery efforts.

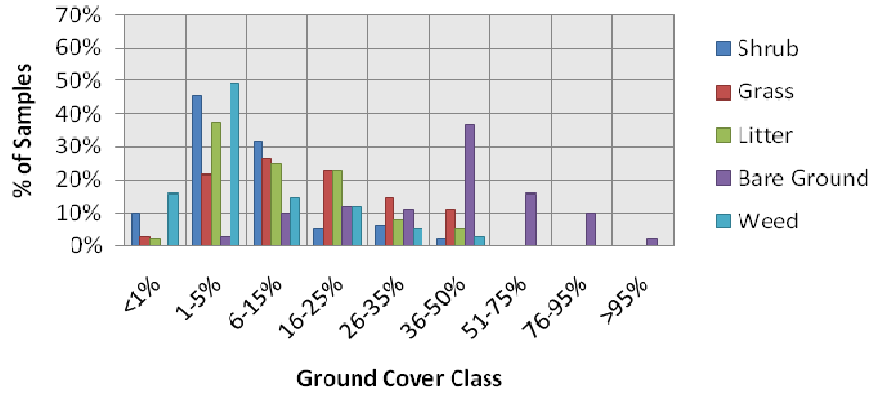

Figure 4. Big Desert ground cover in 2007 (n=101)

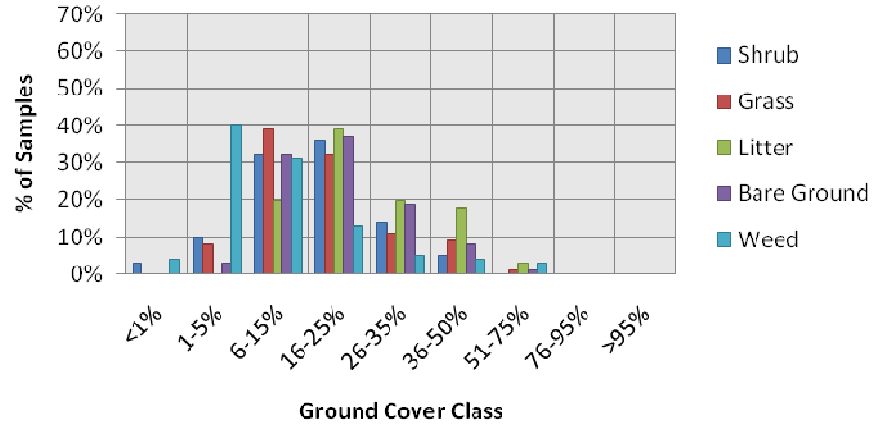

Figure 5. Big Desert ground cover in 2006 (n=100)

Figure 6. Comparison of Big Desert bare ground exposure in 2006 and 2007.

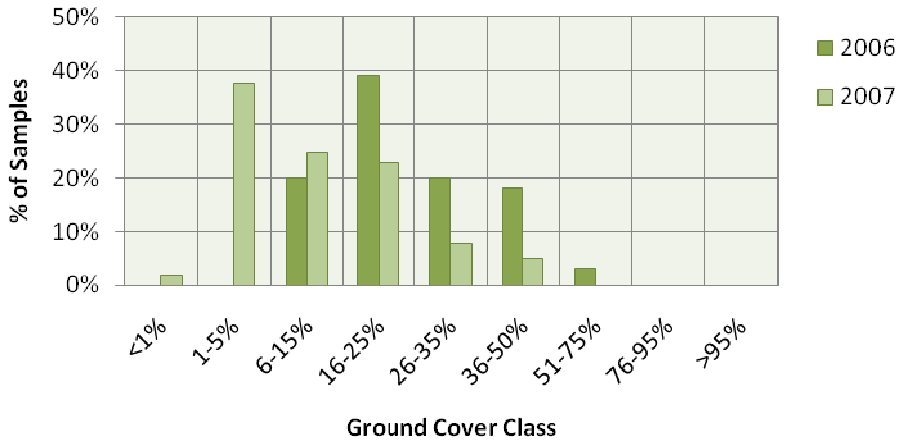

Figure 7. Comparison of litter amounts in the Big Desert between 2006 and 2007.

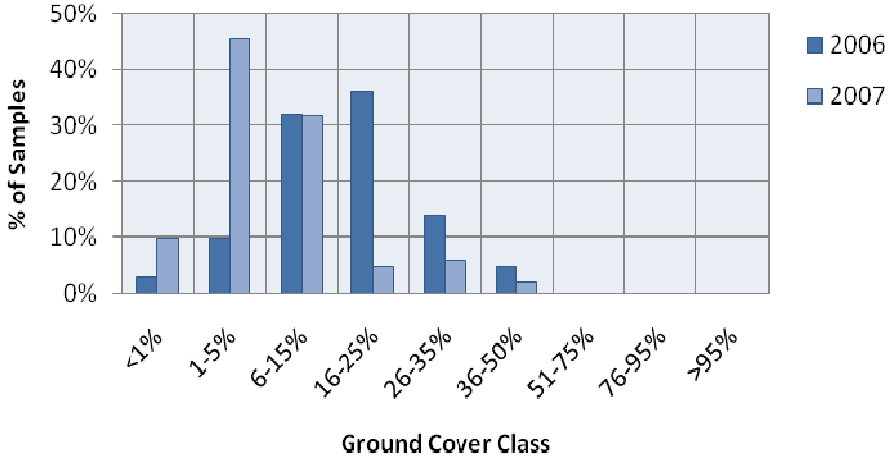

Figure 8. Comparison of shrub cover in the Big Desert Shrub between 2006 and 2007.

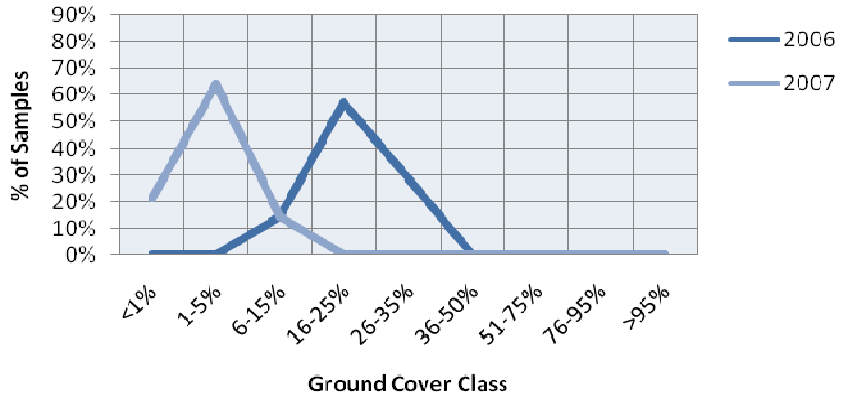

Figure 9. Comparison of pre/post fire shrub cover at sample points within the 2006 Crystal fire perimeter.

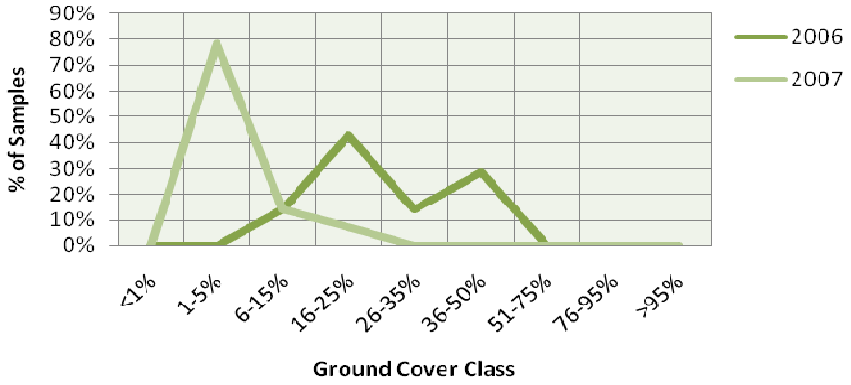

Figure 10. Comparison of pre/post fire litter amounts at sample points within the 2006 Crystal fire perimeter.

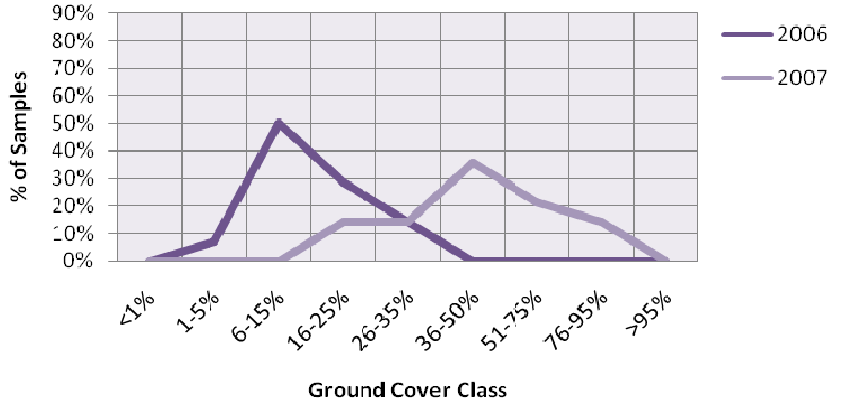

Figure 11. Pre Comparison of pre/post fire bare ground exposure at sample points within the 2006 Crystal fire perimeter.

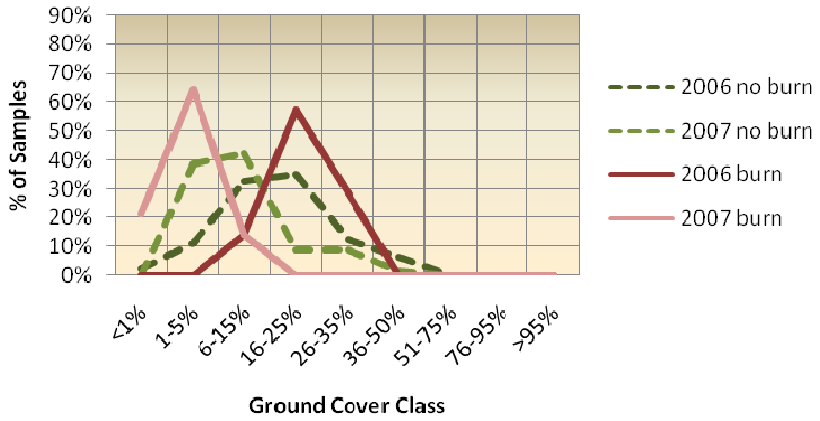

Figure 12. Pre/post burn shrub cover of sample points inside (burn) and outside (no burn) of the Crystal Fire perimeter.

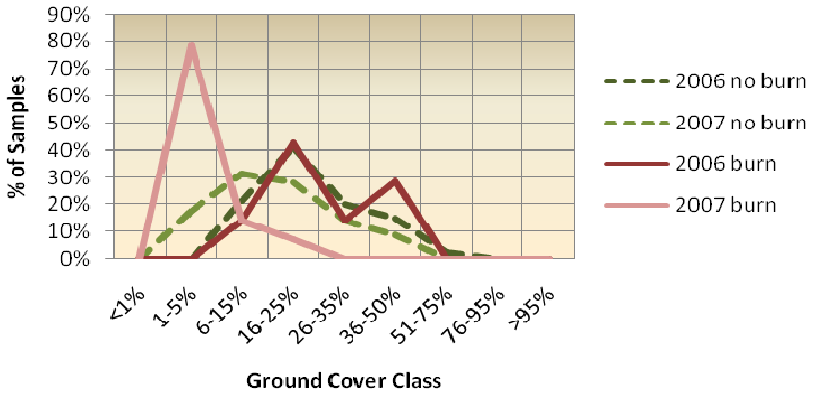

Figure 13. Pre/post burn litter cover of sample points inside (burn) and outside (no burn) of the Crystal Fire perimeter.

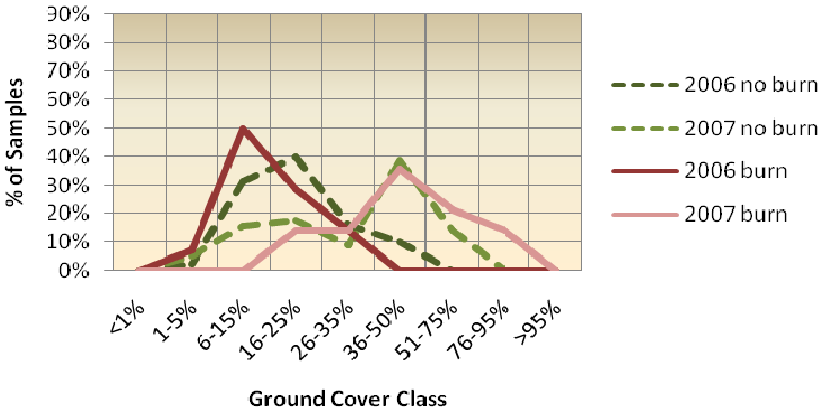

Figure 14. Pre/post burn bareground cover of sample points in and out of the Crystal Fire perimeter.

ACKNOWLEDGEMENTS

This study was made possible by a grant from the National Aeronautics and Space Administration Goddard Space Flight Center. ISU would also like to acknowledge the Idaho Delegation for their assistance in obtaining this grant.

LITERATURE CITED

Anderson, Hal E. 1982. Aids to Determining Fuel Models For Estimating Fire Behavior. USDA For. Serv. Gen. Tech. Rep. INT-122. Ogden, Utah

Gnieting, P., Gregory, J., and Weber, K., 2005, Datum Transforms Involving WGS84. URL visited February 2007. URL: http://giscenter.isu.edu/research/techpg/nasa_tlcc/template.htm

Jennings, Michael. 1997. "Gap Analysis Program". USGS URL: http://www.gap.uidaho.edu

Johnston, Roxanna. 1997. Introduction to Microbiotic Crusts. USDA NRCS Gen. Tech. Rep. Montana State University. "AUM Analyzer" Sheley, Roger. Saunders Steve. Henry, Charles. Reprinted May 2003 URL: http://www.montana.edu/wwwpb/pubs/mteb133.pdf

Perryman, B. L., and R. A. Olson, 2000. Age-stem diameter relationships of big sagebrush and their management implications. J Range Management. 53: 342-346.

Serr, K., Windholz, T., and Weber, K., 2006, Comparing GPS Receivers: A Field Study. *Journal of the Urban and Regional Information Systems Association Volume 18 No. 2*. p19-23.

Development of a Remote Sensing Based Initial Assessment Burn Severity Model

Jill Norton, Idaho State University, GIS Training and Research Center, 921 S. 8th Ave., Stop 8104, Pocatello, Idaho 83209-8104

Keith T. Weber, GISP, Idaho State University, GIS Training and Research Center, 921 S. 8th Ave., Stop 8104, Pocatello, Idaho 83209-8104 (webekeit@isu.edu)

Nancy Glenn, Idaho State University, Boise Center, 322 E. Front St, Suite 240, Boise, ID 83702

ABSTRACT

Two hundred seventy sample points were taken during the summer of 2005 within the USDA-ARS Sheep Experiment Station, DuBois Idaho. Fine-scale vegetation data were collected (n=270) using randomly located ocular estimation methodology (3600m^2, n= 205), point frame methodology (800m^2, n= 45), and twenty stratified-random plots. Ocular estimates included a description of percent cover of shrubs, grasses, forbs, litter, bare ground, and rock as well as an indication of the dominant shrub and weed species, fuel load, sagebrush age, GAP vegetation class, presence/absence of microbial crust, litter type, homogeneity, and four photo points. These estimates and measurements attempted to describe the vegetation within a 60x60m sample area. Point frame estimates included a description of percent cover of shrubs, grasses, forbs, litter, bare ground, and rock using a dot grid (0.5m^2) overlooking underlying vegetation and bare ground. All sample points were stratified by fuel load. Within the study area 64% of the samples indicate a moderate fuel load (~3 tons/acre; n=173), while 21% was low fuel load (n=56) and 15% was high fuel load (n=41). An additional method of shrub cover measurement was incorporated to compare cover results. Ultralight images were taken the week of July 11, 2005 and a classification of shrub cover was made using VegMeasure software. Linear correlation analysis indicates that the best agreement between these estimation methodologies is between the 60x60m ocular methodology and point frame methodology (r 0.7997 for shrub). Correlations between either of these estimation methods and VegMeasure results were poor (60x60m: r 0.1625, point frame: r 0.0224). These correlations were based on a comparison of samples taken within 30 meters of one another. To further examine the relationship between these estimation methods an Inverse Distance Weighted spatial interpolation was performed using shrub cover estimates derived from VegMeasure (point frame: n= 42, 60x60m: n= 195). This was done to predict shrub cover at the exact location where ocular and point-frame estimates were taken, thereby allowing for a more direct comparison of estimation methods. These estimates were compared with both 60x60m ocular and point frame estimates using linear correlation analysis; both relationships resulted in very low R-squared values (R^2 = 0.0049 and 0.0207 respectively).

KEYWORDS: USDA-ARS Sheep Station, ocular estimation, point frame method, percent cover, shrubs, VegMeasure

INTRODUCTION

This study focused on detecting burn severity in a sagebrush-steppe ecosystem using field data and remote sensing techniques. The Normalized Burn Ratio (NBR) is an index based on remote sensing data and is used to calculate the extent and severity of a fire. NBR has been proven to function well in forested ecosystems (Key and Benson, 2004) due to a high contrast of vegetation change before and after the fire. There are two strategies of NBR, initial assessment and extended assessment; with the latter typically considered more representative of fire severity. The difference in assessment strategy is related to the time when post-fire imagery is acquired. This study applied an initial assessment burn severity assessment using multi-spectral imagery following a fall, 2005 prescribed fire at the USDA-ARS U.S. Sheep Experiment Station near Dubois, Idaho. This project uses field and remote sensing data to develop the burn severity assessment specific to semiarid environments. The final model and technique will provide land managers with a tool to assist in accurately describing the characteristics (size, distribution, and severity) of burned areas.

This research also assessed whether pre-fire conditions can reliably predict burn severity in rangeland environments. Regression was used across fuel load categories with their corresponding burn severity ratings to determine possible correlation. The relationship between pre-fire vegetation cover and burn severity, as well as the correlation between burn severity and vegetation re-growth is poorly understood. Once developed and tested, the burn severity model may be applied to current remote sensing data to determine its corresponding burn severity if the area were to burn. To determine if there is a relationship between burn severity and vegetation re-growth, the model may be applied to historical remote sensing data and thus, the results can be compared with the current stages of vegetation re-growth. This opportunity provides the scientific community abundant new data to further explore the relationship between pre-fire vegetation cover and burn severity, and the associated rangeland community dynamics after a fire. This remote sensing application will enhance fire management and recovery efforts across semiarid rangelands worldwide. For example, this information is useful in making assessments on how quickly the landscape will recover, and thus determine what type of treatments land managers can apply to speed recovery in a more efficient and cost effective manner.

For this research, burn severity is defined as the completeness of the burn, or the proportion of biomass removed by the fire. This includes how thoroughly the vegetation was burned, regardless of the pre-existing fuel load. Burn severity was assessed using field data and remote sensing techniques to evaluate the difference in vegetation cover before and after the fire. Both vegetation percent cover field data (n= 10 days) and remote sensing images were acquired shortly before and after the fire. The difference between field vegetation estimates was compared with differenced remote sensing data with the goal of delineating areas of high and low amount of biomass lost as a result of the fire.

An ocular field assessment of burn severity was established based on three field practices for determining burn severity: the composite burn index, (developed by Key and Benson (2004)), the US Park Service field methods (USDI NPS, 2003), and the US Forest Service field methods (USDA FS, 2001, 2002). They were incorporated collectively and modified for application in rangelands. The composite burn index, developed by Key and Benson (2004), as well as the Forest Service and Park Service methods are all post-fire field procedures used to detect and categorize burn severity. Also included in the burn severity analysis will be percent live vegetation cover and litter, as well as exposed rock and bare soil measurements made immediately after the fire. Using field data, multi-temporal imagery, and remote sensing techniques this study aims to develop a reliable burn severity model which can be applied in rangeland ecosystems.

METHODS

Prior to sampling, large-scale (~3.24km^2) vegetation variability and fuel load estimates were assessed across the study area (Figure 1). The variability in fuel load is important to know to adequately sample

across all fuel loads. These large-scale fuel load estimates were performed using the BLM's Determining Fuel Models method (Anderson, 1982), which estimates the amount of fuel in tons/acre. The categories used were very low (0.74 ton/acre=grass only), low-medium (1-2 tons/acre=grass with small, sparse shrubs), medium (3 tons/acre=medium shrubs), and high (4 tons/acre=large, dense shrubs) fuel load categories were observed. These categories were condensed to three total fuel loads: low= 0.74-2 tons/acre, medium= 3 tons/acre, high=4 tons/acre. Seventy-eight polygons with sizes ~8267m^2 were recorded with a Trimble GeoXT GPS receiver (+/- 0.7m @ 95% CI) and labeled with their respective fuel loads category.

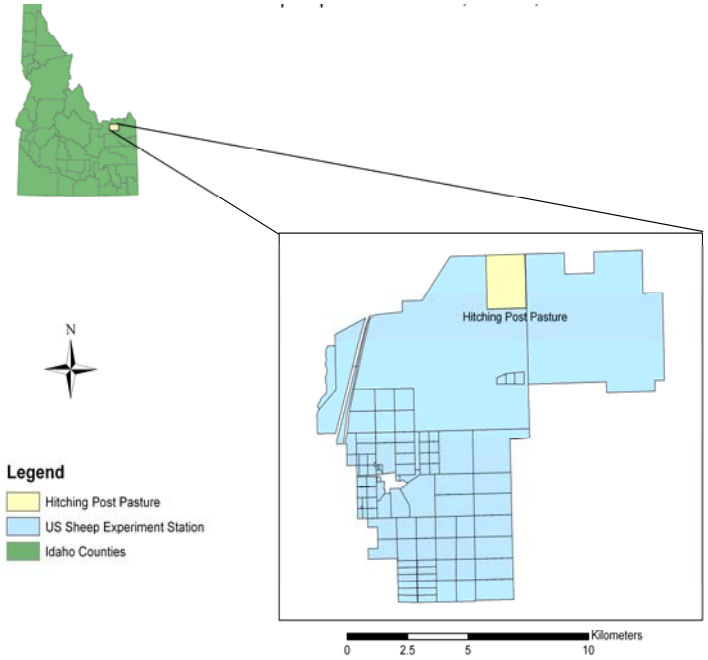

Figure 1: The project study area is within the Hitching Post Pasture of the US Sheep Experiment Station (USSES), Dubois, Idaho.

After large-scale fuel load estimates were completed, fine-scale sampling of the vegetation was evaluated using 60x60m plot areas. Two hundred sample points were randomly generated across the study area using Raster Drilldown (GIS TReC, http://giscenter.isu.edu/software/index.htm) which were navigated to and sampled for percent cover (Table 1), as well as identifying the dominant weed and estimating its abundance (percent cover; Table 1), estimating fuel load (tons per acre) following BLM protocols (Anderson, 1982), and four photo points were taken, one in each cardinal direction. Percent cover (Table 1) of 6 cover categories (shrub, grass, forb, litter, rock, and bare ground) were estimated by walking around the plot and visually estimating/generalizing a cover category for each class (McMahan, et al., 2003). Each plot center location was recorded using a Trimble GeoXT GPS receiver (+/- 0.7m @ 95% CI). At the center of each sample plot, sagebrush was described by its average height and diameter using calipers (+/-1cm) to approximate the age of each plant (Perryman and Olson, 2000). Homogeneity of vegetation cover was assessed across the plot. If vegetation cover was consistent across the entire 60x60m plot it was marked as being homogenous. Each point met the following criteria: 1) >20m from all dozer-created black-lines (for enclosure of the prescribed burn), and 2) >20m from all roads. The 60x60m ocular estimate measurements were taken within all fuel load types.

Table 1: The six cover categories were ocularly measured within these eight cover classes.

None	0
1-5%	1
6-15%	2
15-25%	3
26-35%	4
36-50%	5
51-75%	6
>75%	7

The second method of fine-scale vegetation sampling was the use of 20x40m point frame measurements ($0.5m^2$ each). The point frame technique, designed by Floyd and Anderson (1982) is a well-accepted, accurate sampling method used to determine percent cover of various vegetation types. Designed in sagebrush steppe ecosystems, the point frame establishes a dot grid overlooking underlying vegetation and bare ground. Fifteen point frame observations were collected within each 20x40m plot. The number of point frames was determined by plotting the arithmetic mean and standard deviation for each cover category (Table 1) in relation to the cumulative number of frames used (Figure 2). The corresponding number of frames where the arithmetic mean and standard deviation start to level off was interpreted as the number of point frame observations needed to capture the population's variability for that particular cover type. Because each 20x40m plot results in different frame numbers, an over-estimation of fifteen was chosen as a safety measure. The example in Figure 2 indicates 9 frames would be needed to account for the variability in grass. Note that the number of frames needed cannot actually be acquired until the field data itself has been acquired.

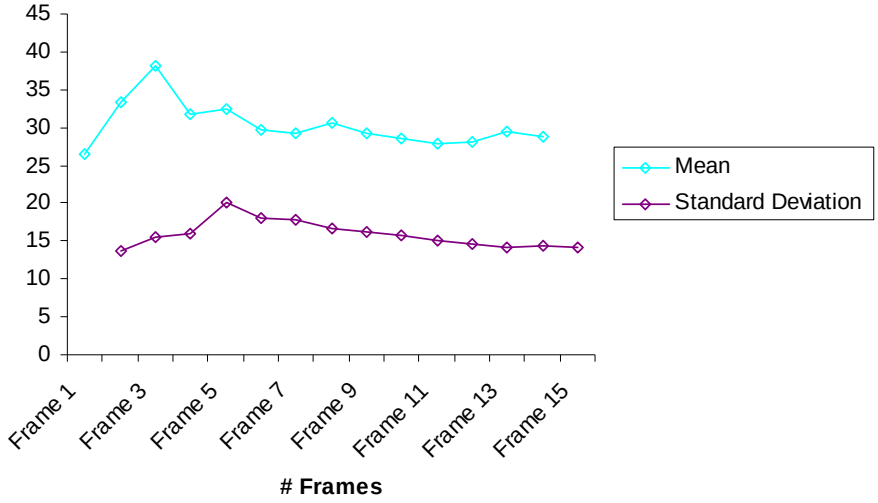

Figure 2: To determine the number of frames needed to accurately depict grass percent cover in each 20x40m plot, one finds where the arithmetic mean (average grass cover for the plot) and standard deviation (standard deviation of grass cover for the plot) "level out" together. In this figure, the statistical values "level out" after sampling approximately nine frames. *Note: grass cover is given on the Y-axis.*

Point frame measurements were taken across all fuel load types (n=3) within the established fuel load polygons (n=78; see large scale field methods above). In total there were 20 stratified random point frame plots established within these fuel load polygons. Each fuel load area (as well as areas designated as unburned relative to the prescribed fire) was characterized using four, 20x40m point frame plots. Forty-five additional point frame plots were established randomly across the pasture. A Trimble GeoXT GPS receiver recorded the 20x40m plot boundaries. At each of these locations four photo points were taken, one in each cardinal direction, homogeneity was described, and fuel load (tons per acre) was estimated following BLM protocols within each plot (Anderson, 1982).

RESULTS

Generally, this pasture was in good rangeland health because there was little bare ground and weeds observed and high percent live vegetation cover (sagebrush, forbs, and grass) throughout. Most of the study area was within the medium fuel load classification (3 tons/acre).

Percent Cover of Litter, Forb, Grass, Shrub, Rock, and Bare Ground: Point Frame

Forty-six percent of all litter, forb, and bare ground cover categories were within the 6-15% cover class for the point frame results (n=65). Forty-three percent of all grass samples were within the 16-25% cover class; thirty-one percent of all shrub samples were within the 26-35% cover class; and sixty-nine percent of all rock samples were within the 1-5% cover class.

Percent Cover of Litter, Forb, Grass, Shrub, Rock, and Bare Ground: 60x60m Ocular Estimate

The majority of litter and rock cover categories were within the cover class of 1-5% for the 60x60m ocular estimate results (n=205): 52% and 75% respectively. Forb and bare ground were mostly within the 6-15% cover class and were 82% and 39% respectively. The majority of grass, within the 16-25% cover class, was 49%. 40% of shrub cover was within the 36-50% cover class.

Big Sagebrush Age Estimation

The mean age of sagebrush plants was 10.62 years (n=205). The minimum age was 6.91 years and the maximum age was 23.52 years. This was determined using stem diameter/age relationships of big sagebrush (Perryman, and Olson, 2000).

Weeds

The dominant weed in the study area was cheatgrass (*Bromus tectorum)* which was found within 18% of all plots (n=205), with 97% of these samples having $\leq 5\%$ cover. Other weeds present in the study area include spotted knapweed (*Centaurea maculosa)*, mullein (*Verbascum thapsus L.*), and leafy spurge (*Euphorbia esula*), within 2%, 9%, and 1% of all plots respectively; all with $\leq 5\%$ cover.

Shrubs

The study area is a sagebrush-steppe ecosystem having two primary subspecies of sagebrush (*Artemisia* ssp.): mountain big sagebrush (*A. tridentata* ssp. *vaseyana*), and threetip sagebrush (*A. tripartita ssp. tripartita*). Other shrub species within the study area were antelope bitterbrush (*Purshia tridentata*), green rabbitbrush (*Chrysothamnus viscidiflorus)*, and horsebrush (*Tetradymia canescens)*.

Shrub cover was estimated using three distinct methodologies. We compared the results of shrub cover estimates to determine if a correlation existed between the methodologies and to help validate/corroborate our estimates. To determine the relationship between 60x60m ocular estimates and point frame estimates, we used 49 sample points located within 10 meters of one another. Using linear correlation analysis, an r of 0.7997 indicates high correlation between these estimation methodologies (Figure 3) for percent shrub cover and this is significant ($P < 0.0001$). Table 2 shows that correlations are good for bare ground as well, 63% of the time (+/-5 %; $P < 0.0001$), and that ocular estimates and point frame methods are not correlated for all other cover categories. These r values and significance ratings are given in Table 3.

An additional method of shrub cover estimation was incorporated for comparison. Aerial ultralight images were taken the week of July 11, 2005 and a classification of shrub cover was made using VegMeasure software. Correlations with the VegMeasure results were poor (Figures 4 and 5). However, compared points (n = 42 and 39) were located within 30 meters.

In an attempt to allow for spatial heterogeneity effects, another shrub cover estimation was derived using the VegMeasure shrub cover estimates to perform a spatial interpolation using inverse distance weighted (IDW) techniques. IDW estimates shrub cover across the entire study area, giving greatest weight to

those sample points nearest the focal pixel being classified (Longley et al., 2005). These results were compared (minimum cells = 12, maximum search distance = 600m, power = 1) to the 60x60m ocular estimates (Figure 6, n = 195) and point frame estimates (Figure 7, n = 42); both show poor agreement (r 0.07 and r 0.1439 respectively).

Other Cover Types

In order to show heterogeneity for each cover type across the study area (Table 4), we compared the arithmetic means for percent cover of each cover category across a 20x40m point frame plot (n=15 samples per plot) with standard error of mean (SEM) bars. The plots are different among the plots, indicating heterogeneity of all cover types across the study area.

Standard deviation around the mean (Table 5) indicates variability within each 20x40m plot. A SPOT pixel (10x10m) has smaller spatial resolution than the point frame, therefore cover is variable among pixels as well (Figure 9). This is important to know when using the imagery for modeling.

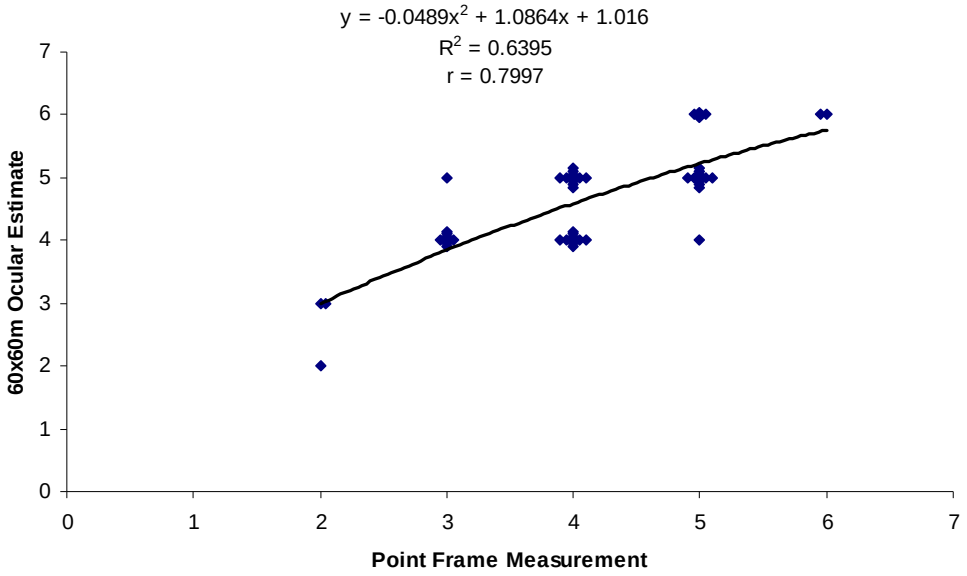

Figure 3: Shrub percent cover estimates were compared using two sampling methods: 60x60m ocular estimates and point frame estimates (n = 48). This correlation uses sample points within 10m. A second order polynomial trendline has been added.

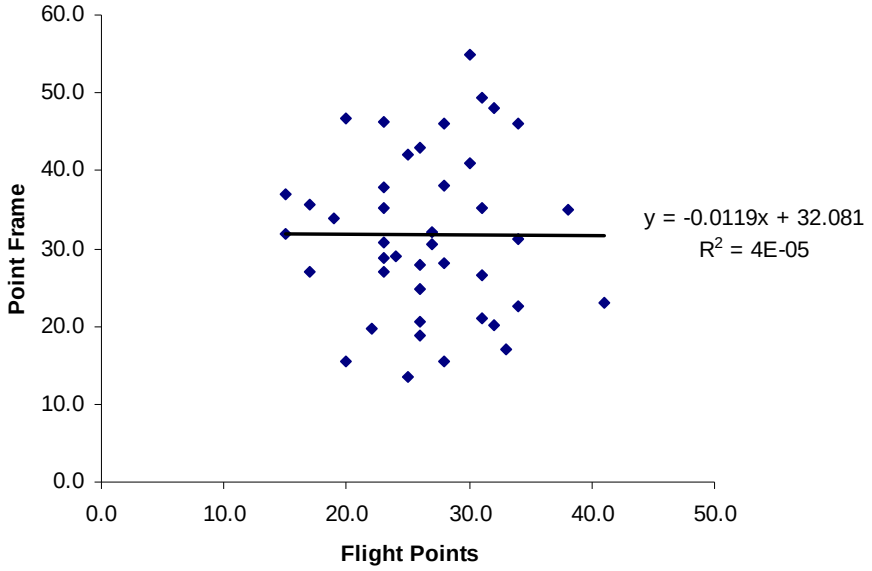

Figure 4: Comparison of shrub percent cover estimates using two sampling methods: aerial photography interpretation (n = 42) and point frame estimates (n = 42). This analysis uses sample points within 30m.

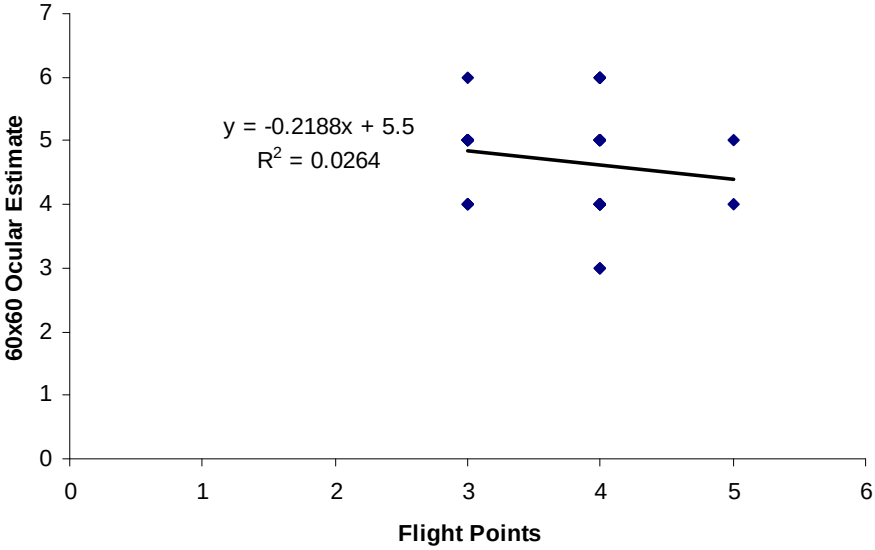

Figure 5: Comparison of shrub percent cover estimates using two sampling methods: aerial photography interpretation (n = 39) and 60x60 ocular estimates (n = 39). This analysis uses sample points within 30m.

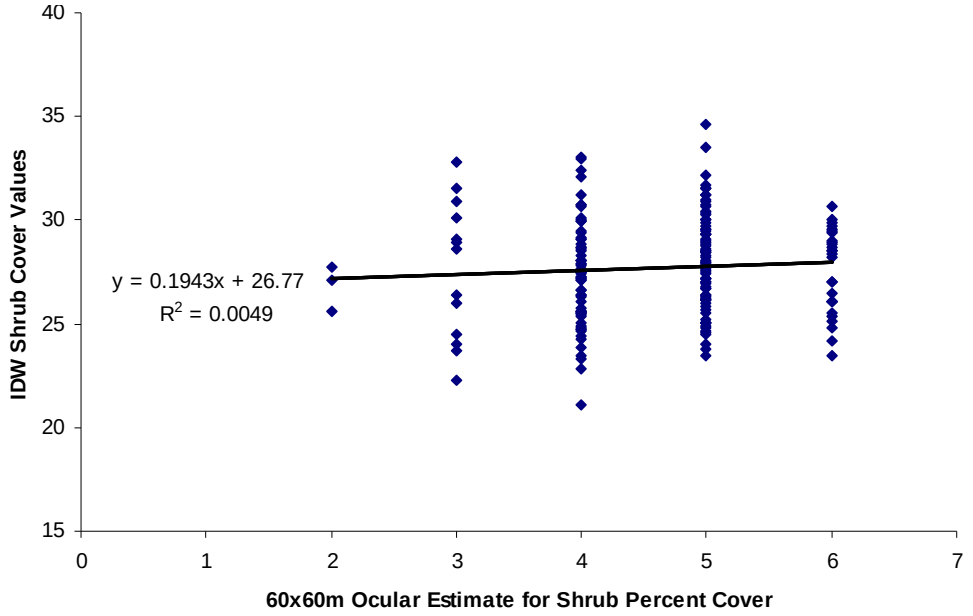

Figure 6: The relationship between 60x60m ocular estimates for percent shrub cover (n = 195) and the inverse distance weighting (IDW) values (n = 195). The linear relationship (y=0.1943x + 26.77) does not explain much of the variation in percent cover of shrub values.

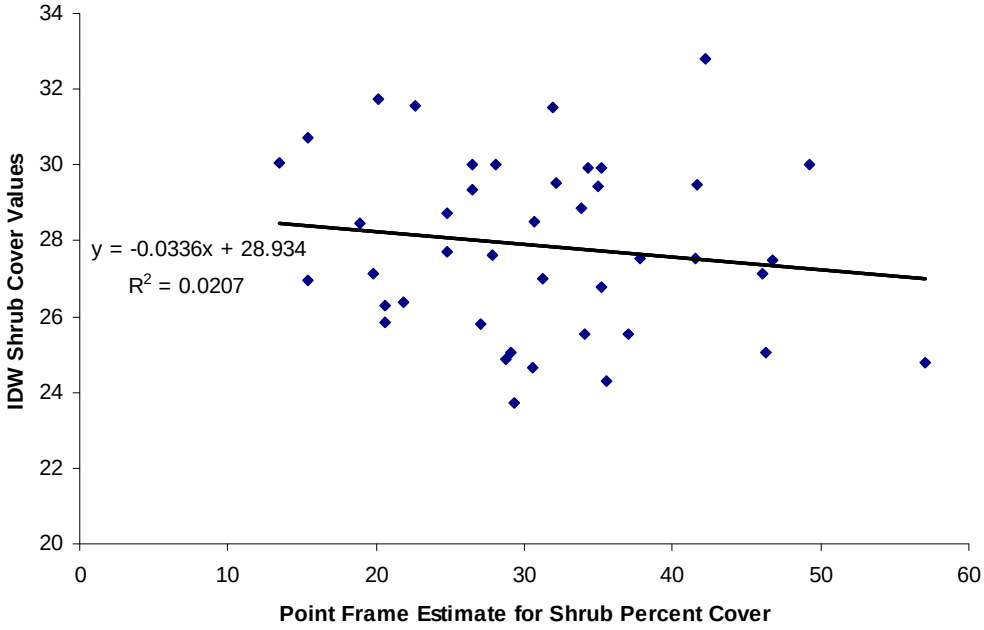

Figure 7: There is a negative correlation between the point frame percent shrub cover estimates (n = 42) and the inverse distance weighting (IDW) values (n = 42). The linear relationship (y=-0.0336x + 28.934) does not explain much of the variation in percent cover of shrub values.

Table 2: Point frame cover estimates were correlated with ocular estimates (n=49) from the same general area (+/-10m). Second order polynomial trendlines have been added.

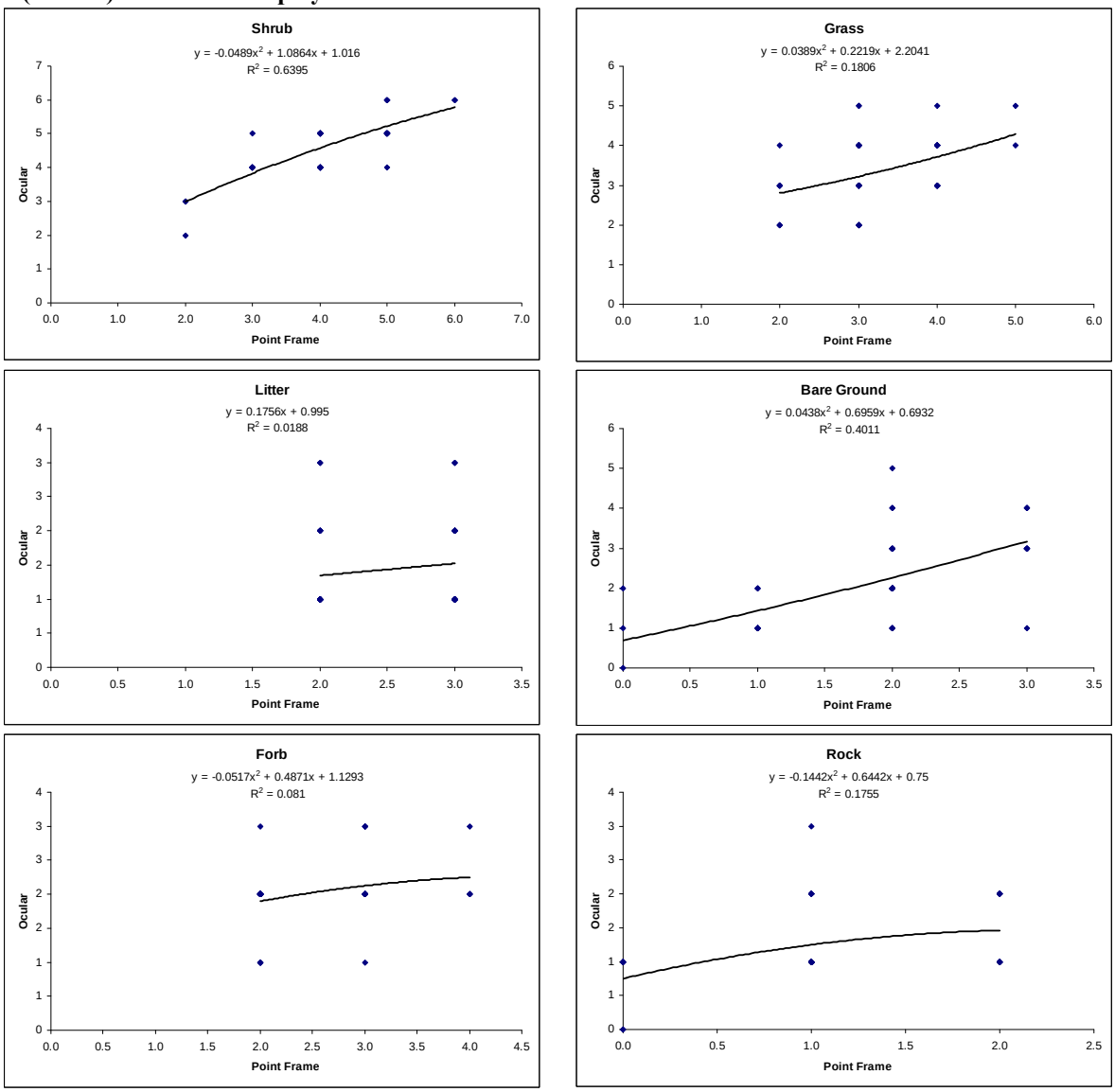

Table 3: Result of statistical analysis comparisons for all cover classes. All were highly significant correlations (*) except the forb cover class, which is marginally significant, and the litter cover class which is most likely due to its fine-scale presence.

Cover Category	r Value	*P* Value	
Shrub	0.7997	<0.0001	*
Grass	0.4249	0.0024	*
Forb	0.2846	0.0504	
Litter	0.1371	0.3473	
Bare Ground	0.6333	<0.0001	*
Rock	0.4189	0.0046	*

Table 4: Spread of mean percent cover for each cover class (+/- 1 standard error of mean (SEM)) using the Point Frame method (n=65). Comparing two shrub cover means at a time (multiple comparisons) as part of an ANOVA indicates that some point frames were significantly different than others (95% CI). There is heterogeneity among most cover categories across the study area.

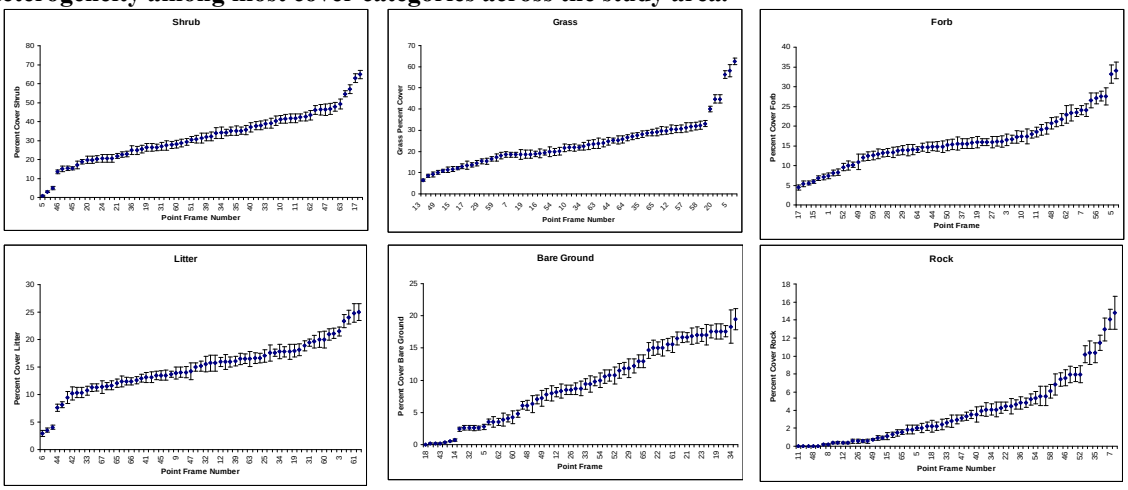

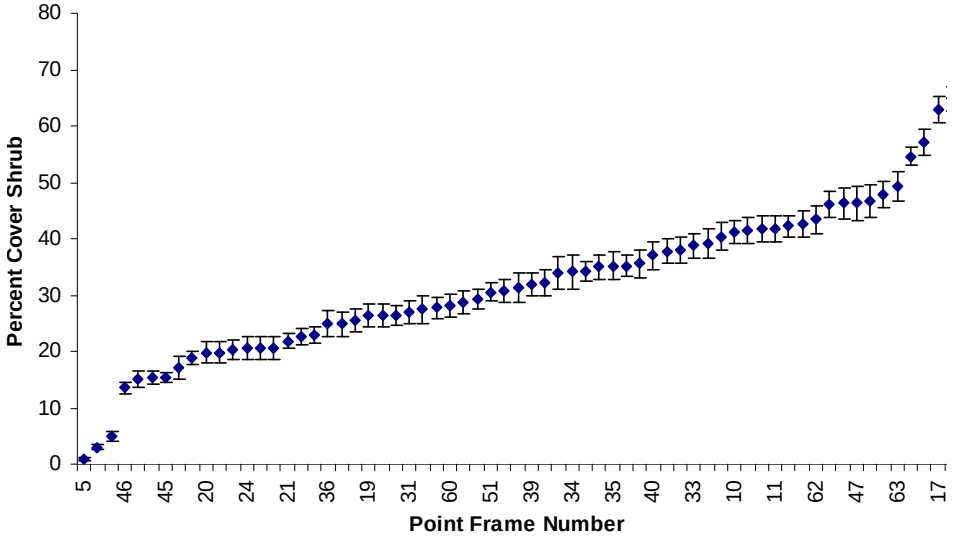

Figure 8: Spread of the means (+/- 1 SEM) of percent shrub cover in 65 plots based on the point frame estimation method. Pair-wise mean comparisons (Tukey HSD) found that only 8% of the pairs differed at an experiment-wide error rate (α) = 0.05. The study area shrub cover was homogenous.

Table 5: Average percent cover for all cover categories with 2 standard deviations (95%) indicating variability amid each 20x40m plot.

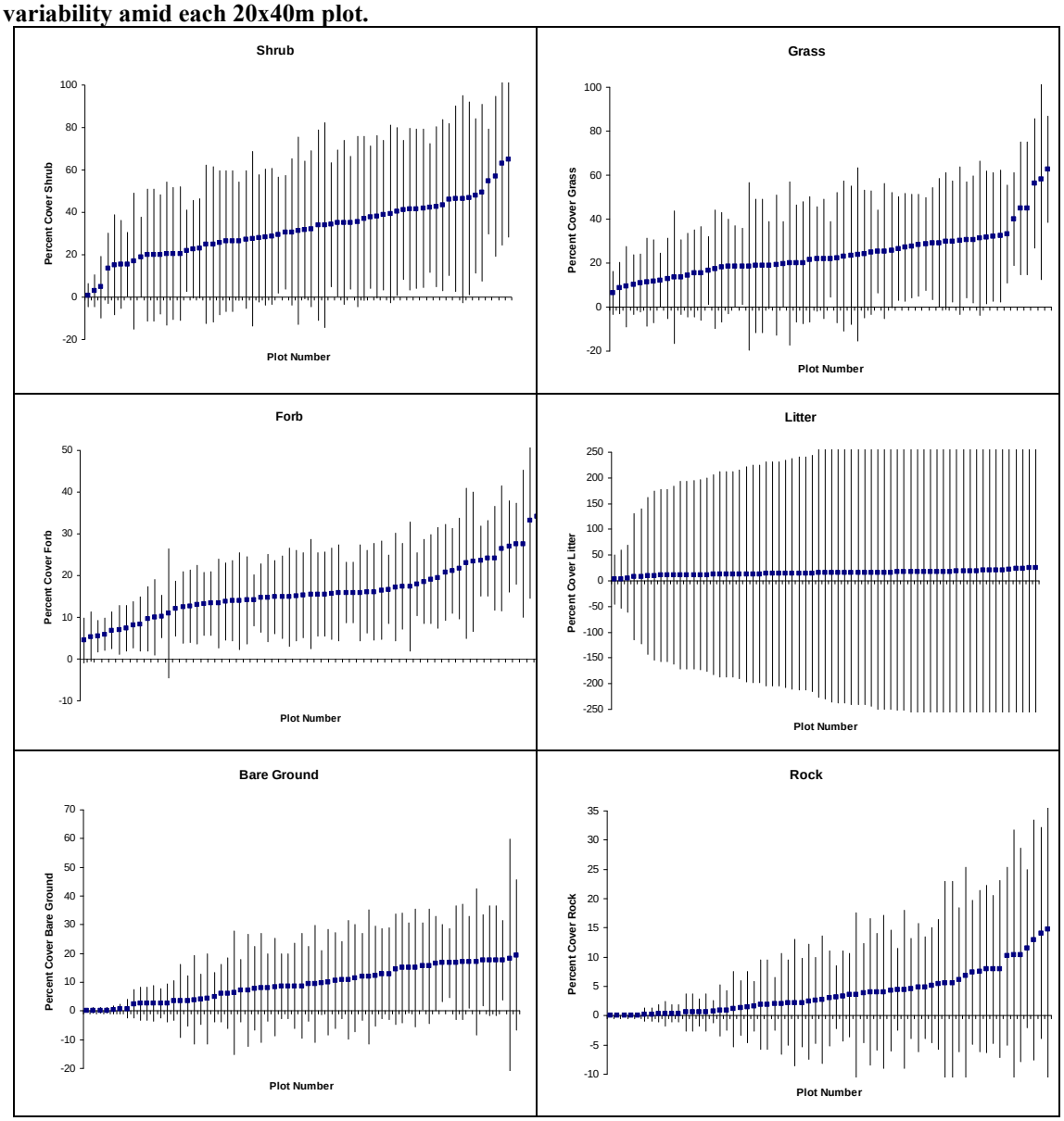

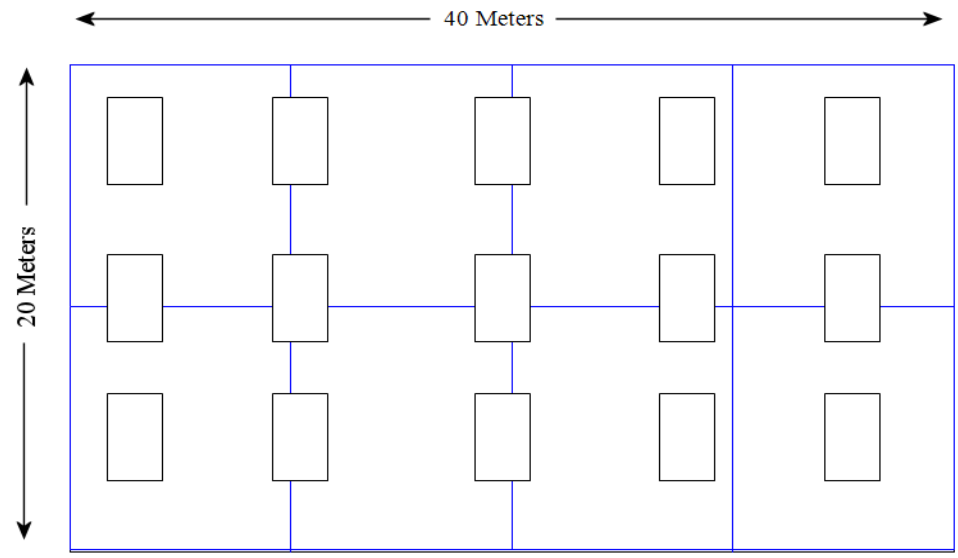

Figure 9: Approximate location of 15 point frames within each 20x40m plot. Blue lines indicate potential SPOT pixel 10x10m placement.

CONCLUSIONS

Due to low R^2 values for the correlations between the ultralight Veg Measure points/ IDW values and other cover estimate methods, we conclude that point frame and 60x60m ocular estimates were better measures of cover. However, this result may be premature. To gather a large enough sample to compare with other analyses (ocular estimation and point frame) we were required to select points within +/- 30m of one another, and used a maximum distance of 600m to produce the IDW spatial interpolation grid. This is in contrast to using points within 10m of one another when comparing point frame and ocular estimates. The 60x60m ocular estimates and point frame estimates explained very little (0.49% and 2.07%) of the variation in IDW values. Ideally, point frame and ocular estimates should have been collected at the same location as the VegMeasured points. This was not done because 1) a poor correlation was not expected and 2) the purpose of this study was not to compare estimation methods but to compile data describing the vegetation and fuels present within the study area. In comparing the mean percent shrub cover for the point frames with SEM, only some (158/2080 ≈ 8%) of the point frames were different at a 95% confidence interval using pair-wise mean comparison (Tukey HSD). This indicates that the study area's shrub cover is homogeneous. However, this is an extremely conservative test of significance because the sample size is so large.

The best correlations between point frame and ocular estimates were for shrub cover where an 80% correlation between these estimates exists. Ocular estimates compared well with point frame measurements for all cover categories except litter (forb was marginal), however; ocular estimates were somewhat coarse (≈ 14% increments), were inherently subjective, and their precision varied among cover types. We found that within each 20x40m plot there was high variability for each cover type, and subsequently, there will be variability within each SPOT pixel as well.

LITERATURE CITED

Anderson, H. E. 1982. Aids to Determining Fuel Models for Estimating Fire Behavior. Ogden, (UT): USDA Forest Service, Intermountain Forest and Range Experiment Station. General Technical Report INT-122. 22 p.

Floyd, D.A., and Anderson, J.E. 1982. A New Point Interception Frame for Estimating Cover of Vegetation. *Vegetation* 50:185-186.

Floyd, D.A., and Anderson, J.E. 1987. A Comparison of Three Methods for Estimating Plant Cover, *Journal of Ecology* 75:221-228.

Longley, P.A., Goodchild, M.F., Maguire, D.J., and Rhind, D.W. 2005. Geographic Information Systems and Science. John Wiley & Sons Ltd, England.

Johnson, D.E., Vulfson, M., Louhaichi, M., and Harris, N.R. 2003. VegMeasure Version 1.6 User's Manual. Department of Rangeland Resources, Oregon State University, Corvallis, OR.

Key, C. and N. Benson. 2004. FIREMON Landscape Assessment V4.

McMahan, B., D. Narsavage, and K. T. Weber. 2003. "The Pole Cam": Corroborating field estimations with High Spatial Resolution Imagery. URL: http://giscenter.isu.edu/research/techpg/nasa_wildfire/Final_Report/Documents/Chapter3.pdf.

Perryman, B.L., and Olson, R.A. 2000. Age-stem diameter relationships of big sagebrush and their management implications. *Journal of Range Management*. 53:342-346.

Wagtendonk, J.W. van, Root, R., and Key, C. 2004. Comparison of AVIRIS and Landsat ETM+ Detection Capabilities for Burn Severity. *Remote Sensing of Environment* 92:397-408.

[THIS PAGE LEFT BLANK INTENTIONALLY]

Comparison of Field Methods

Jill Norton, Idaho State University, GIS Training and Research Center, 921 S. 8th Ave., Stop 8104, Pocatello, Idaho 83209-8104

ABSTRACT
Numerous types of field sampling protocols and procedures have been developed to estimate vegetation characteristics in semi-arid rangelands throughout the world. This study compared two methods commonly used in rangeland studies 1) ocular estimates and 2) point frame estimates. Both methods estimated percent cover of shrubs, grasses, forbs, litter, bare ground, and exposed rock. Statistical analyses were performed to compare these estimation methods which suggest that some cover type estimates tend to correlate well (e.g. shrubs) between sampling methodologies, while others (e.g, forbs) do not. Both methods appear adequate to support remote sensing based studies and additional correlative work is required to fully understand the effects, biases, and error propagation of sampling procedures *(abstract written by editor).*

KEYWORDS: GIS, sampling, remote sensing

INTRODUCTION

Collecting field data from an entire study site is often not practical, thus sampling is often performed. Sampling takes measurements on small plots that are representative of the larger study site. Most sampling methods are quantitative and can include measures of frequency, biomass, and/or cover. The latter measure, canopy cover is a measure of percentage of all ground cover such as vegetation, litter, and bareground. Cover is a measure of abundance that is not biased by the size and distribution of individuals (Floyd and Anderson, 1987; Floyd and Anderson, 1982). A challenging aspect of cover measurements is relating percent canopy cover to remote sensing data and measurements. Cover can be measured in many ways in the field; common methods include ocular estimate (Peterson, 2005), point (Friedel and Chewings, 1988), line (Rahman and Gamon, 2004), or quadrat (Hanley, 1978), surveys. Ocular estimation is most often represented as the percentage of total cover (Carlsson et al., 2005) within a plot as opposed to point, line, and quadrat methods which are direct measurements (Hanley, 1978).

Several studies have compared cover methods in grasslands and rangelands to assess the agreement between them (Hanley, 1978; Stohlgren et al., 1998; Carlsson, 2005). Within sagebrush (*Artemisia* ssp.) steppe ecosystems, Hanley (1978) and Floyd and Anderson (1987) concluded that line and point interception are more precise than visual (ocular) estimation. Kinsinger et al. (1960) determined that line interception was most accurate compared with two other canopy coverage techniques. Furthermore, Floyd and Anderson (1982) determined that point and line intercept methods provided similar results but that the line intercept required 32% more time for the same precision. Their 1987 study compared sampling time and precision between three cover estimate techniques and it revealed that point interception is the most efficient. The point frame technique is a well-accepted, accurate sampling method (Hanley, 1978; Floyd and Anderson, 1982; Floyd and Anderson, 1987; Inouye, 2002). Prior to its design, line interception was one of the most widely used cover methods in shrubby vegetation (Floyd and Anderson, 1982). Created by Floyd and Anderson (1982) in sagebrush steppe ecosystems, the point frame establishes a dot grid overlooking underlying vegetation and bare ground.

There are several types of ocular methods; each can be modified based on the users' sampling needs and experimental design. They typically involve a walk-about viewing the vegetation, soil, and other ground cover across the plot then estimating their percentages. The ocular method typically estimates the percent cover of the top canopy layer, as would be viewed by a satellite sensor. Although ocular estimates may provide a less precise and less accurate estimation of cover than other methods, their advantages include the ease and efficiency of data collection and potential for being most applicable to the spatial resolution of remote sensing images (e.g. 10-30 m). Though the ocular method is more time efficient during data collection than the point frame, it requires copious training time in order to minimize user bias. Ocular methods can involve viewing ground cover from different viewpoints such as panoramic and planimetric views. Germino et al., (2001) state that there is poor correlation between panoramic and planimetric landcover methods and that planimetric methods are better than panoramic methods for landcover studies due to perspective distortions.

We chose the point frame method for comparison to the ocular method because the near nadir view of the vegetation while sampling with a point frame emulates the view of a satellite. The point frame also provides an objective method for comparison to the ocular method. As Floyd and Anderson (1987) pointed out, absolute ground coverages are unknown, therefore it is difficult to compare coverage techniques with absolute certainty.

This study compares a point sighting frame method with an ocular estimation method using two data sets in the same area (+/- 5 m) before and after a prescribed burn (pre-fire n = 44, post-fire n = 42). We aim to determine the correlations between the two methods as well as their applicability for application to 10-30 m remote sensing imagery in rangeland ecosystems. Ground reference data (e.g. cover measurements) are often applied to remote sensing data to 1) aid in the analysis/interpretation of remotely sensed data, 2)

calibrate a sensor, and or 3) verify information extracted from remote sensing data (accuracy assessment) (Lillesand, 2004). Although Landsat data have been correlated to ground data for decades, there are few studies that relate precise ground truth data with remote sensing data. While many remote sensing studies use ground-truth data, no well accepted and published guide is available detailing how to routinely collect vegetation cover in rangeland environments to relate to remote sensing imagery. We compared the results of these two cover methods in order to determine which one would be favorable in future rangeland applications. It was hypothesized that the point frame method would be more accurate in estimating ground cover based on the discussion above. The proportion of intercepted points averages the cover of that cover type and thus provides a better measurement for remote sensing accuracy assessment. There is flexibility in adjusting both point frame and ocular plot sizes to the scale of the imagery, yet the precision of the point frame is higher than that of an ocular estimate of ground cover.

METHODS

The study area is the Hitching Post pasture, a 3.24 km^2 fenced parcel within the U.S. Sheep Experiment Station (USSES) located in Clark County, Idaho (Fig. 1). The pasture is a sagebrush steppe ecosystem characterized by extreme seasonal variability and a co-dominance of *Artemisia* with several grass species (West and Young, 2000). This semiarid area has an elevation of 1463 m, an average annual precipitation of 250-530 mm, and average annual temperatures of 5°-6°C, with a 70 to 90 day frost-free season. The majority of the study area has gradual slopes (0%-1.5%). Soils are mixed, fine-loamy, frigid Calcic Argixerolls derived from residuum, alluvium, or windblown loess (Seefeldt, 2005; Natural Resources Conservation Service, 1995). Cattle and horses have grazed this pasture for the last decade, but it has been rested for the past two and a half years. No fires have occurred in the study area for the past 10 years and most of the area has moderate fuel load (≈ 6722 kg·hectare). The study area was stratified for sampling based on fuel load because vegetation biomass was unaffected by slope, soil type, grazing, or fire history. The pasture is within a sagebrush steppe ecosystem and has two primary subspecies of sagebrush (*Artemisia* ssp.), mountain big (*A. tridentata* ssp. *vaseyana*) and threetip sagebrush (*A. tripartita ssp. tripartita*); other shrub species include antelope bitterbrush (*Purshia tridentata*), green rabbitbrush (*Chrysothamnus viscidiflorus)*, and horsebrush (*Tetradymia canescens)*. There are a few small patches of the exotic forbs leafy spurge (*Euphorbia esula*) and spotted knapweed (*Centaurea maculosa*); the exotic annual, cheatgrass (*Bromus tectorum)*, occurred as a small component (<1%) of the overall plant cover. Lupine (*Lupinus argenteus)* is the most plentiful forb in the pasture, ranging in height from 20 cm to 1 m. During field sampling in summer 2005, sparse bareground was observed, and live vegetation cover (sagebrush, forbs, and grass) was high. This study area was chosen because of the opportunity to participate in a prescribed burn (September 23 and 24, 2005), allowing a high degree of control for pre- and post-fire field sampling.

Though there is not a standard point frame plot size, we determined our plot size to be 20 x 40 m according to the smallest satellite imagery pixel size used in a related study (10-20 m resolution, SPOT 5). This plot size directly relates to at least two (ideally eight with precise georegistration) pixels and therefore provides more accurate comparisons between field data and remote sensing data. Vegetation and/or soil in point frames were assigned to six categories: shrub, grass, forb, litter, rock, and bareground. Shrubs, forbs, and grasses were recorded if photosynthetic tissue fell under a point; shrub stem, dead or alive, and downed combustible debris were recorded as litter if it fell under a point; and rock or bareground were recorded if they were under a point. The necessary number of frames per plot were determined using sample effort curves (Fig. 2), sufficient to capture the variability within the cover types in the study area consisted of 15 frames within each plot. The 15 frames collected within each 20 x 40 m plot used a point frame (0.5 x 1 m with 36 points at 0.1 m intervals) placed ≈1 m aboveground, totaling 540 point observations per plot (Fig. 3). Forty-nine random point frame plots were collected with the following criteria: 1) >20m from all bulldozer-created black-lines (for enclosure of the prescribed burn), and 2) >20m from all roads to mitigate road effects. Before the fire we sampled the 49 random plots, and

post-fire we sampled 42 of the same random plots (within +/- 5 m). Plot boundaries were recorded with a Trimble GeoXT GPS receiver (+/- 0.7m @ 95% CI) (Serr et al 2006).

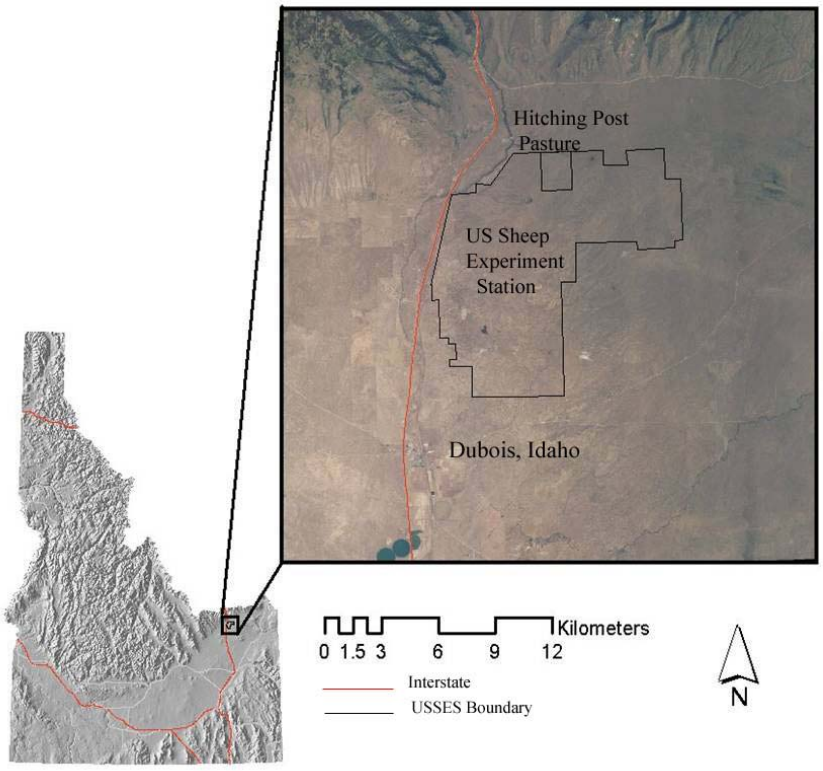

Figure 1. Location of the Hitching Post pasture study area in southeastern Idaho.

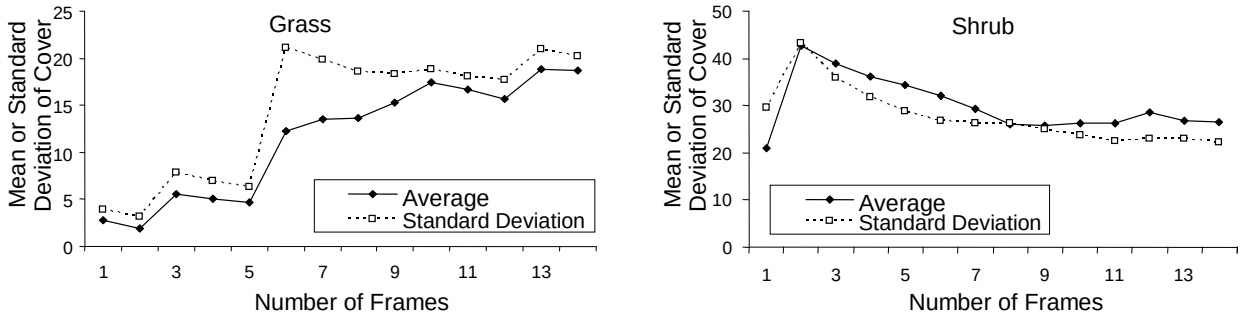

Figure 2. A sample effort curve is used to determine the necessary sampling intensity from one 20 x 40 m plot. Above, the cumulated mean (boxes) and standard deviation (diamonds) of shrub and grass cover for the plot level out around ten, indicating the need for approximately ten frames to estimate shrub and grass cover.

The ocular estimate method used mimics that developed by the ISU GIS TReC (2006) in 1999 and modified by McMahan et al. (2003) for semiarid rangelands in southeastern Idaho. In this method, six cover classes are used to visually assess percent of ground cover by two observers over a 60 m x 60 m plot which ideally covers four Landsat 30 x 30 m pixels or at least two pixels. Each person starts in the plot center and paces 30 m in opposite directions to the plot boundary. After walking the plot circumference, they proceed to walk in a spiral pattern within 3-4 m of the previous track back towards the plot center while observing plot attributes. At the center, each plot attribute is discussed until agreed upon. The six cover classes collected include shrub, grass, forb, litter, bare ground, and rock. Categorical

groups (Table 1) are used to assess percent cover for each cover class (McMahan et al., 2003). The same 42 random plots (as point frame plots) were navigated to both pre- and post-fire for this method so that cover class correlations could be fairly assessed. Each plot center location was recorded using a Trimble GeoXT GPS receiver (+/- 0.7m @ 95% CI) (Serr et al. 2006). Other attributes of the point frame method (Table 2) are compared with the ocular method attributes.

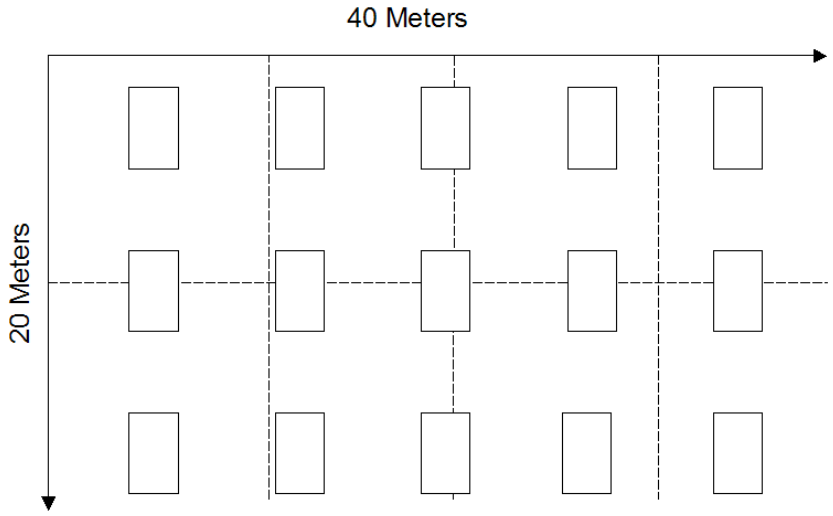

Figure 3. Approximate location of 15 point frames within each 20 x 40 m plot. Dashed lines indicate potential SPOT pixel 10 x 10 m placement.

Polynomial correlation was used to analyze the variability between the ocular and point frame estimates of ground cover. Before remote sensing could be performed, this was the most appropriate statistical technique for preliminary data analysis. Since both variables (point frame estimates and ocular estimates) were response variables and there was no assumption that one would predict the other, correlation was chosen over regression. Significances for ground cover were compared by applying analysis of variance (ANOVA) for each cover category in each data set (pre-fire data set n = 49; post-fire data set n = 42) using SAS (SAS Institute Inc., 2005).

Table 1. Categorical groups of percent cover.

Percent Cover	Cover Class
None	0
1-5%	1
6-15%	2
15-25%	3
26-35%	4
36-50%	5
51-75%	6
>75%	7

Table 2. Point frame plot field attributes collected with Trimble GeoXT GPS receiver and ArcPad customized form.

Attributes
Plot ID and its boundary location
Fuel load (3 categories) or Burn Severity
Plot homogeneity (as described in Field Methods)

RESULTS

Correlation analyses between the point frame and ocular estimates were performed with the pre-fire and post-fire field collected data sets. Data show that shrub has the best correlation coefficient for both pre-fire and post-fire data sets (Figures 4 and 5). For the pre-fire data, shrub is the only cover that has fair correlation 79%; bare ground has the next best correlation, a weak 65%. However, for the post-fire data, shrub, forb, and bare ground have strong correlation, 89%, 83%, and 81% respectively. Litter and rock correlations are poor for pre-fire data (38% and 45% respectively), yet post-fire correlations improve to 74% and 53% respectively. Therefore, point frame and ocular estimate correlations improved after the prescribed burn.

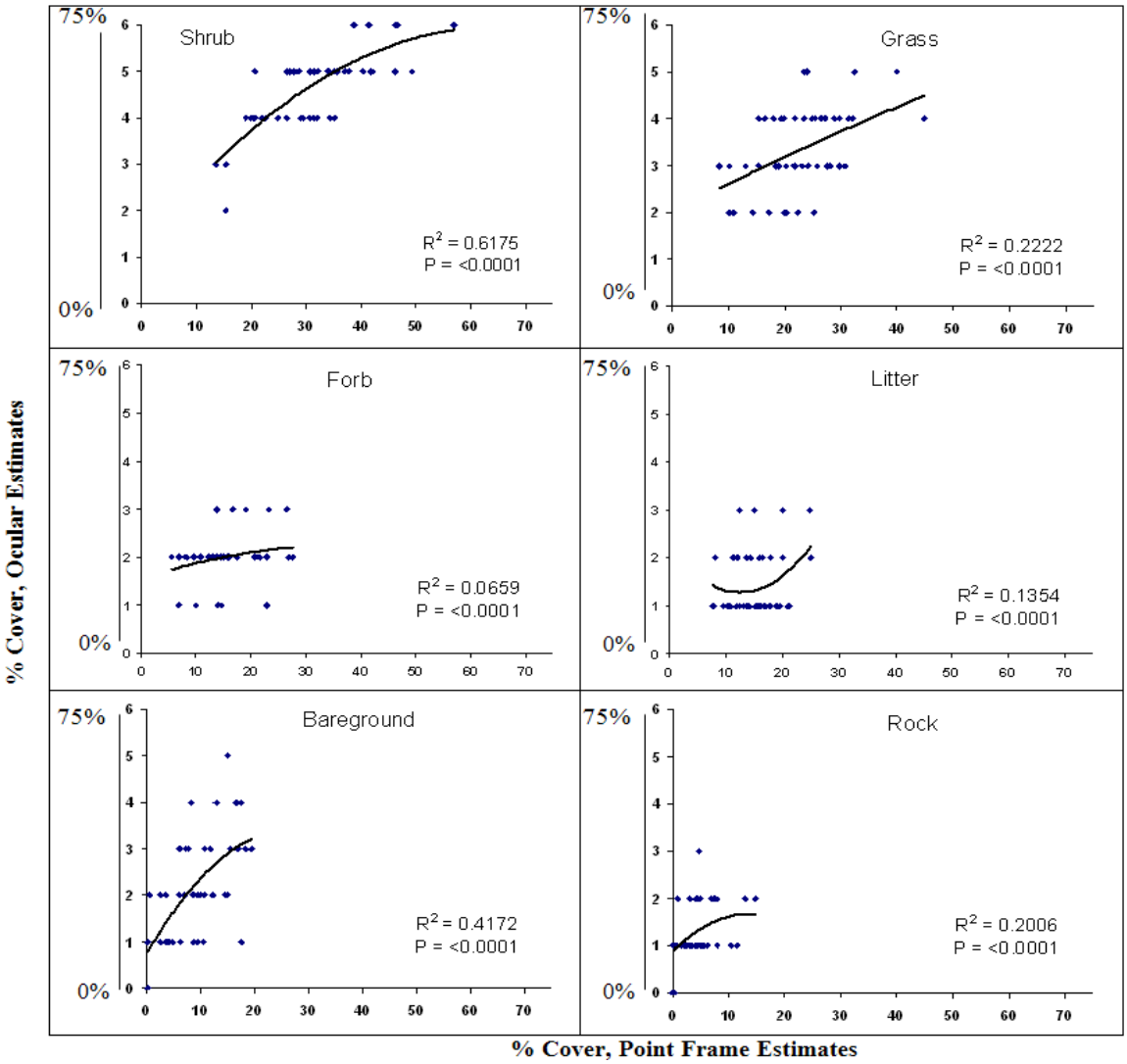

Figure 4. Using the pre-fire data set, point frame estimates are fairly correlated with ocular estimates (n = 49) in the same area for shrub and bareground.

DISCUSSION AND CONCLUSIONS

The shrub cover had the best correlation between ocular and point frame estimates, likely because of its relatively large size (scale) and thus easy for the human eye to estimate total cover. Our lowest correlations with pre-fire data were with litter and rock, hypothesized to be due to their fine scale and thus difficulty to interpret. All post-fire correlations were higher between field methods, most likely because visually assessing cover on the same plane (i.e. burned landscapes) is easier than assessing cover with

multiple canopy levels (i.e. vegetated landscapes).

The shrub cover class has overwhelmingly more height and depth than the other classes. Grass and forbs also have height and depth but they are much shorter and not as broad. Litter, bareground, and rock have relatively little height or depth; these classes are at ground level (except for some litter and shrub stem) and tend to cover a more continuous area than the vegetation classes. These characteristics are pertinent to the perspective of the observer(s).

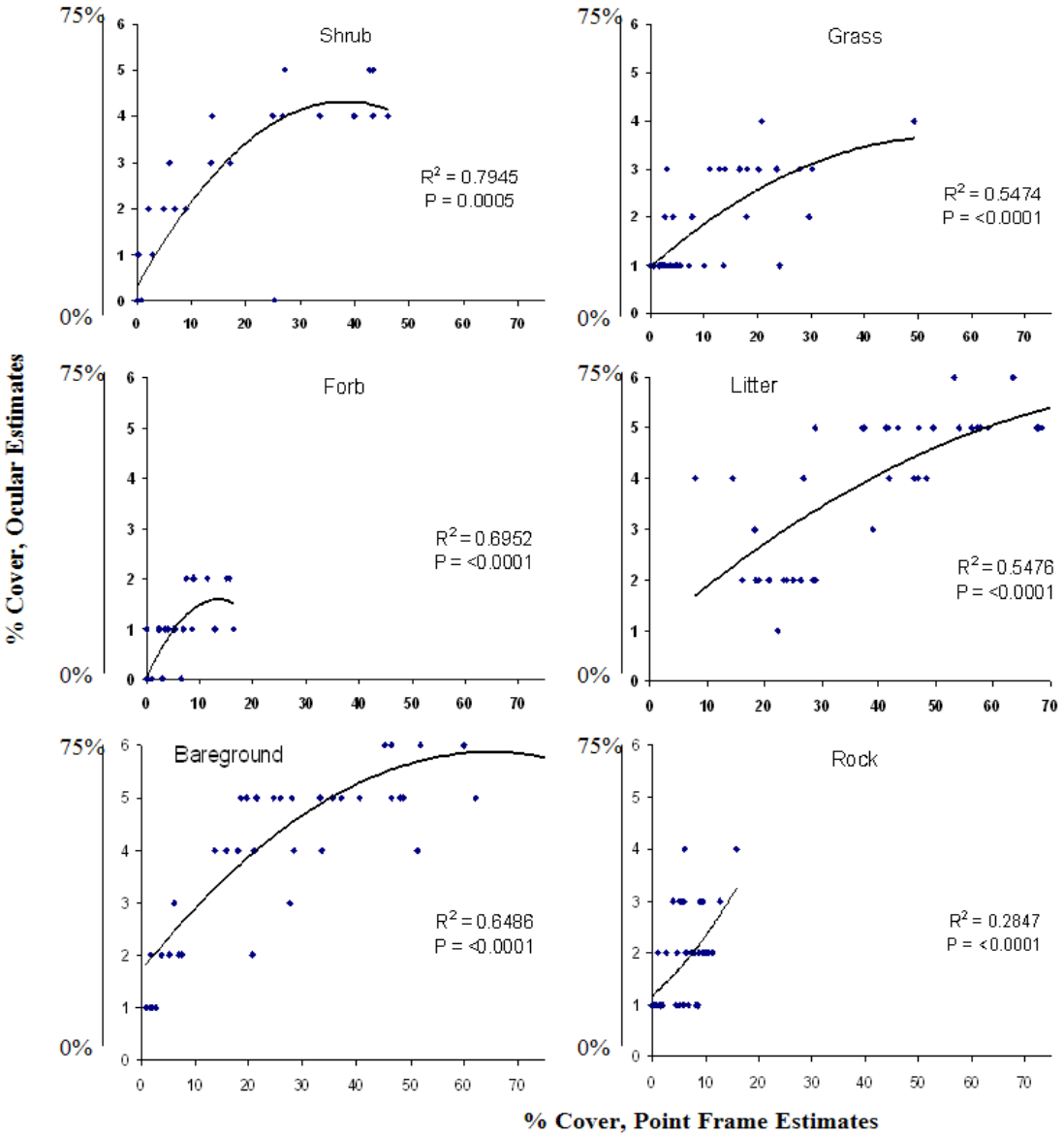

Figure 5. Using the post-fire data set, the best correlation between point frame estimates and ocular estimates are for shrub (best overall correlation) and forb.

Because pre-fire vegetation at our study site had a variety of height and depth characteristics, panoramic observations through the ocular method are likely poor estimates. Though our ocular estimates involved walking the plot extensively, we didn't have a completely nadir view upon the ground cover, as the point frame did. Thus the point frame results have better accuracy in the pre-fire estimates. On the other hand, the post-fire ground cover had fewer canopy levels (often just one), with less vegetation and more

exposed litter, bare ground, and rock. As our post-fire correlation results show, it was easier to ocularly estimate cover with fewer canopy levels and more continuous cover.

Field methods for determining ground cover must take into account perspective distortions such as line of sight and distance effects (Germino et al., 2001). For example, observations taken only from the plot center are error prone. Thus a nadir view of underlying vegetation is necessary to mitigate these effects. Therefore if ocular methods are used, the viewer must walk the plot in a small-scale, grid-like fashion in order to view in nadir the vegetation across the whole plot. The ocular estimations could be improved by decreasing the grid size and using a complete nadir observation stance. The point frame observations were taken at a small scale (0.5 x 1.0 m) with 15 frame estimates across the plot. More point frames may increase the accuracy and precision through observing more of the plot.

The intention of this project was to correlate two field methods for estimating ground cover in rangelands in order to determine the best method for application with 10-30 m remote sensing data. A method which correlates with remote sensing data will enhance training data and thus provide better accuracy assessments. We show that the point frame may be more accurate for dense vegetation, whereas the ocular method may be more appropriate in single canopy or extremely sparse vegetation. The only exception to this is the shrub category which had high correlation; therefore it may be applicable to estimate its cover alone for application to remote sensing imagery. The point frame method is a practical option because it provides better overall accuracy, no subjectivity/user bias is introduced, and it has good repeatability which is essential in multi-temporal studies. It takes only two to three times more sampling time (Table 3) than ocular methods, with relatively no training time. Because ocular estimates require less field time for each plot and thus more area can be covered, it is also an attractive option for ground truthing purposes. We've shown that both methods are feasible for ground truthing purposes as long as scale, number of canopy levels, and perspective distortions are taken into consideration so that ground cover units are not compromised (Tables 4 and 5). The results of this analysis are the backbone for future correlational studies between cover methods and application to remote sensing data.

Table 3. Attributes of the ocular and point frame vegetation cover field methods.

	Ocular	Point Frame
Time per plot	15-20 minutes	30-40 minutes
Accuracy	Low	0.5 x 1.0 m
Precision (repeatability)	Poor	High
Scale (extent)	60 m x 60 m	20 m x 40 m

Table 4. Maximum percent cover (within each cover class) using ocular and point frame estimate data collected pre-fire.

	Ocular Estimates						Point Frame Estimates					
	Shrub	Grass	Forb	Litter	Bare-ground	Rock	Shrub	Grass	Forb	Litter	Bare-ground	Rock
0%												
1-5%				65%	31%	71%						57%
6-15%			80%						53%	59%	49%	
16-25%		43%						53%				
26-35%							41%					
36-50%	45%											
51-75%												
>75%												

Table 5. Maximum percent cover (within each cover class) using ocular and point frame estimate data collected post-fire.

	Ocular Estimates						Point Frame Estimates					
	Shrub	Grass	Forb	Litter	Bare-ground	Rock	Shrub	Grass	Forb	Litter	Bare-ground	Rock
0%	48%		57%				55%		50%			
1-5%		60%				45%		43%				
6-15%												55%
16-25%											21%	
26-35%												
36-50%				48%	36%					31%		
51-75%										31%		
>75%												

ACKNOWLEDGEMENTS

This study was made possible by a grant from the National Aeronautics and Space Administration Goddard Space Flight Center. ISU would also like to acknowledge the Idaho Delegation for their assistance in obtaining this grant.

LITERATURE CITED

Carlsson, A.L.M., Bergfur, J., and Milberg, P. 2005. Comparison of data from two vegetation monitoring methods in semi-natural grasslands. *Environmental Monitoring and Assessment*, 100, 235-248

Floyd, D. and J. Anderson. 1982. A New Point Frame for Estimating Cover of Vegetation. *Vegetatio* 50: 185-186.

Floyd, D. and J. Anderson. 1987. A Comparison of Three Methods for Estimating Plant Cover. *Journal of Ecology* 75: 221-228.

Friedel, M.H. and Chewings, V.H. 1988. Comparison of crown cover estimates for woody vegetation in arid rangelands. *Austral Ecology*, 13, 463-468

Germino, M.J., Reiners, W.A., Blasko, B.J., McLeod, D., and Bastian, C.T. 2001. Estimating Visual Properties of Rocky Mountain Landscapes Using GIS. *Landscape and Urban Planning* 53: 71-83.

GIS TReC. 2006. GIS Training and Research Center. URL: http://giscenter.isu.edu/software/index.htm Last accessed: October 16, 2006.

Hanley, T.A. 1978. A Comparison of the Line-Interception and Quadrat Estimation Methods of Determining Shrub Canopy Coverage. *Journal of Range Management* 31:60-62.

Inouye, R. 2002. Sampling Effort and Vegetative Cover Estimates in Sagebrush Steppe. *Western North American Naturalist* 62(3): 360-364.

Kinsinger, F.E., Eckert, R.E., and Currie, P.O. 1960. A comparison of the line-interception, variable-plot, and loop methods as used to measure shrub crown cover. *Journal of Range Management*, 13, 17-21

Lillesand, T.M., Kiefer, R.W., and Chipman, J.W. 2004. *Remote Sensing and Image Interpretation.* (pp.1-500). New York: Wiley

McMahan, J.B., Narsavage, D., and Weber, K.T. 2003. "The Pole Cam": Corroborating field estimations with High Spatial Resolution Imagery. URL Http://giscenter.isu.edu/research/techpg/nasa_wildfire/Final_Report/Documents/Chapter3.pdf.

Natural Resources Conservation Service (NRCS). 1995. Soil investigation of Agriculture Research Service, United States Sheep Experiment Station headquarters range, US Department of Agriculture. (pp. 133). Rexburg, ID: NRCS

Peterson, E.B. 2005. Estimating cover of an invasive grass (Bromus tectorum) using tobit regression and phenology derived from two dates of Landsat ETM+ data. International Journal of Remote Sensing 26, 2491-2507.

Rahman, A. and Gamon, J. 2004. Detecting biophysical properties of a semi-arid grassland and distinguishing burned from unburned areas with hyperspectral reflectance *Journal of Arid Environments,* 58, 597-610

SAS Institute Inc., 2005. Cary, NC, USA

Seefeldt, S.S. 2005. Consequences of selecting rambouilllet ewes for mountain big sagebrush (*Artemisia tridentata ssp. vaseyana*) dietary preference. *Rangeland Ecology and Management,* 58, 380-384

Serr, K., Windholz, T., and Weber, K., 2006, Comparing GPS Receivers: A Field Study. Journal of the Urban and Regional Information Systems Association Volume 18 No. 2. p19-23.

Stohlgren, T.J., Bull, K.A., and Otsuki, Y. 1998. Comparison of rangeland vegetation sampling techniques in the central grasslands. *Journal of Range Management*, 51, 164-172

West N.E. and Young, J.A. 2000. Intermountain Valleys and Lower Mountain Slopes. In M.G. Barbour and W.D. Billings (Ed.), *North American Terrestrial Vegetation* (pp. 255-284). Cambridge, UK: Cambridge University Press

The Use of Remote Sensing Indices to Determine Wildland Burn Severity in Semiarid Sagebrush Steppe Rangelands Using Landsat ETM+ and SPOT 5

Jill Norton, Idaho State University, GIS Training and Research Center, 921 S. 8th Ave., Stop 8104, Pocatello, Idaho 83209-8104

ABSTRACT

This study evaluates ten remote sensing indices to detect burned areas and burn severity in a southeastern Idaho study area. While fire-related studies have been performed in forested ecosystems, few have been conducted in sagebrush steppe rangelands. Burn severity, defined as the completeness of aboveground vegetation removal during the burn, is useful in determining the type and location of treatment(s) that land managers can implement to speed recovery, and thus assess effectiveness and speed of landscape recovery. This study utilizes pre- and post-fire field based sampling as ground control for image processing of Landsat ETM+ and SPOT 5 multispectral imagery. Single and multi-date indices were validated through accuracy assessment techniques. Remote sensing indices comparing burned with unburned areas had better overall, user's, and producer's accuracies than indices comparing levels of burn severity. The best burn versus unburned index was the Soil Adjusted Vegetation Index (SAVI; 100% overall accuracy) derived from SPOT imagery, and the best burn severity index was the relative differenced Normalized Burn Ratio (RdNBR; 73% overall accuracy) derived from Landsat imagery. These two indices provided the highest user's and producer's accuracies.

KEYWORDS: fire, GIS

INTRODUCTION

Introduction and Statement of the Problem

Roughly 35-40% of the terrestrial earth's surface is comprised of arid and semi-arid lands (Rahman and Gamon, 2004; Anderson and Inouye, 2001; McGwire et al., 2000). Specifically, sagebrush steppe is the largest semiarid vegetation type in North America, yet it is critically endangered (Anderson and Inouye, 2001). In order to properly manage rangelands, it is essential to have a clear understanding of their ecological processes, functions, and the mechanisms driving change. For instance, fire has a powerful influence on ecosystem function and dynamics. Wildland fire is the primary cause of destruction in sagebrush steppe, where erosion hazard is high, vegetation is dry, and perennial vegetation recovery rates are slow (Ruiz-Gallardo et al., 2004; Whitford, 2002; and Wright and Bailey, 1982). Fire frequencies range from 15-100 years in sagebrush steppe ecosystems (Wright and Bailey, 1982; Ratzlaff and Anderson, 1995; Miller and Rose, 1999; Harniss and Murray, 1973; Watts and Wambolt 1996; and Brown et al., 2000). Moreover, fire frequencies have increased due to an abundance of fire-prone introduced annuals (i.e. *Bromus* tectorum) or short-lived perennials, and due to fuel loading following many years of fire suppression (Anderson and Inouye, 2001; Keeley et al., 1999; Diaz-Delgado et al., 2002; Obrist et al., 2003; Whisenant, 1990; Brown et al., 2000). From 1995 to 2005 wildland fires burned approximately 24,277,866 ha in the US compared with 19,828,021 ha burned between 1960 to 1970 (NIFC, 2006). When managing rangelands, the multitude of fire effects need to be accounted for and monitored to update fuel model/vegetation data bases, and to assess ecosystem damage and benefit, the success or failure of a treatment, the possible need for rehabilitation, and vegetation change effects for wildlife concerns or erosion potential (Lutes et al., 2003). The need for information about burned areas (i.e. perimeter and area) has increased; moreover, it is essential to understand the heterogeneity of burn severity patterns within a fire perimeter (van Wagtendonk et al., 2004). Burn modeling and maps (severity, frequency, pattern, size, etc.) provide useful information for land planning, risk assessment, and evaluation of ecological conditions such as the structure, composition, and function of ecosystems (Morgan et al., 2001). Knowledge of within-burn variability fosters understanding of fire's effects such as burn severity, vegetation recovery, and succession enhancing post-fire rehabilitation and remediation efforts (Roy et al., 2006). For example, burn severity information is useful in determining the type and location of treatment(s) that land managers can implement and later assess effectiveness and rate of landscape recovery. Simple and cost-effective techniques need to be established to map fire effects, such as burn severity and extent, within rangelands. Remote sensing with satellite imagery offers the ability to evaluate burned areas across multi-temporal and multi-spatial scales (Morgan et al., 2001). Satellite data are useful for examining fire effects because 1) they can be used to qualitatively and quantitatively evaluate vegetation over multi-temporal and spatial scales, 2) they can be relatively low in cost, 3) they can systematically cover large and inaccessible areas (in many instances fires are located in remote areas), and 4) they can capture data from parts of the electromagnetic spectrum that humans cannot sense (i.e. infrared), which provide useful information specific to vegetation and soils.

Definitions of burn severity differ, as well as the amount of time elapsed between a fire occurrence and when burn severity is assessed (Ryan and Noste, 1983; Miller and Yool, 2002; Roy et al., 2006; Key and Benson, 2006); however, for this research, burn severity is defined as the completeness of the burn, or the damage to the vegetation immediately after the fire. Often confused with the term burn *intensity* which refers to the level of heat produced and flame length, our definition of burn severity includes how thoroughly the vegetation was burned, regardless of the pre-existing fuel load.

This study hypothesizes that burn severity can be modeled with remote sensing techniques using either single date imagery or multi-temporal differencing incorporated with pre- and/or post-fire field data. A sub-study to this project includes testing the hypothesis that pre-fire fuel loads are correlated with burn severity levels.

BACKGROUND

Remote Sensing

Remote sensing is the science of collecting data about a feature(s) on earth without being in physical contact with the subject of interest. Lillesand et al. (2004) describe it as the science and art of acquiring information about an object, area, or phenomenon by analyzing data that is acquired by a device not in contact with that which it is observing. Biophysical characteristics and human activities can be measured and monitored with this technology (Jensen, 2000). Images are taken of the earth's surface capturing energy (i.e. light) from the electromagnetic spectrum. The spectral composition of this radiated energy represents information about the physical properties of vegetation, soil, and water. Parts of the electromagnetic spectrum (i.e. visible bands and infrared bands) are separated from the remaining data and analyzed using remote sensing software. The spectral information from the feature of interest is put into an interpretable form with remote sensing segmentations, techniques, and indices. We can detect change over time applying multi-temporal remote sensing techniques, which is comparing imagery from different time periods.

Remote Sensing of Vegetation in Semi-Arid Environments

Special remote sensing problems need to be considered in rangeland ecosystems due to the variability within the vegetation (or the lack of) and the presence and high reflectance of soil. These rangeland characteristics contribute to the unreliability of remote sensing of vegetation along with: nonlinear mixing due to multiple scattering of light, evolutionary adaptations (making desert plants spectrally dissimilar and lacking a strong red edge), spectral variability within the same species (due to spatially discontinuous precipitation patterns), open shrub canopies (affecting near infrared (NIR) reflectance), small plant canopies, and varying phenological status of plant canopies across space and time (Asner and Heidebrecht, 2002; Okin et al., 2001). Because there tends to be an abundance of bareground in sagebrush steppe rangeland ecosystems and soil reflectance is often brighter than vegetation reflectance, bareground 'dilutes' the vegetation signature. There are many vegetation indices used to detect vegetation parameters; however, problems exist with using these in rangeland ecosystems because they do not account for soil background variations (Qi et al., 1994). This phenomenon of soil influencing the interpretation of vegetation has been well documented (Bannari et al., 1995; Huete, 1988; Huete, 1989; Qi et al., 1994; Schmidt and Karnieli, 2001). It has also been shown that the variation in soil brightness (i.e. wet vs. dry, and different soil association characteristics) can affect the results of vegetation indices (Schmidt and Karnieli, 2001; Asner, 2004). Examples of indices used in semiarid environments include the normalized difference vegetation index (NDVI), soil adjusted vegetation index (SAVI), and modified soil adjusted vegetation index (MSAVI).

The normalized difference vegetation index (NDVI; equation 1), attributed to Rouse et al. (1973), is a remote sensing technique used to estimate vegetation biomass. The NIR band of the electromagnetic spectrum make this measure sensitive to the physiological activity of plants and the red band is sensitive to vegetation and soil discrimination (Jensen, 2000). Though vegetation has been monitored on global scales using the NDVI, it is a poor indicator of vegetation biomass when vegetation cover is low, such as in semiarid rangelands (Huete et al., 1987; Schowengerdt, 1997). This index varies between negative 1 to positive 1.

$$\frac{NIR - Red}{NIR + Red} \qquad (1)$$

The soil adjusted vegetation index (SAVI) is a transformation technique which minimizes soil brightness and soil variations using the red and near-infrared wavelengths as well as a constant soil adjustment factor L. Huete (1988) found that an adjustment factor of 0.5 reduced soil noise across a range of broad-leaf cotton and narrow-leaf grass canopy densities. Huete determined that an adjustment factor of 0.5 could be used across different vegetation densities and different soil types.

The inductive modified soil adjusted vegetation index (MSAVI) is useful to detect vegetation in arid environments because of its ability to account for high bareground reflectance using a *variable* soil adjustment factor L (Qi et al., 1994). The MSAVI remote sensing index uses an iterative inductive equation to calculate L. Furthermore, MSAVI iteratively calculates L until the soil cannot be minimized any more.

Remote Sensing of Burns and Burn Severity

The application of remote sensing for burned area analysis has increased recently utilizing several different sensors, resolutions, and techniques (Garcia and Chuvieco, 2004). Many studies have been performed in forested ecosystems to determine burn severity within a burn perimeter (Patterson and Yool, 1998; Wimberly and Reilly, in press; Turner et al., 1994; White et al., 1996; van Wagtendonk et al., 2004; Brewer et al., 2005; Epting and Verbyla, 2005; Epting et al., 2005), but few have been carried out specifically in areas with reduced vegetation cover (Smith et al., 2005; Roy et al., 2006) or specifically within semiarid sagebrush steppe ecosystems.

The traditional technique to detect burned areas and burn severity is by estimating biomass loss with the NDVI (Salvador et al., 2000; Flasse et al., 2004; Diaz-Delgado et al., 2003). However, bands in the visible spectrum can be susceptible to atmospheric interference and less sensitive to changes in burned landscapes than infrared bands. The NDVI was used until about 1999, when Lopez Garcia and Caselles (1991) developed an algorithm later coined by Key and Benson as the normalized burn ratio (NBR; equation 2) using Landsat imagery (Key and Benson, 1999b; Salvador et al., 2000; Key and Benson, 2004a; Key and Benson, 2006). Since then, it is the most widely used method on large fires (>500 acres) for perimeter and burn severity detection on public lands (Cocke et al., 2005; Key and Benson, 2006).

$$\frac{Band\ 4 - Band\ 7}{Band\ 4 + Band\ 7} \qquad (2)$$

Where: Band 4 = Landsat Band 4 (.76-.90 μm)
Band 7 = Landsat Band 7 (2.08-2.35 μm)

The NBR algorithm was developed in a mild-warm/subtropical climate study area composed of 2/3 forest and 1/3 scrub/bush using Landsat 5 (TM) (Lopez Garcia and Caselles, 1991). A correlation matrix of the reference and burned area was performed to determine the most uncorrelated pair of Landsat bands. The shortwave infrared (SWIR) band increases most after fire, and the near infrared band decreases most after fire. As a result, their technique uses the near-infrared and shortwave infrared bands because these bands correspond best with vegetation change due to fire in the forested ecosystem in which it was developed. Later the algorithm was put to ardent use by Key and Benson (1999b, 2004a, 2006) within forested ecosystems using Landsat TM/ETM+ imagery (NBR, equation 2). Landsat data have been traditionally used to map burned areas and fire severity (White et al., 1996; Patterson and Yool, 1998; Key and Benson, 1999b, 2004a; Santos et al., 1999; Salvador et al., 2000; Miller and Yool, 2002; Diaz-Delgado et al., 2003; Garcia and Chuvieco, 2004; Howard and Lacasse, 2004; van Wagtendonk et al., 2004; Brewer et al., 2005; Epting et al., 2005; Cocke et al., 2005; Roy et al., 2006). The NBR index is evaluated by correlating the index with field-based composite burn index (CBI) values. Performed in the field, the CBI was developed by Key and Benson (1999a, 2004b) as an ocular measurement of fire severity within each study plot that corresponds with sensor radiometric response data. CBI data include percent of foliage and litter/moss consumed, as well as percent of re-sprouting vegetation.

A differenced NBR (dNBR) is used to offer a quantitative measure of environmental change due to the fire, or temporal difference (Key and Benson, 1999b; Key and Benson, 2004a). The dNBR represents a

scaled index of the magnitude of change caused by fire (van Wagtendonk et al., 2004). To do this, the post-fire NBR data set is subtracted from the pre-fire NBR data set (equation 3).

$$dNBR = NBR_{pre\text{-}fire} - NBR_{post\text{-}fire} \qquad (3)$$

There are two types of dNBR severity measures, an initial assessment and an extended assessment. The initial assessment represents immediate change: the post-fire scene is acquired immediately after the fire. However, the extended assessment represents recovery of the plant community. The post-fire scene is not acquired until the next growing season, which could be as early as a few weeks or 11 months after the fire, depending on the season of fire (Key and Benson, 2004a). The pre-fire scenes for each assessment are taken within the same seasonal period, either the same year or an earlier year (to match phenological timing).

The NBR and dNBR may or may not be applicable in rangeland ecosystems due to vegetation re-growth times with respect to the seasonality of the burn. For instance, it takes longer for forested ecosystems to recover to pre-fire conditions (i.e., having the same reflectance) than rangelands. Alternatively, depending on pre-fire condition and the season of the burn in rangelands, vegetation can recover as early as the end of the same growing season, or as up to 10 years following the fire.

Several single date and multi-date approaches have been compared for the assessment of burn severity in forests such as those by Epting et al. (2005) and Brewer et al. (2005). Epting et al. (2005) evaluated 13 remote sensing techniques as both single date and multi-date analyses including: three Landsat TM and ETM+ band ratios (bands 7/4, 7/5, 4/5); three vegetation indices (NDVI, SAVI, MSAVI); two multivariate transformations (a Kauth-Thomas Tasseled Cap transformation including greenness and wetness components, and Second Principal Components Analysis); normalized burn ratio (NBR; and differenced normalized burn ratio (dNBR)), and single TM bands 4, 6, and 7. Though Epting et al. (2005) had highest results (correlating field measures of fire severity with mapped fire severity) with the dNBR in forested areas, they determined that the dNBR may not be appropriate for estimating burn severity in non-forested areas. Brewer et al. (2005) compared six remote sensing indices: two principal components analyses; two artificial neural network classifications (a back propagation and a k-nearest neighbor); and two normalized difference indices (NBR and a modified NBR which replaced Landsat band 7 with band 5). Out of the six methods compared, Brewer et al. (2005) determined that the dNBR was the simplest method that does not introduce analyst input error (i.e., human bias) with the advantage that it can be used anywhere in the continental U.S. They separated forest (unburned, low severity, and high severity classes), shrub, and grass vegetation (unburned and burned classes), and resulted in 100% user accuracies for the burned/unburned shrub categories when compared with National Land Cover Data. Roy et al. (2006) agree that the dNBR is suboptimal in non-forested areas because of its insensitivity to burn severity. Miller and Thode (in revision) found that a Landsat relative dNBR (Table 1; RdNBR) performs better than the absolute dNBR at detecting high burn severity areas from moderate burn severity in a mixed forest/shrubland study area. Gerard et al. (2003) developed an algorithm coined the normalized difference SWIR (NDSWIR; Table 1) to map fire scar burns using pre-fire and post-fire SPOT NIR (0.84 µm) and SWIR (1.66µm) bands. The SPOT SWIR band is useful for the detection of old fire scars and canopy moisture content (Gerard et al., 2003).

Study Area

This study takes place within the Hitching Post pasture, a 3.24 km^2 fenced parcel within the U.S. Sheep Experiment Station (USSES) located in Clark County, Idaho at an elevation of approximately 1800 m (Fig. 1). Average annual precipitation ranges from 250-530 mm with up to seventy percent falling as snow (Seefeldt, 2005). Average annual temperatures are 5-6 °C, with a 70 to 90 day frost-free season. The majority of the pasture has gradual slopes (0-1.5 %), with the greatest slope being approximately 9 % excluding rocky outcrops. The pasture is a sagebrush steppe ecosystem characterized by extreme seasonal

variability and a co-dominance of *Artemisia* with several grass species (West and Young, 2000). The Hitching Post pasture has two primary subspecies of sagebrush (*Artemisia* ssp.): mountain big (*A. tridentata* ssp. *vaseyana*), and threetip (*A. tripartita* ssp. *tripartita*). Mountain big sagebrush is a more mesic subspecies located between 1525 m and 3050 m elevation (Wright and Bailey, 1982). It is between 0.73 - 1.22 m tall in precipitation zones varying between 355 - 510 mm per year. Threetip sagebrush is typically found below 1830 m in dry soils receiving between 255 - 400 mm of precipitation per year (Wright and Bailey, 1982). This subspecies is a weak sprouter (grows from the meristem). Other shrub species within the pasture are antelope bitterbrush (*Purshia tridentata*), green rabbitbrush (*Chrysothamnus viscidiflorus)*, and horsebrush (*Tetradymia canescens)*. There are a few small patches of the exotic forbs leafy spurge (*Euphorbia esula*) and spotted knapweed (*Centaurea maculosa)*. The exotic annual, cheatgrass (*Bromus tectorum)*, occurs as a small component (<1%) of the overall plant cover. Lupine (*Lupinus argenteus)* is the most plentiful forb in the pasture, ranging in height from 20 cm to 1 m; graminoids present are thickspike wheatgrass (*Elymus lanceolatus)*, bluebunch wheatgrass (*Pseudoroegneria spicata*), and plains reedgrass (*Calamogrostis montanensis* Scribn.). Soils are mixed, fine-loamy, frigid Calcic Argixerolls derived from residuum, alluvium, or windblown loess (Seefeldt, 2005; NRCS, 1995). Sheep and horses have grazed this pasture for the last decade, but grazing has not occurred for the past 2.5 years prior to the burn.

Table 1. Remote sensing indices that were explored to find the best burn/no burn algorithm and the best burn severity algorithm.

Remote Sensing Index	Algorithm	Sensor	References
SAVI	$\frac{(1+L)(NIR-Red)}{NIR+Red+L}$ (L = 0.5)	Landsat: NIR = band 4 Red = band 3 SPOT: NIR = band 3 Red = band 2	Huete, 1988
MSAVI	$\frac{2*(NIR)+1-\sqrt{(2*(NIR)+1)2-8*(NIR-Red)}}{2}$	Landsat: NIR = band 4 Red = band 3 SPOT: NIR = band 3 Red = band 2	Qi et al., 1994
pNDSWIR	$\frac{NIR-SWIR}{NIR+SWIR}$	Landsat: NIR = band 4 SWIR = band 5	
NDSWIR	Pre-fire NDSWIR – Post-fire NDSWIR	SPOT: NIR = band 3 SWIR = band 4	Gerard et al., 2003
NBR	$\frac{NIR-SWIR}{NIR+SWIR}$	Landsat: NIR = band 4 SWIR = Band 7	Lopez Garcia and Caselles, 1991; Key and Benson, 1999b; 2004a
dNBR	Pre-fire NBR –Post-fire NBR		
RdNBR	$\frac{Pre\text{-}fireNBR-Post\text{-}fireNBR}{\sqrt{prefireNBR}}$	Landsat: NIR = band 4 SWIR = band 7	Miller and Thode, in revision

Remote Sensing Index	Algorithm	Sensor	References
Modified NDVI	$\frac{SWIR - Red}{SWIR + Red}$	SPOT: Red = band 2 SWIR = band 4	None
rModNDVI	$\frac{Pre\text{-}fireModNDVI - Post\text{-}fireModNDVI}{\sqrt{Pre\text{-}fireModNDVI}}$		

This study area was chosen because it offered an opportunity to participate in a prescribed burn, allowed a high degree of control for pre- and post-fire field sampling, and because it contained a sagebrush steppe rangeland environment. The prescribed burn occurred September [14 and 15], 2005, and is described in more detail below.

METHODS

Introduction

This study utilizes pre- and post-fire field-based sampling as training sites for establishing locations of sample sites along with a description of the vegetation, bareground, and burn severity observed at each site. The pre-fire field assessments were collected by two people together between mid-June and early August 2005, and post-fire sampling followed the September 2005 prescribed burn for approximately 1.5 months. Burn severity is assessed using a combination of field and satellite data that evaluate the vegetation lost due to fire. These field vegetation estimates are compared with remote sensing data with the goal to delineate areas of high and low amounts of live vegetation cover post-fire. The parameters we use to determine burn severity in the field are: 0% = no area burned, <50% = <50% area burned, >50% = >50% area burned, and 100% = all area burned.

Prior to the vegetation surveys, large-scale (~8000 m^2) vegetation variability and fuel load estimates were performed across the pasture to design a sampling regime which adequately sampled across all fuel loads. Fuel loads were sampled to get an accurate representation of pre-fire vegetation communities. Because the vegetation communities (i.e. fuel load and species type) were similar on all soils, elevations, and aspects in the pasture, further stratification of sampling was not necessary. Upon walking the entire pasture, three main types of vegetation cover (fuel load) were observed. There were patches of grass only (with bareground); patches of small, sparse shrubs (with grass and forbs); and patches of tall, dense shrubs (with grass and forbs). These qualitative observations are based on the work of the BLM's Determining Fuel Models method, which ocularly estimates the vegetation across a shrubland landscape in tons/acre (Anderson, 1982). Though biomass measurements are never made, this technique estimates biomass visually based primarily on grass and shrub (size and density) cover in rangelands. According to a USDA fuel load guidelines study, Anderson (1982) found that grass-only parts of shrublands equate to less than 1 ton/acre, and their shrublands averaged 4 tons/acre. Our fuel load categories correspond with Anderson's observations: grass-only patches are considered very low fuel load while high fuel load is characterized by tall, dense shrub areas. A transitional category of medium was formed, which is small to medium-sized shrubs with grass and forbs. During this process, 78 polygons ~8267 m^2 each (with consistent fuel loads) were recorded with a Trimble GeoXT GPS receiver (+/- 0.7m @ 95% CI (Serr, unpublished)) and labeled with their respective fuel loads. These polygons are hereafter named 'large scale, homogenous fuel load polygons'.

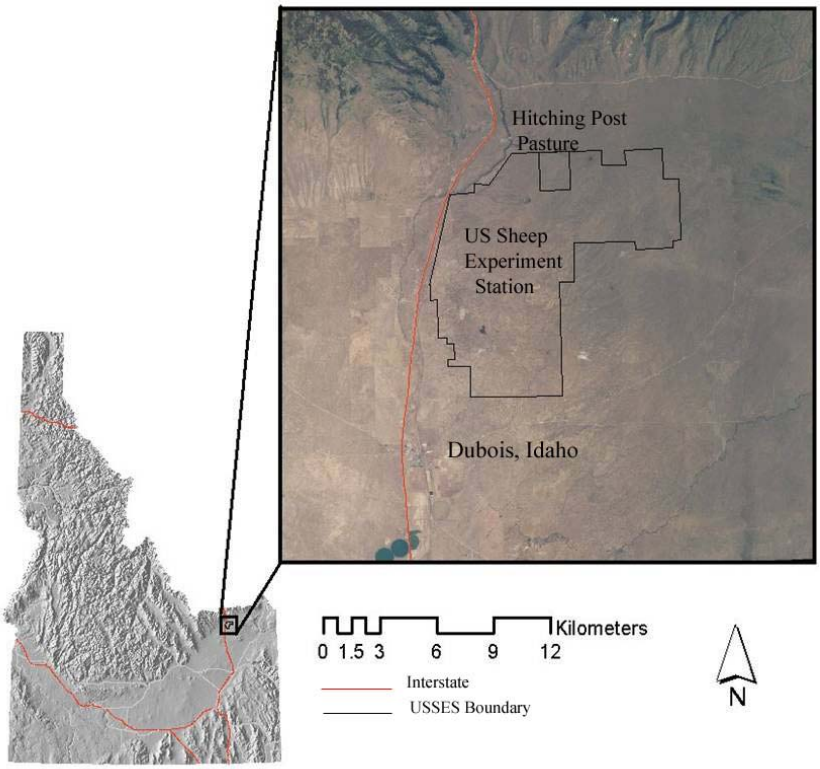

Figure 1. Location of the Hitching Post pasture study area in southeastern Idaho.

After the large-scale fuel load estimates were performed, two different methods for fine scale sampling of the vegetation were performed. These include: 1) 60 m x 60 m plot ocular estimates of vegetation and bareground percent cover, and 2) 20 m x 40 m plot point frame measurements. The ocular method is used for quickly collecting percent cover of the upper-most canopy and comparing the results with remote sensing data. Percent cover of shrub, grass, forb, litter, rock, and bareground are estimated over a 60 m x 60 m plot, after thoroughly walking the area. The point frame method takes longer in the field; however, it provides a more accurate representation of true ground cover (Floyd and Anderson, 1982; Floyd and Anderson, 1987). The point frame method was used because: 1) it serves as a complimentary method for coupling ground data with remote sensing data; 2) it provides fine resolution field data roughly equivalent to the resolution of the SPOT imagery (10 m); and 3) the near-nadir view while sampling the vegetation emulates the view of a satellite.

Pre-Field Operations

ESRI's ArcPad, (6.0.2, 1990-2000), a mobile GIS software installed on the GPS unit allowed seamless data collection between GPS locations and field attributes. ArcPad Application Builder in ArcPad Studio (6.0.0.24U, 2002) was used to customize an attributed form associated with each shapefile collected in the field. Pre-established categorical groups were used to assess percent cover (Table 2) for each cover class (shrub, grass, litter, bareground, rock, and forb) (McMahan et al., 2003).

Table 2. Categorical groups of percent cover.

Percent Cover	Cover Class
None	0
1-5%	1
6-15%	2
15-25%	3
26-35%	4
36-50%	5
51-75%	6
>75%	7

Field-Based Ocular Estimates

The ocular estimate method used was developed by the ISU GIS Training and Research Center (TReC) and modified by McMahan et al. (2003) for semiarid rangelands in southeastern Idaho. Plots are approximately 60 m x 60 m in order to encompass approximately four Landsat pixels (30 m x 30 m). This method has been used by the TReC as a cover method for remote sensing interpretation/classification since 1999 (McMahan et al., 2003; Russell and Weber, 2003; and Weber and McMahan, 2003). Two hundred random sampling locations were generated using the Raster Drilldown tool (GIS TReC, 2006) across the pasture that met the following criteria: 1) >20m from all bulldozer-created black-lines (for enclosure of the prescribed fire), and 2) >20m from all roads to ensure roads were not within plots, to mitigate 'road effects', and to eliminate sampling bias. Six additional plots were created in order to have adequate replication within unburned areas and fuel load classes. These 60 m x 60 m ocular estimate plots were located within all fuel load categories and adequate (≥ 30) representation was insured for each category. In total, 206 ocular plots were navigated to using the GPS receiver. Each person started in the plot center and paced 30 m in opposite directions to the plot boundary. After walking the plot circumference, they proceeded to walk in a spiral pattern within 3-4 m of the previous track back towards the plot center while observing plot attributes (Table 3). At the center, each plot attribute was discussed until agreed upon. Percent cover for six categorical categories (shrub, grass, forb, litter, rock, and bareground) were estimated. Each plot center location was recorded using the GPS receiver, and here sagebrush was described by its average height and diameter using calipers (+/-1cm) to approximate the age of each plant (Perryman and Olson, 2000). Four photo points were taken as well from the plot center, one in each cardinal direction. This method also includes identifying the dominant weed and estimating its abundance (percent cover). Fuel load (tons per acre) was estimated following BLM protocols (described above) over the 60 m x 60 m plot. Homogeneity of vegetation cover was assessed across each plot, and a plot was considered homogeneous if vegetation type and percent canopy cover was consistent at visually-based 10 m^2 increments across an entire plot. Therefore, if a 10 m^2 portion of the plot was different than the remaining areas within a plot, then the plot as a whole was not considered homogenous.

Field-Based Point Frame Measurements

Because the study uses 10 m SPOT imagery, a finer scale field method (versus the 60 m plot estimates) was sought for comparison with the imagery. Thus we chose point frame measurements made over a 20 x 40 m plot size which can encompass eight SPOT pixels. This plot size allows a benefit over a smaller plot size because there are more pixels in the plot tolerating some georegistration error. Though ocular estimates are time efficient and easy, they can be less precise (than point or line methods) and inherently subjective. In addition, the somewhat coarse and unequal (~ 14%) categorical increments (Table 2) used can be difficult to relate to absolute remote sensing measurements. It is important to determine a field method that is applicable to remote sensing in rangelands, and furthermore that is reliable, user-friendly, and lacks user bias. Because the field data are an integral part of remote sensing models, it must be accurate enough relative to the imagery resolution. It is important to note; however, that because exact vegetation coverages are unknown (using plots due to the time constraints of collecting cover across the whole study area), it is difficult to compare coverage techniques with absolute certainty.

Table 3. Field attributes for all ocular estimates collected with an ArcPad customized form within a Trimble GeoXT GPS receiver.

Attributes
Plot ID and its center point location
Date
Percent cover of: dominant shrub
Percent cover of: other shrubs present
Average shrub height (Low: <51cm, Medium: 51-100cm, Tall: >100cm)
Percent cover of: grass
Percent cover of: litter
Percent cover of: bareground
Percent cover of: rock
Percent cover of: forb
Percent cover of: dominant weed
Fuel load (Low: Grass only, Medium: small to medium sized shrubs, High: tall, dense shrubs)
Sage diameter measured once in each cardinal direction
Photos taken in 4 cardinal directions & their ID #
Presence of microbiotic crust
Observed vegetation type (GAP classification category which was 'Sagebrush Grassland', defined by the Idaho GAP 2 data set (2000),
Litter type (oxidized gray or biologically brown)
Plot homogeneity (as described in Field Methods)

The point frame technique, designed by Floyd and Anderson (1982) is a well accepted, accurate sampling method used to visually determine vegetation percent cover (Floyd and Anderson, 1987; Inouye, 2002). Designed in sagebrush steppe ecosystems, this frame establishes a dot grid overlooking underlying vegetation and bareground. Observers view vegetation from a near-nadir standing position and record the cover types that are beneath 36 intercepted points (cross-hairs). A number of point frames are collected within each pre-defined plot size; the sampling intensity necessary to capture variability within each plot was determined using a sample effort curve (Fig. 2). Based on sample effort curves from all cover categories, a maximum of 15 frames of point data were needed at each plot to ensure adequate representation of ground cover in this study area. The location of the 15 frames within each plot were selected at 7 m intervals across the 40 m-axis of the plot, then placed at 3 m, 5 m, and 7 m perpendicular to each interval along the 20 m-axis (Fig. 3). The 20 x 40 m plot boundary was established with a field tape and recorded with the GPS. In addition to the ground cover class identified (at each cross-hair) in the frame, fuel load (tons per acre) was estimated following BLM protocols (same as above), and homogeneity was assessed at the 20 m x 40 m scale. Each plot's attributes (Table 4) were entered into the GPS.

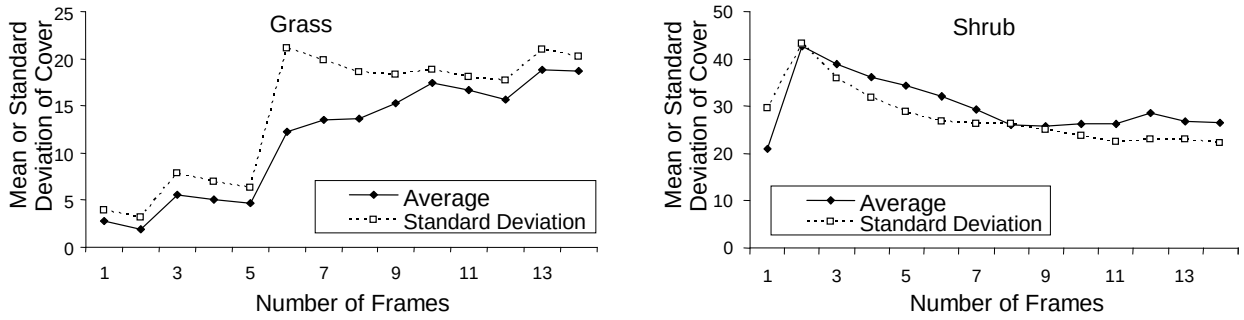

Figure 2. A sample effort curve is used to determine the necessary sampling intensity from one 20 x 40 m plot. Above, the cumulated mean (boxes) and standard deviation (diamonds) of shrub and grass cover for the plot level out around ten, indicating the need for approximately ten frames to estimate shrub and grass cover.

.

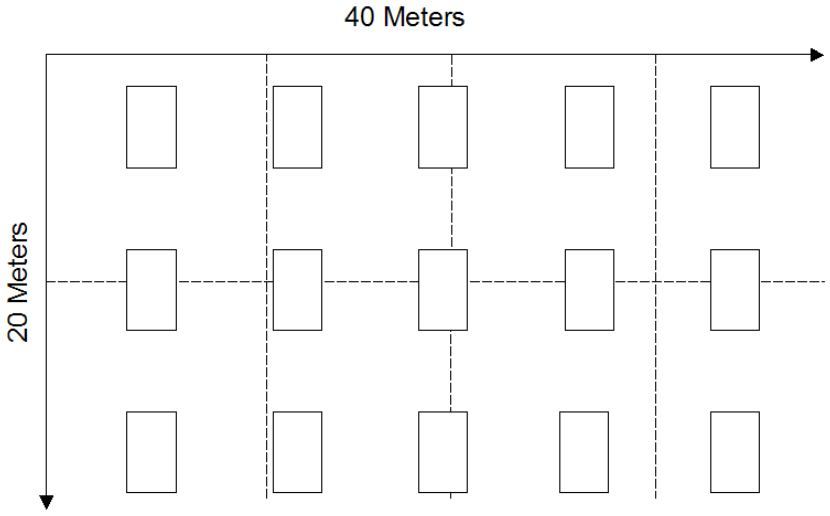

Figure 3. Approximate location of 15 point frames within each 20 x 40 m plot. Dashed lines indicate potential SPOT pixel 10 x 10 m placement.

Table 4. Point frame plot field attributes collected with Trimble GeoXT GPS receiver and ArcPad customized form.

Attributes
Plot ID and its boundary location
Fuel load (3 categories) or Burn Severity
Plot homogeneity (as described in Field Methods)

Field Methods--Sampling Stages

Pre-fire Sampling

Pre-fire ground cover sampling was performed primarily for hypothesis #2 to determine correlation between pre-fire fuel loads and burn severity levels. During pre-fire sampling, the ocular estimate method was performed at 206 random plots across the pasture (Fig. 4; points). In conjunction with the ocular estimates, point frame data (Fig. 4; rectangles) were collected at 45 of the 206 sample sites. These 45 plots were centered within the ocular plots that were determined homogenous. In order to ensure replication, 20 additional stratified random point frame plots were set up within the previously established large scale, homogenous fuel load polygons. Each of the three fuel load categories were represented by at least four, 20 m x 40 m point frame plots and four plots were established within the proposed unburned area for replication.

Figure 4. Pre- and post-fire sampling plot locations, prescribed fire boundaries, and bulldozer-created fireline.

Prescribed Fire

The prescribed fire was performed September [14 and 15], 2005 by Targhee Fire, a contract crew through the USSES. The fire crews burned most of the northern 4/5 of the pasture (approximately 2.82 km^2; Fig. 4) consistently. They ignited vegetation in the southeast and northwest corners simultaneously while walking the dozerline with a drip torch towards the southwest corner. These two fires came together in the southwest corner and progressively moved toward the northeast with the wind. Using a hand-held anemometer, winds were observed around 20 m/sec throughout most of this northern burn. Nine strip burning/spot fires were ignited in the southern portion of the pasture to ensure replication (south of the middle bulldozer line; Fig. 4). The prescribed fire in September burned approximately 85% of the pasture area including 173 of the sampling sites.

Post-Fire Sampling

Post-fire field surveys, performed within 1.5 months after the fire, were intended to provide field validation of burn severity levels. All of the pre-fire sampling sites were re-sampled after the fire. The same field methods as pre-fire sampling (ocular estimates and point frame measurements) were repeated at the same scales and within 3-5 m of the original locations (by navigating with the GPS unit). Data were collected consistent to the pre-fire methods, except fuel load attributes and sagebrush age data. In addition, a burn severity rating (unburned, low, moderate, and high) was assigned to each ocular and point frame plot. This project assessed burn severity with a modified ocular method based on combining the works of the US Forest Service field methods (USDA FS, 2001), the US Park Service field methods (USDI NPS, 2003), and Key and Benson's (Key and Benson, 1999a; 2004b) composite burn index (CBI). Each of these post-fire field methods incorporates qualitative and quantitative measurements to detect and categorize burn severity; we incorporated and modified the three methods above according to the burn conditions on our study area in the context of a semiarid rangeland site. Since most of the vegetation and

organic soil material was consumed by the fire the burn severity assessment became solely qualitative; no attribute was physically measured. However, attributes such as litter condition, shrub condition, surface rock (USDA FS), organic substrate, and vegetation (USDI NPS) were incorporated from the USDA and USDI burn severity assessments. Key and Benson's (1999a; 2004b) CBI places a ≈50% change in the herb/low shrub/tall shrub strata into the moderate burn severity category. The study area predominantly fits into Key and Benson's shrub strata, so we incorporated this ≈50% change burn severity category.

After the burn, we walked the entire pasture to assess the burn severity variability using the attributes that were applicable to the prescribed burn. For instance, we did not use any tree measurements (there were no trees) or measurements of standing litter (all burned areas had standing burned stumps). In most instances, the fire either burned all vegetation (except stumps) or none; there was a very small amount of incompletely burned vegetation.

Severity at each plot was assessed based on the percent cover of consumed, above-ground vegetation and litter versus the amount of bareground and rock, as a satellite would interpret each plot's reflectance. If there were patches of partly consumed vegetation within the plot its percent cover was assessed and a severity category was assigned. Each study plot was classified with an ocular burn severity rating (0-3) based on the amount of remaining above-ground live vegetation within the plot: 0 = Unburned, no vegetation change; 1 = <50% burned, little above ground consumption; 2 = >50% burned, most of above ground vegetation was consumed; and 3 = 100% burned, all above-ground vegetation mortality. Of 271 total plots, only 13 were <50% burned. The corresponding remote sensing values were not significantly different than the unburned or moderate severity classes and there were not enough plots for validation. These data were incorporated and analyzed with the >50% category (2) (Table 5) because the sample size was too low to have its own class and subsequently considered moderate severity or 'incompletely burned'.

Table 5. Description of burn severity categories based on an ocular estimate.

Burn Severity Value	Category	Definition
Unburned	1	Vegetation is in same condition as pre-fire
Moderate	2	Vegetation was burned within the plot
High	3	100% vegetation was burned within plot

Post-Field Operations

Differential correction/post processing was performed to minimize clock (satellite and receiver), atmospheric, and ephemeris errors of the GPS data. Trimble's GPS Pathfinder Office 3.10 was used for differential correction and shape correct. The real time CORS stations located in Mammoth, WY and at the Idaho National Laboratory (INL) (depending on which was available) were preferred for the differential correction. However, when necessary, CORS stations located further away (i.e. Pocatello, ID) were used.

Remote Sensing Methods

Image Acquisition

Landsat ETM+ and SPOT 5 imagery were chosen for this work due to their reasonable cost, spatial and spectral resolution, and because their data are continuously collected. Both Landsat and SPOT satellite images were acquired within one month after the prescribed fire. Landsat has three visible (blue, green, red), one near-infrared (NIR), and two shortwave infrared (SWIR) bands (1.65 μm and 2.21 μm) at 28.5 m spatial resolution. While Landsat provides more spectral resolution (especially in the SWIR where burn severity is likely to be distinguishable), the spatial resolution is lower than SPOT-5 and its long-term future data availability is questionable. SPOT-5 has three multispectral bands (green, red, and NIR) at 10 m spatial resolution and one SWIR band (~1.66 μm) at 20 m spatial resolution. Because the SPOT SWIR band has a spatial resolution of 20 m and the visible and NIR data have a spatial resolution of 10 m, the

SWIR data were resampled to 10 m and analyzed together with the visible and NIR data. A total of 2 Landsat (July 4 and October 24, 2005) and 2 SPOT (August 27 and September 28, 2005) images were acquired (Table 6): all images were chosen as close to the prescribed burn (September [14 and 15], 2005) as possible with the smallest percentage of cloud cover.

Table 6. Dates and location of SPOT and Landsat imagery.

Imagery	Date	Scene ID/Path Row
SPOT 5 Pre-fire	27-Aug-05	547-260
SPOT 5 Post-fire	28-Sep-05	547-260
Landsat ETM+ Pre-fire	4-Jul-05	39/29
Landsat ETM+ Post-fire	24-Oct-05	39/29

Overview of Image Processing

Several remote sensing methods are explored and compared in this study using Landsat and SPOT imagery. In order to test the hypothesis that burn severity can be predicted with remote sensing data, ten remote sensing indices are explored and compared through accuracy assessments. The indices include: 1) an original Landsat dNBR and one relative dNBR using pre- and post-burn imagery; 2) one relative modified NDVI using pre- and post-fire imagery; 3) one original normalized difference shortwave-infrared index (NDSWIR), and two modified NDSWIR using multi-imagery and post-fire imagery; 4) two SAVIs using an adjustment factor of 0.5 with both the Landsat and SPOT post-fire images; and 5) two MSAVIs using post-fire Landsat and post-fire SPOT imagery.

Using homogenous point frame study plots (n=36) we investigated the differences in the pre- and post-fire SPOT and Landsat images (Figures 5 and 6). We averaged the reflectance values from the 36 plots for each of the pre- and post-fire images and compared the differences. The SPOT data had small changes in reflectance values between the pre-and post-fire images. The red reflectance decreased after the fire approximately 0.84% and the NIR reflectance increased approximately 1.8% after the fire. The green reflectance increased 1.6% and the SWIR reflectance increased approximately 0.81%. In the Landsat data the NIR decreased 3% and the SWIR (2.21 μm) reflectance increased 5.5% after the fire. Blue, green, and red reflectances decreased less than 1% and the SWIR (1.66 μm) increased 0.85%.

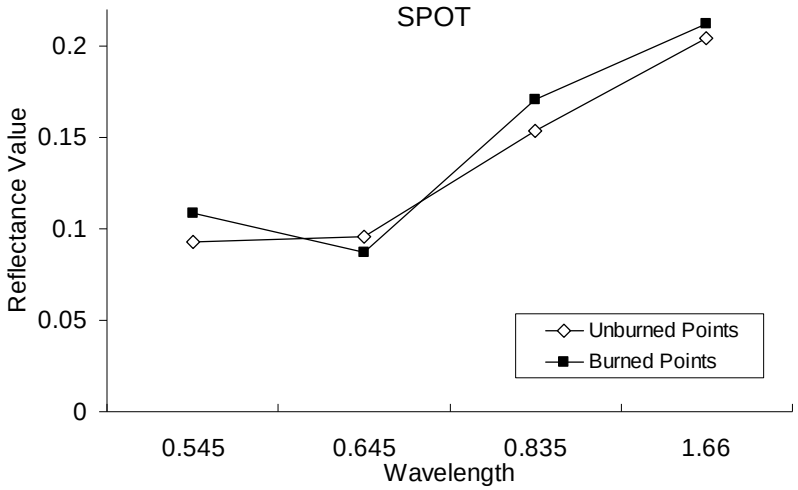

Figure 5. Pre-fire and post-fire SPOT imagery is used to demonstrate homogenous point frame plot (n = 36) reflectance averages.

Interpretation of the reflectance values from the homogeneous plots indicates that the SPOT data demonstrate a smaller amount of change between pre- and post-fire in comparison to the Landsat data. The post-fire Landsat data was collected approximately one month after the fire while the SPOT data was collected less than two weeks after the fire. The Landsat post-fire response (a decrease in NIR reflectance and an increase in SWIR reflectance) is consistent with a loss of vegetation and an increase in soil exposure. On the other hand, the SPOT green and NIR reflectances increased, albeit less than 2%. The response of the SPOT data in the red and SWIR bands is similar to that of corresponding bands in the Landsat data. Regardless of the green and NIR increases, we chose to analyze the SPOT data and compare results with Landsat.

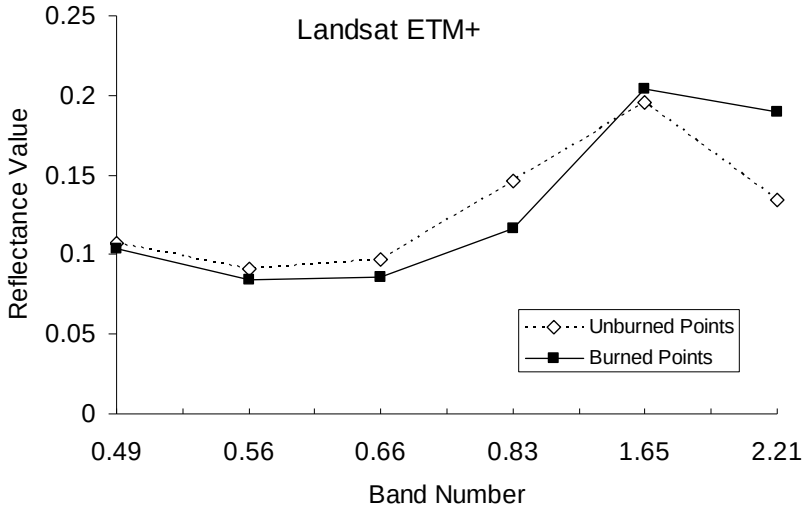

Figure 6. Pre-fire and post-fire Landsat imagery is used to demonstrate homogenous point frame plot (n=32) reflectance averages.

Because resource management decisions are made with maps it is important to know their quality of information. Accuracy assessment is conducted to identify how well the remotely sensed data represents earth's features and provides a measure of quality that remotely sensed data describes of land cover (Congalton and Green, 1999). Validation of the remote sensing burn severity was performed following traditional accuracy assessment techniques by placing field data (reference data) and remote sensing data (classified data) into an error matrix (Congalton and Green, 1999). The standard error matrix reports users, producer's, and overall accuracies, as well as a kappa statistic (KHAT). The overall accuracy, reported as the accuracy assessment statistic, is the sum of the correctly classified pixels divided by the total number of pixels in the error matrix (see below; Congalton and Green, 1999). Producer's and users accuracies are a better representation of accuracy because they represent the individual category accuracies, and are not biased by the overall sample size. The producer's accuracy reports the percentage of pixels which accurately represent the landscape (on the map). The users accuracy represents the chances of, when going to an area on the ground, that the map will be classified correctly. The KHAT is a measure of how well the remotely sensed data agree with the validation data and provides insight into how much better the classification is than a random classification (Congalton and Green, 1999).

A pairwise test of significance (Congalton and Green, 1999; equation 4) was run for the matrices that had highest accuracies as well as for those which shared similar overall accuracies. This test is a Kappa analysis that determines if two error matrices are significantly different by comparing their KHAT statistics.

$$Z = \frac{|K1 - K2|}{\sqrt{\text{var}(K1) + \text{var}(K2)}} \quad (4)$$

Where: K1 and K2 = Kappa statistic for error matrix 1 and 2
var(K1) and var(K2) = estimates of variance for matrix 1 and 2

Pre-processing of Imagery
Radiometric Correction
All imagery were processed to at-satellite reflectance using ENVI software (RSI, 2005) to reduce between-scene variability. This was an important step since multi-temporal imagery was used. Both Landsat images were processed using ENVI's Landsat TM Calibration Utility; the SPOT images were processed using band math in ENVI with algorithms (4) (SPOT, 2005) and (5) (Landsat 7, 2006) as follows:

$$\text{Radiance} = \frac{\text{Digital Number}}{\text{Absolute Calibration Gain}} \quad (5)$$

$$\text{Reflectance} = \frac{\Pi * \text{radiance} * \text{sun-earth distance}^2}{\text{solar equivalent irradiance} * \cos(\text{solar angle})} \quad (6)$$

Where: *Radiance* = spectral radiance at the sensor's aperture
Digital Number = the digital number of each pixel ranging from 0-255
Absolute Calibration Gain = the sensor processing procedure to maximize the instrument's radiometric resolution without saturating the detectors; each band's gain is provided by the image metadata
Sun-Earth Distance = Earth-Sun distance in astronomical units from nautical handbook
Solar Equivalent Irradiance = mean solar exoatmospheric irradiances in watts/(meter squared * μm) provided by SPOT Image Corp. for each band
Solar Angle = solar zenith angle in degrees

On May 31, 2003 the Landsat ETM+ scan line corrector (SLC) which compensates for forward motion of the spacecraft failed (Howard and Lacasse, 2004). This mechanical failure cannot be repaired, thus, portions of the ground are collected redundantly or missed entirely. While a linear transform of the data from another scene date can be used to estimate the missing DN values (Howard and Lacasse, 2004) this was not necessary because our study area was not located in an area affected by the SLC failure.

Geometric Correction
Image rectification was performed using ground control points (GCPs) and the Image to Map Registration tool in ENVI. Image rectification was performed after the remote sensing indices (see below) in order to reduce error during resampling. Spatial interpolation was performed using GCPs selected from the index images and matched with the primary 'Dozerline' GPS GCP file. This GPS file was collected around the periphery of the controlled burn, which could easily be matched with the burn periphery in the index images. Where necessary, GCPs from roads and pasture corners were also used. Both the GCP files and index image files were in a Transverse Mercator projection (SPOT = IDTM; Landsat = UTM) and the GCPs were located spatially throughout the study area. Each image was then subset to the study area.

Resampling during the image rectification process was implemented using the nearest neighbor first order polynomial interpolation. The output pixel size was set to the same size as the input image file. This method was chosen because it assigns the closest brightness value to the output pixel, rather than an average of the surrounding pixels (Jensen, 1996; Lillesand et al., 2004), therefore maximizing spectral and spatial integrity of the data. The resulting Root Mean Square Error (RMSE) was less than ½ pixel for both the Landsat and SPOT imagery (Table 7) during the image rectification process.

Table 7. Root Mean Square Error (RMSE) of the Landsat and SPOT data.

Imagery	RMSE	Distance off (m)
Landsat	0.2621	7.9
SPOT	0.3489	3.5

Remote Sensing Indices

Several remote sensing indices were implemented (Table 1) including single image and multi-image manipulation. A burn versus no burn algorithm was first sought to differentiate the areas that were burned from the areas that were not burned. Subsequently, an algorithm was sought to determine areas of differing levels of burn severity. There is a possibility of introducing inherent error when comparing multi-temporal datasets and using them in band ratios due to spatial mis-interpolation, therefore; single image segmentation was performed to reduce this occurrence. Multi-date indices were performed in order to show change detection from pre-burn conditions to post-burn conditions. This temporal image differencing technique uses the same bands from each image; the same algorithm is applied twice for each image; and the post-fire result is subtracted from the pre-fire result. Algorithms compared with Landsat imagery were: soil adjusted vegetation index (SAVI) and modified soil adjusted vegetation index (MSAVI) single date indices, and differenced normalized burn ratio (dNBR), normalized difference SWIR (NDSWIR), and relative dNBR multi-date images. Algorithms compared with SPOT imagery were: SAVI, MSAVI, and post-fire NDSWIR single date indices, and relative modified normalized difference vegetation index (NDVI) and NDSWIR multi-date indices.

Single Date Indices

Single date indices represent change by using only the post-fire satellite image. For initial assessment of burn severity, it is best to use imagery as close after the fire date as possible. The Landsat and SPOT post-fire images were used to produce three remote sensing indices: SAVI, MSAVI, and NDSWIR. These single date indices were applied to determine burned from unburned areas, and then assessed to differentiate burn severity.

The SAVI remote sensing index was appropriate to try in our rangeland application with both the Landsat and SPOT post-fire images because of the inherent amount of high bareground after a fire. Huete (1988) suggests that a soil adjustment factor of 0.5 can be used across different ecosystem types with differing biomass amounts. The SAVI output values range between 0-1: values near zero represent less vegetation (high burn severity) and increasing values represent more vegetation (low burn severity or unburned vegetation).

The MSAVI was used (with Landsat and SPOT post-fire images) because it has increased sensitivity to vegetation where total vegetation cover is low (i.e. after a fire) (Qi et al., 1994). The MSAVI output values range between -1 to 1. It is expected that this algorithm is successful at discriminating vegetation associated with unburned and moderate severity burns because of its ability to minimize soil's high reflectance.

We chose to assess the accuracy of the post-fire NDSWIR (pNDSWIR), described in better detail below. This index uses SPOT NIR and SWIR bands and no visible bands; therefore, potentially less susceptible to atmospheric interferences.

Multi-Date Indices

Multi-image manipulation was first performed to identify burned from unburned areas and then to differentiate burn severity levels within a burn perimeter. This process detects vegetation change from pre-burn to post-burn conditions using two images. Typically multi-date indices require an algorithm to be applied to both pre-fire and post-fire images before the final algorithm is performed (i.e. differenced). Areas of no change have values equal to, or close to zero. For instance, a pre- and post-NBR is performed and then differenced resulting with the dNBR (Table 1). As established, Landsat bands 4 and 7 are applied in the dNBR with values typically ranging from negative 1 to positive 1; negative values represent increased vegetation productivity in the post-fire scene or clouds in the pre-fire scene, positive values represent fire effects or clouds in the post-fire scene. We applied a dNBR to the Landsat data.

We also used Landsat data for a relative differenced NBR (RdNBR; Miller and Thode, in revision). RdNBR values range from -1 to 1; negative values represent increased vegetation (unburned or low severity), and positive values represent a decrease in vegetation (high severity) after the fire. The relative dNBR was not used with SPOT data because the pre-fire NBR results have negative values and this index requires the division of the square root of the pre-fire NBR results. Therefore because the pre-fire NBR has negative values it cannot be performed without scaling the pre-fire data to positive values. The aim of this research was to test indices without additional need of processing (e.g. rescaling).

The NDSWIR results are compared with the results of the post-fire pNDSWIR (above). Because spectral proximity of the Landsat band 5 (1.65 μm) is similar to SPOT's SWIR (1.66μm), the NDSWIR index (Gerard et al., 2003) was modified to include the Landsat imagery. It was expected that the Landsat and SPOT NDSWIR indices would have similar results because of the SWIR bands' spectral proximity. However, because the SPOT spatial resolution is higher than the Landsat spatial resolution, it was expected that the SPOT NDSWIR may provide an increased level of delineation.

To incorporate SPOT's SWIR band, the NDVI was modified by replacing the NIR with the SWIR band which was previously found useful for fire scar detection (Gerard et al, 2003). We performed the modifiedNDVI (Table 1) with the pre-fire and post-fire SPOT images in order to produce a relative modified NDVI index (rModNDVI).

Accuracy assessment (described below) was used to provide an assessment of how well the remotely sensed indices corresponded with the field data. Accuracy results were then compared between the 10 remote sensing indices.

Accuracy Assessment

Relating Remote Sensing Indices to Field Data

Training data were used to relate remote sensing index values to field data. Using field plot data and the Spatial Analyst function in ArcMap 9.1 (Extract Values to Points; ESRI, 2005) burn severity index values were extrapolated for each training plot. The Extract Values to Points function acquires the pixel value under the plot center point. The Interpolate Values at Point Locations option was checked in order to account for the surrounding plot size. The value of the point is calculated using the adjacent cells with a bilinear interpolation method (ESRI, 2005). Burn severity index values were separated into burn severity classes by first placing all plot values into their respective burn severity classes as determined in the field. Then the minimum, maximum, and mean index values of each class were determined. Overlapping index values were separated by splitting the difference between the maximum of one class with the minimum of the next class. Likewise, if there was a gap between burn severity class data values, then a break was

determined by splitting the difference between the maximum of one class with the minimum of the next class. A total of 119 plots were used for the training including both ocular and point frame plot index values. High burn severity had 89 plots; moderate burn severity ('incompletely burned') had 16 plots; and the unburned class had 14 plots. To encompass the variability across the study area, training plots were randomly selected within each burn severity class and the same training plots were used within each burn severity class for each index. A categorical scatterplot of burn severity classes and remote sensing index values was created to show the breaks and overlap in the remote sensing data (Fig. 7).

Validation

Fifty plots were reserved for the validation of each class (n=150), as recommended by Jensen (1996) (Table 8). No training data were used in the validation. An error matrix was created to compare the field validation plots with their corresponding index values. Overall accuracy, as well as the users and producer's accuracy are presented in the error matrix table (Table 9). Error matrices for all ten remote sensing indices were established and Kappa analysis was performed. A pairwise test of significance was run for the matrices that had highest accuracies as well as for those which shared similar overall accuracies.

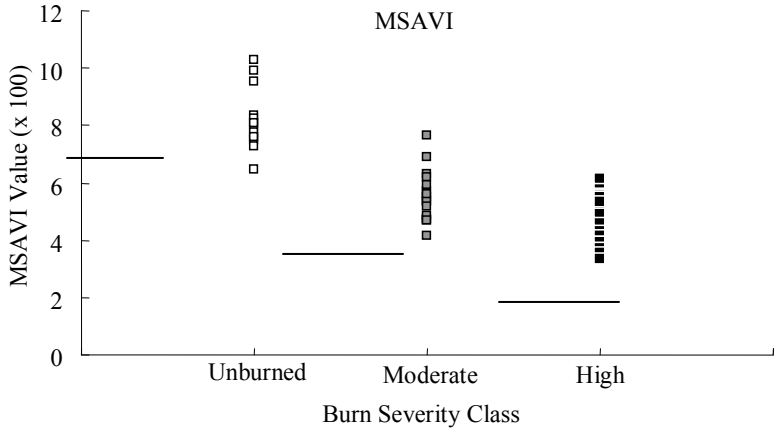

Figure 7. Example of a categorical scatterplot of burn severity classes versus the Landsat MSAVI index. Dashes indicate mean index values of the burn severity class.

Table 8. Number of training plots and validation plots when assessing all remote sensing indices.

Burn Severity Value	Category	# of Training Plots	# of Validation Plots
Unburned	1	14	50
Moderate	2	16	50
High	3	89	50

RESULTS

The remote sensing indices comparing burned with unburned areas had better overall, users, and producer's accuracies than indices comparing burn severities (Tables 10, 12 - 14). Based on a homoscedastic, two-tail t-Test comparing the overall accuracies of 10 single date and 10 multi-date indices (with SPOT and Landsat data), the single date and multi-date indices do not differ in mean overall accuracy ($P = 0.4073$).

Table 9. An example of an error matrix table with Kappa results: the Landsat relative dNBR burn severity index.

	Unburned	Moderate	High	Total
Unburned	43	1	0	44
Moderate	6	28	12	46
High	1	21	38	60
Total	50	50	50	150
Overall Accuracy	73%			
Users Accuracy	86%	56%	76%	
Producer's Accuracy	98%	61%	63%	
KHAT	0.49			
Variance	0.0033			
Z Statistic	8.4339			

Table 10. Burned versus unburned remote sensing index accuracies and kappa statistics using SPOT 5 imagery.

Accuracy Type	dNDSWIR	pNDSWIR	RelModNDVI	MSAVI	SAVI
Overall Accuracy	65%	96%	94%	95%	100%
Producer's Unburned	49%	96%	94%	98%	100%
Users Unburned	82%	92%	88%	86%	100%
Producer's Burned	86%	96%	94%	93%	100%
Users Burned	57%	98%	97%	99%	100%
KHAT	0.3333	0.9091	0.862944	0.8763	1.0000
Variance	0.0068	0.0013	0.001955	0.0017	0.0000
Z Stat	4.0239	25.0211	19.51918	20.6704	*

Burn versus Unburned Index Results

Landsat remote sensing indices of dNBR, NDSWIR, MSAVI, SAVI, and RdNBR, and SPOT indices of dNDSWIR, pNDSWIR, rModNDVI, MSAVI, and SAVI were compared using all field data for accuracy assessment. The burned versus unburned indices generated using SPOT imagery (pNDSWIR, rModNDVI, and MSAVI), and the Landsat-derived burned versus unburned indices (dNBR, RdNBR, MSAVI, and SAVI) had relatively consistent results (~ 95% overall accuracy). Three burned vs. unburned SPOT-derived indices (pNDSWIR, MSAVI, and SAVI) have 95% or better overall accuracies (Table 10). The highest overall accuracy for the burn vs. unburned indices was the SPOT SAVI at 100% (Table 11). The pNDSWIR had an overall accuracy of 96% and had a slightly higher KHAT value than the MSAVI results. Upon performing a pairwise test for significance between the pNDSWIR and MSAVI SPOT error matrices, the z-statistic ($Z = 0.599$) reveals that they are not significantly different. Three burned vs. unburned Landsat indices (RdNBR, MSAVI, and SAVI) performed nearly equally well at 95% overall accuracy (Table 12). Table 12 reports the same values (to the 100^{th}) of KHAT, variance, and z-statistics for these three indices, indicating they have equal classification accuracies (Congalton and Green, 1999); therefore, a pairwise test for significance is not necessary. The z-statistic values indicate that all three indices were significantly better than a random result. The remote sensing indices that assessed burned versus unburned areas had better overall, users, and producer's accuracy results than those detecting burn severity.

Table 11. An example of an error matrix table: the SPOT SAVI index with 100% overall accuracy.

		Reference Data		
		Unburned	Burned	Total
Remote Sensing Data	Unburned	50	0	50
	Burned	0	100	100
	Total	50	100	150
	Overall			100%
	Users	100%	100%	
	Producers	100%	100%	

Table 12. 'Burned versus unburned' remote sensing index accuracies and kappa statistics using Landsat ETM+ imagery.

Accuracy Type	dNBR	RdNBR	NDSWIR	MSAVI	SAVI
Overall Accuracy	94%	95%	89%	95%	95%
Producer's Unburned	96%	98%	90%	94%	94%
Users Unburned	86%	86%	74%	90%	90%
Producer's Burned	93%	93%	88%	95%	95%
Users Burned	98%	99%	96%	97%	97%
KHAT	0.8615	0.8763	0.7329	0.8788	0.8787
Variance	0.0019	0.0018	0.0036	0.0017	0.0017
Z Stat	19.3140	20.6704	12.1327	21.1018	21.1017

Table 13. 'Burn severity' remote sensing index accuracies and kappa statistics using Landsat ETM+ imagery.

Accuracy Type	dNBR	RdNBR	NDSWIR	MSAVI	SAVI
Overall Accuracy	66%	73%	58%	66%	67%
Producer's Unburned	96%	98%	90%	94%	94%
Producer's Moderate	50%	61%	37%	50%	52%
Producer's High	55%	63%	52%	55%	57%
Users Unburned	86%	86%	74%	90%	90%
Users Moderate	38%	56%	34%	42%	44%
Users High	74%	76%	66%	66%	68%
KHAT	0.4900	0.5900	0.37000	0.4900	0.5100
Variance	0.0033	0.0030	0.00375	0.0034	0.0033
Z Stat	8.4339	10.7668	6.04186	8.4456	8.8829

Burn Severity Index Results

The best burn severity index (differentiating unburned, moderate, and high) was the Landsat RdNBR with a 73% overall accuracy and users and producer's accuracies of 56% and 61%, respectively, for the moderate category and 76% and 63%, respectively for the high category (Table 13). The best overall accuracy for the SPOT burn severity indices was the SAVI index at 71% (Table 14). The pNDSWIR index closely followed at 69% and a pairwise test for significance (Z = 0.381) revealed that the two matrices are not significantly different. Z statistics indicate that all Landsat and SPOT indices (except the dNDSWIR) had significantly better results than if randomly classified.

Table 14. 'Burn severity' remote sensing index accuracies and kappa statistics using SPOT 5 imagery.

Accuracy Type	dNDSWIR	rModNDVI	pNDSWIR	MSAVI	SAVI
Overall Accuracy	65%	67%	69%	67%	71%
Producer's Unburned	95%	94%	96%	98%	100%
Producer's Moderate	49%	58%	56%	51%	61%
Producer's High	56%	54%	58%	55%	55%
Users Unburned	82%	88%	92%	86%	100%
Users Moderate	40%	28%	40%	38%	38%
User's High	74%	86%	76%	76%	76%
KHAT	0.4800	0.5100	0.5400	0.5000	0.5700
Variance	0.0034	0.003223	0.0032	0.0033	0.0030
Z Stat	0.0819	8.983351	9.6167	8.6376	10.391

DISCUSSIONS AND CONCLUSIONS

While studies have been performed in forested ecosystems to reliably detect burn severity with remote sensing data, there have not been any established in sagebrush steppe rangelands. This study compares the results of 10 remote sensing indices to delineate burned areas and burn severity within rangelands immediately following a fire using medium resolution satellite imagery. We used bands in the electromagnetic spectrum that correspond with vegetation change after a fire and algorithms sensitive to high reflectance of bareground that occurs in rangelands. It is important to note that overall accuracy cannot be relied upon completely because it can be biased by large sample sizes of one category versus another. For instance, the unburned results have much higher accuracies than the other burn severity classes resulting in inflated overall accuracies. As indicated by the highest users and producer's accuracies, the best index for determining burned from unburned areas was the SPOT SAVI (100% users and producer's accuracies for all categories) and the best index for differentiating burn severity within a burn was the Landsat RdNBR.

Consistent with Sannier (1999), Epting et al. (2005), and Miller and Yool (2002) accuracies were better with fewer burn severity categories. In all cases (except the SPOT dNDSWIR; Tables 10 and 13) the unburned versus burned indices had better results than the burn severity indices. We were able to successfully determine if an area was burned or not in rangelands using the SPOT pNDSWIR, rModNDVI, MSAVI, and SAVI indices and the Landsat dNBR, RdNBR, NDSWIR, MSAVI, and SAVI indices.

Our best burn severity index, the Landsat RdNBR (Fig. 8), supported Miller and Thode's (in revision) results. In a mixed ecosystem study area, they concluded that this index performed better at separating

high burn severity from other burn severity classes. Our moderate and high burn severity users (56%, 76%, respectively) and producer's (61%, 63%, respectively) accuracies for the RdNBR were higher than all other indices. These results are important to land managers given that high severity areas require more recovery effort. Therefore, there is a need for high producer and user's accuracies in high severity areas (Miller and Thode, in revision).

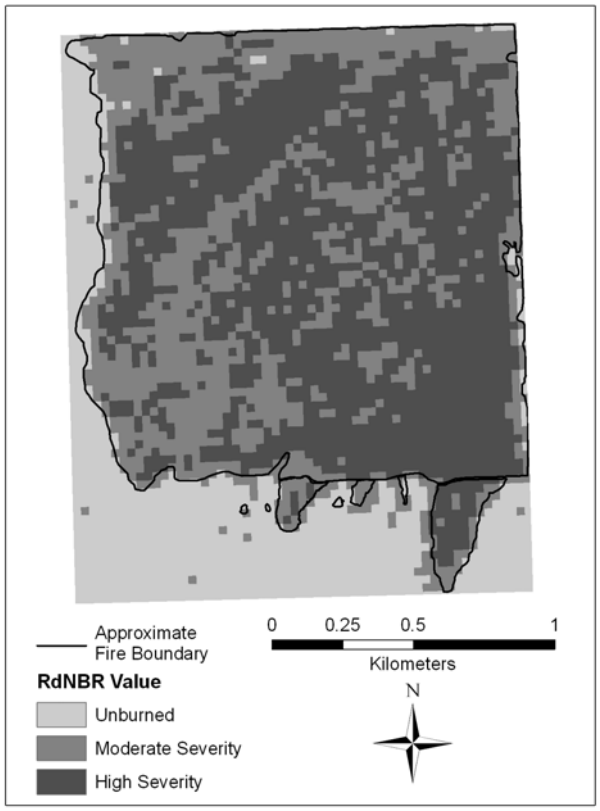

Figure 8. The relative differenced NBR using Landsat data.

Mapping burn severity patterns at a scale that is coarse enough to capture landscape scales for management, yet fine enough to provide the spectral differentiation between burn severity classes is needed. Though we did not test spatial variables between Landsat and SPOT, we can compare results of indices used on each dataset. For example, in comparing the NDSWIR, the SPOT index provides more spatial detail and morphology of the burn categories (Fig. 9). Therefore, even though SPOT didn't provide as high accuracies as the Landsat RdNBR for burn severity levels, its spatial resolution may provide other attributes that are useful to land managers. Landsat provides a practical scene size of 170 x 183 km and costs are reasonable if more than one image needs to be purchased. The results of the Landsat RdNBR verify that the Landsat 30 m spatial resolution is high enough to capture the spectral variability between burn severity classes in rangelands. However, it is up to the land manager to decide the level of detail needed to determine burn severity and thus the scale of fire recovery efforts.

Spatial correlation of ground cover and low RMS error (less than ½ a pixel) reduce the likelihood of classification error, however, they do not excuse the possibility of error. Therefore, although error is introduced with multitemporal data sets and spatial mis-interpolation occurs, these effects did not significantly alter the overall accuracies.

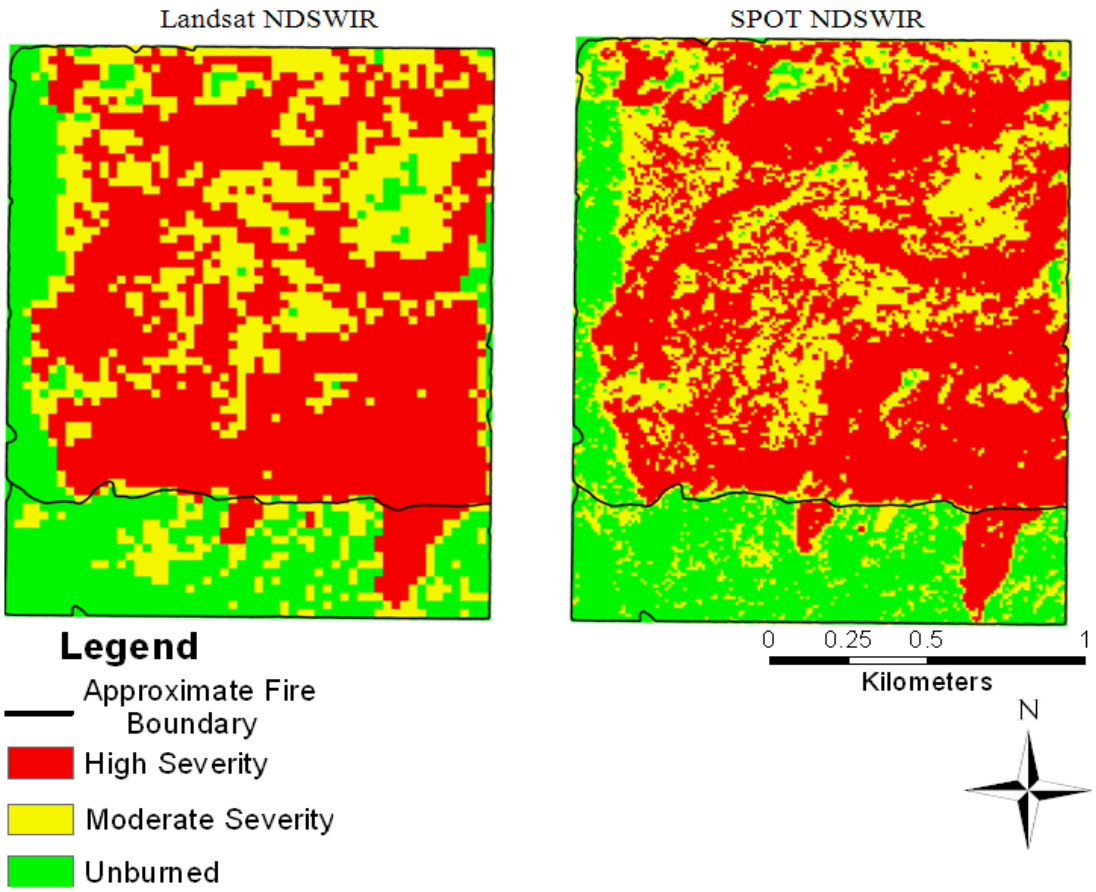

Figure 9. Comparison of the burn severity Landsat and SPOT NDSWIR results.

Timing of imagery acquisition is important in relation to the fire date and field sampling due to phenological vegetation changes. It is difficult to fairly compare remote sensing index results when timing of pre-fire and post-fire data sets vary. Naturally, a data set with more time between images will translate to more change in the index value. Our Landsat imagery had 112 days between the pre-fire and post-fire scenes as well as approximately 1 month between the burn and post-fire image, whereas the SPOT imagery had 32 days between imagery and only 4-5 days between the burn and post-fire image. Images acquired closest after a fire will likely show more immediate fire effects than images acquired for sometime after the fire. The multi-temporal indices between Landsat and SPOT carry different relationships. The shorter time gap between SPOT images and their acquisition dates (close to field data collection) coupled with the increased spatial resolution explains, in part, why the SPOT NDSWIR accuracy is slightly better than the Landsat NDSWIR. The higher sensitivity of the Landsat bands explains the higher accuracies for the burn severity levels. Recovery time is different in forests and rangelands and often depends on seasonal timing of fire. This should be considered when collecting imagery in order to model effects specific to fire.

In the pre-fire images, the SPOT and Landsat reflectance values are essentially the same (where their bands overlap). However, in the post-fire images, the SPOT and Landsat data differ. The green and NIR bands increase in the SPOT post-fire image (only four days after the fire) while the green and NIR Landsat bands decrease. The Landsat data is consistent with an increase in soil exposure and a loss of vegetation cover. On the other hand, the SPOT post-fire reflectances are counter-intuitive to an increase in soil exposure and a decrease in vegetation cover. These differences are most likely due to sensor characteristics (i.e. sensor angle, sun angle, and acquisition time) rather than data collection windows.

The SWIR 1.66 µm data is essentially the same between the SPOT and Landsat pre- and post-fire data. The fact that Landsat provided a better discrimination of burn severity is likely due to the better spectral resolution (e.g. inclusion of the longer-wave SWIR band (band 7, 2.21 µm) and less importantly the blue band (band 1)). This result is expected as the longer SWIR bands are notably more sensitive to increased soil exposure than the shorter SWIR bands. As previously noted, the value in use of the SPOT data may be the higher spatial resolution, allowing for better discrimination of the burn boundaries.
The magnitudes of the SPOT data are slightly higher than Landsat for both NIR and SWIR bands. This may be due to the higher spatial resolution of SWIR and influence of soil. Because SPOT pixels have smaller spatial resolution they may be more sensitive to the reflection of bareground, thus their values are higher. Higher SPOT values may be also the result of the sensors' calibration. Most importantly, the SPOT results indicate that spectrally, it is less sensitive to post-fire effects such as burn severity than Landsat.

Our fire took place in the fall when vegetation was already senesced. Though it was proper to have imagery close to the fire dates, reflectance (and changes in reflectance) values were not as high as if the fire occurred in a spring or mid-summer fire. For example, because the SPOT SWIR (1.66µm) is sensitive to canopy moisture content, the band did not represent as much change because vegetation was dry in both pre-fire and post-fire images. Perhaps a study with an earlier fire date would show more definite results with the burn severity indices that used the SWIR (1.66µm) band.

An unknown level of bias was introduced in the field measure of burn severity because it was qualitative. A quantitative measure of burn severity would provide a more precise and accurate field assessment and enable comparison across multiple studies. Such an assessment needs to be established for rangeland application that is easy to learn and quick to perform in the field. Other possible errors include the timing of field sampling. Due to phenological changes, it is possible that a plot's fuel load could be mis-labeled. The pre-fire sampling was spread out over approximately 6 weeks, starting the end of June through August 5th. Craddock and Forsling (1938) determined that grass and forb growth is largely completed by July 1st. However we did note growth in lupine (*Lupinus argenteus)* and in birds beak (*Cordylanthus ramosus)*. Therefore, vegetation cover was slightly greater toward the end of the sampling season. However, this would only affect the results of the second hypothesis. Likewise, after the fire, grass established quickly. There was never more than 5% grass cover in a plot, but new cover was noted. It is important to note, however, that the burn severity attribute and remote sensing indices were not affected by pre-fire sampling time because the pre-fire data were not used in those analyses.

Georegistration errors between the imagery and field data may be another source of error. An RMS error less than ½ a pixel is not much of a shift, but may be just enough to produce errors in the error matrix. Furthermore, (for hypothesis #2) during the post-fire surveys, we attempted to put plots in the same location using the GPS. Stakes were not used to delineate plot centers or boundaries due to regulations at the USSES. It was easier to have better accuracy with the point frame plots because we were able to lay out the perimeter based on a polygon shapefile in the GPS; however, the ocular estimates were located using only a point. Because of this, there is likely more georegistration error introduced in the ocular plots, which consisted of most of our field data. This would not affect the index results; it would only affect the results of the second hypothesis. Although a high precision GPS instrument was used (+/- 0.7m @ 95% CI) (Serr, unpublished) atmospheric effects may have also contributed to georegistration errors.

This study used 269 field plots for training and validation. Additional studies could be done to show the optimal number of training points for sufficient or better classification of burn severity.

The biggest limitation to our study is that the results are based on one burn and that it was a prescribed burn rather than natural. Because there were more than normal amounts of fine fuels (due to a wet spring) and because there were high winds during the fire, the majority of the burn was high burn severity. There

was not a sufficient number of post-fire field plots in the low burn severity class to justify having more categories, such as unburned, low, moderate, and high burn severity classes for classification. The few low burn severity plots were incorporated into the moderate burn severity class and considered 'incompletely burned' because the sample size was too low to have its own class. Inclusion of the low burn severity data in the moderate class may have skewed the data resulting in misrepresented moderate severity data. One possibility would have been to discard the low severity data all together. It would be useful to develop a burn severity classification with more detailed categories such as unburned, low, moderate, and high. Because there were not enough unburned and low burn severity plots within the burn perimeter, the hypothesis #2 sub-study (which correlated pre-fire fuel loads with burn severity) could only be performed between the moderate and high burn severity plots.

Hyperspectral imagery should be further explored to detect burn severity in rangelands because it may have wavelengths and corresponding bandwidths that are more sensitive to fire effects. For instance, AVIRIS channels 60 and 148, as suggested by van Wagtendonk et al. (2004), may discriminate fire effects better than Landsat bands 4 and 7 in rangelands. Another area for further study is performing an extended assessment of burn severity (the spring following the burn). It may be possible that rangeland burn severity is best detected with an extended assessment. An extended assessment may delineate areas of high burn severity better, either where perennial vegetation has not recovered or where introduced annuals have established.

The best burn severity index using SPOT imagery was the SAVI index (Fig. 10). However, our results with SAVI are contradictory with Epting's et al. (2005) results whereas their SAVI and MSAVI indices performed worse than their indices incorporating mid-infrared bands. Their study area is in a coastal, cloudy region (Alaska) with potentially more atmospheric haze making the red band ineffective. More importantly, their study area was in a forested ecosystem. As suggested by White et al. (1996), Epting et al. (2005), and Roy et al. (2006) different burn severity indices may be needed across different ecosystem types. Furthermore, if better burn severity accuracies (>76% users and >63% producer's) are needed for recovery purposes within high burn severity areas, then a different algorithm should be sought.

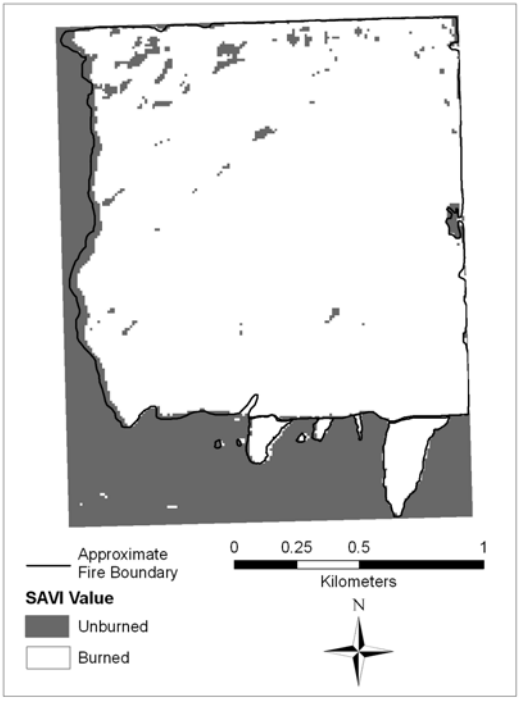

Figure 10. The SAVI burned versus unburned index using SPOT data.

The remote sensing indices used in this study are reproducible and straightforward. We chose to focus on remote sensing methods that incorporate satellite imagery and fit the needs of land managers (reasonable cost and practical spatial and spectral resolution) and methods that would not require the user to incorporate *large* amounts of field studies. This, after all, is the intent of remotely sensed models. The spatial resolution of imagery is ultimately determined by the necessary scale of fire recovery efforts. Because fire recovery efforts vary according to remoteness, economic impacts of the burn, and burn severity, land managers may require different types of satellite imagery. Though our best results are with the burned versus unburned algorithms, a 73% overall accuracy for the RdNBR burn severity index encourages future research. The RdNBR provided the best initial assessment users and producer's accuracies for this rangeland prescribed burn indicating its usefulness to land managers. These accuracies show moderate agreement between the index burn severity classes and the field-based burn severity classes. Before this index is entirely recommended, however, more studies need to be performed using the RdNBR in rangelands that have heterogeneous fuel loads, and within burns that have variable burn severities. Future research entailing an extended assessment and the application of hyperspectral imagery is necessary to contribute to our understanding of burn severity in rangeland ecosystems and vegetation recovery.

ACKNOWLEDGEMENTS

I am indebted to Dr. Nancy Glenn, my major advisor for her insightful guidance, endless help, and benevolent patience throughout my graduate career. I am thankful to Dr. Matt Germino for his frequent edits and guidance in addition to providing accommodation in his supportive lab facility. I am grateful, as well to my other committee members, Tony Stocks and Steve Seefeldt, for believing in me and inspiring self-confidence.

To my family and friends, near and far, thank you for your compassion, love, and support throughout my academic career. I could not have done it without you! Mom, Dad, Paule, April, and James thank you for the tremendous amount of support and love you've given me. Dan, Erik, Jane, Jen, Jesse, John, Monique, Penny, Ru, Sara, Tony, and the many others involved in my graduate experience—thank you so very much!

This project would not have been possible without the funding from the National Aeronautics and Space Administration (NASA) grant #NNG05GB05G. The U.S. Sheep Experiment Station in Dubois, Idaho offered their facilities and friendly support during the field seasons. I thank Bret Taylor and Ada Williamson for helping with and encouraging the success of two field seasons; and I thank Steve Seefeldt for facilitating with the prescribed burn.

LITERATURE CITED

Anderson, H.E. 1982. Aids to determining fuel models for estimating fire behavior. General Technical Report INT-122. Intermountain Forest and Range Experiment Station Ogden, UT.

Anderson, J.E. and Inouye, R.S. 2001. Landscape-scale changes in plant species abundance and biodiversity of a sagebrush steppe over 45 years. *Ecological Monographs,* 71, 531-556

Asner, G.P. 2004. Biophysical remote sensing signatures of arid and semiarid ecosystems. Remote Sensing for Natural Resource Management and Environmental Monitoring. 3 ed., ed S. L. Ustin, 53-109. Vol. 4. Hoboken, New Jersey: John Wiley and Sons.

Asner, G.P. and Heidebrecht, K.B. 2002. Spectral unmixing of vegetation, soil and dry carbon cover in arid regions: comparing multispectral and hyperspectral observations. International Journal of Remote Sensing, 23:19, 3939-3958

Bannari, A., Morin, D., Bonn, F., and Huete, A.R. 1995. A review of vegetation indices. Remote Sensing Reviews, 13, 95-120

Brewer, C.K., Winne, J.C., Redmond, R.L., Opitz, D.W., and Mangrich, M.V. 2005. Classifying and mapping wildfire severity: A comparison of methods. Photogrammetric Engineering and Remote Sensing, 71:11, 1311-20

Brown, James K.; Smith, Jane Kapler, eds. 2000. Wildland fire in ecosystems: effects of fire on flora. Gen. Tech. Rep. RMRS-GTR-42-vol. 2. Ogden, UT: U.S. Department of Agriculture, Forest Service, Rocky Mountain Research Station. 257 p. URL: http://www.fs.fed.us/rm/pubs/rmrs_gtr42_2.pdf; Last accessed July 28, 2006.

Cocke, A.E., Fule, P.Z., and Crouse, J.E. 2005. Comparison of burn severity assessments using differenced normalized burn ratio and ground data. International Journal of Wildland Fire, 14, 189-98

Congalton, R. and Green, K. 1999. Assessing the accuracy of remotely sensed data: principles and practices. (pp. 137). Washington, D.C.: CRC Press, Inc.

Craddock, G.W. and Forsling, C.L. 1938. The influence of climate and grazing on spring-fall sheep range in southern Idaho. United States Department of Agriculture Technical Bulletin No. 600. URL: http://warp.nalusda.gov/ref/USDApubs/tb.htm#sortnbr; Last accessed September 28, 2006.

Diaz-Delgado, R., Lloret, F., Pons, X., and Terradas, J. 2002. Satellite evidence of decreasing resilience in mediterranean plant communities after recurrent wildfires. Ecology, 83, 2293-2303

Diaz-Delgado, R., Lloret, F., and Pons, X. 2003. Influence of fire severity on plant regeneration by means of remote sensing imagery. International Journal of Remote Sensing, 24:8, 1751-1763

Epting, J. and Verbyla, D. 2005. Landscape-level interactions of pre-fire vegetation, burn severity, and post-fire vegetation over a 16-year period in interior Alaska. Canadian Journal of Forest Research, 35:6, 1367-1377

Epting, J., Verbyla, D., and Sorbel, B. 2005. Evaluation of remotely sensed indices for assessing burn severity in interior alaska using Landsat TM and ETM+. Remote Sensing of Environment, 96, 328-339

Flasse, S., Trigg, S., Ceccato, P., Perryman, A., Hudak, A., Thompson, M., Brockett, B., Dramé, M., Ntabeni, T., Frost, P., Landmann, T., and le Roux, J. 2004. Remote sensing of vegetation fires and its contribution to a fire management information system. In J.G. Goldammer and C. de Ronde (Ed.), Wildfire Management Handbook for Sub-Sahara Africa (pp.158-211). The Hague, Netherlands: SPB Publishing

Floyd, D.A. and Anderson, J.E. 1982. A new point interception frame for estimating cover of vegetation. Vegetatio, 50, 185-186

Floyd, D.A. and Anderson, J.E. 1987. A comparison of three methods for estimating plant cover. Journal of Ecology, 75, 221-228

Garcia, M. and Chuvieco, E. 2004. Assessment of the potential of SAC-C/MMRS imagery for mapping burned areas in Spain. Remote Sensing of Environment, 92, 414-423

Gerard, F., Plummer, S., Wadsworth, R., Ferreruela Sanfeliu, A., Iliffe, L., Balzter, H., and Wyatt, B. 2003. Forest fire scar detection in the boreal forest with multi-temporal SPOT-VEGETATION data. Geoscience and Remote Sensing, IEEE Transactions on, 41:11, 2575-2585

GIS Training and Research Center (TReC). 2006. URL: http://giscenter.isu.edu/software/index.htm Last accessed: October 16, 2006

Harniss, R.O. and Murray, R.B. 1973. 30 Years of Vegetal Change Following Burning of Sagebrush-Grass Range. Journal of Range Management, 26, 322-325

Howard, S.M. and Lacasse, J.M. 2004. An evaluation of gap-filled Landsat SLC-Off imagery for wildland fire burn severity mapping. Photogrammetric Engineering and Remote Sensing, 701:8, 877-880

Huete, A.R., Jackson, R.D., and Post, D.F. 1987 Spectral response of a plant canopy with different soil backgrounds. Remote Sensing of Environment, 17:11, 37-54

Huete, A.R. 1988. A soil-adjusted vegetation index (SAVI). Remote Sensing of Environment, 25, 295-309

Huete, A.R. 1989. Soil influences in remotely sensed vegetation-canopy spectra. In G. Astrar (Ed.), Theory and Applications of Optical Remote Sensing (pp.107-41). New York: Wiley, Wiley

Inouye, R.S. 2002. Sampling effort and vegetative cover estimates in sagebrush steppe. Western North American Naturalist, 62, 360-364

Jensen, J.R. 1996. Introductory Digital Image Processing: A Remote Sensing Perspective. (pp. 318). New Jersey, USA: Prentice-Hall, Inc.

Jensen, J.R. 2000. Remote Sensing of the Environment: An Earth Resource Perspective. (pp. 544). New Jersey, USA: Prentice-Hall, Inc.

Keeley, J.E., Fotheringham, C.J., and Morais, M. 1999. Reexamining fire suppression impacts on brushland fire regimes. Science, 284, 1829-1832

Key, C.H. and Benson, N.C. 1999a. The Composite Burn Index (CBI): Field Rating of Burn Severity. URL: http://www.nrmsc.usgs.gov/research/cbi.htm;Last accessed July 28, 2006

Key, C.H. and Benson, N.C. 1999b. The Normalized Burn Ratio (NBR): A Landsat TM Radiometric Index of Burn Severity. URL: http://www.nrmsc.usgs.gov/research/ndbr.htm; Last accessed July 28, 2006

Key, C.H. and Benson, N.C. 2004a. Remote Sensing Measure of Severity: The Normalized Burn Ratio. FIREMON Landscape Assessment (LA) V4 Sampling and Analysis Methods. pp. LA1-16

Key, C.H. and Benson, N.C. 2004b. Ground Measure of Severity: The Composite Burn Index. FIREMON Landscape Assessment (LA) V4 Sampling and Analysis Methods pp. LA_CBI_Plot-1-9

Key, C.H. and Benson, N.C. 2006. Landscape Assessment (LA) Sampling and Analysis Methods. USDA Forest Service Gen. Tech. Rep. RMRS-GTR-164-CD. pp. 55

Lillesand, T.M., Kiefer, R.W., and Chipman, J.W. 2004. Remote Sensing and Image Interpretation. (pp. 1-500). New York: Wiley

Lopez Garcia, M.J. and Caselles, V. 1991. Mapping burns and natural reforestation using thematic mapper data. Geocarto International, 6, 31-37

Lutes, D.C., Keane, R.E., Caratti, J.F., Key, C.H., Benson, N.C., Sutherland, S., and Gangi, L.J. 2003. FIREMON: Fire Effects Monitoring and InventorySystem, Extended abstract submitted to: American Meteorological Society 2nd International Wildland Fire Ecology and Fire Management Congress, November 2003, Orlando, FL. URL:http://ams.confex.com/ams/pdfpapers/65637.pdf Last accessed October 16, 2006

McGwire, K., Minor, T., and Fenstermaker, L. 2000. Hyperspectral mixture modeling for quantifying sparse vegetation cover in arid environments. Remote Sensing of Environment, 72, 360-374

McMahan, J.B., Narsavage, D., and Weber, K. 2003. The "Pole Cam": corroborating field estimations with high spatial resolution imagery. In K. Weber (Ed.), Final Report: Wildfire Effects on Rangeland Ecosystems and Livestock Grazing in Idaho (pp. 18-22). Idaho State University URL: http://giscenter.isu.edu/research/techpg/nasa_wildfire/template.htm Last accessed October 16, 2006

Miller, J.D. and Thode, A.E. (in revision). Quantifying burn severity in a heterogeneous landscape with a relative version of the delta Normalized Burn Ratio (dNBR). Remote Sensing of Environment

Miller, J.D. and Yool, S.R. 2002. Mapping forest post-fire canopy consumption in several overstory types using multi-temporal Landsat TM and ETM data. Remote Sensing of Environment, 82, 481-96

Miller, R.F. and Rose, J.A. 1999. Fire history and western juniper encroachment in sage-brush steppe. Journal of Range Management, 52, 550-559

Morgan, P., Hardy, C.C., Swetnam, T.W., Rollins, M.G., and Long, D.G. 2001. Mapping fire regimes across time and space: Understanding coarse and fine-scale fire patterns. *International Journal of Wildland Fire,* 10, 329–342

National Interagency Fire Center (NIFC). 2006. Wildland Fire Statistics. URL: http://www.nifc.gov/stats/fires_acres.html; Last accessed September 26, 2006

Natural Resources Conservation Service (NRCS). 1995. Soil investigation of Agriculture Research Service, United States Sheep Experiment Station headquarters range, US Department of Agriculture. (pp. 133). Rexburg, ID: NRCS

Obrist, D., Delucia, E.H., and Arnone, J.A. 2003. Consequences of wildfire on ecosystem CO2 and water vapour fluxes in the Great Basin. Global Change Biology, 9, 563-74

Okin, G.S., Roberts, D.A., Murray, B., and Okin, W.J. 2001. Practical limits on hyperspectral vegetation discrimination in arid and semiarid environments. Remote Sensing of Environment, 77, 212-225

Patterson, M.W. and Yool, S.R. 1998. Mapping fire-induced vegetation mortality using Landsat Thematic Mapper data: A comparison of linear transformation techniques. Remote Sensing of Environment, 65, 132-42

Perryman, B.L. and Olson, R.A. 2000. Age-stem diameter relationships of big sagebrush and their management implications. Journal of Range Management, 53, 342-346

Qi, J., Chehbouni, A., Heute, A.R., Kerr, Y.H., and Sorooshian, S. 1994. A modified soil adjusted vegetation index. Remote Sensing of Environment, 48, 119-126

Rahman, A. and Gamon, J. 2004. Detecting biophysical properties of a semi-arid grassland and distinguishing burned from unburned areas with hyperspectral reflectance Journal of Arid Environments, 58, 597-610

Ratzlaff, T.D. and Anderson, J.E. 1995. Vegetal recovery following wildfire in seeded and unseeded sagebrush steppe. Journal of Range Management, 48, 386-391

Rouse, J.W., Haas, R.H., Schell, J.A., and Deering, D.W. 1973. Monitoring vegetation systems in the great plains with ERTS'. Third ERTS Symposium, NASA SP-351 I, 309-317

Roy, D.P., Boschetti, L., and Trigg, S.N. 2006. Remote sensing of fire severity: Assessing the performance of the normalized burn ratio. *IEEE Geoscience and Remote Sensing Letters*, 3, 112-116

RSI. 2005. ENVI user's guide (Version 4.2). Research Systems Incorporated (pp. 1201). Boulder, Colorado

Ruiz-Gallardo, J.R., Castańo, S., and Calera, A. 2004. Application of remote sensing and GIS to locate priority intervention areas after wildland fires in Mediterranean systems: a case study from south-eastern Spain. International Journal of Wildland Fire, 13, 241-252

Russell, G. and Weber, K. 2003. Field collection of fuel load, vegetation characteristics, and forage measurements on rangelands of the upper Snake River Plain, ID for wildfire fuel and risk assessment models. In K. Weber (Ed.), Final Report: Wildfire Effects on Rangeland Ecosystems and Livestock Grazing in Idaho (pp. 4-11). Idaho State University URL: http://giscenter.isu.edu/research/techpg/nasa_wildfire/template.htm Last accessed October 16, 2006

Ryan, K.C. and Noste, N.V. 1983. Evaluating prescribed fires. In: J.E. Lotan, B.M. Kilgore, W.C. Fischer, and R.W. Mutch, Tec. Coord. Proc. Symposium and Workshop on Wilderness Fire. USDA Forest Service General Tec. Rep. INT-182. Intermountain Forest and Range experiment Station, Ogden, UT. 230-238

Salvador, R., Valeriano, J., Pons, X., and Diaz-Delgado, R. 2000. A semi-automatic methodology to detect fire scars in shrubs and evergreen forests with Landsat MSS time series. International Journal of Remote Sensing, 21, 655-71

Sannier, C. 1999. Strategic monitoring of crop yields and rangeland conditions in southern Africa with remote sensing. PhD Thesis, Cranfield University: Silsoe College

Santos, T.G., Caetano, M.R., Barbosa, P.M., and Paúl, J.U. 1999. A comparative

study of vegetation indices to assess land cover change after forest fires. Remote Sensing for Earth Science, Ocean, and Sea Ice Applications, 3868, 232-240

Schmidt, H. and Karnieli, A. 2001. Sensitivity of vegetation indices to substrate brightness in hyper-arid environment: the Makhtesh Ramon Crater (Israel) case study. International Journal of Remote Sensing, 22, 3503-3520

Schowengerdt, R.A. 1997. Remote Sensing: Models and Methods for Image Processing. (pp. 182-355). San Diego: Academic Press

Seefeldt, S.S. 2005. Consequences of selecting rambouilllet ewes for mountain big sagebrush (Artemisia tridentata ssp. vaseyana) dietary preference. Rangeland Ecology and Management, 58, 380-384

Smith, A.M.S., Wooster, M.J., Drake, N.A., Dipotso, F.M., Falkowski, M.J., and Hudak, A.T. 2005. Testing the potential of multi-spectral remote sensing for retrospectively estimating fire severity in African savannahs. Remote Sensing of Environment, 97, 92-115

Turner, M.G., Hargrove, W.W., Gardner, R.H., and Romme, W.H. 1994. Effects of fire on landscape heterogeneity in Yellowstone National Park, Wyoming. Journal of Vegetation Science, 5, 731-42

USDA Forest Service. 2001. Field measurements for the training and validation of burn severity maps from spaceborne, remotely sensed imagery. Remote Sensing Applications Center, Salt Lake City, (UT): USDA Forest Service, Final Project Report, Joint Fire Science Program-2001-2. Project # 01B-2-1-01, pp. 15 URL:http://www.fs.fed.us/eng/rsac/baer/jfs.html Last accessed October 15, 2006

USDI National Park Service. 2003. Fire monitoring handbook. Boise, (ID): Fire Management Program Center, National Interagency Fire Center. pp. 274

van Wagtendonk, J.W., Root, R.R., and Key, C.H. 2004. Comparison of AVIRIS and Landsat ETM+ detection capabilities for burn severity. Remote Sensing of Environment, 92, 397–408

Watts, M.J. and Wambolt, C.L. 1996. Long-term recovery of Wyoming big Sagebrush after four treatments. Journal of Environmental Management, 46, 95-102

Weber, K. and McMahan, J.B. 2003. Field collection of fuel load and vegetation characteristics wildfire risk assessment modeling: 2002 field sampling report. In K. Weber (Ed.), Final Report: Wildfire Effects on Rangeland Ecosystems and Livestock Grazing in Idaho (pp. 12-16). Idaho State University URL: http://giscenter.isu.edu/research/techpg/nasa_wildfire/template.htm Last accessed October 16, 2006

West, N.E. and Young, J.A. 2000. Intermountain Valleys and Lower Mountain Slopes. In M.G. Barbour and W.D. Billings (Ed.), North American Terrestrial Vegetation (pp. 255-284). Cambridge, UK: Cambridge University Press

Whisenant, S. 1990. Changing fire frequencies on Idaho's Snake River plains: Ecological and management implications. p. 4-10, in Proceedings from the Symposium on Cheatgrass Invasion, Shrub Dieoff, and Other Aspects of Shrub Biology and Management. U.S. Forest Service General Technical report INT-276

White, J.D., Ryan, K.C., Key, C.C., and Running, S.W. 1996. Remote sensing of forest fire severity and vegetation recovery. International Journal of Wildland Fire, 6, 125-36

Whitford, W. 2002. Ecology of Desert Systems. (pp. 343). California: Academic Press

Wimberly, M.C. and Reilly, M.J. (in press). Assessment of fire severity and species diversity in the southern appalacians using Landsat TM and ETM+ imagery. Remote Sensing of Environment (in press).

Wright and Bailey. 1982. Fire Ecology. (pp.528). New York: Wiley

APPENDIX I: RESULTS OF TEN REMOTE SENSING INDICES

Table 15. Results of all SPOT burned versus unburned remote sensing indices.

SAVI		Reference Data		
		Unburned	Burned	Total
Remote	Unburned	50	0	50
Sensing	Burned	0	100	100
Data	Total	50	100	150
	Overall	100%		
	Users	100%	100%	
	Producers	100%	100%	

pNDSWIR		Reference Data		
		Unburned	Burned	Total
Remote	Unburned	46	2	48
Sensing	Burned	4	98	102
Data	Total	50	100	150
	Overall	96%		
	Users	92%	98%	
	Producers	96%	96%	

RelMod		Reference Data		
NDVI		Unburned	Burned	Total
	Unburned	44	3	47
Remote	Burned	6	97	103
Sensing	Total	50	100	150
Data	Overall	94%		
	Users	88%	97%	
	Producers	94%	94%	

MSAVI		Reference Data		
		Unburned	Burned	Total
Remote	Unburned	45	3	48
Sensing	Burned	5	97	102
Data	Total	50	100	150
	Overall	95%		
	Users	86%	99%	
	Producers	98%	93%	

dNDSWIR		Reference Data		
		Unburned	Burned	Total
Remote	Unburned	41	43	84
Sensing	Burned	9	57	66
Data	Total	50	100	150
	Overall	65%		
	Users	82%	57%	
	Producers	49%	86%	

Table 16. Results of all Landsat burned versus unburned remote sensing indices.

dNBR		Reference Data		
		Unburned	Burned	Total
Remote	Unburned	43	2	45
Sensing	Burned	7	98	105
Data	Total	50	100	150
	Overall	94%		
	Users	86%	98%	
	Producers	96%	93%	

NDSWIR		Reference Data		
		Unburned	Burned	Total
Remote	Unburned	37	4	41
Sensing	Burned	13	96	109
Data	Total	50	100	150
	Overall	89%		
	Users	74%	96%	
	Producers	90%	88%	

MSAVI		Reference Data		
		Unburned	Burned	Total
Remote	Unburned	45	3	48
Sensing	Burned	5	97	102
Data	Total	50	100	150
	Overall	95%		
	Users	94%	95%	
	Producers	90%	97%	

RdNBR		Reference Data		
		Unburned	Burned	Total
Remote	Unburned	43	1	44
Sensing	Burned	7	99	106
Data	Total	50	100	150
	Overall	95%		
	Users	86%	99%	
	Producers	98%	93%	

SAVI		Reference Data		
		Unburned	Burned	Total
Remote	Unburned	45	3	48
Sensing	Burned	5	97	102
Data	Total	50	100	150
	Overall	95%		
	Users	90%	97%	
	Producers	94%	95%	

Table 17. Results of all SPOT burn severity remote sensing indices.

SAVI		Reference Data			
		Unburned	Moderate	High	Total
Remote	Unburned	50	0	0	50
Sensing	Moderate	0	19	12	31
Data	High	0	31	38	69
	Total	50	50	50	150
	Overall	71%			
	Users	100%	38%	76%	
	Producers	100%	61%	55%	

pNDSWIR		Reference Data			
		Unburned	Moderate	High	Total
Remote	Unburned	46	2	0	48
Sensing	Moderate	4	20	12	36
Data	High	0	28	38	66
	Total	50	50	50	150
	Overall	69%			
	Users	92%	40%	76%	
	Producers	96%	56%	58%	

RelMod		Reference Data			
NDVI		Unburned	Moderate	High	Total
	Unburned	44	3	0	47
Remote	Moderate	3	14	7	24
Sensing	High	3	33	43	79
Data	Total	50	50	50	150
	Overall	67%			
	Users	88%	28%	86%	
	Producers	94%	58%	54%	

MSAVI		Reference Data			
		Unburned	Moderate	High	Total
Remote	Unburned	45	3	0	48
Sensing	Moderate	4	21	17	42
Data	High	1	26	33	60
	Total	50	50	50	150
	Overall	67%			
	Users	86%	38%	76%	
	Producers	98%	51%	55%	

dNDSWIR		Reference Data			
		Unburned	Moderate	High	Total
Remote	Unburned	41	2	0	43

Sensing	Moderate	8	20	13	41
Data	High	1	28	37	66
	Total	50	50	50	150
	Overall	65%			
	Users	82%	40%	74%	
	Producers	95%	49%	56%	

Table 18. Results of all Landsat burn severity remote sensing indices.

dNBR		Reference Data			
		Unburned	Moderate	High	Total
Remote	Unburned	43	2	0	45
Sensing	Moderate	6	19	13	38
Data	High	1	29	37	67
	Total	50	50	50	150
	Overall	66%			
	Users	86%	38%	74%	
	Producers	96%	50%	55%	

NDSWIR		Reference Data			
		Unburned	Moderate	High	Total
Remote	Unburned	37	4	0	41
Sensing	Moderate	12	17	17	46
Data	High	1	29	33	63
	Total	50	50	50	150
	Overall	58%			
	Users	74%	34%	66%	
	Producers	90%	37%	52%	

MSAVI		Reference Data			
		Unburned	Moderate	High	Total
Remote	Unburned	45	3	0	48
Sensing	Moderate	4	21	17	42
Data	High	1	26	33	60
	Total	50	50	50	150
	Overall	67%			
	Users	90%	42%	66%	
	Producers	94%	50%	55%	

RdNBR		Reference Data			
		Unburned	Moderate	High	Total
Remote	Unburned	43	1	0	44
Sensing	Moderate	6	28	12	46
Data	High	1	21	38	60
	Total	50	50	50	150
	Overall	73%			
	Users	86%	56%	76%	

	Producers	98%	61%	63%	

SAVI

		Reference Data			
		Unburned	Moderate	High	Total
Remote Sensing Data	Unburned	45	3	0	48
	Moderate	4	22	16	42
	High	1	25	34	60
	Total	50	50	50	150
	Overall	66%			
	Users	90%	44%	68%	
	Producers	94%	52%	57%	

APPENDIX II: OTHER REMOTE SENSING INDICES APPLIED

Two other remote sensing indices using the modified NDVI index were performed to test their accuracy and compare their results with other indices. Results presented previously were limited to the best indices. Because the SWIR band is useful for fire detection, it was incorporated into the NDVI index by replacing the NIR band. The post-fire SPOT image was used to create the post modified NDVI (pModNDVI) (Table 19). The differenced modified NDVI (dModNDVI) was created using both the pre-fire and post-fire SPOT images (Table 19).

The dModNDVI and rModNDVI (presented previously) had the same overall accuracy for burn severity results (Tables 20 and 14, respectively), but the dModNDVI had slightly lower overall accuracy for the burned versus unburned results (Table 21). Though the pModNDVI overall accuracy results for burned versus unburned (Table 21) were similar to results already presented, its burn severity results were very poor.

Table 19. Other remote sensing indices to detect burn severity.

Remote Sensing Index	Algorithm	Sensor
pModNDVI	$\frac{SWIR - Red}{SWIR + Red}$	SPOT: Red = band 2 SWIR = band 4
dModNDVI	Pre-fire ModNDVI – Post-fire ModNDVI	

Table 20. 'Burn severity' accuracies and kappa statistics for other remote sensing indices using SPOT 5 imagery.

Accuracy Type	pModNDVI	dModNDVI
Overall Accuracy	53%	67%
Producer's Unburned	100%	98%
Users Unburned	32%	80%
Producer's Moderate	35%	53%
Users Moderate	42%	42%
Producer's High	58%	58%
User's High	84%	80%
KHAT	0.3	0.5100
Variance	0.004045	0.0033
Z Stat	4.716899	8.8441

Table 21. 'Burned versus unburned' accuracies and kappa statistics for other remote sensing indices using SPOT 5 and imagery.

Accuracy Type	pModNDVI	dModNDVI
Overall Accuracy	84%	93%
Producer's Unburned	100%	98%
Users Unburned	34%	80%
Producer's Burned	82%	91%
Users Burned	100%	99%
KHAT	0.435897	0.8272
Variance	0.007515	0.0024
Z Stat	5.02837	16.6233

APPENDIX III: DETAILS OF THE LANDSAT AND SPOT SENSORS

Table 22. Comparison of Landsat 7 and SPOT 5 sensor characteristics (Lillesand et al., 2004).

	Landsat 7 ETM+	SPOT 5
Dates	August 27, 2005 September 28, 2005	July 4, 2005 October 24, 2005
Spatial Resolution	30 mpp-- multispectral 60 mpp-- Thermal 15 mpp-- Panchromatic	10 mpp-- multispectral 20 mpp-- SWIR 2.5 mpp-- Panchromatic
Bands and Spectral Resolution (μm)	1 0.45 - 0.52 (Blue) 2 0.52 – 0.60 (Green) 3 0.63 – 0.69 (Red) 4 0.76 – 0.90 (NIR) 5 1.55 – 1.75 (SWIR) 6 10.4 – 12.5 (Thermal) 7 2.08 – 2.35 (MIR) 8 0.52 – 0.90 (Panchromatic)	1 0.50 – 0.59 (Green) 2 0.61 – 0.68 (Red) 3 0.78 – 0.89 (NIR) 4 1.58 – 1.75 (SWIR) 5 0.48 – 0.71 (Panchromatic)
Cost/100 km^2	$275 (gap-filled)	$406
Operational Altitude (km)	705	832
Swath Width (km)	185	60-80
Phase Orbit	16 Days	26 Days
Launch	April 15, 1999	May 3, 2002
Image Area (km^2)	31,450	3600

APPENDIX IV: ASSESSMENT OF HYPOTHESIS #2: CAN BURN SEVERITY BE PREDICTED WITH FUEL LOAD?

It is hypothesized that fuel load can be used to reliably predict burn severity, and thus pre-burn conditions can be derived (post-burn) using remote sensing derived burn severity. Only moderate and high burn severity data (n = 193 plots) could be used in this analysis because the unburned data locations were biased. Except for two plots within the burn, the unburned plots were chosen and intentionally NOT burned. Taking into consideration georegistration errors, two unburned plot samples are not enough to include in the data analysis. Therefore, the question became: can moderate and high burn severity be predicted with fuel load?

A Spearman correlation method was used (because there is a non-parametric distribution) to assess the correlation between fuel load ocular estimates and remote sensing index burn severity values. Fuel load categories were 1, 2, and 3, and the burn severity category was continuous. The Landsat relative dNBR values are significantly correlated with fuel load ($P < 0.001$) but moderately (rho = 0.292). SPOT SAVI values are also significantly correlated with fuel load ($P < 0.0001$), however, these values do not predict fuel load well (rho = -0.362).

In addition, a Spearman correlation method was used (because there is a non-parametric distribution) to assess the correlation between fuel load ocular estimates and remote sensing index burn severity values that were put into ordinal categories. Index values were placed into ordinal categories (unburned, moderate severity, and high severity) the same as described above. Fuel load categories were 1, 2, and 3, and burn severity categories were 2 and 3. Burn severity is not significantly correlated with fuel load ($P = 0.5273$, rho = 0.046) using the SPOT SAVI data; and fuel load does not predict burn severity significantly nor well ($P = 0.2049$, rho = 0.092) using the Landsat relative dNBR data.

These results conclude that pre-burn conditions cannot be derived post burn using remote sensing data. This may be due to a combination of factors such as timing of field data collection, timing of imagery, span of time between pre-and post-fire images and georegistration errors. Additionally, SPOT lacks the spectral resolution for adequate burn severity classification and although Landsat demonstrated a greater sensitivity of burn severity, fuel load still did not have a significant effect, perhaps due to Landsat's spatial resolution. Higher-than-normal amounts of pre-fire fuel load and high winds during the fire contributed to most of the study area having high burn severity. Though the nature of fire is sporadic and pre-fire fuel loads cannot be controlled, a more orthogonal design may better detect the relationship between fuel load and burn severity. Also, before the fire, fuel load was fairly homogenous across the study area. This study could be improved by having more sample plots in the unburned area and not so heavily weighted with high burn severity plots.

[THIS PAGE LEFT BLANK INTENTIONALLY]

Field Evaluation and Hyperspectral Imagery Analysis of Fire-Induced Water Repellent Soils and Burn Severity in Southern Idaho Rangelands

Charles D. Finley, Idaho State University, GIS Training and Research Center, 921 S. 8th Ave., Stop 8104, Pocatello, Idaho 83209-8104

ABSTRACT

This study utilizes spectroscopy and field analysis to classify and detect burn severity and fire-induced soil water repellency following a rangeland wildfire in Southern Idaho. To map the distribution of burn severity and water repellency, hyperspectral imagery was collected over the study site and classified with the Spectral Angle Mapper (SAM) and Mixture Tuned Match Filtering (MTMF) algorithms. Prior to the analysis, burn severity was assessed at the study area, and water repellency was evaluated with a mini-disc infiltrometer (MDI) and the water drop penetration test (WDPT). Field information was recorded with a GPS and used as training data for the spectroscopic classifications.

Analysis of the field data indicated significant increases in water repellency with respect to increasing burn severity, but repellency decreased in high severity areas. The SAM classification correctly classified low severity shrub and grass areas, as well as high severity grass areas with producer's accuracies between 74% and 92%, but the differentiation of moderate and high burn severity areas was ambiguous, resulting in producer's accuracies between 39% and 54%. A MTMF classification of soil water repellency resulted in a representative map of soil water repellency distribution. The analysis techniques conducted in this project signify spectroscopy to be beneficial for differentiating soil characteristics and fire severity classes in burned rangeland areas, where mostly bare, spectrally homogenous soils exhibit slight changes in reflectance.

KEYWORDS: remote sensing, fire, wildfire

Introduction and Background

Statement of Problem

Wildland fires are a naturally occurring phenomenon throughout the rangelands of the Intermountain West. The physiology of the vegetative communities and the hot, dry summer climate make the region extremely susceptible to fire. Frequent occurrences of dry lightning storms regularly ignite wildland fires in the rugged western country. Rangeland ecosystems have adapted to the frequent occurrences of fire in such manners as regulating the buildup and decomposition of litter and organic matter (DeBano et al., 1998). Wildland fires have been documented to increase forage production of rangeland grasses by reducing the cover of sagebrush and other shrubs (Raper et al., 1984).

As a result of the natural occurrence of fires, vegetative communities exhibit fire regimes, which refer to the nature of fire occurrences over time in an ecosystem, as well as the short and long-term effects (Smith, 2000). Natural and human-influenced alterations like climate change, invasive species, and increased fuel loads can lead to variations in an environment's natural fire regime, often resulting in an increase of severe fire events. These events, whether accelerated or naturally occurring, can destroy litter accumulation and organic layers on forest and rangeland floors, and induce or enhance soil water-repellency, which leads to increased soil erosion, watershed degradation, flooding, and debris flows (DeBano, 2000). Severe fires can alter entire ecosystems by wiping out vegetation stands, displacing and killing wildlife, inflicting damage to organic soil layers, restricting plant regeneration, and forcing the environment to deviate from its original fire regime (Odion et al., 2004).

A significant factor influencing erosion, sedimentation events, and watershed processes after wildfires is the presence of water repellent layers within the soils. Past research has indicated that the formation of soil water repellency after fires is a result of several factors, including fire behavior, temperature and burn severity (DeBano, 2000). The severity of a wildland fire describes the consequences of a fire on the soils, vegetation, and ecological processes of the affected area (DeBano et al., 1998). Though the comprehensively described severity of a wildland fire includes its effects on soil, the post-fire soil characteristics and subsequent ecological and physical processes are a causal effect of the temperature and intensity at which vegetation, litter, and organic material burns. Therefore it is important to assess the components of burn severity and soil water repellency independently of one another, as well as comprehensively. The independent assessment of these factors is necessary for susceptibility modeling of wildfire areas, particularly in assessing debris flow and increased sedimentation risks, which are common problems associated with wildfire-affected areas.

This project consists of two components: a field regimen that assesses the severity, or ecological alteration of the landscape, caused by a rangeland wildfire, and its cause-and-effect relationships with fire-induced soil water repellency. This study also develops a method to extract spectral signatures of burn severity classes and water repellent soils from high spectral resolution imagery to classify and map these parameters in a rangeland wildfire setting at a landscape scale. The use of hyperspectral imagery for mapping soil effects of wildfires in rangeland areas provides a detailed window into the subtle changes of spectra among ground targets in arid landscapes. Certain fundamental problems have been noted by past researchers when applying remote sensing techniques in arid areas; these include a high background soil reflectance that crowds out the contribution of vegetation and other spectra (Okin et al., 1999b), and the tendency for desert vegetation of the same species to often have high spectral variability (Okin et al., 2001). Through field assessments of wildfire burn severity and soil water repellency, coupled with statistical tests, and subsequent hyperspectral spectroscopy analysis, this research project evaluates the effects of fire-induced soil water repellency in a rangeland environment. The two hypotheses of this study are (a) water repellency will be evident to the highest degree in areas of moderate burn severity and (b) hyperspectral spectroscopy will discern water repellent soils of varying degrees, as well as wildfire burn severity classes, in a rangeland wildfire area.

Past studies of relationships between wildfire severity and soil water repellency have indicated higher repellency is found in moderate burn severity areas due to extended burn times and temperatures (Davis and Holbeck, 2001; DeBano, 2000; Lewis et al., 2004). The majority of the described research, however, has been conducted in Rocky Mountain West forested ecosystems, where the dominant vegetation is pine and conifer stands, and soils tend to be shallow, rocky, and poorly developed. This study was conducted in the Clover fire area of the southern Idaho rangelands, within which the primary vegetation is sagebrush and grass and the soils are composed of loamy sands to clays, typically derived from basalts and rhyolites, with varying depths of wind-blown loess deposits (Wright, 1985). Because of inherent ground and climatic conditions, soils in these areas often exhibit slight water repellency even in the absence of fire. Based on the principles of fire temperature and residency times as described by DeBano (2000), this research project similarly hypothesizes that rangeland soils will exhibit highest incidences of water repellency in areas of moderate burn severity, and lowest occurrences in low severity and unburned areas. Soils in high burn severity areas will display inconsistent and variable rates of water repellency, because of rapid burn times that may not burn vegetation long enough to release water repellent compounds, or because the fire may burn so hot that water repellent compounds break down altogether (DeBano, 2000). In addition to field analysis, this research project involves mapping and classifying burn severity and soil water repellency with hyperspectral images, also known as spectroscopy. Our hypothesis predicts that spectroscopy will discern burn severity and water repellent soils of varying degrees within rangeland wildfire areas. While the spectroscopy of a rangeland fire area is expected to evaluate the burn severity, the most challenging portion of the analysis is the assessment of fire-induced soil water repellency based on the spectral characteristics of the soil. By evaluating the spatial distribution and relationships of soil water-repellency and burn severity with field methods and spectroscopy, this research will provide insight into the dynamics of rangeland wildfire, which are exceedingly unique in comparison to wildland fires of forested ecosystems. The objective of this project is not to craft a comprehensive model of post-fire erosion susceptibility, but to facilitate standardization of methodologies for precisely assessing the input variables of rangeland burn severity and soil water repellency. This methodology will provide a tool for assessing field variables on a landscape scale with remote sensing imagery. By standardizing the classification and assessment of variables, rangeland managers can more effectively evaluate post-fire effects, and input parameters for susceptibility modeling can be more specified.

Study Area

The primary study area for this project is the Clover Fire area (Fig. 1.1), approximately 39 km west of Twin Falls, Idaho, USA. The Clover fire was a lightning-caused rangeland wildfire, ignited on 15 July, 2005 and contained on 20 July, 2005. The fire boundary encloses 192,846 acres (~ 780 km^2), and was the largest wildland fire in Idaho in the 2005 fire season. It extends from Salmon Falls Creek at its eastern boundary, about 8 km west of Castleford, ID, in a northwesterly direction into the Saylor Creek Air Force Range at its western boundary. The elevation of the study area ranges from around 750 m in the northern lowlands, to 1355 m atop Castleford Butte in the southeastern portion of the fire boundary.

The fire boundary is primarily on BLM land, and is adjacent to the Bruneau Desert. Several irrigated farm fields are on the northeast boundary of the area, and the northwest end of the fire boundary is in the Saylor Creek range, a tactical target range utilized by the US Air Force. The topography of the study area is characterized by flat, shallow drainages, bordered by gradually-sloping buttes and ridges.

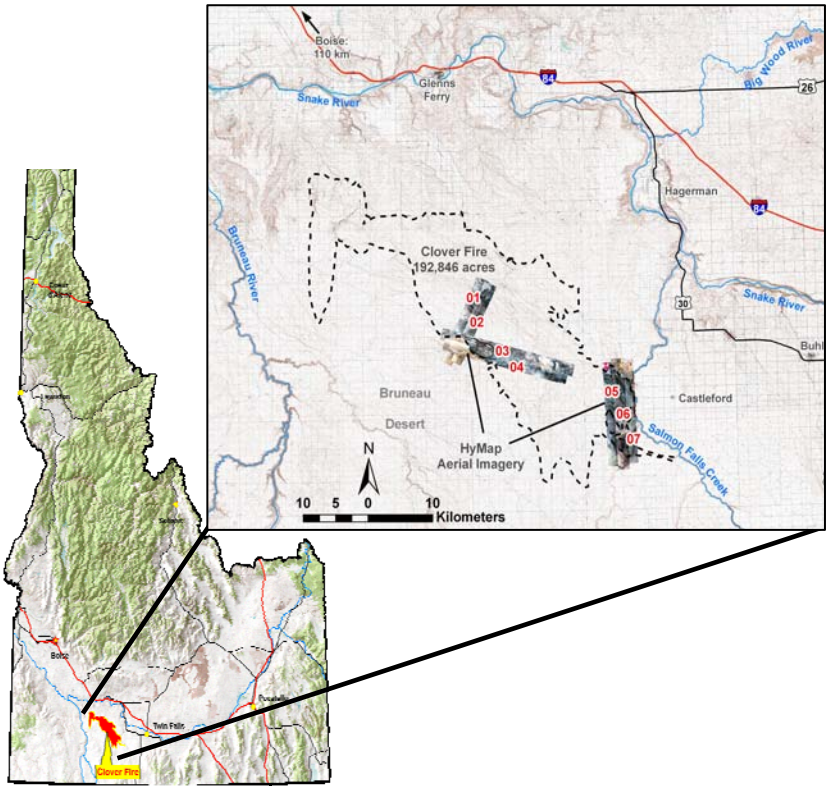

Figure 1.1. Clover fire, Idaho, with hyperspectral flight

Intermittent stream beds lie in steep gullies feeding Salmon Falls Creek and the intermittent Saylor Creek. Pre-fire vegetation within the burn area ranges from seeded areas of crested wheatgrass in the northern end, to dense sagebrush in the southern end. Cheatgrass is abundant throughout the sagebrush areas. Soils range from sandy, gravelly loams in the northern end to silt and loam throughout the middle section. The southern end of the fire boundary is typified by deep silt loam soils. Basaltic rock outcrops are located throughout the study area and along the gullies and stream canyons. The Clover fire area was susceptible to debris flows and excess sedimentation after the fire in the case of heavy rainfall. No significant rain events were observed in the area, however, for at least three months following the fire (Appendix 2).

The field sampling and remote sensing classification took place within 3 sections of designated flight lines inside the study area. HyMap hyperspectral imagery was collected over these sections on August 26, 2005. The 3 sections cover 175 km^2, of which 117 km^2 are inside the burn area, encompassing approximately 15% of the burn area. The slope within the sampling boundaries ranges from 0^o to 57^o, with the mean slope being 3^o. In addition, several canyons and gullies have vertical cliff walls up to 30 m in height.

The study area was chosen based on previously-determined criteria. Personal communications with various experts in the field of wildfire research in Idaho (F.Pierson, USDA Agricultural Research Station; P. Robichaud and C. Luce, USDA-Forest Service Rocky Mountain Research Station), all concur that it is best to assess fire areas for water-repellency as soon after the fire as possible. DeBano (2000) indicates that low severity fires, particularly prescribed burns, exhibit fire-induced water-repellency for less than one year, but water-repellent layers in moderate and high severity wildland fire areas can persist for several years after a fire. Wildland fire areas tend to have excess fuel build-up, in contrast to prescribed burn areas, which cause the fires to burn hotter and with greater volatility. Wildland fires tend to burn during the hottest and driest times of the summer months, and typically burn in steep, often unstable watersheds. In contrast, prescribed fires are typically held in calm weather conditions in the spring or fall season, and the boundaries are controlled so as not to allow the fire to extend uncontrollably into steep, highly erosive basins.

The extent and amelioration of water-repellency is dependent on treatment, including seeding, mulching, mechanical, and chemical treatments, as well as natural responses, particularly meteorological events. Intermountain rangeland environments are known to receive intense thunderstorms during the summer months (Wondzell and King, 2003), that, dependent upon rainfall intensity, can initiate excessive erosion or debris flows and erode water-repellent soil layers (DeBano et al., 1998). Though some rainfall was

recorded in the study area**,** most erosion occurred as a result of severe windstorms between September 1, 2005 and October 30, 2005. The windstorms occurred as a result of Pacific frontal weather systems moving east across the southern Idaho plains, and they developed large dust clouds after encountering the burned area (Fig. 1.2). As a result, scouring and aeolian transport of ash, soils and litter occurred. By late October 2005, the high plateau areas of the study area had experienced at least 4 severe windstorms and all of the topsoil, ash and litter had been removed, leaving only the hard, concrete-like calcic horizon. Because of the variable and unpredictable nature of wildland fire environments, assorted degrees of fire-induced water-repellency were expected at the site, as well as areas of high, moderate and low severity burns. These variable characteristics of the Clover fire provided a reasonable study site for this research project.

Fig. 1.2. A dust storm moves across the Clover fire area, Sept. 16, 2005.

Rangeland Ecosystems

Rangelands have been classified throughout the world, in an agricultural sense, as areas suitable for livestock forage and habitat, yet not agricultural harvest. Covering approximately 50% of the United States, they can vary from forested areas and brushy hillsides to shrubby, near-barren desert land (Holecheck and Pieper, 2001). In the Western USA, rangelands have been typified as primarily public land that is allotted to ranchers for livestock foraging purposes. Public rangelands, however, serve a variety of purposes other than livestock holdings including ecological and wildlife preservation, multi-use recreation, and scientific research.

The vast rangelands of the Intermountain West cover approximately 700,000 km^2 (Knapp, 1995), and are bordered by the Cascade and Sierra Nevada mountain ranges to the West, and the Rocky Mountains to the East. This rangeland area is mostly within the Basin and Range geologic province, a region characterized by numerous fault-block mountain ranges extending in north-south directions, separated by wide flat valleys often wider than 75 km (Knapp, 1995). The physiography of Intermountain West rangelands is exemplified by dry, wind-swept plains, and steep rocky slopes. Precipitation ranges from 25 to 50 cm per year and the climate is typically considered semi-arid above 41^o N, due to more frequent Pacific frontal systems, and arid below 41^o N. (Knapp, 1995).

The Intermountain Western rangelands are further classified into zones based on vegetation and aridity (Holecheck and Pieper, 2001). The most arid rangeland zones are defined lying southeast and southwest of 41^o N in the desert basins of Bonneville, in Central Utah, and Lahontan, in Western Nevada (Knapp,

1995). Vegetation in these areas is typified by shadsscale (*Atriplex confertifolia)* shrubs, horsebrush (*Tetradymia canescens)*, perennial ricegrasses (*Achnatherum hymenoides*) and annual cheatgrass (*Bromus tectorum)*. Primarily south of 41° N is the rangeland zone known as the big sagebrush semi-desert, a sparsely-covered, sagebrush-dominated region with some annual and perennial grasses (Knapp, 1995). North of 41° N is the sagebrush-steppe zone, characterized by semi-arid conditions and higher percentages of vegetation cover. Plant species include big sagebrush (*Artemisia tridentata* Nutt.) shrubs as the dominant overstory, perennial bunchgrasses like crested wheatgrass (*Agropyron cristatum)*, needlegrass (*Achnatherum nelsonii)*, Idaho fescue (*Festuca idahoensis* Elmer), and annuals such as the invasive cheatgrass and medusahead (*Taeniatherum caput-medusae)*. The largest contiguous region of sagebrush-steppe rangeland in the USA is located in eastern Oregon, northern Nevada, southern Idaho, northern Utah, and southwestern Wyoming. Most of the sagebrush vegetation in these locations is found at elevations ranging from 610 to 2135 m (Wright, 1985). Typical soils of sagebrush-steppe zones vary from loamy sand to silty clay, and are a mix of volcanic-derived basalts and rhyolites, as well as windblown loess deposits (Wright, 1985). In areas of higher elevation within the sagebrush-steppe, plant communities may be grass-dominated, often by cheatgrass, and intermixed with pine timber and Western Juniper (*Juniperus occidentalis)* (Knapp, 1995).

Dynamic rangeland environments are exemplified by communities of vegetation that include annual and perennial grass communities and populations of woody shrubs, and by exterior driving factors such as rainfall, fire and grazing by herbivores (Noy-Meir, 1973). The vegetation communities of rangelands are especially susceptible to fire because of drought, high temperatures and steady winds. Due to these factors, single fires within rangelands may easily extend over several thousand hectares when burning a virtually uniform fuel supply. Periodic occurrences of dry lightning storms ignite rangeland fires throughout the Intermountain West. Additionally, humans have utilized fire as a management tool for centuries. Early explorers of the United States West documented native inhabitants setting fire to the plains and forests as a method of enhancing wildlife forage quality by subduing shrubbery, improving access to plant foods, and facilitating travel by clearing underbrush in forests. Across grass and shrub lands, the natives would regularly ignite fires as a means of driving game for harvest. Fire was also an effective tool of communication and battle (Shinn, 1980). While it is well known that native inhabitants of the West definitely utilized fire as a multi-use tool, the extent and frequency with which it was used by the natives is unclear. This is because native populations were sparsely settled in many areas, due to the immense size of the region, and many areas contained meager resources (Shinn, 1980). Thus, certain areas of the Intermountain West likely have experienced more frequent intentional burning than others. Various researchers have attempted to determine the historical frequency of fire across the Intermountain West. Houston (1973) observed scars of tree rings to determine an average historical fire frequency of 32 to 70 years in northern Yellowstone National Park, and smaller plots within that area may have burned every 17 to 41 years. Natural fire-return intervals of lower elevation sagebrush stands may range from 50 years to as low as 100 years. (Whisenant, 1990; Wright, 1985; Young and Evans, 1981). Many plants within semi-arid rangelands have adapted to intermittent fires by developing means of fire resistance, and rangelands continually influenced by fire have become accustomed to lightning-caused and customary burns (Shinn, 1980; Smith, 2000).

After the settlement of western lands by European descendants, the established fire return intervals of the Intermountain West were disrupted due to careless burning by pioneers (Shinn, 1980), and eventual negative attitudes toward uncontrolled fires, leading to strategies of rapid fire suppression. When the federal government established forest reserves in the U.S. in 1891, a policy of total fire exclusion was adopted (Shinn, 1980). Other damaging elements of traditional rangeland fire regimes in the Intermountain West include: the swift introduction of the invasive annual cheatgrass (Whisenant, 1990); the expansion of Western Juniper, which has increased fuel loads and fire dangers in rangelands (Young and Evans, 1981); and disruption of grazing strategies due to the displacement of native herd animals by domestic livestock (Shinn, 1980). It is estimated that the average historic fire return interval of 35 to 100

years on Idaho's Snake River Plain has been reduced to 2 to 4 years due to the increased fine fuel load of cheatgrass populations and the impact of livestock (Whisenant, 1990). This was determined by examining the records of known fire history and regenerative strategies of plant communities on 12 sites in southern Idaho.(Whisenant, 1990).

Rangeland researchers have studied the effects of wildland fires and prescribed burns throughout the past century, particularly focusing on the effects of fire on successional elements of plants and plant communities within rangelands. The predominant and most defining plant species of rangeland environments is big sagebrush (*Artimesia tridentate* Nutt.). Big sagebrush is well-suited to habitation in arid rangeland environments because its deep root system allows the plant to draw water from deep soil layers during the heat of summer. This quality allows the sagebrush to grow throughout the dry season, after all moisture is gone from the upper soil layers. Annual grasses present in rangelands typically grow early in the season because they retain their moisture from the upper soil layers. During growing seasons that are wetter than normal, annual grasses can exploit more water than usual, resulting in an increased, denser stand (Knapp, 1995). These dense stands of annual grasses present a relatively uniform, high fine fuel load, which result in more combustible and severe fires when ignited. A negative impact of increased fuel loads from fine fuels like cheatgrass is that, when burned, the potential for unburned remnant patches of sagebrush and native grasses to remain in the affected area decreases (Whisenant, 1990). When unburned patches remain, sagebrush has been observed to reestablish from seed within 4-6 years, and cover may return to preburn levels within 15 to 25 years of the fire (Bunting, 1985). In completely burned areas, range managers will often reseed big sagebrush because the population cannot reestablish on its own if no unburned areas are available for seed redistribution (Britton and Clark, 1985). Though rabbitbrush shrub populations tend to dominate most soon after fire, if grazing and fire are restricted and controlled, sagebrush will eventually dominate the area. However, if fires return more frequently due to increased fine fuel loads, especially within the first 4-6 years when sagebrush seedlings are establishing, sagebrush stands may be further affected and annual grass stands will continue to dominate (Wright, 1985). When fires occur during late summer or early fall, perennial forbs and grasses appear relatively unaffected, and subsequent productivity may actually be enhanced (Bunting, 1985). While monitoring an 11,000 ha burn site in south central Utah, researchers found cheatgrass cover to be near 100% the year following the burn (West and Hassan, 1985). Two years following the burn, perennial bunchgrass populations appeared to be near preburn conditions. Though native rangeland plant populations can effectively recover from fire, altered conditions such as increased fine fuel load, reduced patchiness and ensuing fires returning much sooner will rapidly break down the ecosystem dynamics by altering plant communities, successional patterns, and fire regimes.

Wildland fires throughout the American West have increased significantly in size, severity, and damage since the early part of the 20th century (Odion et al., 2004). Along with this increase, ensuing research has steadily analyzed fire patterns, behavior, history, and effects. Though a handful of researchers have scrutinized rangeland fires and fire events at lower mountain elevations, particularly in sagebrush-steppe and pinyon-juniper ecosystems (Cannon, 2001; Cannon et al., 2001; Pierson et al., 2001; Pierson et al., 2003), the majority of wildfire-related research has been in forested settings (Odion et al., 2004; Pierce et al., 2004; Robichaud et al., 2003; Wondzell and King, 2003).

Post-fire Sedimentation Processes

The hydrological impacts following rangeland fire can often be severe. Reduction of vegetation, litter, and organic layers on forest and rangeland floors by fire reduces rainfall interception, leading to increased soil erosion and overland flow (Ice et al., 2004). Soil infiltration rates can be decreased by the formation of water-repellent soil layers, and the removal of litter and organic layers (DeBano et al., 1998). These are key factors in the increase of soil erosion in burned areas, and are influenced by fire severity (DeLuis et al., 2002). Post-fire hillslope erosion can also lead to sediment-laden stream flow and debris flows. Debris flows can cover exceedingly large areas, having been known to surpass 10^9 m^3 of volume (Iverson,

1997), and the fluidity of some debris flows can allow for significant runout lengths. Debris flows often occur with little warning, possessing such force that even small flows can transport vast amounts of sediment, inflict damage to infrastructure, and imperil human lives (Cannon, 2001).

Many rangeland environments affected by wildfire are considered susceptible to debris flows because they cover steep topography where vegetation has been removed. Most common to burned watersheds are debris flows that initiate through progressive bulking of sediment within high-order channels and on hillslopes, usually occuring within a short period of the fire (Cannon et al., 2001). The majority of debris flows (93%) on Storm King Mountain, CO noted by Cannon et al. (2001) were traced to zero and first order channels and hollows where noteworthy erosion and runoff was observed. Analysis of a burned rangeland canyon in southeast Idaho identified increased overland flow, resulting from heavy rainfall on hillslopes as the primary initiator of an erosion debris flow that shut down a major transportation corridor (Tucket et al., 2004). Similar debris flow characteristics of progressive bulking sediment flows were identified in Yellowstone National Park after the destructive fires of 1988 (Meyer and Wells, 1997). Cannon (2001) distinguishes two types of fire-related debris flows recognized throughout the Southwest; type 1, a poorly-sorted mixture of boulders and similar-sized material, with significant height, and sharp, distinct margins, having a matrix of fine-grained materials, and type 2 flows, consisting principally of sandy, gravelly materials, with a charcoal and ash-abundant matrix. The sediment-rich type 2 debris flows are differentiated from sediment-laden stream flow because of the lack of hydraulic sorting that would remove the fine material.

Debris flows may also occur as a result of a stable, intact mass of sediment becoming saturated and subsequently moving downhill (Summerfield, 1991). The paths can usually be traced up an easily identifiable channel to a source, known as a soil-slip scar (Cannon et al., 2001) or colluvial failure (Meyer et al., 2001). In previously burned forested areas, soil-slip flows are most often observed five or more years following the fire, because the decaying of tree and shrub roots that anchor colluvium has reduced soil cohesion (Meyer et al., 2001). In contrast, type 1 and 2 debris flows are more likely to occur within a month to a year after the fire event (Cannon et al., 2001; Meyer and Wells, 1997; Tucket et al., 2004).

A detailed analysis of post-fire erosional debris flows involves assessing each of the parameters that affect flow generation. In a relative hazard ranking model, Sprague-Wheeler (2001) attempted to evaluate wildfire areas in Central Idaho based on the parameters of geology, burn severity, slope angle, and aspect. A setback with assigning ordinal rankings to each of the parameters is the preponderance for subjectivity while assessing the variables and it also doesn't effectively represent the physical processes involved. For a susceptibility analysis to be accurate and applicable, the parameter assessment should be standardized prior to input in a comprehensive study. For these particular reasons, this study analyzes two particular variables (burn severity and soil water repellency) that influence debris flow generation. Even though our study area was not at high risk of debris flow generation (primarily because of the lack of precipitation; Appendix 2), by conducting an in-depth analysis of the particular debris flow parameters, future vulnerability studies will be more robust.

In a study of 95 burned basins in the American Southwest, Cannon (2001) identified geology, soil conditions, basin morphology, burn severity, and precipitation as the primary initiating factors of debris flows. Several other conditions that affect slope stability and cause increased sedimentation include decreased soil infiltration rates due to the formation of water-repellent layers and the removal of vegetation, a result of burn severity, which decreases interception and evapotranspiration of water (Cannon et al., 2001). An extensive review of relevant literature has identified fire-induced soil water repellency and wildfire burn severity as two crucial parameters of post-fire debris flow generation that are in need of research in rangeland environments.

Water Repellent Soils

A major dynamic influencing sedimentation events in burned areas is the presence of water repellent soil layers. Soil water repellency is a phenomenon that has been the focus of intense research for over 30 years (DeBano, 1981; DeBano, 2000). These soils are found around the world, in agricultural fields, grasslands, brushlands, and forests (Dekker and Ritsema, 1994). Numerous studies have identified water repellent soils in different plant communities, ranging from soils between grass bunches in Australia, underneath citrus canopies in Florida, around the decaying roots of shrubs in the Sierra Nevada, below aspen stands in Wisconsin, and in Southern California chapparal communities where dense litter layers were present (DeBano, 1981). Johnson and Beschta (1981) noted a seasonal variation in soil water repellency, pointing out that Western Oregon soils exhibited increased repellency during the summer months, due to greater vegetation cover that protected the soil surface, and higher temperatures hardening the soil surface and reducing the viscosity of water. A water repellent soil layer is recognizable because water droplets will ball up and sit on top of the layer, often for longer than five minutes and sometimes over 1 hour (Cannon, 2001; DeBano, 1981; Dekker and Ritsema, 2000), without soaking into the soil.

Rangeland soils sometimes exhibit soil water repellency in the absence of fire because of dry climatic conditions, compaction, unevenly-spaced vegetation, and organic layers that naturally contain hydrophobic compounds (DeBano, 1981). These conditions can lead to water input exceeding soil infiltration rates, resulting in overland flow (Pierson et al., 2001; Wondzell and King, 2003). Water repellent soils may occur for a number of different reasons, but the primary factors affecting it involve organic matter, soil texture (DeBano, 1981), soil water content (DeBano, 2000; Doerr and Thomas, 2000), and plant-soil relationships (DeBano, 2000; DeLuis et al., 2002). Formation of a layer can occur because of the irreversible drying of organic matter, and the leaching of organic substances from litter and mineral particles. Additionally, hydrophobic organic matter can mix with mineral soil particles during heating, creating and/or enhancing water repellency in the soils (DeBano et al., 1998), and at very high temperatures (220^{o}-275^{o}C) (Moody and Smith, 2005), cementation by clay oxide occurs over the soils. Soil water repellency tends to have varying degrees of persistence and intensity, but it is often noted that fire-induced water repellency is more severe in its persistence (DeBano, 1981) and the hydrological effects incurred from it. Water repellent layers in soil are often found at or below the surface, and exhibit variable spatial characteristics. In natural soil conditions, repellency can be present below the surface, but soil remains penetrable because of cracks, root holes, and animal burrow holes that allow preferential flow, and the presence of litter layers above the soil absorbs water, thus, the risk of overland flow is low (Doerr et al., 2006). In burned soils, a subsurface layer can be present at depths of 6 cm or greater, and is much less penetrable, because the litter layer is destroyed, and preferential flow spots are often choked with fine particles from post fire erosion (Doerr et al., 2006).

When a rangeland area is affected by wildfire, organic matter, which often contains hydrophobic compounds, combusts, producing aliphatic hydrocarbons (DeBano et al., 1998; Lewis et al., 2004), that are detectable in the burned soils. The depth and thickness of water repellent soils after fire depends on the severity of the fire. Typically fires with higher burn severity produce a deeper repellent layer, but very hot fires destroy the compounds responsible for the repellency. Laboratory testing by DeBano (2000), observed changes in soil water repellency after heating soils with temperatures similar to those observed in wildland fires. Results indicated that soils exhibited little, if any, change when they were heated no more than 175^{o}C. When soils were heated between 175 and 200^{o}C, water repellency of high intensity was observed, and when soils were heated between 280^{o} and 400^{o}C, water repellency was destroyed. Although it is unclear from the literature which soil types may exhibit higher degrees of repellency, it is stated that the heating of translocated substances within the soil, and not the soil itself, is generally responsible for the presence of water repellency (DeBano, 1981; DeBano, 2000). The texture of soils, however, does play a significant role in the induction of soil water repellency; when organic matter is mixed with coarse-textured soils or sands, and heated, water transport is restricted severely, as opposed to finer soils, in which the organic materials enhance water and air movement (DeBano, 1981). A unique

attribute in the formation of water repellent soils is the tendency of hydrophobic compounds to move downward in dry soils due to temperature gradients in the upper mineral soils (DeBano et al., 1998). After the fire has passed, the heat may continue to move downward, causing more of the hydrophobic substances to volatize, thus thickening the water repellent layer (DeBano, 2000). This characteristic is an important dynamic in the relationship of burn severity and associated burn times to sedimentation events because a water repellent layer deep below the surface that has abundant erosive soil on top of it is capable of producing overland flow following saturation.

Another dynamic relating to the formation of water repellent soils is the cementation of the soil, due to the burning of biomass and the intense heating of the soils chemical properties. While testing the cohesive shear strength of forest soils heated to specific temperatures, Moody et al. (2005), found that the majority of soil water repellency formed because of the heating and volatization of organics occurs at temperatures up to 220^{o} C. At temperatures greater than 220^{o} C, however, the organic repellency is reduced and overtaken by sesquioxide clay cementation, involving the intense heating of aluminum, iron, and titanium oxide clays. This finding is important in relation to post-fire erosion because the sesquioxide clay cementation is responsible for the increase in the size of the eroded soil aggregates after fire. Similar to temperature thresholds for water repellency, Moody et al. (2005) found the critical shear stress of soils to drop abruptly when heated above 275^{o} C, as does the water repellency of soils; and the clay cementation is destroyed, increasing the porosity and erodibility of the soils. The findings of Moody et al. (2005) and DeBano (1981; 2000) indicate that the degree of water repellency can be separated not only between weak, moderate and strong repellency due to the volatization of organics, but also into a category of very strong repellency as a result of sesquioxide clay cementation.

Water repellent soil layers pose serious threats to slope stability after wildfires because of their influence on debris flow generation. When a water repellent layer is present below the surface, there is usually a layer of highly penetrable mineral soil above it. The occurrence of precipitation events over the area can drop heavy amounts of rainfall on the soils, suddenly saturating the soils. Normally, rainfall will infiltrate deep into the soils, but the presence of a water repellent layer presents a barrier to the rainwater. Additionally, the absence of vegetation increases the amount of water falling into the soil, allowing it to erode faster because vegetation does not minimize raindrop impacts through interception. When the upper soil layer reaches saturation, overland flow begins. The increased runoff eventually forms rills, which have a depth to the presence of the water repellent layer. Gradually, the erosive processes within the rills will degrade the water repellent layer, causing it to break down and ultimately become receptive to infiltration (DeBano, 2000). The increased runoff and overland flow, however, can progressively bulk across a watershed and lead to erosional debris flows (Cannon, 2001; Cannon et al., 2001; Meyer and Wells, 1997; Tucket et al., 2004).

Researchers have indicated that water repellent soils can be very difficult to model because of the extreme spatial and temporal variability of the phenomenon (DeBano, 2000; Shakesby and Doerr, 2006). Measurements of fire-induced water repellency in Eucalyptus-dominated catchments in South Africa indicated that vegetation cover was responsible for variations in fire behavior and the variability of water repellency in soils (Scott, 1993). The sparse vegetation that is characteristic of rangelands creates even more variability of water repellency because interspaces between plants are often void of any vegetation, and not directly affected by fire. The areas directly beneath shrubs, known as coppice microsites, are generally the most affected by water repellency during a fire (Pierson et al., 2001). In personal field observations one year after the Red Bull Fire in Spanish Forks Canyon, Utah, water repellent soil layers were observed at very shallow levels (<2 cm) directly below burned shrubs **(Fig. 1.3)**, yet no repellency was observed within 30cm of the burned shrub. In observations at the Clover Fire, soil infiltration was observed to increase with distance from burned vegetation. Fire-induced water repellency is often known to persist near its original intensity to within one year after a fire, but soils generally return to pre-fire conditions within five years of the fire (Pierson et al., 2001).

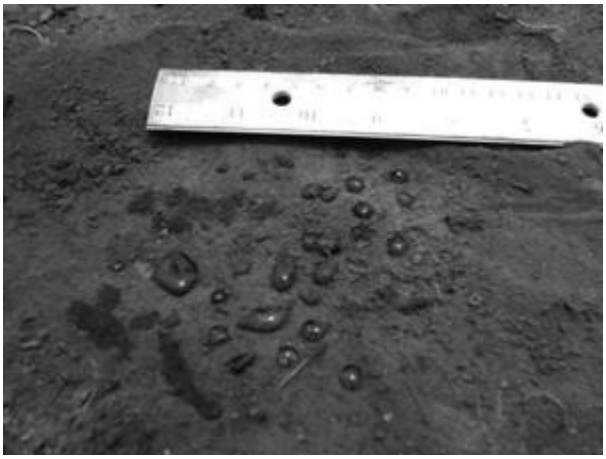

Fig. 1.3. Water repellent soil layers one year after a rangeland wildfire in Uinta NF, Utah.

Remote Sensing

Remote sensing is a science which involves acquiring information about an area on earth, an object, or an occurrence through a device with which it is not in physical contact (Lillesand et al., 2004). In research of natural resources and earth sciences, remote sensing usually involves the acquisition and subsequent processing and analysis of aerial or space-borne imagery covering a portion of the landscape. Remote sensing images hold four forms of resolution: spatial, spectral, temporal, and radiometric. The spatial resolution of an image refers to the smallest quantitative area on the ground that is discernable in the image. Spatial resolution of aerial and space-borne imagery can range from less than one meter (e.g. panchromatic band of Digital Globe, Inc.'s Quickbird imagery), to greater than one kilometer (e.g. NASA's Moderate Resolution Imaging Spectrometer (MODIS)). The spectral resolution of an image describes the range of spectral bands and their associated bandwidths in an image. Traditionally, remote sensing imagery has been panchromatic in nature, capturing brightness values of the ground in a broad band of wavelengths (e.g. from far ultraviolet to near infrared (NIR)) in a grayscale, or multispectral, capturing spectral characteristics of the ground surface through multiple channels of the electromagnetic spectrum. A multispectral image usually contains multiple bands ranging from the visible portion of the spectrum to the NIR, short wave infrared (SWIR) and sometimes thermal infrared (Jensen, 2000). A less traditional and newer sensor type is the hyperspectral sensor, which collects data within hundreds of very narrow, nearly contiguous bands, covering portions of the visible, NIR, and SWIR. Hyperspectral sensors are unique in that the bands are collected adjacent to one another in a near continuous spectrum by oversampling (Lillesand et al., 2004). The bands are typically narrow (e.g. 10 to 15 nm or less), allowing fine absorption features of the earth to be detected. The smaller the spectral window detected in each band, the higher the spectral resolution, (Aspinall et al., 2002). Remote sensing systems have proven valuable in analyzing physical and environmental characteristics of the earth, as well as assessing the effects of natural events and disasters like wildfires, floods, severe storms and earthquakes.

There are a number of challenges related to remote sensing in arid rangelands, foremost being its inherent characteristic of a large soil background that crowds out a low vegetation cover (Okin et al., 2001). The vegetation communities of arid lands often exhibit a reduction of leaf absorption in the visible spectrum, and are intrinsically different in their spectral signature, as compared to humid vegetation (Okin et al., 1999a). These setbacks tend to enhance nonlinear mixing of spectra within pixels and there can be a tendency to misidentify and wrongly estimate the abundance of the materials present within the confines of one pixel. Researchers have utilized hyperspectral image analysis, commonly referred to as spectroscopy, to analyze arid areas in efforts of minimizing the problems associated with spectrally differentiating landscape characteristics.

The science of spectroscopy is unique and beneficial in the fact that the narrow, nearly contiguous wavelengths in spectroscopic images can allow for the spectral signature extraction of specific mineralogical compositions, soil and ground texture, and organic matter. Unlike conventional multispectral remote sensing, spectroscopy requires in-depth analysis of the image spectrum, in order for researchers to understand the contributing composition of materials and their interactions, and to accurately and sufficiently identify the endmember materials in sight. The goal of this project was to identify the unique spectroscopic characteristics of burned rangelands, including burn severity and water repellent soils, and use their spectral signature as training endmembers to determine their distribution across the geographic area of the acquired imagery.

The most important component of spectroscopic imaging is the identification of spectral endmembers to be used for classification of the imagery. Numerous researchers have utilized spectroscopy to identify the unique spectral signatures of materials across an image; most often for mapping soil and mineralogical properties (Chabrillat et al., 2002; Debba et al., 2005; Okin et al., 2001; Palacios-Orueta and Ustin, 1998), and discriminating vegetation types (Bachmann et al., 2002; Glenn et al., 2005; Mundt et al., 2005a; Parker-Williams, 2004). The advantage of mapping mineral distribution, or discriminating vegetation type, is the tendency for individual minerals and plants to exhibit unique and separable spectral signatures. When spectroscopy is utilized over burned rangeland areas, the differentiation of distinct spectral signatures is compounded by the fact that a large soil background is present, and was so before the area was burned, introducing high albedo effects. When a rangeland experiences a wildfire of high severity, the vegetation and fuel is often completely incinerated, leaving much of the area bare of any substantial ground cover, litter, or vegetation, as was the case in much of our study area. Because soils in arid regions tend to be mineralogically similar and bright (Okin et al., 2001), and the burning of vegetated areas leaves little variability across the surface, the distinction and separation of particular soil characteristics in burned areas can be ambiguous. Due to the intricate nature of rangeland wildfire, and its spectral attributes, spectroscopy may have the ability to maximize the obscure differences among them.

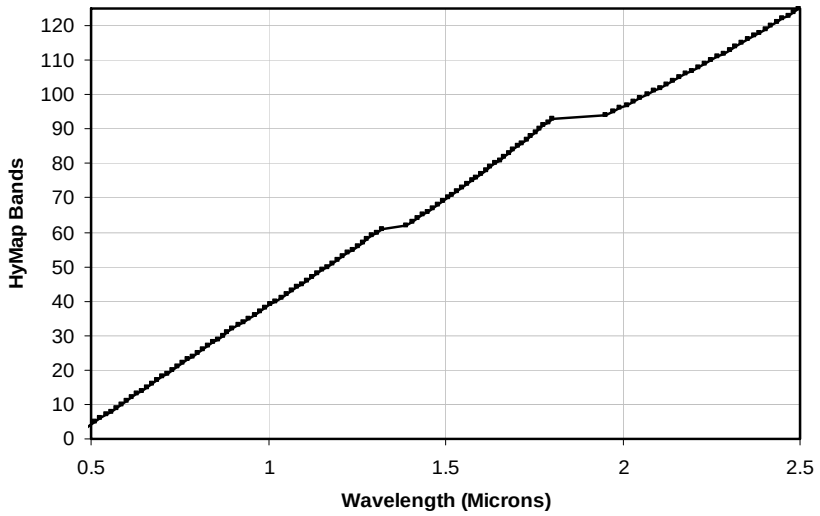

Fig. 1.4. HyMap reflectance

Hyperspectral imagery was used for this study because the seemingly extreme variability often observed with water repellency (Pierson et al., 2001; Shakesby et al., 2003) is undetectable with coarser, traditional sensors. The concurrent collection of full spectral measurements in spectroscopic sensors provides a commanding foundation for the identification of biochemical composition of plants (Ustin et al., 2004), and, when coupled with high spatial resolution, the fine scale, variable absorption features typical of soils can be accurately evaluated (Palacios-Orueta and Ustin, 1998). The HyMap sensor (HyVista Inc., Australia) which was utilized for the current research project, is a hyperspectral sensor capturing 126

spectral bands between 0.45 μm and 2.5 μm, with a spatial resolution of 3 m. The spectral regions covered in HyMap imagery include the visible portion (0.45 μm to 0.7 μm), the NIR (0.7 μm to 1.3 μm), and the SWIR (1.3 μm to 2.5 μm), with the majority of the bands (60-125) lying in the latter **(**Fig. 1.4). Hyperspectral imagery can be associated with a detailed spectral library, a set of spectral signatures of various materials that can be used for matching a feature to its corresponding wavelength in the image (Lillesand et al., 2004). When a spectroscopy project matches imagery to field-collected spectral libraries, a great advantage is the ability to extend the spectral libraries across wide areas and multiple images to identify target materials (Aspinall et al., 2002). The unique spectral characteristics of hyperspectral images and its processing efficiency are beneficial for evaluating landscape scale disturbances, and can prove useful in developing mitigation response plans after such events.

Previous Studies

Commonly, specific procedures and classification methods are employed when undertaking spectroscopy research and a general flow of processes is followed. Methods developed specifically for spectroscopy involve noise reduction procedures like the Minimum Noise Fraction (MNF), endmember selection like the Pixel Purity Index (PPI) and the n-dimensional visualization of endmembers, and finally, spectral mixture analysis. Because spectroscopy is a relatively new technology, researchers are continuously developing new and improved algorithms, classifications, and methods to compliment the analysis. Palacios-Orueta and Ustin (1998) simulated AVIRIS band reflectance to find the best spectral predictors for classification of soil samples using a series of Principal Component (PC) Analyses. The simulated imagery was conducted on soil samples collected from two adjacent valleys near the Southern California Coast. During the laboratory experiments, the researchers found the albedo of the soil to have the greatest effect on spectral variability, though absorption played a role as well, particularly in samples with high amounts of transparent sand particles. The primary difference in reflectance among the samples was caused by iron content and organic matter (OM) content. After experimenting with PC analyses on the data, the researchers were able to accurately summarize the spectral variability of the soils based on the associated OM and iron content after the second and third PCs (eigenvalues).

In ensuing research, Palacios-Orueta et al. (1999) conducted a landscape-scale classification of the same study area, in an attempt to describe soil properties with AVIRIS. The researchers tested a Hierarchical Foreground and Background Analysis (HFBA), in an effort to discriminate the soils typical of the study site. HFBA is a stepwise series of modified spectral mixture analysis techniques; HFBA develops a sequence of vectors based on foreground and background spectral variation defined by the user. The technique essentially links the spectral variations of the imagery with wave-based multiscale resolution in order to classify spectral endmembers according to the variance of the spatial domain (Pinzon et al., 1998). The hierarchical sequence narrows down the variance of the normalized spectral curves into small reliable ranges of easily detectable variability (Palacios-Orueta et al., 1999). Through the HFBA technique, the researchers were able to detect and classify soils with high OM content and iron content in accordance with their spatial location. A downfall of the HFBA is that its tendency to decrease the variability of the imagery reduces its effectiveness across study areas, without having prior knowledge of endmember characteristics.

Rahman and Gamon (2004) utilized the Water Band Index (WBI) (0.97 μm reflectance/ 0.90 μm reflectance) of temporally spaced hyperspectral reflectance images to accurately and successfully identify fresh biomass (regrowth) and water content in burned and unburned areas at a grassland fire site in Southern California. Their temporal classification study took advantage of the spectral change due to spring regrowth one season after a fire. Statistical procedures tested the performance of a WBI classification in comparison to known indices like the Normalized Difference Vegetation Index (NDVI) and the Photochemical Reflectance Index (PRI), as well as field-gathered data. The WBI correlated

significantly with the NDVI and field-assessed biomass ('r' = 0.67 and 0.79), demonstrating the ability of hyperspectral data to collect biophysical information across the spectrum.

Several studies have demonstrated the power of hyperspectral imagery for the identification and classification of noxious weeds in arid lands. Parker Williams and Hunt (2004) utilized AVIRIS hyperspectral imagery and the reflectance of the noxious weed leafy spurge to determine its occurrence with the Mixture Tuned Matched Filtering (MTMF) spectral mixture analysis procedure at a study site in Northeastern Wyoming. The researchers found differences in their classifications dependent on the preset detection thresholds, which yielded either false positives or false negatives. Out of three land cover types (mixed prairie, riparian, and conifer); leafy spurge was detected best within mixed prairie and riparian areas, with an overall accuracy of 95%.

At a research site in southwest Idaho, Mundt et al. (2005a) used Spectral Angle Mapper (SAM) and MTMF classifications to search for the noxious weed hoary cress with HyMap hyperspectral data. Comparisons of SAM and MTMF classifications found no statistical difference in the two, though visual interpretation indicated that SAM produced a better classification. The researchers found that a multiple endmember SAM classification on MNF transformed data detected hoary cress occurrence with 86% overall accuracy in areas of 30% cover or more. These results are similar to those in Glenn et al. (2005) using HyMap hyperspectral imagery with MTMF to identify low cover infestations of leafy spurge in Swan Valley, Idaho. Spectroscopy is a well-suited method for the detection of noxious weeds in arid lands because of the ability to detect the spectral signatures of the weeds aiding in the identification and treatment of small infestations. Researchers have indicated that hyperspectral imagery is essential for detecting noxious weeds in areas of low percent cover (<30%) within a 3m resolution pixel (Mundt et al., 2005a; Mundt et al., in press) .

In example of the continuing development of new spectroscopic techniques, Mundt et al. (2006) combined the analytical strength of high spatial resolution hyperspectral imagery with Light Detection and Ranging (LiDAR) data to map the distribution and structure of sagebrush stands in the Eastern Snake River Plain, Idaho. The researchers utilized the MTMF classification technique and mean heights of LiDAR pulses to assess the location and heights of sagebrush, increasing the accuracy of sagebrush classifications by 14% to an overall accuracy of 89%. In addition to ordinarily classifying the sagebrush stands, the LiDAR fusion assessments provided information on the stands' health and response to disturbances like wildfires.

While the noticeable spectral characteristics of invasive weeds and other vegetation have allowed scientists to classify them with spectroscopy, the analysis of bare ground and soils in arid lands presents greater challenges because of the subtle spectral distinctions among soils and their inherent high reflectance (Okin et al., 2001). Furthermore, when low cover arid areas are burned in common rangeland fires, the spectral signature of the soil is affected. Burned soils are often blackened, and can be easily detected with remote sensing imagery, but the variation of soil's spectral characteristics in relation to fire-induced effects, like the degree of water repellency, are often ambiguous. In a former study, hyperspectral imagery was collected over the Hayman fire in Colorado, and analyzed for the remote identification of water repellent soils (Lewis et al., 2004). Regions of interest were selected for slight, moderate and high water repellency, based on field examinations, and used as training data for classification. The researchers utilized a PC transform and SAM to detect water repellent soil layers at 80% accuracy, but failed to detect the degree of repellency (Lewis et al., 2004). Researchers in this project used water repellency data collected at 4 m circle plots in the field as regions of interest for detecting strong and moderate and weak water repellency. The majority of the strong and moderate repellency plots were in areas classified as moderate or high burn severity. When the classification was conducted using only the circle plots as training data, the resulting classification accuracy was quite low (17%, 27% and 0% for slight, moderate, and high water repellency). The researchers then increased the

size of the plots with a 3x3 adjacent pixel window for inclusion of the water repellency (WR), and, using 50% of the sample plots for validation (slight WR: n=6; moderate WR: n=11; high WR: n=9), the accuracies increased to 67%, 55%, and 45% for slight, moderate, and high repellency, respectively. Although the repellency degree could not be detected to a finer degree than slight, moderate, or high, the researchers deemed the findings successful because the classification identified regions of water repellency at a landscape scale that could be mitigated for erosion control.

Though the accuracy of the Lewis et al. (2004) classification was strengthened by the inclusion of training plot pixel windows, the pre-fire forest vegetation structure was such that the soil water repellency would likely be more consistent across the forest floor. In a rangeland setting, the spacing of shrubs and other vegetation introduces a unique dynamic that causes fire-induced soil water repellency to be much more variable across the rangeland floor. The buffering of training areas, as done by Lewis et al. (2004) would increase the possibility of false positive classifications with the imagery over our study area.

At the same site, hyperspectral imagery was used to assess burn severity by adapting the Normalized Burn Ratio (NBR; Key and Benson, 2002) and the Normalized Differenced Vegetation Index (NDVI) to Short Wave Infrared (SWIR) hyperspectral bands, and through use of a partial linear unmixing technique (Laes et al., 2004). They found the NBR adaptation to be a fast and effective method of mapping burn severity with minimal fieldwork involved, however, the thresholds and cutoff values for the input bands differed among separate images. Laes et al. (2004) also used field spectrometry information as endmembers to assess the burn severity among the Hayman Fire with partial linear unmixing. Though no validation other than field comparison was presented, the pixel unmixing results were used to represent the abundance of certain materials (ash, scorched vegetation, green vegetation, soil, and rock) across the image in an unconventional burn severity map. In both of the Hayman fire studies the authors indicated that spectral characteristics of soils may be better analyzed for repellency degree if greater soil reflectance was visible, as is the case in a non-forested rangeland area. Our study has taken into account the achievements and pitfalls of previous-related studies, specifically those involving wildland fire and arid environments, to develop methods of reliably evaluating the burn severity and soil water repellency of rangeland wildfire areas with hyperspectral imagery.

MATERIALS AND METHODS

Field sampling at the Clover fire site began in late August 2005, and was completed by the end of October 2005. Following an initial drive-through survey of the burned area, 3 study sections were designated (Fig. 2.1), across which HyMap hyperspectral imagery was collected. Within the 3 sections, we field-assessed burn severity using 9 m x 9 m sample plots across four classes (unburned, low, moderate, and high). Burn severity was assessed using methods of the United States Forest Service (USFS) Burned Area Emergency Response (BAER) teams, as described by Bobbe et al. (2001), which involved ocular ground estimates of vegetation and soil damage, ground cover, and excess sedimentation risk. The burn severity classes were further broken down by the dominant vegetation group (shrub and grass). Additionally, soil water repellency was evaluated at each sample plot using a mini-disc infiltrometer (MDI), and the Water Drop Penetration Time (WDPT) test. A field spectrometer was used to collect supplemental spectral characteristics of endmembers (features to be mapped) within the study area. With the aid of a hand-held global positioning system (GPS) device, these measurements were used as ground control points and spectral reference for the remote sensing classification study. We also conducted a supplemental sampling experiment that analyzed infiltration with the MDI at set-length intervals from burned sagebrush.

Initial Field Survey

We visited the area and conducted a visual survey and assessment of the overall severity and character of the fire and the ecological and geomorphologic characteristics of the landscape. Three regions were designated as the most suitable for acquiring aerial images (flight lines); these regions were selected

based on the range of characteristics among the assessed variables (Fig. 2.1). The easternmost flight line was designated as section A because it was the first section to be sampled. The middle flight line was designated as section B, and the western-most section, which was also the last section to be sampled, was designated as section C. Within each section sample plots were evaluated and assigned burn severity, and 3 points in each plot were tested for soil water repellency.

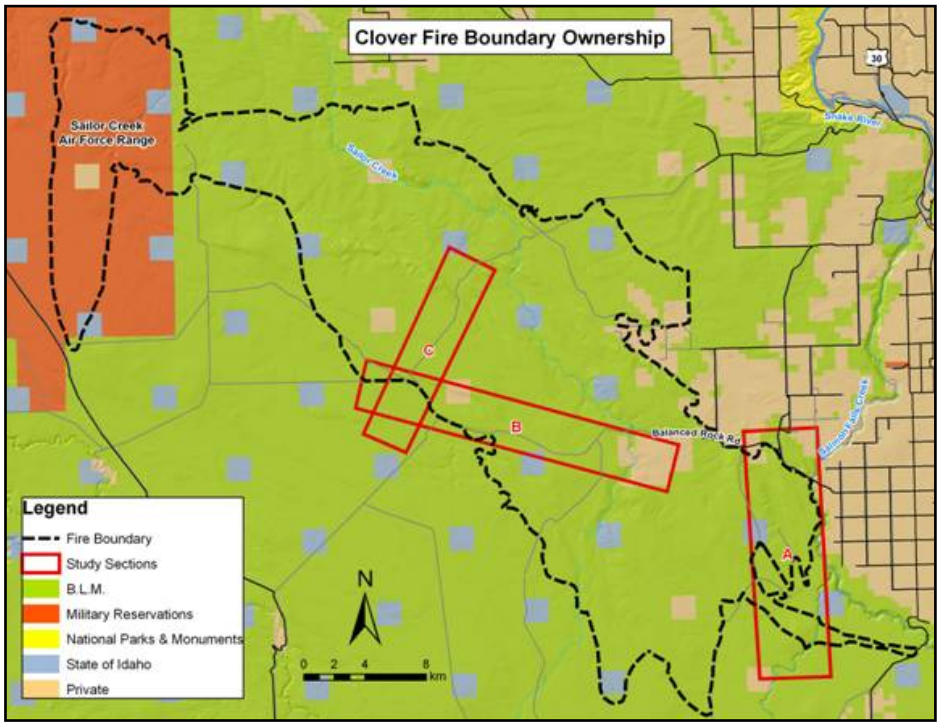

Fig. 2.1. Clover fire boundary and ownership. Field study sections A, B, and C shown in red.

Section A

Sampling of section A began on August 27, 2005, and was completed by September 12, 2005. Within section A burn severity and soil water repellency was assessed at 41 plots. Section A is just west of Salmon Falls Creek and extends from north of the Balanced Rock Road approximately 16.5 km south to the geographic feature known as the Devil Creek Butte. The section is 4.8 km wide, with an area of 482 km^2. The majority of Section A is within BLM boundaries, and is allotted rangeland, while a portion on the eastern side of Salmon Falls Creek, and in the northernmost corner of Section A, is privately owned farmland. The pre-fire vegetation in section A consisted of sagebrush in various stages of growth, perennial bunchgrasses, and stands of annual cheatgrass. Significant amounts of bare ground are present throughout section A. Salmon Falls Creek and Devil Creek are the two drainages within section A, though Salmon Falls Creek is the only perennial stream.

The elevation of Section A ranges from 1038 m, in Salmon Falls Creek Canyon, to 1349 m, atop Devil Creek Butte, with a mean elevation of 1233 m. Section A is relatively flat, with an average slope of about 4^o, the drainages of Salmon Falls Creek and Devil Creek canyons are quite steep, however, with slopes near 57^o. Salmon Falls Creek also has vertical canyon walls in excess of 30 m in places. Other areas that exhibit relatively steep slopes are the hillsides adjacent to the large grass-covered basin known as the Blue Gulch, slopes around Devil Creek Butte, and several intermittent drainage gullies across the section (Fig. 2.2 A).

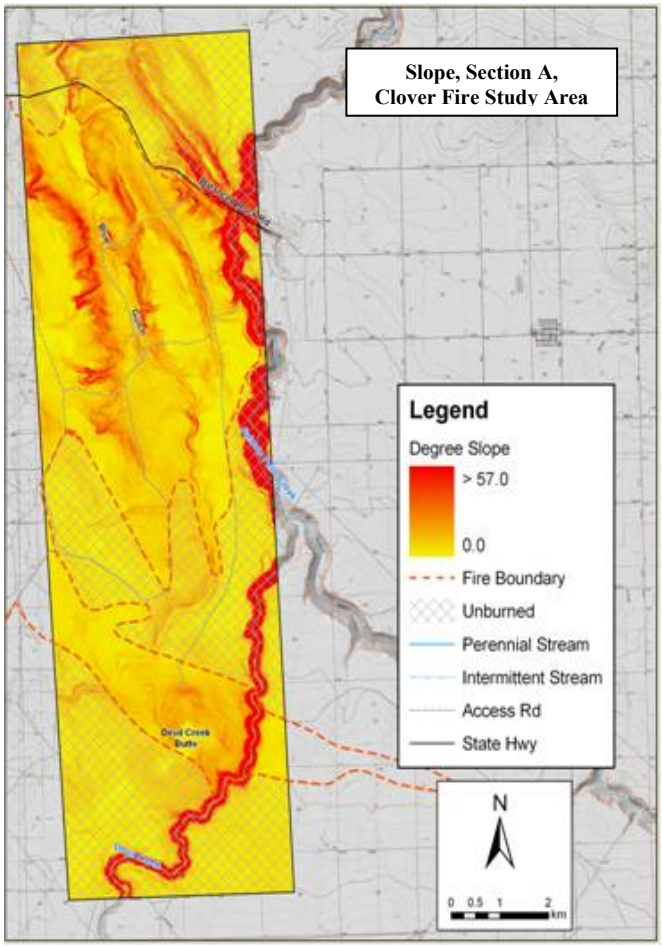

Figure 2.2 A. Slope, section A

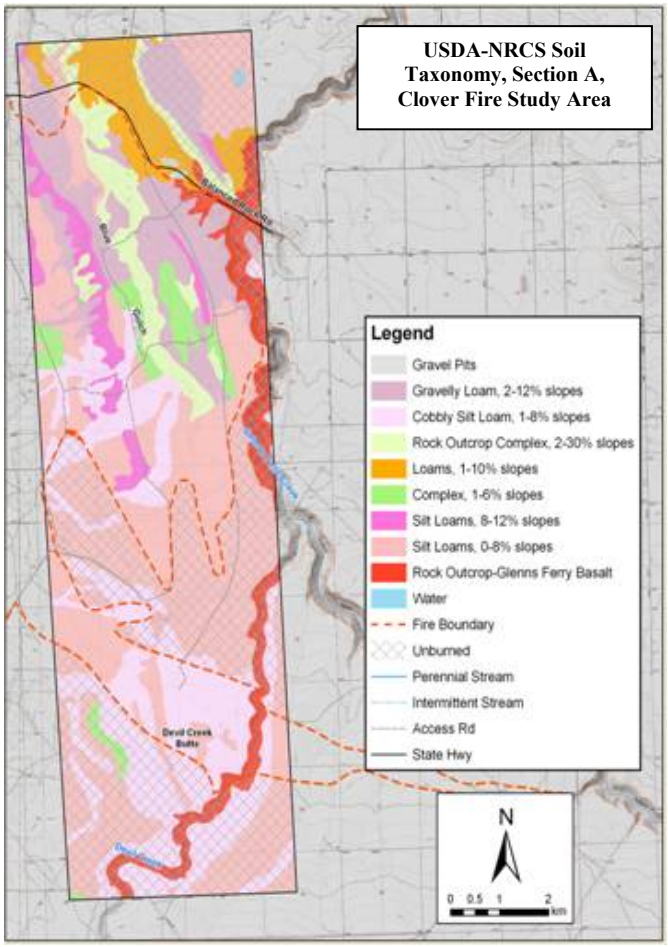

Figure 2.2 B. Soils, section A

The northern portions of section A consist mostly of loam and gravely loam soils, with some areas of silt loam. Rock outcrop complexes are present along the slopes of the Blue Gulch and within the Salmon Falls Creek canyon. The southern portion of Section A is primarily silt loam, with cobbly silt loam present around the Devil Creek Butte. A steep rock outcrop complex (Glenn's Ferry basalt formation) is present within the Devil Creek canyon (Fig. 2.2 B) (USDA-NRCS, 2005).

Approximately 47% of Section A was burned during the Clover fire. Because the fire spread in an easterly direction, section A was one of the last areas to burn. The deep Salmon Falls Creek canyon acted as a natural fire barrier, preventing the flames from crossing it and affecting the agricultural areas to the east. South of the Balanced Rock Road and east of the BLM access road, the fire burned in a large sagebrush stand at moderate severity levels and at high severity levels within the grass covered basin known as the Blue Gulch. The fire continued in an easterly direction, burning very hot in the sagebrush stands to the western edge of Salmon Falls Creek canyon. For approximately 7 km south of the Balanced Rock Road, high severity fire scars were visible in sagebrush stands, and a large area of homogeneous, high burn severity was visible where annual grass stands existed before the fire. About halfway down the section, the fire burned in grassy areas at low severity, and actually stopped burning at this point. The southern half of Section A has a wide swath of unburned sagebrush, punctuated only by south and east-running fingers of burn scars, most likely spot burns across the plain. One more significant fire run is noticeable near the southern edge of the section, where the fire burned severely in sagebrush and grass across the front and on top of the Devil Creek Butte. This last run, approximately 1.5 km wide, and 10 km long, terminates in a flat sagebrush area at the western edge of Salmon Falls Creek canyon (Fig. 2.3).

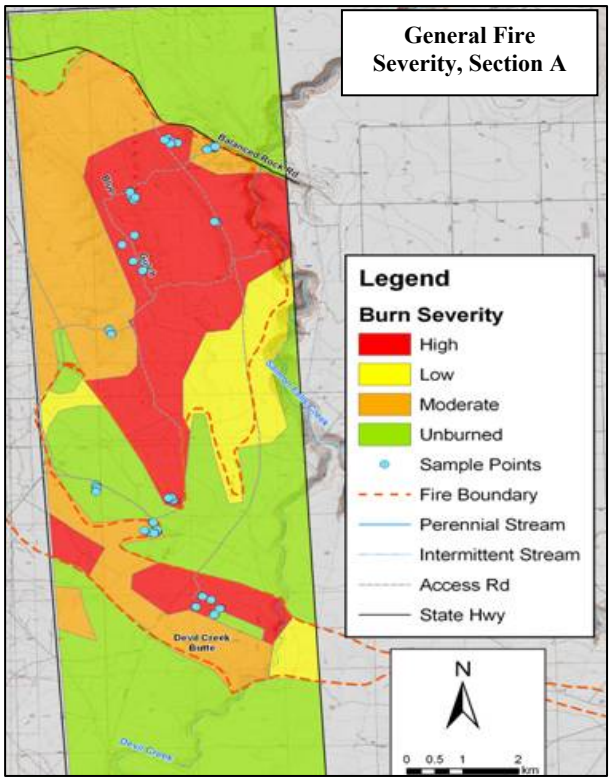

Figure 2.3. General fire severity, section A

Section B

Section B extends approximately 21 km from the southern edge of the geographic feature known as the Big Hill, at the Crows Nest Flat area, in an east-southeast direction, along the Pot Hole Creek drainage, following the Balanced Rock road. The eastern end of the section crosses a portion of the intermittent Sailor Creek drainage. Section B is approximately 3.2 km wide and covers approximately 68 km^2. Field sampling of section B began on September 16, 2005, and ended on October 1, 2005. Within section B, a total of 33 plots were evaluated. About halfway through the sampling period in Section B major dust storms developed (September, 2005), severely altering the soil structure, and removing litter and the top soil layers.

Section B exhibited the most heterogeneity of burn characteristics and vegetation communities within the study area. All of section B is allotted rangeland on BLM property, except for a small area of private property east of Sailor Creek. The western end of section B, which overlaps section C, known as the Crows Nest Flat, is an area of thick sagebrush cover, much of which was unburned during the fire. Further east, up the Pot Hole Creek drainage, a large stand of annual and perennial grass was present prior to the burn. East of the Pot Hole Creek drainage, pre-fire vegetation of Section B consisted of typical rangeland communities, with sagebrush, perennial grasses, and annual grasses. On the west side of the Sailor Creek canyon, a large stand of seeded perennial bunchgrass is present, with intermittent patches of rabbitbrush and sagebrush.

The elevation of Section B varies from 1180 m in the Crows Nest Flat area to 1298 m above the southern edge of the flat, and the Sailor Creek canyon drops to an elevation of 1167 m. The mean elevation of the section is 1224 m asl. The average slope of section B is 2.8^o, although the hillsides along the southern edge of the Big Hill, north of Pot Hole Creek, slope up to 15^o, and parts of the Sailor Creek canyon exhibit slopes of 25^o (Fig. 2.4A).

The central portion of Section B mostly consists of silt loam soils and stony silt loams, while the eastern portion exhibits complex soil groups. The slopes around the Crows Nest Flat area are stony silt loam and very stony fine sandy loam. The slopes of the Big Hill and within the Sailor Creek canyon are steep rock outcrop complexes (Glenn's Ferry Basalt Formation). West of Sailor Creek canyon, stony silt loams and complex soil groups exist (Fig. 2.4B) (USDA-NRCS, 2005).

Approximately 80% of section B was burned during the Clover Fire (Fig. 2.5). The Crows Nest Flat area is outside of the burn area and heavy sagebrush and grass stands are present. East of the flats, along the Pot Hole Creek drainage, high and moderate severity burns were observed. Above the Pot Hole Creek drainage, a large sagebrush area was moderately burned on the north side of Section B, and high severity burn damage was observed on the south side. Just west of the Sailor Creek canyon, low, moderate, and high severity burns were noticeable, and variable burns were found within the canyon as well. East of the canyon, patchy burn scars were observed, although access to that area was limited because it sits on private property.

Section C

The final section of the study area, section C, is 3 km wide, and extends from the Crows Nest Flat area north approximately 13.4 km, across the Big Hill plateau, along the Crows Nest Road to the Sailor Creek basin, within the BLM Wild Horse and Burro management area. All of section C is on BLM land, and covers nearly 43 km^2. Field sampling of section C began on October 1, 2005, and was completed on October 21, 2005. Only 6 plots were evaluated in Section C because conditions were severely altered by the dust storms; the plateau-like geography of the Big Hill had been raked by strong winds, and the top soil layers were removed. All that was left of the soils on the Big Hill was the hard, concrete-like subsurface calcic horizon layer that was seemingly unaffected by the fire.

The northern end of section C is in a wide basin, which was covered by patchy grass and sagebrush vegetation prior to the burn. On the southern side of this basin, the Big Hill rises abruptly from the valley floor, and gradually slopes southward towards the Crows Nest Flats. Thick sagebrush and rabbitbrush were visible on the northern slope of the Big Hill. Atop the Big Hill and along the plateau, light and moderate sagebrush cover was present prior to the burn, along with perennial bunchgrasses and annual grasses, as well as significant portions of bare ground. The southern end of section C overlaps with section B where the Big Hill loses elevation, sloping into the Crows Nest Flats.

The mean elevation of section C is 1171 m asl. The lowest point is 1000 m, in the northern portion of section C, in the Sailor Creek basin. The elevation on the Big Hill rises to approximately 1230 m, and then drops to near 1180 m in the Crows Nest Flats, before rising abruptly to 1298 m on Crows Nest Butte, at the southern end of section C. While the mean slope of section C is only 2.5^o, the northern edge of the Big Hill has slopes between 20^o and 27^o (Fig. 2.4A).

The soil groups within the northern portion of section C, in the Sailor Creek basin, are predominantly complex groups, with some areas of sandy loams and stony silt loams, with some rock outcrops. The steep, northern slope of the Big Hill is another band of complex soil groups. Atop the Big Hill, a large area of silt loam exists, and south of that more complex groups are present (Fig. 2.4B) (USDA-NRCS, 2005).

Approximately 70% of section C was burned during the Clover fire. In the northern portion, within the Sailor Creek basin, patchy areas of high, moderate, and low severity burns are present. Along the steep northern slope of the Big Hill, low and moderate burn scars are apparent. Atop the Big Hill, the flat plateau appeared to have burned with high severity to the west, and moderate to low severity to the east. This area was extensively damaged by the windstorms as well. The southern end of section C, the Crows Nest Flat, was not burned (Fig. 2.5).

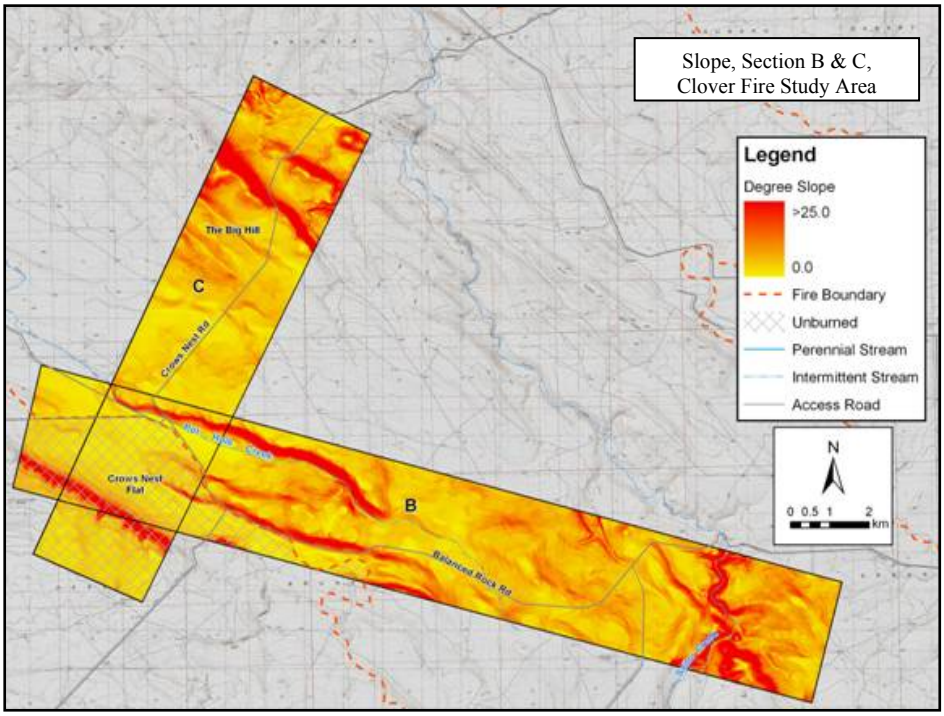

Fig. 2.4A. Slope, section B and C.

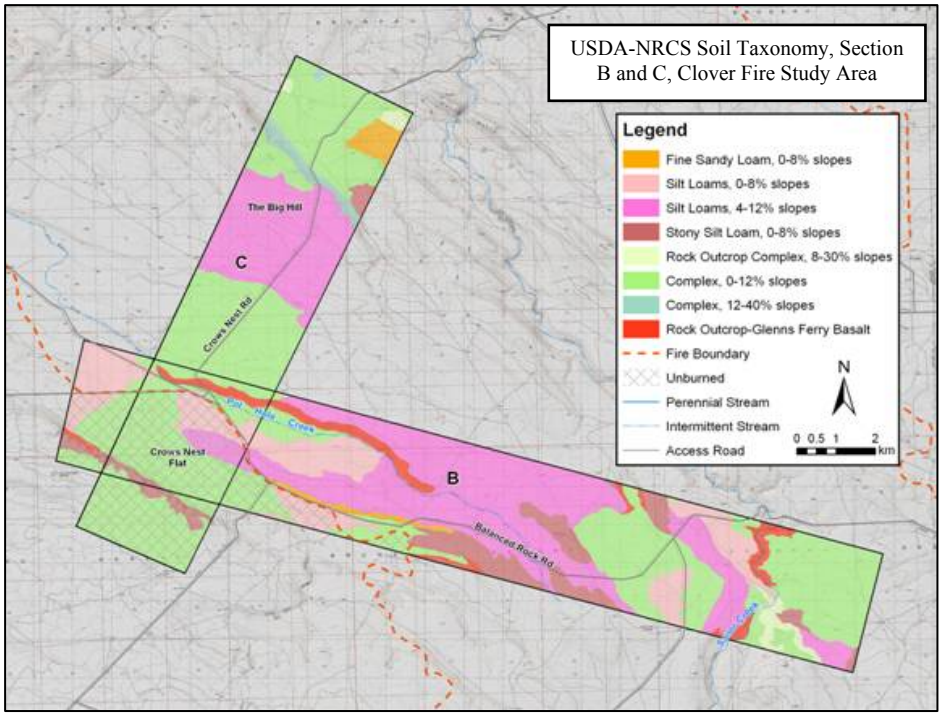

Fig. 2.4B. Soils, section B and C

Field Methods

Sampling Scheme

Prior to conducting field tests, 9 m by 9 m sample plots (Fig. 2.6) were identified and staked out in areas representing the different burn severity categories, which was assessed as described in the following sections. The size of the sample plot was determined based on the accuracy and resolution of the hyperspectral imagery. The HyMap imagery has a pixel resolution of 3 m by 3 m, and thus the field

sample plot encompassed a 9 pixel area. This allowed for errors in georegistration and spectral anomalies within the imagery. The boundary of the plot was recorded with the GPS in a polygon format. Soil conditions and vegetation burn severity most representative of the sample plot were evaluated. Within the 9 m x 9 m sample plot, three sample points were tested for water repellency and infiltration capacity, and the locations recorded with GPS in point format. The water repellency tests were conducted three times within each sample point. Because the accuracy of the Trimble GeoXT hand-held GPS device is no more than 1 meter (Steede-Terry, 2000), water repellency tests (MDI and WDPT) were conducted within 1 meter of the GPS sample point to ensure georegistration of the field-collected data.

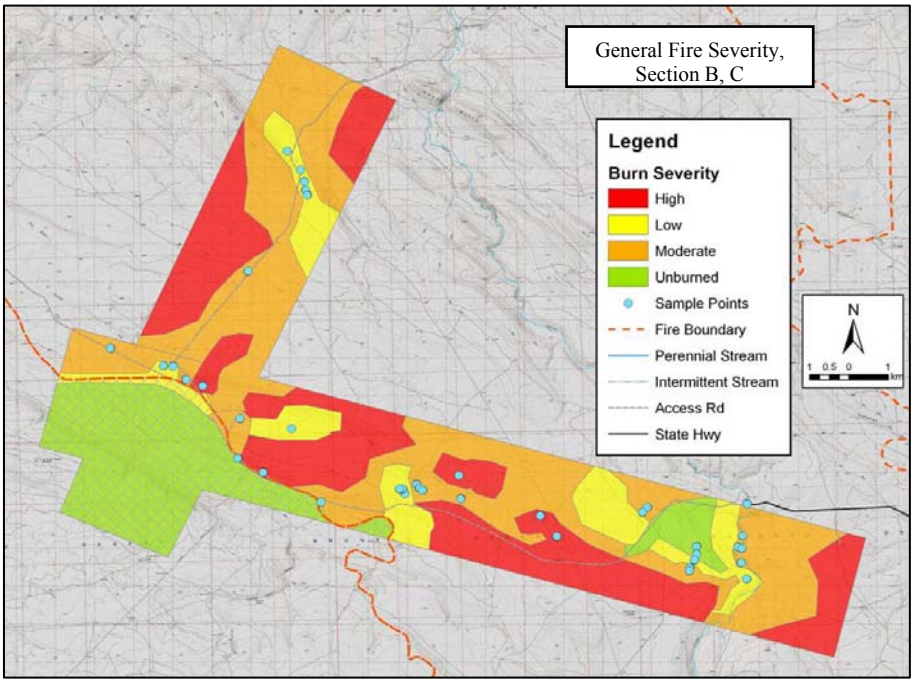

Fig. 2.5. General fire severity, section B and C.

Burn severity

This study assessed the effects of wildfire burn severity on soil properties, particularly the infiltration characteristics of the soil and the formation of water repellent soil layers. Burn severity is the effect the fire has on the soils, vegetation, and all other ecological aspects within the fire area, it is a relative measure of the change endured by the affected ecosystem and is expressed in terms of the share of vegetation killed by the fire as well as that regenerating in the following season (Davis and Holbeck, 2001). Physical and chemical changes of the soils are also taken into account (DeBano et al., 1998), though not comprehensively by most standard methods (Shakesby and Doerr, 2006). A standardized method of assessing burn severity in the field was developed by Key and Benson (2004); this method, however, is primarily meant for analysis of a burned forest ecosystem during the season following the fire, and documents changes in the environment in comparison to pre-burn conditions. The USDA Forest Service (USFS) and National Park Service (NPS) utilize initial and extended burn severity assessments to classify the conditions immediately after a fire (Bobbe et al., 2001; Switky, 2003), often in areas where pre-fire information is unavailable. Areas susceptible to post-fire sedimentation events are most susceptible within the same season as the fire (Cannon, 2001; Cannon et al., 2001; Tucket et al., 2004), thus it was essential for this project that the burn severity assessment take place soon after the fire. Most importantly, burn severity assessment methods like the Normalized Burn Ratio landscape assessment methods (Key and Benson, 2004) are not entirely suited for rangeland ecosystems, and researchers have indicated the need to restructure burn severity classifications relevant to soil changes (Shakesby and Doerr, 2006). The classification of burn severity across our study area, even using the USFS guide,

proved somewhat subjective and ambiguous, based on the pre-fire vegetation load and density, the vegetation group, and the character of the fire. We initally found the separation of unburned, low, and high burn severity to be quite straightforward, while the separation of moderate and high burn severity was at times difficult. Besides the fact that the ground characteristics were altered by wind soon after the fire, areas of high burn severity were often interspersed with less severely burned areas. In addition, the distribution of coppice microsites, or the area directly beneath the shrub canopy, and the interspace microsites between them, caused intermixing of severely burned and lesser burned shrubs and grass in many areas. Even though the separation of burn severity classes was at times subjective, as is the nature of ocular representations, by assessing the effects of the fire on the vegetation in accordance with the soil characteristics, a comprehensive representation of rangeland burn severity was determined.

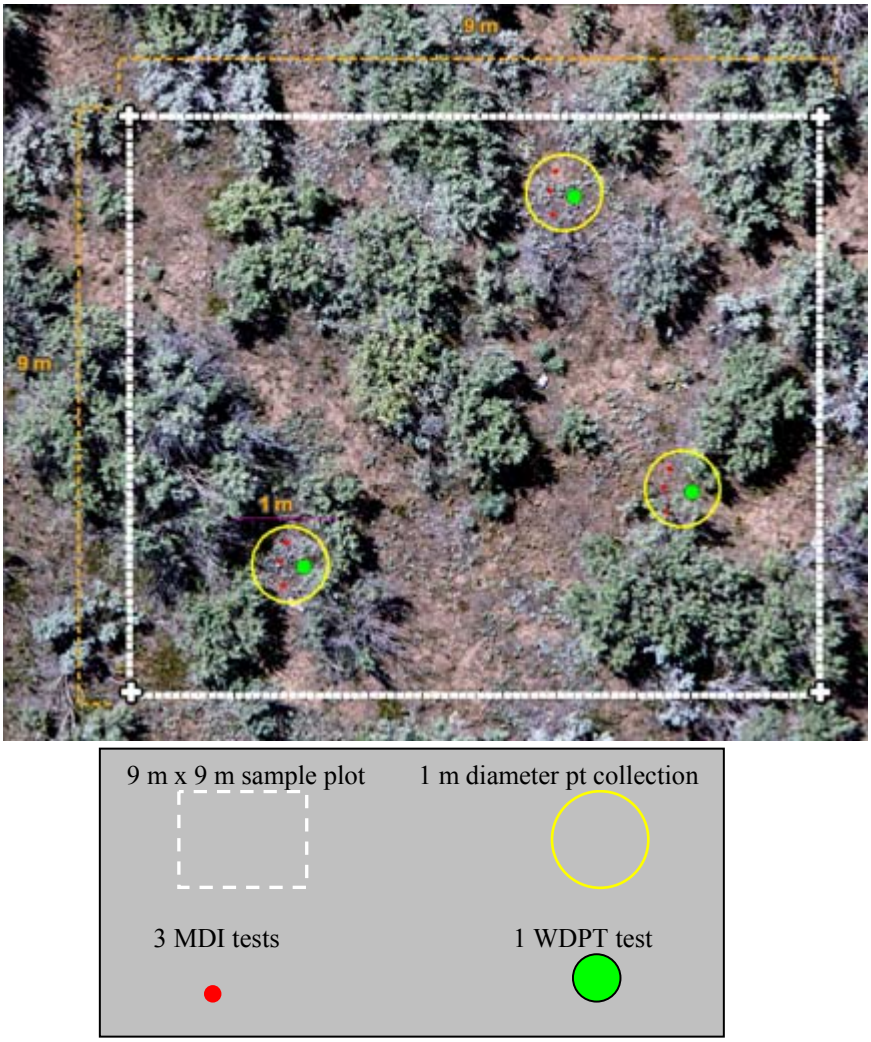

Fig. 2.6. Sampling Scheme

For this project, a burn severity assessment method similar to that used by the USFS BAER teams and the NPS was utilized (Bobbe et al., 2001; Switky, 2003), as the assessment was conducted in the same season as the fire event, and the soil and vegetation had not been assessed prior to the fire. Burn severity was classified into four broad categories: unburned, low, moderate, and high (Table 2.1**)**. The classes were further broken down by the dominant vegetation group of the area, namely grass and shrub, because observations indicated that burn severity and water repellency differed among these two different vegetation groups (Fig. 2.7, A-H).

Table 2.1. Burn severity classifications

Burn Severity	Vegetation	Description
Unburned	**Shrub**	Area not affected by fire
Low	**Shrub**	Foliage singed or consumed, branches still intact, <60% canopy consumed
Moderate	**Shrub**	Foliage, twigs, some branches consumed, branches up to 1cm diam. remain, 40-80% canopy consumed
High	**Shrub**	All shrub parts consumed, only stubs or stumps >1cm diam. remain
Unburned	**Grass**	Area not affected by fire
Low	**Grass**	Stalks & blades may remain slightly blackened, may be burned with at least 5 cm unburned stubble remaining
Moderate	**Grass**	Unburned stubble <5cm tall remains, forb foliage consumed, plant base burned near ground, burns uniform throughout area
High	**Grass**	No unburned grasses visible above root crown, all plant parts of forbs consumed, burns uniform throughout area

Fig. 2.7 A. Low severity shrub

Fig. 2.7 B. Low severity grass

Fig. 2.7 C. Moderate severity shrub.

Fig. 2.7 D. High severity grass

Fig. 2.7 E. High severity shrub

Fig. 2.7 F. High severity shrub

Fig. 2.7 G. High severity grass

Fig. 2.7 H. High severity grass

Assessing Water Repellency

A well-known and commonly used technique for identifying water repellency in soils is the Water Drop Penetration Time (WDPT) test (DeBano, 1981). The WDPT is used extensively because the method is fairly simplistic, enabling users to quickly identify water-repellent soil conditions. This method involves placing a drop of water on to the soil and watching to see if it infiltrates, or balls up and is repelled by the soil. Prior to placing the water drop, the top layer of loose soil, or duff, should be brushed aside because, if not removed, that layer will easily absorb water, and produce misleading results. Researchers have questioned the WDPT, however, because the size and surface tension of the water drop can vary with temperature, and a level of subjectivity is involved in differentiating strongly water-repellent soils (60 s), from extremely water repellent soils (>3600 s) (Dekker and Ritsema, 2000). Numerous variations of the WDPT test have been used. The USDA Forest Service classification standards indicate that if water remains for less than 10 seconds, the water-repellency is considered weak, 10 to 40 seconds indicates a moderate water-repellent layer, and water remaining for longer than 40 seconds is indicative of strong water-repellency (Davis and Holbeck, 2001). Krammes and DeBano (1965) indicated water-repellency if water did not penetrate after 5 seconds, mentioning that most soils repelling water for over 5 seconds generally tended to repel water for several minutes. Cannon (2001) indicated water-repellency if water did not penetrate the surface after 30 seconds, indicating that a 5-second threshold may only reflect the reluctance of water to infiltrate an extremely dry soil. The WDPT is well-suited for identifying the presence of water-repellent soils, but it is ambiguous for analyzing the degree of water-repellency (Dekker and Ritsema, 1994).

The WDPT was conducted at each MDI sample point to validate, correlate values and determine thresholds of the MDI tests. The WDPT involved digging an approximately 10 cm deep, terraced hole and testing the soils at various depths within the hole. Using a dropper or squirt bottle, water was dripped

on the soil at the surface, and depths of 2, 4, 6, and 8 cm. A water repellent layer was apparent if the water beaded up and sat or rolled off of the soil surface.

For this study, water-repellency was indicated in the field if the water drop remained on the soil for longer than thirty seconds (Cannon, 2001). In an effort to classify the degree of water-repellency, and correlate it with the MDI results, the water drop was allowed to remain on the surface for 360 seconds, and drops lasting longer were assigned that threshold value. A WDPT of 30-60 seconds indicated weak water-repellency, 61 to 180 seconds moderate water repellency, and 181 to 360 seconds indicated high water repellency. These values were used in previous studies by Dekker and Ritsema (1994), and Lewis et al. (2006). WDPT values were recorded in correspondence with the infiltration tests at each sample point location.

A newer method for water repellency analysis utilized by researchers at the USDA Forest Service (Lewis et al., 2006) is the Mini-Disc Infiltrometer (Decagon Devices, 1998). The Mini-Disc Infiltrometer (MDI) is a device that measures the infiltration of water into soil (Fig. 2.8). The MDI is a 22.5 cm long, 3 cm diameter hard plastic tube, gradated by milliliters up to 100. A rubber stopper is positioned approximately 5 cm below the top of the tube, creating a separate compartment that controls air suction. A 1 cm-wide steel tube passes from above the stopper to the bottom of the tube, above a stainless-steel porous disk. Another steel tube protrudes from the top, allowing air to escape when the disk is placed on the soil. When the two compartments of the MDI are filled with water, it is under tension, allowing the water to stay in place and not flow out of the disk. When the disk is placed on the soil, the water is pulled through the disk by capillarity, infiltrating the soil (Kirkham, 2005). The inner steel tube allows air to escape from the lower compartment into the upper compartment in a bubble, which then escapes from the top of the MDI by the other steel tube. The time until infiltration and amount of infiltration with the MDI is recorded.

A series of steps was followed for assessing water-repellency with the MDI, and results were correlated with the better-known Water Drop Penetration Time (WDPT) test. With a small shovel, any obstructing debris or rocks were removed to expose the soil surface. Additionally, the loose soil, or duff is cleared to expose the bare mineral soil. The burned areas of the site tended to have little ground cover, other than broken branches or brushes, because it was either consumed by the flames or removed by wind transport after the fire. If the sample site was located on a very steep slope, a small, level shelf was constructed, allowing for an accurate MDI reading without water seeping out of the sides of the disk. When the MDI was set on the top of the soil surface, the water within the tube began to infiltrate the soil through the porous disk and the soil, and a stopwatch was started. The time was recorded as soon as the first bubble entered the infiltrometer, and the MDI was held in place for one minute duration. At the end of the minute, the amount of water, in milliliters, that infiltrated the soil within that time frame was recorded. To compensate for local variability within the soil at the sample site, the MDI test was conducted three times at each sample site, within 50 cm of each other, and the average value of the three measurements was utilized for further analysis. Thus, there were 3 average MDI values within each sample plot. The rate of infiltration measured by the MDI was the primary measurement referred to for water repellency identification.

Daily weather observations at Castleford, ID were obtained for the months of August, September, and October from the National Climatic Data Center (NCDC, 2005) Records indicate that for the three months that sampling took place at the study site, monthly precipitation totals did not exceed 2 mm during August and September, and October received 6.36 mm of precipitation, mostly during the final days of the month, when field sampling was nearly complete (Appendix 2).

Researchers in Portugal found that water repellency in Eucalyptus soils was not present after being thoroughly moistened from wet winter conditions (Doerr and Thomas, 2000). Their study implied a moisture threshold of soils, above which repellency is not a factor, indicating temporal variability with the phenomenon. Because very little rain, which could affect the repellency and infiltration properties of the soil, was recorded during the sampling period, no samples were taken for laboratory analysis of moisture content and water repellency.

Fig. 2.8. The Mini-Disc Infiltrometer by Decagon Devices. Pullman, WA.

A quantitative method of detecting water repellent layers beneath the soil is by digging lateral trenches in the soil after wetting it with a rain simulator (Pierson et al., 2001), or after a rainstorm. By digging a trench and examining the soil layers beneath the surface, subsurface layers can be detected by differentiating the wet soil from the dry soil. Though the trench method gives a greater understanding of the spatial variability of water repellent soil layers and the preferential flow characteristics of rangeland soils, it was impractical in the dry rangeland study area where the amount of water needed for a rain simulator was inaccessible. To reduce the tendency for preferential flow beneath the MDI, the tube was held firmly on the soil surface, so as to keep water from escaping below the side of the porous disk. This, coupled with a multi-depth analysis by the WDPT, provided surficial and subsurface characteristics of soil water repellency in lieu of trenching.

The variability of the soil water repellency in the burned area was analyzed by assessing the infiltration with the MDI at measured intervals away from a burned brush. Pierson et al (2001) observed that soils in the burned rangeland areas tended to exhibit lower water repellency in the spaces between the burned brushes, called interspace microsites, due to the lack of combustible litter and organic material that induce water repellency when burned, within those areas. Additionally, the interspace microsites would not exhibit natural water repellency caused by sagebrush shrubs because they are outside the area of influence. Background repellency levels were measured during this study in unburned areas to obtain infiltration characteristics in an undisturbed setting. This experiment compared MDI measurements at lengths of 25, 50, 75, 100, and 200 cm out from burned sagebrush, to observe the changes in soil water repellency as the proximity to the brush decreases. The transects were sampled in a location and direction where the spacing of adjacent brush was wide enough that collateral effects from the other brush was minimized. This experiment strengthened the understanding of the perceived variability of water repellent soils within a burned rangeland area by demonstrating the spatial characteristics of water repellent soils induced by fire, and affected by vegetation dynamics.

Data Analysis

Following the acquisition of field data, the water repellency values and burn severity classes were statistically analyzed to assess their importance to the research. Initially, descriptive statistics of the MDI values within each burn severity class were calculated. Because the use of the MDI for assessing soil water repellency has only been documented one time (Lewis et al., 2006), the relation of its values (ml/min) were tested with results of the more traditional, and well documented, WDPT test. Due to the more subjective nature of the WDPT, a strong correlation was not expected, primarily due to the threshold of values (360 s) for high water repellency, and the fact that the MDI rate and WDPT essentially measure two different parameters (time of the water drops persistency and amount of infiltration). In addition, the relationship between the WDPT time (s) and the time till infiltration with the MDI (s) was tested, but again, a strong correlation was not expected due to the threshold of the WDPT. In addition, many of the WDPT values were 0, and even in a water repellent soil, the MDI generally began infiltrating quickly. To help understand the significance of the field data and to test the relationship of the MDI-assessed water repellency with burn severity, a linear mixed model called the Proc Mixed analysis was used in SAS (SAS Institute, 2005). The advantage of the Proc Mixed is that it tests the variance/covariance structure of the field data, while allowing for possible errors created by spatial correlation of the data across the study area (SAS Institute, 2005). The model established the burn severity classes as the subject level, or the lowest information criterion, and the average MDI value at each sample point as the dependent variable.

The first step of the model was to perform a Least Squares adjustment of the mean MDI values of each burn severity class, which chooses a best fit curve of the data based on the least sum of the deviations squared. The model then computed the difference between all pairs of the least squares mean MDI values among the matrix of burn severity/vegetation classes. The resulting t-test levels of significance (p-values) were then adjusted with the Kramer multiple comparison adjustment method for false positives (SAS Institute, 2005). When independent observations (MDI values) are subject to the same criterion (burn severity classes) the chance for false positives increase. The Kramer adjustment is a method of countering the possibility of false positives. If the p-value is less than the alpha value of 0.05, then the null hypothesis that the two variables are the same is rejected, and their relationship is considered significant.

Field Spectrometry

Spectral signatures of endmembers for burn severity and soil water repellency were collected in the field with a handheld spectroradiometer. The purpose of collecting the field spectrometry was to acquire spectral signatures of endmembers within the field for imagery control, and to assess the differences among the endmembers' spectral characteristics. Endmember signatures of bare ground, gravel, basalt rock, unburned grass and shrub, low severity grass and shrub, moderate severity shrub, and high severity grass and shrub were collected.

A FieldSpec Pro spectroradiometer, made by Analytical Spectral Devices Inc. (2004) was used and collects spectrometry information in-situ at a range of 350 to 2500 nm (Fig. 2.9). The device has a 25^{o} field of view (bare fiber) with a sampling interval of 100 milliseconds (Analytical Spectral Devices, 2004); when held waist high, the sensor acquires a spectral signature of approximately 1 m^2 on the ground. A fiber optic sensor relays the data to a notebook computer where the input spectral data is saved. After collecting the field spectrometry, the spectra (reflectance versus wavelength) were imported into ENVI, where the values were plotted in the spectral library viewer. The values were then resampled to match the spectral scale of the HyMap hyperspectral imagery, in micrometers (μm).

Before collecting the field spectrometry, the device was calibrated with a white spectralon plate to calibrate and normalize the data collection for reflectance. Optimally, field spectrometry should be collected on the same day as the aerial imagery if it is to be used for endmember control when classifying

hyperspectral imagery. The lack of instrument availability and logistics prevented same day data collection; however, the field spectrometry was collected within two weeks of the aerial imagery, and it was collected on a cloudless day, near solar noon, so as to limit atmospheric dust, water vapor, and shadows.

Fig. 2.9. The FieldSpec Pro by Analytical Spectral Devices.

GPS Data Collection and Processing

This research project relied heavily on Geographic Information Systems (GIS) as a data collection, analysis, and organization tool. GIS utilizes digital spatial information with relational attributes to efficiently manage multiple layers of data in similar map projections. While conducting field sampling, a hand held Trimble GeoXT (Trimble Navigation, 2005) global positioning system (GPS) device recorded the boundary of the sampling plots as polygon shapefiles, along with the points at which the soil water repellency tests were conducted in the form of point shapefiles. The data were collected in Universal Transverse Mercator (UTM) Projection; zone 11 north, with the North American Datum of 1983. The GPS records of each sample point and plot were used as ground-truth verification for the remote sensing analysis.

A total of eighty sample plots were evaluated and their position recorded with the GPS, and the three sample point locations within each plot were also recorded, totaling 235 (several plots contained less than 3 points because the GPS did not receive an ample signal to record their locations). After collecting the field data with GPS, the information was downloaded onto a workstation, post-processed, and differentially corrected for inherent geometric error using Trimble Pathfinder (Trimble Navigation, 2005) software. The data was then input into ArcGIS (ESRI, 2005), where the records were assessed, edited, and additional fields were added. Finally, the GIS shapefiles were imported into a geodatabase, which is a centralized collection of relevant geospatial data. The geodatabase included the field-collected sample point and polygon shapefiles and point locations at which the ASD spectradiometer data was collected, along with their attribute tables, and ground control points (GCP's). Other data included in the geodatabase were the fire boundary, local soil classifications, roads, elevation, slope, and generalized burn severity. The attributes included with the point and polygon field-collected data are listed in Table 2.2.

Table 2.2. GIS attribute table of field-collected data

Sample point attributes	
1	Point number
2	Burn Severity
3	Ground Cover at point
4	Dominant Vegetation (in plot)
5	MDI time till infiltration (seconds)
6	MDI rate of infiltration (ml/min)
7	WDPT value (2, 4, 6, 8 cm)
8	Water repellent layer present (yes/no)
9	Depth of water repellent layer
10	Sample Date
11	Average MDI value
12	WDPT repellency rating
13	UTM X coordinates
14	UTM Y coordinates
15	NRCS soil classification
Sample plot attributes	
1	Plot number
2	Burn Severity
3	% ground cover across plot (ocular estimate)
4	Dominant vegetation
5	Comments
6	Sample Date

Transect Repellency Experiment

In order to strengthen the understanding of water repellency in a rangeland wildfire setting, we conducted a supplemental experiment that examined the infiltration capacity of soils at predetermined distances from a burned shrub. The experiment was designed to show that the infiltration of soil increases, or the water repellency decreases, as the distance from the brush increases. Soil infiltration was tested with the MDI. The experiment was conducted on various-sized shrubs, with canopy edge ranging from 25-100 cm from the center of the shrub.

To conduct the experiment, a burned shrub was identified, and flags staked at lengths of 25 cm, 50 cm, 75 cm, 100 cm, and 200 cm from the shrub (Fig. 2.10). At each flag location, the MDI test was conducted three times, within 20 cm perpendicular to the measured transect. The three measurements at each increment were averaged and input into a table (Table 2.2**)**. The tests were conducted on October 15 and October 21, 2005. On October 21, the ASD FieldSpec Pro spectroradiometer was used to collect field spectra at the transect sites. Spectra were collected at 25 cm, 50 cm and 100 cm. Because of weather conditions (cloudy sky), the FieldSpec Pro could not be used on October 15.

Spectroscopy Methods

Hyperspectral data was acquired over the study area with the HyMap sensor, by HyVista, Inc. A total of seven flight lines were flown over the three study sections (Fig. 2.11). The flight lines are approximately 10-15 km long and 1-2 km wide. The HyMap imagery consists of 125 bands, with a contiguous spectral range from 0.45 to 2.5 μm. Bandwidths range from 0.015 μm in the visible and NIR to 0.020 μm in the SWIR, and the imagery has a pixel size of 3 m. The data were collected on August 26, 2005, between 12:00 noon MST and 12:33 MST. The geographic locations of study sections and flight lines were chosen based on the variability of fire effects and local geography observed within the areas.

Hyperspectral Processing Flow

Spectroscopic research generally follows a standard processing sequence (Fig. 2.12). After selecting a study area and acquiring hyperspectral imagery, an initial assessment of the imagery is conducted. This is done by visually assessing individual bands within the imagery, examining various color composites, and evaluating individual band statistics to assess the signal-to-noise ratio, to determine if any areas of the data contain null data values or are missing lines, and to evaluate the geometry of the imagery for any visual flaws (Jensen, 2005). After an initial assessment of the imagery, radiometric and geometric correction of the imagery is carried out (in this case by the vendor, HyVista).

Fig. 2.10. Sagebrush transect

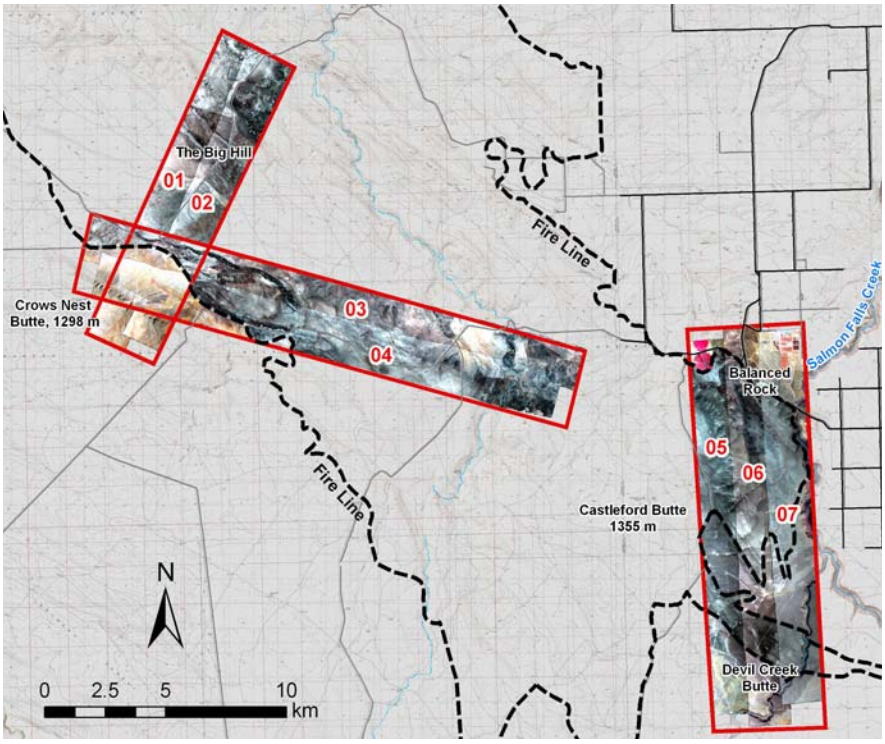

Fig. 2.11. HyMap flight lines (01-07) collected over the study area.

Following radiometric and geometric correction of the imagery, the dimensionality of the data is reduced to find relative bandwidths for analysis. Hyperspectral datasets are very rich in information, due to the large amount of spectral bands, or data dimensionality (Jensen, 2005) within them. Because all of the bands may not be pertinent for a specific analysis, standardized methods have been developed to reduce the dimensionality of hyperspectral imagery. This is completed through the use of statistical methods that delete and transform bands with redundant and unnecessary information. A statistical algorithm for reducing hyperspectral data dimensionality is the Minimum Noise Fraction (MNF) transform, which is a two-phase principal components analysis performed on the data to reduce noise and determine the useful, coherent bands to be used (Jensen, 2005). The MNF output results in a 125 band transformed data set with the noise as the unit variance and no wavelength correlation. The resulting 125 band images are eigenvalues and are sequentially reorganized according to data coherency. After examining the eigenvalue plots and images, the 125 images can be separated between coherent and noise-dominated bands.

Following data reduction, the pixels of the imagery are analyzed and reduced to subsets of only pure pixels, or those pixels containing only one material, also known as extreme pixels. In a 3 m x 3 m pixel, for example, the area on the ground a pixel covers may contain a certain percentage of litter, vegetation, rock and bare ground. In this case, the pixel would not be considered pure, because of the existence of multiple endmembers or materials within its geographic confines. If another pixel contained the spectral signature of 100% bare ground, or 100% rock, or 100% litter, then that pixel would be considered pure, as it contains only one material. Pure pixels are important for identifying endmembers present in the imagery and are later used as training data to find similar pixels through the use of the n-Dimensional Visualizer (n-DV), and classification techniques like the Spectral Angle Mapper. Identification of pure pixels is first implemented using Pixel Purity Indexing (PPI) in ENVI. The PPI repeatedly projects scatter plots of image spectra onto random unit vectors in n-dimensions (n=number of bands) for a set number of iterations (10,000 or more), and records the outliers as extreme, or pure pixels. A user-defined threshold sets the range of pixel digital number (DN) values that will be grouped with the identified extreme pixels for each projection of vectors. The more iterations completed during the PPI, the greater the likelihood one will find all of the most extreme pixels in the image. At the end of the iterations, the pixels that have been marked extreme the highest number of times are considered pure. After the pure pixels are identified, those that are most extreme (representing the highest portions of the accumulated distribution percentage), are assessed to determine what portion of the spectrum, and which endmembers, they represent. The spectral qualities of the extreme pixels are analyzed with the n-DV.

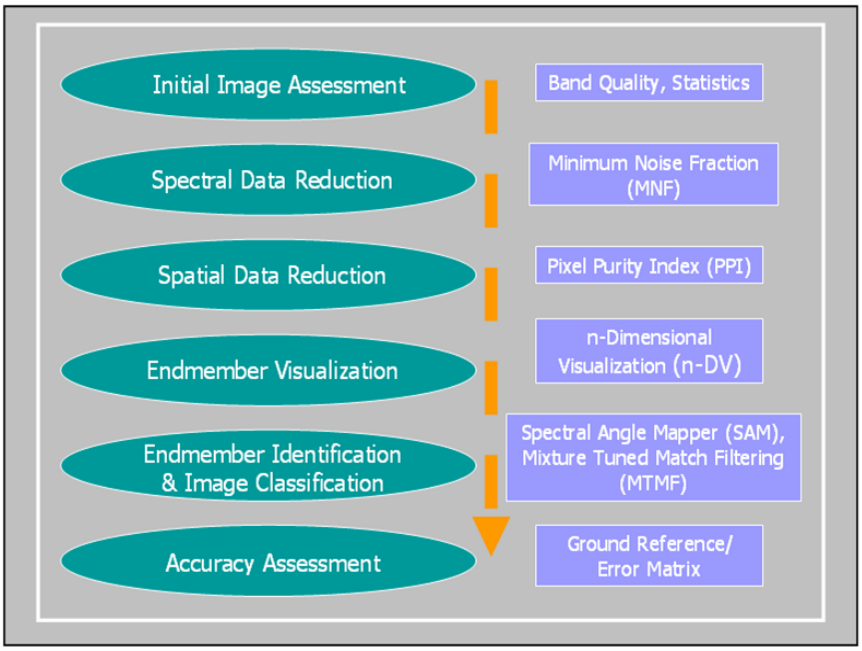

Fig. 2.12. The hyperspectral processing flow (adapted from Jensen, 2005).

After identifying the extreme pixels in an image with the PPI process, the pixels' spectra can be multi-dimensionally visualized in the n-DV. Through the use of the n-DV in ENVI, a collection of spectra can be plotted and visualized in a point cloud of n dimensions. By rotating the point cloud in accordance with the selected band axes, spectra of specific endmembers will appear in clumps within the point cloud (Jensen, 2005). According to the total number of endmembers, those that are pure will fall at vertex points. For example, with two endmembers, the pure spectra will appear at two ends of a line, and the mixed spectra in the middle. Likewise, with three endmembers, mixed pixels will appear inside of a triangle, with the pure spectra at the triangle points, and so on. Because the mixed pixels appear inside the endmember vertices and the extreme pixels as outliers, the pure pixels are readily identified (Kruse et al., 1997). After the purest pixels are located, ground collected spectral information, spectral libraries, and/or ground-based user knowledge are employed to determine what each pure pixel represents. After identifying the endmembers within the imagery, classification techniques are applied to map the material they represent across the remainder of the image. This can range from endmember classification within a single pixel, or sub-pixel, to the application of specific classification techniques developed for spectroscopy. One such classification method often utilized in spectroscopy is the Spectral Angle Mapper (SAM). SAM allows efficient classification based on the similarity of image spectra to a spectral reference (Kruse et al., 1993). When the SAM is computed, vectors of reference spectra are projected in n-dimensional space (n = number of bands), and a specified angle is set for which pixels falling within that angle are placed within the category of that certain reference spectra. Depending on the size of the reference angle, the classification can be generalized when large reference angles are used, or specialized when a small angle is used. The smaller the angle, however, the more likely it will be that portions of the image will be unclassified. One advantage SAM has over other classifiers is that only the length of the reference (and unknown) vectors and not the angles of the vectors are affected by the albedo within the imagery. This means that changes in albedo across an image (e.g. from topography or sun angles) will not affect the classification of a target material.

While SAM is a presence/absence classifier, examples of methods of detecting sub-pixel abundance include Linear Spectral Unmixing (LSU) and Mixture Tuned Match Filtering (MTMF). LSU is an automated attempt to unmix single pixels that have various materials and spectral properties within them (Kruse et al., 1997). MTMF is a more advanced form of spectral unmixing, in that it does not require knowledge of all the endmember signatures to map the sub-abundance of a pixel (Aspinall et al., 2002). The MTMF results in a matched filter (MF) score (a linear measure of abundance) and an infeasibility value (indication of false positives). Between the MF and infeasibility value, there is potential to identify subpixel abundances. To locate the endmembers being mapped by the MTMF, the MF and infeasibility values are simultaneously analyzed in a 2-dimensional scatter plot. The analyst can interactively select and/or threshold pixels in the scatter plot representing the desired target. After mapping and classification of the imagery, an accuracy assessment is normally carried out to statistically quantify and analyze the integrity of the results.

The most typical accuracy assessment conducted on remote sensing classifications is the confusion matrix, or error matrix (Jensen, 2005). The confusion matrix is a method of categorically assessing the accuracy of a remote sensing-derived classification map by comparing it with ground truth information. The matrix outputs a square matrix indicating which classes on the map fall within the ground truth reference classes. The overall accuracy of the map is computed, as well as producer's and user accuracies, the kappa coefficient, and errors of commission and omission. Producer's and users accuracies refer to how well individual categories have been mapped; the producer's accuracy indicates the probability, as percentage, that a pixel of a certain classification actually falls where the ground truth area of that same class is, and is determined by dividing the total number of correctly classified pixels in each category by the total number of training set pixels used for that particular category (Lillesand et al., 2004). The users accuracy is computed by dividing the total number of correctly classified pixels in each class by the total number of pixels placed in that category (row total). The users accuracy indicates the

probability that a particular classified pixel on the map is actually represented by the same class on the ground (Lillesand et al., 2004). Errors of commission and omission indicate the percentage of a class that is wrongly included in a class (commission error) and the percentage of a class that is wrongly excluded from its category (omission error) (Congalton and Green, 1999). The Kappa coefficient of agreement (K_{hat}), is a multivariate accuracy assessment technique (Jensen, 2005) that indicates the measure of agreement between the actual agreement of the classified map (indicated by the error matrix) and the chance agreement of the reference data (the row and column totals). A Kappa value greater than 0.80 indicates strong agreement, 0.40-0.80 represents moderate agreement, and values less than 0.40 indicate poor agreement) (Congalton and Green, 1999).

The processing and classification of the imagery for this study followed the described hyperspectral processing flow. The objective of processing the imagery was to classify the burn severity of the study sections in accordance with the burn severity assessment made in the field. After accurately classifying the burn severity, endmembers representing high water repellency were identified and a separate set of classifications was conducted to map areas of high water repellency, and thus, likely at risk of elevated erosion levels. A total of 7 images were collected over the three sections of the Clover fire study area. The image that had been most thoroughly field sampled within its boundaries was image 6, of section A. The proceeding section describes the processing and classifications of image 6.

Processing, Image 6

Initial Image Assessment

Preliminary image processing was conducted by the vendor and included geometric and radiometric (atmospheric) correction. The HYCORR algorithm was used to atmospherically correct the imagery, and the images were refined with the Empirical Flat Field Optimal Reflectance Transformation (EFFORT), an algorithm commonly used after the initial atmospheric correction of the imagery. The EFFORT spectral polishing technique further improves the data accuracy and accounts for errors within the HyCorr algorithm, due to anomalies and accuracy limits (Jensen, 2005), by applying a linear correction to each individual band in the scene. The imagery was converted from radiance values to reflectance values, and spatially projected to the UTM Projection, zone 11, with the WGS 84 datum. A preliminary evaluation of all the bands indicated them to be spectrally correct. After acquiring the HyMap data, all image analysis was conducted with ENVI software (RSI, 2005).

Minimum Noise Fraction

To reduce the dimensionality of the dataset, a minimum noise fraction (MNF) transform was computed. The result of the MNF is a transformed data set with noise as the unit variance, and eigenvalue images arranged according to noise correlation. The most optimal image processing is made possible by using the bands that display the most dominant and coherent variance. Although all the transformed bands in a MNF may have some useful information, it is more feasible and practical to subset the images to those bands containing the high amounts of variance. Additionally, at least two of the image bands were almost completely noise-dominated (bands 62 and 63). By examining the output eigenvalue plots of individual band variance in comparison with the cumulative MNF band variance, the percentage of band variance to be utilized for further processing can be determined (Fig. 2.13). Typically, the decision of which bands to utilize is made by determining where the eigenvalue plot flattens out and coherent data is lost, and choosing the corresponding variance and band threshold (Mundt et al., 2005a). To begin, a subset of 30 MNF bands was used, corresponding to a threshold of 77% cumulative variance (Fig. 2.13). The subsequent PPI failed to identify all extreme pixels, however, so it was decided to utilize the full 125 band MNF for processing. Despite the fact that several of the bands were noise-dominated, they were still included in the MNF because of the possibility that those bands may have viable data identified by the MNF.

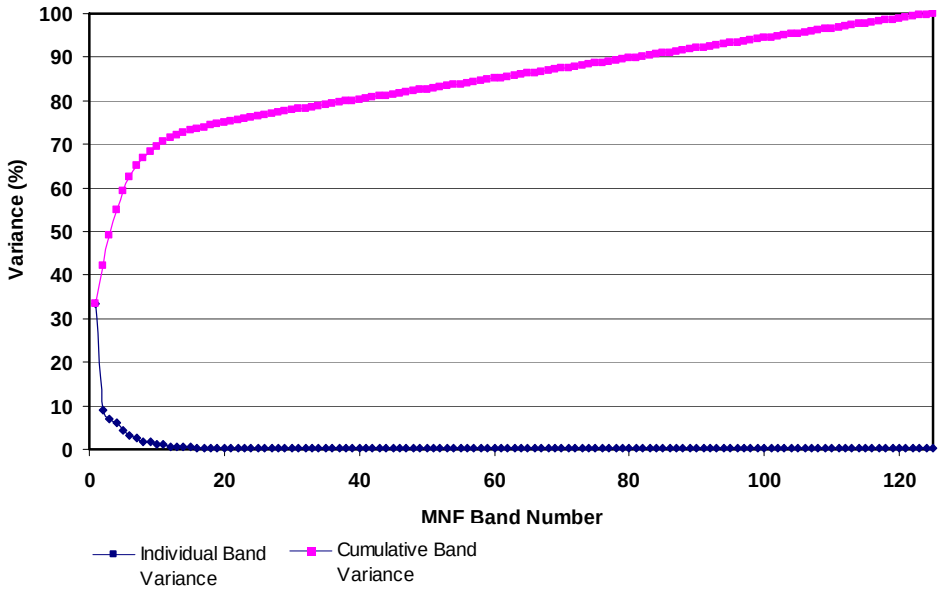

Fig. 2.13. Individual vs. cumulative band variance, MNF-transform. 30 bands = 77% cumulative variance.

Image Masking

Because the study aimed to classify only the burned areas, the unburned areas of the image were isolated from the burned areas, and a mask was applied over them for further analysis. Using band 1 of the MNF image, the burned area was easily isolated from the unburned areas using an interactive image histogram stretching technique (Fig. 2.14 A-C). The histogram of brightness values for band 1 of the MNF has two peaks and a trough in the middle between the positive values of the burned area, and the negative values of the unburned areas. By stretching the histogram to encompass only the positive brightness values, the unburned area is blacked out. The values below 0 were then thresholded to a region of interest (ROI) and subsequently used as a mask. By applying the mask to the MNF image, a new image was created with brightness values for the burned area only, and all unburned areas that previously had negative brightness were set to 0. Setting the unburned areas brightness values to 0 removed them from analysis, and allowed subsequent image processing to be performed on only the burned area.

Pixel Purity Indexing (PPI)

The purpose of the Pixel Purity Index is to identify the extreme, or pure, pixels within the MNF-transformed image. As mentioned, the PPI was originally computed on the subset, 30 band MNF image (considered the most coherent). After masking out the unburned areas of the image, the first PPI was run with 10,000 iterations, with a pixel threshold of 3.

When completed, the PPI routine results in a plot illustrating the total extreme pixels selected in relation to the total iterations (**Fig. 2.15**). A typical PPI curve should rise sharply and then flatten out near the end of the iterations after all of the extreme pixels have been found. As Fig. 2.15 demonstrates, the plot of iterations versus extreme pixels did not flatten out, even though 65,000 pixels were identified as extreme. The primary reason is likely due to the homogeneity of the burned area brightness values across the image. For example, a histogram of MNF band 1 (**Fig. 2.16**) shows the DN brightness values of the image ranging from -25.00 to 22.00. In comparison, the DN values of band 1 of the original reflectance image range from 0 to 1600. After experimenting with a range of iterations and various threshold values and obtaining similar results, it was presumed that the homogeneous, spectral similarity of the target materials within the burned area increased the difficulty for the PPI to distinguish pure pixels among the image

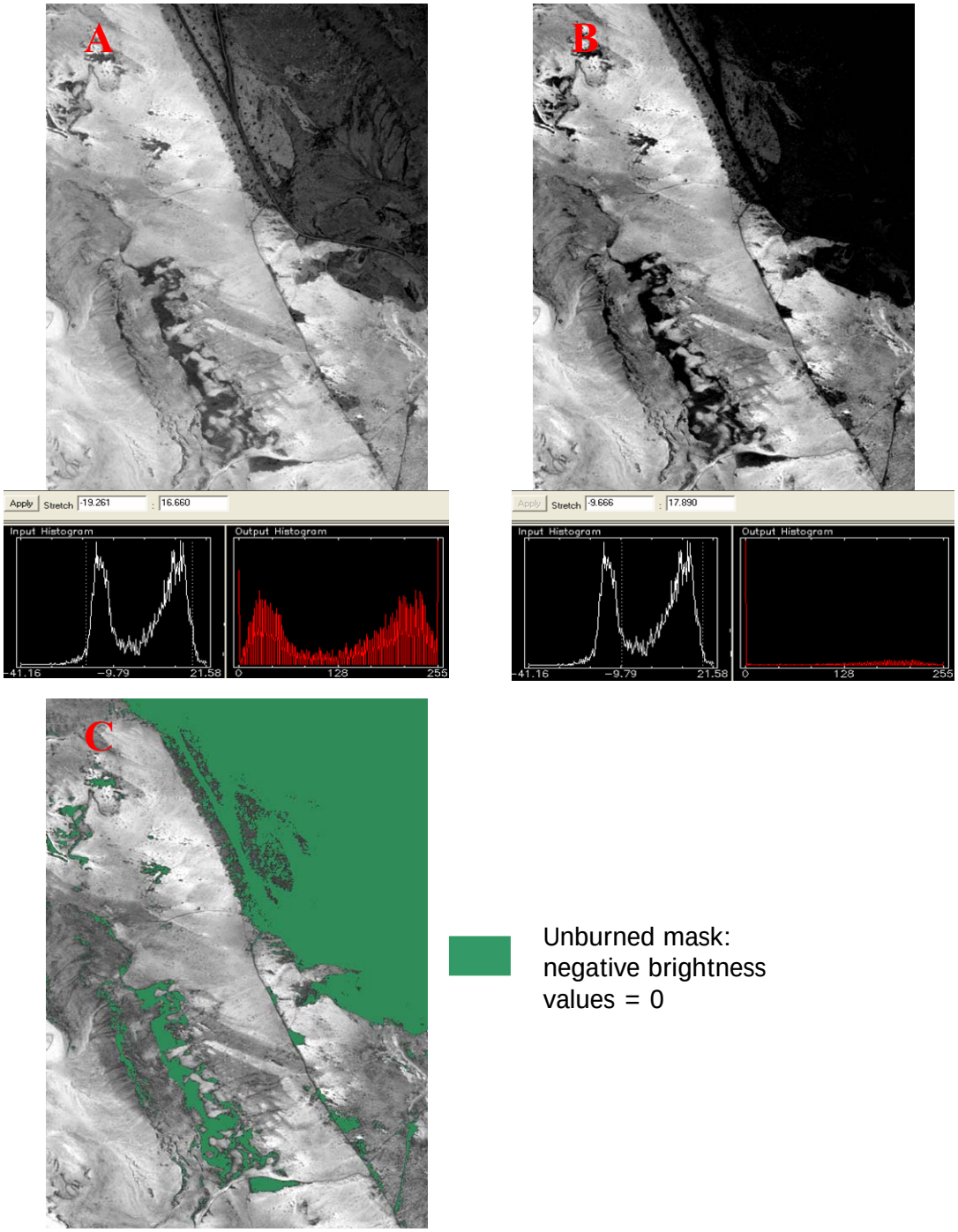

Fig. 2.14. Isolating the burned area with Band 1 of the MNF. A: Unadjusted histogram; B: Stretched histogram; C: Mask applied over unburned area after thresholding negative values and setting them to 0.

The utilization of the 125 band MNF compensated for the difficulty of identifying extreme pixels, by allowing the maximum variance of pixel and data coherency to be considered for extreme pixel detection. This second PPI with the 125 MNF bands was run at 30,000 iterations, with a threshold of 2.5 pixels (**Fig. 2.17**). Though this resulted in an acceptable PPI, it was very heavy on resources, taking approximately 24 hours to compute and maximizing the computer-allocated memory in excess of 1400 MB. Due to the

large allocation of memory and time needed for this computation, this was the only image in which a PPI was computed using all 125 bands. The other flight lines on which PPI's were computed used the first 50 MNF bands (~85% variance) (**Appendix 3**). The tradeoff of discarding the top 15% of data variance for performance was worthwhile because it was determined that the use of the remaining variance would not considerably increase the results of extreme pixel identification. The primary factor in identifying the extreme pixels was the amount of iterations (30,000) conducted with the PPI, as subsequent PPIs on other images with 50 MNF bands would demonstrate.

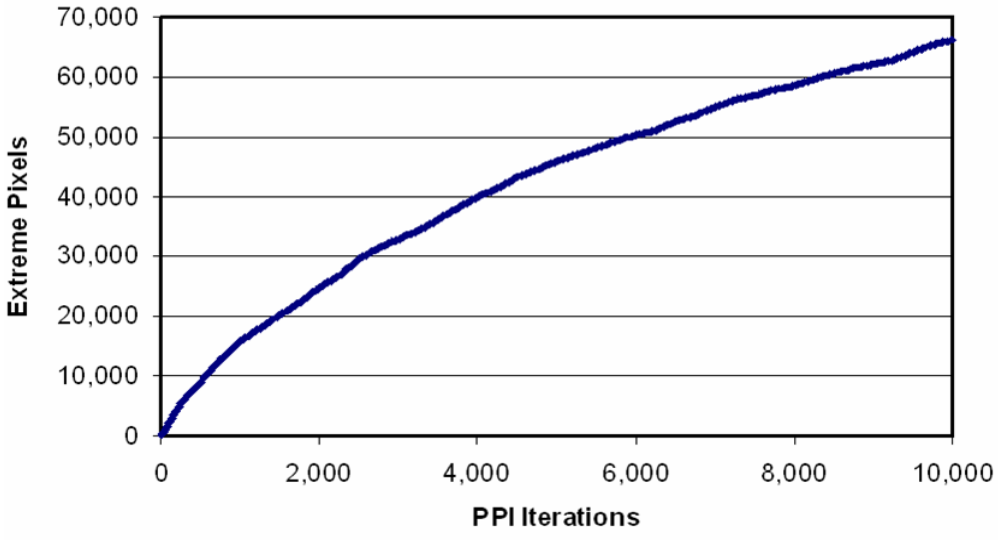

Fig. 2.15. PPI plot of 30 band MNF, 10,000 iterations, threshold 3.

The 125 band PPI identified 1,517,669 pixels out of 2,182,656 total pixels (**Fig. 2.17**). Of those total pixels, 1,365,902 were discarded, because they constituted the lower 90% of the accumulated percentage of extreme pixels found. This was done because the most extreme (pure) pixels are likely to be in the upper portions of the accumulated percentage of pixel distribution. After discarding the lower 90%, approximately 152,000 pixels remained to be analyzed for endmember identification. To identify the extreme pixels of the image, the PPI band values were thresholded to DN values between 73 and 10,879 (highest), corresponding to the top 152,000 extreme pixels. This resulted in a threshold of 151,386 pixels in the upper cumulative 10% of the frequency distribution (**Fig. 2.17**).

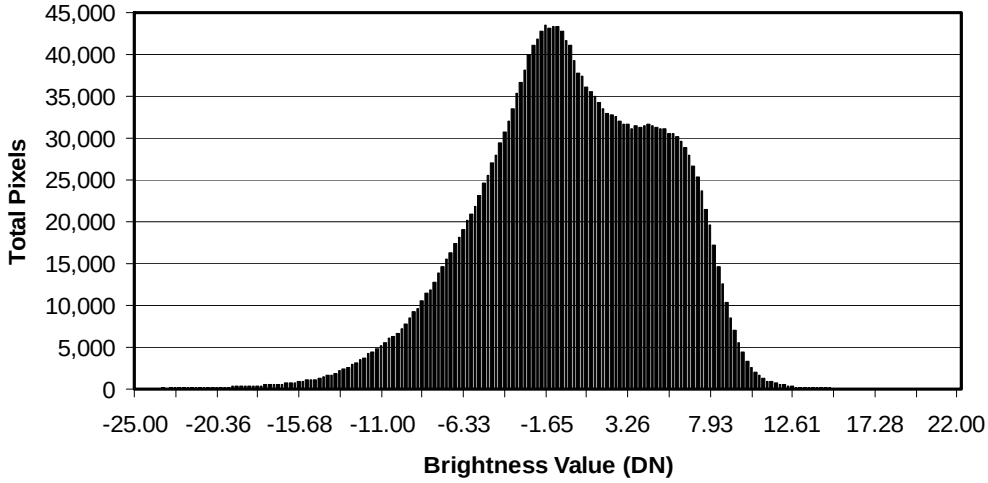

Fig. 2.16. MNF band 1 (masked) brightness value histogram.

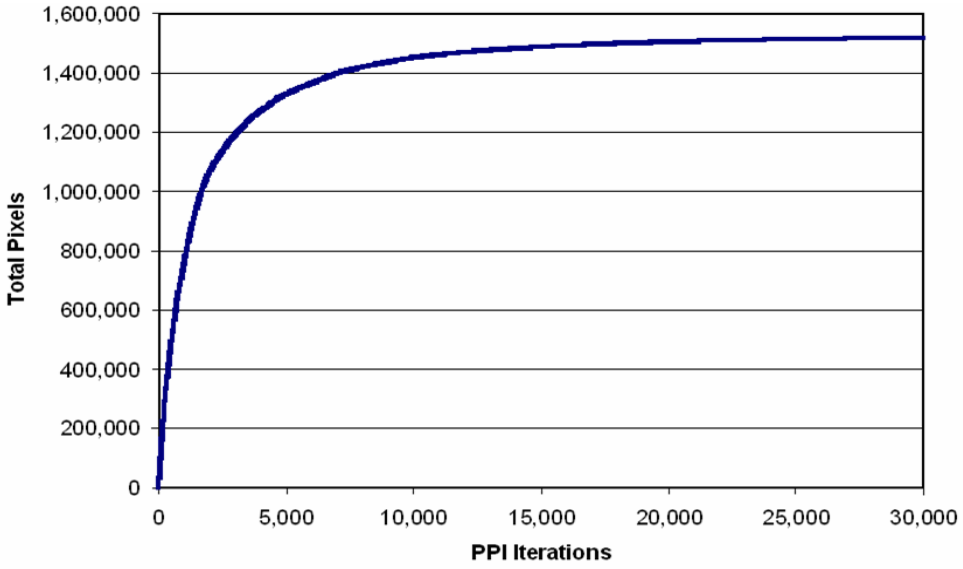

Fig. 2.17. PPI plot of 125 MNF, 30,000 iterations, threshold 2.5.

n-Dimensional Visualization

After discarding the lower 90% of cumulative pure pixels, the 152,000 remaining pixels were analyzed with the n-DV to identify extreme pixels. The number of pixel spectra projected in the n-DV should not be so high that the visualizer is overcrowded and its capability reduced. Because 152,000 pixels were too many for projecting at one time, they were viewed in increments of about 25,000 pixels (Table 2.3), between the DN values of 73 and 10,879 (Fig. 2.18 A-G).

Table 2.3. Pixel increments for n-Dimensional Visualization

Pixel increment	DN value range	Total pixels
1	73-80	24,416
2	81-91	25,526
3	92-107	25,801
4	108-133	25,218
5	134-191	25,011
6	192-10,879	25,413

After viewing each pixel increment in the n-DV at dimensions up to n=125, it was evident that extreme pixels could not be distinguished until the highest value increments were visualized. Using the autocluster option, ENVI selected 46 classes of extreme pixels in the n-DV from the spectral cloud of DN 134 – 10,879, the two highest pixel increments. After the 46 extreme pixel classes were detected the remaining pixel spectra were manually examined, and 6 additional classes were selected. The 52 extreme pixel classes identified in the n-DV were then exported back to the image as regions of interest (ROI's), and a geographic projection was applied to them, so that they could be identified and related to ground truth information.

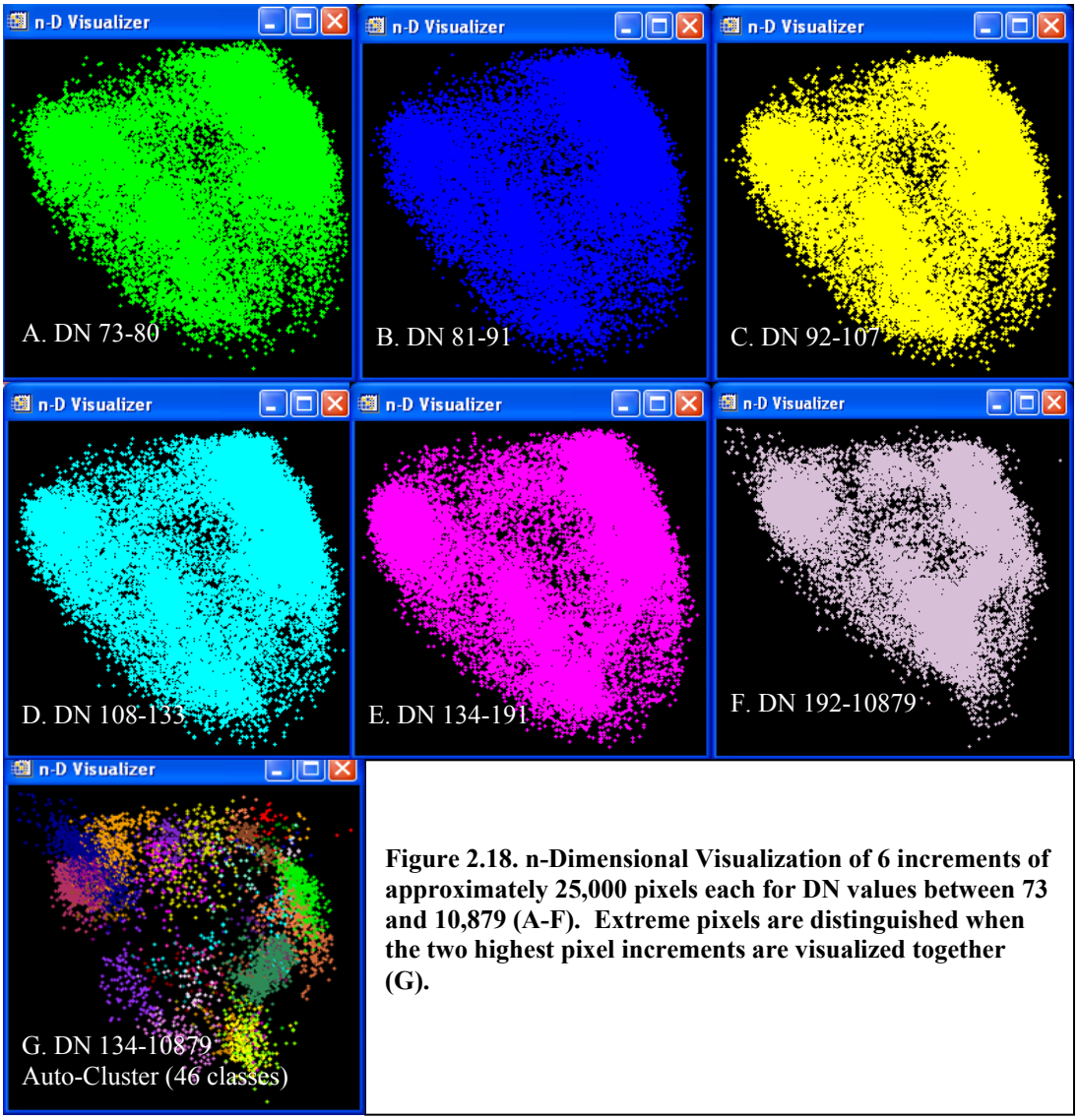

Figure 2.18. n-Dimensional Visualization of 6 increments of approximately 25,000 pixels each for DN values between 73 and 10,879 (A-F). Extreme pixels are distinguished when the two highest pixel increments are visualized together (G).

Identifying Burn Severity Endmembers

The most difficult and time-consuming portion of spectroscopy is the identification of endmembers. This study utilized the functionality of ArcMap GIS to interactively view the extreme pixels identified in the HyMap image in the same geographic projection as the field-collected ground truth data, as well as other geospatial data, to identify the extreme pixels that could be used as endmembers. After the extreme pixels were selected in ENVI, they were converted to a class image, and then to a vector dataset, and saved as a shapefile. The shapefiles, which represented the 52 categories of extreme pixels found in the n-DV, were overlaid with the ground truth information collected in the field, as well as 2004 National Agriculture Imagery Program (NAIP) ortho-rectified digital color aerial photos (USDA-FSA, 2005). A supervised classification portraying the dominant pre-fire vegetation groups of shrub or grass was created from the aerial photos and supplementally used as a guide for identifying the dominant vegetation group of the extreme pixels pre-fire vegetation group (Appendix 4). The NAIP ortho imagery is representative of the study area approximately one year before the fire, and its true color, high resolution (1 m) allows for accurate visual detection of vegetated areas, bare ground, roads, and other man-made features. Prior to analysis, the geo-registration of the HyMap imagery was assessed in comparison with the ortho-rectified NAIP ortho imagery, and found to have a mean error of 6.4 m (Appendix 1). The average shift difference between the Hymap and NAIP imagery was an acceptable difference for the purpose of identifying burn

severity endmembers, particularly since many of the burned areas tended to cover large, homogeneous areas.

The extreme pixel classes were assigned their respective burn severity endmember (e.g. unburned, low, moderate, high) by assessing the geographic location of the extreme pixels with respect to other ground truth information. When pixels were found near a sample plot (10-20 m), the underlying vegetation classification was consulted to verify the dominant vegetation group (e.g. shrub, grass), and the pixels were assigned the vegetation group and burn severity of that plot. Extreme pixels were also spectrally matched to endmembers by examining the average spectral profile of the pixels in comparison to the spectra of the sample plots. Some burn severity classes exhibited unique spectral signatures (e.g. low severity grass) that extreme pixels could easily be matched to, while others displayed signatures that were virtually indistinguishable from the typical spectra of the image (e.g. moderate and high severity shrub). This introduced a certain level of subjectivity to the assignment of moderate and high burn severity training endmembers that likely evoked error in the classifications. Extreme pixels that could not be identified based on their spatial association to other GIS layers or their spectral association with training plots were discarded for further use. Of the 52 extreme pixel classes analyzed in ArcGIS, 10 were discarded because their material could not be confidently identified, resulting in 42 extreme pixel classes, of which the similar classes were merged together for input into the classification algorithms.

Identifying Water Repellent Soil Endmembers

A considerable portion of the remote sensing analysis for this project involved analyzing the spectral characteristics of the soils across the burned area; within various burn severity zones, at points designated as having high water repellency and no repellency, and across areas of different pre-fire vegetation characteristics. The predominant spectral characteristic across the entire burned area is the high reflectance within the short wave infrared (SWIR; 1.5-2.5 μm). A typical spectral profile from the hyperspectral imagery of burned soil at the study area (Fig. 2.19) exhibits reflectance between 5% and 10% at the beginning of the visible spectrum (0.5 μm), and rises steadily to about 35% reflectance around 1.75 μm in the SWIR, where it flattens out; the curve then demonstrates a rise up to about 40% reflectance around the clay absorption band at 2.3 μm (which demonstrates a dip in the signature due to the water retention capabilities of clay minerals) (Chabrillat et al., 2002), and then levels off around 37% reflectance (the absorption near 1.4 μm and 1.9 μm are due to atmospheric water absorption and noise). The majority of the spectral signatures across the burned area, and particularly in the moderate and high severity shrub areas, display a similar curve, with most of the variation in the SWIR. To depict the locations of water repellent soils in the image, the spectral profile had to be defined and used as training endmembers. None of the extreme pixels overlapped the water repellent sample plots, indicating that water repellent soils did not demonstrate a pure spectral signature, as identified by the PPI, which could be used as a training endmember. To define spectral signatures for the soils, the ground-collected data was overlaid on the projected HyMap reflectance data in ENVI, and spectral profiles of sites representing high water repellency were recorded. Initially, the average spectral signature of each sample plot containing water repellent soils was recorded. After analyzing the average spectra of the sample plots, it was apparent that plots having weak to moderate repellency or high repellency only at points, did not always demonstrate a clear spectral difference from plots without repellency. These plots did have slightly lower reflectance (~5%) in the SWIR portion of the spectrum, however. It was clear, however, that plots with very strong water repellency throughout (e.g. average MDI rate of all 3 points were MDI = 0-3 ml/min) exhibited a noticeable decrease of 5% - 10% less reflectance in the SWIR portion of the spectrum than those with weak or moderate water repellency, and up to 15% lower SWIR reflectance than sites with no repellency (Fig. 2.20).

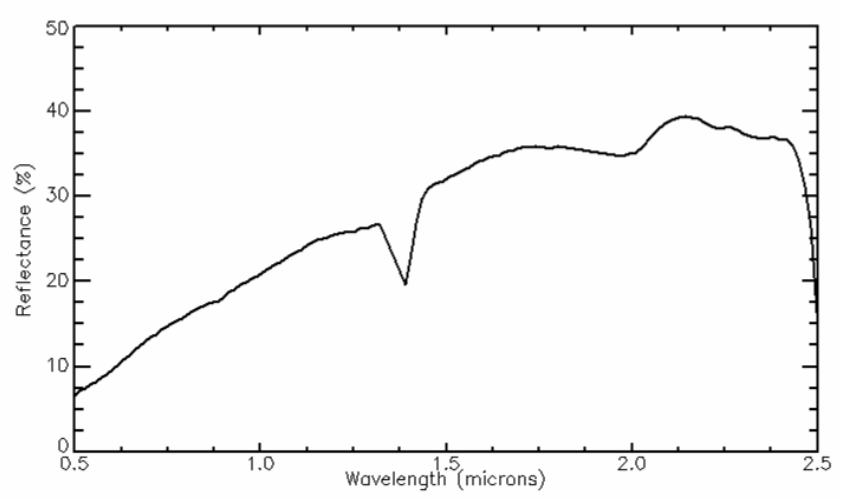

Fig. 2.19. Typical spectral profile of soil in burned area

An ideal goal of the spectroscopic analysis was to identify features of the reflectance spectrum that were unique to fire-induced water repellent soils. Two features of fire-induced water repellency that may introduce a unique spectral characteristic are aliphatic hydrocarbons, which are created through the combustion of organic matter (DeBano, 1998), and the reduction of the clay absorption layer at 2.3 μm, due to the cementation of clay oxides in the soil after a fire burns at very hot temperatures (220°-275°) (Moody et al., 2005). An indication of aliphatic hydrocarbons would likely be noticeable in the spectral regions typical of absorption by organic compounds. These regions include the NIR and SWIR region of the spectrum between 1.4 μm and 2.1 μm (Hummel et al., 2001; Lewis et al., 2004). Fire-induced soil cementation due to intense heating of clay oxides (AlOH, FeOH) would be indicated by absorption in the clay absorption band at 2.3 μm (Fig. 2.20). The reflectance spectrum of the soils was carefully analyzed at these wavelengths, and no noticeable difference of absorption within the NIR and SWIR (other than a general decrease in reflectance) was observed that would indicate a change in the organic chemistry of the soil. It is most probable that any change in reflectance or absorption due to organic compound alterations in this region of the spectrum was blocked by the presence of charred soils and ash on the surface. No difference in absorption caused by intense heating of the soils was detected at the clay absorption band (2.3 μm) other than the decreased reflectance among the moderate and high water repellent soil sites.

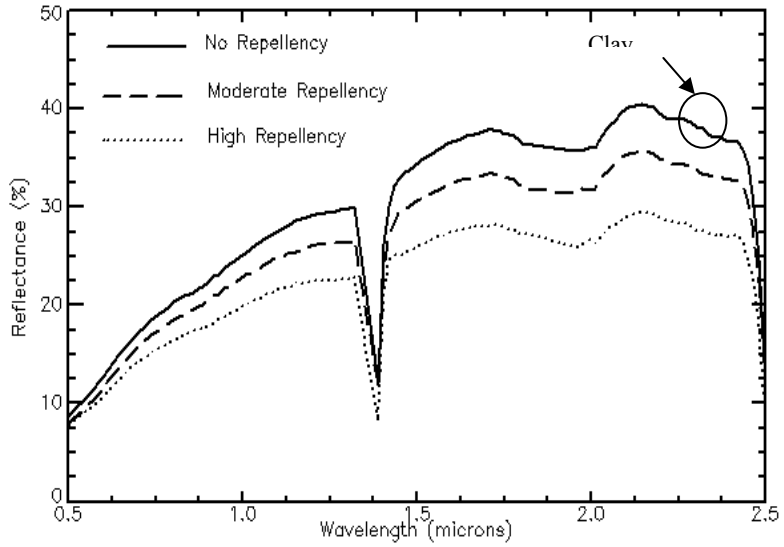

Fig. 2.20. Spectral signatures of non water repellent, moderately water repellent, and highly water repellent soils within the burned area.

A field-collected spectral signature of highly water repellent soils (Fig. 2.21) was used as a guide for the identification of those materials on the image, and sample plots that were assessed as highly water repellent were compared to it. The field-collected spectral signature of the water repellent soil is unique in that its peak reflectance at the clay absorption band (2.3 μm) is only 25%, and the SWIR portion of the curve displays minimum variation save for the slight bump in reflectance at about 2.0 μm. The overall low reflectance of the entire spectral curve is not surprising because the field spectrometry was acquired only 1 m above the burned, blackened soil, and thus it was not as affected by atmospheric noise or the albedo of the surrounding brighter, less severely burned soils. Though the field collected spectra of water repellent soil demonstrated lower average reflectance than other highly repellent sites assessed in the imagery, its general shape and reflectance values served as a guide for the detection of strongly water repellent soil spectra in the imagery. After detecting and recording the spectral profiles of the water repellent sample sites, their spectral signatures were saved in a spectral library in order to be used as endmembers for classification.

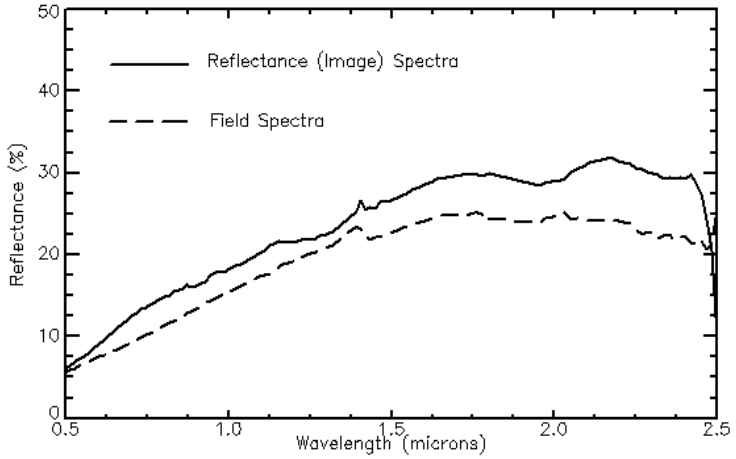

Figure 2.21. Field-collected spectra of water repellent soil (dashed), and HyMap reflectance spectra from the same location (solid).

Unsupervised Classification

As a first cut classification of the imagery, the Iterative Self-Organizing Data Analysis Technique (ISODATA) unsupervised classification was performed on the masked MNF image. After the desired number of classes is established by the user, the ISODATA classification calculates the mean class values within a dataset, and classifies all the remaining pixels with a minimum distance technique (RSI, 2005). Five classes were established for the ISODATA classification to compute, in order to separate the burn severity classes of low severity grass and shrub, moderate severity shrub, high severity grass and shrub, and bare ground. The user does not determine endmembers or training classes for an unsupervised classification. This has some advantages in heterogeneous systems (e.g. rangelands) because the data is statistically categorized without user bias. However, because the ISODATA classification is unsupervised, it is unclear what endmembers the resulting classes represent. The primary reason for conducting the unsupervised classification was to determine the separability of the burned areas brightness values prior to more rigorous classification procedures.

Burn Severity Classifications

The Spectral Angle Mapper (SAM) and Mixture Tuned Match Filtering (MTMF) classification methods were conducted to independently classify burn severity and areas of high water repellency. The spectra of the identified extreme pixels were used as input endmembers (reference spectra) for a SAM classification of burn severity and included the following: bare ground, rock, low, moderate, and high severity grass, and low, moderate, and high severity shrub. The bare ground endmember was included because patches of bare ground, which portrayed high reflectance and albedo, were naturally present across the area, even

though they were minimally affected by the fire (due to the lack of vegetation present on them). It is noted that unburned areas were not included as endmembers in the classification because those areas had been masked out for further analysis. In addition, bands of basalt (rock) were visually identified among the extreme pixels, but no ground truth information was available to verify their presence. The SAM classification was conducted using a maximum angle of 1 radian for all of the endmember classes. The single angle value was used because of the high number of reference classes input for the classification, and it was not yet known which classes would over- or under-classify. After the SAM classification was computed, similar endmember classes were combined, and a confusion matrix was conducted to assess the accuracy of the classification image.

A separate classification for each burn severity class (unburned, low, moderate, high shrub and grass) was then conducted on the image using the MTMF technique, and the extreme pixels as endmembers. The MTMF outputs 2 images for each endmember; a matched filter score image and an infeasibility score image. The results are interpreted by plotting the MF score versus the infeasibility values in a 2-dimensional scatter plot. The MF scores of the MTMF typically have a mean value around 0, which indicates no match of spectra was detected in the pixel. Pixels with a MF score of 1.0 are considered a perfect match, containing 100% pixel abundance, pixels scored greater than 1.0 have been overestimated or misinterpreted due to noise, however they are still considered to have 100% abundance (MF scores of 0-1 represent linear abundance of 0 - 100%), and MF scores of 0 or less are background and not considered target components (Mundt et al, 2006; In Press). The values of the infeasibility image, which can range from 0 to the 100's, are output in noise sigma units, and indicate the feasibility that the MF scored pixel is indeed of its expressed value (RSI, 2005). The infeasibility values of the MTMF are advantageous to the accuracy of the classification because high values (>2) indicate the possibility of pixels being false positives and not matching the target, although their MF score is high (RSI, 2005). The most accurately mapped pixels of a MTMF classification will have a MF score near 1, and a low infeasibility value. After assessing the pixel distribution in the 2-D scatter plot, the user determines a threshold for infeasibility and the acceptable MF score (pixel abundance) that can be considered as presence of the target material.

After computing the MTMF for each burn severity endmember and assessing the 2-D scatter plot, the best thresholds for each endmember were established (Fig. 2.22 A, B, Table 2.4), and subsequently converted to vector files in ENVI. All of the severity classes were included in the MTMF except for moderate severity grass, which was determined to be too spectrally dissimilar from low severity grass, and therefore not classifiable. The vectors of the thresholded pixels were then exported to ArcGIS as shapefiles, where an accuracy assessment was conducted on them. Because the most important function of the MTMF is to map the abundance of an endmember in a particular pixel, a traditional classification map portraying the algorithmic spatial detection of all the endmembers (as with the SAM) would fall short of portraying its unique and prevailing quality. This is because the MF scores of the pixels are scaled according to the amount of a particular endmember's spectra within each pixel (Fig. 2.22C). In addition, since many pixels in an image are a mixture of multiple endmember spectra, mapping multiple endmember MF scores would result in overlapping of MF scores on pixels, and an incorrect portrayal of the classification.

Although the MF score results can be related to a measure of subpixel abundance of an endmember, the proportion of an endmember within a pixel is difficult to quantify and verify without a large number of extremely precise field measurements. For the purpose of identifying areas of soil water repellency, we did not attempt to quantify the subpixel abundance of their quantity, but instead utilized the MTMF to predict their presence. The best way to interpret and validate a target material's presence with the MTMF is by thresholding the output band to the desired spectral quantity within the pixel, and performing an accuracy test that verifies a presence or absence of the endmember within the thresholded pixel.

Table 2.4. MF score and Infeasibility thresholds for the MTMF burn severity classification, Image 6

Endmember Class	MF Score Threshold	Infeasibility Threshold
High Severity Shrub	0.65 - 2.00	> 20
Moderate Severity Shrub	0.85 - 2.00	> 20
Low Severity Shrub	0.50 – 1.50	> 20
High Severity Grass	0.50 – 2.00	> 20
Low Severity Grass	0.50 – 1.50	> 15
Bare Ground	0.40 - 2.00	> 20

Performing a presence/absence error assessment involves overlaying the thresholded pixels in projected space with the ground truth reference polygons or points (collected with GPS) of the corresponding classes to indicate presence of the target material, as well as ground truth polygons or points representing a separate class to indicate absence of the endmember. A matrix is established, in which one of the following is denoted: True positive, when a reference polygon is inside of the classification, indicating the classification to be correct in that area; false positive, when an absence polygon falls inside the classification, indicating the classification to be incorrect in that area; false negative, when an reference polygon falls outside of the classification, indicating an incorrect classification in that area; and true negative, when an absence polygon falls outside of the classification, indicating a correct classification (or absence of) in that area.

Water Repellency Classifications

A separate set of classifications was conducted to identify the presence of water repellent soils in the imagery. The average spectra of the moderate and highly water repellent training sites (Fig. 2.20) were used as training endmembers for the SAM and MTMF classification of water repellent soils. The training spectra for the moderate and high water repellent soils did not indicate any unique change in spectral composition from the surrounding areas, but they were separable due to their decreased reflectance in the SWIR portion of the spectrum. The highly water repellent soils were expected to be detected more accurately because their SWIR reflectance was 10%-15% lower in reflectance than the non-water repellent areas. The moderately repellent soils, however, only exhibited 5%-10% less reflectance in the SWIR than non-repellent soils, and their classification was not expected to be as accurate, because of their spectral similarity to non-repellent soils.

Since the spectral analysis of the water repellent endmembers indicated most of the variability of the data to be in the SWIR region, the original reflectance image was subset to the SWIR wavelengths of 1.43 μm – 2.5 μm (bands 65-125) for the classifications. The remaining 61 bands were MNF-transformed and masked, as described in section 3.3.2, and the supervised classifications were conducted on them. Following the classifications of water repellency, a confusion matrix and a presence/absence error matrix was performed to test the accuracy of the classifications.

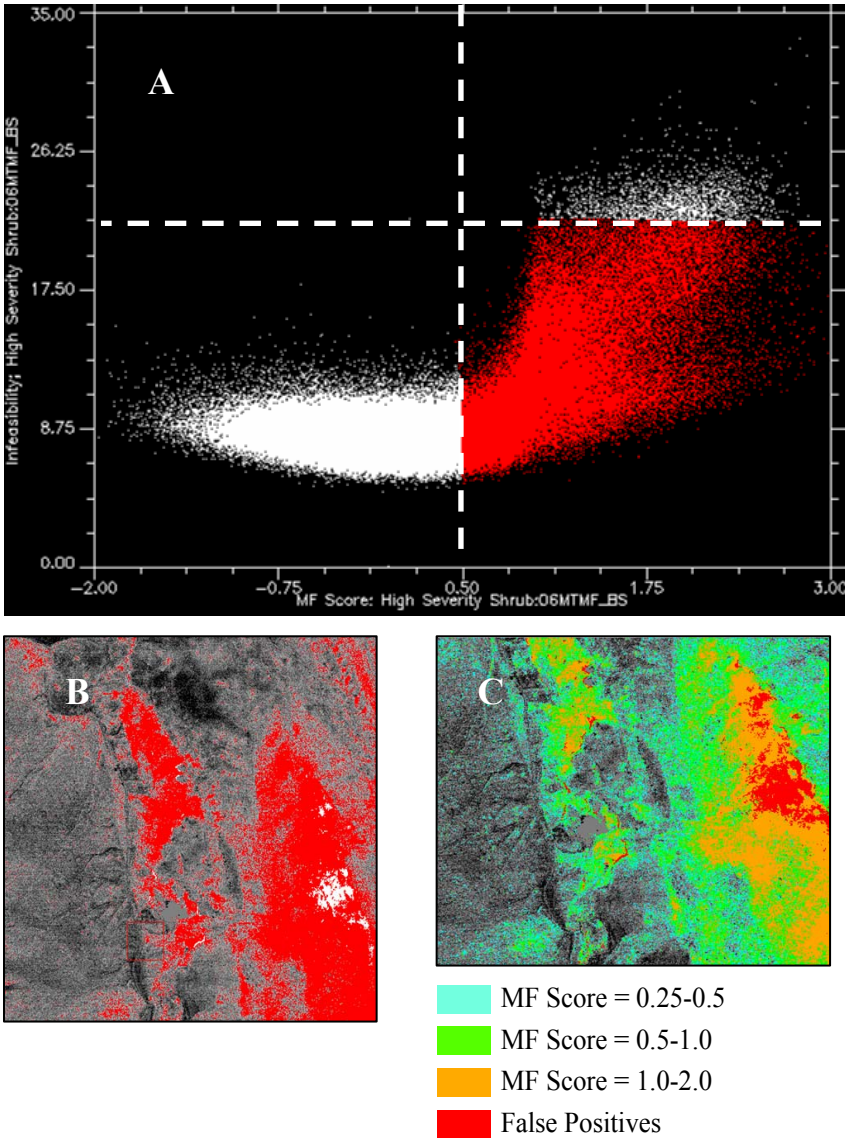

Figure 2.22 A, B, C. 2-D scatter plot of MF score vs. Infeasibility value (high severity shrub). Red indicates pixels most likely to be high severity shrub (A). Corresponding pixel selection of 2-D scatter plot in a portion of image 6 (B). Thresholded MTMF pixel abundance values (MF Scores), in a high severity shrub area of image 6 (C).

RESULTS

Field Data Results

Across the 3 sections of the study area, 235 total points were assessed for water repellency within 80 sample plots. The water repellency was assessed at three points within the sample plots with the Mini-Disc Infiltrometer (MDI) and the Water Drop Penetration Test (WDPT). Of the 235 points, 61 were located in high burn severity, 81 in moderate severity, 69 in low severity, and 24 in unburned. Initial data review indicated that infiltration differed within similar burn severity classes of different vegetation groups, therefore the classes were further broken down by the dominant vegetation group, namely grass and shrub, of the area being sampled. According to the burn severity classes broken down by vegetation, 12 points were recorded in unburned shrub, 51 in low burn severity shrub, 63 in moderate severity shrub, and 41 in high severity shrub. Within the grass vegetation groups, 12 points were in unburned grass, 18

in low severity grass, 18 in moderate severity grass, and 20 in high severity grass (Table 3.1). Most of the water repellent soils were found in the top 2 cm of the soil layers. Mean values and standard deviations of the MDI values were computed for each burn severity class (Table 3.1). In addition, the descriptive statistics of the MDI sample points were listed in accordance with the corresponding WDPT rating at the sample point location (Table 3.2). The WDPT ratings assisted in designating the class ranges of the MDI values. Soils with a WDPT value of 30s-60s were classified as having weak water repellency. Soils with a WDPT value of 61s-180s were classified as moderately water repellent, and soils with a WDPT greater than 180s were strongly water repellent (Dekker and Ritsema, 1994; Lewis et al., 2006).

Table 3.1. Descriptive statistics and standard deviation (SD) of MDI measurements (ml/min), describing infiltration characteristics (as measured by MDI) in each burn severity class.

Burn Severity Class	Count	Min MDI	Max MDI	Mean MDI	SD MDI
Unburned Shrub	12	4.00	16.67	9.89	3.38
Low Severity Shrub	51	3.00	12.67	6.57	2.12
Moderate Severity Shrub	63	1.00	8.33	4.47	1.95
High Severity Shrub	41	1.33	15.00	5.81	2.73
Unburned Grass	12	2.67	12.00	5.31	2.65
Low Severity Grass	18	2.33	8.00	5.22	1.56
Moderate Severity Grass	18	0.00	8.00	4.31	2.33
High Severity Grass	20	2.33	13.00	7.32	2.66
All Data	**235**	**0.00**	**16.67**	**5.78**	**2.70**

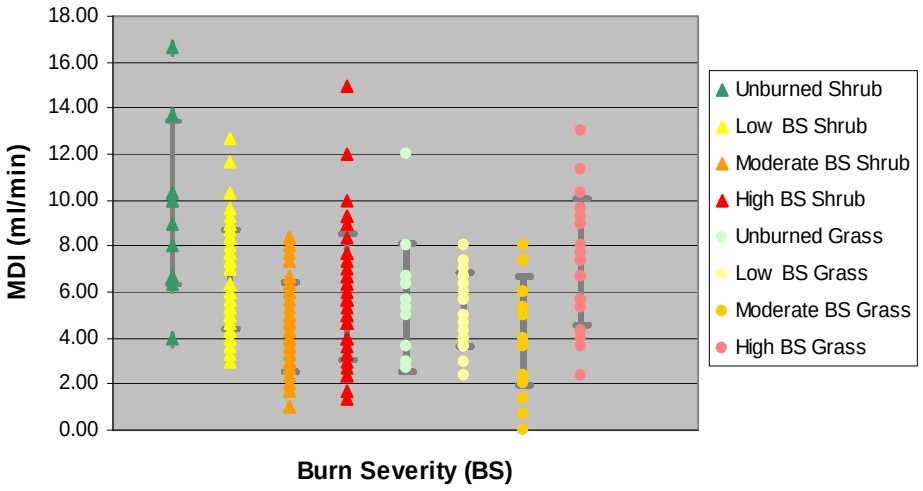

Fig. 3.1. Soil water repellency distribution of MDI values (ml/min) among burn severity (BS) classes

The MDI measures the amount of water infiltrating the soil per 1 minute (ml/min). The highest MDI value (16.67 ml/min) was recorded in an unburned shrub section, and the lowest value (0 ml/min) was recorded in a moderately burned grass area. Mean MDI values were consistently lower in the moderately burned shrub (4.47 ml/min) and grass areas (4.31 ml/min), and highest in unburned shrub areas (9.89 ml/min). Areas of high severity shrub, low severity grass, and unburned grass all had similar MDI values between 5 and 6 ml/min, and areas of low severity shrub and high severity grass had moderate MDI values of 6.57 ml/min and 7.32 ml/min (Fig. 3.1). Because the use of the MDI for assessing soil water repellency has only been documented by one other study (Lewis et al., 2006), its values were correlated with the results of the more traditional, and well documented, WDPT test. Due to the subjective nature of

the WDPT, a strong relationship was not expected, primarily due to the threshold of values (360 s) for high water repellency. Soils that were highly water repellent often had WDPT values greater than 360 s, but were assigned a value of 360 s. In addition, there were numerous data points that exhibited WDPT values of 0. Although there was a broader range of WDPT values between 0 s and 125 s, most points either exhibited no water repellency (0 s) or water repellency lasting longer than 360 s. A comparison of the MDI repellency range with respect to WDPT time values at the 103 points in the burned portion of section A (Fig. 3.2) indicates a moderate inverse trend ($r^2 = 0.50$) between the two. Because the WDPT values of 360 s are thresholded values and are not considered real values, a separate analysis was conducted without the 360s values. The resulting fit was no better than that indicated in Fig. 3.2 and is not shown.

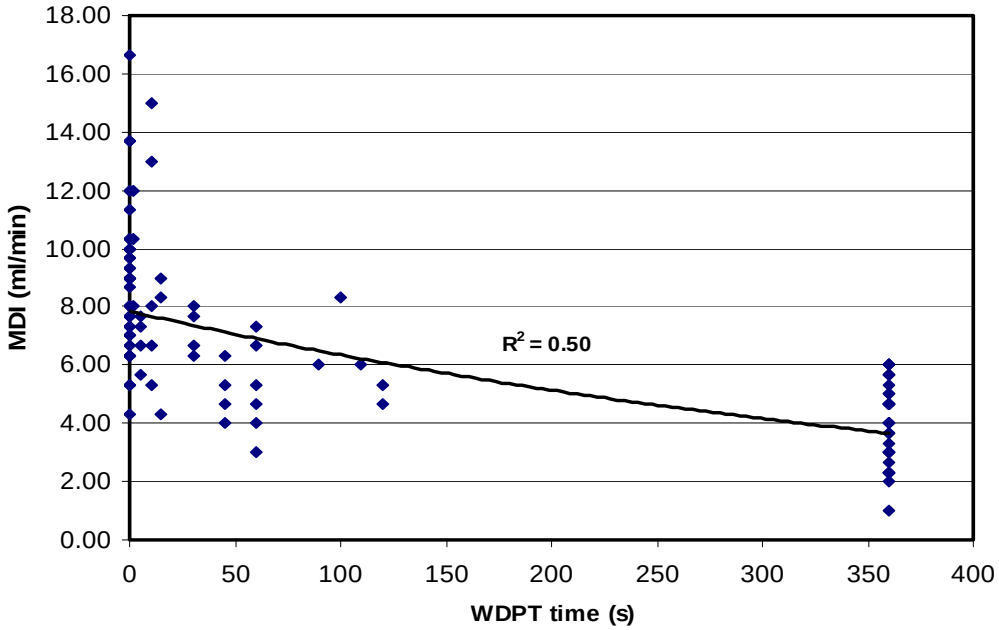

Fig. 3.2. Comparison of MDI repellency values with respect to WDPT time values at sample points in Section A. WDPT times lasting longer than 6 minutes were assigned a value of 360 s. The R^2 value of 0.50 indicates a slight inverse trend between the variables.

The MDI time till infiltration was also tested against the time of the WDPT (Fig. 3.3) and included the bias due to the 0 and 360 values of the WDPT. Soils with no water repellency would be expected to infiltrate right away with the MDI, while soils with high water repellency often take time to allow water to infiltrate. A slight trend was detected with this comparison as well, indicating that highly water repellent soils are resistant to infiltration. Even though a slight relationship was detected, the capillarity of the soils often allowed infiltration to begin faster with the MDI test, even on soils that repelled a water drop. Extremely high water repellent soils (WDPT >360 s) that were tested, however, had high MDI time values as well, indicative of the relationship between the two testing methods. The WDPT measures the persistence (in seconds) of a water drop on the soil surface, and is a reliable indicator of the presence of a water repellent layer. Of the 13 points assessed in unburned shrub areas, only 1 point exhibited weak water repellency (WDPT 30s-60s). Of the 51 points assessed in low burn severity shrub areas, 1 point exhibited weak water repellency, and 3 points exhibited strong water repellency (WDPT >181s). Of the 63 points assessed in moderate severity shrub areas, 9 points exhibited

weak water repellency, 16 points exhibited moderate water repellency (WDPT 61s-180s), and 29 points exhibited strong water repellency. Of the 41 points assessed in high severity shrub areas, 6 points exhibited weak water repellency, 5 points exhibited moderate water repellency, and 15 points exhibited strong water repellency. None of the 12 points assessed in unburned grass exhibited water repellency with the WDPT. Within low burn severity grass areas, 1 of the 18 points assessed exhibited weak water repellency, and 1 exhibited strong water repellency. Within the moderate severity grass areas, 5 of the 18 points assessed exhibited moderate repellency by the WDPT, and 11 points exhibited strong repellency. Of the 20 points assessed within the high severity grass areas, 4 exhibited weak repellency, 2 exhibited moderate repellency, and 3 exhibited strong repellency (Table 3.2). Though the high severity grass areas did not exhibit strong water repellency when tested at the surface with the MDI, the WDPT test indicated repellency in the soils at depths of 2 cm or deeper, below a layer of highly penetrable, loose soil (Appendix 6). The subsurface layers of soil was likely a result of the downward transfer of heat during the fire (DeBano et al, 1998), causing hydrophobic substances to volatize below the burned organic matter, and create a water repellent layer. The WDPT measurements proved useful for identifying subsurface water repellent layers within the study area that were unrecognized by the MDI measurements; they also supplemented the MDI measurements when ranges were established indicating the soils' strength of repellency.

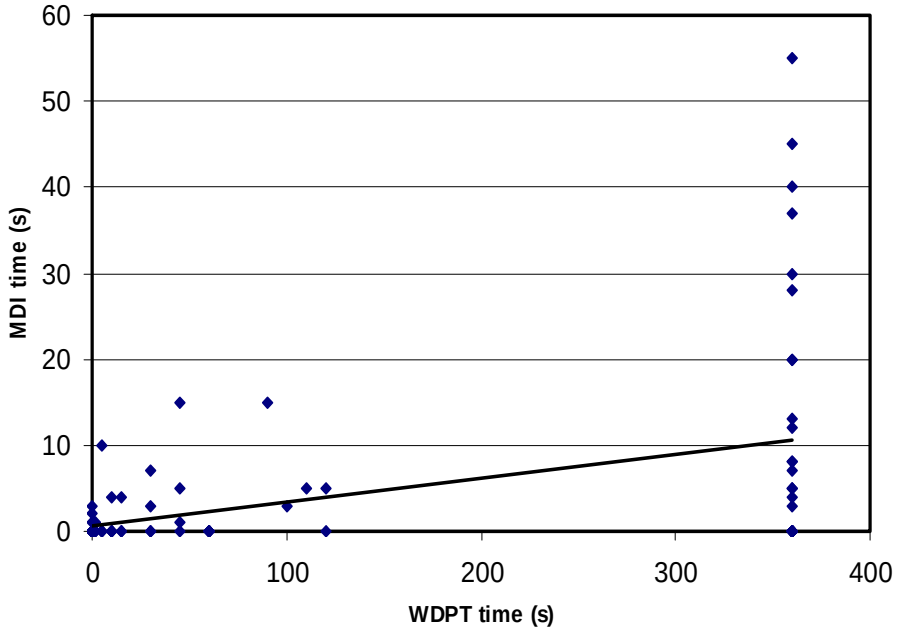

Figure 3.3. Comparison of MDI time till infiltration with WDPT time values in Section A

A mixed model analysis was computed in SAS to assess the relationship of the MDI-assessed water repellency with burn severity. The first step of the model was to perform a Least Squares adjustment of the mean MDI values of each burn severity class (Fig. 3.4, Table 3.3). The model then computed the difference between all pairs of the least squares mean MDI values among the matrix of burn severity/vegetation classes (Column A/B - Column C/D; Table 3.4). The resulting t-test p-values (unadjusted p-value) were adjusted with the Kramer multiple comparison adjustment method (adjusted p-value) to reduce the chance of false positives among independent observations. For those comparisons with p-values below the alpha level of 0.05, the null hypothesis of the two variables being the same was rejected, indicating the difference between those classes to be significant (SAS Institute, 2005) (Table 3.4). In the mixed model, the denominator degrees of freedom were equal to the number of samples (n=79) minus the rank (XZ) matrix, where XZ = burn severity (4 classes) x vegetation (2 classes), and is established by the software to be the same for all comparisons throughout each iteration of the model (SAS Institute, 2005).

Table 3.2. MDI values (ml/min) and WDPT repellency ratings among burn severity classes

Water Repellency (WR) rating	Count	Min MDI (ml/min)	Max MDI (ml/min)	Mean MDI (ml/min)	SD MDI (ml/min)
Unburned Shrub					
No WR	12	4	16.67	10.18	3.55
Weak WR	1			6.67	
Moderate WR					
Strong WR					
Low Severity Shrub					
No WR	47	3	12.67	6.61	2.2
Weak WR	1			7.67	
Moderate WR					
Strong WR	3	4.67	7	5.67	1.2
Moderate Severity Shrub					
No WR	9	3	8.33	5.07	1.68
Weak WR	9	2	8.33	4.63	1.83
Moderate WR	16	1	8.33	5.06	2.13
Strong WR	29	1	8	3.91	1.92
High Severity Shrub					
No WR	15	4	15	7.62	3.01
Weak WR	6	2.67	9.33	6.28	2.34
Moderate WR	5	4	8.33	5.67	1.65
Strong WR	15	1.33	6.67	3.85	1.51
Unburned Grass					
No WR	12	2.67	12	5.31	2.76
Weak WR					
Moderate WR					
Strong WR					
Low Severity grass					
No WR	16	2.33	8	5.25	1.64
Weak WR	1			6.33	
Moderate WR					
Strong WR	1			3.67	
Moderate Severity Grass					
No WR	2	5.33	8	6.67	1.89
Weak WR					
Moderate WR	5	0	7.33	4.93	2.85
Strong WR	11	0.67	7.33	3.61	2.08
High Severity Grass - Includes subsurface values at ~ 2 cm.					
No WR	11	6.67	11.33	8.7	1.43
Weak WR	4	3.67	13	6.25	4.51
Moderate WR	2	5.33	6.67	6	0.95
Strong WR	3	2.33	5.67	4.56	1.93

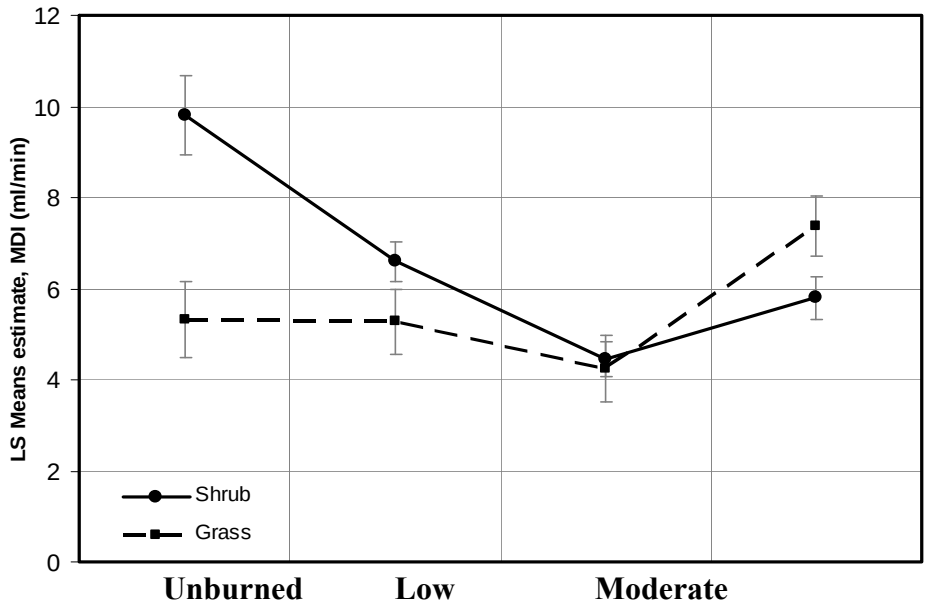

Fig. 3.4. Least squares adjusted means of MDI values (ml/min) among burn severity classes.

Burn severity classes exhibiting significant differences of repellency between each other are unburned grass and unburned shrub (p=0.0098), unburned shrub and low severity grass (p=0.0036), unburned shrub and low severity shrub (p=0.0296), unburned shrub and moderate severity grass (p=0.0001), unburned shrub and moderate severity shrub (p<0.0001), unburned shrub and high severity shrub (p=0.0032), low severity shrub and moderate severity shrub (p=0.0073), moderate severity grass and high severity grass (p=0.0414), and moderate severity shrub and high severity grass (p=0.0062). Aside from the clear significant differences between the unburned shrub and all other classes, the mixed model demonstrated the tendency for repellency to increase significantly with respect to burn severity within shrub areas; while grass areas did not exhibit significant changes in repellency until those areas experienced high severity burns, at which point the repellency significantly decreased.

Table 3.3. Least squares adjusted means of MDI values

Burn Severity	Vegetation	Least Squares Means Estimate (ml/min)	Standard Error
Unburned	Grass	5.3306	0.8433
Unburned	Shrub	9.8134	0.8744
Low	Grass	5.28	0.7185
Low	Shrub	6.5938	0.4221
Moderate	Grass	4.2496	0.7206
Moderate	Shrub	4.4456	0.3794
High	Grass	7.3788	0.6636
High	Shrub	5.8021	0.471

The decrease in initial repellency in the high severity grass areas, as measured by the MDI, is slightly misrepresented, however, because subsurface repellency was found at several points in high severity grass areas at or below a depth of 2 cm (Fig. 3.4). The subsurface repellency within the high severity grass areas was found near a depth of 2 cm with the WDPT.

Table 3.4. Results of Proc Mixed Analysis Difference of Least Square Means calculation. Adjusted P-values less than α = 0.05 in bold indicate significant class differences.

A. Burn Severity	B. Vegetation	C. Burn Severity	D. Vegetation	Estimate	Standard Error	Degrees Freedom	t-Value	Unadjusted P-value	Adjusted P
Unburned	**Grass**	**Unburned**	**Shrub**	**-4.4827**	**1.2148**	**71**	**-3.69**	**0.0004**	**0.0098**
Unburned	Grass	Low	Grass	0.05067	1.1079	71	0.05	0.9636	1
Unburned	Grass	Low	Shrub	-1.2632	0.943	71	-1.34	0.1847	0.8804
Unburned	Grass	Moderate	Grass	1.081	1.1092	71	0.97	0.3331	0.9766
Unburned	Grass	Moderate	Shrub	0.8851	0.9247	71	0.96	0.3417	0.9789
Unburned	Grass	High	Grass	-2.0482	1.0731	71	-1.91	0.0603	0.5497
Unburned	Grass	High	Shrub	-0.4715	0.9659	71	-0.49	0.627	0.9997
Unburned	**Shrub**	**Low**	**Grass**	**4.5334**	**1.1318**	**71**	**4.01**	**0.0002**	**0.0036**
Unburned	**Shrub**	**Low**	**Shrub**	**3.2195**	**0.9709**	**71**	**3.32**	**0.0014**	**0.0296**
Unburned	**Shrub**	**Moderate**	**Grass**	**5.5637**	**1.1331**	**71**	**4.91**	**<.0001**	**0.0001**
Unburned	**Shrub**	**Moderate**	**Shrub**	**5.3678**	**0.9532**	**71**	**5.63**	**<.0001**	**<.0001**
Unburned	Shrub	High	Grass	2.4345	1.0977	71	2.22	0.0298	0.3539
Unburned	**Shrub**	**High**	**Shrub**	**4.0113**	**0.9932**	**71**	**4.04**	**0.0001**	**0.0032**
Low	Grass	Low	Shrub	-1.3139	0.8334	71	-1.58	0.1193	0.7624
Low	Grass	Moderate	Grass	1.0303	1.0176	71	1.01	0.3148	0.9711
Low	Grass	Moderate	Shrub	0.8344	0.8126	71	1.03	0.308	0.9687
Low	Grass	High	Grass	-2.0989	0.9781	71	-2.15	0.0353	0.3966
Low	Grass	High	Shrub	-0.5222	0.8591	71	-0.61	0.5453	0.9987
Low	Shrub	Moderate	Grass	2.3442	0.8352	71	2.81	0.0065	0.1096
Low	**Shrub**	**Moderate**	**Shrub**	**2.1483**	**0.5676**	**71**	**3.79**	**0.0003**	**0.0073**
Low	Shrub	High	Grass	-0.785	0.7865	71	-1	0.3216	0.9733
Low	Shrub	High	Shrub	0.7917	0.6325	71	1.25	0.2147	0.913
Moderate	Grass	Moderate	Shrub	-0.1959	0.8144	71	-0.24	0.8106	1
Moderate	**Grass**	**High**	**Grass**	**-3.1292**	**0.9796**	**71**	**-3.19**	**0.0021**	**0.0414**
Moderate	Grass	High	Shrub	-1.5525	0.8609	71	-1.8	0.0756	0.6199
Moderate	**Shrub**	**High**	**Grass**	**-2.9333**	**0.7644**	**71**	**-3.84**	**0.0003**	**0.0062**
Moderate	Shrub	High	Shrub	-1.3566	0.6048	71	-2.24	0.028	0.3396
High	Grass	High	Shrub	1.5767	0.8138	71	1.94	0.0567	0.5305

Transect Repellency Experiment

The transect repellency experiment analyzed the infiltration of the soil at set lengths away from a burned brush. The values of the MDI (ml/min) at the lengths of 25, 50, 75, 100 and 200 cm are listed in Table 3.5. All the transects except transect 1 on October 15, demonstrated a general increase in infiltration as distance from the burned shrub increased (Fig. 3.5A). In the case of transect 1 on October 15, the soil was apparently disturbed at 25 cm, presumably from animals, allowing infiltration at that location. The transect exhibited little variation in infiltration, ranging from 3.7 ml/min to 5.0 ml/min. The values of transects 2, 3, and 4 on Oct. 15 had similar values of infiltration at 25 cm, ranging from 1.0 ml/min to 1.7 ml/min. Infiltration in transect 2 rose sharply to 4.0 ml/min at 50 cm, then to 6.0 ml/min at 100 cm, before dropping down to 4.0 cm at 200 cm. Transect 3 demonstrated a general increase in infiltration from 25 cm to 200 cm, with the values steadily climbing from 1.3 ml/min to 4.0 ml/min. Transect 4 rose sharply between 25 cm and 75 cm, from 1.0 ml/min to 4.7 ml/min, then dropped back down to 3.3 ml/min at 100 cm, where the infiltration was constant to 200 cm.

The transect values from October 21 (Fig. 3.5B) demonstrated analogous increases in infiltration with distance. All of the transects behaved similarly when they were within the coppice area (soils that had were beneath the canopy of the brush prior to the fire). Typically, the soil was blackened beneath the canopy of the shrub, due to the heat and flames enveloping it. Outside of this area, soil qualities were likely not as affected from the heat of the flames. For example, in the case of transect 3, the edge of canopy was at 25 cm, and the remaining infiltration measurements were within 2 ml/min. This

experiment demonstrated that water repellency in rangeland areas can be assessed based on the distance between shrubs, or the size of the interspaces.

The October 21 transect measurements were supplemented with measurements of field spectrometry at distances of 25 cm, 50 cm and 100 cm, radially from the burned brush (Fig. 3.6A-C). For all three transects, the 25 cm location exhibited the lowest reflectance, beginning near 5% in the visible portion of the spectrum, and consistently staying below the other reflectance values into the NIR spectrum portion. The anomalies in reflectance near 1.4 and 2.7 µm are due to atmospheric water absorption.

Table 3.5. MDI values (ml/min) at set transect lengths, Oct. 15 and Oct. 21 plots.

	15-Oct				21-Oct		
	Plot 1	Plot 2	Plot 3	Plot 4	Plot 1	Plot 2	Plot 3
25 cm	4	2	2	2	1	2	2
25 cm	7	1	1	1	1	5	3
25 cm	4	2	1	0	3	4	5
Average	**5.0**	**1.7**	**1.3**	**1.0**	**1.7**	**3.7**	**3.3**
50 cm	4	5	1	2	4	5	5
50 cm	4	3	0	2	4	4	5
50 cm	4	4	3	3	4	5	3
Average	**4.0**	**4.0**	**1.3**	**2.3**	**4.0**	**4.7**	**4.3**
75 cm	3	5	3	5	5	7	4
75 cm	4	4	1	5	4	4	4
75 cm	4	4	1	4	3	5	4
Average	**3.7**	**4.3**	**1.7**	**4.7**	**4.0**	**5.3**	**4.0**
100 cm	5	7	3	4	6	5	5
100 cm	6	6	2	3	6	5	5
100 cm	4	5	3	2	6	5	5
Average	**5.0**	**6.0**	**2.7**	**3.0**	**6.0**	**5.0**	**5.0**
200 cm	4	3	4	2	5	8	5
200 cm	6	5	3	4	6	8	4
200 cm	4	4	5	4	6	10	3
Average	**4.7**	**4.0**	**4.0**	**3.3**	**5.7**	**8.7**	**4.0**
Canopy Edge	**50**	**50**	**75**	**50**	**100**	**50**	**25**

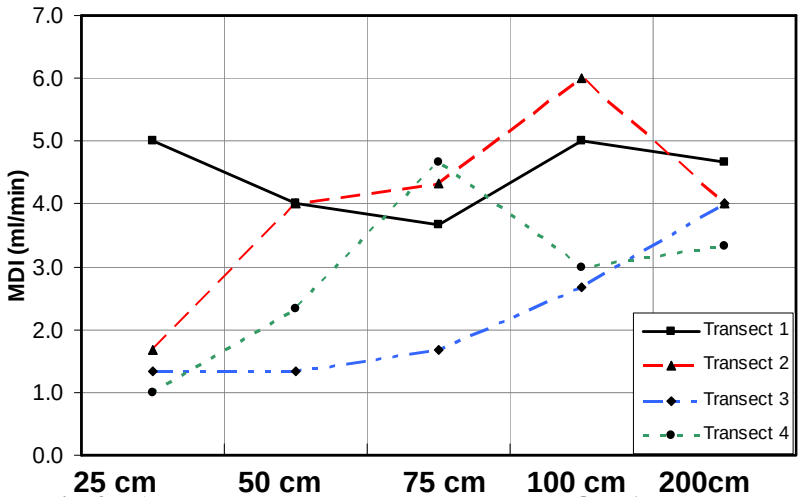

Fig. 3.5 A. MDI values at set transect lengths, Oct. 15 plot

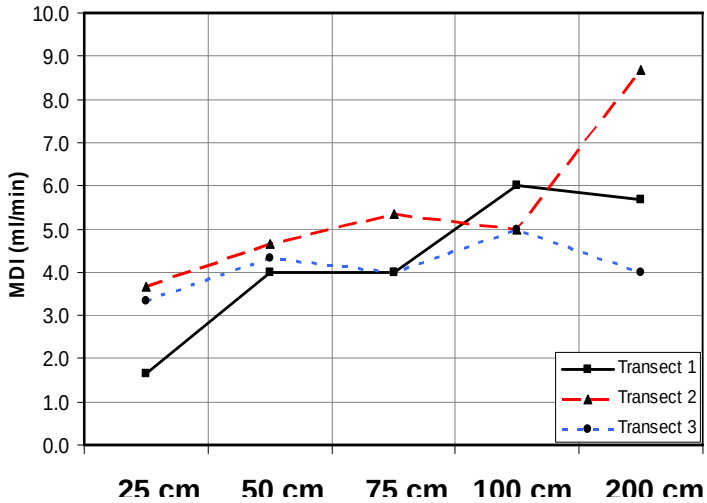

Fig. 3.5 B. MDI values at set transect lengths, Oct. 21 plot

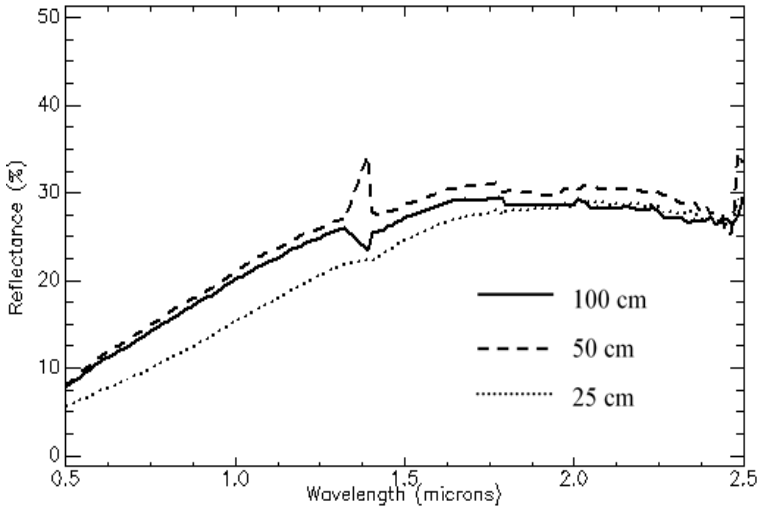

Fig. 3.6 A. Transect 1, spectral signatures at sampled intervals

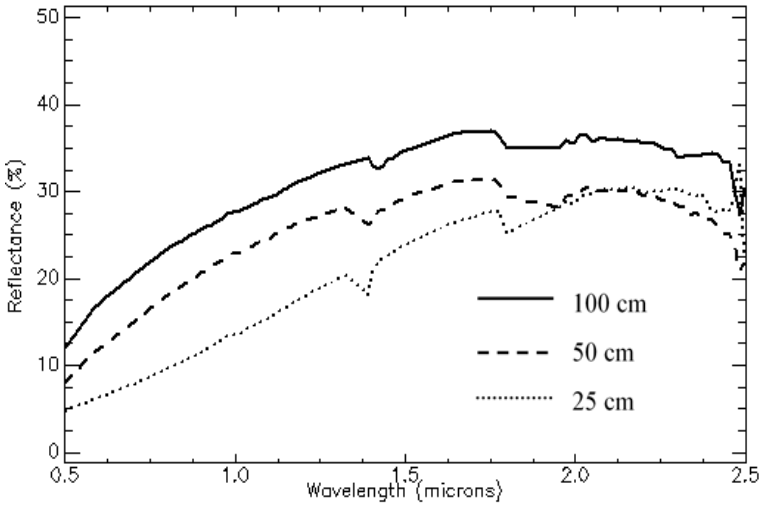

Fig. 3.6 B. Transect 2, spectral signatures at sampled intervals

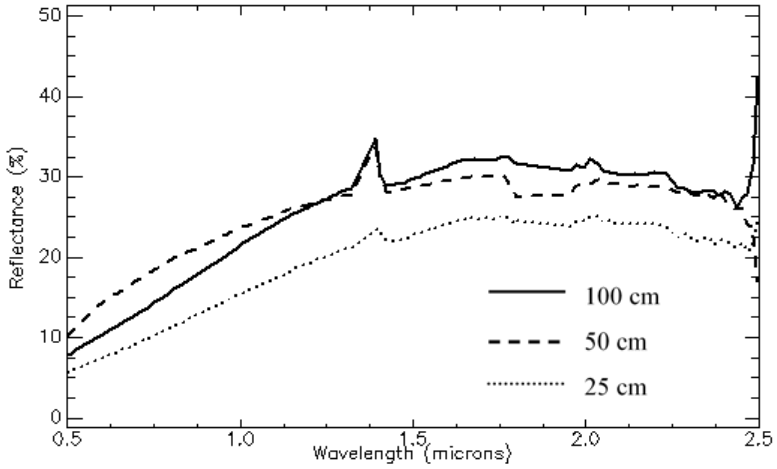

Fig. 3.6 C. Transect 3, spectral signatures at sampled intervals

Field Spectroscopy

Endmember signatures collected with the field spectrometer included unburned grass and shrubs (sagebrush), low severity grass and shrubs (sagebrush), moderate severity shrubs (sagebrush), high severity grass and shrubs (sagebrush), gravel, basalt rock, and bare ground (Fig. 3.7A, B). Bare ground areas included patches of soil exhibiting high reflectance, with no vegetation, and little to no litter cover. The endmembers portraying the highest reflectance were the grassy areas (Fig. 3.7A), including the unburned grass, which had the highest reflectance in the NIR, and the low and high severity grass. Other endmembers exhibiting high reflectance were the bare ground, rock and gravel areas. The signatures that exhibited the least reflectance were the unburned and burned sagebrush (Fig. 3.7B) because of the reduced reflectance among the leaves of the unburned shrubs, and the blackened soil from the burned shrubs, respectively. All signatures exhibit spikes in reflectance near 1.4, 1.9, and 2.7 μm because of the atmospheric noise and water absorption at those wavelengths. The signature of bare ground (not pictured) displayed excess noise across the entire signature, due to the extremely high albedo, or increased reflectance among the entire spectrum of the bright, bare ground.

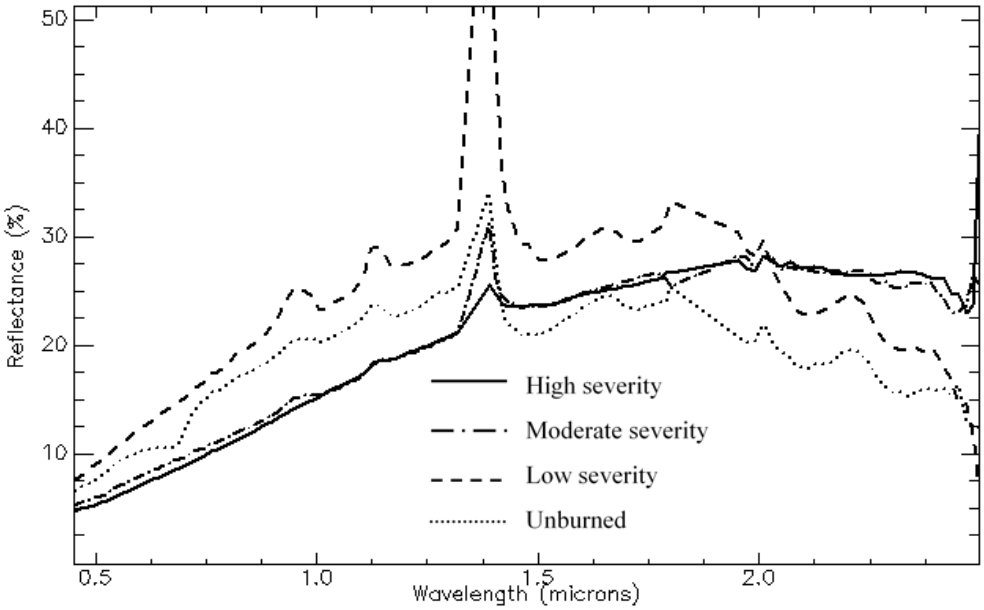

Figure 3.7A. Field collected spectral signatures of high severity shrub burn (solid line), moderate severity shrub burn (dash-dot line), low severity shrub burn (dashed line), unburned shrub (dotted line).

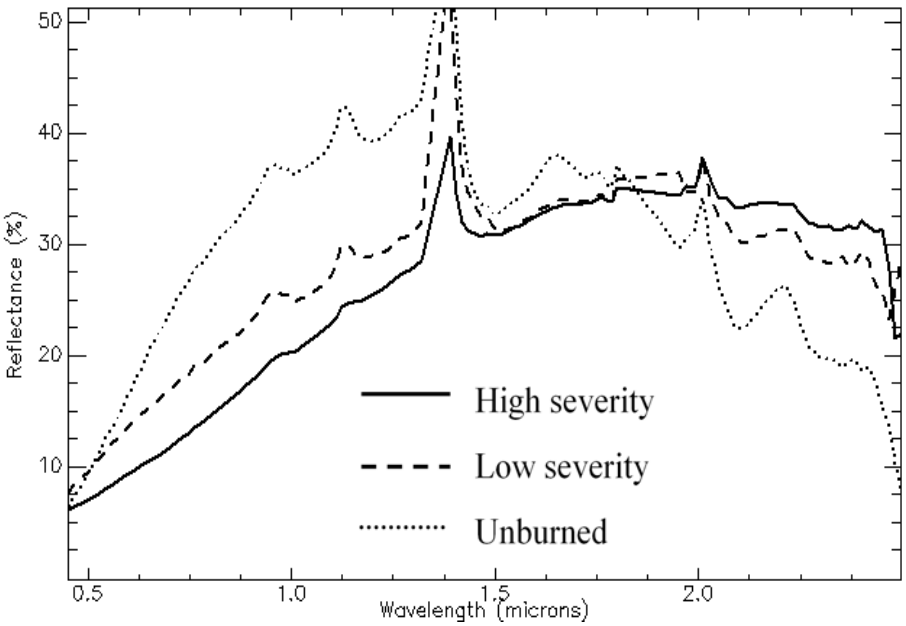

Fig. 3.7B. Field collected spectral signatures of high severity grass burn (solid line), low severity grass burn (dashed line), unburned grass (dotted

Spectroscopy Results

Unsupervised Classification of Burn Severity

The ISODATA unsupervised classification was performed on the masked MNF-transformed image 6. The unsupervised classification method detected 7 mean classes among the image, given a user specified input range of 5-10 classes. After the image was classified, a projection was applied to it, and the ground truth training plots were overlaid to match the classes (Fig. 3.8). The visual assessment of the classification with the ground truth plots indicated that the unsupervised classification separated the classes primarily among high severity shrub and moderate severity shrub, and high severity grass and low severity grass/shrub. The burn severity that was best separated among the image was high severity grass. Moderate severity shrub areas were confused and classified with areas of high severity shrub. The classifier also mixed areas of low severity grass with low severity shrub. A confusion matrix error assessment was not conducted on the class image because the ground truth regions of interest (ROI's) were used to identify the classes and it was evident that the accuracy would be low within each class because more than one burn severity ground truth endmember was present. As a first look at the image, the unsupervised classification demonstrated that the image could be generally classified among high and low burn severity areas based on the separability of the MNF-transformed spectra.

Supervised Classification of Burn Severity

The Spectral Angle Mapper (SAM) and mixture tuned matched filtering (MTMF) algorithms were conducted on the image to classify the burn severity of the study area. The results of the two classification techniques were displayed and compared to determine the most suitable method, and confusion matrices were computed to assess their accuracy. The SAM confusion matrices, computed in ENVI, calculated the total pixels within the ground truth reference plots that fell within each burn severity class. The error matrices computed for the MTMF were conducted manually, and indicated the presence or absence of classified pixels within a sample plot. Therefore, the cell totals of the MTMF error matrix were much lower, because they only equaled the number of sample plots input for the matrix, and not the total pixels within the plots.

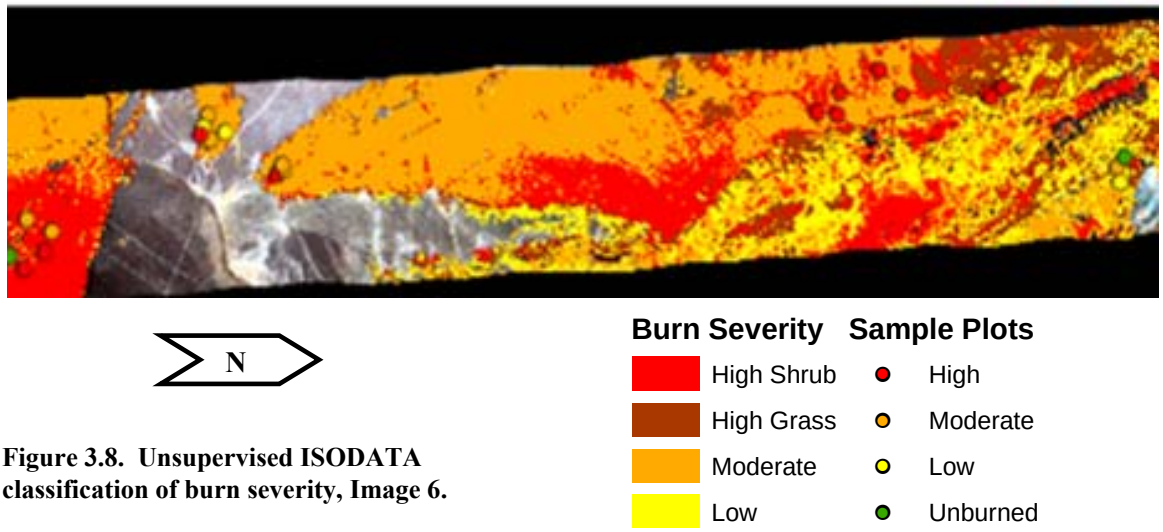

Figure 3.8. Unsupervised ISODATA classification of burn severity, Image 6.

Spectral Angle Mapper (SAM) Classification

The first burn severity classification utilized the SAM algorithm (Fig. 3.9A); the SAM designates spectral classes within the image based on a user-specified angle set around a reference spectra in n-dimensional space. The reference endmembers used in the SAM classification were the extreme pixels found and designated to a burn severity class through n-dimensional visualization. A maximum spectral angle of 1 radian was set for each endmember as designation of that burn severity class. After the algorithm was computed and the extreme pixel endmember classes representing the same severity classes were combined, a confusion matrix was conducted (Tables 3.6 A, B). The confusion matrix was built using the field-assessed sample plots (Fig. 3.9B) with their assigned burn severity as ground truth. The confusion matrix calculated an overall accuracy of 72%. A kappa coefficient of 0.65 indicated a moderate agreement that the classification was better than a classification resulting strictly from chance agreement.

The producer's and users accuracies indicate acceptable values for all of the classes, except for the high (39% and, 66%, respectively) and moderate (54% and 39%, respectively) severity shrub classes. It is important to examine the producer's and users accuracies in an error matrix report, because examining the overall accuracy alone can be misleading. Although the overall accuracy of the error matrix is quite high, the low producer's and users accuracies for high and moderate severity shrub areas indicate that the SAM had trouble differentiating moderate severity shrub areas from high severity shrub areas, and is supported by the spectral signatures obtained with the field spectrometry which recorded nearly identical signatures for the high and moderate shrub areas (Fig. 3.7B). Low severity grass areas were also confused with bare ground areas, because of the high reflectance in both areas. No moderate severity grass areas were detected with the SAM. For the purpose of classifying soil reflectance exhibiting water repellency, it was acceptable for high and moderate shrub areas to be confused in the classification, because field data statistics indicated no significant difference in repellency values between moderate severity shrub areas (mean MDI = 4.45 ml/min) and high severity shrub areas (mean MDI = 5.8 ml/min). The moderate and high severity areas that were confused were combined for a second accuracy assessment, and the overall accuracy increased to 78%, and producer's and users accuracies for the merged high and moderate severity shrub area increased to 81% and 87%, respectively, and the Kappa value increased to 0.72 (Table 3.7).

Table 3.6A. SAM burn severity classification error matrix and results

Class (pixels)	Ground Truth (pixels)						
	Bare Ground	**High Severity Shrub**	**High Severity Grass**	**Low Severity Shrub**	**Low Severity Grass**	**Moderate Severity Shrub**	**Total**
Unclassified	24	6	8	4	130	19	191
Bare Ground	**271**	6	1	0	0	1	279
High Severity Shrub	0	**52**	0	8	0	19	79
High Severity Grass	0	0	**107**	0	0	2	109
Low Severity Shrub	12	6	0	**123**	0	3	144
Low Severity Grass	56	0	0	0	**406**	0	462
Moderate Severity Shrub	3	63	0	16	0	**52**	134
Total	366	133	116	151	536	96	**1398**
Overall Accuracy = 72% (1011/1398)							
Kappa Coefficient = 0.65							

Table 3.6B. SAM burn severity classification producer's and users accuracy

Class	Commission (%)	Omission (%)	Producer's Accuracy (%)	Users Accuracy (%)
Bare Ground	2.87	25.96	74.04	97.13
Low Severity Grass	12.12	24.25	75.75	87.88
High Severity Grass	1.83	7.76	92.24	98.17
High Severity Shrub	34.18	60.9	39.1	65.82
Low Severity Shrub	14.58	18.54	81.46	85.42
Moderate Severity Shrub	61.19	45.83	54.17	38.81

Table 3.7. Producer's and users accuracies after merging the SAM classes of moderate and high burn severity, overall accuracy 78%, K = 0.72

Class	Commission (%)	Omission (%)	Producer's Accuracy (%)	Users Accuracy (%)
Bare Ground	2.87	25.96	74.04	97.13
Low Severity Grass	12.12	24.25	75.75	87.88
High Severity Grass	1.83	7.76	92.24	98.17
High/Moderate Severity Shrub	12.68	18.78	81.22	87.32
Low Severity Shrub	14.58	18.54	81.46	85.42

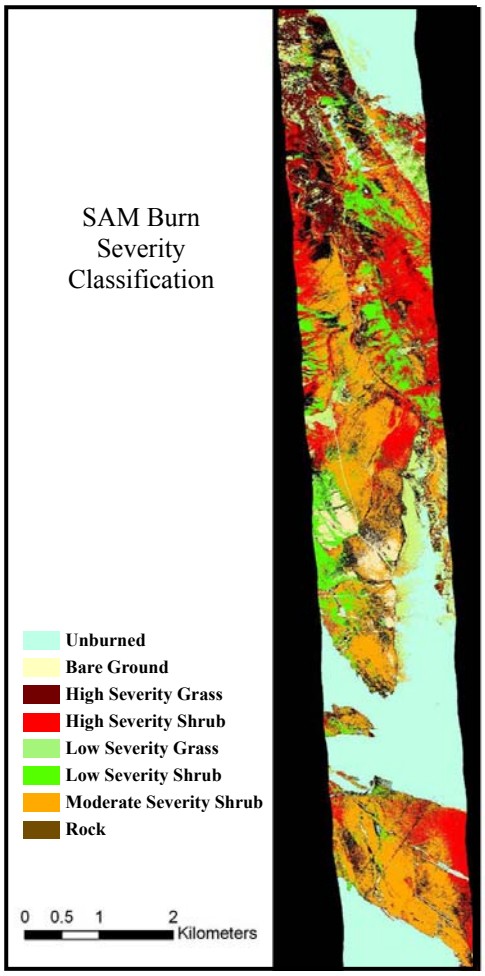

Fig 3.9A. SAM burn severity classification

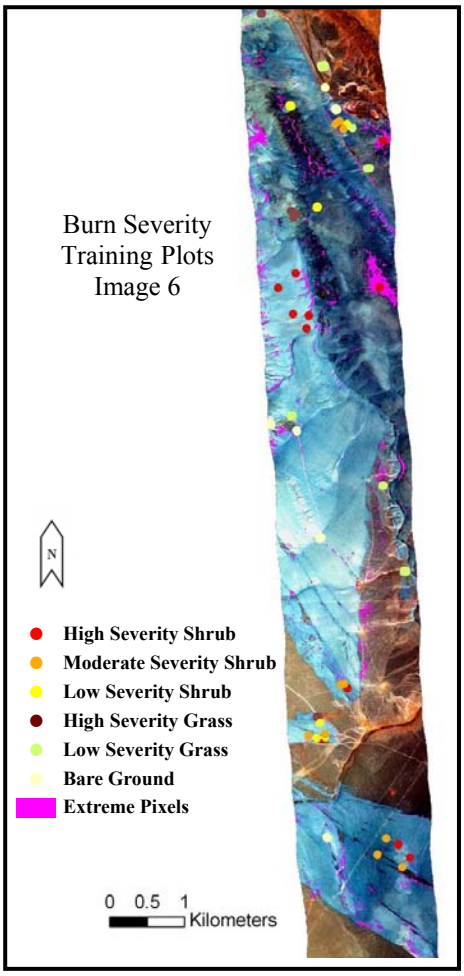

Figure 3.9B. Burn severity training plots overlaid on false color composite of image 6

Mixture Tuned Matched Filtering (MTMF) classification

The next burn severity classification used the MTMF method. MTMF classifications of burn severity were computed on image 6, using input spectra from the extreme pixels representing all of the burn severity categories, and bare ground. The MF scores were plotted in the 2-D scatter plot (as described above and in Fig. 2.22A-C) and after interactively assessing the locations of pixels within the scatter plot, band thresholds were determined for each endmember class in the MTMF (Table 3.8). Ideally, the lower value of the MF thresholds represent the percent abundance of a pixel that is designated to represent the endmember being mapped, and the infeasibility threshold represents the values of the output infeasibility image above which the classified pixels are considered false positives. Figure 3.10 (A-G) illustrates the MTMF image for each burn severity class, and the determined MF score and infeasibility value threshold, as listed in Table 3.8. After the MF Score and infeasibility values were thresholded for each burn severity class, a presence/absence error matrix was calculated (Table 3.9A-D). Because the MTMF classification technique is basically an identifier of one specific endmember class with respect to every other material in the image, the most suitable method of assessing the accuracy of the classification is by assessing the presence or absence of the endmember material being mapped with respect to a ground truth reference location.

Table 3.8. MF Score and infeasibility thresholds for the MTMF burn severity classification, Image 6

Endmember Class	MF Score Threshold	Infeasibility Threshold
High Severity Shrub	0.65 - 2.00	> 20
Moderate Severity Shrub	0.85 - 2.00	> 20
Low Severity Shrub	0.50 – 1.50	> 20
High Severity Grass	0.50 – 2.00	> 20
Low Severity Grass	0.50 – 1.50	> 15
Bare Ground	0.40 - 2.00	> 20

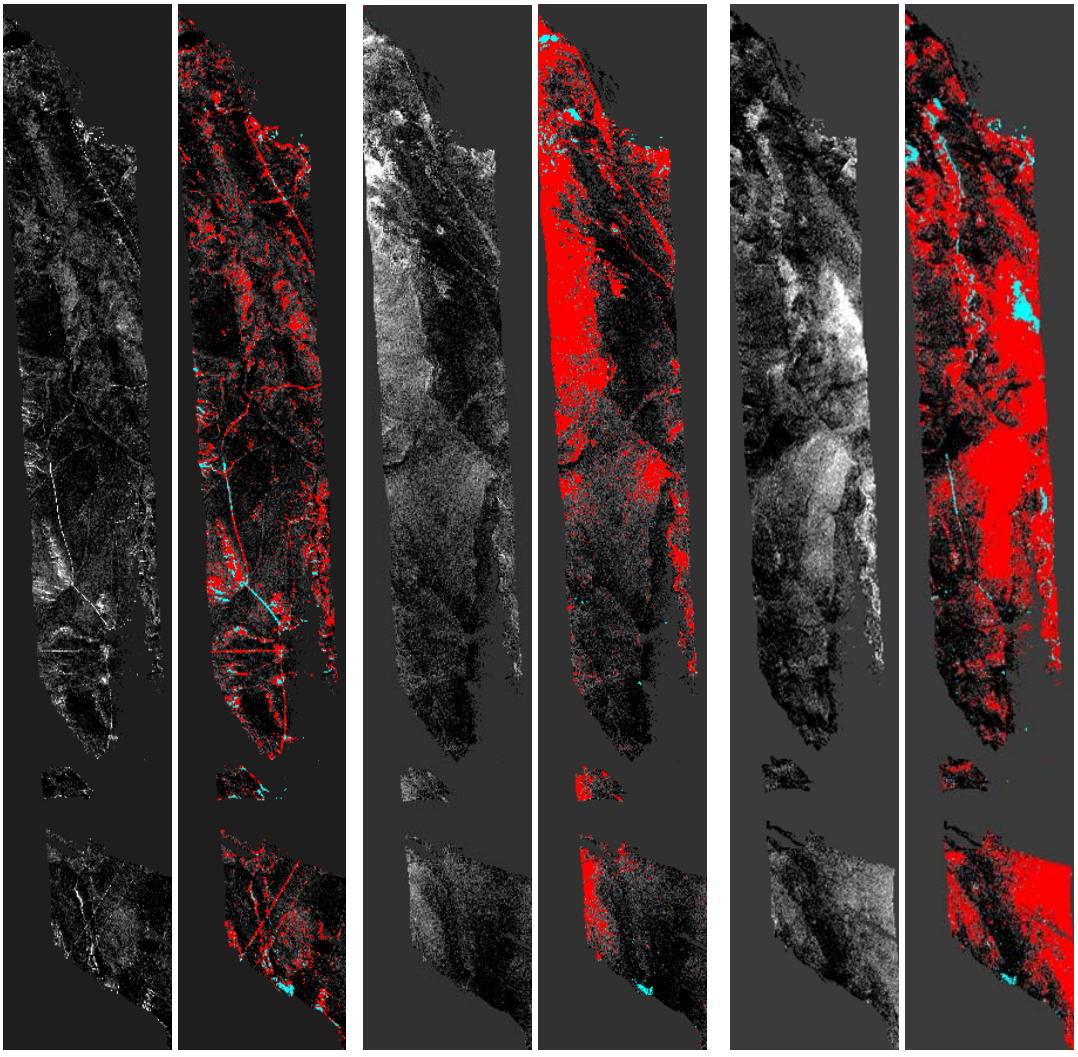

A. Bare Ground **B.** High Severity Grass **C.** High Severity Shrub

Figure 3.10, A-C (above) & D-F (next page). MTMF burn severity classification output images (left image) and thresholded MF Scores in red and infeasibility scores in cyan (right image).

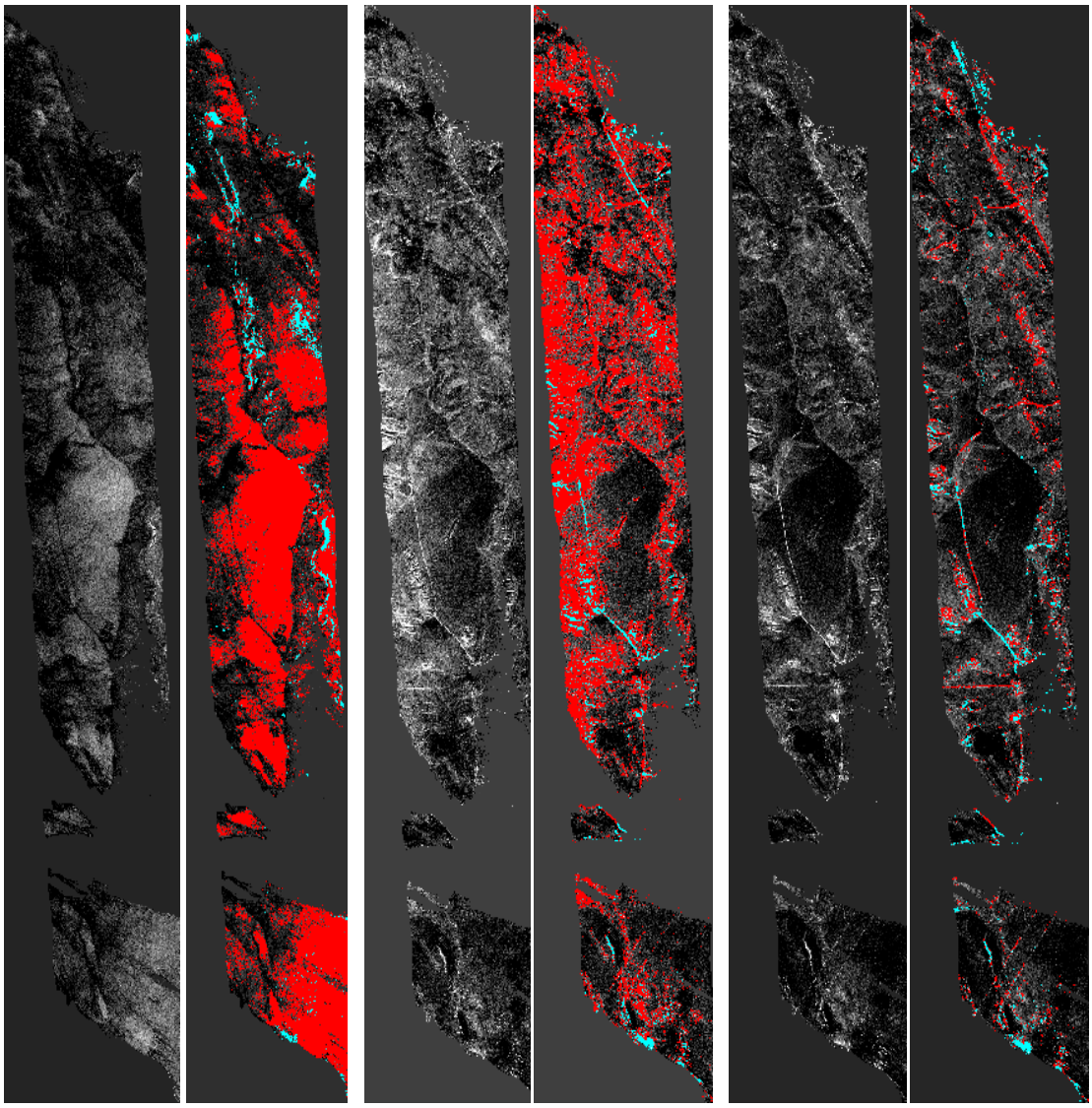

D. Moderate Severity Shrub

E. Low Severity Shrub

F. Low Severity Grass

Table 3.9 A-D. Presence/Absence matrices for MTMF classification of burn severity (indicating plots within or outside of classified areas).

A. Class 1: High Severity Shrub			
MTMF Class	**Reference Positive**	**Reference Negative**	**Users Accuracy**
Classified Positive	**6**	4	60%
Classified Negative	3	**5**	62.50%
Producer's Accuracy	66%	55%	**61%**

B. Class 2: Moderate Severity Shrub			
MTMF Class	**Reference Positive**	**Reference Negative**	**Users Accuracy**
Classified Positive	**5**	4	55%
Classified Negative	5	**4**	44%
Producer's Accuracy	50%	50%	**50%**

C. Class 3: Low Severity Shrub			
MTMF Class	**Reference Positive**	**Reference Negative**	**Users Accuracy**
Classified Positive	**2**	4	33%
Classified Negative	2	**4**	33%
Producer's Accuracy	50%	50%	**50%**

D. Class 4: High Severity Grass			
MTMF Class	**Reference Positive**	**Reference Negative**	**Users Accuracy**
Classified Positive	**4**	3	57%
Classified Negative	0	**5**	100%
Producer's Accuracy	100%	63%	**75%**

The MTMF display and accuracy is dependent on thresholding; while smaller MF score thresholds increase the accuracy of endmember presence in a pixel, the displayed abundance of the endmember is increased, resulting in overlapping of classes. The overall accuracies of the MTMF classes (bottom right values in Table 3.9 A-D) are a quotient of the correctly classified reference plots with respect to the total reference plots.

The cell totals of the presence/absence accuracy assessment demonstrate low values in comparison to the cell totals of the traditional confusion matrix performed on the SAM, because the cell values here represent the number of ground-assessed reference plots present or absent in the classification, while the values of the SAM error assessment represent total pixels present within an endmember class. Plot totals were used in the presence/absence error matrices, instead of pixel totals, because the presence/absence error matrix was conducted manually (by the user), while the SAM error matrix was conducted in ENVI, allowing the software to accurately total the number of pixels present in a class. An error matrix was not conducted for the class of low severity grass because there were too few ground truth training sites for input, and the classified area was minimal (Fig. 3.10F), as the endmember was mainly detected around the fringes of the burn area, and moderate severity grass was not classified. The error matrices for the MTMF-classified burn severity classes demonstrate the accuracy of the classification based on the presence or absence of ground-referenced plots within or outside of the classified area.

Supervised Classifications of Water Repellency

After identifying soils in the field that exhibited the presence of soil water repellency, their spectral signatures were used as training endmembers to classify soil water repellency with the SAM and MTMF

classification algorithms. The spectral endmembers used as training in the classifications represented strong and moderate fire-induced water repellency, and were located in moderate and high burn severity areas. The average spectra were obtained from two plots each of strong and moderate soil water repellency that had been identified in the field, and had consistent levels of repellency throughout the plots. The results of the two classification techniques were displayed and compared to determine the most suitable method, and accuracy assessments were conducted on them.

Table 3.10A. Confusion matrix of SAM water repellency classification, Image 6 (pixels)
Overall Accuracy = 51% Kappa = 0.31

Class (pixels)	Strong Repellency	Moderate Repellency	Total
Unclassified	40	0	40
Strong Repellency	15	0	15
Moderate Repellency	23	51	74
Total	78	51	129

Spectral Angle Mapper (SAM) Classification

The first SAM classification was conducted with a maximum spectral angle of 0.65 radian for accepting spectra of that endmember class, and was applied to both endmembers (strong and moderate repellency). The initial classification result failed to classify at least 50% of the image, and the overall accuracy was below 25%. To increase the amount of area being classified, as well as the accuracy, the SAM classification was conducted again with a maximum angle of 0.75 radian for each endmember. The results categorized 52% of the burned area as having moderate water repellent soils, 23% as having strong water repellent soils, and 25% of the image was unclassified (Fig. 3.11). A confusion matrix was calculated on the SAM using the ground locations of 8 moderate water repellent sample plots and 9 strongly water repellent sample plots (not including those input for training data), and the resulting overall accuracy was 51% (Table 3.10A, B). The low overall accuracy and the Kappa value of 0.31 suggest the SAM may not be the best method for classifying soil water repellency.

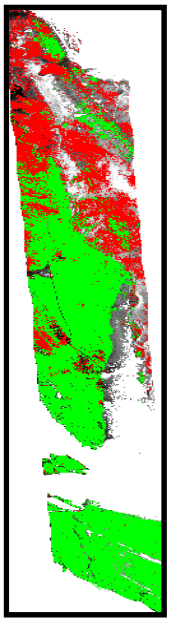

Figure 3.11. SAM classification of strong (red) and moderate (green) water repellent soils, Image 6.

Table 3.10B. Commission and omission errors and producer's and users accuracies for SAM water repellency classification, Image 6

Class	Commission Error (%)	Omission Error (%)	Producer's Accuracy (%)	Users Accuracy (%)
Strong Repellency	0	80.77	19.23	100
Moderate Repellency	31.08	0	100	68.92

MTMF Classification of Water Repellency

The MTMF algorithm was conducted on the imagery to classify moderate and high water repellent soils. The same training spectra were used for the MTMF classification as was used in the SAM classification. The MF scores and infeasibility values of each mapped endmember were plotted in a 2-D scatter plot (Fig. 3.12) to determine the thresholds of the pixels' endmember abundance and false positive values that would be displayed. After examining the 2-D scatter plot, a MF score threshold of 1-2 was chosen for display the pixels with 100% abundance of the soil water repellency endmember (Fig. 3.12, in red). For the strong water repellency classification, pixels with infeasibility scores greater than 16 were determined to be areas most likely to have false positives, most of which were high reflectance bare ground areas.

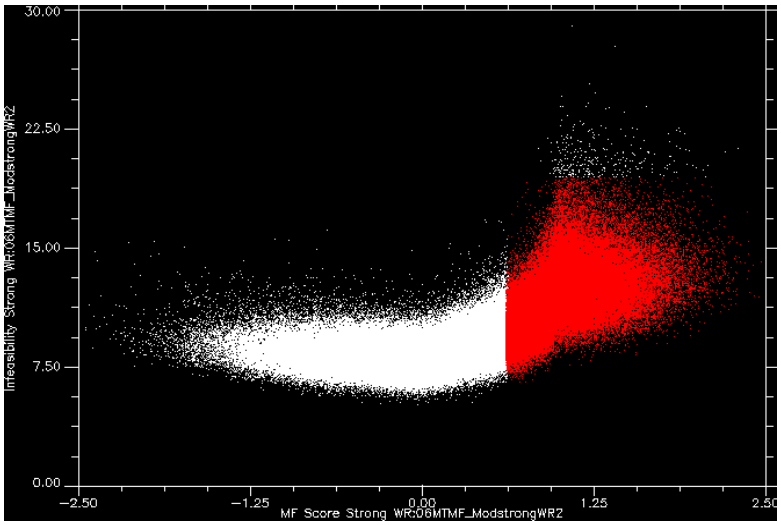

Figure 3.12. 2-D scatter plot of strong water repellency MF scores (x-axis) vs. Infeasibility scores (y-axis). Red area depicts thresholded pixels with MF score (pixel abundance) of 0.5-2.0, and infeasibility scores less than 20, indicating values above 20 to be false positives.

After the pixel thresholds were determined and displayed as ROI's, the ground truth sample plots were overlaid on the image in order to determine the accuracy of the classification. A presence/absence matrix was conducted using 9 sample plots that displayed high water repellency (presence endmembers), and 8 sample plots that displayed moderate water repellency (absence endmembers). The error matrices were conducted for the moderate and high water repellency at MF score thresholds of 0.3-2.0, 0.5-2.0, and 1.0-2.0 (Table 3.11A-C; Table 3.12A-C, respectively), representing endmember abundance within a pixel of 30%, 50%, and 100%, respectively.

For the described image, MF Score thresholds (subpixel abundance of endmembers) of 100% abundance, 50% abundance, and 30% abundance all indicated an overall accuracy of 65% (Table 3.11A-C). Within the threshold ranges of 100%

and 50% abundance, the producer's accuracy of reference positives, or training sites present in the positive classification area was 55%, while the accuracy of negative reference sites not being present was higher, at 75%. When the threshold was increased to include 30% pixel abundance, the positive reference accuracies increased to 78%, while the accuracies of negative reference sites decreased to 50%. The change in producer's accuracy indicates that with the increase in subpixel abundance (or a lower MF score threshold), there is a higher likelihood that pixels classified as strong water repellency will be overlaid by ground truth plots representing strong water repellency as well.

Table 3.11A-C. Presence/absence matrices for MTMF classification of strong water repellency (indicating plots within or outside of classified areas).

A. MF score threshold = 1.0-2.0 (88,321 pixels classified at this threshold)			
MTMF Class	**Reference Positive**	**Reference Negative**	**Users Accuracy**
Classified Positive	5	2	71%
Classified Negative	4	6	60%
Producer's Accuracy	55%	75%	**65%**

B**. MF score threshold = 0.5-2.0 (191,399 pixels classified at this threshold)**			
MTMF Class	**Reference Positive**	**Reference Negative**	**Users Accuracy**
Classified Positive	5	2	71%
Classified Negative	4	6	60%
Producer's Accuracy	55%	75%	**65%**

C**. MF score threshold = 0.3-2.0 (542,403 pixels classified at this threshold)**			
MTMF Class	**Reference Positive**	**Reference Negative**	**Users Accuracy**
Classified Positive	7	4	64%
Classified Negative	2	4	67%
Producer's Accuracy	78%	50%	**65%**

For the MTMF classification of moderate water repellency, 8 positive references and 9 negative references were input for validation of the high repellency classification, and MF Score thresholds of 100% abundance, 50% abundance, and 30% abundance indicated overall accuracies of 65%, 35% and 35%, respectively. The overall accuracy was higher for the original MF Score threshold of 1.0 – 2.0 primarily because no negative references were among the 5,942 pixels in that threshold. When the MF score threshold was reduced to 0.5 or 0.3 (50% or 30% abundance), the overall accuracies decreased; this was because the total number of thresholded pixels substantially increased, presenting negative reference points among them. Although the MTMF classifications of water repellency did not have strong accuracies for verification, it's output is an accurate representation of water repellency across the study area because it demonstrates the discontinuous nature of soil water repellency in burned rangeland areas.

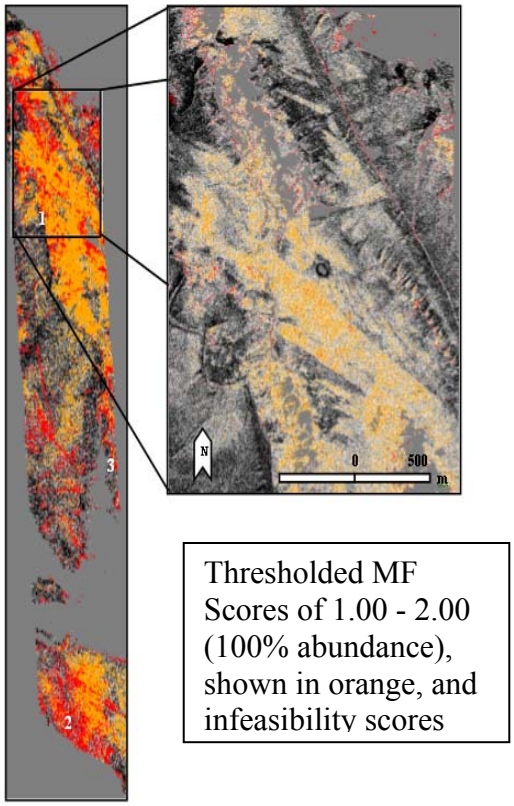

Figure 3.13. MTMF classification of high water repellency, Image 6

Table 3.12 A-C. Presence/Absence matrices for MTMF classification of moderate water repellency

A. MF score threshold = 1.0-2.0 (5942 pixels)			
MTMF Class	**Reference Positive**	**Reference Negative**	**Users Accuracy**
Classified Positive	2	0	100%
Classified Negative	6	9	60%
Producer's Accuracy	25%	100%	**65%**

B. MF score threshold = 0.5-2.0 (169,910 pixels)			
MTMF Class	**Reference Positive**	**Reference Negative**	**Users Accuracy**
Classified Positive	3	6	33%
Classified Negative	5	3	38%
Producer's Accuracy	38%	33%	**35%**

C. MF score threshold = 0.3-2.0 (393,151 pixels)			
MTMF Class	**Reference Positive**	**Reference Negative**	**Users Accuracy**
Classified Positive	3	6	33%
Classified Negative	5	3	38%
Producer's Accuracy	38%	33%	**35%**

DISCUSSION AND CONCLUSIONS

This study presents a technique for mapping burn severity and fire-induced soil water repellency in a burned rangeland area of the Intermountain West. The utilization of high spatial and spectral resolution imagery proved crucial for this project due to the lack of spectral separability across the burned portion of the study area. The SAM burn severity classification detected classes of low, moderate and high severity shrub areas, and low and high severity grass with an overall accuracy of 72%; the MTMF algorithm detected water repellent soils in over 30% of the burned area with an overall accuracy of 65%. Additionally, the field evaluations demonstrated pertinent methods for assessing burn severity and water repellency in burned rangelands, and analytical results provide valuable insight to the dynamics of rangeland fire related to pre-fire vegetation cover and vegetation type. The image-wide classification of burn severity and detection of water repellent soils is useful for locating areas susceptible to increased sedimentation, and in need of treatment or preventative measures.

The primary difficulty of assessing burn severity in rangelands is the apparent homogeneity throughout many areas of the burn. Despite the fact that native rangeland vegetation often exhibits ample spacing of bare ground interspaces among shrubs and native bunch grasses, annual grasses like the invasive cheatgrass often grow within them. The presence of annual grass among interspaces serves as a bridge in the case of fire, allowing it to burn rapidly through the interspaces, reaching other coppice microsites more readily. This dynamic of rangelands often results in very uniform burns throughout large areas, of which a severity description is ambiguous. In the case of rangelands that have been previously burned, the uniformity of successive burns is much more pronounced, as annual grasses have become more prevalent and shrubs are often immature, and the low fuel load is wholly incinerated.

In this study, the time lag between the fire and the image acquisition and field study was approximately one month, and may have attributed to errors in the field assessment and remote sensing classification of burn severity. A more accurate assessment of burn severity might have been possible had the sampling begun closer to the fire date. Local weather records indicated only 1.2 mm rainfall during the month of August (NCDC, 2005). Disturbance by wind and aeolian transport was more likely than precipitation, however, but not quantifiable.

The important contributions of the field analyses were the indications of water repellency variability among various burn severity classes. The significant differences of repellency values between all the burn severity classes of shrub, as well as unburned shrub, indicate a general increase in water repellency among shrub areas as burn severity increases and a drop in repellency after being burned at high severity. This indicates that water repellency is likely to reduce in a high severity burn due to the destruction of aliphatic hydrocarbons by excess heat. The repellency observed in grass areas was consistently strong in unburned, low and moderate severity areas, but decreased significantly in high severity areas, and is indicative of natural water repellency in grass areas, often noted even in the absence of fire (Pierson et al., 2001). When grass is burned at high severity, however, the organic matter inducing the natural water repellency is seemingly incinerated along the surface, resulting in non-water repellent soil. Several of the high severity grass areas exhibited subsurface water repellency, however, at a depth of 2 cm indicative of a downward heat gradient, often noticed in high temperature fires. The presence of subsurface water

repellent layers, as well as the behavior or water repellency in respect to changes in fire severity is supportive of DeBano's (2000) findings. Because grass areas have considerably less vegetation prior to fire, fire-induced water repellency within those areas is not expected to be as high as in shrub areas. This is contradicted, however, by the observation of the lowest mean MDI being in moderately burned grass (MDI = 4.31 ml/min). This value is not an anomaly, however, and is probably due to the fact that, as stated, the grass areas demonstrate natural repellency in the absence of fire. The fact that the mean MDI value of the moderate severity grass is not significantly different from low severity or unburned grass areas also indicates that the soil is not greatly affected by moderate burn severity. Conversely, the mean MDI value of moderate severity shrub areas (MDI = 4.47 ml/min), which is nearly identical to that of moderate severity grass, is more indicative of fire-induced water repellency, because of its significant difference from other unburned, low, and high severity shrub areas. The statistical analysis of the field data was beneficial for this study because it indicated relationships between burn severity and water repellency that proved useful in the subsequent remote sensing analysis classification, and also provided insight to the dynamics of rangeland wildfire effects.

The use of the MDI for assessing water repellency is valuable because it indicates the degree of repellency among a soil in a less subjective manner than the WDPT. In the case of subsurface soil water repellency, however, the MDI results may be misleading if the above layer of penetrable soil is not removed. The WDPT values served to indicate which MDI values represented very strong repellency. Even though the correlation of the MDI with the WDPT times was not strong, a slight inverse relationship was present between the two. Observations of the WDPT indicated that the water drop usually soaked in immediately, or was present for longer than 360 s. Even though the threshold of the WDPT at 360 s seemed to censor its correlation with the MDI by clustering the highly repellent measurements at that time value, a slight trend was discovered when the two methods were tested against each other. Even after removing the values at 360 s, however, the methods' relationship did not improve, suggesting that the perceived censoring of the threshold values did not have as great an effect on the validity of the WDPT results. Longer observations of the WDPT would have resulted in a more normal distribution of the time values, and likely a greater correlation. Other methods have been used for assessing fire-induced water repellency that account for preferential flow within the soil. The use of rain-simulators and trench analysis (Pierson et al., 2003) assesses sub-surface water repellency, and provides an indication of its spatial variability across an area, as opposed to the point scale measurement by the MDI. The dry conditions of the study area and logistical incompatibility deemed the use of rain simulators infeasible for this project. A comparison of the rain simulator and trench analysis with MDI measurements would be an important contribution to water repellency research.

The inception of soil water repellency across burned rangelands is largely dependent on the pre-fire vegetation. In the discontinuous vegetation distribution of rangelands, the interspaces are not nearly as affected by fire and water repellency as the areas where shrubs are rooted. The variability among interspace microsites is also confounded, however, by the amount and density of pre-fire vegetation, which affects the severity and temperature of the fire, and in turn the formation of water repellent soil layers. The presence and amount of biomass differed across our study area, which in turn affected the distribution and inception of soil water repellency, resulting in its sporadic, discontinuous distribution. Because of the discontinuous nature of vegetation communities across the study area, it was presumed prior to field analysis that the spatial distribution and presence of soil water repellency would vary considerably. In areas of more mature pre-fire vegetation, where the interspersion of coppice and interspace microsites was prevalent, 1-2 m wide black spots were noticeable across the high severity burn areas. These spots represented sites where shrubs had been incinerated, and typically demonstrated higher repellency than the lighter reflectance areas around it. The transect repellency experiment conducted around burned sagebrush proved that soil water repellency is not spatially homogenous by indicating that repellency of the soil decreased as distance from a burned shrub increased. The results of the experiment suggested that soil water repellency was most influenced by the burned shrub when under

its canopy edge, which was evident by the blackening of the soil. When the soil was out of the canopy influence (which was usually between 50 and 100 cm) the repellency of the soil tended to decrease. The final measurements at 200 cm were incomparable among transects because at that distance various other unknown factors were influencing the soil, other than the burned brush. The findings of the transect repellency experiment suggest that water repellency distribution, pre- or post-fire, can be depicted based on the distribution and spacing of shrubs.

The classification of burn severity with the hyperspectral data was compounded by the fact that the extreme pixels of the image (used as classification endmembers) were primarily in areas of extremely high and low reflectance. Their spatial examinations showed few of them actually overlying any of the study plots, and most were further away from the study plots than the imagery's georegistration difference would displace them. Though the extreme pixel classes were assigned their respective burn severity based on their spatial association with the ground truth plots as well as the spectral association among them, a certain level of subjectivity was involved in the assignments. While the assignments were more confident among spectrally unique classes, like low and high severity grass, and low severity shrub, the differentiation of moderate and high severity shrub and moderate severity grass areas was much less distinct. The spectral signatures of moderate and high severity shrub areas are virtually analogous in most cases, and it is difficult for the untrained eye to differentiate the classes in the field. The low users and producer's accuracies of the moderate and high burn severity SAM classifications exhibit this. No moderate severity grass areas were detected in the burn severity classification, in part because few extreme pixels were matched to the moderate grass areas. Additionally, the spectral characteristics of moderately classified grass areas are quite similar to low severity grass areas, due to the lack of charring among the soil, the presence of root crowns, and the high reflectance among the areas. The increased accuracy that was achieved after combining the moderate and high severity shrub areas demonstrates that the SAM classification technique is best for differentiating areas of low severity from moderate or high severity (of which the spectral signatures are very similar).
The results of the field spectrometry provided supplemental understanding of the burn severity classifications by indicating the spectral separability among the classes. The unburned and low severity grass areas were separable from other classes because the senesced (unburned) grass in those areas presented higher reflectance in the NIR than other areas. Their high soil background portrayed higher reflectance in the SWIR as well, and was not reduced due to excess charring. Classes that low severity grasses were most confused with included moderate severity grass and bare ground, both of which had high reflectance in the NIR and SWIR as well. The high severity grass areas still demonstrated higher reflectance than burned shrub areas because the soils were not as damaged and charred as soils within shrub areas. The field spectrometry also indicated very similar reflectance in the high and moderate shrub areas, as was demonstrated in the classifications. The signatures acquired with the field spectrometer were sometimes dissimilar from signatures of the same material acquired from the imagery because the field spectrometer's small field of view (25^{o}) acquired an approximate reflectance area of 1 m^2 data. This presents discrepancies with image reflectance, especially in unburned or low severity areas, because, while the field spectrometry predominantly acquires the material in target (dependent upon height of acqusition), the image pixel acquires the target along with background material(s).

Aside from the confusion of moderate and high severity shrub areas, the SAM algorithm was a better method of assessing burn severity using extreme pixels as endmembers, due to its ability to detect continuous zones of burn severity across the landscape. Results of an MTMF classification of burn severity indicated a low overall accuracy of 50% for all classes except high severity grass. One reason for the low accuracies among the MTMF is because the user-determined pixel thresholds indicate the abundance of an endmember within a pixel. Due to the spectral similarity of the image, and the ambiguity of some burn severity endmembers, it was most probable that the endmembers mixed and overlapped among pixels. A more rigorous field study with more sample plots for verification would likely improve the accuracy of the MTMF, yet endmember overlap would probably still occur. The

benefits of the MTMF are more pronounced in the classification of a single endmember, such as soil water repellency.

The spectral classification of soil water repellency was dependent on materials exhibiting specific spectral features indicative of their presence. In locations where dense shrub had been incinerated, the ground displayed blackened, charred soil. Water repellency was often noted in the charred soils, which exhibited spectral signatures of 10% – 15% less reflectance in the SWIR portion of the spectrum than soils from non-water repellent areas. This decreased reflectance was noted in areas of high water repellency, contrary to areas classified as moderate or high burn severity, in which the reflectance values varied. Although these areas of low reflectance were not the only areas to display high water repellency, they were the only water repellent areas that could be differentiated spectrally. Even though no spectral feature was found strictly unique of water repellent soils, the lowered reflectance typical of incinerated, dense vegetation was indicative of their presence.

The narrow bandwidths of the hyperspectral imagery enabled the detection of the charred soils across the image, and their presence was best mapped using the MTMF algorithm. The success of the SAM classification varied according to the maximum spectral angle established. Various angles were experimentally used and the shift between 0.60 and 0.70 radians was the principal angle difference for under- or over-detection of endmembers. While a SAM classification with a maximum angle of 0.65 classified small portions of the image, it did not cover enough of the image to be verifiable.

The MTMF algorithm was beneficial in locating areas of high water repellency. The output of pixel abundance is a more detailed and accurate representation of the soil water repellency, because it replicates the intermittent nature of water repellency across a burned area. The resulting accuracies from the subpixel abundance representation of strong soil water repellency with the MTMF ranged from 55% to 78% (producer's accuracy) among different values of pixel abundance. The changes in accuracy indicate that with increases in subpixel abundance (lower MF threshold), the more likely it is that portions of the image classified as strongly water repellent will be overlaid by ground truth plots representing that endmember.

Although the MF score results of the MTMF can be related to a measure of subpixel abundance of an endmember, for the purpose of identifying areas of soil water repellency, we did not attempt to quantify the subpixel abundance, but instead utilized the MTMF to predict the endmembers' presence. Given the inherent spatial errors of the imagery and the field-acquired GPS data, an accurate representation of subpixel abundance value would not be practical below the 3 m pixel resolution scale. In addition, the verification of subpixel abundance values would prove difficult to verify given the scale of the 9 m x 9 m sample plots, because the area of the sample plots was meant to encompass 9 pixels (to account for inherent georegistration errors), and the soil water repellency was tested at a 1 m point level within the sample plots.

Unlike the results of the field assessment, in the spectroscopic classification the high soil water repellency was depicted primarily in high severity burn areas, even though more repellency was found in moderate severity areas during the field season. A probable reason for this is because the absence of litter and vegetation in the high severity areas allows for imaging of the soil reflectance. In the moderate severity areas, however, litter and standing vegetation, though burned, is often present, which introduces spectral interference among the image. In addition, the field classification of burn severity has a degree of subjectivity, and moderate and high burn severity classifications may have been confused in the field. Other sources of spectral interference and confusion include shade within the gullies and canyons and the presence of basalt rocks on the surface, which likely contribute to reduced reflectance; some portions of the study area were more rock-strewn than others, like the gullies and slopes of the butte. The infeasiblity scores of the MTMF were decisive for differentiating these materials from water repellent soils. On the

bottom portion of the MTMF image (Fig. 3.13) a substantial amount of high infeasibility is present on the slopes of Devil Creek Butte (2), which was observed to have a considerable covering of basalt stones across the slopes. High infeasibility is also present in the shade of Devil Creek Canyon (3), and in the high reflectance bare ground areas (1). Another important point to note is that, even though the hyperspectral imagery can discern subtle variations of spectra across the surface of the soil, it cannot detect sub-surface soil characteristics. Because fires often cause heat to migrate downward in the soil, a water repellent layer is often present at depths below the surface, and was found at depths up to 2 cm below the surface soil, primarily in areas of high severity grass. A detection of areas likely to have subsurface water repellency with the MTMF classification is possible by detecting areas of high severity grass where the layers are common, but the actual repellent layer would not be detected.

We analyzed the spectra of the burned area in search of additional spectral features that may indicate the presence of fire-induced water repellency; in particular, the lack of a clay oxide absorption band at 2.3 μm, and the indication of aliphatic hydrocarbons. After heating forest soils to various temperatures, Moody et al. (2005) found that the surface of soils heated to very high temperatures (220^{o}-275^{o}) exhibited cementation due to the cooking of the clay oxides within the soils. Because of the high water retention capabilities of clay minerals, the spectral signatures of soils often exhibit a noticeable dip in the spectral signature at 2.3 μm, where clay oxides are detected. If the clays were cemented in a fire due to intense heating, the clay absorption feature would be dissolved from the signature because of the removal of the water. We examined the clay absorption band in spectra from water repellent sample plots at our study area but no noticeable change in the signature was substantiated. In addition, no evidence of clay cementation in the soils was found at the study site. It was concluded that the relatively sparse cover and fuel load in the rangeland did not burn hot enough to induce clay cementation. No evidence of aliphatic hydrocarbons was observed during the analysis of the NIR and SWIR. The charring of the soils, due to the incineration of organic matter, likely muted any spectral evidence of the compounds.
This project demonstrates the potential for spectroscopy to supplement an analysis of post-fire effects on soil properties and rangeland fire dynamics through the use of classification algorithms like the SAM and MTMF. Future research can be built onto these findings to refine the analysis procedures. The SAM classification is best for classifying burn severity across the image because the output classes are more continuous in trait, and express the uniform nature of burn severity across rangelands. The MTMF proved optimal for classifying water repellency because the subpixel abundance output is indicative of the discontinous, unpredictable character of water repellency across burned rangelands. A pitfall of the hyperspectral sensor, though not unexpected, is its inability to detect sub-surface water repellency. Higher accuracy of the classifications may be obtained by implementing a more rigorous field study across the study area. While the MTMF classification algorithm is useful for depicting the presence of water repellency, the degree of repellency is difficult to detect, mainly because the burned, darkened soils within the areas of soil water repellency dominate the spectral reflectance. A future development of this research that may enhance the results could involve the migration of a spatial analysis, using GIS, in conjunction with the described spectral analysis. The addition of a spatial analysis such as kriging, or probability mapping, may better interpolate the spatial variability of soil water repellency across the study area in association with burn severity.

We conclude from this research that water repellent soils are most likely to be found in moderately high to high severity areas of rangelands. Field analysis indicated water repellent soils are likely to be found in moderate severity areas, though this is likely biased by the subjective nature of in-situ burn severity analysis, especially in moderate and high areas. This same confusion was demonstrated in the spectroscopic classification of burn severity and water repellency, but the detection of water repellency among the high severity burned, blackened soils confidently indicates it to be evident in high severity areas. Due to potential discrepancies involving the vegetation burn severity assessment, the methods used for this research could be improved upon in rangelands by examining the parameters of burn severity classes, or perhaps classifying burn severity in a different manner altogether. Though the abolition of

low, moderate, and high severity classes may go against protocol, recent literature (Doerr et al., 2006; Shakesby and Doerr, 2006) has suggested that a more comprehensive range of burn severity assessment, involving more than just the destruction of biomass, may better describe the effects of wildland fire. For example, a greater understanding of hydro-geomorphic impacts across a wider variety of fire landscapes is needed, as is the development of severity indices relating to hydrological, geomorphological, and soil changes across fire landscapes. The utilization of the MDI for assessing water repellency improved the understanding of the phenomenon throughout the burned area by quantifying the degree of repellency among burn severity classes, while the WDPT test was useful for identifying the presence of water repellent soils.

Aside from the success of the spectroscopic classifications, results of this research indicate that rangeland wildfires are dynamic in nature, and their effects on soil properties are consequential of pre-fire vegetation type and condition, fuel load abundance and previous fire history. Although numerous other factors affect fire behavior (e.g. temperature, humidity, wind, slope, aspect), the principal factors influencing the formation of water repellent soils are the presence and amount of biomass available for consumption. Results of this or a similar analysis may be useful parameters in a predictive model of erosion and debris flow susceptibility following rangeland wildfire; the results also prove beneficial for rangeland management and planning practices.

ACKNOWLEDGEMENTS

This thesis is dedicated to my Father, William W. Finley, whose legendary accomplishments and work ethic will never be matched. In addition, my Mother has given me wonderful love and encouragement over the past two years, and her mail-order brownies and banana bread have been a lifesaver. Many thanks go to my older siblings for their support over the past 2 years, especially John, whose sage advice persuaded me to pursue graduate school.

My advisor, Nancy Glenn has been fantastic, and I thank her tremendously for the help, encouragement and confidence she instilled in me while completing my thesis. Many thanks go to the rest of the committee: Glenn, Jen, and John, for their insightful input, and Terry for stepping in at the last minute. Great thanks go to Keith Weber, Laurie Lindsay and the GIS center for employing and supporting me. The ISU Geosciences department deserves great appreciation, especially Melissa for cheerfully handling my inquiries. The geosciences professors are top-notch and deserve a well-rounded appreciation for their hard work, masterful education, and genuine friendliness. In addition, Dr. James Mahar of Engineering deserves a special note for providing the "most bang for the buck" in graduate education. I would like to thank John Ash of the BLM Twin Falls Office for assisting me with field inquiries. Forest Service researchers Peter Robichaud, Charlie Luce, and Fred Pierson, were helpful in the formulation of my thesis.

I am indebted to all of the wonderful people and long-lasting friends I have met and known here at ISU and in Idaho, and will continue to bond with. Finally, I consider myself lucky and fortunate that I was allowed to conduct research in a state as unique, accommodating, and indisputably beautiful as that of Idaho.

This study was made possible by a grant from the National Aeronautics and Space Administration Goddard Space Flight Center. ISU would also like to acknowledge the Idaho Delegation for their assistance in obtaining this grant.

LITERATURE CITED

Analytical Spectral Devices, I., 2004, http://www.asdi.com/.

Aspinall, R.J., Marcus, W.A., and Boardman, J.W., 2002, Considerations in collecting, processing, and analysing high spatial resolution hyperspectral data for environmental investigations: Journal of Geographic Systems, v. 4, p. 15-29.

Bachmann, C.M., Donato, T.F., Lamela, G.M., Rhea, W.J., Bettenhausen, M.H., Fusina, R.A., Bois, K.R.D., Porter, J.H., and Truitt, B.R., 2002, Automatic Classification of Land Cover on Smith Island, VA, Using HyMAP Imagery: IEEE Transactions on Geoscience and Remote Sensing, v. 40, p. 2313-2330.

Bobbe, T., Finco, M.V., Quayle, B., and Lannon, K., 2001, Field Measurements for the Training and Validation of Burn Severity Maps from Spaceborne, Remotely Sensed Imagery: Salt Lake City, Utah, 18 pp., USDA Forest Service, Remote Sensing Applications Center, p. 18.

Britton, C.M., and Clark, R.G., 1985, Effects of fire on sagebrush and bitterbrush, *in* Durham, J., ed., Rangeland Fire Effects; A Symposium: Boise, ID, USDI-BLM, p. 22-26.

Bunting, S.C., 1985, Fire in sagebrush ecosystems: Successional changes, *in* Durham, J., ed., Rangeland Fire Effects; A Symposium: Boise, ID, USDI-BLM, p. 7-11.

Cannon, S.H., 2001, Debris-Flow Generation from Recently Burned Watersheds: Environmental & Engineering Geoscience, v. 7, p. 321-341.

Cannon, S.H., Kirkham, R., and Parise, M., 2001, Wildfire-Related Debris Flow Initiation Processes, Storm King Mountain, Colorado: Geomorphology, v. 39, p. 171-188.

Chabrillat, S., Goetz, A.F.H., Krosley, L., and Olsen, H.W., 2002, Hyperspectral images in the identification and mapping of expansive clay soils and the role of spatial resolution: Remote Sensing of Environment, v. 82, p. 432-445.

Clark, M.L., Clark, D.B., and Roberts, D.A., 2004, Small-footprint estimation of sub-canopy elevation and tree height in a tropical rain forest landscape: Remote Sensing of Environment, v. 91, p. 68-89.

Cocke, A.E., Fulé, P.Z., and Crouse, J.E., 2005, Comparison of burn severity assessments using Differenced Normalized Burn Ratio and ground data: International Journal of Wildland Fire, v. 14, p. 189-198.

Congalton, R.G., and Green, K., 1999, Assessing the accuracy of remotely sensed data: principles and practices: Boca Raton, Florida, CRC Press, 137 p.

Davis, M., and Holbeck, C., 2001, Nuts and bolts of BAER soil and watershed assessments, *in* Harmon, D., ed., Crossing Boundaries in Park Management: 11th Conference on Research and Resource Management in Parks and on Public Lands: Hancock, MI, p. 5.

DeBano, L.F., 1981, Water Repellent Soils: a state-of-the-art: Berkeley, CA, 22 pp., Pacific Southwest Forest and Range Experiment Station, p. 22.

DeBano, L.F, 2000, The role of fire and soil heating on water repellency in wildland environments: a review: Journal of Hydrology, v. 231-232, p. 195-206.

DeBano, L.F., Neary, D.G., and Pfolliott, P.F., 1998, Fire's Effects on Ecosystems: New York, John Wiley and Sons, 333 p.

Debba, P., Ruitenbeek, F.J.A.v., Meer, F.D.v.d., Carranza, E.J.M., and Stein, A., 2005, Optimal field sampling for targeting minerals using hyperspectral data: Remote Sensing of Environment, v. 99, p. 373-386.

Decagon Devices, I., 1998, URL: http://decagon.com/, accessed 06/01/05.

Dekker, L.W., and Ritsema, C.J., 1994, How water moves in a water repellent sandy soil 1. Potential and actual water repellency: Water Resources Research, v. 30, p. 2507-2517.

Dekker, L.W., and Ritsema, C.J., 2000, Wetting patterns and moisture variability in water repellent Dutch soils: Journal of Hydrology, v. 231/232, p. 148-164.

DeLuis, M., Gonzalez-Hidalgo, J.C., and Raventos, J., 2002, Effects of fire and torrential rainfall on erosion in a mediterranean gorse community: Land Degradation and Development, v. 14, p. 203-213.

Doerr, S.H., Shakesby, R.A., Blake, W.H., Chafer, C.J., Humphreys, G.S., and Wallbrink, P.J., 2006, Effects of differing wildfire severities on soil wettability and implications for hydrological response: Journal of Hydrology, v. 319, p. 295-311.

Doerr, S.H., and Thomas, A.D., 2000, The role of soil moisture in controlling soil water repellency: new evidence from forest soils in Portugal: Journal of Hydrology, v. 231/232, p. 134-147.

ESRI, I., 2005, http://www.esri.com

Fraser, R.H., and Li, Z., 2002, Estimating fire-related parameters in boreal forest using SPOT VEGETATION: Remote Sensing of Environment, p. 95-110.

Gimeno-Garcia, E., Andreu, V., and Rubio, J.L., 2004, Spatial patterns of soil temperatures during experimental fires: Geoderma, v. 118, p. 17-38.

Glenn, N.F., Mundt, J.T., Weber, K.T., Prather, T.S., Lass, L.W., and Pettingill, J., 2005, Hyperspectral data processing for repeat detection of small infestations of leafy spurge: Remote Sensing of Environment, v. 95, p. 399-412.

Holecheck, J.L., and Pieper, R.D., 2001, Range management: Principles and practices: Saddle River, NJ, Prentice Hall Inc.

Houston, D.B., 1973, Wildfires in Yellowstone National Park: Ecology, v. 54, p. 1111-1117.

Hummel, J.W., Sudduth, K.A., and Hollinger, S.E., 2001, Soil moisture and organic matter prediction of surface soils using an NIR soil sensor: Computers and electronics in agriculture, v. 32, p. 149-165.

Ice, G.G., Neary, D.G., and Adams, P.W., 2004, Effects of wildfire on soils and watershed processes: Journal of Forestry, v. 102, p. 16-20.

Iverson, R.M., 1997, The physics of debris flows: Reviews of Geophysics, v. 35, p. 245-296.

Jensen, J.R., 2000, Remote sensing of the environment, an earth resources perspective: Saddle River, NJ, Prentice Hall, Inc., 544 p.

Jensen, J.R., 2005, Introductory digital image processing: A remote sensing perspective: Upper Saddle River, NJ, Pearson Prentice Hall, 526 p.

Johnson, M., and Beschta, R., 1981, Seasonal variation of infiltration capacities of soils in Western Oregon: Corvallis, OR, 6 pp., Pacific Northwest forest and range experiment station, p. 6.

Key, C., and Benson, N., 2004, Landscape Assessment (LA) Sampling and Analysis Methods, FIREMON Landscape Assessment V4.

Kirkham, M.B., 2005, Principles of Soil and Plant Water Relations: San Diego, CA, Elsevier Academic Press, 500 p.

Knapp, P.A., 1995, Intermountain West lightning-caused fires: Climatic predictors of areas burned: Journal of Range Management, v. 48, p. 85-91.

Krammes, J.S., and Debano, L.F., 1965, Soil wettability: a neglected factor in watershed management: Water Resources Research, v. 1, p. 283-286.

Kruse, F.A., Lefkoff, A.B., Boardman, J.B., Heidebrecht, K.B., Shapiro, A.T., Barloon, P.J., and Goetz, A.F.H., 1993, The Spectral Image Processing System (SIPS) - Interactive Visualization and Analysis of Imaging Spectrometer Data: Remote Sensing of Environment, v. 44, p. 145-163.

Kruse, F.A., Richardson, L.L., and Ambrosia, V.G., 1997, Techniques developed for geologic analysis of hyperspectral data applied to near-shore hyperspectral ocean data, ERIM 4th International Conference, Remote Sensing for Marine and Coastal Environments, Volume 1: Environmental Research Institute of Michigan (ERIM), Ann Arbor, p. I-233 - I-246.

Laes, D., Mas, P., Lewis, S., Robichaud, P., and Kokaly, R., 2004, Postfire burn-severity classification of the Hayman fire, CO: Based on hyperspectral data-JFSP RFP 2001-2 Task 1: SLC, UT, Remote Sensing App. Center, p. 29.

Lewis, S.A., Robichaud, P.R., Elliot, W.J., Frazier, B.E., and Wu, J.Q., 2004, Hyperspectral remote sensing of postfire soil properties, Tenth Forest Service Remote Sensing Applications Conference: Salt Lake City, Utah, p. 9.

Lewis, S.A., Wu, J.Q., and Robichaud, P.R., 2006, Assessing burn severity and comparing soil water repellency, Hayman Fire, CO: Hydro. Proc. v. 20, p.1-16.

Lillesand, T.M., Kiefer, R.W., and Chipman, J.W., 2004, Remote Sensing and Image Interpretation: USA, John Wiley & Sons, 763 p.

Meyer, G.A., Pierce, J.L., Wood, S.H., and Hull, A.J.T., 2001, Fire, storms and erosional events in the Idaho batholith: Hydrological Processes, v. 15.

Meyer, G.A., and Wells, S.G., 1997, Fire-related sedimentation events on alluvial fans, Yellowstone National Park, U.S.A.: Journal of Sedimentary Research, v. A67, p. 776-791.

Moody, J.A., and Smith, J.D., 2005, Critical shear stress for erosion of cohesive soils subjected to temperatures typical of wildfires: Journal of Geophysical Research, v. 110, p. 1-13.

Moody, J.A., Smith, J.D., and Regan, B.W., 2005, Critical shear stress of cohesive soils subjected to temperatures typical of wildfires: Journal of Geophysical Research, v. 110, FO1004, p. 1-13.

Mundt, J.T., Glenn, N.F., Weber, K.T., Prather, T.S., Lass, L.W., and Pettingill, J., 2005, Discrimination of hoary cress and determination of its detection limits via hyperspectral image processing and accuracy assessment techniques: Remote Sensing of Environment, v. 96, p. 509-517.

Mundt, J., Glenn, N., Weber, K., Pettingill, J., 2005, Determining target detection limits and accuracy delineation using an incremental technique. Remote Sensing of Environment, in press.

Mundt, J.T., Streutker, D.R., and Glenn, N.F, 2006, Mapping sagebrush distribution using fusion of hyperspectral and lidar classifications: Photogrammetric Engineering & Remote Sensing, v. 72, p. 47-54.

NCDC, 2005, http://www.ncdc.noaa.gov/oa/ncdc.html, Accessed May 24, 2006. Okin, G.S., Roberts, D.A., Murray, B., and Okin, W.J., 2001, Practical limits on hyperspectral vegetation discrimination in arid and semiarid environments: Remote Sensing of Environment, v. 77, p. 212-225.

Noy-Meir, I., 1973, Desert Ecosystems: environment and producers: Annual Reviews in Ecological Systems, v. 4, p. 25-51.

Odion, D.C., Frost, E.J., Strittholt, J.R., Jiang, H., Dellasala, D.A., and Moritz, M.A., 2004, Patterns of fire severity and forest conditions in the Western Klamath Mountains, California: Consevation Biology, v. 18, p. 927-936.

Okin, G.S., Roberts, D.A., Murray, B., and Okin, W.J., 2001, Practical limits on hyperspectral vegetation discrimination in arid and semiarid environments: Remote Sensing of Environment, v. 77, p. 212-225.

Okin, W.J., Okin, G.S., Roberts, D.A., and Murray, B., 1999a, Multiple endmember spectral mixture analysis: application to an arid/semi-arid landscape, *in* Green, R.O., ed., The 1999 AVIRIS Workshop: Pasadena California, p. 291-300.

Okin, W.J., Okin, G.S., Roberts, D.A., and Murray, B., 1999b, Multiple endmember spectral mixture analysis: endmember choice in an arid shrubland, *in* Green, R.O., ed., The 1999 AVIRIS Workshop: Pasadena California, p. 323-332.

Palacios-Orueta, A., Pinzon, J.E., Ustin, S.L., and Roberts, D.A., 1999, Remote Sensing of Soils in the Santa Monica Mountains: II. Hierarchical Foreground and Background Analysis: Remote Sensing of Environment, v. 68, p. 138-151.

Palacios-Orueta, A., and Ustin, S.L., 1998, Remote Sensing of Soil Properties in the Santa Monica Mountains, pt. I: Spectral Analysis: Remote Sensing of Environment, v. 65, p. 170-183.

Parker-Williams, A., and Hunt Jr., R., 2004, Accuracy assessment for detection of leafy spurge with hyperspectral imagery: Journal of Range Management, v. 57, p. 106-112.

Parker-Williams, A.E., 2004, Accuracy assessment for detection of leafy spurge with hyperspectral imagery: Journal of Range Management, v. 57, p. 106-112.

Pierce, J., Meyer, G.A., and Jull, T., 2004, Fire-Induced erosion and millenial-scale climate change in northern ponderosa pine forests: Nature, v. 432, p. 87-90.

Pierson, F.B., Robichaud, P.R., and Spaeth, K.E., 2001, Spatial and temporal effects of wildfire on the hydrology of a steep rangeland watershed: Hydrological Processes, v. 15, p. 2905-2916.

Pierson, F.B., Robichaud, P.R., Spaeth, K.E., and Moffet, C., 2003, Impacts of fire on hydrology and erosion in steep mountain big sagebrush communities, First Interagency Conference on Research in the Watersheds: Benson, AZ.

Pinzon, J.E., Ustin, S.L., Castaneda, C.M., Pierce, J.F., and Costick, L.A., 1998, Robust spatial and spectral feature extraction for multispectral and hyperspectral imagery, *in* Schewel, J., ed., SPIE Int. Soc. Opt. Eng., Volume 3372: Boston, Massachusetts.

Rahman, A.F., and Gamon, J.A., 2004, Detecting biophysical properties of a semi-arid grassland and distinguishing burned from unbuned areas with hyperspectral reflectance: Journal of Arid Environments, v. 58, p. 597-610.

Raper, B., Clark, B., Matthews, M., and Aldrich, A., 1984, Early effects of a fall burn in a Western Wyoming big sagebrush-grass community, *in* Durham, J., ed., Rangeland
fire effects, a symposium: Boise, ID, USDI Bureau of Land Management, p. 88-93.

Robichaud, P., Macdonald, L., Freeouf, J., Neary, D., Martin, D., and Ashmun, L., 2003, Postfire Rehabilitation of the Hayman Fire, USDA Forest Service, p. 293-314.

RSI, 2005, Environmental Systems Research Institute (ENVI) online help documentation, http://www.ittvis.com/index.asp.

SAS Institute, I., 2005, Online Documentation, http://v8doc.sas.com/sashtml/.

Scott, D.F., 1993, The hydrological effects of fire in South African mountain catchments: Journal of Hydrology, v. 150, p. 409-432.

Shakesby, R.A., Chafer, C.J., Doerr, S.H., Blake, W.H., Wallbrink, P., Humphreys, G.S., and Harrington, B.A., 2003, Fire Severity, Water Repellency Characteristics and Hydrogeomorphological Changes Following the Christmas 2001 Sydney Forest Fires: Australian Geographer, v. 34, p. 147-175.

Shakesby, R.A., and Doerr, S.H., 2006, Wildfire as a hydrological and geomorphological agent: Earth-Science Reviews, v. 74, p. 269-307.

Shinn, D.A., 1980, Historical perspectives on range burning in the Inland Pacific Northwest: Journal of Range Management, v. 33, p. 415-423.

Smith, J.K., 2000, Wildland fire in ecosystems: effects of fire on fauna: Ogden, UT, 83 pp., U.S. Department of Agriculture, Forest Service, Rocky Mountain Research Station, p. 83.
Sprague-Wheeler, D.K., 2001, The use of remote sensing imagery for evaluation of post-wildfire susceptibility to landslide and erosion hazards in the Salmon-Challis National Forest, Lemhi County, Idaho: Pocatello ID,, Idaho State University.

Steede-Terry, K., 2000, Integrating GIS and the Global Positioning System: Redlands, CA, Environmental Systems Research Institute, Inc., 95 p.

Summerfield, M.A., 1991, Global Geomorphology: London, England, Pearson Education Ltd., 537 p.

Switky, K.R., 2003, Fire monitoring handbook: Boise, ID, 274 pp., NPS Fire management program center, National Interagency Fire Center, p. 274.

Trimble Navigation, L., 2005, http://www.trimble.com/.

Tucket, T., Beard, J., Fluckiger, M., Rizvi, H., Woodcock, P., and Mahar, W., 2004, Caddy Canyon erosion debris flow and abatement, Proceedings for the 39th annual Symposium of Engineering Geology and Geotechnical Engineering: Butte, MT, 8 pp.

USDA-FSA, 2005, USDA-Farm Service Agency National Agriculture Imagery Program, http://www.apfo.usda.gov/NAIP.html.

USDA-NRCS, 2005, Owyhee, Twin Falls County, ID, Soil Taxonomy database, Volume 2005.

Ustin, S.L., Roberts, D.A., Gamon, J.A., Asner, G.P., and Green, R.O., 2004, Using imaging spectroscopy to study ecosystem processes and properties: Bioscience, v. 54, p. 523-534.

Wagtendonk, J., Root, R., and Key, C., 2004, Comparison of AVIRIS and Landsat ETM+ Detection Capabilities for Burn Severity: Remote Sensing of Environment, v. 92, p. 397-408.

West, N.E., and Hassan, M.A., 1985, Recovery of sagebrush-grass vegetation following wildfire: Journal of Range Management, v. 38, p. 131-134.

Whisenant, S.G., 1990, Changing fire frequencies on Idaho's Snake River Plains: Ecological and management implications, USDA Forest Service, Intermountain Research Station, p. 10.

Wondzell, S., and King, J., 2003, Postfire erosional processes in the Pacific Northwest and Rocky Mountain regions: Forest Ecology and Management, v. 178, p. 75-87.

Wright, H.A., 1985, Effects of fire on grasses and forbs in sagebrush-grass communities, *in* Durham, J., ed., Rangeland Fire Effects; A Symposium: Boise, ID, USDI-BLM, p. 12-21.

Young, J.A., and Evans, R.A., 1981, Demography and fire history of a western juniper stand: Journal of Range Management, v. 34, p. 501-506.

Appendix A. HyMap Georegistration Error Analysis

Table A.1. GCP locations and difference between NAIP and HyMap imagery

GCP	Image	POINT_X	POINT_Y	X Shift (meters)	Y Shift (meters)	Direction (degrees)
1	NAIP	666,102.45	4,715,075.72			
1	Hymap	666,105.87	4,715,073.63	3.42	2.09	328
2	NAIP	666,893.28	4,715,232.65			
2	Hymap	666,886.48	4,715,221.46	6.80	11.19	238
3	NAIP	666,090.55	4,714,050.23			
3	Hymap	666,091.67	4,714,049.09	1.12	1.13	313
4	NAIP	666,548.17	4,713,147.33			
4	Hymap	666,545.50	4,713,141.34	2.67	5.99	240
5	NAIP	667,160.10	4,711,880.29			
5	Hymap	667,156.15	4,711,875.03	3.95	5.26	230
6	NAIP	666,486.12	4,709,334.87			
6	Hymap	666,483.74	4,709,330.91	2.38	3.95	230
7	NAIP	666,158.87	4,708,526.93			
7	Hymap	666,158.46	4,708,522.45	0.41	4.48	265
8	NAIP	667,208.51	4,708,389.00			
8	Hymap	667,202.51	4,708,380.42	6.01	8.58	234
9	NAIP	667,645.14	4,706,835.53			
9	Hymap	667,639.29	4,706,824.72	5.86	10.81	241
10	NAIP	666,973.99	4,706,594.00			
10	Hymap	666,968.56	4,706,588.15	5.43	5.85	228
11	NAIP	667,046.15	4,705,139.67			
11	Hymap	667,043.09	4,705,131.62	3.06	8.06	250
12	NAIP	666,996.98	4,704,364.09			
12	Hymap	666,994.01	4,704,360.58	2.97	3.51	235
13	NAIP	667,904.24	4,704,083.76			
13	Hymap	667,898.02	4,704,074.44	6.22	9.32	236
14	NAIP	666,684.22	4,703,657.20			
14	Hymap	666,682.96	4,703,653.65	1.25	3.55	250
15	NAIP	667,390.52	4,702,319.32			
15	Hymap	667,388.29	4,702,312.07	2.23	7.25	252
16	NAIP	666,371.51	4,702,252.54			
16	Hymap	666,371.28	4,702,252.54	0.23	0.00	180
17	NAIP	667,313.54	4,700,577.16			
17	Hymap	667,314.21	4,700,570.66	0.67	6.51	275
18	NAIP	666,781.14	4,699,651.41			
18	Hymap	666,782.30	4,699,653.72	1.15	2.31	63
		Mean		3.10	5.55	238.22
		Standard Deviation		2.16	3.24	
		Maximum difference		6.80	11.19	
		Minimum difference		0.23	0.00	
		Range		6.57	11.19	

Assessment of the HyMap georegistration was based on measurements between 18 NAIP aerial photograph ground control points (GCP's) and their equivalent locations on HyMap image 06.

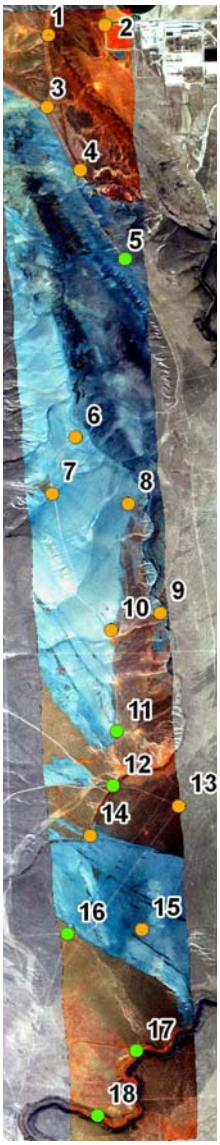

Fig. A.1. GCP's used for georegistration assessment, HyMap image 06

Appendix B. Daily Weather Observations, Castleford, Idaho

Daily weather records for Castleford, Idaho weather station obtained from National Climatic Data Center, US Department of Commerce (NCDC, 2005). Castleford is approximately 6 km east of the Clover Fire study area.

Table A.2. Weather observations, August, 2005

Year	Month	Day	Temp. (deg. F) Max.	Min.	Obs.	Precip (mm)
2005	Aug.	1	94	56	83	0
2005	Aug.	2	88	58	88	0
2005	Aug.	3	89	52	88	0
2005	Aug.	4	94	53	93	0
2005	Aug.	5	97	53	95	0
2005	Aug.	6	99	58	99	0
2005	Aug.	7	99	55	88	0
2005	Aug.	8	92	69	80	Trace
2005	Aug.	9	92	58	82	0
2005	Aug.	10	92	58	91	0
2005	Aug.	11	91	57	88	0
2005	Aug.	12	88	51	85	0
2005	Aug.	13	86	47	80	0
2005	Aug.	14	82	46	81	0
2005	Aug.	15	86	51	85	0
2005	Aug.	16	84	61	74	Trace
2005	Aug.	17	86	51	77	0
2005	Aug.	18	80	56	79	1.02
2005	Aug.	19	85	51	85	0
2005	Aug.	20	93	52	92	0
2005	Aug.	21	96	54	94	0
2005	Aug.	22	94	62	74	Trace
2005	Aug.	23	88	53	83	0
2005	Aug.	24	84	53	76	0
2005	Aug.	25	83	44	82	0
2005	Aug.	26	88	50	87	0
2005	Aug.	27	90	50	89	0
2005	Aug.	28	91	50	90	0
2005	Aug.	29	90	55	85	0
2005	Aug.	30	85	49	69	0
2005	Aug.	31	76	41	75	0
Mean:			**89.1**	**53.4**	**Total:**	**1.02**

Table A.3. Weather observations, September, 2005

Year	Month	Day	Temp. (deg. F) Max.	Min.	Obs.	Precip (mm)
2005	Sept.	1	82	41	81	0
2005	Sept.	2	93	49	92	0
2005	Sept.	3	93	51	86	0
2005	Sept.	4	86	51	83	0
2005	Sept.	5	83	48	79	0
2005	Sept.	6	82	41	81	0
2005	Sept.	7	85	49	83	0
2005	Sept.	8	90	52	77	0
2005	Sept.	9	83	52	77	0
2005	Sept.	10	77	34	57	Trace
2005	Sept.	11	66	34	65	0

2005	Sept.	12	69	44	67	0
2005	Sept.	13	70	33	68	0
2005	Sept.	14	74	39	73	0
2005	Sept.	15	80	48	79	0
2005	Sept.	16	79	45	75	0
2005	Sept.	17	77	48	63	Trace
2005	Sept.	18	70	38	68	0
2005	Sept.	19	76	38	75	0
2005	Sept.	20	79	42	76	0
2005	Sept.	21	78	54	71	0
2005	Sept.	22	79	41	N/A	0
2005	Sept.	23	77	47	70	0
2005	Sept.	24	68	43	55	0
2005	Sept.	25	62	34	62	0
2005	Sept.	26	73	35	70	0
2005	Sept.	27	70	49	66	1.8
2005	Sept.	28	71	39	69	0
2005	Sept.	29	77	37	76	0
2005	Sept.	30	81	45	79	0
Mean:			**77.7**	**43.4**	**Total:**	**1.8**

Table A.4. Weather observations, October, 2005

			Temp. (deg. F)			Precip
Year	Month	Day	Max.	Min.	Obs.	(mm)
2005	Oct.	1	84	48	81	0
2005	Oct.	2	80	41	53	1.8
2005	Oct.	3	57	38	52	Trace
2005	Oct.	4	53	36	50	0.5
2005	Oct.	5	55	27	54	0
2005	Oct.	6	64	28	62	0
2005	Oct.	7	68	33	66	0
2005	Oct.	8	66	46	58	0
2005	Oct.	9	60	39	58	0
2005	Oct.	10	61	32	59	0
2005	Oct.	11	60	31	56	0
2005	Oct.	12	60	42	58	0
2005	Oct.	13	72	33	69	0
2005	Oct.	14	80	38	78	0
2005	Oct.	15	80	52	62	0
2005	Oct.	16	63	42	61	0
2005	Oct.	17	61	38	59	0
2005	Oct.	18	72	35	68	0
2005	Oct.	19	69	46	66	0
2005	Oct.	20	67	42	61	0
2005	Oct.	21	63	35	61	0
2005	Oct.	22	65	33	63	0
2005	Oct.	23	69	35	67	0
2005	Oct.	24	74	37	73	0
2005	Oct.	25	73	40	65	0
2005	Oct.	26	67	48	61	0
2005	Oct.	27	61	42	45	0.76
2005	Oct.	28	55	35	53	3.05
2005	Oct.	29	55	35	52	0.25
2005	Oct.	30	52	30	48	0
2005	Oct.	31	55	27	54	0
Mean:			**65.2**	**37.5**	**Total:**	**6.36**

Appendix C: Additional Image Processing

The efficiency of spectroscopy is demonstrated in its ability to transfer spectra among multiple images in order to classify them without undertaking all of the pre-processing steps required for the initial image classification (PPI & n-DV endmember identification). After conducting the primary image analysis on image 6, the other images were mosaicked together for more efficient processing. Listed below are the image analysis and classification results of mosaicked images 5, 6, and 7, of section A; images 3 and 4 of section B, and images 1 and 2 of section C. Prior to conducting the mosaics, the images were MNF-transformed and saved as 125-band MNF files. After the images were mosaicked, a mask was applied to the image to isolate the burned areas. A SAM classification of burn severity and a MTMF classification of water repellency were conducted on each mosaicked image. Prior to the classification of water repellency, the reflectance images were subset to the SWIR portions of the image (bands 65-125), and the remaining 61 bands were MNF-transformed.

As was the case in image 6, higher accuracies may have been obtained for the MTMF classification of high water repellency had a more complete field assessment been conducted. The classifications do serve to indicate those areas most likely to exhibit soil water repellency, while the infeasibility scores are useful for identifying areas of false positives.

Section A

A SAM classification of burn severity and a MTMF classification of high water repellency were conducted on the mosaicked images 5, 6, and 7 (Fig. A.2 A), comprising section A. The extreme pixel endmembers identified in image 6 were used as training endmembers for burn severity classes. Several sample plots in images 5 and 7 were used as supplemental training sites in order for the classification to completely cover the mosaicked image. Bare ground was not included in the burn severity classification of the mosaicked image because of a lack of ground truth plots outside of image 6 representing bare ground. An error matrix was calculated for the classification using 54 field-collected sample plots from section A (plots used for training were not used as ground truth) as reference. The classification resulted in 66% overall accuracy, and a Kappa coefficient of 0.56 (Table A.5). As with the other classifications, the burn severity classes of moderate and high shrub were confused, as is evident by the lower producer's accuracy. The high severity grass had low accuracy as well, but the primary reason is likely because there were only 3 sample plots available for reference sites in that class, which were confused in themselves with high severity shrub. The accuracies of low severity grass and shrub, and high severity shrub were actually higher for the mosaicked image classification of section A. The probable reason for this is because the ground truth sample plots added to the accuracy assessment for the classified mosaic consisted mainly of these classes, and their presence beneath the correctly classified area increased the accuracy of that class.

The MTMF classification of burn severity detected highly water repellent soils across 12.5% of the burned area when a pixel abundance of 100% was used for presence/absence detection (Table A.6 A). A total of 8 positive reference ground truth plots and 10 negative reference plots were used for the accuracy assessment. When the threshold was lowered to a percentage of material identified within the pixel (Table A.6 B, C), the overall accuracies of the classification increased from 33% to 61% at MF score thresholds of 0.5 and 0.3. Slight reflectance differences among the mosaicked images resulted in over-classification of the bottom portion of the image (Fig. A.2 B) on Devil Creek Butte, but the results still serve to pinpoint areas susceptible to increased sedimentation following the fire.

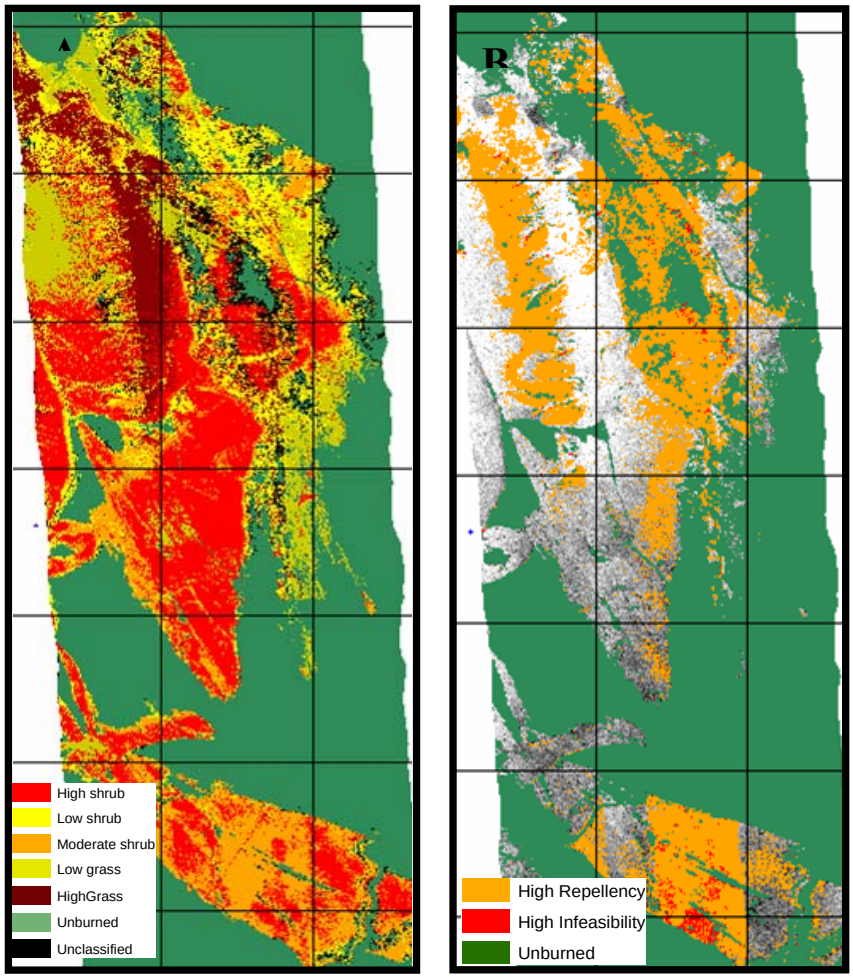

Figure A.2. A. SAM burn severity classification, section A. B. MTMF classification of fire-induced high water repellency, MF score threshold = 0.65-2.0. Infeasibility scores (red) greater than 20. Note: 1 square = 2 km

Table A.5. SAM burn severity classification error matrix, section A

Error Matrix, SAM Burn Severity Classification, Image 5, 6, & 7 Mosaic						
Overall Accuracy = (205/312) 66%						
Kappa Coefficient = 0.56						
Ground Truth (pixels)						
Class	**Low Severity Shrub**	**Moderate Severity Shrub**	**High Severity Shrub**	**Low Severity Grass**	**High Severity Grass**	**Total**
Unclassified	0	6	0	0	0	6
Low Severity Shrub	64	13	5	7	0	89
Moderate Severity Shrub	2	45	20	0	0	67
High Severity Shrub	5	12	50	0	0	67
Low Severity Grass	0	5	1	35	10	51
High Severity Grass	0	2	18	1	11	32
Total	71	83	94	43	21	312

Class	Commission (%)	Omission (%)	Producer's Accuracy (%)	User's Accuracy (%)
Low Severity Shrub	28.09	9.86	90.14	71.91
Moderate Severity Shrub	32.84	45.78	54.22	67.16
High Severity Shrub	25.37	46.81	53.19	74.63
Low Severity Grass	31.37	18.6	81.4	68.63
High Severity Grass	65.63	47.62	52.38	34.38

Table A.6. Presence/absence error matrices of MTMF classification of highly water repellent soils, Section A: A. MF = 1-2.0; B. MF = 0.5 – 2.0; C. MF = .3-2.0

A. MF score threshold = 1.0-2.0 (189,351 pixels) 12.5% of burned area			
MTMF Class	Reference Positive	Reference Negative	User's Accuracy
Classified Positive	3	6	33%
Classified Negative	6	3	33%
Producer's Accuracy	33%	33%	**33%**

B. MF score threshold = 0.5-2.0 (679,134 pixels) 45% of burned area			
MTMF Class	Reference Positive	Reference Negative	User's Accuracy
Classified Positive	5	4	56%
Classified Negative	3	6	67%
Producer's Accuracy	63%	60%	**61%**

C. MF score threshold = 0.3-2.0 (993,927 pixels) 66% of burned area			
MTMF Class	Reference Positive	Reference Negative	User's Accuracy
Classified Positive	5	4	56%
Classified Negative	3	6	67%
Producer's Accuracy	63%	60%	**61%**

Section B

A SAM classification of burn severity was conducted on mosaicked images 3 and 4 (Fig. A.3). The SAM classification used 23 extreme pixel classes representing burn severity categories as endmembers; these were identified on image 4 using the PPI and n-DV endmember identification technique. A maximum angle of 1.0 radian was utilized for the classification. 25 sample plots were utilized for accuracy assessment of the classifications. The SAM classification of burn severity had an overall accuracy of 60% and a kappa coefficient of 0.50 (Table A.7**)**. The burned grass areas were classified accurately in the image, while the moderate and high shrub areas were confused.

A MTMF classification of highly water repellent soils was conducted on the mosaicked images 3 and 4 (Fig. A.4). The MNF-transformed spectra of 2 known water repellent sample plots in section B were input as endmembers in the classification. The presence/absence error matrices of the classification are listed in Table A.8 (A, B, C). For the accuracy assessment of the MTMF classification, 11 positive reference plots were used and 8 negative reference plots. The overall accuracies of the MTMF classifications increased by 10% each time the MF score threshold was lowered to include greater pixel abundance. The infeasibility scores of 20 or higher (Fig. A.4) indicate most false positives to be within the very high and low reflectance areas, like the access roads, and rock-strewn slopes.

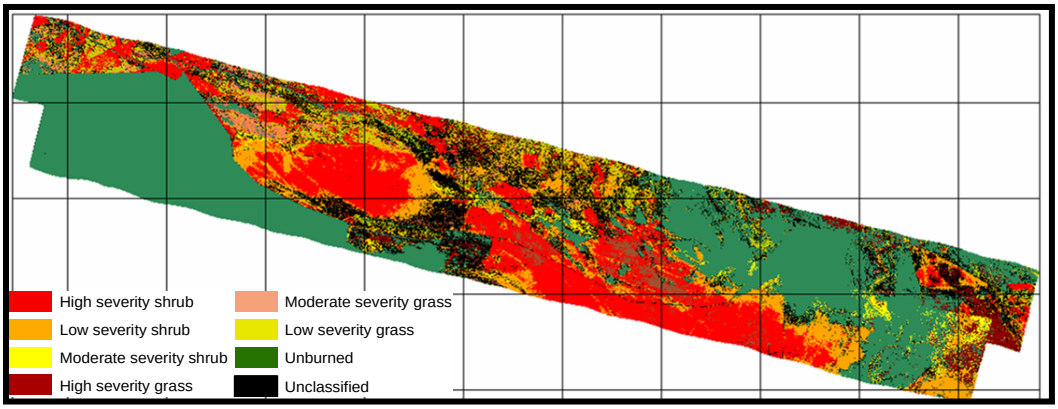

Figure A.3. SAM burn severity classification, section B. 1 square=2 km

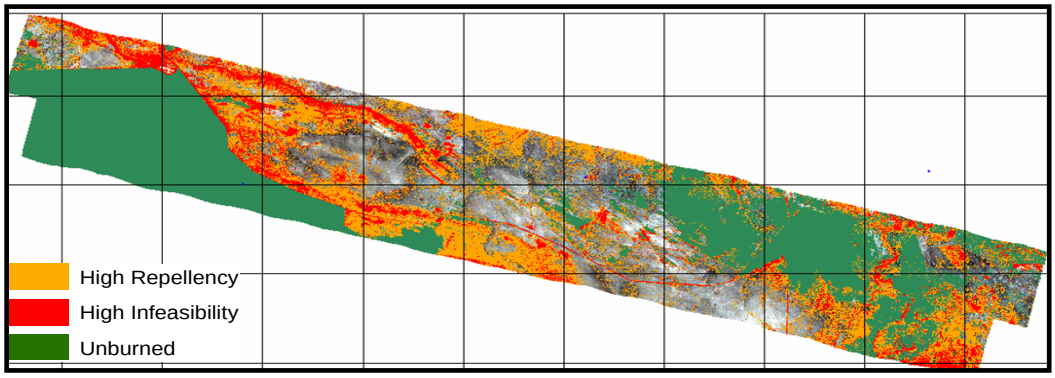

Figure A.4. MTMF classification of fire-induced high water repellency, MF score threshold = 0.65-2.0. Infeasibility scores (red) greater than 20.

Table A.7. SAM burn severity classification error matrix, section B

Error Matrix, SAM Burn Severity Classification, Image 3 & 4 Mosaic							
Overall Accuracy = (131/225) 60%							
Kappa Coefficient = 0.50							
Ground Truth (pixels)							
Class	**Low Severity Shrub**	**Moderate Severity Shrub**	**High Severity Shrub**	**Low Severity Grass**	**Moderate Severity Grass**	**High Severity Grass**	**Total**
Unclassified	5	7	7	17	1	0	37
Low Severity Shrub	13	1	0	0	0	0	14
Moderate Severity Shrub	5	33	9	0	0	0	47
High Severity Shrub	0	20	23	0	0	0	43
Low Severity Grass	0	2	0	38	0	0	40
Moderate Severity Grass	0	8	0	6	16	0	30
High Severity Grass	1	5	0	0	0	8	14
Total	24	76	39	61	17	8	225

Class	Commission (%)	Omission (%)	Producer's Accuracy (%)	User's Accuracy (%)
Low Severity Shrub	7.14	45.83	54.17	92.86
Moderate Severity Shrub	29.79	56.58	43.42	70.21
High Severity Shrub	46.51	41.03	58.97	53.49
Low Severity Grass	5	37.7	62.3	95
Moderate Severity Grass	46.67	5.88	94.12	53.33
High Severity Grass	42.86	0	100	57.14

Table A.8 A, B, C. Presence/absence error matrices of MTMF classification of highly water repellent soils, Section B

A. MTMF score threshold = 1.0-2.0 (142,662 pixels) 3.4% of burned area			
MTMF Class	Reference Positive	Reference Negative	User's Accuracy
Classified Positive	5	6	45%
Classified Negative	6	2	25%
Producer's Accuracy	45%	25%	**37%**

B. MTMF score threshold = 0.5-2.0 (680,674 pixels) 17% of burned area			
MTMF Class	Reference Positive	Reference Negative	User's Accuracy
Classified Positive	5	6	54%
Classified Negative	6	2	33%
Producer's Accuracy	64%	25%	**47%**

C. MTMF score threshold = 0.3-2.0 (1,103,054 pixels) 27% of burned area			
MTMF Class	Reference Positive	Reference Negative	User's Accuracy
Classified Positive	7	4	64%
Classified Negative	4	4	50%
Producer's Accuracy	64%	50%	**58%**

Section C

The field data collection in section C was inadequate for a robust classification, because heavy wind storms had transported large amounts of soil and litter away from the study site, leaving very different conditions than those at the time of image acquisition. These storms resulted in ground conditions that were not representative of conditions in the imagery. Because of this deficiency, the classifications of section C could not be substantially assessed for accuracy.

The field conditions in section C also made it difficult to differentiate high and moderate severity shrub from high and moderate severity grass areas, so the burn severity of the section only differentiated low, moderate and high burn severity. Burn severity endmembers from section B were transferred to section C for the supervised classification. Several of the training sites from the field were input for endmember identification as well. The SAM burn severity classification (Fig. A.5 A) was conducted with a maximum angle of 1 radian. After the classification, an error matrix was calculated for the classification using the field-assessed sample plots (excluding those that were input as training sites). The general burn severity classification of low, moderate and high severity produced a surprisingly high accuracy of 75%. The presented high accuracy may be slightly misleading, however, because the number of training sites for error assessment only totaled 2 for high severity, 3 for moderate severity, 5 for low severity, and 1 for bare ground. Table A.9 lists the error matrix values for the SAM burn severity classification.

Table A.9. SAM burn severity classification error matrix, section C

Error Matrix, SAM Burn Severity Classification, Image 1 & 2 Mosaic					
Overall Accuracy = (117/155) 75% **Kappa Coefficient = 0.66**					
Ground Truth (pixels)					
Class	**High Severity**	**Moderate Severity**	**Low Severity**	**Bare Ground**	**Total**
Unclassified	0	0	2	0	2
High Severity	30	10	1	0	41
Moderate Severity	3	36	14	2	55
Low Severity	0	0	38	0	38
Bare Ground	0	0	6	13	19
Total	33	46	61	15	155
Class	**Commission (%)**	**Omission (%)**	**Producer's Accuracy (%)**	**User's Accuracy (%)**	
High Severity	26.83	9.09	90.91	73.17	
Moderate Severity	34.55	21.74	78.26	65.45	
Low Severity	0	37.7	62.3	100	
Bare Ground	31.58	13.33	86.67	68.42	

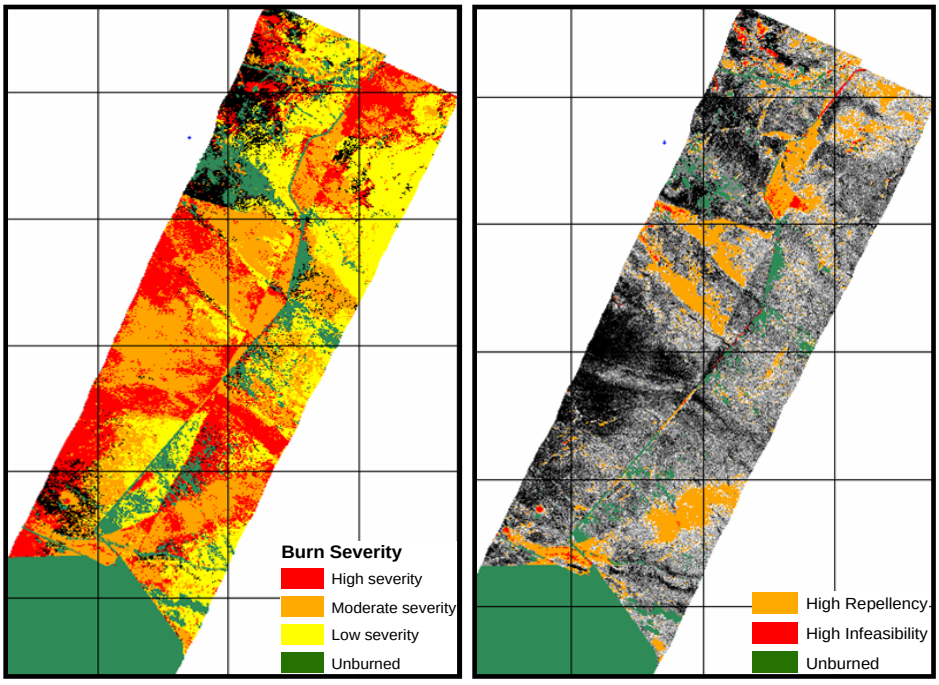

Figure A.5 A (left). SAM burn severity classification, section C.
Figure A.5 B (right). MTMF classification of soil water repellency, section C (MF score threshold 0.65-2.0). 1 square equals 2 km.

The lack of strong water repellency in Section C during field sampling was likely due to damage and dispersion of soil by the windstorms. A MTMF classification of water repellent soils was conducted on the mosaicked images of section C using the spectral endmembers of highly water repellent training sites assessed in section B. Due to the lack of field data, the MTMF could not be verified, but served as an indicator of areas most likely to exhibit soil water repellency (Fig. A.5 B). The MTMF classification detected 3.5% of the burned portion of section C to have highly water repellent soils, when a MF score threshold of 0.65-2 was used.

Appendix D. NAIP Aerial Photography Classification of Vegetation

To verify the areas being classified as shrub and/or grass, a supervised classification of the 2004 USDA National Agriculture Imagery Program (NAIP) true color ortho-photograph was employed to identify areas of shrub, grass, and bare ground, and used as a supplemental endmember identification layer. Because the HyMap imagery of the burned area appeared quite homogeneous and spectrally similar, it was difficult to remotely identify which of the burned areas were of grass, shrub, or a mixed shrub and grass area, especially in severely burned areas. For this reason, the NAIP classification was utilized to identify those areas.

The countywide NAIP images, which were flown in the summer of 2004, were obtained as MR SID compressed image files, subset to the study section areas with ArcGIS, and converted to TIFF format for use in ENVI. In ENVI, an interactive histogram stretch of the RGB brightness values allowed for the differentiation of the green shrub areas, and the higher reflectance, yellow grass areas, as well as areas of bare ground (Fig 1A). Regions of Interest (ROI's) were drawn among 3 classes: High reflectance bare ground, green sagebrush/shrub, and senesced yellow grass**.** Because the imagery was acquired during the summer, the majority of the grass had already reached senescence, allowing accurate detection after adjusting the RGB values.

A SAM classification was conducted of the subset image (Fig. 1B) using digitized ROI's as training areas. A maximum SAM angle of 1 radian was used for the grass and shrub classes, and a SAM angle of 2.5 was used for the bare ground class. The larger angle was used for the bare ground area because they tended to be under-classified, and grouped, or committed to, the grass areas. A comparison of Figure 1A and Figure 1B demonstrates the tendency for the bare ground to be under-classified.

Although the images contained features other than burned vegetation (asphalt, buildings, rock), they were not separated into different classes, because ENVI was unable to differentiate the dark reflectance of rock and asphalt from the shrub areas, and the buildings were inapplicable to the study. The accuracy of the vegetation classification was assessed with ground truth data from the field-collected sample plots of unburned or low severity areas, where the vegetation type was confidently assessed in the field, and the dominant vegetation group identified. The error matrix (Table A.10) indicates an overall accuracy of 90% and a Kappa coefficient of 0.78.

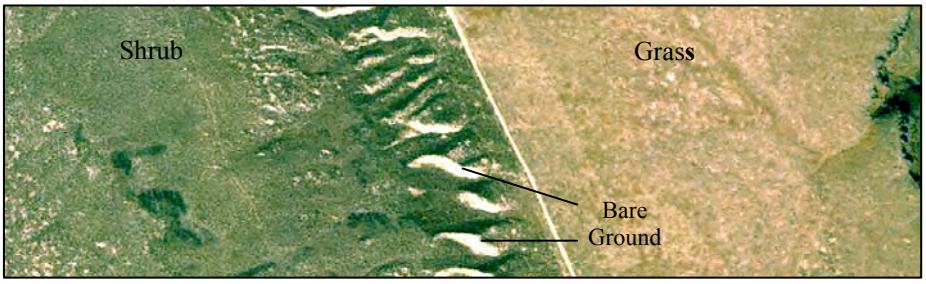

Fig A.6 A. Summer 2004 (pre-fire) NAIP aerial imagery utilized for validation of vegetation specific burn severity.

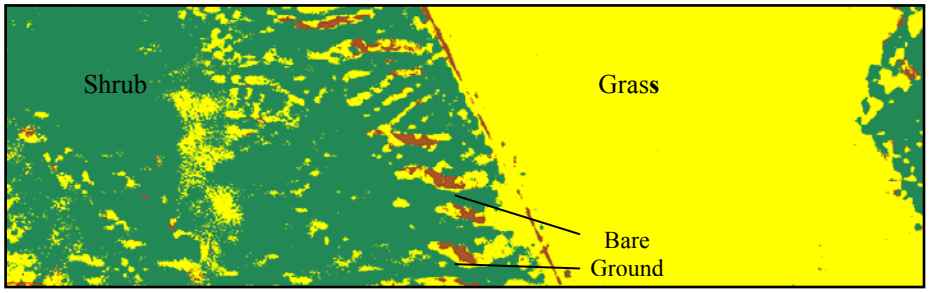

Fig A.6 B. SAM classification of the summer 2004 (pre-fire) NAIP aerial imagery. Yellow = grass, green = shrub, brown = bare ground.

Error Matrix, SAM Vegetation Classification				
Overall Accuracy = (25376/28265) 90% **Kappa Coefficient = 0.7804**				
Ground Truth (pixels)				
Class	**Bare Ground**	**Grass**	**Shrub**	**Total**
Unclassified	0	0	0	0
Bare Ground	4830	1585	62	6477
Grass	12	18427	648	19087
Shrub	392	190	2119	2701
Total	5234	20202	2829	28265
	Ground Truth (%)			
Class	**Bare Ground**	**Grass**	**Shrub**	**Total**
Unclassified	0	0	0	0
Bare Ground	92.28	7.85	2.19	22.92
Grass	0.23	91.21	22.91	67.53
Shrub	7.49	0.94	74.9	9.56
Total	100	100	100	100
Class	**Commission (%)**	**Omission (%)**	**Producers Accuracy (%)**	**Users Accuracy (%)**
Bare Ground	25.43	7.72	92.28	74.57
Grass	3.46	8.79	91.21	96.54
Shrub	21.55	25.1	74.9	78.45

Appendix E. GeoXT Customized GPS Data Collection Forms

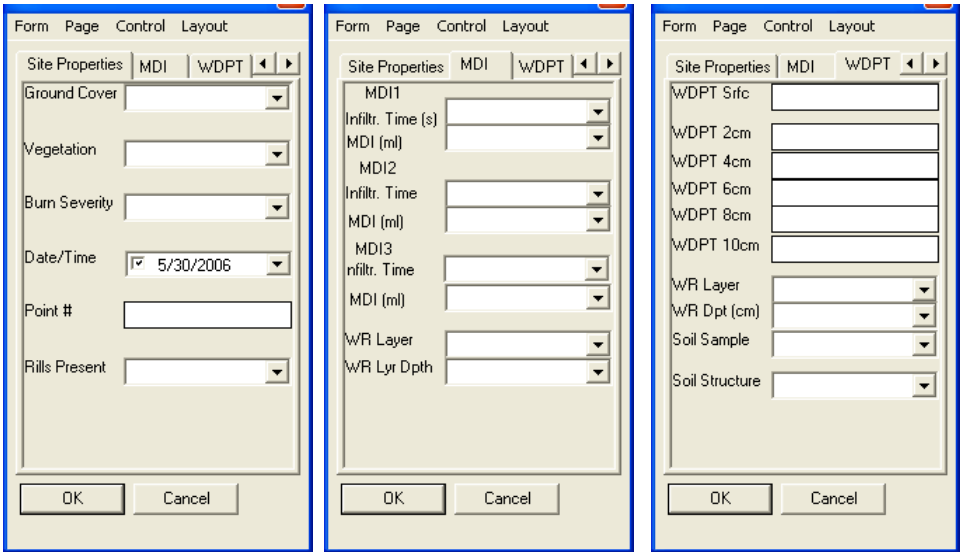

Figure A.7. Customized GeoXT data collection forms

Customized GPS data collection forms were created in ArcPad 6 (ESRI, 2005). The forms included drop-down menus and data entry boxes for the purpose of inputting data values assessed in the field.

Appendix F. Field Data

235 sample points were collected throughout sections A, B, and C. Tables A.11-A.13 list the burn severity and soil water repellency information recorded at each point. The water repellency information was recorded with the Water Drop Penetration Test (WDPT) and the Mini-Disc Infiltrometer (MDI).

Table A.11. Burn severity and soil water repellency field data, Section A.

Point	Vegetation	Severity	WDPT (seconds)				MDI (ml/min)
			Surface	2 cm	4 cm	6 cm	
1	Shrub	Unburned	0	0	0	0	4.00
2	Shrub	Unburned	0	0	0	0	6.33
3	Shrub	Unburned	30	0	0	0	6.67
4	Shrub	Unburned	0	0	0	0	8.00
5	Shrub	Unburned	0	0	0	0	9.00
6	Shrub	Unburned	0	0	0	0	10.00
7	Shrub	Unburned	0	0	0	0	10.00
8	Shrub	Unburned	2	0	0	0	10.33
9	Shrub	Unburned	0	0	0	0	10.33
10	Shrub	Unburned	0	0	0	0	13.67
11	Shrub	Unburned	0	0	0	0	13.67
12	Shrub	Unburned	0	0	0	0	16.67
13	Shrub	Low	360	0	0	0	4.67
14	Shrub	Low	360	0	0	0	5.33
15	Shrub	Low	0	0	0	0	5.33
16	Shrub	Low	0	0	0	0	6.33
17	Shrub	Low	0	0	0	0	6.33
18	Shrub	Low	360	0	0	0	7.00
19	Shrub	Low	0	0	0	0	7.00
20	Shrub	Low	0	0	0	0	7.33
21	Shrub	Low	30	0	0	0	7.67
22	Shrub	Low	0	0	0	0	7.67
23	Shrub	Low	5	0	0	0	7.67
24	Shrub	Low	0	0	0	0	8.67
25	Shrub	Low	0	0	0	0	9.00
26	Shrub	Moderate	360	360	0	0	1.00
27	Shrub	Moderate	360	360	5	0	2.33
28	Shrub	Moderate	360	60	0	0	2.67
29	Shrub	Moderate	60	60	45	0	3.00
30	Shrub	Moderate	360	10	5	0	3.00
31	Shrub	Moderate	360	30	0	0	3.00
32	Shrub	Moderate	30	360	5	0	3.33
33	Shrub	Moderate	30	360	60	5	3.67
34	Shrub	Moderate	360	30	0	0	4.00
35	Shrub	Moderate	360	10	0	0	4.67
36	Shrub	Moderate	120	0	0	0	4.67
37	Shrub	Moderate	360	10	0	0	5.00
38	Shrub	Moderate	60	0	0	0	5.67
39	Shrub	Moderate	360	15	10	0	6.00
40	Shrub	Moderate	360	110	30	5	6.00
41	Shrub	Moderate	360	30	0	0	6.00
42	Shrub	Moderate	60	0	0	0	6.00
43	Shrub	Moderate	10	0	0	0	6.67
44	Shrub	Moderate	360	13	15	15	6.67
45	Shrub	Moderate	360	60	5	0	7.33
46	Shrub	Moderate	60	0	0	0	7.33
47	Shrub	Moderate	60	45	5	0	7.67

48	Shrub	Moderate	360	30	0	0	8.00
49	Shrub	Moderate	120	5	0	0	8.33
50	Shrub	Moderate	360	15	0	0	3.00
51	Shrub	Moderate	30	0	0	0	4.00
52	Shrub	Moderate	20	0	0	0	4.67
53	Shrub	Moderate	360	60	10	0	4.67
54	Shrub	Moderate	30	0	0	0	5.33
55	Shrub	Moderate	60	5	0	0	8.00
56	Shrub	Moderate	60	5	0	0	8.00
57	Shrub	Moderate	15	0	0	0	8.33
58	Shrub	High	360	30	0	0	2.33
59	Shrub	High	360	360	0	0	2.33
60	Shrub	High	360	60	0	0	2.33
61	Shrub	High	360	360	30	0	3.00
62	Shrub	High	360	60	0	0	4.00
63	Shrub	High	60	0	0	0	4.00
64	Shrub	High	60	5	0	0	4.67
65	Shrub	High	360	30	0	0	4.67
66	Shrub	High	360	30	0	0	4.67
67	Shrub	High	360	360	0	0	4.67
68	Shrub	High	360	30	0	0	5.00
69	Shrub	High	0	0	0	0	5.33
70	Shrub	High	60	5	0	0	5.67
71	Shrub	High	30	0	0	0	5.67
72	Shrub	High	360	30	0	0	5.67
73	Shrub	High	5	0	0	0	5.67
74	Shrub	High	0	0	0	0	6.33
75	Shrub	High	0	0	0	0	6.67
76	Shrub	High	360	360	0	0	6.67
77	Shrub	High	30	0	0	0	7.33
78	Shrub	High	0	0	0	0	7.67
79	Shrub	High	30	0	0	0	7.67
80	Shrub	High	0	0	0	0	9.00
81	Shrub	High	30	0	0	0	9.33
82	Shrub	High	0	0	0	0	9.33
83	Shrub	High	0	0	0	0	10.00
84	Shrub	High	0	0	0	0	12.00
85	Shrub	High	10	0	0	0	15.00
86	Grass	Unburned	10	0	0	0	5.33
87	Grass	Unburned	2	0	0	0	8.00
88	Grass	Unburned	2	0	0	0	12.00
89	Grass	Low	0	0	0	0	4.33
90	Grass	Low	15	0	0	0	4.33
91	Grass	Low	30	0	0	0	6.33
92	Grass	Low	0	60	0	0	7.00
93	Grass	Low	0	0	0	0	9.67
94	Grass	Moderate	120	5	0	0	0.00
95	Grass	Moderate	360	25	0	0	2.00
96	Grass	Moderate	360	60	5	0	3.67
97	Grass	Moderate	360	20	0	0	4.00
98	Grass	Moderate	120	5	0	0	5.33
99	Grass	Moderate	360	360	30	0	6.00
100	Grass	Moderate	90	0	0	0	6.00
101	Grass	Moderate	30	0	0	0	6.33
102	Grass	Moderate	0	5	0	0	7.33

103	Grass	Moderate	0	0	0	0	8.00
104	Grass	High	60	0	0	0	5.33
105	Grass	High	360	30	20	0	5.67
106	Grass	High	0	360	60	0	5.67
107	Grass	High	5	60	0	0	6.67
108	Grass	High	60	0	0	0	6.67
109	Grass	High	5	120	0	0	7.33
110	Grass	High	0	0	0	0	7.33
111	Grass	High	0	120	0	0	7.67
112	Grass	High	10	360	0	0	8.00
113	Grass	High	15	60	0	0	9.00
114	Grass	High	0	90	0	0	9.00
115	Grass	High	0	60	0	0	9.33
116	Grass	High	0	120	0	0	9.67
117	Grass	High	0	0	0	0	10.33
118	Grass	High	0	0	0	0	11.33
119	Grass	High	10	15	10	0	13.00

Table A.12. Burn severity and soil water repellency field data, Section B.

			WDPT				
Point	**Vegetation**	**Severity**	**Surface**	**2 cm**	**4 cm**	**6 cm**	**MDI (ml/min)**
1	Shrub	Low	0	0	0	0	4.00
2	Shrub	Low	0	0	0	0	4.33
3	Shrub	Low	20	3	0	0	3.33
4	Shrub	Low	0	0	0	0	7.67
5	Shrub	Low	0	0	0	0	6.33
6	Shrub	Low	0	0	0	0	5.67
7	Shrub	Low	0	0	0	0	8.33
8	Shrub	Low	0	0	0	0	10.33
9	Shrub	Low	0	0	0	0	8.33
10	Shrub	Low	0	0	0	0	9.00
11	Shrub	Low	0	0	0	0	8.33
12	Shrub	Low	0	0	0	0	11.67
13	Shrub	Low	0	0	0	0	6.33
14	Shrub	Low	0	0	0	0	9.00
15	Shrub	Low	0	0	0	0	9.33
16	Shrub	Low	0	0	0	0	12.67
17	Shrub	Low	0	0	0	0	5.33
18	Shrub	Low	20	0	0	0	6.00
19	Shrub	Moderate	30	0	0	0	4.00
20	Shrub	Moderate	60	0	0	0	4.67
21	Shrub	Moderate	60	30	0	0	1.00
22	Shrub	Moderate	30	0	0	0	2.00
23	Shrub	Moderate	360	360	10	0	1.67
24	Shrub	Moderate	0	0	0	0	4.33
25	Shrub	Moderate	360	0	0	0	2.00
26	Shrub	Moderate	0	0	0	0	6.33
27	Shrub	Moderate	360	30	0	0	1.67
28	Shrub	Moderate	60	0	0	0	4.67
29	Shrub	Moderate	60	0	0	0	6.33

30	Shrub	Moderate	360	5	0	0	1.67
31	Shrub	Moderate	60	10	0	0	3.33
32	Shrub	High	15	0	0	0	6.00
33	Shrub	High	360	0	0	0	3.33
34	Shrub	High	0	0	0	0	4.00
35	Shrub	High	60	0	0	0	5.67
36	Shrub	High	0	0	0	0	6.33
37	Shrub	High	60	0	0	0	8.33
38	Shrub	High	0	0	0	0	4.00
39	Shrub	High	0	0	0	0	7.00
40	Shrub	High	360	5	0	0	3.67
41	Shrub	Moderate	30	0	0	0	8.33
42	Shrub	Moderate	360	0	0	0	6.33
43	Shrub	Moderate	0	0	0	0	4.00
44	Shrub	High	30	0	0	0	5.00
45	Shrub	High	360	0	0	0	1.33
46	Shrub	High	30	0	0	0	2.67
47	Shrub	Moderate	60	10	0	0	3.33
48	Shrub	Moderate	360	60	0	0	3.33
49	Shrub	Moderate	120	60	0	0	1.67
50	Shrub	Moderate	360	0	0	0	4.67
51	Shrub	Moderate	60	0	0	0	4.67
52	Shrub	Moderate	60	0	0	0	3.67
53	Shrub	High	360	30	0	0	1.67
54	Shrub	High	360	0	0	0	4.67
55	Grass	Unburned	5	0	0	0	5.67
56	Grass	Unburned	5	0	0	0	6.33
57	Grass	Unburned	0	0	0	0	5.00
58	Grass	Unburned	0	0	0	0	3.67
59	Grass	Unburned	0	0	0	0	2.67
60	Grass	Unburned	0	0	0	0	3.00
61	Grass	Unburned	0	0	0	0	2.67
62	Grass	Unburned	0	0	0	0	2.67
63	Grass	Low	0	0	0	0	6.67
64	Grass	Low	0	0	0	0	3.00
65	Grass	Low	0	0	0	0	3.67
66	Grass	Moderate	120	5	0	0	5.00
67	Grass	Moderate	360	10	0	0	2.33
68	Grass	Moderate	5	0	0	0	5.33
69	Grass	Moderate	360	15	0	0	5.00
70	Grass	Moderate	120	60	0	0	0.67
71	Grass	Moderate	360	60	0	0	1.33
72	Grass	Low	0	0	0	0	4.00
73	Grass	Low	0	0	0	0	7.33
74	Grass	Low	0	0	0	0	5.00
75	Grass	Low	0	0	0	0	4.67
76	Grass	Low	0	0	0	0	2.33
77	Grass	Low	0	0	0	0	4.00
78	Grass	High	0	30	0	0	4.00

79	Grass	High	30	60	0	0	4.33
80	Grass	High	0	30	0	0	3.67
81	Grass	Unburned	15	0	0	0	6.67

Table A.13. Burn severity and soil water repellency field data, Section C.

Point	Vegetation	Severity	WDPT				MDI (ml/min)
			Surface	2 cm	4 cm	6 cm	
1	Shrub	Low	0	0	0	0	4.33
2	Shrub	Low	0	0	0	0	4.67
3	Shrub	Low	0	0	0	0	5.33
4	Shrub	Low	0	0	0	0	4.00
5	Shrub	Low	0	0	0	0	7.67
6	Shrub	Low	0	0	0	0	4.00
7	Shrub	Moderate	60	10	0	0	3.33
8	Shrub	Moderate	360	60	0	0	3.33
9	Shrub	Moderate	120	60	0	0	1.67
10	Shrub	Moderate	360	0	0	0	4.67
11	Shrub	Moderate	60	0	0	0	4.67
12	Shrub	Moderate	60	0	0	0	3.67
13	Shrub	High	360	30	0	0	1.67
14	Shrub	High	360	0	0	0	4.67
15	Shrub	Low	0	0	0	0	5.67
16	Shrub	Low	0	0	0	0	3.67
17	Shrub	Low	0	0	0	0	5.67
18	Shrub	Low	0	0	0	0	3.00
19	Shrub	Moderate	30	0	0	0	4.33
20	Shrub	Moderate	30	0	0	0	3.67
21	Shrub	Moderate	0	0	0	0	4.33
22	Shrub	Moderate	360	30	5	0	5.00
23	Shrub	Moderate	60	10	0	0	2.67
24	Grass	Low	0	0	0	0	4.67
25	Grass	Low	0	0	0	0	2.33
26	Grass	Low	0	0	0	0	4.00
27	Grass	High	30	0	0	0	4.00
28	Grass	High	30	0	0	0	4.33
29	Grass	High	30	0	0	0	3.67
30	Grass	Low	0	0	0	0	5.67
31	Grass	Low	0	0	0	0	8.00
32	Grass	Low	0	0	0	0	5.67
33	Grass	Low	0	0	0	0	6.67
34	Grass	Low	0	0	0	0	6.00
35	Grass	Low	360	0	0	0	3.67

Relative Suitability of Indices Derived from Landsat ETM+ and SPOT 5 for Detecting Fire Severity in Sagebrush Steppe Rangelands

Jill Norton, Blaine County, 219 1st Ave. South, Suite 209, Hailey, ID 83333

Nancy Glenn, Idaho State University, Boise Center, 322 E. Front St, Suite 240, Boise, ID 83702

Matt Germino, Idaho State University, Dept of Biological Sciences, Box 8007, Pocatello, ID 83209

Keith T. Weber, Idaho State University, GIS Training and Research Center, Pocatello, ID 83209

Steven Seefeldt,USDA-ARS Subarctic Agricultural Research Unit, Rm. 355 O'Neill Bldg, University of Alaska Fairbanks, Fairbanks, AK 99775

ABSTRACT
Indices of burn area and fire severity based on remotely sensed data have been developed for forest ecosystems, but not semiarid shrublands in which large wildfires are a common occurrence and a major issue for land management. Our goal was to determine whether available satellite data could be used to remotely sense burn area and fire severity (completeness of vegetation removal) in shrublands. We compared the performance of five remote sensing indices with extensive ground-based cover assessments made before and after the burning of a 3 km^2 area. The different indices were based on either Landsat 7 ETM+ or SPOT 5 data, using either single or multiple dates of imagery. Remote sensing indices delineating burned versus unburned areas had better overall, user, and producer's accuracies than indices delineating levels of fire severity. The Soil Adjusted Vegetation Index (SAVI) calculated from SPOT had the greatest overall accuracy (100%) in delineating burned versus unburned areas. The relative differenced Normalized Burn Ratio (RdNBR) using Landsat provided the highest accuracies (73% overall accuracy) for delineating fire severity. Though SPOT's spatial resolution likely conferred advantages for determining burn boundaries, Landsat's higher spectral resolution (particularly band 7, 2.21 μm) appeared necessary for detecting differences in fire severity.

Keywords: Burn severity, Semi-arid rangelands, Relative differenced Normalized Burn Ratio

INTRODUCTION AND BACKGROUND

Sagebrush steppe communities evolved with regular and extensive wildfires. Fire is a widespread agent of change and has become one of the dominant land management issues today (Arno and Gruell 1983). Remote sensing with satellite imagery offers the ability to evaluate burned areas across multitemporal and multispatial scales, as demonstrated in forest ecosystems (Morgan et al. 2001). Satellite data are useful for examining fire effects because they 1) can be used to qualitatively and quantitatively evaluate vegetation over multi-temporal and -spatial scales, 2) can be relatively low cost, 3) systematically cover large and inaccessible areas (in many instances fires are located in remote areas), and 4) capture data from parts of the electromagnetic spectrum (i.e. infrared) that provide useful information specific to vegetation and soils (Flasse et al. 2004).

Our goal was to determine whether rangeland fire severity could be modeled with remote sensing techniques, using commonly available satellite data and either single date imagery or pre-and post-fire multitemporal differencing incorporated with field data. Definitions of fire severity differ among studies, as does the amount of time elapsed between fires and when severity is assessed (Key and Benson, 2006; Lentile et al. 2006; Miller and Yool, 2002; Roy et al. 2006; and Ryan and Noste, 1983). Fire severity is defined for the current study as the completeness of above-ground vegetation removal due to fire, measured immediately following fire. Thus, remote detection of burns requires sensitivity of imagery and calculations of vegetation change. Fire severity is distinct from burn severity, which incorporates both short- and long-term post-fire effects (Key and Benson, 2006; Lentile et al. 2006). Our study occurred in mountain sagebrush steppe, where wildfires occur frequently from mid-summer through fall. Shrubs and herbs co-dominate foliar cover before fire, while after fires herbs increase in abundance and shrubs are temporarily absent as they reestablish by seed over decades (Harniss and Murray, 1973). Some post-fire green-up by herbs occasionally occurs in the same growth season as the fires.

The objectives of this research were to 1) evaluate the suitability of remote sensing indices for fire severity mapping within a sagebrush steppe rangeland, 2) assess the importance of considering spectral and spatial resolution, and 3) assess the influence of timing of imagery acquisition and seasonality of fire. These objectives are aimed at developing methods for fire severity mapping for land management agencies.

Remote sensing of semiarid vegetation

Several attributes of reflectance to satellite sensors make detecting vegetation change in sparsely vegetated semiarid rangeland ecosystems challenging. These rangeland characteristics contribute to the challenges of remote sensing of vegetation along with: 1) nonlinear mixing due to multiple scattering of light, 2) evolutionary adaptations making desert plants spectrally dissimilar and lacking a strong red edge, 3) spectral variability within the same species due to spatially discontinuous precipitation patterns, 4) open shrub canopies which affect near infrared (NIR) reflectance, 5) low leaf area index, and 6) varying phenological status of plant canopies across space and time (Asner, 2004; Asner and Heidebrecht, 2002; Okin et al. 2001). Because there tends to be an abundance of bare ground in sagebrush steppe rangeland ecosystems and soil reflectance is often brighter than vegetation reflectance, bare ground 'dilutes' the vegetation signature. This is exaggerated in burned ecosystems where soil reflectance is high and little vegetation exists.

Vegetation indices have been developed to detect vegetation and could be used to estimate biomass loss for mapping burn areas and severity (Santos et al. 1999), such as the normalized difference vegetation index (NDVI) (Flasse et al. 2004; Epting and Verbyla, 2005; Roy, 1999; Ruiz-Gallardo et al. 2004; van Wagtendonk et al. 2004; Salvador et al. 2000), soil adjusted vegetation index (SAVI - Huete, 1988; Epting et al. 2005), modified soil adjusted vegetation index (MSAVI - Qi et al. 1994; Epting et al. 2005), atmospherically resistant vegetation index (ARVI) (Kaufman and Tanre, 1992; Santos et al. 1999), and normalized difference shortwave infrared (NDSWIR; Gerard et al. 2003). Alteration of the vegetation:soil

balance is a substantial characteristic of fire; therefore soil adjustments in vegetation indices (e.g. SAVI or MSAVI) are likely to be critical for mapping burn areas and severity. Because SAVI and MSAVI were developed to minimize soil brightness and soil variations using red and near-infrared wavelengths as well as a soil adjustment factor for semiarid vegetation, these indices may be appropriate for rangeland fire applications. NDVI was the primary technique used to detect burn severity until the late 1990s, when Lopez Garcia and Caselles (1991) developed an algorithm later coined as the normalized burn ratio (NBR; equation 1) using Landsat imagery (Key and Benson, 1999b; Key and Benson, 2004a; Key and Benson, 2006; Salvador et al. 2000). Since then, the Landsat-based NBR is the most widely used method on large fires (>200 hectares) for perimeter and burn severity detection (Cocke et al. 2005; Key and Benson, 2006).

$$\text{NBR} = \frac{NIR - SWIR_{(2.21\mu m)}}{NIR + SWIR_{(2.21\mu m)}} \qquad (1)$$

The NBR technique uses the near-infrared (Landsat band 4, 0.76 – 0.90µm) and shortwave infrared (Landsat band 7, 2.08 – 2.35µm) because these bands are generally the most sensitive to vegetation change due to fire, which increases the shortwave infrared band and decreases the near infrared band (Lentile et al. 2006).

A differenced NBR (dNBR) is used to offer a quantitative measure of environmental change due to the fire or other temporal difference (Key and Benson, 1999b; Key and Benson, 2004a). The dNBR represents a scaled index of the magnitude of change caused by fire (van Wagtendonk et al. 2004). The dNBR is composed of the post-fire NBR data set subtracted from the pre-fire NBR data set (equation 2).

$$\text{dNBR} = \text{NBR}_{\text{pre-fire}} - \text{NBR}_{\text{post-fire}} \qquad (2)$$

There are two types of dNBR severity measures, an initial assessment in which post-fire measures occur immediately after fire and are not influenced by biotic recovery, and an extended assessment in which post-fire assessments are made in subsequent growth seasons and thereby reflect recovery. The NBR and dNBR may or may not be applicable in rangeland ecosystems due to vegetation re-growth times with respect to the seasonality of the burn. For instance, it takes longer for forested ecosystems to recover to pre-fire conditions (i.e. having the same reflectance) than rangelands. Likewise, Miller and Thode (2007) found that a Landsat-based relative dNBR (RdNBR, equation 3) performs better than the absolute dNBR at detecting high burn severity areas from moderate burn severity in mixed forest/shrubland study areas.

$$\text{RdNBR} = \frac{\text{dNBR}}{\sqrt{\left|\text{NBR}_{\text{prefire}}\right|}} \qquad (3)$$

Burn (fire) severity has also been assessed by comparing several single-date and multi-date approaches. For instance, Roy et al. (2006) and Epting et al. (2005) agree that the dNBR may not be the most optimal for estimating fire severity in non-forested areas. Yet Brewer et al. (2005) stated the dNBR has the advantage of using it anywhere in the continental U.S. and pointed out that it (stratified by National Landcover data (NLCD)) does not introduce analyst input error (i.e., human bias). In addition, Gerard et al. (2003) developed an algorithm coined the normalized difference SWIR (NDSWIR, equation 4) to map fire scar burns using SPOT NIR (Band 3, 0.78-0.89µm) and SWIR (Band 4, 1.58-1.75µm).

$$\text{NDSWIR} = \frac{NIR - SWIR_{(1.66\mu m)}}{NIR + SWIR_{(1.66\mu m)}} \qquad (4)$$

Many studies have been performed in forested ecosystems to determine burn or fire severity within a burn perimeter (Brewer et al. 2005; Epting and Verbyla, 2005; Epting et al. 2005; Miller and Thode, 2007; Patterson and Yool, 1998; Turner et al. 1994; White et al. 1996; Wimberly and Reilly, 2007). However, few studies have been carried out in areas with reduced vegetation cover (Roy et al. 2006; Smith et al. 2005) or specifically within semiarid sagebrush steppe ecosystems (van Wagtendonk et al. 2004).

MATERIALS AND METHODS

Study area

This study took place within the Hitching Post pasture, a 3.24 km^2 fenced parcel within the U.S. Sheep Experiment Station (USSES) located in Clark County, Idaho, USA, at an elevation of approximately 1800 m (Fig. 1). Average annual precipitation ranges from 250-530 mm with up to seventy percent falling as snow (Seefeldt, 2005). Average annual temperatures are 5-6 °C, with a 70 to 90 day frost-free season. The pasture is a sagebrush steppe ecosystem characterized by extreme seasonal variability and a co-dominance of *Artemisia* with several grass species (West and Young, 2000). The Hitching Post pasture has two primary subspecies of sagebrush (*Artemisia* ssp.): mountain big (*A. tridentata* ssp. *vaseyana*), and threetip (*A. tripartita ssp. tripartita*). Sheep and horses have grazed this pasture for the last decade, but it had not been domestically grazed for 2.5 years prior to the burn. This study area was chosen because it offered an opportunity to take advantage of a prescribed burn, allowing a high degree of control for pre- and post-fire field sampling.

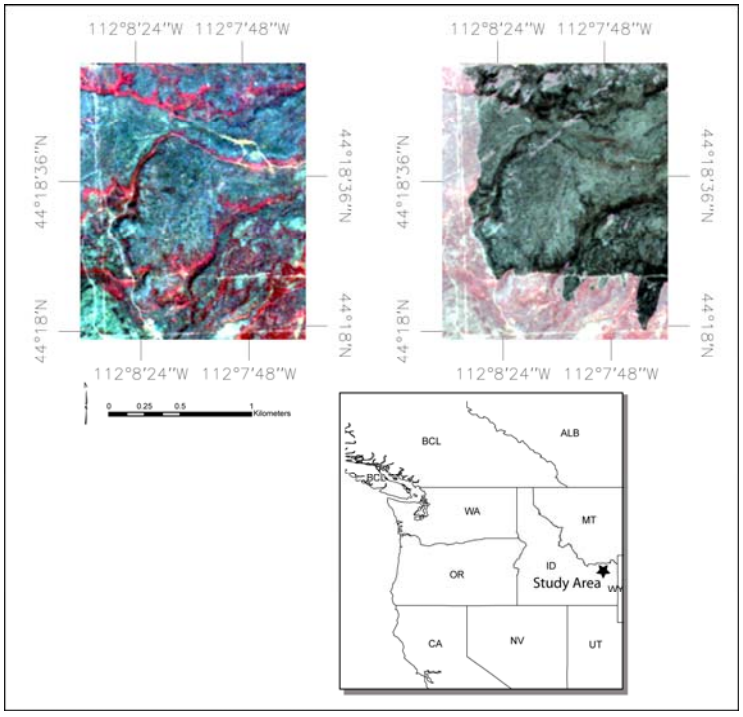

Figure 1. Study area, USDA Sheep Experiment Station, Dubois, Idaho. SPOT 5 images (NIR, red, green) of pre-burn (left) and post-burn (right) of the Hitching Post Pasture.

Fire

The prescribed fire was performed on September 14 and 15, 2005 and consistently burned most of the northern 4/5 of the pasture (approximately 2.82 km^2, Fig. 2) delineated with a bulldozed safety line. Wind direction and speed were monitored throughout the burn every 30 minutes. Using a hand-held anemometer, winds were observed around 20 m/sec in a predominantly northeast direction throughout most of this burn. Flame lengths ranged from approximately 30 cm to 4 m tall as the fire moved from

grass and forbs up to shrubs. Afterward, nine strip burns and spot fires were ignited in the southern portion of the pasture (and burned to the north) (Fig. 2, south of the middle dozerline). The prescribed fire burned approximately 85% of the pasture area including 173 of the sampling sites (described below).

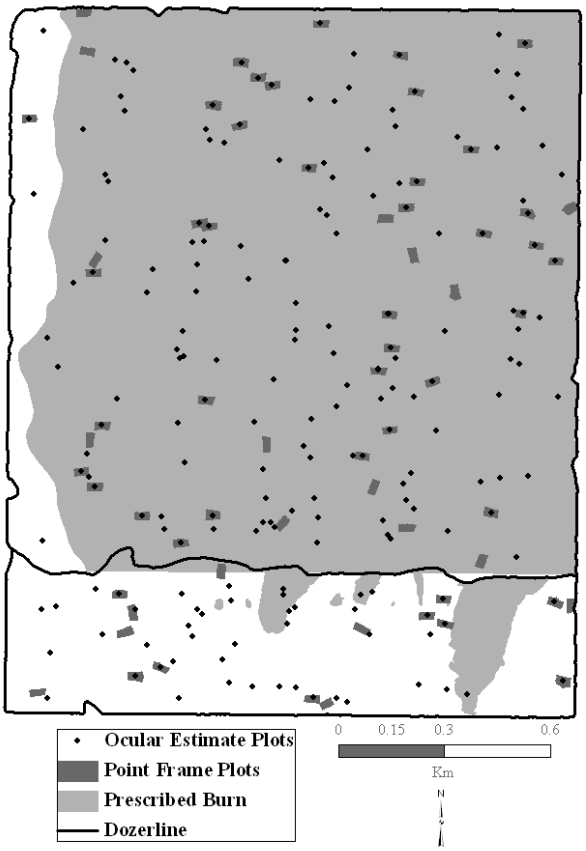

Figure 2. Location of ocular and point frame plots in relation to the fire in the Hitching Post Pasture.

Field methods

This study utilized pre- and post-fire field-based sampling to establish locations of sample sites along with a description of the vegetation, amount of bare ground, and fire severity observed at each site. These data were collected for both training and validation of the remote sensing indices used for the first objective. Two field methods were performed: ocular and point frame. The ocular method was used to quickly estimate percent cover of the upper-most canopy of ground cover across a 60 × 60 m plot with qualitative, coarse resolution. In the ocular method, categorical percent cover (0, 1-5%, 6-15%, 16-25%, 26-35%, 36-50%, 51-75%, >75%) for six categories (shrub, grass, forb, litter, rock, and bare ground) were estimated after thoroughly walking the plot area. Each sample site (n=206) was randomly located within the pasture (Fig. 2; points) to ensure adequate replication across fire severity classes.

The point frame method was also used to provide a relatively more accurate and statistical representation of true ground cover (Floyd and Anderson, 1982; Floyd and Anderson, 1987). The point frame establishes a dot grid overlooking underlying vegetation and bare ground. Observers view vegetation from a near-nadir standing position and record the cover types that are beneath 36 intercepted points (cross-hairs). Plots of 20 × 40 m were sampled with the point frame. The sampling frequency necessary to capture variability was determined using sample effort curves from all cover categories. A maximum of 15 frames of point data were needed within each 20 × 40 m plot to ensure adequate representation of cover in this study area. Point frame data (Fig. 2; rectangles) were collected at 45 of the 206 ocular sample sites

(centered over the sites where ocular estimates were used) as well as 20 additional sample sites (total of 65 point frame samples).

Pre-fire field data collections occurred between mid-June and early August 2005 and included 206 ocular plots and 65 point frame measurements. Post-fire sampling began immediately following the prescribed burn and continued for approximately 1.5 months, prior to any green-up. Post-fire field surveys, intended to provide field validation of fire severity levels, included re-sampling all pre-fire sampling sites. The same field methods as pre-fire sampling (ocular estimates and point frame measurements) were consistently repeated at the same scales and within 3-5 m of the original locations by navigating with a GPS unit. In addition, a fire severity rating (unburned, incompletely burned (moderate), and completely burned (high)) was assigned to each ocular and point frame plot.

We assessed fire severity with a customized ocular method by modifying the field methods of the US Forest Service (Bobbe et al. 2001) and the US Park Service (USDI NPS, 2003), and the composite burn index (CBI) of Key and Benson (1999a; 2004b). Each of these methods incorporates qualitative and quantitative measurements to detect and categorize fire severity; we incorporated and modified the three methods above according to burn conditions in our study area in the context of a semiarid rangeland site. Attributes such as litter condition, shrub condition, surface rock (USDA FS), organic substrate, and vegetation (USDI NPS) were incorporated from the USDA and USDI burn severity. Key and Benson's (1999a) CBI places a ~50% change in the herb/low shrub/tall shrub strata into the moderate burn severity category. The study area predominantly fits into Key and Benson's shrub strata, so we incorporated this ~50% change severity category, referred to herein as 'incompletely burned'. In most plots and pixels, the fire either burned all vegetation (except stumps) or none; there was a very small amount of partly burned vegetation. Therefore, severity at each plot was assessed based on the percent cover of bare ground and rock, and the amount of consumed, above-ground vegetation and litter. Fire severity classes included unburned, incompletely burned (moderate), and completely burned (high).

Remote sensing methods

Image acquisition

Landsat 7 ETM+ and SPOT 5 imagery were chosen for this work due to their reasonable cost, spatial and spectral resolution, and because their data are continuously collected, making them useful and easily available to land/fire managers. In addition to visible and NIR bands, SPOT 5 provides a SWIR band (1.58-1.75µm) with 20m spatial resolution. Pre- and post-fire images were acquired for Landsat (July 4 and October 24, 2005) and SPOT (August 27 and September 28, 2005) (Table 1). All images were chosen as close to the date of the prescribed burn (September 14-15, 2005) as possible with no cloud cover.

Table 1. Dates and location of SPOT and Landsat imagery. The prescribed fire occurred September 14 and 15, 2005.

Imagery	Date	Scene ID/Path Row
SPOT 5 Pre-fire	27-Aug-05	547-260
SPOT 5 Post-fire	28-Sep-05	547-260
Landsat ETM+ Pre-fire	4-Jul-05	39/29
Landsat ETM+ Post-fire	24-Oct-05	39/29

Imagery were processed to at-satellite reflectance using ENVI software (ITT, 2007) to reduce between-scene variability. The SPOT 20 m SWIR band was resampled to 10 m to coregister with the SPOT red and NIR bands of 10 m. Image rectification was performed after remote sensing indices (see below) were calculated in order to reduce error during resampling. The resulting Root Mean Square Error (RMSE) was

less than ½ pixel for both the Landsat (0.2621) and SPOT (0.3489) imagery during the image rectification process. Our study area was not affected by the scan line corrector (SLC) failure in the Landsat images.

Image processing

In order to identify the Landsat and SPOT bands that were most sensitive to changes between the pre- and post-fire images, we investigated 36 field plots in both pre- and post-fire images. These 36 sample sites were chosen for their near homogeneous vegetation cover (type and amount) within each plot pre-fire and similar fire severities within each plot post-fire. Reflectance values for the plots were averaged for each of the pre- and post-fire images and then compared (Figs. 3 and 4).

Based on initial investigations of sensitivity of the SPOT and Landsat data, 5 indices were implemented (Table 2) including single-date and multi-date (pre- and post-burn imagery) manipulation. Indices were applied to determine burned from unburned areas, and then assessed for their ability to differentiate levels of fire severity identified in the field. The multi-date indices include a dNBR (equation 2) and relative dNBR (RdNBR; equation 3) with Landsat imagery. SPOT was not used for the dNBR and RdNBR because of the lack of a SWIR band comparable to Landsat's band 7 (2.21 μm).

Table 2. Remote sensing indices used. Red: Landsat band 3, SPOT band 2; NIR: Landsat band 4, SPOT band 3; SWIR: Landsat band 5 (for NDSWIR), Landsat band 7 (for NBR, dNBR, and RdNBR), SPOT band 4.

Remote Sensing Index	Algorithm	References
SAVI	$\frac{(1+L)(NIR-Red)}{NIR+Red+L}$ (L = 0.5)	Huete, 1988
MSAVI	$\frac{2*(NIR)+1-\sqrt{(2*(NIR)+1)2-8*(NIR-Red)}}{2}$	Qi et al., 1994
NDSWIR	$\frac{NIR-SWIR}{NIR+SWIR}$	Gerard et al., 2003
NBR dNBR	$\frac{NIR-SWIR}{NIR+SWIR}$ Pre-fire NBR –Post-fire NBR	Lopez Garcia and Caselles, 1991; Key and Benson, 1999b
RdNBR	$\frac{dNBR}{\sqrt{\lvert NBR_{prefire}\rvert}}$	Miller and Thode, 2007

The single-date indices, using post-fire imagery only, include the SAVI, MSAVI, and normalized difference shortwave-infrared index (NDSWIR, equation 4). Both Landsat and SPOT imagery were used for all of these indices. As suggested by Huete (1988), we used a soil adjustment factor of 0.5 for the SAVI calculation which can be applied across varying vegetation biomass environments. The MSAVI index calculates a variable soil adjustment factor L (Qi et al. 1994) until soil noise cannot be further removed.

Relating remote sensing indices to field data

Training data were used to relate remote sensing index values to fire severity values. For training purposes, 119 index values from plots (including both ocular and point frame, none of which overlapped) were used. Each field plot was assigned a fire severity rating based on the field methods described above.

Remote sensing index values were acquired at each training site for each index. The fire severity index values were then separated into fire severity classes by first placing all plot values into their respective fire severity classes as determined in the field. The minimum, maximum, and mean index values of each class were determined. The classes were separated by splitting the difference between the maximum of one class with the minimum of the next class. Likewise, if there was a gap between fire severity class data values, then a break was determined by splitting the difference between the maximum of one class with the minimum of the next class. To encompass the variability across the study area, training plots were randomly selected within each burn severity class and the same training plots were used within each burn severity class for each index.

Validation

An accuracy assessment was used to quantitatively determine how well the remotely sensed indices corresponded with the field data. The validation was performed following traditional accuracy assessment techniques (Congalton and Green, 1999). Fifty plots of unburned and 100 plots of burned were used for the unburned versus burned validation. For the fire severity validation, 50 plots for each class (unburned, incompletely burned, completed burned) (n=150) were used for the validation. No training data were used for the validation (Table 3). The remote sensing burn severity values of the validation plots were then compared to the field fire severity classes. Accuracy results were calculated for each index, including a standard error matrix reporting user, producer's, and overall accuracies, kappa statistic, and a Z-test statistic for significance (of a single error matrix) (Congalton and Green, 1999).

Table 3. Number of training and validation plots used to assess remote sensing indices.

Burn Severity Value	# of Training Plots	# of Validation Plots
Unburned	14	50
Moderate	16	50
High	89	50

A pairwise test of significance (equation 5) (Congalton and Green, 1999) was performed for the matrices that had highest accuracies as well as for those that shared similar overall accuracies. This test is a Kappa analysis that determines if two error matrices are significantly different by comparing their KHAT statistics.

$$Z_{pairwise} = \frac{|K_1 - K_2|}{\sqrt{var(K_1) + var(K_2)}} \qquad (5)$$

Where K_1 and K_2 are the Kappa statistics for error matrices 1 and 2 and var(K_1) and var(K_2) are estimates of variance for matrices 1 and 2.

RESULTS

The SPOT and Landsat reflectance values between pre-and post-fire images were different (Figs. 3 and 4). The SPOT green and NIR reflectances had the greatest change, increasing approximately 1.6% and 1.8%, respectively, after the fire. The SPOT red band decreased 0.84% and the SWIR band increased approximately 0.81%. The SPOT pre-fire image was collected in late August, at a time when most herbs/grasses were senesced and soil exposure was high. Alternatively, the Landsat data was acquired at the beginning of July before the onset of seasonal drought and senescence of herbaceous species. In comparing the pre- and post-fire Landsat images, the NIR and SWIR (2.21μm) bands demonstrated the greatest change (Fig. 4). The NIR decreased 3% and the SWIR band increased 5.5% after the fire.

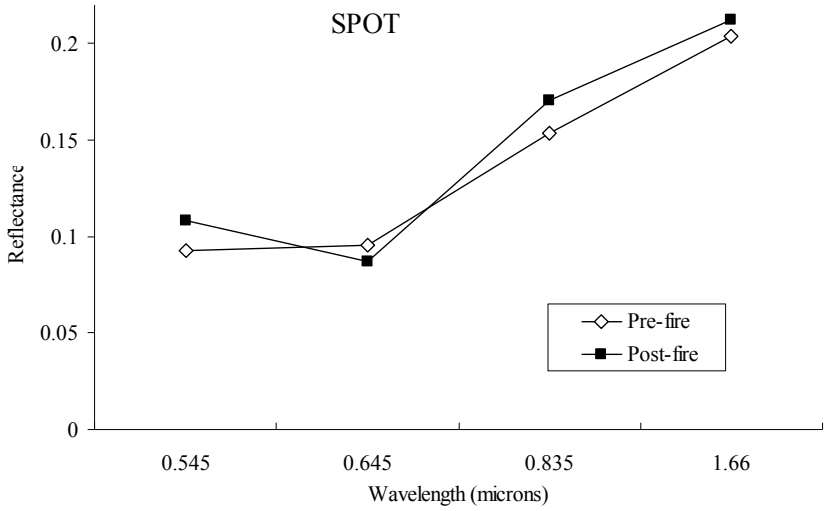

Figure 3. The average value of SPOT 'at satellite' reflectance for 36 plots, pre- and post-fire.

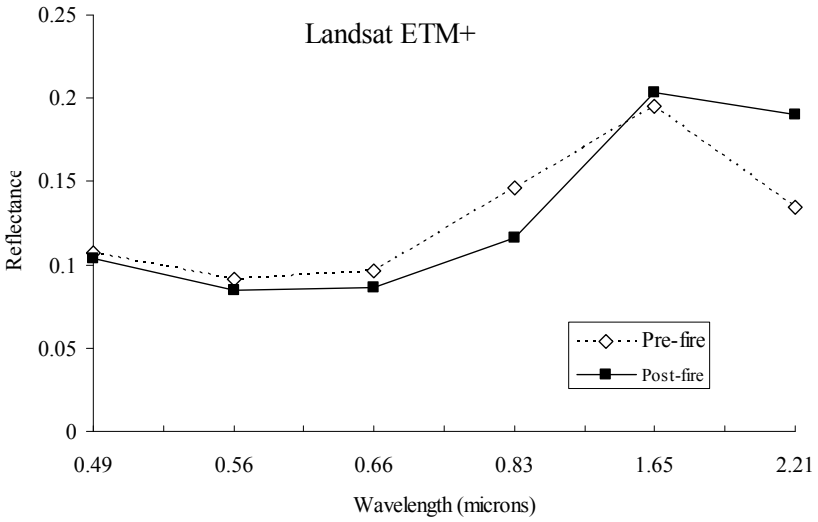

Figure 4. The average value of Landsat 'at satellite' reflectance for 36 plots, pre- and post-fire.

The remote sensing indices assessing burned versus unburned areas had better overall, user, and producer's accuracies (Tables 4 and 5) than those where fire severity was described as unburned, incompletely burned, or completely burned (Tables 6 and 7).

Burned versus unburned

The burned versus unburned indices generated using SPOT imagery (NDSWIR, MSAVI, and SAVI) and the Landsat-derived burned versus unburned indices (dNBR, RdNBR, NDSWIR, MSAVI, and SAVI) had relatively high accuracy (~ 95% overall accuracy). The three burned versus unburned SPOT-derived indices (NDSWIR, MSAVI, and SAVI) had 95% or better overall accuracies (Table 4). SPOT SAVI provided the highest overall, users, and producer's accuracies (100%). Three burned versus unburned Landsat indices (RdNBR, MSAVI, and SAVI) performed nearly equally well at 95% overall accuracy (Table 5). A pairwise test of significance indicated that the SPOT SAVI index was significantly different

than both the SPOT MSAVI and NDSWIR (Table 8). A pairwise test for significance indicates that none of the Landsat-based indices are significantly different. Pairwise tests for significance between the SPOT-based SAVI index and the Landsat-based RdNBR, dNBR, MSAVI, and SAVI indices indicate that the SPOT-based SAVI is significantly better than the Landsat indices (Table 8).

Table 4. 'Burned vs. Unburned' remote sensing index accuracies and kappa statistics using SPOT 5 imagery.

Accuracy Type	NDSWIR	MSAVI	SAVI
Overall Accuracy	96%	95%	100%
Producer's Unburned	96%	98%	100%
Users Unburned	92%	86%	100%
Producer's Burned	96%	93%	100%
Users Burned	98%	99%	100%
KHAT	0.9091	0.8763	1.0000
Z	25.0211	20.6704	*

Table 5. 'Burned vs. Unburned' remote sensing index accuracies and kappa statistics using Landsat ETM+ imagery.

Accuracy Type	dNBR	RdNBR	NDSWIR	MSAVI	SAVI
Overall Accuracy	94%	95%	89%	95%	95%
Producer's Unburned	96%	98%	90%	94%	94%
Users Unburned	86%	86%	74%	90%	90%
Producer's Burned	93%	93%	88%	95%	95%
Users Burned	98%	99%	96%	97%	97%
KHAT	0.862	0.876	0.733	0.879	0.879
Z	19.314	20.670	12.133	21.102	21.102

Fire severity

The best fire severity index differentiating pixels between unburned, incompletely burned, and completely burned was the Landsat RdNBR. This index had a 73% overall accuracy and user accuracies of 56% and 76% for incompletely and completely burned, respectively (Table 6). The producer's accuracy was 61% and 63% for incompletely and completely burned, respectively. The best overall accuracy for the SPOT burn severity indices was the SAVI index at 71% overall accuracy (Table 7). Pairwise tests for significance between matrices indicate that the SPOT fire severity indices were not significantly different from each other; the Landsat fire severity indices were also not significantly different from each other with the exception of the RdNBR and NDSWIR (Table 9). Because the majority of the RdNBR's accuracies (overall, producer's and users) were higher than those of the other Landsat indices, the RdNBR was then compared to the SPOT-based indices. The pairwise test of significance indicated that the RdNBR accuracies were significantly better than the SPOT-based indices (Table 9) for fire severity.

Table 6. Fire Severity (unburned, moderate or incompletely burned, high or completely burned) remote sensing index accuracies using Landsat ETM+ imagery.

Accuracy Type	dNBR	RdNBR	NDSWIR	MSAVI	SAVI
Overall Accuracy	66%	73%	58%	66%	67%
Producer's Unburned	96%	98%	90%	94%	94%
Producer's Moderate	50%	61%	37%	50%	52%
Producer's High	55%	63%	52%	55%	57%
Users Unburned	86%	86%	74%	90%	90%
Users Moderate	38%	56%	34%	42%	44%
Users High	74%	76%	66%	66%	68%
KHAT	0.4900	0.5900	0.37000	0.4900	0.5100
Z	8.4339	10.7668	6.04186	8.4456	8.8829

Table 7. Fire Severity (unburned, moderate or incompletely burned, high or completely burned) remote sensing index accuracies using SPOT 5 imagery.

Accuracy Type	NDSWIR	MSAVI	SAVI
Overall Accuracy	65%	67%	71%
Producer's Unburned	95%	98%	100%
Producer's Moderate	49%	51%	61%
Producer's High	56%	55%	55%
Users Unburned	82%	86%	100%
Users Moderate	40%	38%	38%
User's High	74%	76%	76%
KHAT	0.4800	0.5000	0.5700
Z	8.2319	8.6376	10.391

Table 8. Pairwise test of significance between matrices for burned versus unburned

Pairwise Comparison	**$Z_{pairwise}$ (critical value at 95% confidence interval = 1.96)**
SPOT SAVI vs. SPOT MSAVI	3.0000
SPOT SAVI vs. SPOT NDSWIR	2.5211
SPOT SAVI vs. Landsat RdNBR	2.7727
SPOT SAVI vs. Landsat dNBR	3.0858
SPOT SAVI vs. Landsat MSAVI	2.7056
SPOT SAVI vs. Landsat SAVI	2.7056

DISCUSSION AND CONCLUSIONS

While studies have been performed in forested ecosystems to reliably detect fire severity, there have not been any established efforts in sagebrush steppe rangelands, an ecosystem type in which fire is common, and is a major factor in management. Fire management would benefit profoundly from research and monitoring of fires, which in turn could be enhanced with efficient remote sensing techniques. As

indicated by the highest overall, user, and producer's accuracies, the best index for determining burned from unburned areas was SPOT SAVI (100% overall accuracy) and the best index for differentiating fire severity within a burn was Landsat RdNBR (73% overall accuracy). Statistical testing indicated that SPOT SAVI was significantly different than other burned versus unburned indices. However, testing of fire severity indices indicate SPOT and Landsat-based indices are significantly different but that when compared within each sensor, the indices are not significantly different. While this conclusion is less compelling to place the Landsat-based RdNBR as the best index, the high users and producer's accuracies in the moderate and high fire severity categories indicate its superiority to other indices.

Table 9. Pairwise test of significance between matrices for fire severity.

Pairwise Comparison	$Z_{pairwise}$ (critical value at 95% confidence interval = 1.96)
Landsat RdNBR vs. Landsat NDSWIR	2.6777
Landsat RdNBR vs. SPOT NDSWIR	6.59
Landsat RdNBR vs. SPOT MSAVI	6.8894
Landsat RdNBR vs. SPOT SAVI	7.9487

Consistent with Sannier (1999), Epting et al. (2005), and Miller and Yool (2002), accuracies were better with fewer severity categories. In all cases, unburned versus burned indices had better results than fire severity indices. We were able to successfully determine if an area was burned or not in rangelands using SPOT-based NDSWIR, MSAVI, and SAVI indices and Landsat-based dNBR, RdNBR, NDSWIR, MSAVI, and SAVI indices.

Our best fire severity index, the Landsat RdNBR, supports Miller and Thode's (2007) results. In a mixed ecosystem study area, they concluded that this index performed better at separating high burn severity from other burn severity classes. Our incompletely and completely burned fire severity users' accuracies (56%, 76%, respectively) and producer's accuracies (61%, 63%, respectively) were higher for RdNBR than all other indices. These results are important to land managers given that high severity areas often require greater rehabilitation efforts.

Timing of imagery acquisition is important in relation to the seasonality of fire and field sampling dates due to phenological vegetation changes. Our fire took place in late summer when vegetation had already senesced. Reflectance (and resultantly, changes in reflectance) values were not as high as if the fire occurred in early to mid-summer (although fire in early to mid-summer is less common than fires in late summer in this ecosystem). Comparing the different indices when the sensors sampled on different days creates the possibility for a confounding factor of change in vegetation over time. Landsat imagery had 112 days between pre-fire and post-fire scenes, whereas SPOT imagery had only 32 days. Furthermore the Landsat pre-fire image was acquired when vegetation was not entirely senesced while the SPOT imagery was collected in late summer when there was a greater degree of senesced herbs in the plant community. Additionally, the Landsat post-fire image was collected 39 days after the fire whereas the SPOT post-fire image was collected 13 days after the fire. As demonstrated in Fig. 4, the longer SWIR band (2.21μm) provided the highest sensitivity (compared to other bands) to the burn. This response is consistent with an increase in soil exposure and a loss of vegetation cover. However, the increase in SPOT's green and NIR reflectances in response to an increase in soil exposure and a decrease in vegetation cover after the fire was not what we expected. Furthermore, the low sensitivity to changes in reflectance (~1%) between pre- and post-fire images in the SPOT imagery was also not expected. The low sensitivity and direction of change in reflectances may be explained by white mineral ash (silica) due to timing of imagery acquisition close after the fire (Smith et al. 2005). Another explanation could be that small changes in SPOT reflectance were within the error bound due to a combined effect of sensor signal to noise ratio and atmospheric path radiance. A previous study indicated a minimum difference in reflectance of 0.1% is needed for accurate retrieval of environmental variables (Brando and Dekker, 2003). While the Brando and Dekker (2003) study focused on retrievals from water bodies, a similar

accuracy may also be needed for fire applications. Changes in SPOT's SWIR band pre- and post-fire was similar to Landsat's band 5; this portion of the electromagnetic spectrum may not have the sensitivity of fire effects for rangelands, regardless of the time span between image acquisitions. SPOT does not have a SWIR band equivalent to Landsat band 7 (2.08-2.35µm), which has demonstrated sensitivities to reduced vegetation cover and increased soil exposure. It is worthwhile to note that the shorter time gap between SPOT images and their acquisition dates (close to field data collection) may explain, in part, why the SPOT NDSWIR accuracy is slightly better than the Landsat NDSWIR (for both burned versus unburned and fire severity), regardless of the sensitivity of this SWIR band. In summary, the multitemporal indices between Landsat and SPOT carry different relationships.

Mapping fire severity patterns at a scale that is coarse enough to capture landscape scales for management, yet fine enough to provide the spectral differentiation between fire severity classes is needed. Though SPOT didn't provide fire severity accuracies as high as Landsat (RdNBR), its spatial resolution may provide other attributes that are useful to land managers, such as burn perimeter. Landsat provides a practical scene size of 170 x 183 km and costs are reasonable if more than one image needs to be purchased. The results of the Landsat RdNBR verify that the Landsat 30 m spatial resolution is high enough to capture spectral variability between fire severity classes in rangelands. However, it is up to the land manager to decide the level of detail needed to determine fire severity and thus the scale of fire recovery efforts.

In this study the majority of the study sites were high fire severity where little vegetation reflectance and high amounts of soil should be detected. SAVI may have performed well in part because the algorithm uses NIR and red bands and not SWIR (1.58-1.75µm), which was less sensitive to the fire. The red band decreased most post-burn as bare ground and ash cover likely increased. However, our results with SAVI are contradictory to those of Epting et al. (2005), whereas their SAVI and MSAVI severity indices performed worse than their indices incorporating mid-infrared bands (2.21 µm). Their study areas were in forested ecosystems with higher standing biomass pre-fire.

Spatial correlation of ground cover and low RMS error (less than ½ a pixel) reduce the likelihood of classification error; however, they do not exclude the possibility of error entirely. Therefore, although error is introduced with multitemporal data sets, these effects likely would not have significantly altered reported accuracies. Georegistration errors between GPS field data and imagery may also have occurred for both single- and multi-date indices.

Hyperspectral imagery should be further explored to detect fire severity in rangelands because it may be more sensitive to fire effects for semiarid vegetation. For instance, AVIRIS channels 60 and 148, as suggested by van Wagtendonk et al. (2004), may discriminate fire effects better than Landsat bands 4 and 7 in rangelands. Improvements to this work may also include using the M-statistic to assess the differences between indices and separability of individual bands. Similar work has been accomplished by Kaufman & Remer (1994), Pereira (1999), and Smith et al (2007). In addition, it may be that rangeland fire severity is best detected with an extended assessment (e.g. burn severity). An extended assessment may delineate areas of high severity better, either where perennial vegetation has not recovered or where introduced annuals have established.

The SAVI and RdNBR indices are reproducible and straightforward. We chose to focus on remote sensing methods that incorporate satellite imagery and fit the needs of land managers (reasonable cost and practical spatial and spectral resolution) and methods that would not require the user to incorporate *large* amounts of field studies. Our findings support the use of the SPOT-SAVI combination for delineating burn versus unburned areas and Landsat RdNBR combination for delineating fire severity. If delineating burn versus unburned is a higher priority than fire severity, only post-fire imagery is necessary. However, if fire severity is needed then both pre-fire and post-fire imagery are required. Though our best results are

with the burned versus unburned algorithms, a 73% overall accuracy for the RdNBR fire severity index encourages future research. Before this index is entirely recommended, however, more studies need to be performed using the RdNBR in rangelands that have heterogeneous fuel loads, and within burns that have variable fire severities.

ACKNOWLEDGEMENTS
Funding for this research was provided by NASA grant # NNG05GB05G. The authors would like to thank the United Stated Department of Agriculture Agricultural Research Station's Sheep Experiment Station in Dubois, Idaho, for assistance and coordination with the study area and organizing the prescribed fire. ISU would also like to acknowledge the Idaho Delegation for their assistance in obtaining this grant

LITERATURE CITED

Arno, S.F. and Gruell, G. E., 1983, Fire history at the forest-grassland ecotone in southwestern Montana. *Journal of Range Management,* 36, 332–336.

Asner, G. P., 2004, Biophysical remote sensing signatures of arid and semiarid ecosystems. In *Remote Sensing for Natural Resource Management and Environmental Monitoring, 3 ed.*, vol 4, S. L. Ustin (ed), pp 53-109 (Hoboken, New Jersey: John Wiley and Sons).

Asner, G. P., and Heidebrecht, K.B., 2002, Spectral unmixing of vegetation, soil and dry carbon cover in arid regions: comparing multispectral and hyperspectral observations. *International Journal of Remote Sensing*, 23, 3939-3958.

Bobbe, T., Finco, M., and Sohlberg, R., 2001, Field measurements for the training and validation of burn severity maps from spaceborne, remotely sensed imagery. USDA Joint Fire Science Program Final Project Report JSP RFP-2001-2. Available online at: http://www.fs.fed.us/eng/rsac/baer/jfs.html (accessed 15 October, 2006).

Brewer, C.K., Winne, J.C., Redmond, R.L., Opitz, D.W., and Mangrich, M.V., 2005, Classifying and mapping wildfire severity: A comparison of methods. *Photogrammetric Engineering and Remote Sensing,* 71, 1311-20.

Cocke, A.E., Fule, P.Z., and Crouse, J.E., 2005, Comparison of burn severity assessments using differenced normalized burn ratio and ground data. *International Journal of Wildland Fire,* 14, 189-98.

Congalton, R. and Green, K., 1999, *Assessing the accuracy of remotely sensed data: principles and practices* (Washington, D.C.: CRC Press, Inc).

Epting, J., and Verbyla, D., 2005, Landscape-level interactions of pre-fire vegetation, burn severity, and post-fire vegetation over a 16-year period in interior Alaska. *Canadian Journal of Forest Research*, 35, 1367-1377.

Epting, J., Verbyla, D., and Sorbel, B., 2005, Evaluation of remotely sensed indices for assessing burn severity in interior Alaska using Landsat TM and ETM+. *Remote Sensing of Environment*, 96, 328-339.

Flasse, S. Trigg, S., Ceccato P., Perryman A., Hudak A., Thompson M., Brockett B., Dramé M., Ntabeni, T., Frost, P., Landmann, T., and le Roux, J., 2004, Remote sensing of vegetation fires and its contribution to a fire management information system. In *Wildfire Management Handbook for Sub-Sahara Africa*, J.G. Goldammer and C. de Ronde (eds), pp 158-211 (The Hague, Netherlands: SPB Publishing).

Floyd, D.A. and Anderson, J.E., 1982, A new point interception frame for estimating cover of vegetation. *Vegetatio,* 50, 185-186.

Floyd, D.A. and Anderson, J.E., 1987, A comparison of three methods for estimating plant cover. *Journal of Ecology,* 75, 221-228.

Gerard, F., Plummer, S., Wadsworth, R., Ferreruela Sanfeliu, A., Iliffe, L., Balzter, H. and Wyatt, B., 2003, Forest fire scar detection in the boreal forest with multitemporal SPOT-VEGETATION data. *Geoscience and Remote Sensing, IEEE Transactions on,* 41, 2575-2585.

Harniss, R.O., and R.B. Murray, 1973, Thirty years of vegetal change following burning of sagebrush-grass range. *Journal of Range Management* 26: 322-325.

Huete, A.R., 1988, A soil-adjusted vegetation index (SAVI). *Remote Sensing of Environment,* 25, 295-309.

ITT, 2007, *ENVI user's guide (Version 4.2)* (Boulder, CO, ITT Visual Information Solutions).

Kaufman, Y.J. and Tanre, D., 1992, Atmospherically resistant vegetation index (ARVI) for EOS-MODIS. *IEEE Transactions on Geoscience and Remote Sensing,* 30, 261-270.

Kaufman, Y.J. and Remer, L.A., 1994, Detection of forests using mid-IR reflectance: an application for aerosol studies. *IEEE Transactions on Geoscience and Remote Sensing*, 32, 672-683.

Key, C.H., and Benson, N.C., 1999a, The Composite Burn Index (CBI): Field Rating of Burn Severity. Available online at: http://www.nrmsc.usgs.gov/research/cbi.htm (accessed 28 July, 2006).

Key, C.H., and Benson, N.C., 1999b, The Normalized Burn Ratio (NBR): A Landsat TM Radiometric Index of Burn Severity. Available online at: http://www.nrmsc.usgs.gov/research/ndbr.htm (accessed 28 July, 2006).

Key, C.H., and Benson, N.C., 2004a, Remote Sensing Measure of Severity: The Normalized Burn Ratio. In *FIREMON: Fire Effects Monitoring and Inventory System*, D. C. Lutes, R. E. Keane, J. F. Caratti, C. H. Key, N. C. Benson, & L. J. Gangi (eds), Ogden, UT: U.S. Department of Agriculture, Forest Service, Rocky Mountain Research Station. pp. LA1-16.

Key, C.H., and Benson, N.C., 2004b, Ground Measure of Severity, The Composite Burn Index. In *FIREMON: Fire Effects Monitoring and Inventory System*, D. C. Lutes, R. E. Keane, J. F. Caratti, C. H. Key, N. C. Benson, & L. J. Gangi (eds), Ogden, UT: U.S. Department of Agriculture, Forest Service, Rocky Mountain Research Station. pp. LA_CBI_Plot-1-9.

Key, C.H., and Benson, N.C., 2006, Landscape Assessment (LA) Sampling and Analysis Methods. USDA Forest Service General Technical Report, RMRS-GTR-164-CD. (Ogden,UT). pp. 55.

Lentile, L.B., Holden, Z., Smith, A.M.S., Falkowski, M.J., Hudak, A.T., Morgan, P.,Gessler, P.E. and Benson, N.C., 2006, Remote sensing techniques to assess active fire and post-fire effects. *International Journal of Wildland Fire*, 15, 1-27.

Lopez Garcia, M.J., and Caselles, V., 1991. Mapping burns and natural reforestation using thematic mapper data. *Geocarto International,* 6, 31-37.

Miller, J.D. and Thode, A.E., 2007, Quantifying burn severity in a heterogeneous landscape with a relative version of the delta Normalized Burn Ratio (dNBR). *Remote Sensing of Environment*, 109, 66-80.

Miller, J.D., and Yool, S.R., 2002, Mapping forest post-fire canopy consumption in several overstory types using multi-temporal Landsat TM and ETM data. *Remote Sensing of Environment,* 82, 481-96.

Morgan, P., Hardy, C.C., Swetnam, T.W., Rollins, M.G., and Long, D.G., 2001, Mapping fire regimes across time and space: Understanding coarse and fine-scale fire patterns. *International Journal of Wildland Fire,* 10, 329–342.

Okin, G.S., Roberts, D.A., Murray, B., and Okin, W.J., 2001, Practical limits on hyperspectral vegetation discrimination in arid and semiarid environments. *Remote Sensing of Environment*, 77, 212-225.

Patterson, M.W., and Yool, S.R.,1998, Mapping fire-induced vegetation mortality using Landsat Thematic Mapper data: A comparison of linear transformation techniques. *Remote Sensing of Environment*, 65, 132-42.

Pereira, J.M.C., 1999, A comparative evaluation of NOAA/AVHRR vegetation indexes for burned surface detection and mapping, *IEEE Transactions on Geoscience and Remote Sensing*, 37, 217-226.

Qi, J., Chehbouni, A., Heute, A.R., Kerr, Y.H. and Sorooshian, S., 1994, A modified soil adjusted vegetation index. *Remote Sensing of Environment,* 48, 119-126.

Roy, D.P., 1999, Multi-temporal active-fire based burn scar detection algorithm. *International Journal of Remote Sensing,* 20, 1031-1038.

Roy, D.P., Boschetti, L., and Trigg, S.N., 2006, Remote sensing of fire severity: Assessing the performance of the normalized burn ratio. *IEEE Geoscience and Remote Sensing Letters*, 3, 112-116.

Ruiz-Gallardo, J.R., Castańo, S., Calera, A., 2004, Application of remote sensing and GIS to locate priority intervention areas after wildland fires in Mediterranean systems: a case study from south-eastern Spain. *International Journal of Wildland Fire*, 13, 241-252.

Ryan, K.C., and Noste, N.V., 1983, Evaluating prescribed fires. *In Proceedings of the symposium and workshop on wilderness fire. 15–18 November 1983, Missoula, MT*, J.E. Lotan, B.M. Kilgore, W.C. Fischer, R.W. Mutch (eds) USDA Forest Service, Intermountain Forest and Range Experiment Station General Technical Report INT-GTR-182. (Ogden, UT) pp. 230–238.

Salvador, R., Valeriano, J., Pons, X., and Diaz-Delgado, R., 2000, A semi-automatic methodology to detect fire scars in shrubs and evergreen forests with Landsat MSS time series. *International Journal of Remote Sensing,* 21, 655-71.

Sannier, C., 1999, Strategic monitoring of crop yields and rangeland conditions in southern Africa with remote sensing. PhD dissertation, Cranfield University, Silsoe Bedfordshire, UK.

Santos, T.G., Caetano, M.R., Barbosa, P.M., and Paúl, J.U., 1999, A comparative study of vegetation indices to assess land cover change after forest fires. In *Remote Sensing for Earth Science, Ocean, and Sea Ice Applications*, *Proceedings of SPIE Vol 3868,* G. Cecchi, E.T. Engman, E. Zilioli (eds) (Florence, Italy, 1999), pp. 232-240.

Seefeldt, S.S., 2005, Consequences of selecting rambouilllet ewes for mountain big sagebrush (Artemisia

tridentata ssp. vaseyana) dietary preference. *Rangeland Ecology and Management,* 58, 380-384.

Smith, A.M.S., Wooster, M.J., Drake, N.A., Dipotso, F.M., Falkowski, M.J. and Hudak, A.T., 2005, Testing the potential of multi-spectral remote sensing for retrospectively estimating fire severity in African savannahs. *Remote Sensing of Environment*, 97, 92-115.

Smith A.M.S., Drake, N.A., Wooster, M.J., Hudak, A.T,. Holden, Z.A. and Gibbons C.J., 2007, Production of Landsat ETM+ Reference Imagery of Burned Areas within Southern African Savannahs: Comparison of Methods and Application to MODIS. *International Journal of Remote Sensing*, 28, 2753-2775.

Turner, M.G., Hargrove, W.W., Gardner, R.H., and Romme, W.H., 1994, Effects of fire on landscape heterogeneity in Yellowstone National Park, Wyoming. *Journal of Vegetation Science*, 5, 731-42.

USDI National Park Service., 2003, *Fire monitoring handbook (*Boise, ID, Fire Management Program Center, National Interagency Fire Center).

Van Wagtendonk, J.W., Root, R.R., AND Key, C.H., 2004, Comparison of AVIRIS and Landsat ETM+ detection capabilities for burn severity. *Remote Sensing of Environment,* 92, 397–408.

West N.E. and Young, J.A., 2000, Intermountain Valleys and Lower Mountain Slopes. In *North American Terrestrial Vegetation*, M.G. Barbour and W.D. Billings (eds.), pp. 255-284 (Cambridge, UK: Cambridge University Press).

White, J.D., Ryan, K.C., Key, C.C., and Running, S.W., 1996, Remote sensing of forest fire severity and vegetation recovery. *International Journal of Wildland Fire*, 6, 125-36.

Wimberly, M.C., and Reilly, M.J., 2007, Assessment of fire severity and species diversity in the southern Appalachians using Landsat TM and ETM+ imagery. *Remote Sensing of Environment,* 108, 189-197.

[THIS PAGE LEFT BLANK INTENTIONALLY]

Fire Severity Modeling of Sagebrush-Steppe Rangelands in Southeastern Idaho

Keith T. Weber, GISP, Idaho State University, GIS Training and Research Center, 921 S. 8th Ave., Stop 8104, Pocatello, Idaho 83209-8104 (webekeit@isu.edu)

Steven S. Seefeldt, Research Agronomist, USDA-ARS, SubArctic Agricultural Research Unit, University of Alaska Fairbanks, Fairbanks, Alaska 99775

Jill M. Norton, GIS Specialist, Blaine County Idaho, Hailey, Idaho 83333

Charles Finley, GIS Coordinator, Newmont Environmental, PO Box 669, Carlin Nevada 89822

ABSTRACT
The potential for high severity fires to affect changes in rangelands is considerable, and for this reason, assessing fire severity is critical. We explored fire severity modeling in rangelands by applying post-fire field observations to Satellite Pour l'Observation de la Terre 5 (SPOT 5) imagery using Classification Tree Analysis (CTA) techniques at two 2005 burns. The results of these analyses demonstrate that CTA is equally adept at classifying areas of low severity as well as those with high severity with reliable accuracy (66-100%). Furthermore, the CTA technique is fairly uncomplicated to apply and provides an error assessment upon which land managers can better justify their recommendations.

KEYWORDS: Classification tree analysis, GIS, remote sensing.

INTRODUCTION

Wildland fire is a common occurrence throughout the Intermountain West. While historic vegetation communities may have adapted to this form of disturbance, the frequency and intensity of today's wildfires is different compared to what occurred in the past (DeBano et al. 1998; Thoren and Mattsson 2002). The change in frequency and intensity can be attributed to 1) fire suppression efforts that have inadvertently created fuel stockpiles (Pyne et al. 1996) and 2) the introduction of invasive weeds like *Bromus tectorum* (Cheatgrass), a fire-promoter species (Brooks et al 2004). The consequences of these differences are large-scale changes to vegetation on a landscape scale which, in turn negatively impacts wildlife habitat, forage production, soil erosion (Finley 2006), and the health of rangeland ecosystems (Pyke et al. 2002).

The effect of wildfires is perceived to be substantial and public land managers are required to assess the severity of nearly all fires occurring on public lands and prepare remediation plans for high severity burns (Sharon Paris, pers. comm. [21-September-2007]; Department of Interior 2004), especially in cheatgrass infested areas. However, due to the broad extent and distribution of wildfires in the Intermountain West the ability of land managers to closely evaluate each and every fire is sometimes logistically difficult if not impossible. For these reasons, the application of remote sensing models that accurately and reliably describe fire severity may be useful (Lentile et al 2006).

Several image processing methods have been used to model fire severity (Garcia and Chuvieco, 2004) with most designed for forested ecosystems (Turner et al. 1994; White et al. 1996; Patterson and Yool, 1998; Van Wagtendonk et al. 2004; Brewer et al. 2005; Epting et al. 2005). Prior to 1999, the most widely used fire severity modeling method was an NDVI-based technique to estimate biomass loss, and hence, fire severity (Salvador et al. 2000; Diaz-Delgado et al. 2003; Flasse et al. 2004). In 1999, the normalized burn ratio (NBR) technique was developed and has been widely applied and accepted (Garcia and Casseles 1991; Key and Benson 1999; Salvador et al. 2000; Key and Benson, 2006). Another form of the NBR model is known as a differenced NBR (dNBR). It estimates fire severity by comparing a pre-burn NBR model to that of a post-burn NBR model. The result is a model where the magnitude of change has been normalized by pre-burn landscape characteristics (Key and Benson 1999; Key and Benson, 2004; Van Wagtendonk et al. 2004; Cocke et al. 2005)

Few techniques have been specifically developed to model fire severity in semi-arid rangelands (Smith et al. 2005; Roy et al. 2006), and to some extent, it has been accepted that the techniques applied in forested ecosystems should be equally applicable within other ecosystems. More recent studies, however, indicate this is not the case and alternative methods are required to assess fire severity within semi-arid rangeland ecosystems (Epting et al. 2005; Norton 2006). The primary reason why models developed for forests do not translate well within rangelands is the prevalence of exposed soil, in both pre- and post-burn conditions, contributing to the spectra acquired by the sensor (Okin et al 1999). In addition, a scale effect may exist related to the proportional area occupied by individual plants relative to the size of each pixel (e.g., a sagebrush plant occupies perhaps 1% of a Satellite Pour l'Observation de la Terre 5 (SPOT 5) pixel [10x10m] whereas a Douglas-fir can cover 100% of the same pixel). Consequently, the majority of pixels used in remote sensing projects over semi-arid rangelands exhibit heterogeneity within each pixel (i.e., mixed pixels or mixels), making accurate differentiation more difficult (Okin et al 2001).

Recent fire severity studies within sagebrush-steppe ecosystems in southeastern Idaho have investigated two approaches to model fire severity using image classification techniques. The first used the HyMap hyperspectral sensor (Finley 2006) while the second used SPOT 5 and Landsat 7 multispectral sensors (Norton 2006). In both cases, overall classification accuracy between low and high severity fire areas was good (72% and 67% overall accuracy respectively [K_{hat} = 0.69 and 0.33, respectively) but unfortunately, neither quite achieved the level of reliability ($\geq$75%) cited in the literature (Congalton

1991; Goodchild et al. 1994). Because of the nature of fire data (non-normal and multivariate due to the interactive effect of soil, slope, aspect, and wind) classification results better than these are not likely when using probabilistic classification techniques. Therefore, an alternative technique for fire severity modeling was investigated.

Classification tree analysis (CTA) is a non-probabilistic, non-parametric statistical technique well-suited to modeling skewed, non-normal data and phenomena (Breiman et al. 1998; Friedl and Brodley 1997; Lawrence and Wright 2001; Miller and Franklin 2001). CTA algorithms select useful spectral and ancillary data which optimally reduce divergence within a response variable (Lawrence and Wright 2001) such as fire severity observations. CTA uses machine-learning to perform binary recursive splitting operations and ultimately yields a classification tree diagram that is used to produce a model of the response variable. There are various splitting algorithms common to CTA: 1) entropy, 2) gain ratio, and 3) Gini. The entropy algorithm has a tendency to over-split and thereby creates an unnecessarily complex tree (Zambon et al. 2006). The gain ratio algorithm, addresses the over-splitting problem through a normalization process, while the Gini algorithm attempts to partition the most homogeneous clusters first using a measure of impurity (McKay and Campbell 1982; Weber et al. 2006; Zambon et al. 2006).

The goal of this study was not to directly compare CTA to other classification techniques and attempt to prove one or the other is better, but to explore the use of CTA to model fire severity in semi-arid rangelands. Since the acquisition of fire perimeters is already part of federal agency post-fire protocols, it was not necessary to use image processing techniques to delineate where a fire has occurred. Rather, focus was placed upon accurately identifying high fire severity areas to assist land managers in post-fire recovery plans and remediation efforts.

METHODS

Study Area

This study focuses upon two 2005 fires in southeastern Idaho: 1) the Hitching Post pasture fire at the US Sheep Experiment Station (USSES) near DuBois, Idaho (a prescribed fire) and 2) the Clover Fire(Clover), 39 km west of Twin Falls, Idaho (a lightning-ignited wildfire). The USSES (Figure 1) includes nearly 40,000 ha of land (Seefeldt and Laycock 2006) that have been assigned to the USSES or leased from the Department of Energy, USDA-Forest Service, or the Department of Interior-Bureau of Land Management. The USSES spans four Major Land Resource Areas (NRCS 2006) including the Central Rocky Mountains, Snake River Plain, Lost River Valleys and Mountains, and Eastern Idaho Plateaus. This area has been used for rangeland research since 1925 and the research that has been conducted there has contributed greatly to our understanding of western rangelands.

Mean annual precipitation varies considerably across the USSES as elevation ranges between 1615-2900 m. The dominant plant species in the sagebrush-steppe communities are Mountain Big Sagebrush (*Artemisia tridentata* Nutt. ssp. *vaseyana* (Rydb.) Beetle.), threetip sagebrush (*Artemisia tripartita* Rydb.), Antelope bitterbrush (*Purshia tridentata* (Pursh) DC.), bluebunch wheatgrass (*Pseudoroegneria spicata* (Pursh) A. Löve), thickspike wheatgrass (*Elymus lanceolatus* (Scribn. & J.G. Sm.) Gould), Sandberg bluegrass (*Poa secunda* J. Presl), arrowleaf balsamroot (*Balsamorhiza sagittata* (Pursh) Nutt.), and tapertip hawksbeard (*Crepis acuminata Nutt*. ssp. *acuminata*) (West and Young, 2000, Wright and Bailey, 2004). The Hitching Post pasture is a 324 ha fenced parcel within the Headquarters Unit of the USSES (Figure 1) at an elevation of approximately 1800 m. Mean annual precipitation ranges between 250-530 mm with most (as much as 70%) falling as snow (Seefeldt, 2005). Soils are mixed, fine-loamy, frigid Calcic Argixerolls (NRCS, 1995). Sheep and horses have grazed this pasture for the past decade, but grazing had not occurred for 2.5 yr prior to the burn. The USSES fire was a series of prescribed fires that began on September 14th and were extinguished on September 15th, 2005. The fire boundary encompassed 244 ha.

The Clover study site (Figure 1) spans two Major Land Resource areas (NRCS 2006), namely the Snake River Plain and Owyhee High Plateau. The mean annual precipitation is 175-400mm which varies somewhat with elevation which ranges between 950 and 1375 m. The site is dominated by big sagebrush (*Artemisia tridentata* Nutt.), perennial bunchgrasses such as crested wheatgrass (*Agropyron cristatum)*, needlegrass (*Achnatherum nelsonii*), and Idaho fescue (*Festuca idahoensis* Elmer). Annuals plants found at this site include cheatgrass and medusahead (*Taeniatherum caput-medusae)* (Wright 1985). Soils vary from loamy sand to silty clay, and are a mix of volcanic-derived basalts and rhyolites as well as windblown loess deposits (Wright 1985). The Clover fire was a lightning-caused wildfire which began on July 15 and was contained on July 20, 2005. The fire boundary encloses 78,042 ha, the largest wildland fire in Idaho in 2005.

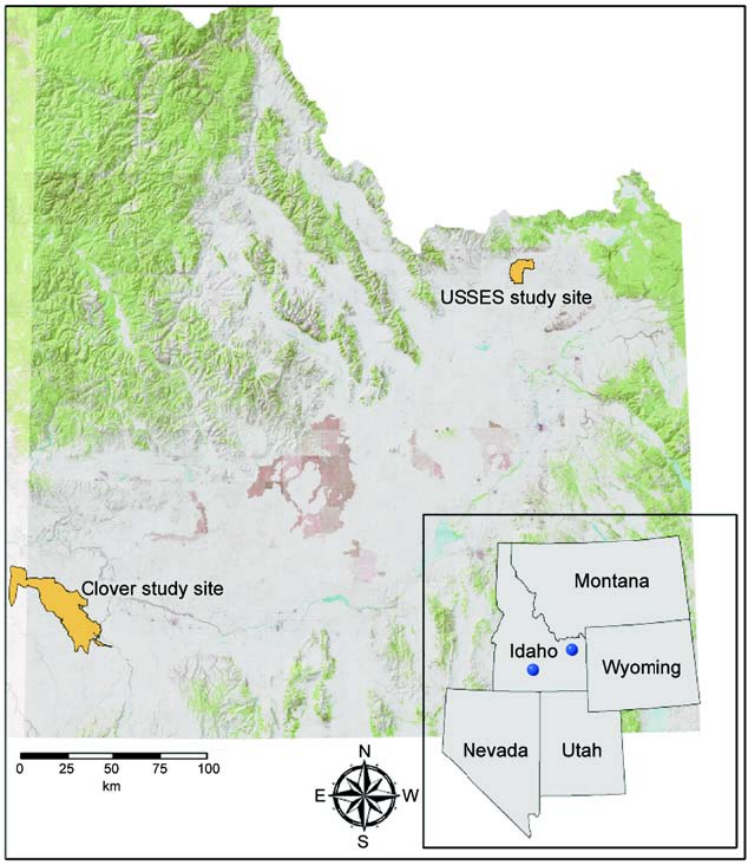

Figure 1. Location of sites compared in this study

Field Data

A standard protocol for field fire severity assessment has been developed for forested ecosystems (Key and Benson 2004). Assessing fire severity within sagebrush-steppe ecosystems cannot follow the exact procedure and for this reason fire severity was assessed using a modified ocular method based on combining the methods described by Key and Benson (1999; 2004), the USDA Forest Service BAER teams (Bobbe et al. 2001) and the US National Park Service (Switky 2003). Fire severity assessments were made beginning one week after the fire was contained and ending within two months after the fire. A total of 512 (n=277 at the USSES study site and n=235 at the Clover study site) points were randomly located within the study sites and navigated to using a Trimble GeoXT GPS receiver (+/-0.9 m @ 95% CI; Serr et al. 2007). Fire severity was then classified as either 1) unburned, 2) low severity (understory removed while shrubs retained green leaves), or 3) high severity (understory removed and shrubs charred or removed by the fire) for CTA modeling. Some aspects of fire severity can be quantified but

classification of general severity has proven difficult. Classification of burn or fire severity, based on post-fire appearances of litter and soil (Ryan and Noste 1983), are useful for placing severity into broadly defined, discrete classes, ranging from low to high. A general burn severity classification developed by Hungerford (1996) in forest situations relates burn severity to soil resource response and has three classes; low, moderate, and high. In rangeland ecosystems the medium and high severity classes described by Hungerford merge as there are not large woody component and deep duff layer, whose response to burning differentiates the classes. Therefore, we chose a simple classification of low or high severity.

All unburned sample points were omitted from subsequent processing. This was done 1) to simplify the classification process (Jensen 1996), 2) because fire perimeters were already available using more cost-effective methods such as field collection using GPS, and 3) because fire perimeter delineation was outside the scope of this study. The potential error was that unburned areas within the fire perimeter would not be identified and the authors acknowledge that some of the predicted low severity sites may indeed be unburned sites. This error was allowed because 1) the focus of this study was to correctly identify high fire severity areas to assist land managers in post-fire recovery plans and remediation efforts and 2) very few unburned sites were found within the fire perimeters.

Image Processing

SPOT 5 satellite imagery was acquired for both the USSES (September 28, 2005) and Clover (September 1st, 2005) study sites. The acquisition dates for these data reflect post-fire scenes corresponding to only 12 days post-fire (USSES) and 43-days post-fire (Clover). The imagery was georectified (RMSE = 3.48 for the USSES study site and RMSE = 0.298 for the Clover study site) using nearest neighbor resampling and then atmospherically corrected using the Cos(t) algorithm in Idrisi Kilimanjaro (Chavez 1996). The imagery was then projected into Idaho Transverse Mercator (NAD 83).

Using reflectance data, normalized difference vegetation index (NDVI), normalized burn ratio (NBR), and biomass estimates (the ratio of the short-wave infrared band divided by the visible green band [Mirik et al. 2005]) were calculated within Idrisi. In addition, topography data was assembled for use as ancillary data within the CTA process (Elumnoh and Shrestha 2000). The elevation data for both study sites was acquired from the shuttle radar topography mission (SRTM) and was resampled to 10m to match the spatial resolution of the SPOT 5 imagery. Slope and aspect models were derived from the elevation models using Idrisi Kilimanjaro.

Polygon shapefiles describing the fire perimeters were rasterized and used as a mask for all raster data. Field observations were similarly masked and only those points falling inside the fire perimeter were used in the CTA. This masking process was done to help facilitate classification by prudently applying ancillary knowledge to better inform the classifier. This process is a well accepted technique referred to as "cluster busting" (Jensen 1996; Hunter 2004). CTA was performed using the Gini splitting algorithm (Zambon et al. 2006) with ten input images available for the classification process: green, red, near-infrared (NIR), and shortwave-infrared (SWIR) reflectance bands (1-4), NDVI, NBR, and biomass band-ratios, and elevation, slope, and aspect topography layers.

To absorb georegistration error within the SPOT imagery for the USSES study site (RMSE=3.48) and ensure sample points fell within representative pixels (Weber 2006) the USSES sample points were buffered by 5m (note: this process was not required for the Clover study site as georegistration error of the SPOT imagery was quite low [RMSE=0.298]). The resulting layers were rasterized using ArcGIS 9.1 and subset into training and validation sites. A total of 474 training sites (i.e., pixels) (n=385 at the USSES study site and n=89 at the Clover study site) and 288 validation sites (n=207 at the USSES study

site and n=81 at the Clover study site) were created. These data were then used within Idrisi Kilimanjaro for CTA.

RESULTS AND DISCUSSION

The USSES and Clover study sites differed in most every factor (elevation, precipitation, and soils) including fire type, seasonality, and size. These differences increase the challenges of developing a fire severity model, especially when trying to determine explanatory variables that would be consistent.

While ten input images were available for the classification, CTA consistently selected biomass, NBR, and NDVI band-ratio, NIR, and slope layers (note: layers are listed alphabetically and the order listed is not indicative of the layer's importance). The biomass layer is a simple ratio-type vegetation index where reflectance values from the short-wave infrared region (band) are divided by reflectance values from the green band. While Mirik et al. (2005) demonstrated a strong empirical relationship ($R^2 = 0.87$) between this index and total rangeland biomass, the relationship of the biomass index and actual rangeland biomass was not performed as part of this study. The biomass index differs from the normalized difference infrared index (NDII [Hunt and Yilmaz 2007]) in that the biomass index is a simple ratio-type index as opposed to a normalized difference-type index and the biomass index does not make use of the infrared band as does NDII. Another related normalized difference-type index is the normalized difference water index (NDWI) which uses the ratio of the difference between the near infrared and thermal infrared bands divided by the sum of these same bands (Gu et al. 2007). Neither the NDII nor NDWI were used in this study (NDWI cannot be used with SPOT imagery as this sensor does not include a thermal infrared band).

Using these five layers, high fire severity areas were correctly identified in most cases, having a user accuracy of 100% and 79% at the USSES and Clover study sites, respectively (Tables 1 and 2). These results improve upon previous fire severity classifications for the same study sites (Finley 2006; Norton 2006) in nearly all cases such as calculated overall accuracy (72% compared with 86% using CTA at the Clover study site; 67% compared with 97% using CTA at the USSES study site) and the Kappa statistic (0.69 compared with 0.65 at the Clover study site; 0.33 compared with 0.78 at the USSES study site [Congalton 1991]).

Table 1. CTA results for the USSES study site.

		Known validation sites			
		Low fire severity	High fire severity	Total	User accuracy
Model results	Low fire severity	14	7	21	0.66
	High fire severity	0	186	186	1.00
	Total	14	193	207	
	Producer's accuracy	1.00	0.96		Overall = 0.97

Kappa index of agreement = 0.78

Assessment of error and bias

While the resulting overall accuracies were better than those reported using more traditional, probabilistic classification techniques such as maximum-likelihood (Norton 2006) and spectral angle mapper (Finley 2006), using CTA for fire severity modeling in sagebrush-steppe rangelands was fairly simple and straightforward, requiring only post-fire imagery and ground observations. Achieving satisfactory results appears to be a function of sample size as in both cases the class (low fire severity or high fire severity) with a larger number of samples resulting in better classification accuracy. The

minimum number of observations to maintain accuracy will need to be determined and provided to land managers.

Table 2. CTA results for the Clover study site.

		Known validation sites			
		Low fire severity	High fire severity	Total	User accuracy
Model results	Low fire severity	50	7	57	0.88
	High fire severity	5	19	24	0.79
	Total	55	26	81	
	Producer's accuracy	0.90	0.73		Overall = 0.85

Kappa index of agreement = 0.65

At the USSES study site, the prescribed fire burned relatively dense vegetation at close to optimal burn conditions (low humidity, high temperature, slight breeze) resulting in 92% of the field observations rating a high fire severity compared to 8% at a low severity. In contrast, field observations for the Clover study site were opposite, with 33% high fire severity compared to 67% low fire severity (Figure 2). Fire severity is primarily a function of the fire's behavior which is closely tied to factors such as the amount and type of fuels and the weather during the fire (Pyne et al. 1996). Model proportions of high and low severity areas were the same as estimated by observation (Figure 2). The similarity of these results (Table 3) indicates the model is robust in comparing a large range of overall fire severities.

Table 3. Comparison between the proportion of field observations and fire severity areas as modeled.

	Proportion of total fire area (and field observations)	
Study site	Low severity fire	High severity fire
USSES	0.08 (0.08)	0.92 (0.92)
Clover	0.67 (0.68)	0.33 (0.32)

There were other potential differences between the fires at the two study sites which could have caused a potential bias such as:

1) The post-fire SPOT imagery acquired for the USSES study site was collected only 12 days after the fire, while the imagery for the Clover study site was not collected until 43 days after the fire. This difference could not be avoided due to the widespread smoke and haze caused during the early parts of the 2005 fire season (July and August). As a result the earliest clear imagery available (coincident with a SPOT imaging date) was September 1st. However, lack of precipitation reduced changes to post-fire vegetation at the Clover site.
2) The fire at the USSES study site was a prescribed fire whereas the fire at the Clover study site was a lightning ignited "natural" fire.
3) The scale of the two fires was different with the USSES fire covering 244 ha whereas the Clover fire covered over 78,000 ha.
4) The seasonality of the two fires was also different with the USSES fire occurring in September while the Clover fire occurred in July. While both occurred in the same year, we correctly expected that a late season fire (under continued dry/drought conditions) would yield a fire of higher severity as the fuels had become increasingly desiccated.

Given all the differences listed above, the fire severity models, which were prepared in nearly identical ways using post-fire field observations collected in a very similar fashion (although by two separate field teams) were quite robust. As a result, CTA was able to produce fire severity models with good user accuracy (mean = 83% [note: this is the mean of all user accuracy values]), indicating the resiliency of this modeling technique (see Figure 3 for a step-by-step approach of this technique).

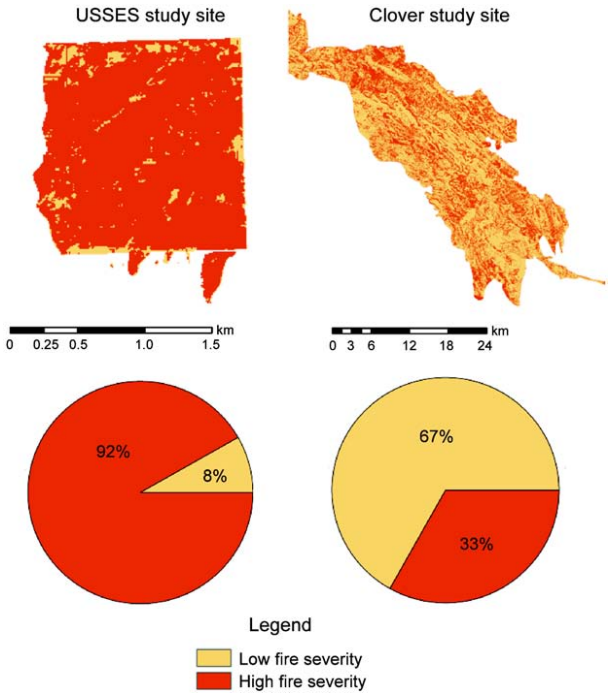

Figure 2. The resulting fire-severity models were different, with the USSES fire having a much larger proportion of high-fire-severity areas (92%) relative to the Clover fire with only 33% considered high fire severity

CONCLUSIONS

Time of fire, fire severity, climate before and after fire, and vegetation before fire all influence vegetation recovery after fire in sagebrush steppe rangelands (DeBano et al. 1998). Only one of these influences, fire severity, cannot be determined using relatively easy to obtain records. The large sizes of many fires in sagebrush steppe rangelands increase the difficulty of mapping burned and unburned areas, let alone delineating low and high burn severity areas. Yet many land management agencies are charged with developing remediation plans for high severity burn areas. The model described in this manuscript uses easy to obtain satellite imagery (SPOT 5) that can be rapidly analyzed to identify those high severity burn areas. This model, as opposed to NBR, does require some field observations, but the required data (location [GPS point] and observed fire severity rating [unburned, low, or high]), can be collected fairly quickly and accurately. The advantage of collecting field data is that managers will have an error assessment that validates the model. The model is equally effective in picking out the few high severity spots in a large low severity fire as in picking out the few low severity spots in a large high severity fire in the sagebrush steppe.

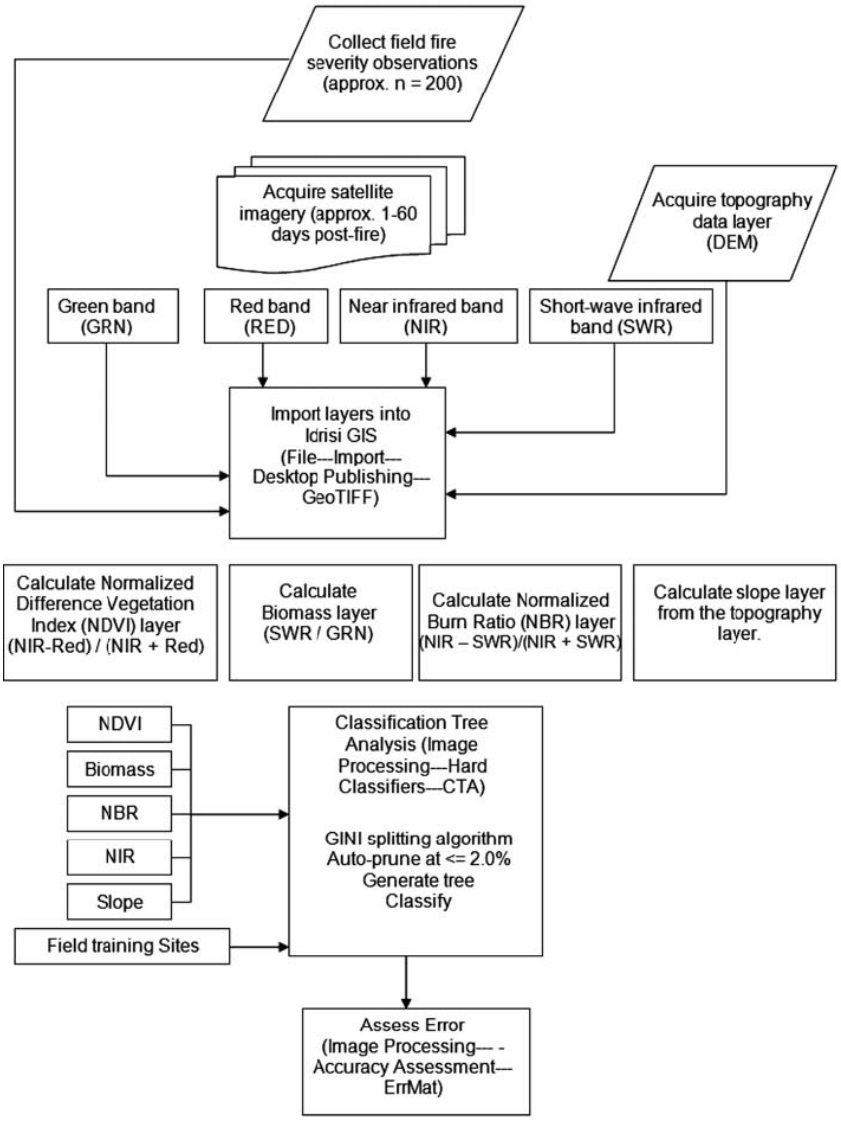

Figure 3. Cartographic model of the process followed to produce a fire-severity model using classification tree analysis at both the Clover and USSES study sites.

ACKNOWLEDGEMENTS

We would like to acknowledge the Idaho Delegation for their assistance in obtaining this grant from the National Aeronautic and Space Administration (NASA) and the assistance of Jamen Underwood and Penny Gneiting for their field data collection efforts and research in rangeland fire severity modeling. Idaho State University would also like to acknowledge the Idaho Delegation for their assistance in obtaining this grant.

LITERATURE CITED

Bobbe, T., Finco M. V., Quayle, B., and Lannon, K. 2001, Field measurements for the training and validation of burn severity maps from spaceborne, remotely sensed imagery. Remote Sensing Applications Center, Salt Lake City, Utah: USDA Forest Service, Final Project Report, Joint Fire Science Program-2001-2. Project # 01B-2-1-01, pp. 15 URL: http://www.fs.fed.us/eng/rsac/baer/final_report_01B-2-1-01.pdf Visted April 2007.

Breiman, L., Friedman, J. H., Olshen, R. A., and Stone C. J., 1998, Classification and Regression Trees. Chapman and Hall, CRC press, Boca Raton, Florida. 358 pp.

Brewer, C.K., Winne J. C., Redmond R. L., Opitz D. W., and Mangrich M. V. 2005, Classifying and mapping wildfire severity: A comparison of methods. *Photogrammetric Engineering and Remote Sensing*, 71:11, 1311-20

Brooks, M. L., D'Antonio, C. M, Richardson, D. M., Grace, J. B., Keeley, J. E, DiTomaso, J. M., Hobbs, R. J., Pellant, M., and Pyke. D. 2004, Effects of Alien Plants on Fire Regimes. *Bioscience.* 54(7):677-688.

Chavez, P. S. 1996, Image based atmospheric corrections- revisited and improved. *Photogrammetric Engineering and Remote Sensing*, *62*, 1025-1036.

Cocke, A.E., Fule, P. Z., and Crouse, J. E. 2005, Comparison of burn severity assessments using differenced normalized burn ratio and ground data. *International Journal of Wildland Fire*, 14: 189-98

Congalton, R. G. 1991, A Review of Assessing the Accuracy of Classifications of Remotely Sensed Data, Remote Sensing of Environment, 37:35–46.

DeBano, L.F., Neary, D.G., and Pfolliott, P.F. 1998, *Fire's Effects on Ecosystems*. New York: John Wiley and Sons, 333 pp.

Department of the Interior (DOI) 2004, Departmental Manual, Part 620 Chapter 3, Burned Area Emergency Stabilization and Rehabilitation (620DM3), 16 pp.

Diaz-Delgado, R., Lloret, F., and Pons, X. 2003, Influence of fire severity on plant regeneration by means of remote sensing imagery. *International Journal of Remote Sensing*, 24 (8) 1751-1763

Epting, J., Verbyla, D., and Sorbel, B. 2005, Evaluation of remotely sensed indices for assessing burn severity in interior Alaska using Landsat TM and ETM+. *Remote Sensing of Environment*, 96, 328-339

Elumnoh A. and Shrestha R. P. 2000, Application of DEM Data to Landsat Image Classification: Evaluation in a Tropical Wet-Dry Landscape in Thailand. *Photogrammetric Engineering and Remote Sensing*. 66(3):297-304.

Flasse, S., Trigg, S., Ceccato, P., Perryman, A., Hudak, A., Thompson, M., Brockett, B., Dramé, M., Ntabeni, T., Frost, P., Landmann, T., and le Roux, J. 2004, Remote sensing of vegetation fires and its contribution to a fire management information system. In. Goldammer, J.G. and de Ronde, C. (Eds.), *Wildfire Management Handbook for Sub-Sahara Africa*. The Hague, Netherlands: SPB Publishing, pp.158-211.

Finley, C. D. 2006, Field evaluation and hyperspectral imagery analysis of fire-induced water repellent soils and burn severity in southern Idaho rangelands. Idaho State University. URL: http://giscenter.isu.edu/Research/techpg/nasa_tlcc/to_pdf/cfthesis.pdf visited April 2007. 237pp.

Friedl, M. A. and Brodley, C. E., 1997, Decision tree classification of land cover from remotely sensed data. Remote sensing of environment. 61(3):399-409.

García, M. J. L. and Caselles, V. 1991, Mapping burns and natural reforestation using thematic mapper data. *Geocarto International*, 6:31-37.

Garcia, M. J. L. and Chuvieco, E. 2004, Assessment of the potential of SAC-C/MMRS imagery for mapping burned areas in Spain. *Remote Sensing of Environment*, 92, 414-423.

Goodchild, M. F., Biging, G.S., Congalton, R.G., Langley, P.G., Chrisman, N.R. and Davis, F.W. 1994, Final report of the accuracy assessment task force. *California Assembly Bill AB1580*, Santa Barbara: University of California, National Center for Geographic Information and Analysis (NCGIA).

Gu, Y., Brown, J. F., Verdin, J. P., and Wardlow B. 2007, A five-year analysis of MODIS NDVI and NDWI for grassland drought assessment over the central Great Plains of the United States. Geophysical Research Letters, 34(L06407). 6 pp.

Hungerford, R.D. 1996, Soils. Fire in Ecosystem Management Notes: Unit II-I. USDA Forest Service, National Advanced Resource Technology Center, Marana, Arizona

Hunt, E. R. and Yilmaz, T. 2007, Remote sensing of vegetation water content using shortwave infrared reflectance. Summaries of International Society for Optical Engineering. URL: http://ars.usda.gov/research/publications/publications.htm?seq_no_115=209592 visited January 2008.

Hunter, B. 2004, Overview of Methodology for Remote Sensing/GIS Analysis of Lakes Lewisville and Grapevine Shoreline Management Project. University of North Texas, URL: http://www.swf.usace.army.mil/Pubdata/notices/EA/Appendices/AppendixCOverviewofMethodologyforGIS.pdf visited January 2008. 9 pp.

Jensen, J. R. 1996, Introductory Digital Image Processing. Prentice Hall, New Jersey. p. 238

Key, C.H. and Benson, N. C. 1999, The Normalized Burn Ratio (NBR): A Landsat TM Radiometric Index of Burn Severity. URL: http://www.nrmsc.usgs.gov/research/ndbr.htm visited April 2007.

Key, C.H. and Benson, N. C. 2004, Remote Sensing Measure of Severity: The Normalized Burn Ratio. FIREMON Landscape Assessment (LA) V4 Sampling and Analysis Methods. pp. LA1-16

Key, C.H. and. Benson, N. C. 2006, Landscape Assessment (LA) Sampling and Analysis Methods. USDA Forest Service Gen. Tech. Rep. RMRS-GTR-164-CD. pp. 55

Lawrence, R. L. and Wright, A. 2001. Rule-based Classification Systems Using Classification and Regression Tree (CART) Analysis. *Photogrammetric Engineering and Remote Sensing*. 67(10):1137-1142.

Lentile, L. B., Holden. Z. A, Smith, A. M. S., Falkowski, M. J., Hudak, A. T., Morgan, P., Lewis, S. A., Gessler, P. E., and Benson, N. C. 2006, Remote Sensing Techniques to Assess Active Fire Characteristics and Post-Fire Effects. *Intlernational Journal of Wildland Fire* 15(3):319-345.

McKay, R.J. and Campbell, N.A. 1982, Variable selection techniques in discriminant analysis II: Allocation, *British Journal of Mathematical and Statistical Psychology*, 35, 30-41

Miller, J. and Franklin, J. 2001, Modeling the distribution of four vegetation alliances using generalized linear models and classification trees with spatial dependence. *Ecological Modeling*, 157: 227–247.

Mirik, M., Norland, J. E., Crabtree, R. L., and Biondini, M. E. 2005, Hyperspectral One-Meter-Resolution Remote Sensing in Yellowstone National Park, Wyoming: II Biomass. *Rangeland Ecology and Management*. 58(5):459-465.

Natural Resources Conservation Service (NRCS). 1995, Soil investigation of Agriculture Research Service, United States Sheep Experiment Station headquarters range, US Department of Agriculture. Rexburg, ID: NRCS. 133pp.

Natural Resources Conservation Service (NRCS). 2006, Land Resource Regions and Major Land Resource Areas of the United States, the Caribbean, and the Pacific Basin. United States Department of Agriculture Handbook, 296 pp.

Norton, J. 2006, The Use of Remote Sensing Indices to Determine Wildland Burn Severity in Semiarid Sagebrush Steppe Rangelands Using Landsat ETM+ and SPOT 5. Idaho State University. URL: http://giscenter.isu.edu/Research/techpg/nasa_tlcc/to_pdf/jnthesis.pdf visited April 2007. 111pp.

Okin, W.J., Okin, G.S., Roberts, D.A., and Murray, B. 1999, Multiple end member spectral mixture analysis: end member choice in an arid shrubland, *in* Green, R.O., ed., *The 1999 AVIRIS Workshop*: Pasadena California, p. 323-332.

Okin, G. S., Roberts, D. A., Murray, B., and Okin, W. J., 2001, Practical limits on hyperspectral vegetation discrimination in arid and semiarid environments. *Remote Sensing of Environment*, 77, 212-225.

Patterson, M.W. and Yool, S. R. 1998, Mapping fire-induced vegetation mortality using Landsat Thematic Mapper data: A comparison of linear transformation techniques. *Remote Sensing of Environment*, 65, 132-42

Pyke D. A., Herrick, J. E., Shaver, P., and Pellant, M. 2002, Rangeland health attributes and indicators for qualitative assessment. *Journal of Range Management* 55:584-597.

Pyne, S. J., Andrews, P. L., and Laven, R. D. 1996, *Introduction to Wildland Fire*. New York: John Wiley and Sons, 769 pp.

Roy, D. P., Boschetti, L., Trigg, S. N. 2006, Remote sensing of fire severity: assessing the performance of the normalized burn ratio. *IEEE Geoscience and Remote Sensing letters*. 3:112-116.

Ryan, K. C.; Noste, N. V. 1983, Evaluating prescribed fires. Pages 230-238 in Lotan, J. E.; Kilgore, B. M.; Fischer, W. C.; Mutch, R. W. (tech. cords.), *Proceedings, symposium and workshop on wilderness fire*. General Technical Report INT-182. Ogden, UT: U.S. Department of Agriculture, Forest Service, Intermountain Research Station.

Salvador, R., Valeriano, J., Pons, X., and Diaz-Delgado, R. 2000, A semi-automatic methodology to detect fire scars in shrubs and evergreen forests with Landsat MSS time series. *International Journal of Remote Sensing*, 21, 655-71

Seefeldt, S.S. 2005, Consequences of selecting rambouilllet ewes for mountain big sagebrush (*Artemisia tridentata* ssp. vaseyana) dietary preference. *Rangeland Ecology and Management*, 58: 380-384

Seefeldt, S.S. and Laycock, W. 2006, The United States Sheep Experiment Station: Shedding light on rangeland ecosystems. *Rangelands* 28(2):30-35.

Serr, K., Windholz, T. K., and Weber K. T. 2006, Comparing GPS Receivers: A Field Study. *URISA Journal*. 18(2):19-24.

Smith, A. M. S., Wooster, M. J., Drake, N. A., Dipotso, F. M., Falkowski, M. J., and Hudak, A. T. 2005, Testing the potential of multi-spectral remote sensing for retrospectively estimating fire severity in African savanna environments. *Remote sensing of environment* 97:92-115.

Switky, K.R. 2003, *Fire monitoring handbook*: Boise, ID, 274 pp., NPS Fire management program center, National Interagency Fire Center, 274pp.

Thoren, F.and Mattsson, D. 2002, Historic Wildfire Research in Southeastern Idaho. URL: http://giscenter.isu.edu/research/techpg/blm_fire/historic/wildfire_report.pdf visited April 2007. 16pp.

Turner, M.G., Hargrove, W. W., Gardner, R. H., and Romme, W. H. 1994, Effects of fire on landscape heterogeneity in Yellowstone National Park, Wyoming. *Journal of Vegetation Science*, 5, 731-42

Van Wagtendonk, J.W., Root R. R., and Key, C. H., 2004, Comparison of AVIRIS and Landsat ETM+ detection capabilities for burn severity. *Remote Sensing of Environment*, 92: 397–408

Weber, K. T. 2006, Challenges of Integrating Geospatial Technologies Into Rangeland Research and Management. *Rangeland Ecology and Management*. 59(1):38-43.

Weber, K. T., Glenn, N. F., Mundt, J. T., and Gokhale, B. 2006, A Comparison Between Multi-spectral and Hyperspectral Platforms for Early Detection of Leafy Spurge in Southeastern Idaho. Pages 185-196 in Weber, K. T. (Ed.), *Final: Report: Detection, Prediction, Impact, and Management of Invasive Plants Using GIS*. 196pp.

West, N.E. and Young, J. A., 2000, Intermountain Valleys and Lower Mountain Slopes. Pages 255-284 in Barbour, M.G. and Billings, W.D. (Ed.), *North American Terrestrial Vegetation*. Cambridge, UK: Cambridge University Press.

White, J.D., Ryan, K. C., Key, C. H., and Running, S. W. 1996, Remote sensing of forest fire severity and vegetation recovery. *International Journal of Wildland Fire*, 6, 125-36

Wright, H. E. and Bailey, A. W. 2004, *Fire Ecology: United States and Southern Canada*. Wiley Interscience. 528pp.

Wright, H.A. 1985, Effects of fire on grasses and forbs in sagebrush-grass communities, pages 12-21 in Durham, J. (Ed.), *Rangeland Fire Effects*; A Symposium: Boise, ID, USDI-BLM.

Zambon, M., Lawrence, R., Bunn, A., and Powell, S. 2006. Effect of alternative splitting rules on image processing using classification tree analysis. *Photogrammetric Engineering and Remote Sensing*, 72(1): 25–30.

[THIS PAGE LEFT BLANK INTENTIONALLY]

Comparing Fire Severity Models from Post-Fire and Pre/Post-Fire Differenced Imagery

Keith T. Weber, GISP, Idaho State University, GIS Training and Research Center, 921 S. 8th Ave., Stop 8104, Pocatello, Idaho 83209-8104 (webekeit@isu.edu)

Steven Seefeldt, Research Agronomist, USDA-ARS, SubArctic Agricultural Research Unit, University of Alaska Fairbanks, Fairbanks, Alaska 99775

Corey Moffet, Research Rangeland Scientist, USDA-ARS, U.S. Sheep Experiment Station, Dubois, Idaho 83423

Jill Norton, GIS Specialist, Blaine County, Hailey, ID 83333

ABSTRACT

Wildland fires are common in rangelands worldwide. The potential for high severity fires to affect long-term changes in rangelands is considerable, and for this reason assessing fire severity shortly after the fire is critical. Such assessments are typically carried out following Burned Area Emergency Response teams or similar protocols. These data can then be used by land managers to plan remediation and future land uses. To complement these procedures and explore fire severity modeling of sagebrush steppe rangelands, we compared models developed using 1) post-fire imagery only with 2) differenced imagery (pre-fire minus post-fire imagery). All models were developed from Classification Tree Analysis (CTA) techniques using Satellite Pour l'Observation de la Terre 5 (SPOT 5) imagery and Shuttle Radar Topography Mission (SRTM) elevation data. The results indicate that both techniques produced similar fire severity models (model agreement = 98.5%) and that little improvement in overall accuracy was gained by using differenced imagery (0.5 %). Therefore, we suggest the use of CTA models developed using only the post-fire imagery. The analyses and techniques described in this paper provide land managers with tools to better justify their recommendations and decisions following wildland fires in sagebrush steppe ecosystems.

KEYWORDS: classification tree, remote sensing, wildfire, GIS

INTRODUCTION

Wildland fires are a common occurrence throughout the Intermountain West. While historic plant communities may be adapted to fire, the frequency and intensity of today's wildfires is different compared to what occurred in the past (DeBano et al., 1998; Thoren and Mattsson 2002). The change in frequency and intensity can be attributed to 1) fire suppression efforts that have inadvertently created fuel stockpiles (Pyne et al 1996) and 2) the conversion of sagebrush-grass communities to fire-promoting cheatgrass (*Bromus tectorum* L.) dominated communities (Brooks et al 2004). The consequences of these differences are manifest in various impacts on wildlife habitat, forage production, potential soil erosion (Pierson et al., 2001; Finley, 2006; Moffet et al., 2007), and rangeland health (Pyke et al., 2002).

Assessing the effect of wildfires is important to land management agencies to minimize threats to life/property and prevent unacceptable degradation of natural and cultural resources (Sharon Paris, pers. comm.; Department of Interior 2004). However, due to the broad extent and distribution of wildfires in the Intermountain West the ability of land managers to closely evaluate each and every fire can be logistically difficult if not impossible. For these reasons, the application of remote sensing models that accurately and reliably classify fire severity may be useful (Lentile et al 2006).

Several image processing methods have been used to model fire severity (Garcia and Chuvieco, 2004); most have been designed for forested ecosystems (Turner et al., 1994; White et al., 1996; Patterson and Yool, 1998; Van Wagtendonk et al., 2004; Brewer et al., 2005; Epting et al., 2005). Prior to 1999, the most widely used fire severity modeling method was an NDVI-based technique to estimate biomass loss, and hence, fire severity (Salvador et al., 2000; Diaz-Delgado et al., 2003; Flasse et al., 2004). In 1999, the normalized burn ratio (NBR) technique was developed and has been widely applied and accepted (Key and Benson 1999; Salvador et al., 2000; Key and Benson, 2006).

Another form of the NBR model is known as a differenced NBR (dNBR). It estimates fire severity by comparing a pre-burn NBR model to that of a post-burn NBR model. The result is a model where the magnitude of change has been normalized by pre-burn landscape characteristics (Key and Benson 1999; Key and Benson, 2004; Van Wagtendonk et al., 2004; Cocke et al., 2005).

While fire severity studies reported by Finley (2006) and Norton (2006) suggest the NBR techniques may not be well-suited to sagebrush-steppe ecosystems, more recent research (Weber and Seefeldt, 2008) has demonstrated the application of classification tree analysis (CTA) for fire severity modeling of rangelands with favorable results. CTA is a non-probabilistic, non-parametric statistical technique well-suited to modeling skewed, non-normal data and phenomena (Breiman et al. 1998; Friedl and Brodley 1997; Lawrence and Wright 2001; Miller and Franklin 2001). The CTA algorithms select useful spectral and ancillary data which optimally reduce divergence in a response variable (Lawrence and Wright 2001) such as fire severity observations. CTA uses machine-learning to perform these binary recursive splitting operations and ultimately yields a classification tree diagram that is used to produce a model of the response variable. Splitting algorithms common to CTA include entropy, gain ratio, and Gini. The entropy algorithm has a tendency to over-split and thereby creates an unnecessarily complex tree (Zambon, et al., 2006). The gain ratio algorithm addresses the over-splitting problem through a normalization process while the Gini algorithm attempts to partition the most homogeneous clusters first using a measure of impurity (McKay and Campbell 1982; Zambon et al., 2006).

A previous study reported by Weber et al (2008) described fire severity models created using post-fire satellite imagery only. The goals of this study were to model fire severity in semi-arid rangelands and compare the results derived using post-fire imagery only with results from differenced imagery (i.e., derived from pre- and post-fire differenced imagery). Specifically, we will test whether the CTA model

derived using post-fire only imagery satisfactorily classifies high severity fire areas in the sagebrush steppe.

METHODS

Study Area

This study focuses upon the Hitching Post pasture burn at the U. S. Sheep Experiment Station (USSES) near Dubois, Idaho (Figure 1). The prescribed burn was begun September 14th and was extinguished September 15th, 2005. The fire boundary encompassed 2.44 km^2 within the Hitching Post pasture (112° 7' W 44° 19' N), a 3.24 km^2 fenced parcel on the USSES that ranges in elevation from 1765 to 1800 m. Mean annual precipitation (1971 to 2000) at the Dubois Experiment Station (112° 12' W 44° 15'N, elevation, 1661 m) is 331 mm with 60% falling during April through September. Soils are mapped as complexes of Maremma (Fine-loamy, mixed, superactive, frigid Calcic Pachic Argixerolls), Pyrenees (Loamy-skeletal, mixed, superactive, frigid Typic Calcixerolls), and Akbash (Fine-loamy, mixed, superactive, frigid Calcic Pachic Argixerolls) soils on slopes less than 20 percent, but mostly 0 to 12 percent (NRCS 1995).

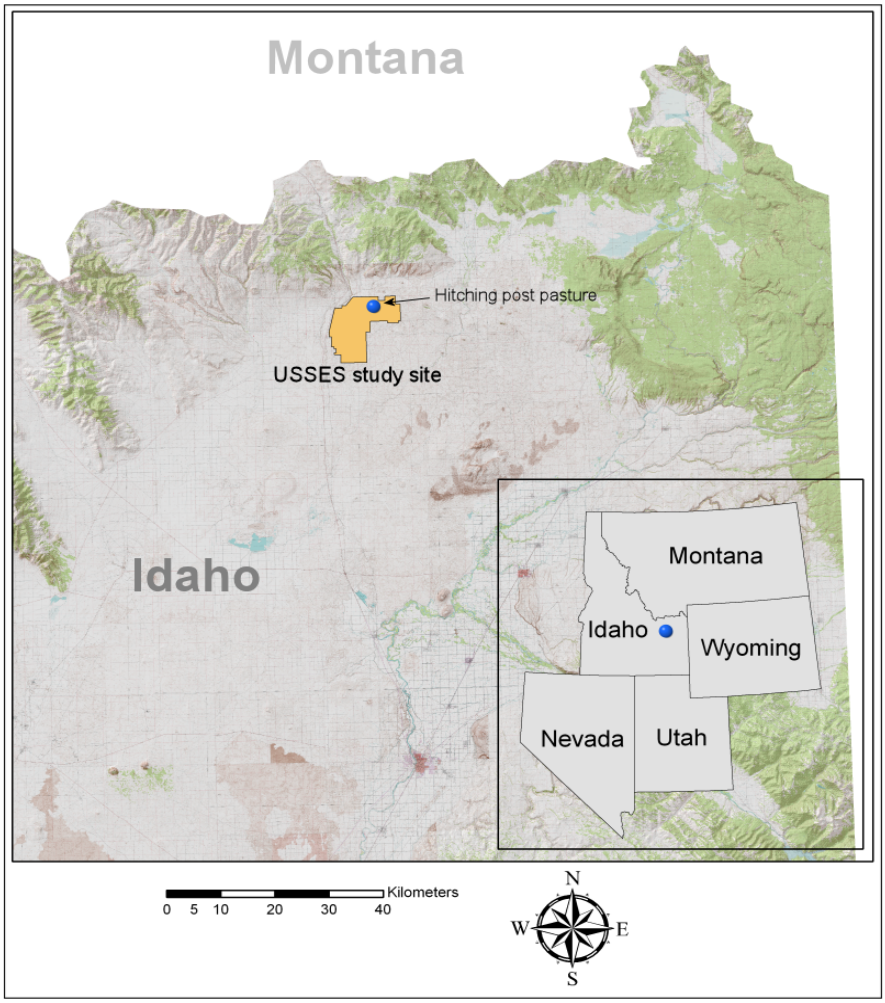

Figure 1. Location of the USDA ARS Sheep Experiment Station and site of the prescribed fire used in this study.

Vegetation on the study site is a sagebrush-grass community that is dominated by mountain big sagebrush (*Artemisa tridentata* ssp. *vaseyana* [Rydb.] Beetle) and threetip sagebrush (*A. tripartita* Rydb.). Subdominant shrub species include antelope bitterbrush (*Purshia tridentata* [Pursh] DC.),

yellow rabbitbrush (*Chrysothamnus viscidiflorus* (Hook.) Nutt.), and spineless horsebrush (*Tetradymia canescens* DC.). There are a few small patches of the exotic forbs leafy spurge (*Euphorbia esula* L.) and spotted knapweed (*Centaurea stoebe* L. ssp. *micranthos* [Gugler] Hayek) and trace amounts (<1% of overall plant cover) of the exotic annual cheatgrass. Lupine (*Lupinus argenteus* Pursh) is the most plentiful forb on the study site and the graminoids present are thickspike wheatgrass (*Elymus lanceolatus* [Scribn. & J.G. Sm.] Gould ssp. *lanceolatus*), bluebunch wheatgrass (*Pseudoroegneria spicata* [Pursh] A. Löve ssp. *spicata*), and plains reedgrass (*Calamagrostis montanensis* Scribn. ex Vasey).

The management of this pasture for the past decade has been light, short duration, grazing with sheep and horses in spring and/or fall. There was no grazing in this pasture during the 2.5 years prior to the prescribed burn.

Field Sampling

Beginning one week after the prescribed burn, 277 randomly selected sample areas (60 x 60 m) were visited to assess fire severity. The sample areas were located on the ground by navigating to the preselected area with a GPS receiver using real-time positioning. These positions were later post process differentially corrected to achieve a horizontal positional accuracy of <1m (Serr et al. 2006). While subjective, a fire severity rating (0 = Unburned, no vegetation change; 1 = little vegetation/fuel consumption by the fire; 2 = most of the vegetation was consumed; and 3 = burned (the area was considered a completely consumed by the fire) was assigned to each area visited following methods modified from the combined work of US Forest Service field methods (Bobbe et al., 2001), the US Park Service field methods (Switky 2003), and Key and Benson's (Key and Benson 1999; 2004) composite burn index (CBI). Groups one (n=13) and two (n=57) were later combined because only 13 areas were assigned to group one which was insufficient for validation. In addition, some aspects of fire severity can be quantified but classification of general severity has proven difficult. Classification of burn or fire severity, based on the post-fire appearance of litter and soil (Ryan and Noste 1983), are useful for placing severity into broadly defined, discrete classes, ranging from low to high. A general burn severity classification developed by Hungerford (1996) in forest situations relates burn severity to soil resource response and has three classes; low, moderate, and high. In rangeland ecosystems the medium and high severity classes described by Hungerford merge as there are not large woody component and deep duff layer, whose response to burning differentiates the classes. Therefore, we chose a simple classification of low or high severity and as a result, three classes remained: 0 (unburned), 1 (low fire severity), and 2 (high fire severity).

It was not an objective of this study to separate burned from unburned areas and for this reason all unburned sample areas were omitted from subsequent processing. We recognize that the few unburned areas within the fire perimeter (n=9) would not be classified as unburned, but most likely, would be classified as low fire severity areas based upon preliminary classification results (i.e., using unburned areas in the analysis). Preliminary analyses further indicated that spectral signatures of unburned and low fire severity sites were very similar and spectrally indistinct (Richards 1993; Lillesand and Kiefer 2000). This potential for error however, was considered acceptable because the focus of the study was to develop a model that would correctly identify high fire severity areas so land managers performing post-fire recovery planning and remediation could focus their resources on high fire severity areas.

Image Processing

Pre- and post-fire Satellite Pour l'Observation de la Terre 5 (SPOT 5) satellite imagery (10m x 10m pixels) was acquired for the USSES study site for August 27, 2005 and September 28, 2005, respectively. The imagery was georectified using 1 m National Agricultural Imagery Program orthophotography for the study area (RMSE = 3.48) using the same set of control points within ArcGIS,

corrected for atmospheric effects and projected into Idaho Transverse Mercator (NAD 83) using a first order affine transformation and nearest neighbor resampling.

Normalized difference vegetation index (NDVI), normalized burn ratio (NBR), and biomass estimates (the ratio of the short-wave infrared band divided by the visible green band [Mirik et al. 2005]) were calculated within Idrisi Kilimanjaro using SPOT reflectance data. The biomass layer is a simple ratio-type vegetation index where reflectance values from the short-wave infrared region (band) are divided by reflectance values from the green band. While Mirik et al. (2005) demonstrated a strong empirical relationship ($R^2 = 0.87$) between this index and total rangeland biomass, the relationship of the biomass index and actual rangeland biomass was not performed as part of this study. The biomass index differs from the normalized difference infrared index (NDII [Hunt and Yilmaz 2007]) in that the biomass index is a simple ratio-type index as opposed to a normalized difference-type index and the biomass index does not make use of the infrared band as does NDII. Another related normalized difference-type index is the normalized difference water index (NDWI) which uses the ratio of the difference between the near infrared and thermal infrared bands divided by the sum of these same bands (Gu et al. 2007). Neither the NDII nor NDWI were used in this study (NDWI cannot be used with SPOT imagery as this sensor does not include a thermal infrared band).

In addition, topography data were assembled for use as ancillary data within the CTA process (Elumnoh and Shrestha 2000). Elevation data were acquired from the shuttle radar topography mission (SRTM) and was resampled to 10m to match the spatial resolution of the SPOT 5 imagery. Slope and aspect models were derived from these elevation data using Idrisi Kilimanjaro.

Polygon shapefiles describing the fire perimeters were rasterized and used as a mask for all raster data. Field observations were similarly masked and only those points falling inside the fire perimeter were used in the CTA. This masking process was done to help facilitate classification by prudently applying ancillary knowledge to better inform the classifier. This process is a well accepted technique referred to as "cluster busting" (Jensen 1996; Hunter 2004). CTA was performed using the Gini splitting algorithm (Zambon et al., 2006) with five input images. The post-fire condition dataset contained near-infrared (NIR), NDVI, NBR, and biomass band-ratios, along with the slope layer. The pre-post fire differenced dataset contained differenced NIR (dNIR), differenced NDVI (dNDVI), differenced NBR (dNBR) (Key and Benson 1999; Key and Benson, 2004; Van Wagtendonk et al., 2004; Cocke et al., 2005), differenced biomass, and the same slope layer. In each case, image differencing was performed by subtracting the post-fire imagery from the pre-fire imagery.

To absorb georegistration error within the SPOT imagery (RMSE=3.48) and ensure correct and representative pixels were included in the analysis, all sample areas were buffered by 5m (Weber 2006). The resulting layers were rasterized using ArcGIS 9.1 and subset into training and validation sites. As a result, a total of 385 training site pixels and 207 validation site pixels were created. The CTA was performed with Idrisi Kilimanjaro using these data.

RESULTS AND DISCUSSION

The CTA model developed using five post-fire satellite imagery layers (NIR, NDVI, NBR, biomass, and slope) correctly identified all 186 high fire severity validation areas (n = 186, user accuracy = 100%) (Figure 2a, Table 1). Similarly, using five differenced input layers (dNIR, dNDVI, dNBR, differenced biomass, and the same slope topography layer) user accuracy was 99.5% (Figure 2b, Table 2). While overall accuracy intially appears to be better using differenced imagery (97.1% compared with 96.6%), this slight difference is considered insignificant. Statistically testing this difference is problematic however as each model exhibits a high degree of autocorrelation (Moran's I = 0.55 and 0.51 for post-fire and differenced imagery, respectively) and due to the large number of pixels within each model, statistical tests like mixed linear models would calculate a very small standard error (due to the high

proportion of pixels in agreement) thereby causing the test to detect differences whether they were practically significant or not (Teri Peterson, pers. comm.). The authors argue that any differences reported here is not of practical significance.

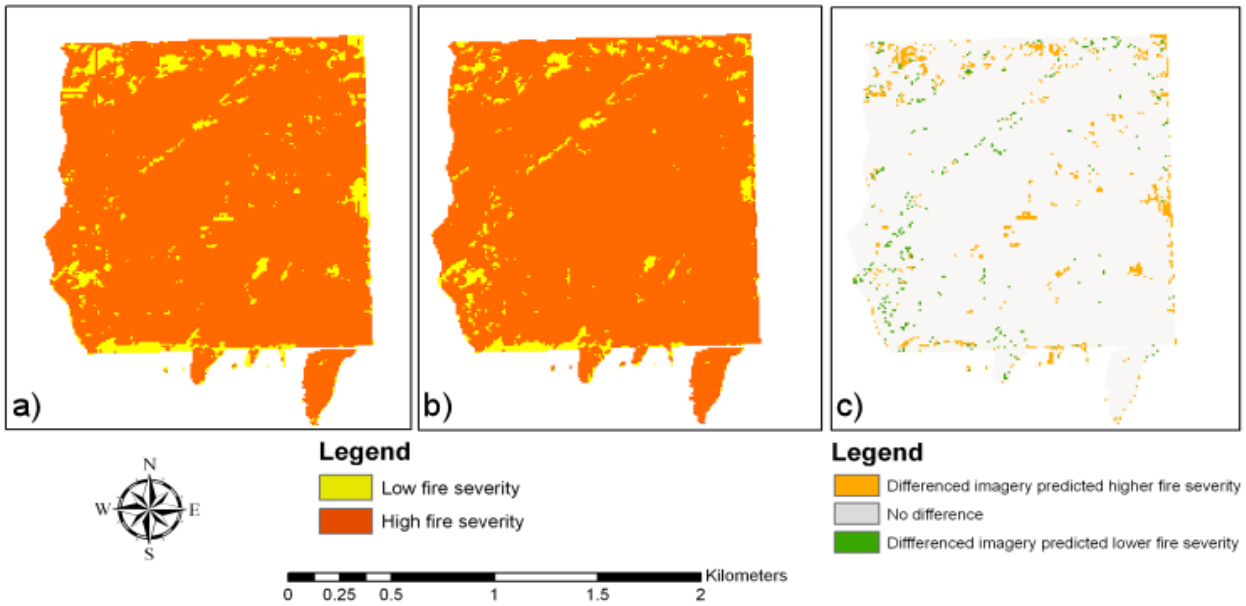

Figure 2. Resulting fire severity models produced using classification tree analysis (CTA) with post-fire imagery (a), differenced imagery (b), and differenced models (c).

Map arithmetic techniques were used to identify those areas (pixels) where the two models predicted different fire severity levels (Figure 2c). Nearly all pixels exhibited agreement in predicted fire severity (98.5%). The majority of the disagreement (73% of all disagreement pixels) was in areas where the differenced imagery model predicted a high fire severity class, but the post-fire imagery model predicted low fire severity (i.e., the differenced imagery model predicted more area burned with high fire severity).

Table 1. Classification tree analysis (CTA) results for fire severity modeling derived using post-fire raster layers.

	Known validation sites			
	Low fire severity	High fire severity	Total	User accuracy
Low fire severity	14	7	21	0.66
High fire severity	0	186	186	1.00
Total	14	193	207	
Producer's accuracy	0.93	0.97		0.97[a]

[a] Overall accuracy

Kappa index of agreement = 0.78

Based on overall accuracies and level of agreement between the two models it is clear that producing a reliable fire severity model in sagebrush steppe ecosystems can be accomplished using just post-fire imagery. Acquiring both pre- and post-fire imagery and producing differenced image layers adds tremendously to the cost and effort with no improvement in the resulting model for this burn; however, this may not be true for all rangelands. Additional studies are merited to determine whether this is true for other rangelands.

Table 2. Classification tree analysis (CTA) results for fire severity modeling derived using differenced raster layers.

	Known validation sites			
	Low fire severity	High fire severity	Total	User accuracy
Low fire severity	13	5	18	0.72
High fire severity	1	188	189	0.99
Total	14	193	207	
Producer's accuracy	0.93	0.97		0.97[a]

[a] Overall accuracy
Kappa index of agreement = 0.80

Assessment of error and bias
Models developed using CTA were able to classify high fire severity areas with good user accuracy (~100%) (cf. Figure 3 for a step-by-step approach and cartographic model of this technique). However, achieving satisfactory results appears to be a function of adequate sample size for each class considered (low fire severity or high fire severity). Initially, it may appear that a disproportionately large number of validation sites were used in high fire severity areas (n=193, 92%; tables 1 and 2). However, as fire severity is primarily a function of the fire's behavior --which is closely tied to factors such as the amount and type of fuels and the weather during the fire (Pyne et al. 1996) -- the proportion of high fire severity sites (used for both modeling and validation) agreed well with field observations where 92% of the study area was recorded as high severity (Figure 2a, b). Indeed when the proportions of the random sampling locations were compared with proportions of fire severity areas, the results appear equitably distributed.

CONCLUSIONS

Post-fire vegetation management in western rangelands should be based on pre-fire vegetation, post-fire weather conditions, soils, available resources (such as seeds, equipment, and personnel), and fire severity. Given the size and distribution of western fires, land managers face an almost impossible task in trying to determining fire severity in a time frame useful for the preparation of remediation plans. The development of GIS layers that combine vegetation information, climate, soils, and fire severity could ease the task of creating predictive models for more effective remediation plan development. The results of this research addresses mapping of fire severity, which can be used as one layer within a GIS-based remediation model. Using easily obtained post-fire SPOT 5 imagery, high severity burn areas can be accurately, rapidly, and inexpensively delineated, resulting in a GIS layer useful for remediation plan development.

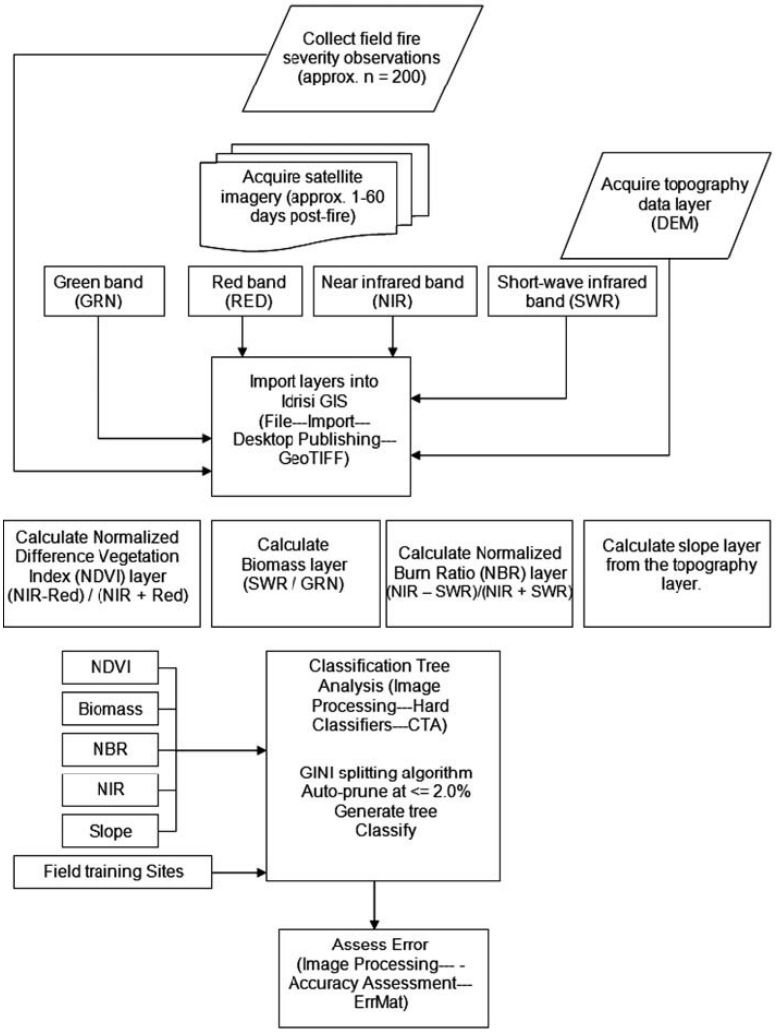

Figure 3. Cartographic model of the process followed to produce a fire-severity model using classification tree analysis at both the Clover and USSES study sites.

ACKNOWLEDGEMENTS

We would like to acknowledge the Idaho Delegation for their assistance in obtaining the grant that supported this work funded through the National Aeronautic and Space Administration (NASA [NNG05GB05G]). In addition, we would like to acknowledge the assistance of Jamen Underwood, and Penny Gneiting for their field data collection efforts and research in rangeland fire severity modeling as well as the statistical consultation of Teri Peterson and the assistance of Sharon Paris.

LITERATURE CITED

Bobbe, T., M. V. Finco, B. Quayle, B., and K. Lannon. 2001. Field measurements for the training and validation of burn severity maps from spaceborne, remotely sensed imagery. Remote Sensing Applications Center, Salt Lake City, Utah: USDA Forest Service, Final Project Report, Joint Fire Science Program-2001-2. Project # 01B-2-1-01, pp. 15 URL: http://www.fs.fed.us/eng/rsac/baer/final_report_01B-2-1-01.pdf Visted April 2007.

Breiman, L., Friedman, J. H., Olshen, R. A., and Stone C. J., 1998, Classification and Regression Trees. Chapman and Hall, CRC press, Boca Raton, Florida. 358 pp.

Brewer, C.K., J. C. Winne, R. L..Redmond, D. W. Opitz, and M. V. Mangrich. 2005. Classifying and mapping wildfire severity: A comparison of methods. Photogrammetric Engineering and Remote Sensing, 71:11, 1311-20.

Brooks M. L., C. M D'Antonio, D. M. Richardson, J. B. Grace, J. E Keeley, J. M. DiTomaso, R. J. Hobbs, M. Pellant, and D. Pyke. 2004. Effects of Alien Plants on Fire Regimes. Bioscience. 54(7):677-688.

Cocke, A.E., P. Z. Fule, and J. E. Crouse. 2005. Comparison of burn severity assessments using differenced normalized burn ratio and ground data. International Journal of Wildland Fire, 14: 189-98.

DeBano, L.F., Neary, D.G., and Pfolliott, P.F., 1998, Fire's Effects on Ecosystems: New York, John Wiley and Sons, 333 pp.

Department of the Interior (DOI). 2004. Departmental Manual, Part 620 Chapter 3, Burned Area Emergency Stabilization and Rehabilitation (620DM3), 16 pp.

Diaz-Delgado, R., F. Lloret, and X. Pons. 2003. Influence of fire severity on plant regeneration by means of remote sensing imagery. International Journal of Remote Sensing, 24:8, 1751-1763.

Epting, J., D. Verbyla, and B. Sorbel. 2005. Evaluation of remotely sensed indices for assessing burn severity in interior Alaska using Landsat TM and ETM+. Remote Sensing of Environment, 96, 328-339.

Elumnoh A. and R. P. Shrestha. 2000. Application of DEM Data to Landsat Image Classification: Evaluation in a Tropical Wet-Dry Landscape in Thailand. Photogrammetric Engineering and Remote Sensing. 66(3):297-304.

Flasse, S., S. Trigg, P. Ceccato, A. Perryman, A. Hudak, M. Thompson, B. Brockett, M. Dramé, T. Ntabeni, P. Frost, T. Landmann, and J. le Roux. 2004. Remote sensing of vegetation fires and its contribution to a fire management information system. In J.G. Goldammer and C. de Ronde (Eds.), *Wildfire Management Handbook for Sub-Sahara Africa* (pp.158-211). The Hague, Netherlands: SPB Publishing.

Finley, C. D. 2006. Field evaluation and hyperspectral imagery analysis of fire-induced water repellent soils and burn severity in southern Idaho rangelands. Idaho State University. URL: http://giscenter.isu.edu/Research/techpg/nasa_tlcc/to_pdf/cfthesis.pdf visited April 2007. 237pp.

Friedl, M. A. and Brodley, C. E., (1997), Decision tree classification of land cover from remotely sensed data. Remote sensing of environment. 61(3):399-409.

Garcia, M. and E. Chuvieco. 2004. Assessment of the potential of SAC-C/MMRS imagery for mapping burned areas in Spain. Remote Sensing of Environment, 92, 414-423.

Gu, Y., Brown, J. F., Verdin, J. P., and Wardlow B. 2007, A five-year analysis of MODIS NDVI and NDWI for grassland drought assessment over the central Great Plains of the United States. Geophysical Research Letters, 34(L06407). 6 pp.

Hungerford, R.D. 1996, Soils. Fire in Ecosystem Management Notes: Unit II-I. USDA Forest Service, National Advanced Resource Technology Center, Marana, Arizona

Hunt, E. R. and Yilmaz, T. 2007, Remote sensing of vegetation water content using shortwave infrared reflectance. Summaries of International Society for Optical Engineering. URL: http://ars.usda.gov/research/publications/publications.htm?seq_no_115=209592 visited January 2008.

Hunter, B. 2004, Overview of Methodology for Remote Sensing/GIS Analysis of Lakes Lewisville and Grapevine Shoreline Management Project. University of North Texas, URL:

Inouye, R. 2002. Sampling Effort and Vegetative Cover Estimates in Sagebrush Steppe. *Western North American Naturalist* 62(3): 360-364.

Jensen, J. R. 1996, Introductory Digital Image Processing. Prentice Hall, New Jersey. p. 238

Key, C.H. and N. C. Benson. 1999. The Normalized Burn Ratio (NBR): A Landsat TM Radiometric Index of Burn Severity. URL: http://www.nrmsc.usgs.gov/research/ndbr.htm; visited April 2007.

Key, C.H. and N. C. Benson. 2004. Remote Sensing Measure of Severity: The Normalized Burn Ratio. FIREMON Landscape Assessment (LA) V4 Sampling and Analysis Methods. pp. LA1-16.

Key, C.H. and N. C. Benson. 2006. Landscape Assessment (LA) Sampling and Analysis Methods. USDA Forest Service Gen. Tech. Rep. RMRS-GTR-164-CD. pp. 55.

Lawrence, R. L. and A. Wright. 2001. Rule-based Classification Systems Using Classification and Regression Tree (CART) Analysis. Photogrammetric Engineering and Remote Sensing. 67(10):1137-1142.

Lentile, L. B., Z. A Holden, A. M. S. Smith, M. J. Falkowski, A. T. Hudak, P. Morgan, S. A. Lewis, P. E. Gessler, and N. C. Benson. 2006. Remote Sensing Techniques to Assess Active Fire Characteristics and Post-Fire Effects. Intl. Journal of Wildland Fire. 15(3):319-345.

Lillesand T. M. and R. W. Kiefer. 2000. Remote Sensing and Image Interpretation. 4th Ed. John Wiley and Sons, New York, NY. 724pp.

McKay, R.J. and Campbell, N.A. 1982. Variable selection techniques in discriminant analysis II: Allocation, British Journal of Mathematical and Statistical Psychology, 35, 30-41.

Miller, J. and J. Franklin, 2001. Modeling the distribution of four vegetation alliances using generalized linear models and classification trees with spatial dependence. Ecological Modeling, 157: 227–247.

Mirik, M., J. E. Norland, R. L. Crabtree, and M. E. Biondini. 2005. Hyperspectral One-Meter-Resolution Remote Sensing in Yellowstone National Park, Wyoming: II Biomass. Rangeland Ecology and Management. 58(5):459-465.

Moffet, C.A., F.B. Pierson, P.R. Robichaud, K.E. Spaeth, and S.P. Hardegree. 2007. Modeling soil erosion on steep sagebrush rangeland before and after prescribed fire. Catena, 71:218-228.

Natural Resources Conservation Service (NRCS). 1995. Soil investigation of Agriculture Research Service, United States Sheep Experiment Station headquarters range, US Department of Agriculture. Rexburg, ID: NRCS. 133pp.

Norton, J. 2006. The Use of Remote Sensing Indices to Determine Wildland Burn Severity in Semiarid Sagebrush Steppe Rangelands Using Landsat ETM+ and SPOT 5. Idaho State University. URL: http://giscenter.isu.edu/Research/techpg/nasa_tlcc/to_pdf/jnthesis.pdf visited April 2007. 111pp.

Patterson, M.W. and S. R. Yool. 1998. Mapping fire-induced vegetation mortality using Landsat Thematic Mapper data: A comparison of linear transformation techniques. Remote Sensing of Environment, 65, 132-42.

Pierson, F.B., P.R. Robichaud, and K.E. Spaeth. 2001, Spatial and temporal effects of wildfire on the hydrology of a steep rangeland watershed. Hydrological Processes, 15:2905-2916.

Pyke D. A., J. E. Herrick, P. Shaver, and M. Pellant. 2002. Rangeland health attributes and indicators for qualitative assessment. Journal of Range Management 55:584-597.

Pyne, S. J., P. L. Andrews, and R. D. Laven. 1996. Introduction to Wildland Fire. John Wiley and Sons, New York. 769 pp.

Richards, J.A., 1993. Remote Sensing Digital Image Analysis, Springer-Verlag, New York, NY. 363 pp.

Ryan, K. C.; Noste, N. V. 1983, Evaluating prescribed fires. Pages 230-238 in Lotan, J. E.; Kilgore, B. M.; Fischer, W. C.; Mutch, R. W. (tech. cords.), *Proceedings, symposium and workshop on wilderness fire*. General Technical Report INT-182. Ogden, UT: U.S. Department of Agriculture, Forest Service, Intermountain Research Station.

Salvador, R., J. Valeriano, X. Pons, and R. Diaz-Delgado. 2000. A semi-automatic methodology to detect fire scars in shrubs and evergreen forests with Landsat MSS time series. International Journal of Remote Sensing, 21, 655-71.

Serr, K., Windholz, T. K., and Weber K. T. 2006. Comparing GPS Receivers: A Field Study. URISA Journal. 18(2):19-24.

Switky, K.R. 2003. Fire monitoring handbook: Boise, ID, 274 pp., NPS Fire management program center, National Interagency Fire Center, 274pp.

Thoren, F.and D. Mattsson. 2002. Historic Wildfire Research in Southeastern Idaho. URL: http://giscenter.isu.edu/research/techpg/blm_fire/historic/wildfire_report.pdf visited April 2007. 16pp.

Turner, M.G., W. W. Hargrove, R. H. Gardner, and W. H. Romme. 1994. Effects of fire on landscape heterogeneity in Yellowstone National Park, Wyoming. Journal of Vegetation Science, 5, 731-42.

Van Wagtendonk, J.W., R. R. Root,., and C. H. Key. 2004. Comparison of AVIRIS and Landsat ETM+ detection capabilities for burn severity. Remote Sensing of Environment, 92: 397–408.

Weber, K. T. 2006. Challenges of Integrating Geospatial Technologies Into Rangeland Research and Management. Rangeland Ecology and Management. 59(1):38-43.

Weber, K. T., S. S. Seefeldt, J. Norton, and C. Finley. 2008. Fire Severity Modeling of Sagebrush-steppe Rangelands in Southeastern Idaho. GIScience and Remote Sensing (*in press*).

White, J.D., K. C. Ryan, C. H. Key, and S. W. Running. 1996. Remote sensing of forest fire severity and vegetation recovery. International Journal of Wildland Fire, 6, 125-36.

Wright, H. E. and A. W. Bailey. 2004. Fire Ecology: United States and Southern Canada. Wiley Interscience. 528pp.

Zambon, M., R. Lawrence, A. Bunn, and S. Powell. 2006. Effect of alternative splitting rules on image processing using classification tree analysis. Photogrammetric Engineering and Remote Sensing, 72(1): 25–30.

Fire Severity Model Accuracy Using Short-term, Rapid Assessment Versus Long-term, Anniversary Date Assessment

Keith T. Weber, GISP, Idaho State University, GIS Training and Research Center, 921 S. 8th Ave., Stop 8104, Pocatello, Idaho 83209-8104 (webekeit@isu.edu)

Steven Seefeldt, Research Agronomist, USDA-ARS, SubArctic Agricultural Research Unit, University of Alaska Fairbanks, Fairbanks, Alaska 99775

Corey Moffet, Research Rangeland Scientist, USDA-ARS, U.S. Sheep Experiment Station, Dubois, Idaho 83423

ABSTRACT

Fires are common in rangelands and after a century of suppression, the potential exists for fires to burn with high intensity and severity. In addition, the ability of fires to affect long-term changes in rangelands is considerable and for this reason, assessing fire severity after a burn is critical. Such assessments are typically carried out following Burned Area Emergency Response team or similar protocols. These data are then used by land managers to plan remediation efforts and future land uses. To complement these procedures and explore fire severity modeling of sagebrush steppe rangelands, we compared fire severity models developed using 1) short-term post-fire imagery (i.e., imagery collected within 30 days of the fire) with 2) long-term post-fire imagery (i.e., imagery collected on or about the one year anniversary date of the fire). All models were developed using Classification Tree Analysis (CTA) and Satellite Pour l'Observation de la Terre 5 (SPOT 5) imagery as well as Shuttle Radar Topography Mission (SRTM) elevation data. The results indicate that while anniversary date imagery can be used to assess fire severity (overall accuracy ~90%) it is not as accurate as using short-term imagery (overall accuracy ~97%). Furthermore, using short-term imagery allows remediation strategies to be crafted and implemented shortly after the fire. Therefore, we suggest rangeland fire severity is best modeled using CTA with short-term imagery and field based fire severity observations. The analyses and techniques described in this paper provide land managers with tools to better justify their recommendations and decisions following fires in sagebrush steppe ecosystems.

KEYWORDS: classification tree, remote sensing, wildfire, GIS

INTRODUCTION

Fires are a common occurrence throughout the Intermountain West. While historic plant communities may be adapted to fire, the frequency and intensity of today's wildfires is different compared to what occurred in the past (DeBano et al., 1998; Thoren and Mattsson 2002). The change in frequency and intensity can be attributed to 1) fire suppression efforts that have inadvertently created fuel stockpiles (Pyne et al 1996) and 2) the conversion of sagebrush-grass communities to fire-promoting cheatgrass (*Bromus tectorum* L.) dominated communities (Brooks et al 2004). The consequences of these differences are manifest in various impacts on wildlife habitat, forage production, potential soil erosion (Pierson et al., 2001; Finley, 2006; Moffet et al., 2007), and rangeland health (Pyke et al., 2002). Assessing the effect of wildfires is important to land management agencies to minimize threats to life/property and prevent unacceptable degradation of natural and cultural resources (Sharon Paris, pers. comm.; Department of Interior 2004). However, due to the broad extent and distribution of wildfires in the Intermountain West the ability of land managers to closely evaluate each and every fire can be logistically difficult if not impossible. For these reasons, the application of remote sensing models that accurately and reliably classify fire severity may be useful (Lentile et al 2006).

Several image processing methods have been used to model fire severity (Garcia and Chuvieco, 2004) with most being designed around forested ecosystems (Turner et al., 1994; White et al., 1996; Patterson and Yool, 1998; Van Wagtendonk et al., 2004; Brewer et al., 2005; Epting et al., 2005). Prior to 1999, the most widely used fire severity modeling method was an NDVI-based technique to estimate biomass loss, and hence, fire severity (Salvador et al., 2000; Diaz-Delgado et al., 2003; Flasse et al., 2004). In 1999, the normalized burn ratio (NBR) technique was developed and has been widely applied and accepted (Key and Benson 1999; Salvador et al., 2000; Key and Benson, 2006).

Another form of the NBR model is known as a differenced NBR (dNBR). It estimates fire severity by comparing a pre-burn NBR model to that of a post-burn NBR model. The result is a model where the magnitude of change has been normalized by pre-burn landscape characteristics (Key and Benson 1999; Key and Benson, 2004; Van Wagtendonk et al., 2004; Cocke et al., 2005). Yet another fire severity modeling approach that has worked well within forested ecosystems relies upon long-term imagery or anniversary date imagery to fully assess the severity of the fire. This approach is based upon the concept that tree mortality is not always evident immediately after a fire and that total tree mortality (including indirect mortality [where a tree is made susceptible to insect infestation and/or disease due to the fire]) may be best determined by examining the fire area a full growing season after the fire (Fraser and Li 2002).

Recent fire severity studies reported by Finley (2006) and Norton (2006) suggest the fire severity modeling techniques developed for forested ecosystems are not well-suited to sagebrush-steppe ecosystems, and research by (Weber et al. 2008) has demonstrated the application of classification tree analysis (CTA) for fire severity modeling of rangelands with favorable results. CTA is a non-probabilistic, non-parametric statistical technique well-suited to modeling skewed, non-normal data and phenomena (Breiman et al. 1998; Friedl and Brodley 1997; Lawrence and Wright 2001; Miller and Franklin 2001). The CTA algorithms select useful spectral and ancillary data which optimally reduce divergence in a response variable (Lawrence and Wright 2001) such as fire severity observations. CTA uses machine-learning to perform these binary recursive splitting operations and ultimately yields a classification tree diagram that is used to produce a model of the response variable. Splitting algorithms common to CTA include entropy, gain ratio, and Gini. The entropy algorithm has a tendency to over-split and thereby creates an unnecessarily complex tree (Zambon, et al., 2006). The gain ratio algorithm addresses the over-splitting problem through a normalization process while the Gini algorithm attempts to partition the most homogeneous clusters first using a measure of impurity (McKay and Campbell 1982; Zambon et al., 2006).

The goal of this study was to compare a fire severity model derived using short term post-fire imagery versus one derived from long-term (anniversary date) post-fire imagery. Specifically we tested which model best described fire severity, defined as the amount of fuel (e.g., vegetation and litter) removed within the fire perimeter.

METHODS

Study Area

This study focuses upon a prescribed fire at the Hitching Post pasture at the U. S. Sheep Experiment Station (USSES) near Dubois, Idaho (Figure 1). The prescribed burn was begun September 14th and extinguished September 15th, 2005. The fire boundary encompassed 2.44 km^2 within the Hitching Post pasture (112° 7' W 44° 19' N), a 3.24 km^2 fenced parcel on the USSES that ranges in elevation from 1765 to 1800 m. Mean annual precipitation (1971 to 2000) at the Dubois Experiment Station (112° 12' W 44° 15'N, elevation, 1661 m) is 331 mm with 60% falling during April through September. Soils are mapped as complexes of Maremma (Fine-loamy, mixed, superactive, frigid Calcic Pachic Argixerolls), Pyrenees (Loamy-skeletal, mixed, superactive, frigid Typic Calcixerolls), and Akbash (Fine-loamy, mixed, superactive, frigid Calcic Pachic Argixerolls) soils on slopes less than 20 percent, but mostly 0 to 12 percent (NRCS 1995).

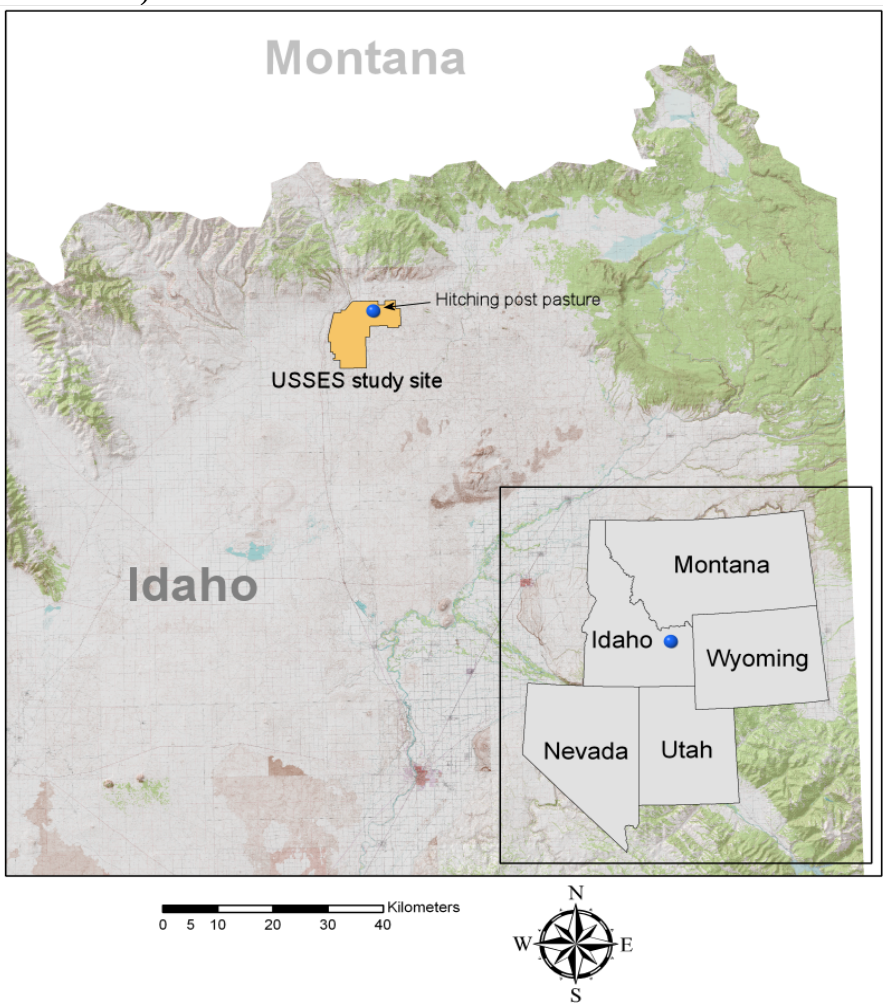

Figure 1. Location of the USDA ARS Sheep Experiment Station and site of the prescribed fire used in this study.

Vegetation on the study site is a sagebrush-grass community dominated by mountain big sagebrush (*Artemisa tridentata* ssp. *vaseyana* [Rydb.] Beetle) and threetip sagebrush (*A. tripartita* Rydb.). Subdominant shrub species include antelope bitterbrush (*Purshia tridentata* [Pursh] DC.), yellow rabbitbrush (*Chrysothamnus viscidiflorus* (Hook.) Nutt.), and spineless horsebrush (*Tetradymia canescens* DC.). There are a few small patches of the exotic forbs leafy spurge (*Euphorbia esula* L.) and spotted knapweed (*Centaurea stoebe* L. ssp. *micranthos* [Gugler] Hayek) and trace amounts (<1% of overall plant cover) of the exotic annual cheatgrass. Lupine (*Lupinus argenteus* Pursh) is the most plentiful forb on the study site and the graminoids present are thickspike wheatgrass (*Elymus lanceolatus* [Scribn. & J.G. Sm.] Gould ssp. *lanceolatus*), bluebunch wheatgrass (*Pseudoroegneria spicata* [Pursh] A. Löve ssp. *spicata*), and plains reedgrass (*Calamagrostis montanensis* Scribn. ex Vasey).

The management of this pasture for the past decade has been light, short duration, grazing with sheep and horses in spring and/or fall. There was no grazing in this pasture during the 2.5 years prior to the prescribed burn of September 14th and 15th, 2005.

Field Sampling

Beginning one week after the prescribed burn, 277 randomly selected sample areas (60 x 60 m) were visited to assess fire severity. The sample areas were located on the ground by navigating to the preselected area with a GPS receiver using real-time positioning. These positions were later post-process differentially corrected to achieve a horizontal positional accuracy of <1m (Serr et al. 2006). While subjective, a fire severity rating (0 = Unburned, no vegetation change; 1 = little vegetation/fuel burned; 2 = most of the vegetation was burned; and 3 = burned (all vegetation was considered completely burned) was assigned to each area visited following methods modified from the combined work of US Forest Service field methods (Bobbe et al., 2001), the US Park Service field methods (Switky 2003), and Key and Benson's (Key and Benson 1999; 2004) composite burn index (CBI). Groups one (n=13) and two (n=57) were later combined as the13 areas assigned to group one were insufficient for validation. Furthermore, some aspects of fire severity can be quantified but classification of general severity has proven difficult. Classification of burn or fire severity, based on post-fire appearances of litter and soil (Ryan and Noste 1983), are useful for placing severity into broadly defined, discrete classes, ranging from low to high. A general burn severity classification developed by Hungerford (1996) in forest situations relates burn severity to soil resource response and has three classes; low, moderate, and high. In rangeland ecosystems the medium and high severity classes described by Hungerford merge as there is not a large woody component and a deep duff layer, whose response to burning differentiates the classes. Therefore, we chose a simple classification of low or high severity and as a result, three classes remained, 0 (unburned), 1 (low fire severity), and 2 (high fire severity).

It was not an objective of this study to differentiate burned from unburned areas with remote sensing/image processing techniques and for this reason all unburned sample areas (n=9) were omitted from subsequent processing.

Image Processing

Post-fire Satellite Pour l'Observation de la Terre 5 (SPOT 5) imagery (10m x 10m pixels) was acquired for the USSES study site on September 28, 2005 (short term post-fire imagery) and September 27, 2006 (long term post-fire imagery). The imagery was georectified using 1 m National Agricultural Imagery Program orthophotography for the study area (RMSE = 3.48 and 4.71) using ArcGIS 9.1, corrected for atmospheric effects using Idrisi and projected into Idaho Transverse Mercator (NAD 83) using a first order affine transformation and nearest neighbor resampling.

Normalized difference vegetation index (NDVI), normalized burn ratio (NBR), and biomass estimates (Mirik et al., 2005) were calculated within Idrisi Kilimanjaro using SPOT reflectance data. The biomass layer is a simple ratio-type vegetation index where reflectance values from the short-wave infrared region (band) are divided by reflectance values from the green band. While Mirik et al. (2005) demonstrated a strong empirical relationship ($R^2 = 0.87$) between this index and total rangeland biomass, the relationship of the biomass index and actual rangeland biomass was not performed as part of this study. The biomass index differs from the normalized difference infrared index (NDII [Hunt and Yilmaz 2007]) in that the biomass index is a simple ratio-type index as opposed to a normalized difference-type index and the biomass index does not make use of the infrared band as does NDII. Another related normalized difference-type index is the normalized difference water index (NDWI) which uses the ratio of the difference between the near infrared and thermal infrared bands divided by the sum of these same bands (Gu et al. 2007). Neither the NDII nor NDWI were used in this study (NDWI cannot be used with SPOT imagery as this sensor does not include a thermal infrared band). Topography layers were also assembled for use as ancillary data within the CTA process (Elumnoh and Shrestha 2000). Elevation data were acquired from the shuttle radar topography mission (SRTM) and resampled to 10m to match the spatial resolution of the SPOT 5 imagery. Slope and aspect models were derived from these elevation data using Idrisi Kilimanjaro.

Polygon shapefiles describing the fire perimeters were rasterized and used as a mask for all raster data. Field observations were similarly masked and only those points falling inside the fire perimeter were used in the CTA. This masking process was done to help facilitate classification by prudently applying ancillary knowledge to better inform the classifier. This process is a well accepted technique referred to as "cluster busting" (Jensen 1996; Hunter 2004). CTA was performed using the Gini splitting algorithm (Zambon et al., 2006) with five input images. The datasets contained near-infrared (NIR), NDVI, NBR, and biomass band-ratios, along with the slope layer. These layers were selected based upon performance results from previous work reported in Weber et al. 2008.

To absorb georegistration error within the SPOT imagery (RMSE=3.48 and 4.71) and ensure correct and representative pixels were included in the analysis, all sample areas were buffered by 5m (Weber 2006). The resulting layers were rasterized using ArcGIS 9.1 and subset into training and validation sites. As a result, a total of 385 training site pixels and 207 validation site pixels were created. The CTA was performed with Idrisi Kilimanjaro using these data.
The resulting fire severity models were compared using a full cross-classification/cross tabulation procedure in Idrisi. Cramer's V and the Kappa Index of Agreement were used to determine the level at which the models agreed with one another (Rosenfield and Fitzpatrick-Lins 1986; Cartensen 1987).

RESULTS AND DISCUSSION

The CTA model developed using short-term post-fire imagery (NIR, NDVI, NBR, biomass, and slope), correctly identified all 186 high fire severity validation areas (n = 186, user accuracy = 100%). Similarly, the CTA model developed using long-term post-fire imagery correctly identified 179 of the 186 high fire severity validation areas (user accuracy = 93%). However, user accuracy of the low fire severity area decreased from 66% using short-term imagery to 39% using long-term imagery (Tables 1 and 2, respectively). In addition, the Kappa index of agreement similarly declined from 0.78 to 0.44 respectively.

The confusion with the low fire severity class was most likely due to the regrowth of vegetation following the fire. Field observations made during the summer of 2006 (n = 233) recorded over 100 sample points with 16-25% cover of grasses. In addition, nearly 100 sample points were recorded having 6-15% shrub cover, the majority of which was rabbitbrush (*Chrysothamnus spp*.) that established following the fire. Yet another factor affecting ground cover at the USSES was the presence of a large

amount of forbs, primarily lupine. Ninety six of 233 sample points had forb cover estimates (i.e., lupine) between 16-25%.

Table 1. Classification tree analysis (CTA) results for fire severity modeling derived using short term post-fire raster layers.

	Known validation sites			
	Low fire severity	High fire severity	Total	User accuracy
Low fire severity	14	7	21	0.66
High fire severity	0	186	186	1.00
Total	14	193	207	
Producer's accuracy	0.93	0.97		0.97[a]

[a] Overall accuracy

Kappa index of agreement = 0.78

Table 2. Classification tree analysis (CTA) results for fire severity modeling derived using long term (anniversary date) post-fire raster layers.

	Known validation sites			
	Low fire severity	High fire severity	Total	User accuracy
Low fire severity	9	14	23	0.39
High fire severity	5	179	184	0.97
Total	14	193	207	
Producer's accuracy	0.64	0.93		0.91[a]

[a] Overall accuracy

Kappa index of agreement = 0.44

Cross-classification and cross-tabulation of these models showed 87.6% overall agreement due to the similarity in how these two models predicted high fire severity areas. This comparison further reinforced a disagreement regarding low fire severity areas. As mentioned above, a number of areas exhibited a relatively rapid re-growth of lupine which accounts for the change classification of high severity fire in the short-term model to a low severity fire in the long-term model. In contrast, a less well understood change in classification was also brought to attention through the cross-tabulation procedure; nearly 16 ha (6%) of the study area changed from low fire severity (in the short-term model) to high fire severity in the long-term model (Figure 2 and Table 3). Since field-based data corroborates the predictions of the short-term model better than the long-term model, one is left to speculate about what may have occurred in these areas during the year following the fire. Analysis of 2006 field data and photo points offer a few possible explanations: While the mean bare ground cover class recorded in all areas considered low fire severity in the short-term model was 16-25% (n=16), the mean shrub cover class in areas in agreement for low fire severity was 6-15% while those areas in disagreement for low fire severity had a mean shrub cover of 1-5%. This may indicate that some of the areas within the perimeter of the fire recovered more slowly (which could be as much attributable to environmental factors as to the severity of the fire) it must be remembered that this speculation is based upon only 16 field observations. Further post-fire sampling should be conducted to monitor the recovery of these areas and determine if any real differences truly exist.

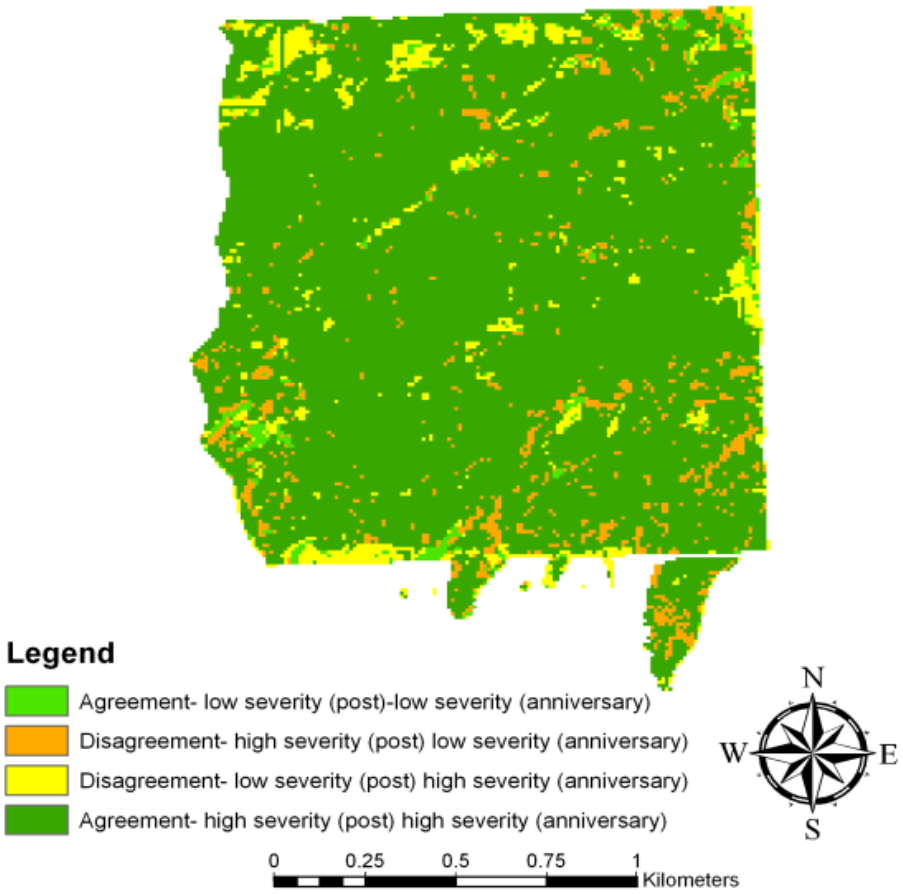

Figure 2. Cross-tabulation between short-term (post-fire imagery) and long-term (anniversary date imagery) fire severity models.

Table 3. Cell-by-cell cross-tabulation comparison of fire severity models produced using short-term (post fire) imagery (columns) and long-term (anniversary date) imagery (rows). Percent of pixels in each category are given in parenthesis.

		Short-term (post-fire) imagery		
		Low fire severity	High fire severity	Total
Long-term (anniversary date) imagery	Low fire severity	432 (2%)	1452 (6%)	1884 (8%)
	High fire severity	1580 (6%)	20941 (86%)	22521 (92%)
	Total	2012 (8%)	22393 (92%)	24405 (100%)

Based on the comparison of accuracies and overall agreement between the two models it seems clear that performing a fire severity assessment one year after a fire in sagebrush steppe rangelands yields little benefit for the land manager. In both cases, most high fire severity areas remain clearly distinguishable (further corroborating the accuracy of the short-term fire severity model) even one year post-fire, but the benefit of having an accurate fire severity model to plan remediation efforts shortly after a fire offers numerous distinct advantages for land managers such as starting remediation before winter and developing plans and collecting resources in the winter for early spring restoration activities.

Assessment of error and bias

Models developed using CTA were able to classify high fire severity areas with good user accuracy (~100%) (cf. Figure 3 for a step-by-step approach and cartographic model of this technique). However, achieving satisfactory results appears to be a function of adequate sample size for each class considered (low fire severity or high fire severity). Initially, it may appear that a disproportionately large number of validation sites were used in high fire severity areas (n=193, 92%; Tables 1 and 2). However, as fire severity is primarily a function of the fire's behavior --which is closely tied to factors such as the amount and type of fuels and the weather during the fire (Pyne et al. 1996) -- the proportion of high fire severity sites (used for both modeling and validation) agreed well with field observations where 92% of the study area was recorded as high severity (Figure 4). Indeed when the proportions of the random sampling locations were compared with proportions of fire severity areas, the results appear equitably distributed.

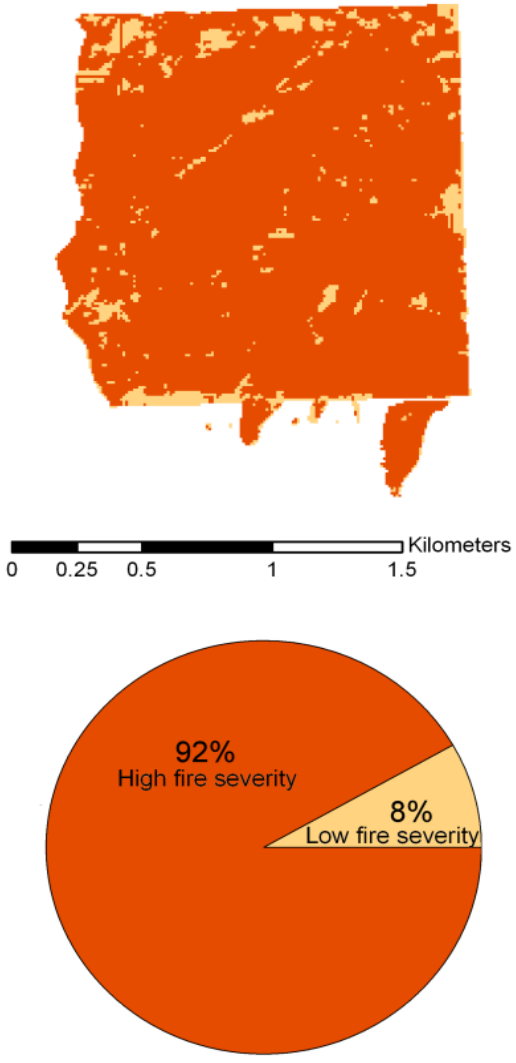

Figure 3. Relative proportions of fire severity.

Management Implications

Land managers who are tasked with assessing fire severity in rangelands and developing remediation plans within a short time of fire control cannot rely on field inspection to provide adequate coverage, especially on large fires. The use of easily obtained SPOT 5 satellite imagery, soon after the fire,

combined with a moderate amount of field sampling will result in an accurate delineation of high severity burn areas where remediation efforts will need to be focused. The cost of obtaining the imagery will be recouped by the savings from reduced field time and the speed with which remediation plans of improved quality and accuracy can be developed.

CONCLUSIONS

Post-fire vegetation management in western rangelands should be based on pre-fire vegetation, post-fire weather conditions, soils, available resources (such as seeds, equipment, and personnel), and fire severity. Given the size and distribution of western fires, land managers face an almost impossible task in trying to determine fire severity within a time frame useful for the preparation of remediation plans. The development of GIS layers that combine vegetation information, climate, soils, and fire severity could ease the task of creating predictive models for more effective remediation plan development. The results of this research addresses mapping of fire severity, which can be used as one layer within a GIS-based remediation and decision support model. Using easily obtained post-fire SPOT 5 imagery, high severity burn areas can be accurately, rapidly, and inexpensively delineated; resulting in a GIS layer useful for remediation plan development.

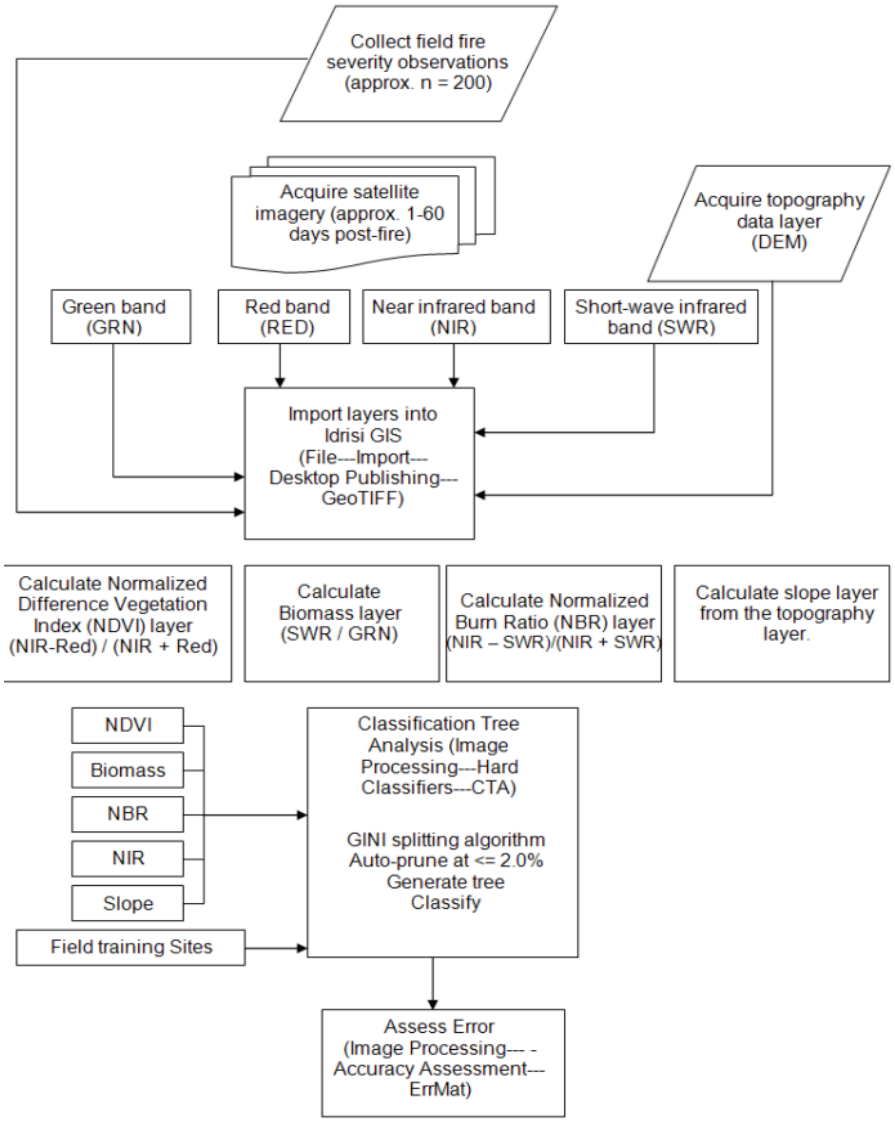

Figure 4. Cartographic model of the process followed to produce a fire severity model using classification tree analysis at the USSES study site.

ACKNOWLEDGEMENTS
We would like to acknowledge the Idaho Delegation for their assistance in obtaining the grant that supported this work funded through the National Aeronautic and Space Administration (NASA NNG05GB05G). In addition we would like to acknowledge the assistance of Jill Norton, Jamen Underwood, and Penny Gneiting for their field data collection efforts and research in rangeland fire severity modeling, the statistical consultation of Teri Peterson, and the assistance of Sharon Paris.

LITERATURE CITED

Anderson, H.E. 1982. Aids to Determining Fuel Models for Estimating Fire Behavior, USDA Forest Service General Technical Report INT-122.

Bobbe, T., M. V. Finco, B. Quayle, B., and K. Lannon. 2001. Field measurements for the training and validation of burn severity maps from spaceborne, remotely sensed imagery. Remote Sensing Applications Center, Salt Lake City, Utah: USDA Forest Service, Final Project Report, Joint Fire Science Program-2001-2. Project # 01B-2-1-01, pp. 15 URL: http://www.fs.fed.us/eng/rsac/baer/final_report_01B-2-1-01.pdf Visted April 2007.

Breiman, L., Friedman, J. H., Olshen, R. A., and Stone C. J., 1998, Classification and Regression Trees. Chapman and Hall, CRC press, Boca Raton, Florida. 358 pp.

Brewer, C.K., J. C. Winne, R. L..Redmond, D. W. Opitz, and M. V. Mangrich. 2005. Classifying and mapping wildfire severity: A comparison of methods. Photogrammetric Engineering and Remote Sensing, 71:11, 1311-20.

Brooks M. L., C. M D'Antonio, D. M. Richardson, J. B. Grace, J. E Keeley, J. M. DiTomaso, R. J. Hobbs, M. Pellant, and D. Pyke. 2004. Effects of Alien Plants on Fire Regimes. Bioscience. 54(7):677-688.

Carstensen, L.W., 1987. A Measure of Similarity for Cellular Maps, In The American Cartographer, 14(4), 345-358.

Cocke, A.E., P. Z. Fule, and J. E. Crouse. 2005. Comparison of burn severity assessments using differenced normalized burn ratio and ground data. International Journal of Wildland Fire, 14: 189-98.

DeBano, L.F., Neary, D.G., and Pfolliott, P.F., 1998, Fire's Effects on Ecosystems: New York, John Wiley and Sons, 333 pp.

Department of the Interior (DOI). 2004. Departmental Manual, Part 620 Chapter 3, Burned Area Emergency Stabilization and Rehabilitation (620DM3), 16 pp.

Diaz-Delgado, R., F. Lloret, and X. Pons. 2003. Influence of fire severity on plant regeneration by means of remote sensing imagery. International Journal of Remote Sensing, 24:8, 1751-1763.

Epting, J., D. Verbyla, and B. Sorbel. 2005. Evaluation of remotely sensed indices for assessing burn severity in interior Alaska using Landsat TM and ETM+. Remote Sensing of Environment, 96, 328-339.

Elumnoh A. and R. P. Shrestha. 2000. Application of DEM Data to Landsat Image Classification: Evaluation in a Tropical Wet-Dry Landscape in Thailand. Photogrammetric Engineering and Remote Sensing. 66(3):297-304.

Flasse, S., S. Trigg, P. Ceccato, A. Perryman, A. Hudak, M. Thompson, B. Brockett, M. Dramé, T. Ntabeni, P. Frost, T. Landmann, and J. le Roux. 2004. Remote sensing of vegetation fires and its contribution to a fire management information system. In J.G. Goldammer and C. de Ronde (Eds.), *Wildfire Management Handbook for Sub-Sahara Africa* (pp.158-211). The Hague, Netherlands: SPB Publishing.

Floyd, D. and J. Anderson. 1982. A New Point Frame for Estimating Cover of Vegetation. Vegetation 50: 185-186.

Floyd, D. and J. Anderson. 1987. A Comparison of Three Methods for Estimating Plant Cover. Journal of Ecology 75: 221-228.

Finley, C. D. 2006. Field evaluation and hyperspectral imagery analysis of fire-induced water repellent soils and burn severity in southern Idaho rangelands. Idaho State University. URL: http://giscenter.isu.edu/Research/techpg/nasa_tlcc/to_pdf/cfthesis.pdf visited April 2007. 237pp.

Fraser, R. H. and Z. Li. 2002. Estimating fire related parameters in boreal forest using SPOT vegetation. Remote Sensing of Environment, 82: 95-110.

Friedl, M. A. and Brodley, C. E., 1997, Decision tree classification of land cover from remotely sensed data. Remote sensing of environment. 61(3):399-409.

Garcia, M. and E. Chuvieco. 2004. Assessment of the potential of SAC-C/MMRS imagery for mapping burned areas in Spain. Remote Sensing of Environment, 92, 414-423.

Inouye, R. 2002. Sampling Effort and Vegetative Cover Estimates in Sagebrush Steppe. *Western North American Naturalist* 62(3): 360-364.

Key, C.H. and N. C. Benson. 1999. The Normalized Burn Ratio (NBR): A Landsat TM Radiometric Index of Burn Severity. URL: http://www.nrmsc.usgs.gov/research/ndbr.htm; visited April 2007.

Key, C.H. and N. C. Benson. 2004. Remote Sensing Measure of Severity: The Normalized Burn Ratio. FIREMON Landscape Assessment (LA) V4 Sampling and Analysis Methods. pp. LA1-16.

Key, C.H. and N. C. Benson. 2006. Landscape Assessment (LA) Sampling and Analysis Methods. USDA Forest Service Gen. Tech. Rep. RMRS-GTR-164-CD. pp. 55.

Lawrence, R. L. and A. Wright. 2001. Rule-based Classification Systems Using Classification and Regression Tree (CART) Analysis. Photogrammetric Engineering and Remote Sensing. 67(10):1137-1142.

Lentile, L. B., Z. A Holden, A. M. S. Smith, M. J. Falkowski, A. T. Hudak, P. Morgan, S. A. Lewis, P. E. Gessler, and N. C. Benson. 2006. Remote Sensing Techniques to Assess Active Fire Characteristics and Post-Fire Effects. Intl. Journal of Wildland Fire. 15(3):319-345.

Lillesand T. M. and R. W. Kiefer. 2000. Remote Sensing and Image Interpretation. 4th Ed. John Wiley and Sons, New York, NY. 724pp.

McKay, R.J. and Campbell, N.A. 1982. Variable selection techniques in discriminant analysis II: Allocation, British Journal of Mathematical and Statistical Psychology, 35, 30-41.

McMahan, J. B., D. Narsavage, and K. T. Weber. 2003. The "Pole-Cam": Corroborating Field Estimations with High-Resolution Imagery. Pages 18-23 in K. T. Weber (Ed.), Final Report: Wildfire Effects on Rangeland Ecosystems and Livestock Grazing in Idaho. 209pp.

Miller, J. and J. Franklin, 2001. Modeling the distribution of four vegetation alliances using generalized linear models and classification trees with spatial dependence. Ecological Modeling, 157: 227–247.

Mirik, M., J. E. Norland, R. L. Crabtree, and M. E. Biondini. 2005. Hyperspectral One-Meter-Resolution Remote Sensing in Yellowstone National Park, Wyoming: II Biomass. Rangeland Ecology and Management. 58(5):459-465.

Moffet, C.A., F.B. Pierson, P.R. Robichaud, K.E. Spaeth, and S.P. Hardegree. 2007. Modeling soil erosion on steep sagebrush rangeland before and after prescribed fire. Catena, 71:218-228.

National Climatic Data Center (NCDC). 2004. CLIM20: Climatography of the United States No. 20 1971-2000. http://cdo.ncdc.noaa.gov/climatenormals/clim20/id/102707.pdf (accessed online September 11, 2007).

Natural Resources Conservation Service (NRCS). 1995. Soil investigation of Agriculture Research Service, United States Sheep Experiment Station headquarters range, US Department of Agriculture. Rexburg, ID: NRCS. 133pp.

Natural Resources Conservation Service (NRCS). 2006. Land Resource Regions and Major Land Resource Areas of the United States, the Caribbean, and the Pacific Basin. United States Department of Agriculture Handbook, 296 pp.

Norton, J. 2006. The Use of Remote Sensing Indices to Determine Wildland Burn Severity in Semiarid Sagebrush Steppe Rangelands Using Landsat ETM+ and SPOT 5. Idaho State University. URL: http://giscenter.isu.edu/Research/techpg/nasa_tlcc/to_pdf/jnthesis.pdf visited April 2007. 111pp.

Patterson, M.W. and S. R. Yool. 1998. Mapping fire-induced vegetation mortality using Landsat Thematic Mapper data: A comparison of linear transformation techniques. Remote Sensing of Environment, 65, 132-42.

Pierson, F.B., P.R. Robichaud, and K.E. Spaeth. 2001, Spatial and temporal effects of wildfire on the hydrology of a steep rangeland watershed. Hydrological Processes, 15:2905-2916.

Pyke D. A., J. E. Herrick, P. Shaver, and M. Pellant. 2002. Rangeland health attributes and indicators for qualitative assessment. Journal of Range Management 55:584-597.

Pyne, S. J., P. L. Andrews, and R. D. Laven. 1996. Introduction to Wildland Fire. John Wiley and Sons, New York. 769 pp.

Richards, J.A., 1993. Remote Sensing Digital Image Analysis, Springer-Verlag, New York, NY. 363 pp.

Rosenfield, G.H., and K. Fitzpatrick-Lins, 1986. A Coefficient of Agreement as a Measure of Thematic Classification Accuracy, In Photogrammetric Engineering and Remote Sensing, 52(2), 223-227

Salvador, R., J. Valeriano, X. Pons, and R. Diaz-Delgado. 2000. A semi-automatic methodology to detect fire scars in shrubs and evergreen forests with Landsat MSS time series. International Journal of Remote Sensing, 21, 655-71.

Sander, L. and K. T. Weber 2006. Range Vegetation Assessment in the Big Desert, Upper Snake River Plain, Idaho. Pages 85-90 in K. T. Weber (Ed), Final Report: Detection, Prediction, Impact, and Management of Invasive Plants Using GIS. 196pp.
URL visited: http://giscenter.isu.edu/research/techpg/nasa_weeds/pdf/field_report.pdf 27-Jun-2007.

Seefeldt, S.S. 2005. Consequences of selecting rambouilllet ewes for mountain big sagebrush (Artemisia tridentata ssp. vaseyana) dietary preference. Rangeland Ecology and Management, 58: 380-384.

Seefeldt, S.S. and W. Laycock. 2006. The United States Sheep Experiment Station: Shedding light on rangeland ecosystems. Rangelands 28(2):30-35.

Serr, K., Windholz, T. K., and Weber K. T. (2006). Comparing GPS Receivers: A Field Study. URISA Journal. 18(2):19-24.

Switky, K.R. 2003. Fire monitoring handbook: Boise, ID, 274 pp., NPS Fire management program center, National Interagency Fire Center, 274pp.

Thoren, F.and D. Mattsson. 2002. Historic Wildfire Research in Southeastern Idaho. URL: http://giscenter.isu.edu/research/techpg/blm_fire/historic/wildfire_report.pdf visited April 2007. 16pp.

Turner, M.G., W. W. Hargrove, R. H. Gardner, and W. H. Romme. 1994. Effects of fire on landscape heterogeneity in Yellowstone National Park, Wyoming. Journal of Vegetation Science, 5, 731-42.

Van Wagtendonk, J.W., R. R. Root, and C. H. Key. 2004. Comparison of AVIRIS and Landsat ETM+ detection capabilities for burn severity. Remote Sensing of Environment, 92: 397–408.

Weber, K. T. 2006. Challenges of Integrating Geospatial Technologies Into Rangeland Research and Management. Rangeland Ecology and Management. 59(1):38-43.

Weber, K. T., S. S. Seefeldt, J. Norton, and C. Finley. 2008. Fire Severity Modeling of Sagebrush-steppe Rangelands in Southeastern Idaho. GIScience and Remote Sensing. 45(1):68-82.

West, N.E. and J. A. Young. 2000. Intermountain Valleys and Lower Mountain Slopes. In M.G. Barbour and W.D. Billings (Ed.), North American Terrestrial Vegetation (pp. 255-284). Cambridge, UK: Cambridge University Press.

White, J.D., K. C. Ryan, C. H. Key, and S. W. Running. 1996. Remote sensing of forest fire severity and vegetation recovery. International Journal of Wildland Fire, 6, 125-36.

Wright, H. E. and A. W. Bailey. 2004. Fire Ecology: United States and Southern Canada. Wiley Interscience. 528pp.

Zambon, M., R. Lawrence, A. Bunn, and S. Powell. 2006. Effect of alternative splitting rules on image processing using classification tree analysis. Photogrammetric Engineering and Remote Sensing, 72(1): 25–30.

[THIS PAGE LEFT BLANK INTENTIONALLY]

Post-fire Recovery of Sagebrush Communities: Assessment using SPOT5 and Very Large-Scale Aerial Imagery

Temuulen Tsagaan Sankey, GIS Training and Research Center, Idaho State University, 921 South 8th Avenue, Stop 8104, Pocatello, ID 83209 (sankteki@isu.edu)

Corey Moffet, Research Rangeland Scientist, USDA-ARS, U.S. Sheep Experiment Station, Dubois, Idaho 83423

Keith T. Weber, GISP, Idaho State University, GIS Training and Research Center, 921 S. 8th Ave., Stop 8104, Pocatello, Idaho 83209-8104 (webekeit@isu.edu)

ABSTRACT

Much interest lies in the long-term recovery rates of sagebrush communities after fire in the western USA as sagebrush communities comprise millions of hectares of rangelands and important wildlife habitat. Little is known about post-fire changes in sagebrush canopy cover over time, especially at a landscape scale. We studied post-fire recovery of shrub canopy cover in sagebrush-steppe communities using spectral mixture analysis. Our study included 16 different fires that burned between 1937-2005 and one unburned site at the U.S. Sheep Experiment Station in eastern Idaho. Spectral mixture analysis was used with September 2006 SPOT5 satellite imagery to estimate percent shrub canopy cover within pixels, an approach that has not been commonly used in sagebrush studies. Very large-scale aerial (VLSA) imagery with 2-cm resolution was used for training and validation. SPOT5 imagery classification was successful and the spectral mixture analysis estimates of percent shrub canopy cover were highly correlated with the shrub canopy cover estimates in the VLSA imagery (R^2= 0.91; p<0.0001). This successful application of spectral mixture analysis has important implications for the monitoring and assessment of sagebrush-steppe communities. Using the percent shrub canopy cover estimates from the classified SPOT5 imagery, we examined shrub canopy recovery rates since different burn years. Using piecewise regression, it was determined that shrub cover in mountain big sagebrush (*Artemisia tridentata* Nutt. ssp. *vaseyana* [Rydb.] Beetle) communities was recovered in 27 years after fire. The recovered shrub cover was 38.6 %. These results are consistent with other field-based studies in mountain big sagebrush communities.

KEYWORDS: Remote sensing, rangelands, photogrammetry

INTRODUCTION

Sagebrush (*Artemisia* spp) communities constitute the largest temperate semi-desert in North America (Anderson and Inouye 2001) and approximately 60 million hectares of rangelands in the western US (Watts and Wambolt 1996). In the Great Basin, sagebrush-steppe occupies approximately 450,000 km^2 area of the Columbia and Snake River Plateaus and provide important habitat for many wildlife species such as sage grouse (Anderson and Inouye 2001). Hundreds of thousands of acres were burned in the Great Basin (Blaisdell and Mueggler 1956) over the latter half of the last century to eradicate sagebrush (Wambolt et al 2001). More recently, the sagebrush-steppe management objectives and values changed and land managers are now concerned about post-fire recovery of sagebrush communities. Meanwhile, fire was suppressed in other areas of the Great Basin and land managers now use prescribed fire as a tool to restore sagebrush communities (Wambolt et al 2001). In both cases, much interest lies in the long-term recovery rates of sagebrush communities after fire. However, little is known about post-fire changes in sagebrush canopy cover over time (Lesica et al 2007), especially at a landscape scale.

Wildfires might have had much larger effects on pre-settlement sagebrush communities than other biotic and abiotic factors (Lesica et al 2007). Post-fire sagebrush recovery has been used as an indicator of pre-settlement fire frequency and to estimate natural fire rotation in sagebrush communities (Baker 2006). Pre-settlement fire return interval varied in sagebrush communities between 12-25 years on more mesic sites and 200 years on more xeric sites (Crawford et al 2004). Pre-settlement fire return intervals were estimated to be 12-25 years for mountain big sagebrush (*Artemisia tridentata* Nutt. ssp. *vaseyana* [Rydb.] Beetle) communities, 30-100 years for Wyoming sagebrush (*Artemisia tridentata* spp. *wyomingensis* Rydb.) communities, and 100-200 years for low sagebrush (*Artemisia arbuscula* Nutt.) communities (Crawford et al 2004). Post-settlement fire regime in sagebrush steppe has been spatially variable, but largely resulted in two common patterns: 1) fire suppression followed by increased shrub cover and tree encroachment by juniper and pinyon species, and 2) annual grass invasion by species such as cheatgrass (*Bromus tectorum*) leading to increased fire frequency (Crawford et al 2004) and a fire-grass feedback loop (Baker 2006). Post-fire sagebrush canopy recovery has been inconsistent among sites and the estimated length of time for recovery has varied greatly among different studies. The documented estimate of time required for canopy cover recovery spans a broad range between 35-100 years for mountain big sagebrush and 50-120 years for Wyoming big sagebrush (Baker 2006). This is partly because post-fire sagebrush recovery can be highly variable in space (Crawford et al 2004) and among species (Lesica et al 2007). Post-fire sagebrush establishment may also be dependent on distance to seed source, availability of viable seed reservoir, availability of moisture, and post-fire weather conditions (Crawford et al 2004). Recovery can also depend upon fire intensity and post-fire land use treatment such as grazing (Baker 2006).

Most sagebrush studies have been based on field measurements and ground observations. Remote sensing and image analysis techniques have not been commonly used. Previous remote sensing-based studies have used AVIRIS data (Kokaly et al 2003) and NOAA/AVHRR data (Kremer and Running 1993) for thematic classification (i.e., a single cover type is assigned to each pixel), and LiDAR data to determine sagebrush presence/absence and height within pixels (Streutker and Glenn 2006). An important research question is whether sagebrush canopy cover can be estimated within pixels using moderate-resolution satellite imagery such as SPOT5. Pixels in SPOT5 imagery are 100 m^2 (10 m x 10 m) in size and thus frequently have a mix of bare ground, herbaceous plants, and shrub in sagebrush-steppe communities. This mix of cover types within pixels poses a fundamental challenge in classifying pixels, since the spectral characteristics of the mixed pixels do not represent any single land cover type (Lillesand and Kiefer 2000). Spectral mixture analysis techniques have been developed to allow estimates of how much of a pixel is comprised by different land cover types (Adams et al 1986; Small 2004; Xiao and Moody 2005). Spectral mixture analysis is most suited when there are a limited number of land cover types and when the spectral properties of these cover types can be assumed to be relatively constant. Spectral mixture analysis characterizes the spectral signatures as a mix of land cover types in each pixel rather than assigning a single land cover type to

each pixel. Each land cover type within the mix is known as a separate "endmember" (Rencz 1999). Once "pure" endmembers (i.e., pure pixels of each cover type) are determined within imagery, endmember fractions or abundance of each cover type within each pixel can be estimated as a mixture (Rencz 1999). A mixture represents a linear combination of the endmembers, weighted by the areal coverage of each endmember in a pixel (Adams et al 1986). The result is an estimate of how much of a given pixel is comprised of different cover types.

We studied sagebrush-steppe communities and their post-fire canopy recovery across the U.S. Sheep Experiment Station's (USSES) Headquarter property in eastern Idaho using SPOT5 satellite imagery and spectral mixture analysis, an approach that has not been used to our knowledge in sagebrush studies. Our objectives were to: 1) determine if spectral unmixing techniques could be used with SPOT5 imagery to estimate percent shrub cover within pixels, and 2) describe post-fire shrub canopy recovery over time using the canopy cover estimates from the classified SPOT5 imagery. We studied 16 fires that burned in different years between 1937-2005 and one site that has not been burned since before 1936 (Table 1). We chose SPOT5 imagery from September 27, 2006. In the sagebrush-steppe of eastern Idaho, grass and forb growth is completed by the beginning of July (Seefeldt and Booth 2006) and herbaceous species are senescent by September. Sagebrush species, however, still actively photosynthesize in September (Billings and Morris 1951; DePuit and Caldwell 1973) and show a second peak in greenness (Kremer and Running 1993) due to overwintering-leaf growth after the ephemeral-leaf drop at the end of the growing season (Bilbrough and Richards 1993). We expected this difference in phenology to allow more prominent spectral discrimination of the shrubs in September, although some shrubs in arid and semi-arid environments have been thought to be spectrally indeterminate from other plant cover types during the growing season (Okin et al 2001).

Table 1. Description of the 16 fires studied.

Burn years	Years since last burn as of 2006	Burn season	Type of fire
0	>70		No fire
1937	69	Unknown	Prescribed
1938	68	Unknown	Unknown
1939	67	Unknown	Unknown
1947	59	Unknown	Prescribed
1974	32	Unknown	Wild
1977	29	Spring	Prescribed
1979	27	Summer	Prescribed
1981	25	Summer	Wild
1990	16	Spring	Prescribed
1993	13	Unknown	Prescribed
1995	11	Fall	Prescribed
1998	8	Fall	Prescribed
1999	7	Fall	Prescribed
2002	4	Fall	Prescribed
2003	3	Fall	Prescribed
2005	1	Summer	Prescribed

METHODS

Study Site Description

The study site is the northwest portion of the USSES headquarters (44º14'44"N, 112º12'47"E) rangeland which has been used for spring and fall grazing by the USSES for more than 70 years. The area is dominated by mountain big sagebrush (*Artemisia tridentata* Nutt. ssp. *vaseyana* [Rydb.] Beetle) with subdominant shrubs of antelope bitterbrush (*Purshia tridentata* [Pursh] DC.), spineless horsebrush (*Tetradymia canescens* DC.), and yellow rabbitbrush (*Chrysothamnus viscidiflorus* [Hook.] Nutt.). The understory is cool season grasses and forbs including bluebunch wheatgrass

(*Pseudoroegneria spicata* [Pursh] A. Löve), Sandberg bluegrass (*Poa secunda* J. Presl), and arrowleaf balsamroot (*Balsamorhiza sagittata* [Pursh] Nutt.). Mean annual precipitation at the nearest weather station is 326 mm. The soils are a complex of sandy loam aeolian deposits of varying depth over lava flows.

Portions of the headquarters property have been subjected to prescribed burning for research since 1936 and these prescribed fires as well as wildfires on the property have been documented. The fire boundaries have been digitized and made available for use in Geographic Information System (GIS) software. We selected 16 different fires (Figure 1) that burned between 1937-2005 (Table 1). We also included one site for which there is neither evidence nor record of fire since the establishment of the USSES and where minimum fire effects were expected.

Imagery and Shrub Classification

SPOT5 images have four spectral bands, centered at 0.55 µm (green), 0.65 µm (red), 0.85 µm (near infrared), and 1.67 µm (middle infrared), and have a spatial resolution of 10 m. The SPOT5 imagery we used was acquired on September 27, 2006, georectified, and corrected for atmospheric effects using Idrisi's ATMOSC module. A subset of this image was used for this project. A set of four very large-scale aerial (VLSA) images were used for training and an independent set of eleven VLSA images were used for validation. The VLSA images were acquired on June 16 and 17, 2006. All VLSA images had 2-cm resolution and each VLSA image was approximately 100 m x 70 m in dimension (approximately 70 SPOT5 pixels). The SPOT5 image subset and VLSA images were both projected in Idaho Transverse Mercator, NAD 83 projection and datum. The VLSA imagery were all co-registered to the SPOT5 imagery (root mean squared errors <1m).

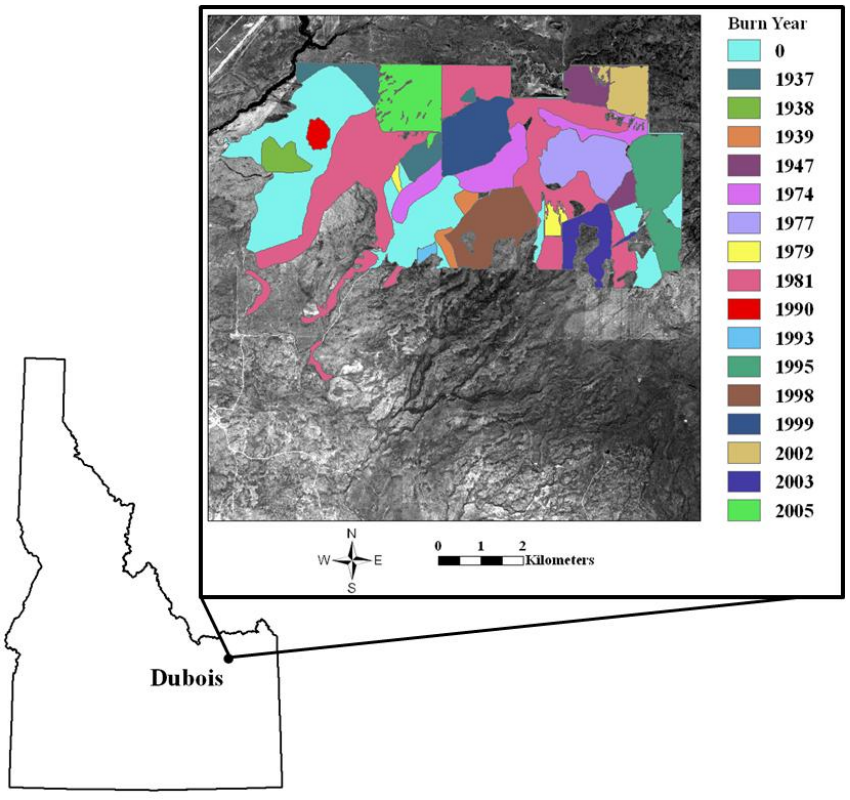

Figure 1. The study site in Idaho showing polygons of mountain big sagebrush ecological sites with fire history defined.

The Matched Filtering Spectral Unmixing technique was used to classify shrubs in the SPOT5 imagery (ENVI Version 4.3, ITT Industries Inc, 2006, Boulder, CO). The Matched Filtering Spectral

Unmixing approach detects a user-defined target cover type in the imagery, while suppressing the spectral signatures of other cover types. Classification training requires identification of pure pixels of the cover class of interest as well as pure pixels that do not have the cover class of interest (i.e., pixels of other cover types). In our case, the target cover type of interest was shrubs, while the other cover types to be suppressed were bare ground and herbaceous cover. Using the four VLSA images, we selected in the SPOT5 imagery 32 pure shrub pixels (shrub endmember) and 30 other pure pixels that clearly had no shrubs (no-shrub endmember), but bare ground and herbaceous cover. A spectral unmixing model was then developed for the SPOT5 image subset to estimate shrub endmember fractions or percent cover of shrubs within each pixel. If constrained to 1, spectral unmixing results produce values ranging 0-1, where 0 indicates 0 percent shrub canopy cover and 1 indicates 100 percent. However, values <0 and >1 are possible when Matched Filtering spectral unmixing technique is used with no constraints. Values <0 and >1 were replaced with 0 and 1, respectively, in our classification model. The accuracy of the resulting classification model was assessed using a linear regression model (Figure 2) and 71 random SPOT5 pixels and 71 windows, 10 m x 10 m in size, placed at the corresponding locations in the eleven VLSA images set aside for validation. The 71 pixel locations were randomly selected using Hawth's tool in ArcMap 9.1. At each random pixel location, an ocular estimate of percent shrub canopy cover was made in the 10 m x 10 m windows placed over the VLSA images. The spectral unmixing model estimates of percent shrub canopy cover within the 71 SPOT5 pixels were extracted from the classified SPOT5 imagery. The two sets of estimates were then correlated in a linear regression model for accuracy assessment.

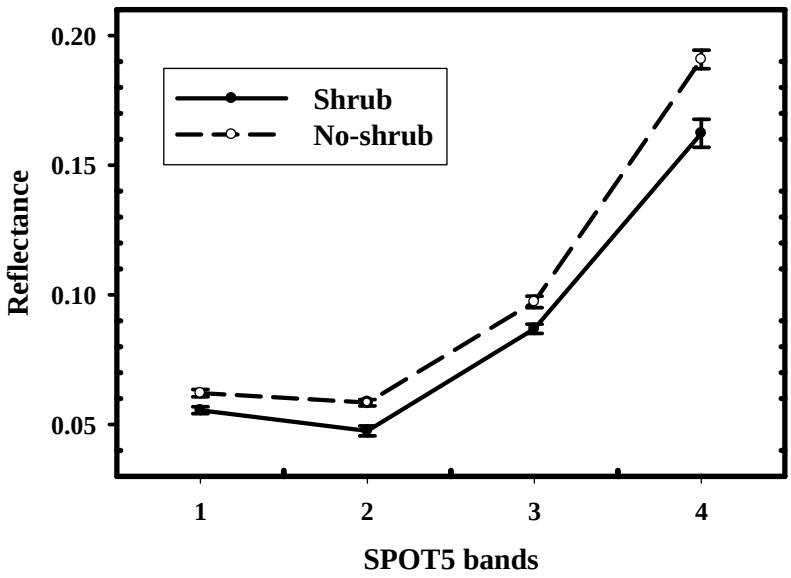

Figure 2. Mean spectral reflectance (+/-1SE) of pure pixels of shrub (n=32) and no-shrub (n=30) endmembers in SPOT5 imagery band 1 (Green), band 2 (Red), band 3 (Near Infrared), and band 4 (Middle Infrared).

Statistical Analysis

The selected 16 fires and one unburned site were represented by 17 sets of polygons. We overlaid the polygons on the classified SPOT5 imagery and generated 100 random points within each polygon to extract the shrub cover estimates from the corresponding 100 pixels in the classified SPOT5 image. The mean of these 100 random pixels were used in the analysis. We used two regression approaches to describe how shrub canopy cover changes with number of years since last burn. The first approach was to model the data with a polynomial regression and the 2nd approach was to model the data with a continuous piecewise regression. For the polynomial regression, we considered linear, quadratic, and cubic terms and selected the lowest order model for which a significant improvement was made by adding the term. The continuous piecewise regression modeled two post-fire phases as follows:

$$\hat{Y} = b_0 + b_1 X_1 + b_2 (X_1 - R) X_2 \quad \textbf{[1]}$$

where $\hat{Y}$ is the predicted shrub canopy cover, X_1 is the number of years since last burn, R is the post-burn year which separates the two phases, X_2 is 1 if $X_1 > R$ and 0 otherwise, b_0 is the predicted shrub cover in the year of a burn, b_1 is the predicted annual increase in shrub cover in phase 1 (recovery), and ($b_1 + b_2$) is the predicted annual increase in shrub cover during phase 2 (recovered). For the piecewise regression, all possible breakpoints (R) were considered and the breakpoint that resulted in a model that fit the data best was selected. The metric used to select the breakpoint for the best piecewise model was the Akaike Information Criterion (AIC) (Akaike 1974). Regardless of the regression approach, we evaluated the normality assumption with the Shapiro-Wilk test on the model residuals and in all cases the data did not warrant rejecting the hypothesis that errors were normally distributed.

RESULTS

Performance of Shrub Classification Model

The spectral reflectance of SPOT5 imagery pixels having shrubs was distinct from pixels that had no shrubs (Figure 2). In all four bands of SPOT5 imagery, the spectral reflectance of pixels having no shrubs was greater than that of pixels having shrubs. The SPOT5 spectral unmixing model performed well when validated using the VLSA image estimates of shrub canopy cover (adjusted $R^2 = 0.91$; $p < 0.0001$; mean error = 0.006 ($\pm$0.10SD) (Figure 3).

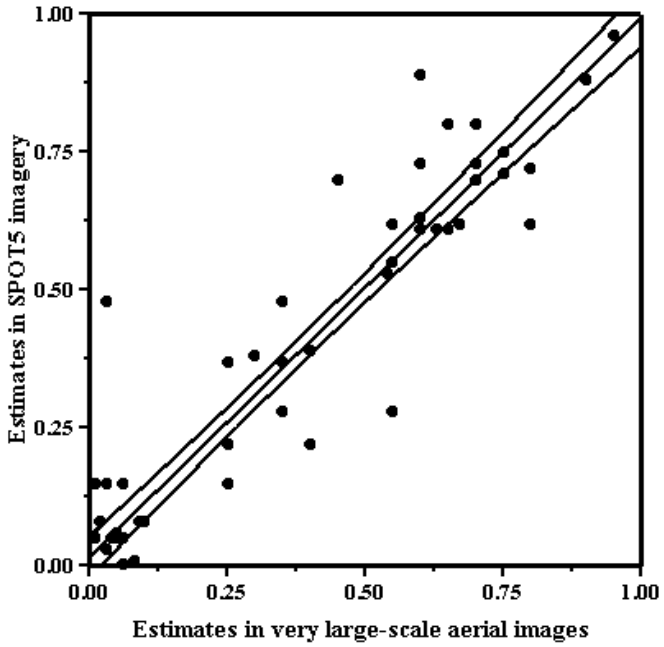

Figure 3. Linear regression of percent shrub cover estimates in SPOT5 and very large-scale aerial images with 95% confidence interval (mean error = 0.006 ($\pm$0.10SD); $R^2 = 0.91$; n = 71).

Post-fire Shrub Canopy Recovery

The 2005 (1 year since last burn) polygon mean was excluded in all analyses performed to describe the relationship between shrub cover and year since last burn, because it was clear that mean shrub cover estimated for this polygon was not a reasonable estimate of the shrub cover.

The piecewise model that best fit the data had a breakpoint at 27 years (Figure 4). The model predicted that shrub cover in the year of burn (year = 0) was 0.47% which was not significantly different from 0. A significant, 1.45 % per year, increase in shrub cover was predicted during phase 1. In phase 2, shrub cover was predicted to decrease by 0.06 % per year, but this estimate was not significantly different from 0. The peak shrub cover at the breakpoint was 38.6 %.

The quadratic model fit the data slightly better than the piecewise regression model on the basis of the AIC and R^2. The R^2 for the best piecewise regression was 0.71, whereas the R^2 for the quadratic model was 0.73. The quadratic regression model had a residual standard error of 8.86 %, whereas the best continuous piecewise regression model had a residual standard error of 9.05 %. The fitted quadratic model was:

$$\hat{Y} = -3.36 + 2.04X - 0.02X^2 \quad \textbf{[2]}$$

where X is the number of years since last burn (Fig 4). This model predicts a negative shrub cover in the year of burn and shrub cover does not become positive until 1.7 years after the burn. Shrub cover increases each year after the burn, but at a decreasing rate, until peak shrub cover of 45 % is reached in year 47. After year 47, shrub cover is predicted to decrease, and is predicted to be less than the cover in year 27 by year 68. In general, the quadratic model and piecewise regression model showed very good agreement in the 0-30 years range after fire and again at around 69 years after fire (Figure 4). The two models had poor agreement between 40 to 50 years after fire where there is no data. The year since last burn was not known for the unburned polygon except that there was no record of fire for the polygon and the first fire records began in 1936, so we arbitrarily assigned it a value of 71 as the number of years since last burn. The model that best fit the data was sensitive to the choice of years since last burn assigned to the unburned polygon. When the value was changed to 91 years, the piecewise regression was the best model. Regardless of the number of years since last burn (>70 years) assigned to the unburned polygon, the fit breakpoint and slopes ahead of and beyond the breakpoint were robust. For the quadratic approach, parameter estimates were not robust to these changes in the years since last burn of the unburned polygons.

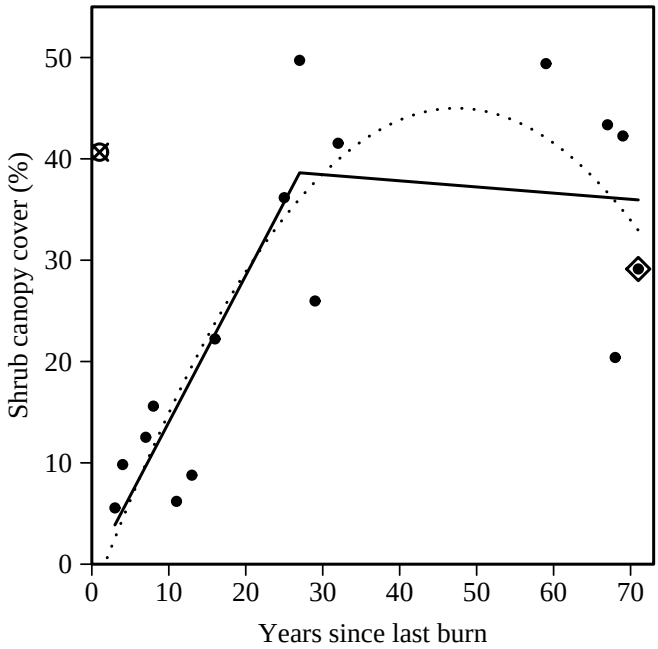

Figure 4. Mean cover estimates from 100 classified SPOT5 pixel samples in each of 17 areas with a different number of years since last burn. The best continuous piecewise regression relationship (solid line) and quadratic relationship (dotted line) are shown. The 1 year since last burn point is shown (⊗) but was not included in the analysis. The >70 years point (• inside the diamond) was plotted at 71 years, but in reality we only know that it is greater than 70.

DISCUSSION

Suitability of SPOT5 and VLSA Imagery for Shrub Classification

The application of SPOT5 imagery in sub-pixel classification of shrubs in sagebrush-steppe communities was successful. The spectral reflectance of shrubs was distinct compared to bare ground and senescent herbaceous cover in the imagery. In all four bands of the SPOT5 imagery, shrub canopy appeared darker than the bright-colored bare ground and herbaceous cover (Fig. 2). We used

a SPOT5 image subset from September because we expected to better distinguish shrubs spectrally in the fall. While herbaceous species are senescent at our study site at this time of the year, shrubs have green leaves year-round. Shrubs produce ephemeral leaves in early spring, which senesce during the growing season, and overwintering leaves later in the growing season, which senesce the following spring (Bilbrough and Richards 1993). Furthermore, sagebrush green vegetation index has been previously shown to be stable between August and October (Chen et al 1998).

Our validation model indicated that the application of spectral mixture analysis in estimating shrub canopy cover within pixels was also successful. The estimated percent shrub canopy cover in the SPOT5 imagery were well correlated to the estimates based on the VLSA imagery. However, there were exceptions. Using visual assessment of the classified SPOT5 imagery and local knowledge, we identified some areas where classification results appeared incorrect. Many pixels with low percent cover of shrubs were classified as having 0 percent shrub cover, when we examined the classified imagery and histogram distribution of pixel values. This pattern supports Okin et al.'s (2001) conclusion that spectral mixture analysis does not provide accurate estimates of vegetation cover, when vegetation cover within a pixel is less than 30 percent. In our observation, shrub cover of less than 15 percent appeared to be commonly classified as having 0 percent shrub cover. Spectral mixture analysis, therefore, might be more appropriate to use in sagebrush-steppe communities, where average shrub cover within pixels is at least greater than 15 percent, if not 30 percent. Furthermore, the estimated shrub canopy percent cover from the SPOT5 imagery within the 2005 fire polygon was unexpectedly high. We suspected this might be due to a high amount of ash on the soil or a high percent cover of velvet lupine (*Lupinus leucophyllus* Dougl. ex Lindl.) in the year following fire. The velvet lupine appeared to have a similar spectral characteristic to sagebrush in the imagery and even appeared similar to sagebrush in the VLSA imagery. Our local familiarity with the site and a field visit to the 2005 fire polygon confirmed this observation.

Availability of the 2-cm-resolution VLSA imagery proved very useful in this study. The VLSA imagery provided accurate and detailed point data that could be used as samples for SPOT5 image training and validation. The results of this successful application of SPOT5 and VLSA imagery in shrub classification have important implications for monitoring and assessment of millions of hectares of sagebrush-steppe in the western United States. Field-based approaches to monitoring post-fire sagebrush canopy cover changes provide highly accurate and valuable results, but they can be labor-intensive, time-consuming, and limited in the spatial extent they can cover. In comparison, the application of remote sensing methods can be more cost-effective and timely due to the large areal extent they cover. Digital imagery also provides opportunities for more robust and comprehensive analysis of change, as the imagery can be easily integrated with other sources of digital data such as maps of fire boundaries and land use.

Post-fire Shrub Canopy Recovery

The best fit regression model considered in this analysis was a quadratic equation, but interpretation of this model made less biological sense than the continuous piecewise regression model. The second order regression model indicated that shrub canopy recovery might continue for 47 years after which shrub cover would decrease. The predicted shrub cover at 47 years after fire would peak at 45 %. The dominant shrub in these sites is mountain big sagebrush and Lesica et al. (2007) reported that mean mountain big sagebrush cover in unburned areas was 28 ± 2 % and that this level of cover was reached by 32 years after fire. Our interpretation of the continuous piecewise regression model that shrub cover was recovered by 27 years after fire was similar to the 32 year mountain big sagebrush recovery period reported by Lesica et al. (2007). Although we didn't consider non-linear regression approaches, Watts and Wambolt (1996) reported that Wyoming big sagebrush cover after fire and other control treatments followed a sigmoid relationship with time. In that study, Wyoming big sagebrush cover had reached >95 % of the expected long-term cover by 30 years. We found the rate of shrub cover increase to be constant during the recovery phase, but Lesica et al. (2007) reported a better fit from a log-linear model where sagebrush cover increased at an increasing rate with time.

Management Implications
Shrub cover in mountain big sagebrush communities is an important attribute for guiding management. This study demonstrated a successful application of SPOT5 imagery, VLSA images, and classification methods in estimating shrub canopy cover. The classification approach described here could enable a more rapid estimate of shrub canopy cover across large areas compared to ground-based measurements, which are both costly and time-consuming. Our results indicated that active shrub canopy recovery might continue for up to 27 years in mountain big sagebrush communities. Using similar methods, post-fire canopy changes in other sagebrush communities can be assessed. Once shrub cover and its changes are estimated, managers can apply post-fire recovery rates to aid their decision making.

ACKNOWLEDGEMENTS

We would like to acknowledge the Idaho Delegation for their assistance in obtaining the grant that supported this work funded through the National Aeronautic and Space Administration (NASA NNG05GB05G).

LITERATURE CITED

Adams, J.B., M.O. Smith, and P.E. Johnson. 1986. Spectral mixture modeling: a new analysis of rock and soil types at the Viking Lander 1 site. *Journal of Geophysical Research* 91:8098-8112.

Akaike, Hirotugu. 1974. A new look at the statistical model identification. *IEEE Transactions on Automatic Control* 19: 716–723.

Anderson, J.E. and R.S. Inouye. 2001. Landscape-scale changes in plant species abundance and biodiversity of a sagebrush steppe over 45 years. *Ecological Monographs* 71:531-556.

Baker, W.L. 2006. Fire and restoration of sagebrush ecosystems. Wildlife Society Bulletin 34: 176-185.

Billings, W.D. and R.J. Morris. 1951. Reflection of visible and infrared radiation from leaves of different biological groups. *American Journal of Botany* 38:327-331.

Bilbrough, C.J. and J.H. Richards. 1993. Growth of sagebrush and bitterbrush following simulated winter browsing: mechanisms of tolerance. *Ecology* 74:481-492.

Blaisdell, J.P. and W.F. Mueggler. 1956. Sprouting of bitterbrush (*Purshia tridentata*) following burning or top removal. *Ecology* 37:365-370.

Crawford, J.A., R.A. Olson, N.E. West, J.C. Mosley, M.A. Schroeder, T.D. Whitson, R.F. Miller, M.A. Gregg, and C.S. Boyd. 2004. Ecology and management of sage-grouse and sage-grouse habitat. *Journal of Range Management* 57:2-19.

Chen, Z., C.D. Elvidge, and D.P. Groeneveld. 1998. Monitoring seasonal dynamics of arid land vegetation using AVIRIS data. *Remote Sensing of Environment* 65:255-266.

DePruit, E.J. and M.M. Caldwell. 1973. Seasonal pattern of net photosynthesis of *Artemisia tridentata*. American Journal of Botany 60:426-435.

Kokaly, R.F., D.G. Despain, R.N. Clark, and K.E. Livo. 2003. Mapping vegetation in Yellowston National Park using spectral feature analysis of AVIRIS data. *Remote Sensing of Environment* 84:437-456.

Kremer, R.G. and S.W. Running. 1993. Community type differentiation using NOAA/AVHRR data within a sagebrush-steppe ecosystem. *Remote sensing of Environment* 46:311-318.

Lesica, P., S.V. Cooper, and G. Kudray. 2007. Recovery of big sagebrush following fire in southwest Montana. *Rangeland Ecology and Management* 60:261-269.

Lillesand, T.M. and R.W. Kiefer. 2000. Remote sensing and image interpretation. Fourth Edition. John Wiley and Sons Inc. New York. Chichester. Weinheim, Brisbane. Singapore. Toronto.

Okin, G.S., D.A. Roberts, B. Murray, and W.J. Okin. 2001. Practical limits on hyperspectral vegetation discrimination in arid and semiarid environments. *Remote Sensing of Environment* 77:212-225.

Rencz, A.N. 1999. Remote sensing for the earth sciences. Wiley and Sons. New York. p.251-307.

Small, C. 2004. The Landsat ETM+ spectral mixing space. *Remote Sensing of Environment* 93:1-17.

Streutker, D.R. and N.F. Glenn. 2006. LiDAR measurement of sagebrush steppe vegetation heights. *Remote Sensing of Environment* 102:135-145.

Wambolt, C.L., K.S. Walhof, and M.R. Frisina. 2001. Recovery of big sagebrush communities after burning in south-western Montana. *Journal of Environmental Management* 61:243-252.

Watts, M.J. and C.L. Wambolt. 1996. Long-term recovery of Wyoming big sagebrush after four treatments. *Journal of Environmental Management* 46:95-102.

Xiao, J. and A. Moody. 2005. A comparison of methods for estimating fractional green vegetation cover within a desert-to-upland transition zone in central New Mexico, USA. *Remote Sensing of Environment* 98:237-250.

Evaluation of Alternative Simple Band Ratios

Shauna Nelson, Idaho State University, Pocatello, Idaho 83209

Keith T. Weber, GISP, Idaho State University, GIS Training and Research Center, 921 S. 8th Ave., Stop 8104, Pocatello, Idaho 83209-8104 (webekeit@isu.edu)

ABSTRACT
Vegetation indices are commonly applied to remote sensing data and their application is based upon well established image processing theory and methodology. Simple band ratio vegetation indices allow for consistent and uniform data processing and analysis. However, it was hypothesized that many of these standard vegetation indices (e.g., SR, NDVI and SAVI) may not produce results any different from other simple ratios calculated from any pair of spectral bands in a given image. To test this, all possible combinations of simple band ratios were created with SPOT 5 imagery using Idrisi software. The resulting simple ratio indices were then correlated against each other and further examined. Results of this study indicate that all simple band ratio combinations are highly correlated with one another and tend to describe the same land surface phenomena.

KEYWORDS: vegetation indices, NDVI, SPOT

INTRODUCTION

Processing digital imagery and the subsequent interpretation of these data can provide valuable information and results in savings in both time and money. The use of vegetation indices to interpret satellite imagery and validate these interpretations with *in situ* data further increases these benefits. However, the effectiveness of vegetation indices is the subject of much scrutiny as scientists continue to experiment with various combinations of band ratios, often times adjusting indices to optimize outcomes under specific soil or vegetation conditions. It is believed that isolating one vegetation index versus another as a single effective derivation of vegetation for all digital images may sacrifice data integrity. Yet, the Normalized Difference Vegetation Index (NDVI) was established for the purpose offering a standardized product that could be uniformly applied worldwide. The NDVI ratio was created using the following calculation (Jensen, 2000):

$$NDVI = \frac{NIR - RED}{NIR + RED}$$

As a simple band ratio (SBR) (meaning that only two bands are involved in the algorigthm and that the index is a result of the quotient of the difference over the sum), consistent in its results, this formula provides uniform vegetation analysis across a variety of data collection scenarios and is applicable to a large number of satellite platforms. Its success and comparative simplicity suggests equally effective indices may be formed with other combinations of spectral bands which may produce similar results.

MATERIALS AND METHODS

To test this, all combinations of SBR indices were calculated using the spectral bands available within SPOT 5 imagery. Once calculated, results were analyzed for each pair of SBR's for correlation (using adjusted R^2) and for their pixel dispersion from the line of best fit (i.e., end members). Results were also analyzed to determine whether a significant difference exists between the derived SBR's. It is noted that other equally well known indices such as the Simple Ratio (SR) and Soil Adjusted Vegetation Index (SAVI) warrant further research as alternative spectral band combinations. However, for the purposes of this evaluation, SBR's were calculated following the standard NDVI equation (i.e., the difference of band A and band B, divided by the sum of band A and band B.

Imagery

Image selection was based on knowledge of the area and vegetation for *in situ* data verification. SPOT 5 satellite imagery was acquired for the U.S. Sheep Experiment Station near DuBois, Idaho on August 5, 2005. The imagery was georectified using nearest neighbor resampling (RMSE = 3.48) and then corrected for atmospheric effects using the Cos(t) algorithm in Idrisi (Chavez 1996). The imagery was then projected into Idaho Transverse Mercator (NAD 83). Vegetation studies of the area indicate the dominant plant species are Mountain Big Sagebrush (*Artemisia tridentata* Nutt. ssp. *vaseyana* (Rydb.) Beetle.), threetip sagebrush (*Artemisia tripartita* Rydb.), Antelope bitterbrush (*Purshia tridentata* (Pursh) DC.), bluebunch wheatgrass (*Pseudoroegneria spicata* (Pursh) A. Löve), thickspike wheatgrass (*Elymus lanceolatus* (Scribn. & J.G. Sm.) Gould), Sandberg bluegrass (*Poa secunda* J. Presl), arrowleaf balsamroot (*Balsamorhiza sagittata* (Pursh) Nutt.), and tapertip hawksbeard (*Crepis acuminata Nutt*. ssp. *acuminata*) (West and Young, 2000, Wright and Bailey, 2004, Weber, et al 2007).

Image Processing and Analysis

Using Idrisi Kilimanjaro's image calculator and the imagery described above, SBR's were systematically determined for all possible combinations of Green, Red, NIR and SWIR bands (Table 1). Regression analysis (REGRESS) was then used to determine the correlation coefficient between all pairs of SBR's (Table 2) and from these analyses the coefficient of determination (R^2) was calculated and used for subsequent comparison.

Table 1. Simple Band Ratios (gray areas indicate SBR's that were not calculated)

	Green	Red	NIR	SWIR
Green		red-grn red+grn	(a) nir-grn nir+grn	swir-grn swir+grn
Red	grn-red grn+red		(b) nir-red nir+red	swir-red swir+red
NIR	grn-nir grn+nir	red-nir red+nir		swir-nir swir+nir
SWIR	(c) grn-swir grn+swir	red-swir red+swir	(d) nir-swir nir+swir	

a. GNDVI (Hunt et al. 2007)
b. NDVI (Tucker 1979)
c. NDII or NDWI (Gao 1996, Hunt and Yilmaz 2007)
d. NDSI (Riggs et. al., 1994, Dozier 1989)

Table 2. All Possible SBR Combinations compared in this study (gray areas indicate redundant combinations)

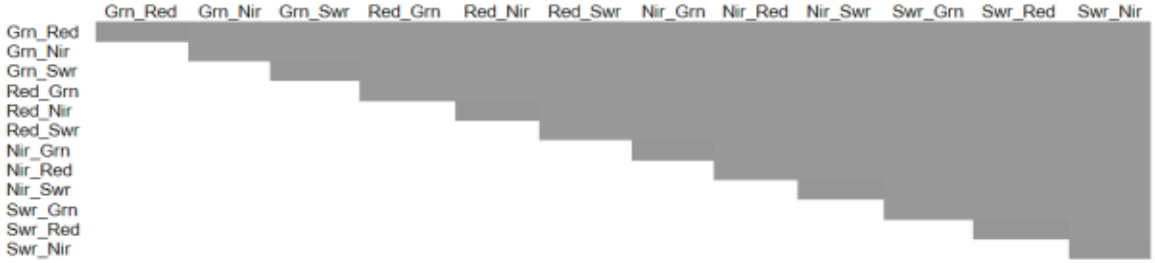

RESULTS AND DISCUSSION

The resulting statistical information (r-values and coefficients of determination [R^2]) and pixel scatter plot distributions were analyzed for variation and similarities between SBRs. Three examples of these results are shown in Figures 1-3.

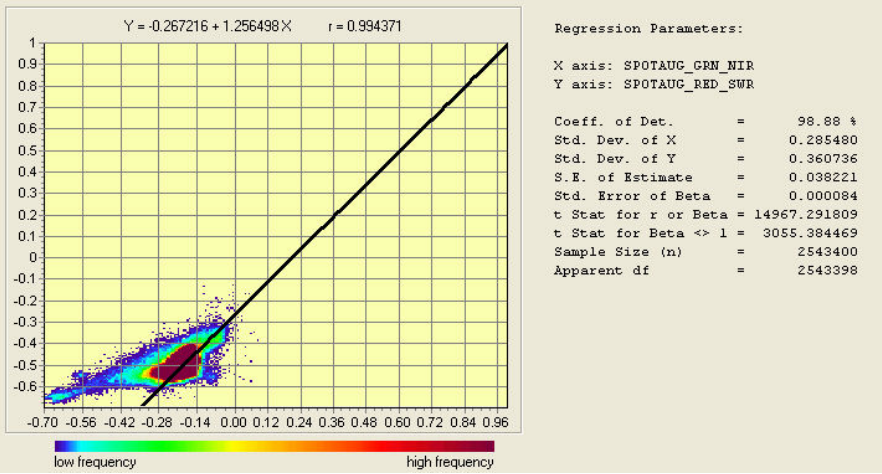

Figure. 1 GRN NIR and RED SWIR pair-wise comparison.

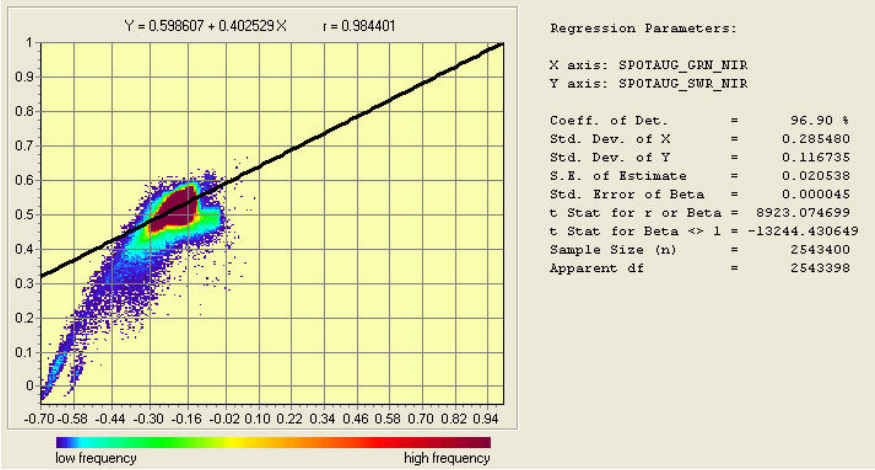

Figure. 2 GRN NIR and SWR NIR pair-wise comparison.

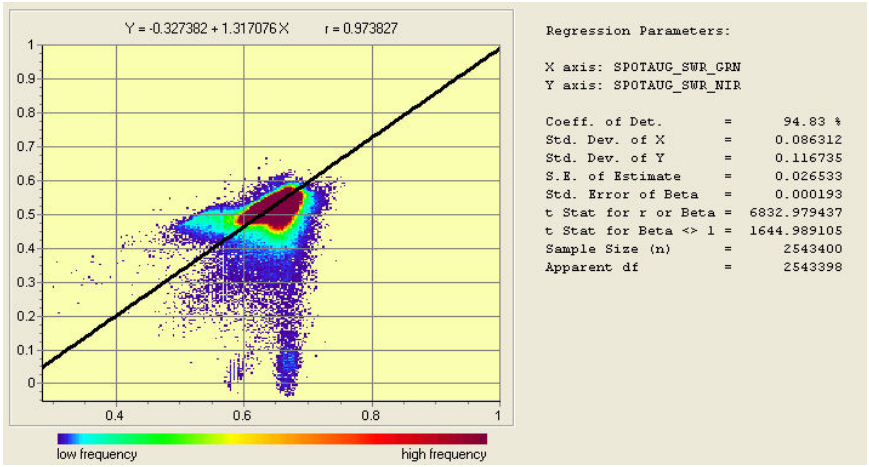

Figure 3. SWIR GRN and SWR NIR pair-wise comparison.

Regression analysis and the resulting R^2 values indicated high correlation between all SBR pairs (Table 3) with coefficients of determination ranging from a low of 0.88 to a high of 0.99.

Table 3 – The R^2 value for all SBR correlation calculations

	Grn_Red	Grn_Nir	Grn_Swr	Red_Grn	Red_Nir	Red_Swr	Nir_Grn	Nir_Red	Nir_Swr	Swr_Grn	Swr_Red	Swr_Nir
Grn_Red												
Grn_Nir	0.98											
Grn_Swr	0.99	0.99										
Red_Grn	0.96	0.97	0.98									
Red_Nir	0.94	0.98	0.97	0.98								
Red_Swr	0.97	0.98	0.99	0.99	0.98							
Nir_Grn	0.97	0.93	0.96	0.95	0.89	0.95						
Nir_Red	0.98	0.92	0.96	0.93	0.88	0.94	0.99					
Nir_Swr	0.98	0.97	0.99	0.98	0.95	0.99	0.98	0.97				
Swr_Grn	0.96	0.92	0.93	0.93	0.89	0.92	0.96	0.99	0.94			
Swr_Red	0.95	0.90	0.91	0.88	0.84	0.88	0.94	0.96	0.91	0.98		
Swr_Nir	0.94	0.96	0.94	0.93	0.95	0.93	0.89	0.89	0.91	0.94	0.92	

A review of paired-SBR plots revealed some emergent characteristics within the majority of pair-wise SBR comparisons. Among the most notable was an isolated segment of pixels (end-members) extending from the central cluster and appearing as a tail (Figure 4).

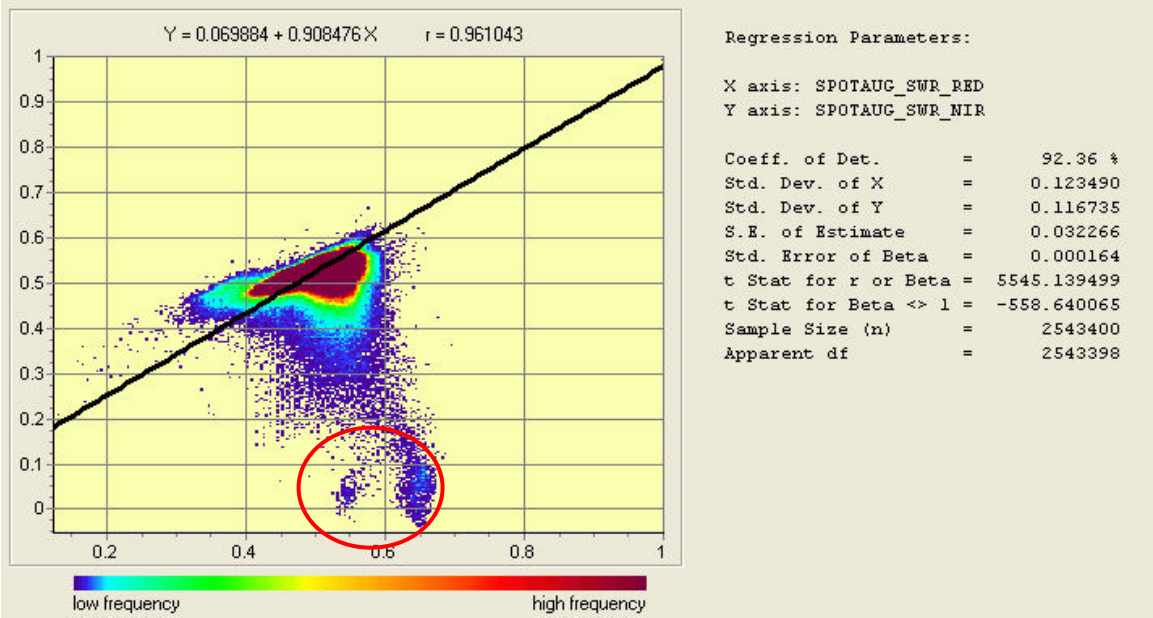

Figure 4. An isolated end-member tail revealed during pair-wise SBR comparisons.

It was hypothesized that some unique land surface characteristic was most likely the cause of the end member tail. To investigate this, the geographic features representing the end member tail needed to be identified and so logical expression was calculated in Idrisi Kilimanjaro to isolate these pixels. To accomplish this (cf. Figure 4) all pixels in the SWR_NIR SBR (cf. Y-axis in the figure 4) with values $\leq$ 0.10 were identified using the Idrisi raster calculator. Next, all pixels in the SWR_RED SBR (cf. X-axis in the figure 4) with values $\geq$ 0.60 were similarly selected. Next, a Boolean AND process was calculated using the results of the first two logical expressions resulting in a new raster layer which isolated the end member tail of interest. The boolean image that was returned had pixel values of one in all areas corresponding to the end member tail and zero's elsewhere.

The resulting boolean image did not appear as a salt-and-pepper scatter of pixels but rather a tight cluster of pixels within the northwest quadrant of the imagery. The raster layer was opened in ArcGIS along with National Agricultural Imagery Program (NAIP) ortho-imagery (acquired in 2004). From this visual analysis it was apparent that the cluster of pixels representing the end-member tail was an irrigated farm field. This was validated in the field by visiting the site and speaking with the land owner about the condition of the field on or around August of 2005 who informed us that the field is (and was) irrigated alfalfa.

CONCLUSIONS

Close and repeated review of image processing results revealed that SBR's derived from combinations of the green, red, NIR, and SWIR bands did not significantly differ from one another regardless of the specific SBR calculated. However, there appears to be some promise of improved land cover differentiation through the use of differenced-SBR's or SBR-quotients. Applying the former to the end-member tail discussed in this paper would yield pixel values near zero for all well correlated pixels (those closest to the line of best fit) and increasing larger values for those pixels representing the end-member tail. Applying the latter (SBR-quotients) would result in pixel values near one for all well correlated pixels and increasingly larger values for the pixels representing the end-member tail. Using the example described in this paper, SBR-quotient values would have a maximum of 31 which, in contrast to the well-correlated pixels (~1.0), is quite different. Additional research appears to be merited into the applicability of SBR-quotients as a means of identifying unique land features.

ACKNOWLEDGEMENTS
This study was made possible by a grant from the National Aeronautics and Space Administration Goddard Space Flight Center. ISU would also like to acknowledge the Idaho Delegation for their assistance in obtaining this grant.

LITERATURE CITED

Chavez, P. S. 1996. Image based atmospheric corrections- revisited and improved. *Photogrammetric Engineering and Remote Sensing, 62*, 1025-1036.

Dozier, J. 1989. Spectral Signature of Alpine Snow Cover from the Landsat Thematic Mapper. IEEE Transactions on Geoscience and Remote Sensing. 22(1989):9-22.

Gao, B. C. and A. F. H. Goetz, 1996. Retrieval of equivalent water thickness and information related to biochemical components of vegetation canopies from AVIRIS data. Remote Sensing of Environment, 52:155-162.

Hunt, E. R., and T. Yilmaz. 2007. Remote Sensing of Vegetation Water Content Using Shortwave Infrared Reflectance. Summaries of International Society for Optical Engineering.

Hunt, E. R., W. Hively, S. Fujikawa, M. Tranchitella, T. Ng, W. Raszula, D. Yoel, C. Daugherty, and G. McCarty. 2007. Remote Sensing of Leaf Area Index from Unmanned Airborne Vehicles (UAV's). Society for Range Management Meeting Proceedings.

Jensen, J. R. 2000. Remote Sensing of the Environment An Earth Resource Perspective. Pages 361-365. Prentice Hall

Tucker, C.J. 1979. Red and photographic infrared linear combinations for monitoring vegetation. Remote Sensing of Environment 8: 127-150.

Riggs, G. A., D. K. Hall, and V. V. Salomonson. 1994. A Snow Index for the Landsat Thematic Mapper and Moderate Resolution Imaging Spectroradiometer. IEEE Transactions on Geoscience and Remote Sensing 4(1994):1942-1944.

Weber, K.T., Seefeldt, S. S., Norton, J.M., Finley, C. 2008. Fire Severity Modeling of Sagebrush-Steppe Rangelands in Southeastern Idaho. GIScience and Remote Sensing. 45(1):83-108.

West, N.E. and Young, J. A., 2000. Intermountain Valleys and Lower Mountain Slopes. Pages 255-284 in Barbour, M.G. and Billings, W.D. (Ed.), *North American Terrestrial Vegetation*. Cambridge, UK: Cambridge University Press.

Wright, H. E. and Bailey, A. W. 2004. *Fire Ecology: United States and Southern Canada*. Wiley Interscience. 528pp.

Resilience of Satellite-Based Measures of Greenness to Fire Decreases with Aridity in Sagebrush-Steppe Rangelands

Ryan E. Baum, Department of Biological Sciences, Idaho State University, Pocatello ID 83209-8007

Matthew J. Germino, Department of Biological Sciences, Idaho State University, Pocatello ID 83209-8007, germmatt@isu.edu, 208-282-3285

ABSTRACT

Satellite measures of greenness were measured in regions differing in synoptic climate, floristics, fire history, and livestock grazing in sagebrush steppe of the upper Snake River Plain of the Great Basin USA. We hypothesized that resilience to fire, as indicated by recovery of greenness to pre-fire levels, would vary among two sagebrush community types that differ in climate, and also with livestock grazing. Study areas were in and around three large areas burned in Wyoming big sagebrush (*Artemesia tridentata* spp. *wyomingensis*) communities, and 13 smaller burn areas in a wetter and cooler region that included higher elevations and a greater occurrence of mountain big sagebrush (*A. t.* spp. *vaseyana*; also having *A. tripartita*) communities. Grazing effects were evaluated in and around a long-term livestock exclosure in Wyoming sagebrush region. The modified soil-adjusted vegetation index ($MSAVI_2$) was calculated from one Landsat scene per year to assess greenness at about the time of peak biomass and greenness, from 1984 to 2004. $MSAVI_2$ was about 50% lower in the Wyoming compared to mountain sagebrush communities, and had transient increases following fire in Wyoming but not mountain sagebrush communities. More persistent effects of fire were apparent in the variability of $MSAVI_2$ among pixels within a scene, and in relationships of this variability to annual precipitation patterns. Variability in $MSAVI_2$ increased for several years following fires in the Wyoming sagebrush region, due to increased sensitivity to annual precipitation (r^2 = 0.47 to 0.70). In contrast, variability in $MSAVI_2$ decreased following fires in the mountain sagebrush region, and was not correlated to annual precipitation. The time required for variability in $MSAVI_2$ to recover to pre-fire levels was greater in grazed compared to ungrazed areas of the Idaho National Laborator study area, but there were otherwise no detectable impacts of grazing on $MSAVI_2$. The less resilient Wyoming sagebrush communities had greater and more enduring changes in greenness after fire. The climatic and biogeographic differences examined here may span a threshold for ecosystem resilience to fire.

KEYWORDS: fire, geographic information systems, grazing, MSAVI, precipitation, remote sensing, sagebrush-steppe, spectral vegetation indices.

INTRODUCTION

Sagebrush (*Artemisia*) steppe ecosystems throughout western North America experience combinations of natural and anthropogenic impacts, such as altered fire regimes and domestic livestock grazing, in addition to natural variation in precipitation (Anderson and Inouye 2001). Fire and livestock grazing cause changes in population and community structure and ecosystem processes that could modify climate-productivity relationships over the vast sagebrush-steppe biome in the Great Basin, USA. The separate effects of fire or grazing disturbances on semiarid rangeland function have been studied (Anderson and Holte 1981, Hosten and West 1994, Anderson and Inouye 2001, Wambolt et al. 2001, Diaz-Delgado et al. 2002, Washington-Allen et al. 2004), but studies of the multiple, potentially interacting effects of such disturbances are scarcer (Valone 2003, Geiger and McPherson 2005). Additionally, ecosystem responses to disturbance have mostly been studied at the small-scale, plot level (e.g., Anderson and Holte 1981, Hosten and West 1994, Anderson and Inouye 2001, West and Yorks 2002), therefore, little quantitative information exists over large spatial and temporal scales (e.g., Washington-Allen et al. 2004) to help address the potentially complex effects of multiple disturbances on ecosystem structure and function. Large scale, landscape-level assessments of the separate and combined effects of weather variation, fire, and livestock grazing disturbances are needed to better match the scale at which rangeland management occurs.

Remote sensing can provide periodic measures of vegetation over large areas that exceed the measurement capabilities of traditional, ground-based assessments (Washington-Allen et al. 2004). Previous studies derived spectral vegetation indices (SVI's) from remotely sensed ratios of red and near-infrared reflectance as a measure of the earth's greenness, which can indicate abundance of rangeland vegetation (e.g., Graetz and Gentle 1982, Pickup and Foran 1987, Graetz et al. 1988, Smith et al. 1990, Pickup et al. 1993, Senseman and Bagley 1996, Elmore et al. 2000, McGwire et al. 2000, Ramsey et al. 2004, Wallace et al. 2004), particularly as it varies in time in response to precipitation and land-use (Paruelo and Lauenroth 1998, Paruelo et al. 2001, Washington-Allen et al. 2004).

This study utilized a 20-year archive of Landsat data to determine how ecosystem greenness responds to fire in two regions that differ in climate on the Upper Snake River Plain of the Great Basin, USA. Both regions are dominated by big sagebrush steppe (*Artemesia tridentata*), but with the mountain big sagebrush (*A. t.* ssp *vaseyana*) and some three-tip sagebrush (*A. tripartita*) community types dominating the relatively cooler and wetter region compared to Wyoming big sagebrush (*A. t.* ssp *tridentata*) communities dominating the warmer and drier region. A lack of recovery following wildfire is perceived to be causing rapid losses of Wyoming sagebrush habitat, whereas mountain sagebrush communities are considered to be more resilient - although few studies have attempted to quantitatively substantiate perceived differences in the functioning of these community types (eg. Chambers et al. 2007). Larger burn areas of fires are increasingly occurring in the Wyoming sagebrush communities, recently attaining about 400 K ha (2007 Murphy Complex Fire in W N America). Widespread acceleration of fire frequencies and corresponding loss of fire-sensitive native perennials such as sagebrush is well known to occur with invasion by exotic annuals such as cheatgrass (*Bromus tectorum*). The fire-cheatgrass cycle can decrease resilience of species assemblages, sometimes altering succession to the extent of causing type conversion from perennial shrub steppe to near monocultures of annual grasses. The subject region has not yet experienced this degree of invasion by cheatgrass, thus providing a rare opportunity to examine fire effects independent of cheatgrass. We also wished determine how domestic livestock grazing, the most extensive land use of the region, affects recovery of greenness following fire in the warmer and drier region. Water availability in these semi-arid rangelands is limited and highly variable in time (Anderson and Inouye 2001), and primary production is linked to variation in rainfall (LeHouerou et al. 1987). Thus, we anticipated variability in greenness to be an important indicator of ecosystem stability. We hypothesized that post-fire recovery of greenness to levels observed in burned areas would occur more quickly in the wetter and cooler region, and in areas in which grazing had been excluded.

Furthermore, we hypothesized that variability in SVI's resulting from fire would result from a greater coupling of vegetation greenness to precipitation patterns.

METHODS

Areas with different fire and grazing histories since 1939 were identified from US Bureau of Land Management (BLM) Geographic Information Systems (GIS) data for lands within or nearby two adjacent regions of the Upper Snake River Plain (Idaho; Figures. 1, 2); the Idaho National Laboratory (INL) and the U.S. Department of Agriculture Sheep Experiment Station (USSES). Both areas were ideal for this study because of their relatively flat topography and large homogenous management units (livestock grazing allotments) where wildfires have occurred frequently over the last two decades. Additionally, both areas have experienced similar livestock grazing. The two study areas are also unique from each other because of their geographic locations; with the USSES situated approximately 100 km north of the INL on the northernmost extent of the Upper Snake River Plain, it is higher in elevation (approx. 1500 – 1950 m) and experienced greater amounts of average yearly precipitation over the 20-year study period (300.5 mm ± 75.1) compared to the INL (approx. 1480 – 1600 m; 192.7 mm ± 60.4; $F_{1, 40} = 26.28$, $P = 0.000$; Figure 3).

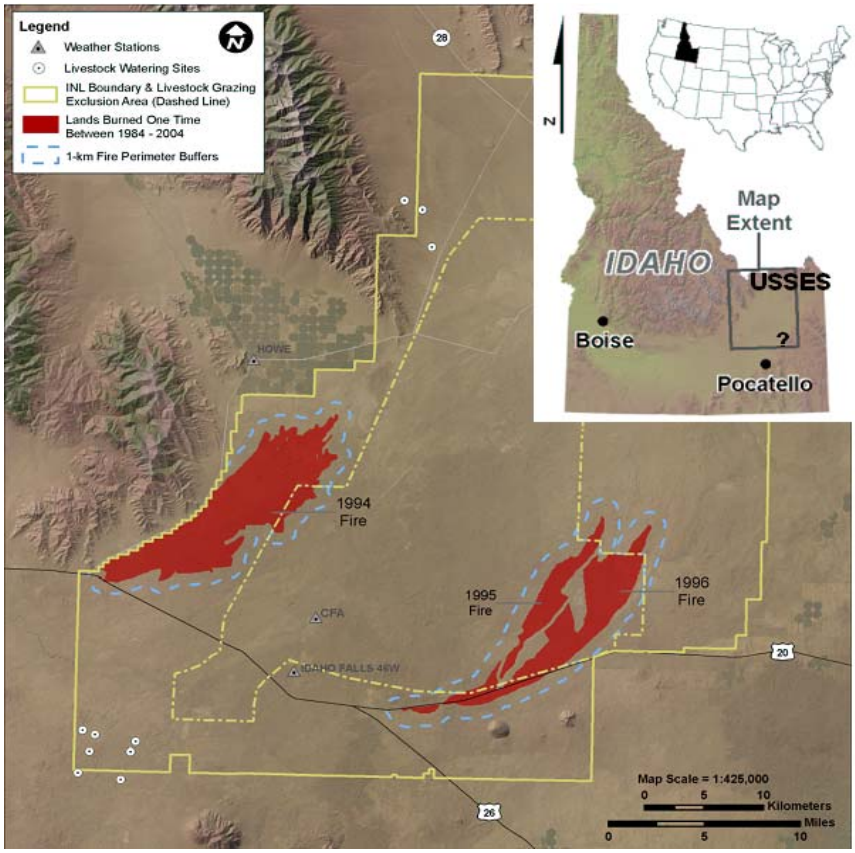

Figure 1. Map of the Idaho National Laboratory (INL) with disturbance history lands for the 1994, 1995, and 1996 fires indicated in red. Dashed blue lines show 1-km fire buffers. Solid yellow line indicates INL boundary with lands closed to livestock grazing since 1950.

Areas within 1 km buffers of wildfire perimeters were categorized as follows: 1) unburned areas where livestock grazing has been excluded since 1950; 2) areas having livestock grazing, in allotments administered by the BLM and referred to here as pasture; 3) ungrazed areas that have been burned once during the study years and not any other time since 1939; and 4) grazed and burned lands. Whereas the INL region offered replicate areas having all of these conditions, there were no ungrazed areas in the USSES region. No pixels within 90 m of boundaries of burn or grazed areas were measured, to avoid

edge effects. Fire years were 1994, 1995, or 1996 on the INL and in 1986, 1988, 1994, or 1998 on the USSES. These burns encompassed significant variation in annual precipitation, and provided 6 – 18 years of recovery from fire. BLM summer stocking rates of domestic grazers (cattle and sheep) varied little over the last 20 years and ranged from 12.4 to 33.5 acres/active animal unit months (AUM). Grazing was excluded from burned areas for two years following fire.

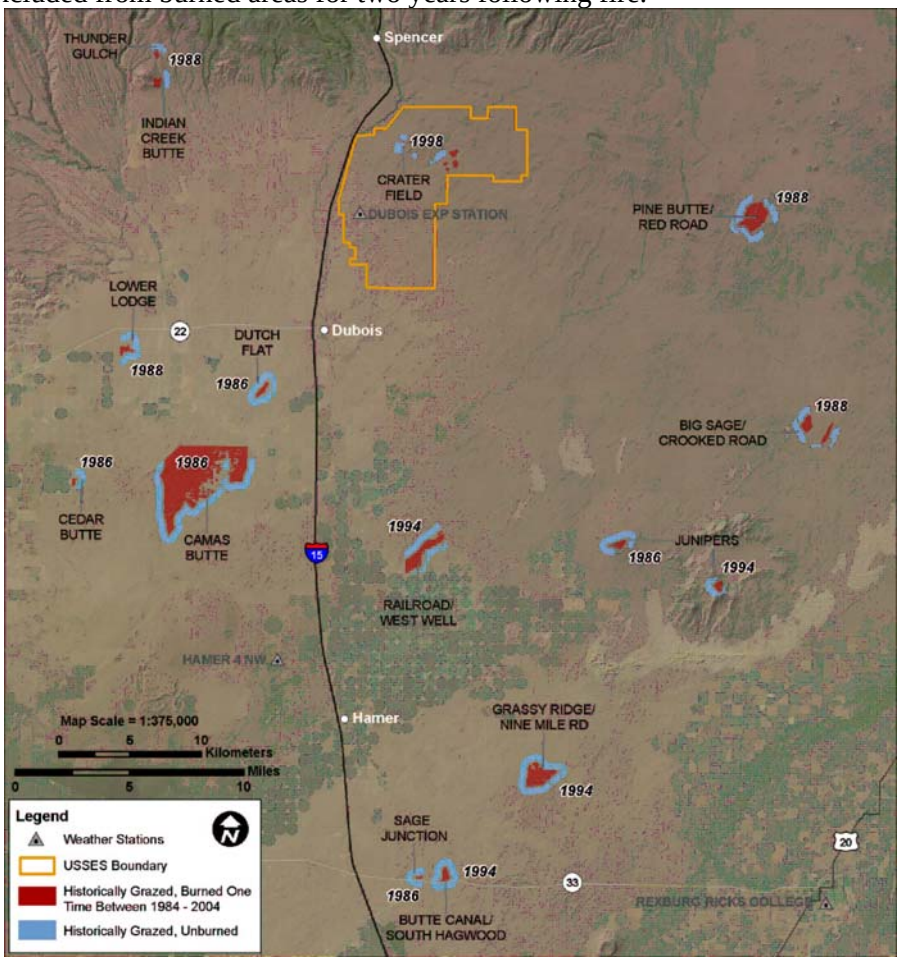

Figure 2. Map of the U.S. Sheep Experiment Station (USSES) located on the northern Upper Snake River Plain (Idaho) with grazed lands that were burned one time by fire in either 1986, 1988, 1994, or 1998 fires indicated in red. Solid blue areas show 1-km fire buffers for historically grazed, unburned areas.

We examined spatial and temporal variability in cloud-free Landsat 5 Thematic Mapper (TM) or 7 Enhanced Thematic Mapper (ETM+) image per year. Image sampling dates were selected for 19 of the years from 1984 – 2004, in a 30-day window centered on 27-June. We were unable to use more sampling dates per year, due to cloud cover or data gaps, and therefore, adjusted our inquiry to avoid complications due to phenological variability among years. The 30-day window evaluated was roughly equivalent to the peak summer growing season for sagebrush-steppe, as estimated by Paruelo and Lauenroth (1995 and 1998) using the maximum normalized difference vegetation index (NDVI) derived from Advanced Very High Resolution Radiometer (AVHRR) data. Pixels (30 m resolution) were converted to at-satellite reflectance, coregistered, and radiometrically normalized with relative corrections for atmospheric attenuation using the empirical, multiple-date, regression method (Jensen 1996).

The second modified soil-adjusted vegetation index ($MSAVI_2$) was calculated to quantify the abundance of sagebrush-steppe vegetation. $MSAVI_2$ increases the dynamic range of the vegetation signal and minimizes soil background influences by enhancing the red (band 3, 630-690 nm) and near-infrared (band

4, 750-900 nm) reflectance ratios (Qi et al. 1994). It was calculated using the equation developed by Qi et al. (1994):

$$MSAVI_2 = \frac{2*(\text{band 4}) + 1 - \sqrt{(2*(\text{band 4}) + 1)^2 - 8*(\text{band 4} - \text{band 3})}}{2}$$

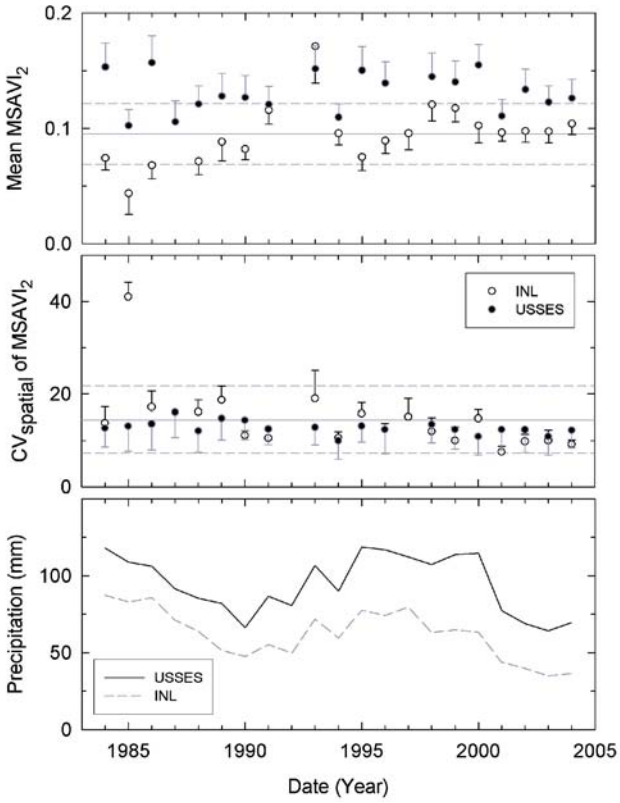

Figure 3. Mean MSAVI2 (+ or - SD) and mean CVspatial of MSAVI2 (+ or - SD) for unburned, grazed pixels of INL (open symbols) and the USSES region (closed) from 1984 - 2004, and sliding, three-year averages of cumulative yearly precipitation (mm) during the study period. Solid lines represent INL group means and dashed lines show ± 1 SD for all years combined (n = 19 years).

Total vegetation cover is commonly less than 50% or even 25% of ground area in sagebrush-steppe at the INL (Anderson and Inouye 2001, R. Blew, unpublished data). MSAVI has been used to quantify sparse vegetation cover in arid and semi-arid rangelands, and significantly correlates to field measures of canopy and areal ground cover (Senseman and Bagley 1996, Purevdorj et al. 1998, McGwire et al. 2000). In arid environments with less than 25% vegetation cover, MSAVI had a higher and more constant sensitivity over the full range of plant cover compared to other soil-adjusted SVI's (Rondeaux et al. 1996). Other soil-adjusted SVI's require constant, empirically defined, soil adjustment factors to minimize soil influences on canopy spectra (e.g., SAVI, TSAVI), and are therefore difficult to apply in assessing impacts of disturbances that alter soil exposure (Rondeaux et al. 1996). Defining an appropriate soil adjustment factor for pixels across an entire image, where the quantity and type of vegetation and soil is not constant, is likely to cause non-systematic errors in estimates of variation in SVI's among pixels that differ in soil exposure due to disturbance regime or variation in precipitation. $MSAVI_2$, a variant of MSAVI avoids this problem by using a dynamic, inductive soil adjustment factor that varies inversely with the amount of vegetation present in each pixel (Qi et al. 1994). $MSAVI_2$'s increased sensitivity to vegetation is important for assessing the year-to-year variability of disturbed sagebrush-steppe rangelands

where the total cover of vegetation is relatively low and soil exposure varies considerably with disturbance and precipitation.

Our analyses focused on calculations of mean $MSAVI_2$, the coefficient of variation (CV) of $MSAVI_2$ among years ("$CV_{temporal}$ of $MSAVI_2$"; CV = SD / mean * 100), and CV of $MSAVI_2$ among pixels with a year (i.e. within one image, "$CV_{spatial}$ of $MSAVI_2$"). Fire effects on $MSAVI_2$ were determined by comparing post-fire mean and CV of $MSAVI_2$ in both burned and non-burned (i.e. grazed) lands the first and subsequent growing seasons after fire. Distances to livestock watering troughs had no effects on $MSAVI_2$, as assessed by examining variation in $MSAVI_2$ among areas that were either within 30 m, or were 30 m to 100 m, 100 m to 500 m, or 500 m to 1000 m from watering troughs (Figure 1). Thus, we examined all pixels within grazing allotments for assessments of disturbance history impacts.

To estimate the potential for shifts from shrub to grass dominance to explain fire effects on $MSAVI_2$, we compared mean and CV of $MSAVI_2$ between lands with history of wildfire and those lands that were not burned and only grazed, and either contained sagebrush or had no sagebrush and were dominated by grasslands. Vegetation communities were identified from previous field surveys and existing vegetation classifications of the INL (Kramber et al. 1992) and USSES (Hanser et al. 2005).

Statistical Analyses

Areas in and around each complex of fires occurring in a year were our unit of replication, with n = 3 blocks for the INL sites burned in either 1994, 1995, or 1996; and n = 4 sets of burn areas lumped together for the USSES region fires of 1986, 1988, 1994, or 1998 (Figure 1). Background differences in mean and $CV_{spatial}$ of $MSAVI_2$ in unburned pasture between regions, and between pasture and ungrazed areas at INL, were determined over all study years using repeated measures MANOVA. Differences in $CV_{temporal}$ of $MSAVI_2$ among the study regions were determined using one-way ANOVA.

Fire effects were assessed using separate ANOVAs for each region, because they could not be consolidated into one experimental design. At the INL, differences in mean and $CV_{spatial}$ of $MSAVI_2$ were determined using ANOVA with grazing, fire, and year as main factors. In the USSES region, the factors were fire and year. Fire effects on $CV_{temporal}$ of $MSAVI_2$ at INL were evaluated with a two-way ANOVA with fire and grazing as main factors, and with a one-way ANOVA in the USSES region.

The significance of relationships between precipitation (PPT) and inter-annual mean $MSAVI_2$ and CV of $MSAVI_2$ were determined using linear least squares regression. Relationships were examined using sliding, three-year averages of yearly PPT (cumulative from January to image date), which had higher correlations with $MSAVI_2$ (higher r^2 values) than did water-year PPT (cumulative from October to image date) and growing season PPT (cumulative from April to image date). Precipitation was determined from historical climate summary data (Western Regional Climate Center, Desert Research Institute, Reno NV) obtained at nearby weather stations (n = 3 each) for the INL (CFA, Howe, and Idaho Falls 46W; Figure 1) and USSES (Dubois Experimental Station, Hamer 4NW, and St. Anthony 1WNW; Figure 2). Three-year sliding averages were calculated by averaging precipitation in the current year up to image dates with that in the two preceding years, respectively, to test for lag effects in vegetation responses to precipitation (Anderson and Inouye 2001). Over the study period, three-year averages of yearly PPT ranged from 246.7 mm to 77.34 mm on the INL and from 394.1 mm to 217.6 mm for the USSES region (Figure 3). One-way ANOVA and Kruskal-Wallis tests were used to detect differences in mean slopes of the relationships between PPT and mean $MSAVI_2$ or CV of $MSAVI_2$ burned and unburned pasture in the INL and USSES regions, using the slope for each replicate burn area at the INL, or clusters of burns for a year at the USSES, as replicates.

RESULTS

Background differences among regions

Mean $MSAVI_2$ in unburned pastures was 28% greater and about 50% less variable among years in the USSES (0.132 ± 0.02 SE, 13.3% $CV_{temporal}$) compared to INL region, over the 20-year period (0.095 ± 0.03, 29.6% $CV_{temporal}$; $P < 0.000$; Figure 3). Variation in $MSAVI_2$ among years ($CV_{temporal}$ of $MSAVI_2$) in the INL region was similar among undisturbed sagebrush (29.6%) and grasslands (31.6%); and ungrazed (29.6%) and grazed (27.8%) areas at INL. $CV_{spatial}$ of $MSAVI_2$ (variation in $MSAVI_2$ among pixels within each image) varied in the INL region from 6.8% to 48.3% among the study years in ungrazed and unburned areas (Figure 3; $P < 0.0001$), and marginally from 7.6% to 41.0% in unburned pasture ($P = 0.11$). In pastures of the USSES region, $CV_{spatial}$ of $MSAVI_2$ (variation in $MSAVI_2$ among pixels within each image) varied from 9.9% to 16.1% among study years (Figure 3; $P = 0.025$). Thus, $MSAVI_2$ tended to be greater and less variable in space and time in the USSES compared to the drier INL region.

Fire effects

There were no differences in mean $MSAVI_2$ (± SD) over all growing seasons after fire, but $MSAVI_2$ increased as much as 39% in the second post-fire year at the INL ($F_{1, 18} = 28.31$, $P < 0.0001$) in grazed and non-grazed pixels, compared to background increases of 14% in unburned areas (Figure 4; $P = 0.0008$). There was no statistical support for increases in $MSAVI_2$ after fires at the USSES.

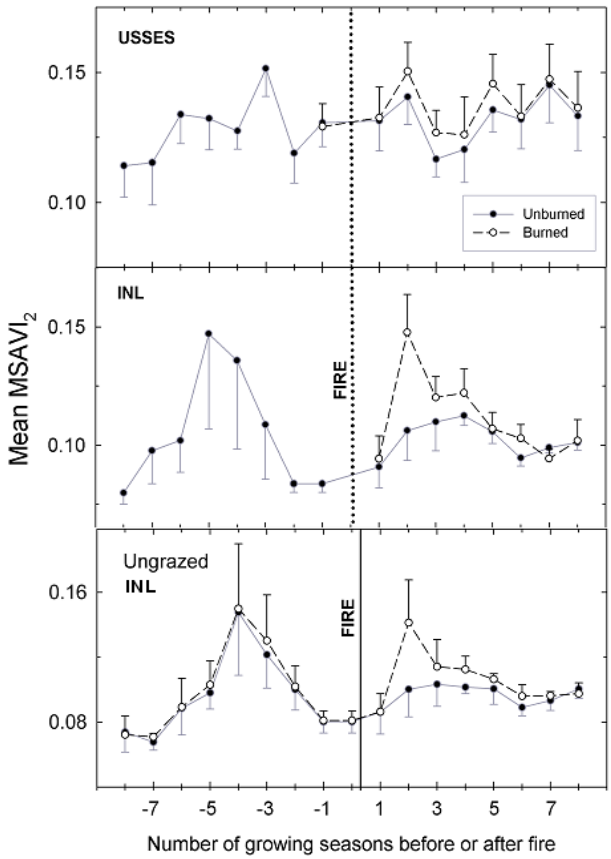

Figure 4. Comparisons of mean $MSAVI_2$ (+ or – 1 SE) from 11 June to 17 July for grazed lands between the USSES (top panel) and INL groups (bottom panel) before or after fire. Vertical line shows time of fire in mid-to-late summer of 1994, 1995, or 1996 for the INL and either 1986, 1988, 1994, or 1998 for the USSES. Scale on the x-axis is year relative to year of fire. Burn-year blocks were N = 3 and N = 4, respectively for the INL and USSES.

As a result of the fire-induced changes in mean $MSAVI_2$, inter-annual variability ($CV_{temporal}$) of $MSAVI_2$ following INL fires was up to 2-fold greater in burned (16%), compared to unburned areas (7%; calculations for Figure 4; $P = 0.04$). In contrast, $CV_{temporal}$ of $MSAVI_2$ following USSES-region fires was similar among burned (7.2%) compared to unburned pasture (6.8%; Figure 4).

Mean $CV_{spatial}$ of $MSAVI_2$ increased 37% in the first post-fire year on INL pastures (Figure 5; $P = 0.09$) and then decreased over years to levels observed in unburned pasture. In contrast, $CV_{spatial}$ of $MSAVI_2$ in the USSES region decreased following fire, and the only statistically supported changes were 35% decreases in years 4-5 following fire ($P = 0.013$). At INL, $CV_{spatial}$ of $MSAVI_2$ recovered to levels observed in unburned areas more quickly in ungrazed areas compared to pasture.

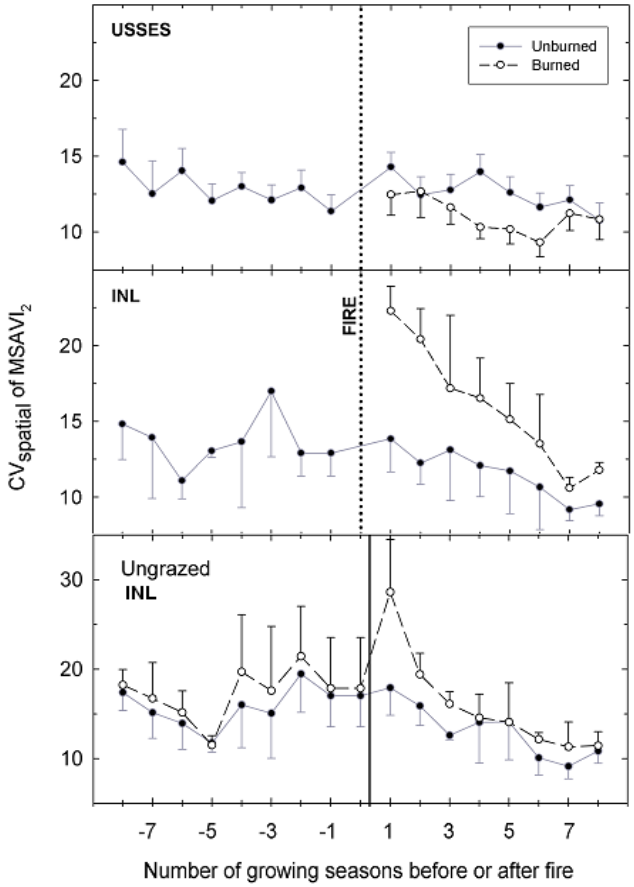

Figure 5. Comparison of mean CV of $MSAVI_2$ (+ or – 1 SE) among pixels ($CV_{spatial}$) of historically grazed lands on the USSES (top panel) and INL (bottom panel) study areas before or after fire. See Fig. 4 for plotting details. N = 3 burn-year blocks for INL and N = 4 for USSES.

Relationships to precipitation

No relationships of mean $MSAVI_2$ and yearly PPT were significant at the 0.05 level (not shown). In the USSES region, $CV_{spatial}$ of $MSAVI_2$ was mostly not correlated with annual precipitation, with the exceptions being small slopes of the relationship in 1994 for both burned and unburned sites (Figure 6, Table 1). In contrast, the slope of the relationship between $CV_{spatial}$ and PPT nearly doubled following fire on pastures at the INL ($F_{3, 11} = 10.80$, $P = 0.03$, Fig. 6, Table 1. The relationship between $CV_{spatial}$ and PPT was significantly for all burn sites on INL, with mean slopes of 0.132 on pasture compared to 0.123 on ungrazed areas. In contrast, the relationship on unburned areas, as well as overall unburned areas of INL was only significant in 1994, and moreover had small slopes (Table 1). In the unburned areas of INL

that had no shrubs, the slopes (mean = 0.154) were greater than on areas with the greatest abundances of sagebrush (mean = 0.109; $P < 0.000$, Table 1).

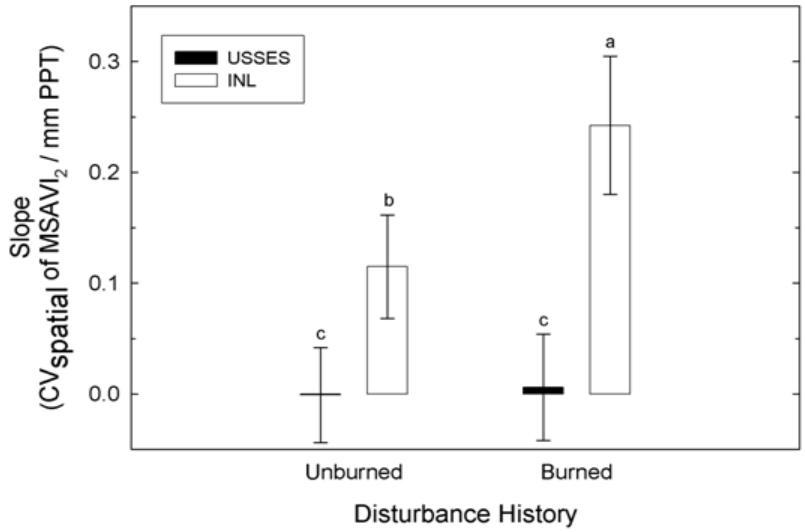

Figure 6. Mean slopes (+ or – 1 SD) of relationships between sliding three-year averages of cumulative yearly precipitation (PPT, from April 1 to image date) and post-fire $CV_{spatial}$ of $MSAVI_2$ among pixels to 2004, for unburned and burned pastures. Replicates were the three INL burn blocks, for areas burned in 1994, 1995, and 1996; and four clusters of burns in the USSES region, including areas burned in 1986, 1988, 1994, or 1998. Letters denote significantly different slopes according to MANOVA.

Table 1. Correlations of sliding three-year averages of cumulative yearly precipitation (from January to image date) and post-fire $CV_{spatial}$ of $MSAVI_2$ among pixels. N indicates the number of post-fire years up to 2004 included in regression analyses.

Region	Condition	Burn	r^2	*P*	Slope	N
USSES	Grazed	1986	0.0275	0.695	0.016	16
		1988	0.1406	0.360	-0.039	14
		1994	0.6764	**0.052**	0.012	9
		1998	0.1609	0.431	-0.039	6
	Grazed/Burned	1986	0.0017	0.922	-0.004	16
		1988	0.0389	0.640	-0.024	14
		1994	0.609	**0.022**	0.077	9
		1998	0.1678	0.420	-0.025	6
INL	Grazed	1994	0.647	**0.005**	0.058	10
		1995	0.080	0.460	0.015	9
		1996	0.064	0.545	0.014	8
	Grazed/Burned	1994	0.701	**0.003**	0.124	10
		1995	0.465	**0.043**	0.086	9
		1996	0.556	**0.034**	0.186	8
	Ungrazed/Burned	1994	0.631	**0.006**	0.080	10
		1995	0.568	**0.019**	0.105	9
		1996	0.556	**0.034**	0.186	8
	Ungrazed/Unburned	1994	0.466	**0.030**	0.057	10
		1995	0.355	0.091	0.075	9
		1996	0.456	0.066	0.064	8
	Ungrazed/Unburned	1994	0.545	**0.015**	0.104	10
	Sagebrush	1995	0.440	**0.051**	0.098	9
		1996	0.633	**0.018**	0.124	8
	Ungrazed/Unburned	1994	0.505	**0.021**	0.149	10
	Grassland	1995	0.392	**0.071**	0.137	9
		1996	0.576	**0.029**	0.175	8

DISCUSSION

Sagebrush steppe of lower elevations that are warmer, drier, and dominated by the Wyoming big sagebrush community type are commonly perceived to be more vulnerable than higher and wetter mountain big sagebrush communities to grazing and fire impacts. Whereas some field studies point to this assertion (e.g., Seefeldt et al. 2007), there have been few quantitative comparisons of fire effects in the two sagebrush types. Our findings that SVIs were greater, less variable, and quicker to recover following fire in mountain big sagebrush than Wyoming big sagebrush thus stands uniquely as evidence of less destabilizing effects of fire in smaller patches it occurs in, in the higher and cooler communities. Significantly, SVIs were constant among annual precipitation variations, nearly irrespective of fire occurrence, in the mountain big sagebrush. These findings indicate the possible existence of an ecosystem threshold in resilience and resistance to fire in this sagebrush biome, in which the drier Wyoming sagebrush appears to have strong responses to fire, but these responses (e.g., increased coupling of productivity to annual precipitation) are absent in the mountain big sagebrush.

Many studies have measured mean changes in plant cover of sagebrush-steppe in response to wildfire or grazing disturbances (e.g., Laycock 1967, Brotherson and Brotherson 1981, Humphrey 1984, Hosten and West 1994, Wambolt 2001, West and Yorks 2002). However, we found that variability in $MSAVI_2$, rather than average trends in $MSAVI_2$, was more sensitive to disturbance than mean $MSAVI_2$, for 8 – 10 years following fire. The immediate responses to fire in initial post-fire years were consistently observed despite climate variations among the burn years. In addition to these shorter-term responses, longer-term variability following fire for INL study areas appeared to result from increased coupling of $CV_{spatial}$ of $MSAVI_2$ to inter-annual changes in precipitation. Fire and grazing influenced the stability or spatio-temporal constancy of $MSAVI_2$ measures in sagebrush-steppe, in ways that were more persistent than their direct, immediate effects of vegetation removal. In contrast, we observed no changes in mean $MSAVI_2$ in any years following fire, and moreover observed variability to decrease post-fire and to be relatively insensitive to yearly precipitation in the USSES region.

Although mean $MSAVI_2$ significantly increased among burned lands the second growing season following fire on the INL, it appeared to recover to levels similar to nearby unburned lands by the third growing season after fire, irrespective of study area. These results contrast previous findings of post-fire vegetation recovery in Mediterranean oak-pine ecosystems, where NDVI derived from Landsat decreased substantially following fire but recovered to pre-fire levels after about a decade (Diaz-Delgado et al. 2002). Post-fire increases in SVI's in sagebrush-steppe compared to decreases in forests may be attributable to greater standing biomass and corresponding leaf area before fire in forests. In sagebrush-steppe ecosystems, resprouting species, especially herbs, tend to increase in abundance in response to fire (Humphrey 1984, Hosten and West 1994, West and Yorks 2002), probably in compensation to overall reductions of dominant sagebrush, a non-resprouting species that recovers slowly after fire. The lack of significant differences in $MSAVI_2$ after fire in the USSES region may reflect greater constancy in herb production, as would be expected with more reliable and abundant precipitation. Our observations of greater mean $MSAVI_2$ among grassland compared to sagebrush pixels, and in burned compared to unburned pixels agree with previous findings of greater SVI values in grassland compared to sagebrush communities (Kremer and Running 1993, Paruelo and Lauenroth 1995, Weiss et al. 2004, Bradley and Mustard 2005).

Increased variability in burned areas might reflect exclusion of shrubs and site dominance by herb cover. $MSAVI_2$ in sites dominated by sagebrush was less responsive to inter-annual variations in precipitation, compared to herb-dominated communities. Similarly, NDVI variability in time was greater in areas dominated by annual grass compared to shrubs (Bradley and Mustard 2005). Long-term field plots on the INL with higher shrub densities tended to exhibit less inter-annual variability in cover than plots with low shrub densities over 45 years (Anderson and Inouye 2001). Additional ground-based studies demonstrate that Wyoming big sagebrush cover varies less than herbaceous or annual species in response to drought

(estimated from data in Passey et al. 1982 and West and Yorks 2002). Less spatio-temporal variability of $MSAVI_2$ in sagebrush compared to herb dominated communities could result from the evergreen habit of sagebrush, which enables the plant to produce leaf area during favorable conditions and retain the foliage during less favorable periods. Thus, increased temporal and spatial variability (i.e. lower stability) among fire-disturbed lands on the INL could be partly due to reductions of shrub cover and compensating increases in herbaceous, and especially grass cover. While in contrast, decreased temporal and spatial variability (i.e. higher stability) among fire-disturbed lands on the INL could be partly due to reduced responses of herbaceous and grass cover.

Increases in $CV_{spatial}$ of $MSAVI_2$ after fire on INL pasture were more persistent than fire effects on ungrazed lands, and may be attributable to more than conversion of shrubs to grasses alone. Greater standing crop results from promotion of shrub over grass cover, leading to greater fuel loads and amplified intensity and severity of fire (DeBano et al. 1998). Increased fire severity may lead to greater site alterations (e.g. changes in soil physical properties) rather than just exclusion of shrubs and could thereby contribute to greater spatial and temporal variability in $MSAVI_2$. Interactions of fire and grazing thus appear to affect sagebrush-steppe communities in ways that are not detectable by simple assessments of mean responses, and moreover, cannot be predicted from linear combinations of the separate effects of grazing and fire.

Our data suggest that fire and grazing can have synergistic effects on the stability of vegetation indices in sagebrush-steppe, primarily by increasing the sensitivity of communities to variability in precipitation, especially in more arid regions where the amount and frequency of precipitation is less consistent. Burning on the INL influenced the long-term response of vegetation in grazed lands differently from ungrazed lands by causing greater increases in the variability of $MSAVI_2$ with increased precipitation. However, this relationship was not observed in grazed lands that burned on the USSES. There was no coupling of $MSAVI_2$ to precipitation, possibly a result of more reliable pre-summer wetting in the USSES region compared to the INL. It is likely that the INL findings could result from pre-fire alterations of community composition by livestock that tend to decrease variability in $MSAVI_2$ until after fire, when variability in $MSAVI_2$ becomes even greater than in burned areas that were not grazed before fire. While changes in precipitation occur due to climate change, the response of sagebrush-steppe rangelands to changes in precipitation may be particularly dependent upon the history of fire and grazing, especially for lands that experience significantly less annual precipitation, such as the INL. Our results indicate that studies seeking to determine fire and grazing impacts should encompass multiple years, consideration of different levels of variation in spatial heterogeneity among sites with different histories of disturbance, and precipitation in sampling among years. Similarly, large-scale assessments linking climate variability and ecosystem productivity will likely reflect disturbance legacies.

ACKNOWLEDGEMENTS

This research was funded by a NASA grant. Ronald C. Rope at INL, and Glenn Guenther and Brett Herres of the BLM provided site or livestock grazing information. ISU would also like to acknowledge the Idaho Delegation for their assistance in obtaining this grant.

LITERATURE CITED

Adler, P.B., and W.K. Lauenroth. 2000. Livestock exclusion increases the spatial heterogeneity of vegetation in Colorado shortgrass steppe. Applied Vegetation Science 3: 213-222.

Adler, P.B., D.A. Raff, and W.K. Lauenroth. 2001. The effect of grazing on the spatial heterogeneity of vegetation. Oecologia. 128: 465-479.

Anderson, J.E., and K.E. Holte. 1981. Vegetation development over 25 years without grazing on sagebrush-dominated rangeland in southeastern Idaho. J. Range Manage. 34(1): 25-29.

Anderson, J.E., and R.S. Inouye. 2001. Landscape-scale changes in plant species abundance and biodiversity of a sagebrush steppe over 45 years. Ecological Monographs. 71(4): 531-556.

Bradley, A.B., and J.F. Mustard. 2005. Identifying land cover variability distinct from land cover change: Cheatgrass in the Great Basin. Remote Sens. Environ. 94: 204-213.

Brotherson, J.D., and W.T. Brotherson. 1981. Grazing impacts on the sagebrush communities of central Utah. Great Basin Naturalist. 41(3): 335-340.

Daddy, F., M.J. Trlica, and C.D. Bonham. 1988. Vegetation and soil water differences among big sagebrush communities with different grazing histories. Southwestern Naturalist. 33(4): 413-424.

DeBano, L.F., D.G. Neary, and P.F. Ffolliott. 1998. Fire's effects on ecosystems. John Wiley & Sons, Inc., New York, NY. 333 pp.

Diaz-Delgado, R., L. Francisco, X. Pons, and J. Terradas. 2002. Satellite evidence of decreasing resilience in Mediterranean plant communities after recurrent wildfires. Ecology. 83(8): 2293-2303.

Foran, B.D., and G. Pickup. 1987. The use of spectral and spatial variability to monitor cover change on inert landscapes. Remote Sens. Environ. 23: 351-363.

Geiger, E.L., and G.R. McPherson. 2005. Response of semi-desert grasslands invaded by non-native grasses to altered disturbance regimes. J. Biogeography. 32: 895-902.

Graetz, R.D., and M.R. Gentle. 1982. The relationships between reflectance in the Landsat wavebands and the composition of an Australian semi-arid shrub rangeland. Photo. Eng. Rem. Sens. 48: 1721-1730.

Hanser, S., S. Knick, J. Hak, and J. Kagan. 2005. Current Distribution of Sagebrush and Associated Vegetation in the Columbia Basin and Southwestern Regions Edition: version 1.0. USGS, Forest and Rangeland Ecosystem Science Center, Snake River Field Station. http://sagemap.wr.usgs.gov

Hosten, P.E., and N.E. West. 1994. Cheatgrass dynamics following wildfire on a sagebrush semidesert site in central Utah. Proceedings–Ecology and management of annual rangelands. INT-GTR-313. Ogden, UT: U.S. Department of Agriculture, Forest Service, Intermountain Research Station: 56-62.

Humphrey, L.D. 1984. Patterns and mechanisms of plant succession after fire on Artemisia-grass sites in southeastern Idaho. Vegetatio. 57: 91-101.

Jensen, J.R. 1996. Introductory digital image processing. Prentice-Hall, Inc., Upper Saddle River, NJ. 318 pp.

Kramber, W.J., R.C. Rope, J.E. Anderson, J. Glennon, and A. Morse. 1992. Producing a vegetation map of the Idaho National Engineering Lab using Landsat thematic mapper data. American Society for Photogrammetry and Remote Sensing/American Congress on Surveying and Mapping Annual Meeting Technical Papers Vol. 1:217-226.

Kremer, R.G., and S.W. Running. 1993. Community type differentiation using NOAA/AVHRR data within a sagebrush-steppe ecosystem. Remote Sens. Environ. 46: 311-318.

Lauenroth, W.K., and O.E. Sala. 1992. Long-term forage production of North American shortgrass steppe. Ecological Applications. 2(4): 397-403.

Laycock, W. 1991. Stable states and thresholds of range condition on North American rangelands: A viewpoint. J. Range Manage. 44: 427-433.

Laycock, W.A. 1967. How heavy grazing and protection affect sagebrush-grass ranges. J. Range Manage. 20: 206-213.

Le Houerou, H.N., R.L. Bingham, and W. Skerbek. 1988. Relationship between the variability of primary production and the variability of annual precipitation in world arid lands. J. Arid Environ. 15: 1-18.

Magnuson, J.J., Kratz, T.K., Frost, T.M., Browser, C.J., Benson, B.J., and Nero, R. 1991. Expanding the temporal and spatial scales of ecological research and comparison of divergent ecosystems: Roles of LTER in the United States. *Long term ecological research: an international perspective* (ed. By P.G. Risser). Scope 47. John Wiley and Sons, Chichester.

McGwire, K., T. Minor, and L. Fenstermaker. 2000. Hyperspectral mixture modeling for quantifying sparse vegetation cover in arid environments. Remote Sens. Environ. 72: 360-374.

Milchunas, D.G., and W.K. Lauenroth. 1993. Quantitative effects of grazing on vegetation and soils over a global range of environments. Ecol. Monogr. 63(4): 327-366.

Passey, H.B., V.K. Hugie, E.W. Williams, and D.E. Ball. 1982. Relationships between soil, plant community, and climate on rangelands of the Intermountain West. Technical Bulletin Number 1669. USDA Soil Conservation Service, Washington, D.C., USA.

Paruelo, J.M., I.C. Burke, and W.K. Lauenroth. 2001. Land-use impact on ecosystem functioning in eastern Colorado, USA. Global Change Biology. 7: 631-639.

Paruelo, J.M., and W.K. Lauenroth. 1998. Interannual variability of NDVI and its relationship to climate for North American shrublands and grasslands. J. Biogeography. 25: 721-733.

Paruelo, J.M., and W.K. Lauenroth. 1995. Regional patterns of normalized difference vegetation index in North American shrublands and grasslands. Ecology. 76(6): 1888-1898.

Pickett, S.T.A., and P.S.E. White. 1985. The ecology of natural disturbance and patch dynamics. Academic Press, Orlando, FL.

Pickup, G., V.H. Chewings, and D.J. Nelson. 1993. Estimating changes in vegetation cover over time in arid rangelands using Landsat MSS data. Remote Sens. Environ. 43: 243-263.

Pickup, G. and B.D. Foran. 1987. The use of spectral and spatial variability to monitor cover changes on inert landscapes. Remote Sens. Environ. 23: 351-363.

Purevdorj, T., R. Tateishi, T. Ishiyama, and Y. Honda. 1998. Relationship between percent vegetation cover and vegetation indices. Int. J. Remote Sens. 19(18): 3519-3535.

Qi, J., A. Chehbouni, A.R. Huete, H. Kerr, and S. Sorooshian. 1994. A modified soil adjusted vegetation index. Remote Sens. Environ. 48: 119-126.

Ramsey, R.D., D.L. Wright, Jr., and C. McGinty. 2004. Evaluating the use of Landsat 30m Enhanced Thematic Mapper to monitory vegetation cover in shrub-steppe environments. Geocarto International. 19(2): 39-47.

Reed, B.C., J.F. Brown, D. VanderZee, T.R. Loveland, J.W. Merchant, and D.O. Ohlen. 1994. Measuring phenological variability from satellite imagery. J. Vegetation Science. 5: 703-714.

Rondeaux, G., M. Steven, and F. Baret. 1996. Optimization of soil-adjusted vegetation indices. Remote Sens. Environ. 55: 95-107.

Senseman, G.M. and C.F. Bagley. 1996. Correlation of rangeland cover measures to satellite-imagery-derived vegetation indices. Geocarto International. 11(3): 29-38.

Skidmore, A.K., B.O. Oindo, and M.Y. Said. 2003. Biodiversity assessment by remote sensing. In: Proceedings of the 30th International Symposium on Remote Sensing of the Environment: Information for Risk Management and Sustainable Development, November 10-14, 2003, Honolulu, Hawaii. 4 pp.

Small, C.J., and B.C. McCarthy. 2003. Spatial and temporal variability of herbaceous vegetation in an eastern deciduous forest. Plant Ecology. 164(1): 37-48.

Stohlgren, T.J., D. Binkley, G.W. Chong, M.A. Kalkhan, L.D. Schell, K.A. Bull, Y. Otsuki, G. Newman, M. Bashkin, and Y. Son. 1999. Exotic plant species invade hot spots of native plant diversity. Ecological Monographs. 69(1): 25-46.

Valone, T.J. 2003. Examination of interaction effects of multiple disturbances on an arid plant community. Southwestern Naturalist. 48(4): 481-490.

Wallace, J.F., P.A. Caccetta, and H.T. Kiiveri. 2004. Recent developments in analysis of spatial and temporal data for landscape qualities and monitoring. Austral Ecology. 29: 100-107.

Wambolt, C.L., K.S. Walhof, and M.R. Frisina. 2001. Recovery of big sagebrush communities after burning in south-western Montana. J. Environ. Manage. 61: 243-252.

Washington-Allen, R.A., R.D. Ramsey, and N.E. West. 2004. Spatiotemporal mapping of the dry season vegetation response of sagebrush steppe. Community Ecology 5(1): 69-79.

Weiss, J.L., D.S. Gutzler, J.E. Allred Coonrod, and C.N. Dahm. 2004. Long-term vegetation monitoring with NDVI in a diverse semi-arid setting, central New Mexico, USA. J. Arid Environ. 58: 248-271.

West, N.E., and T.P. Yorks. 2002. Vegetation responses following wildfire on grazed and ungrazed sagebrush semi-desert. J. Range Manage. 55: 171-181.

West, N.E., and J.A. Young. 2000. Intermountain valleys and lower mountain slopes. In: M.G. Barbour and W.D. Billings (eds), *North American Terrestrial Vegetation*. 2nd ed. Cambridge Univ. Press, New York, NY. pp. 255-284.

West, N.E., K.H. Rea, and R.O. Harniss. 1979. Plant demographic studies in sagebrush-grass communities of southeastern Idaho. Ecology. 60: 376-388.

Whitford, W.G. 2002. Ecology of Desert Systems. Academic Press, London. 343 pp.

Improving Classification Accuracy Assessments with Statistical Bootstrap Resampling Techniques

Keith T. Weber, GIS Director, Idaho State University GIS Center, 921 S. 8th Ave. Stop 8104, Pocatello, Idaho 83209-8104, webekeit@isu.edu

Jackie Langille, Central Washington University, 2203 Brooksfield Ellensburg, WA 98926, langille@geology.cwu.edu

ABSTRACT
The use of remotely sensed imagery to generate land cover models is common today. Validation of these models typically involves the use of an independent set of ground-truth data which are used to calculate an error matrix resulting in estimates of omission, commission, and overall error. However, each estimate of error contains a degree of uncertainty itself due to 1) conceptual bias, 2) location/registration and co-registration errors, and 3) variability in the sample sites used to produce and validate the model. In this study, focus was not placed upon describing land cover mapping techniques, but rather the application of bootstrap resampling to improve the characterization of classification error, demonstrate a method to determine uncertainty from sample site variability, and calculate confidence limits using statistical bootstrap resampling of 500 sample sites acquired within a single Landsat 5 TM image. The sample sites represented one of five land cover categories (water, roads, lava, irrigated agriculture, and rangelands) with each category containing 100 samples. The sample set was then iteratively resampled (n=200) and 65 sites were randomly selected (without replacement) for use as classification training sites while the balance (n=35) were used for validation. Imagery was subsequently classified using a maximum likelihood technique and the model validated using a standard error matrix. This classification-validation process was repeated 200 times. Confidence intervals were then calculated using the resulting omission and commission errors. Results from this experiment indicate that bootstrap resampling is an effective method to characterize classification uncertainty and determine the effect of sample bias.

KEYWORDS: Remote sensing, accuracy assessment, uncertainty, error, confidence intervals

INTRODUCTION

Classification of remotely sensed imagery provides a means to model the earth's surface (Lillesand and Kiefer 2004). Studies implementing this technology have ranged from mapping weeds (Glenn et al., 2005; Lass et al., 2005; Gokhale and Weber, 2006) to modeling wildfire susceptibility (Ercanoglu et al., 2006), forecasting urban growth (McMahan et al., 2002), and a multitude of other applications. In theory, and based upon the results of other scientists (Boardman, 1993; Ray and Murray, 1998; Roberts et al., 1998) classification accuracy is a function of a pixel's spectral similarity to the training sites (pixels with a high proportion of target material). As a result, pixels having high proportions of the target (more spectrally pure) will generally classify correctly more often than pixels containing a lower proportion of target material (spectrally mixed), assuming uniform reflectance characteristics of all objects within each pixel (Mundt et al., 2006).

Regardless of the scale, scope, or resolution of image classification, error assessment is a critical step in the analysis and interpretation process (Stehman and Czaplewski, 1998;, Janssen and van der Wel, 1994). The development of current error assessment techniques has occurred in three stages (Congalton and Green, 1999): 1) no constraint, 2) qualitative general assessments (non-site specific), and 3) quantitative site specific assessments. Longley et al. (2005) similarly describe uncertainty and its assessment as beginning with one's conception of the real-world as this affects how one perceives, observes, defines, and categorizes the world. In turn, one's paradigm influences, and perhaps even drives, measurements and representations which consequently affect nominal classification accuracy assessments. We fully realize this inherent error exists and is an important consideration when one attempts to model natural systems using crisp logic (Sauder et al., 2003). Thus, the quantification of classification error contains both true classification error (the classification algorithm made a mistake) and conception error (how one observes the natural world during the acquisition of training sites) which are inextricably linked together.

Today, classification accuracy is frequently determined using an error matrix of predicted (classified) versus known (reference) occurrences of a target (Congalton, 1991). These tabulations produce estimates of omission, commission, and overall error, and may also be used to calculate statistical measures of accuracy such as Kappa, Tau, and Z-statistics (Titus et al., 1984; Ma and Redmond, 1995; Congalton and Green, 1999; Foody 2002, 2004). While an error matrix is commonly used to tabulate classification accuracy, the number of samples necessary to validate the model is debated, because sample size relates directly to power of analysis (Cohen, 1992, Taylor and Gerrodette, 1993), which is a function of sample site variability, and total project cost. Congalton (1991) stated that "sufficient samples must be acquired to be able to adequately represent the confusion" (i.e., the categories and types of errors committed in the model). One option to accommodate high variability and to assess its effect on classification results is the use of bootstrap resampling. Applying bootstrap resampling does not imply that classifications should be made with an insufficient number of samples. Rather, bootstrap resampling presents a methodology to make better use of the samples available and more easily determine the adequacy of the existing sample set. The authors note that this paper does not attempt to determine minimum sample size as other resources are currently available to aid in this decision such as the recent work published by Van Niel et al. (2005) and Foody et al (2006) and Foody and Mathur (2006).

To improve the reliability of error calculations and better characterize uncertainty, statisticians have applied various techniques including bootstrap resampling (Good, 2005; Efron, 1979). This technique has also been applied with spatial data (Mahalanobis, 1946; Hall, 2003) and remote sensing studies (Okeke and Karniele, 2006; Verbyla and Boles 2000; McMahan and Weber 2003). The general idea behind bootstrap resampling is that with a sufficiently large set of samples one can treat the sample set as representative of a population. By dividing the sample set into classification and validation sub-sets one can perform a classification and then validate the resulting classification to arrive at an estimate of classification accuracy using only a single sample set. To reduce the effects of bias (i.e., the difference in

the type of samples chosen for training versus validation), the sample set can be iteratively resampled to draw new classification and validation sub-sets. Using this process a more robust estimation of uncertainty can be achieved as the user retains the use of all samples and consequently, statistical power, while producing a better characterization of classification error where confidence intervals are calculated directly (cf. Snedecor and Cochran, 1967). This paper explores a parallel approach to classification error assessment and applies iterative bootstrap resampling to improve the characterization of classification error and better represent bias within the sample set (Jones, 1956; Efron, 1979; Good, 2005). An interesting alternative to this and other methods based upon the standard error matrix is the fuzzy error matrix described by Binaghi et al. (2005) and the calculation of misclassification probability as described by Steele et al (1998). The latter applies Kriging and a lattice of training locations to construct an accuracy model similar to a contour map. This tool, however, has not been as broadly applied or accepted as the error matrix.

METHODS

To explore the use of iterative bootstrap resampling to improve error assessment of remote sensing classifications, we designed an experiment using 500 sample points collected from one of five distinct land cover categories (water, roads, lava, irrigated agriculture, and rangelands, respectively) within a study area in southeastern Idaho (Figure 1). One-hundred points (pixels) were acquired within each category using standard on-screen digitizing and one Landsat 5 TM scene (path 39, row 30) acquired on 7-July-2003. One meter digital orthophotos were used to ensure each sample point was clearly located within the correct land cover type. In addition, sample points were corroborated using field observations made during the summer of 2003 (n=253). For each class, sixty-five sample points were randomly selected without replacement for use as training sites while the remainder (n=35) were used for validation. These points were then rasterized using the same spatial parameters as the satellite imagery used for classification (28.5 x 28.5 m).

Landsat imagery was prepared for classification by generating a normalized difference vegetation index (NDVI) and principal component analysis (PCA) images (Eastman, 2003) from raw radiance values (brightness values or DN). The first two PCA bands (PCA-C1 and PCA-C2) contained >95% of the unique spectral variance, therefore the NDVI and two PCA raster images were used for classification. This approach is justified because previous studies have found these data reliable (Rouse et al., 1973; Kriegler et al., 1969) and have applied these data for land cover characterization with positive results (Ingebritsen and Lyon 1985, Singh 1989, Collins and Woodcock 1996, Savage 2005). Two-hundred classification-validation iterations were completed using maximum-likelihood classification in Idrisi Kilimanjaro software (Eastman, 2003). For each iteration, accuracy was assessed using standard error matrices. Each classification-validation iterations included 65 training samples and 35 validation samples, respectively. The goal of this study was not to produce perfect classification results, but rather to explore the use of bootstrap resampling to better assess classification error and bias within the sample set while applying well documented classification techniques. We assumed that sample sites exhibited some degree of autocorrelation (Tobler 1970, Miller 2004) but due to the size of the study area (approximately 35,144 km^2) and distribution of sample sites, spatial autocorrelation was not considered a confounding factor. Geo-registration and co-registration of training and validation sample sites were also considered and explored as a source of error. To explore potential error we used on-screen techniques where we zoomed into each site (approximate scale = 1:1,000) and using both Landsat imagery and NAIP orthoimagery (true color 1-m spatial resolution) were able to verify the category assigned to each site. It should be noted that the categories used in this study were general (water, roads, lava, irrigated agriculture, and rangelands) and thereby, easily verified and differentiated from one another. Thus, the above errors were considered minimal for two reasons; 1) sites were acquired using careful on-screen digitizing and verification and 2) the size of each pixel (28.5 x 28.5 m) made it relatively easy to place a sample site point within it, thereby minimizing co-registration error (Weber, 2006).

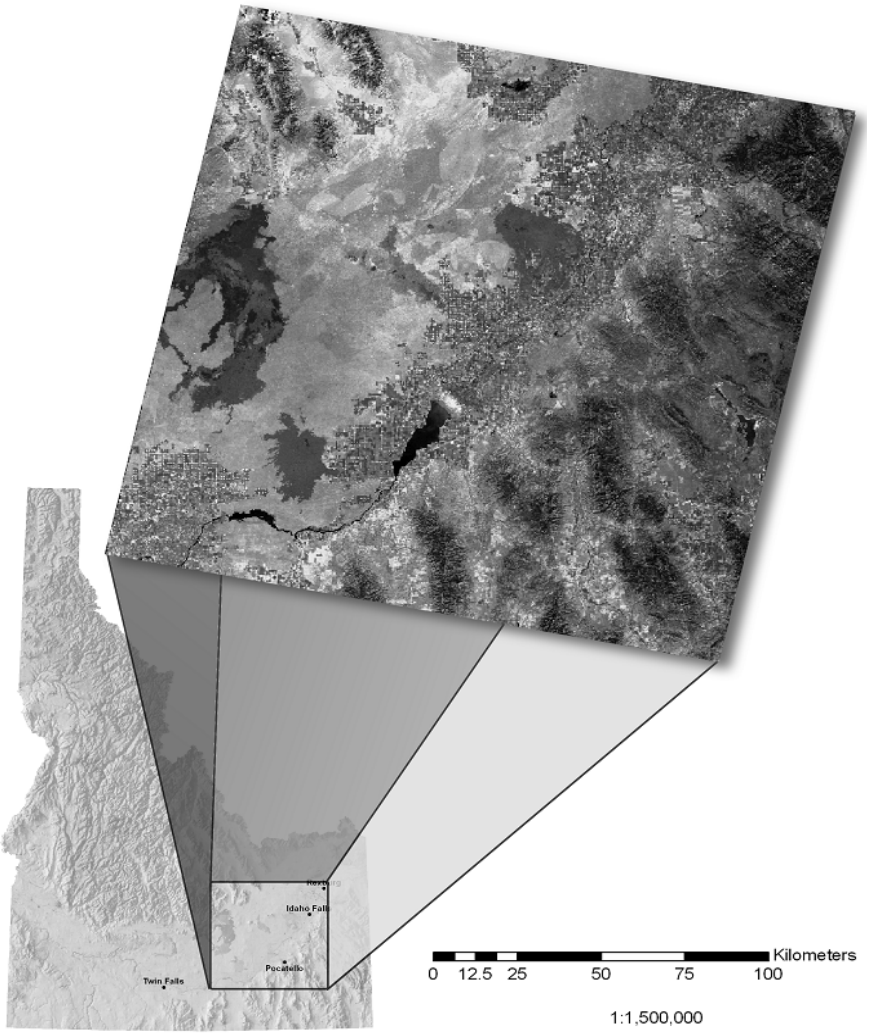

Figure 1. The study area location and Landsat 5 TM imagery used in this research (path 39, row 30, acquired 7-July-2003).

The resulting omission and commission errors from each classification error assessment were then entered into a Microsoft Excel spreadsheet. To determine the minimum number of iterations required for classification error characterization, various statistical techniques have been used such as the cumulative variance approach described by Mundt et al. (2005). We applied an approach similar to Mundt et al. (2005) where cumulative standard deviation (standard error) was graphed for omission and commission errors. The resulting graphs were then investigated to determine the first point at which a "practical sill" has been achieved. The practical sill was defined as the point where the curve developed by the standard error plot has dropped to within 5% of the asymptote, or conversely, has dropped 95% of the difference observed between maximum and minimum standard error (Isaaks and Srivastava 1990) (Equation 1). The number of classification-validation iterations required to achieve the "practical sill" can then be determined by calculating a line of best fit using either inverse or exponential functional forms. This was accomplished in Microsoft Excel by fitting a trend line to the curve and using the equation of the line and its R^2 value. If the fit is sufficient (we suggest a threshold R^2 of 0.70) the minimum number of iterations is then calculated by finding X when Y (i.e., S_p) is known. Alternatively, the number of iterations can be read from the figure itself. Ultimately, all methods are in some ways subjective in that the user must decide the threshold or point at which inflection occurs or where the variance curve "flattens". Using a

Microsoft Excel spreadsheet containing all classification/validation iterations (n=200) also enabled us to directly calculate the 95% confidence interval describing classification error (Good, 2005, NBII, 2006).

$$R = SE_{max} - SE_{min}$$
$$S_p = SE_{max} - 0.95R \quad \text{Eq. 1}$$

Where R is the range and S_p is the practical sill.

RESULTS AND DISCUSSION

The resulting error from two of the 200 classification iterations were randomly selected and given in Tables 1 and 2. These classification results illustrate the variability in accuracies where a randomly selected subset (n=65) of training sites were used for classification. The variability between the two example classification results illustrates a scenario where one or more of the target features exhibit overlapping spectral signatures. To visualize the characteristics of these spectral signatures (n=65), we used spectral comparison charts where each cover class' minimum, maximum, and mean value was displayed for each band (e.g., PCA-C1, PCA-C2, and NDVI). Referring to the signature comparison charts (Figure 2) one can see the water class overlaps with or encompasses several other classes. We speculate this is because some of the water training sites may have been located in shallow water where vegetation, rocks, or substrate affected the spectra. However this did not adversely affect the goal of this study as the authors sought to understand the effect of training site selection and resampling selections on classification accuracy. Indeed this variability and difficulty aided the author's in their goal. Further, some of the training sites may have been in areas where algae or turbidity affected the spectra. In cases like this, where seperability (Richards, 2005) is problematic, one can apply statistical purification (McKay and Campbell, 1982; Eastman, 2003) to the training sites and/or use canonical correlation analysis (Eastman, 2003) of the imagery instead of the principal components analysis used in this study. Purifying spectral signatures effectively makes the signatures more homogenous or uniform by removing training sites that fall outside the typicality threshold. This may not be a viable option, however, if reducing the sample size (i.e., training sites) results in loss of statistical power (Cohen 1992, Taylor and Gerodette, 1993) as it would have been in this case.

Table 1. Sample of percent classification error where 65 points were randomly selected for classification and 35 points were used for validation from a total sample set of 100 points per class.

Class	Water	Roads	Lava	Irrigated Agriculture	Rangelands	Sum	Commission Error (%)
Water	2	0	0	0	0	2	0
Roads	4	25	1	0	2	32	22
Lava	7	0	33	0	0	40	18
Irrigated Agriculture	3	0	0	31	0	34	9
Rangelands	7	3	0	0	29	39	26
Unclassified	12	7	1	4	4	28	
Sum	35	35	35	35	35	175	
Omission Error (%)	94	29	6	11	17		31

Table 2. Sample of percent classification error where a second set of 65 randomly selected points were used for classification and 35 points were used for validation from the same sample set of 100 points per class.

Class	Water	Roads	Lava	Irrigated Agriculture	Rangelands	Sum	Commission Error (%)
Water	35	0	0	0	0	35	0
Roads	0	32	1	0	0	33	3
Lava	0	0	34	0	0	34	0
Irrigated Agriculture	0	0	0	34	0	34	0
Rangelands	0	1	0	0	35	36	2
Unclassified	0	2	0	1	0	3	
Sum	35	35	35	35	35	175	
Omission Error (%)	0	8	2	2	0		2

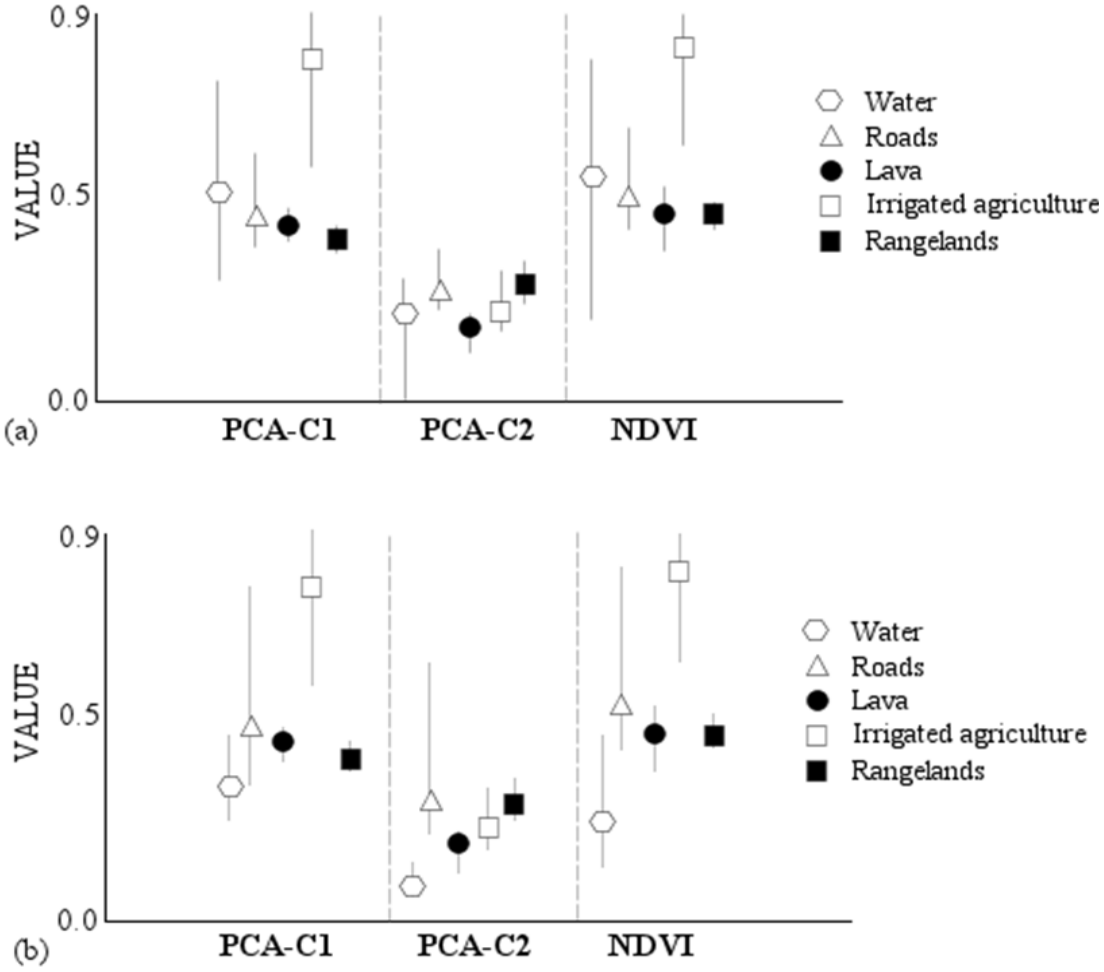

Figure 2. (a,b) Minimum, maximum, and mean spectral signature values for the training sites (n=65) used in this study. Fig 2a represents signatures used to produce classification results reported in table one. Fig. 2b represents signatures used to produce classification results reported in table two.

Based upon the results of bootstrap resampling, a 95% confidence interval was calculated using all classification-validation iterations (n=200) (Table 3). Not surprisingly, the water class had very broad

commission and omission errors. Other classes performed better resulting in a tighter range of commission and omission errors.

Table 3. Calculated error (at 95% confidence) for each class based upon 200 classification-validation iterations.

Class	Commission error	Omission error
Water	0.00 - 0.50	0.01 - 0.97
Roads	0.00 - 0.26	0.08 - 0.31
Lava	0.00 - 0.27	0.00 - 0.14
Irrigated agriculture	0.00 - 0.23	0.02 - 0.18
Rangelands	0.00 - 0.26	0.00 - 0.20

The use of additional sample points (pixels) or the use of sample polygons instead of sample points may have improved classification results and reduced the number of iterations required to achieve the "practical sill". However, the methods used to explore and understand training site variability (bootstrap resampling) and determine the practical sill would remain unchanged.

By inspecting graphs of cumulative standard error (SE) for omission error (producer's accuracy), the minimum number of classification-validation iterations required to capture classification variability was determined as the point where SE met the practical sill (Figure 3). The least number of iterations required to achieve the "practical sill" was 82 iterations for the lava land cover class. Table 4 gives calculated error at 95% confidence where only the first 82 classification-validation iterations were used for all cover classes. Notice that the other cover classes responded differently and required from 91 to 656 classification-validation iterations to achieve their "practical sill" (Table 5). While the authors only performed 200 classification-validation iterations, the value of 656 was derived synthetically using the regression line was fitted to SE curve, and solving for the number of iterations required to achieve the practical sill. To minimize repetition in the rest of this paper, only results from the lava cover class will be discussed. Further, as this technique was designed to improve the characterization of classification error and determine the effect of sampling bias due to training site heterogeneity, we will focus upon omission error (producer's accuracy).

Table 4. Calculated error (at 95% confidence) for the each land cover class based upon 82 classification-validation iterations[1].

Class	Commission error (%)	Omission error (%)
Water	0.0 – 75.0	4.0 – 97.0
Roads	2.0 – 23.0	11.0 – 27.0
Lava	0.0 – 25.0	0.0 – 15.0
Irrigated agriculture	0.0 – 21.0	3.0 – 18.0
Rangelands	2.0 – 26.0	3.0 – 23.0

1- Eighty-two classification-validation iterations were used as the minimum number of iterations necessary to achieve the "practical sill" derived from the standard error curve for the lava cover class (figure 3).

Table 5. The minimum number of classification-validation iterations required to achieve the practical sill[1]

Class	Iterations required	R^2 for line of best fit
Water	210[2]	0.894
Roads	102	0.380
Lava	82	0.989
Irrigated agriculture	656[2]	0.470
Rangelands	91	0.923

1. Based upon the cumulative standard error calculated from omission error.
2. These values were derived synthetically using the regression equation to estimate the number of iterations required to achieve the practical sill.

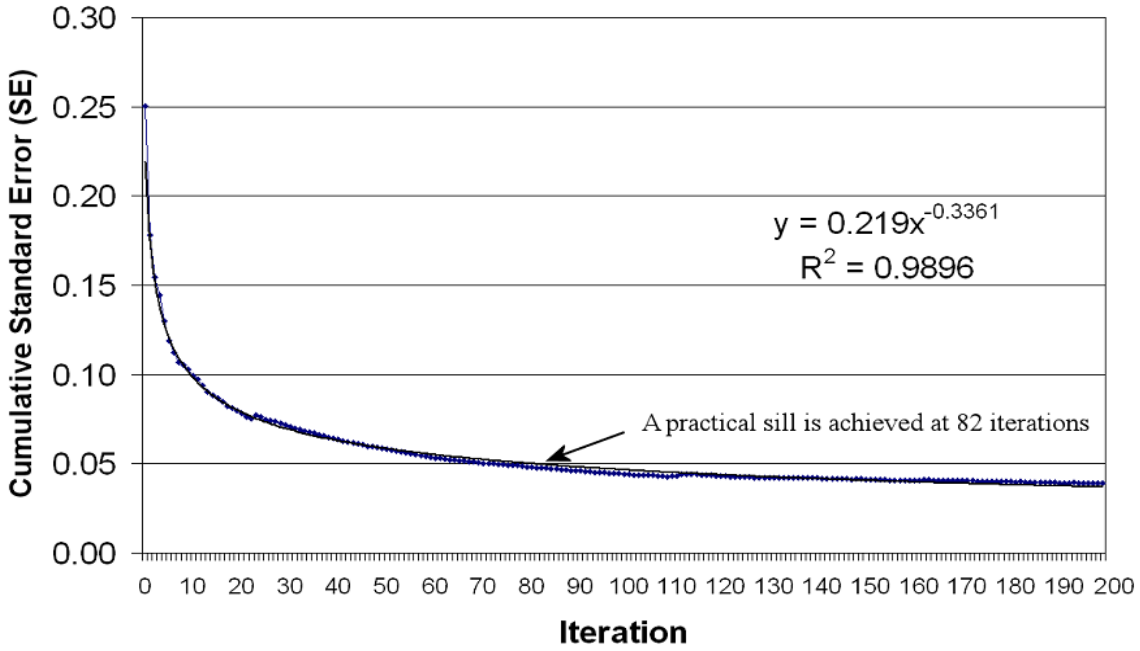

Figure 3. Example of how the minimum number of iterations required to capture the variability in classification error was determined (note: this graph represents cumulative standard error of omission error for the lava cover class). The equation describing the exponential line of best fit is given along with the R-squared value.

The difference between calculated error using 200 versus 82 classification-validation iterations is shown in Figure 4 for the lava land cover class. Based upon these results we concluded that 82 classification-validation iterations were an adequate number to characterize classification error within this cover class. It should be pointed out that –like the other land cover classes used in this paper-- other data sets may require more or perhaps fewer classification-validation iterations. Following the procedures described in this paper, one can easily determine a "practical sill" from SE curves and hence, the minimum number of iterations required for classification error characterization. From these data, one can infer a great deal about sample set bias as the number of iterations required is a function of training site variability (high variability training sites will require additional iterations) along with imagery characteristics such as radiometric, spatial, and spectral resolution, as well as scale of analysis.

CONCLUSIONS

The study was performed to better understand the effect of training site selection and subset resampling on classification accuracy. As a result of this focus, the authors were not concerned about classification accuracy or the development of a reliable land cover mapping technique. Rather, this study focused upon the application of bootstrap resampling to improve the characterization of classification error and hence, uncertainty is a time-consuming process. However, based upon the results of this study, bootstrap resampling greatly improved our understanding of classification uncertainty because variability of classification accuracy was determined, which led to a better understanding of the influence of training site heterogeneity (sample bias). This study indicates that after calculating standard error for any number of classification-validation iterations, if one notices a cumulative standard error that approximates an exponential curve it should be clear that the heterogeneity within the training sites is large and may have significant effects upon classification results. Further, if the asymptote or practical sill is not reached with the number of iterations performed (note the associated low R^2 value (Table 5) for the line fitted to the cumulative SE curve), this indicates the training sites are extremely heterogeneous, requiring the application of either 1) spectral signature purification, 2) spectral mixture analysis, 3) some form of data reduction technique, or 4) additional sample points. We note that this process, like all other statistically-based techniques, requires a sufficient number of observations per class/category to allow subsets to be created that retain statistical power of analysis. Bearing this in mind, bootstrap resampling can be applied to improve the characterization of classification error regardless of the type of imagery, satellite sensor, or classification methodology used.

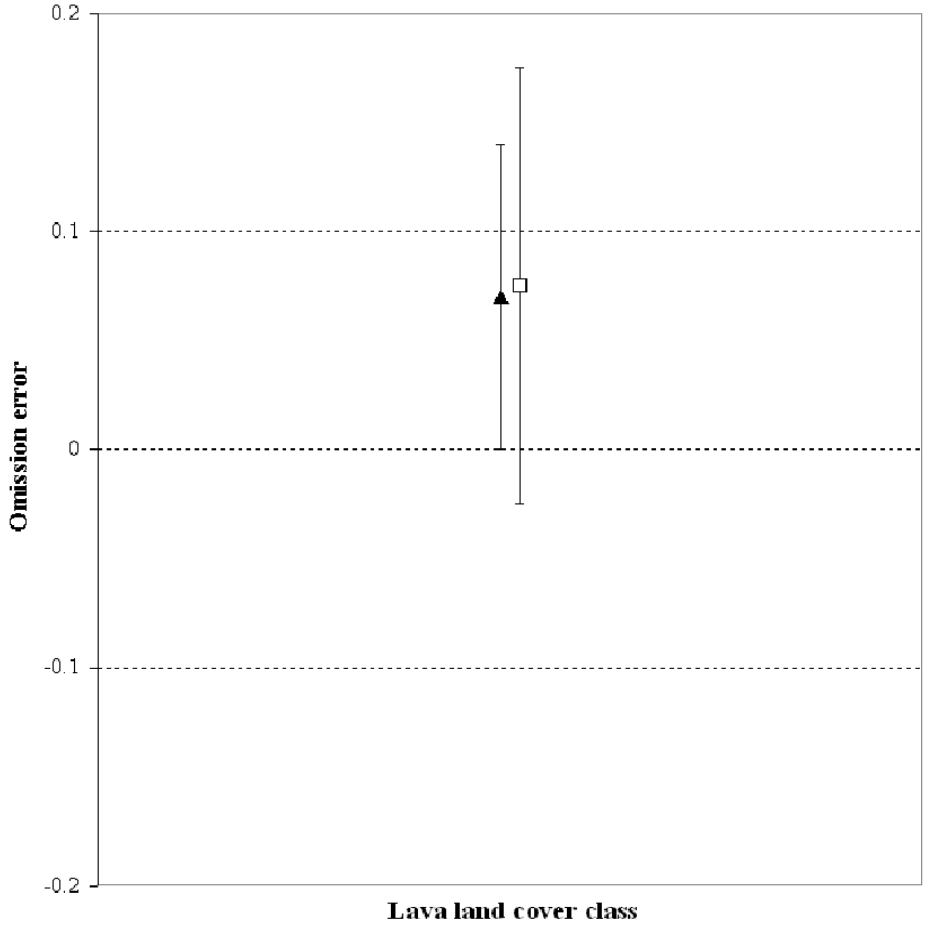

Figure 4. Differences between calculated omission error based upon 200 classification-validation iterations (triangles) and 82 classification-validation iterations (squares). Note: the marker symbol is used to indicate the mean while the whiskers represent a 95% confidence interval of the estimated distribution of errors.

ACKNOWLEDGEMENTS
This study was made possible by a grant from the National Aeronautics and Space Administration Goddard Space Flight Center. ISU would also like to acknowledge the Idaho Delegation for their assistance in obtaining this grant and the assistance of Nancy Glenn, Jacob Mundt, John Welhan and Teri Peterson for their assistance and advice.

LITERATURE CITED

Binaghi E., P. A. Brivio, P. Ghezzi, and A. Rampini. 1999. A fuzzy set-based accuracy assessment of soft classification. Pattern Recognition Letters 20 (1999) 935-948.

Boardman J.W. 1993. Automating spectral unmixing of AVIRIS data using convex geometry concepts. In: Summaries of the Fourth Annual JPL Airborne Geoscience Workshop. pp. 11-14. JPL Publication 93-26, Arlington, VA.

Cohen, J. 1992. Statistical Power Analysis for the Behavioral Sciences. LEA. 567 pp.

Collins, J.B. and C.E. Woodcock. 1996. An assessment of several linear change detection techniques for mapping forest mortality using multitemporal Landsat TM data. Remote Sensing of Environment, 56: 66-77.

Congalton R.G. 1991. A review of assessing the accuracy of classifications of remotely sensed data. Remote Sensing of Environment, 37, 35-46.

Congalton R.G. and K. Green. 1999. Assessing the Accuracy of Remotely Sensed Data: Principles and Practices. Boca Raton: Lewis Publishers. 160pp.

Eastman R. J. 2003. Idrisi Kilimanjaro Guide to GIS and Image Processing. Clark University Laboratory.

Efron B. 1979. Bootstrap methods: Another Look at the Jackknife. Annals of Statistics. 7(1):1-26

Ercanoglu, M., K. T. Weber, J. M. Langille, and R. Neves. 2006. Modeling Wildland Fire Susceptibility Using Fuzzy Systems. GIScience and Remote Sensing 43(3):268-282.

Foody G. M. 2002. Status of land cover classification accuracy assessment. Remote Sensing of Environment, 80, 185-201.

Foody G. M. 2004. Thematic map comparison: Evaluating the statistical significance of differences in classification accuracy. Photogrammetric Engineering and Remote Sensing, 70, 627-633.

Foody, G. M., and A. Mathur. 2006 The use of small training sets containing mixed pixels for accurate hard image classification: Training on mixed spectral responses for classification by a SVM. Remote Sensing of Environment. 103(2006) 179-189.

Foody, G. M., A. Mathur, C. Sanchez-Hernandez, and D. S. Boyd. 2006. Training set size requirements for the classification of a specific class. Remote Sensing of Environment, 104 (2006) 1-14.

Glenn N.F., J. T. Mundt, K. T. Weber, T. S. Prather, L. W. Lass, and J. Pettingill. 2005. Hyperspectral data processing for repeat detection of small infestations of leafy spurge. Remote Sensing of Environment, 95, 399-412.

Gokhale, B. and K. T. Weber. 2006. Modeling Cheatgrass using Quickbird Imagery. Pages 77-84 in K. T. Weber (ed.), Final Report: Detection, Prediction, Impact, and Management of Invasive Plants using GIS. 196 pp.

Good, P. I. 2005. Resampling Methods: A Practical Guide to Data Analysis. 3rd Edition. Birkhauser. 218 pp.

Hall, P. 2003. A short prehistory of the boostrap. Statistical Science. 18(2):158-167.

Ingebritsen, S.E. and R. J. P. Lyon. 1985. Principal components analysis of multitemporal image pairs. International Journal of Remote Sensing, 6(5): 687-696.

Isaaks, E. H. and Srivastava, R. M. 1990. Introduction to Applied Geostatistics. Oxford University Press, NY. 592 pp.

Janssen, L. L. F. and F. J. M. van der Wel. 1994. Accuracy Assessment of Satellite Derived Land-Cover Data: A Review. Photogrammetric Engineering and Remote Sensing, 60(4): 419-426.

Jones, H. L. 1956. Investigating the properties of a sample mean by employing random subsample means. J. Amer. Statist. Assoc. 51:54--83.

Kriegler, F.J, W. A.Malila, R. F. Nalepka, and W. Richardson. 1969. Preprocessing transformations and their effects on multi-spectral recognition. In: Proceedings of the Sixth International Symposium on Remote Sensing of Environment. University of Michigan, Ann Arbor, MI., USA, 97-131.

Lass, L. W., T. S. Prather, N. F. Glenn, K. T. Weber, J. T. Mundt, J. Pettingill. 2005. A review of remote sensing of invasive weeds and example of the early detection of spotted knapweed (Centaurea maculosa) and babysbreath (Gypsophila paniculata) with a hyperspectral sensor. Weed Science, 53:242-251

Lillesand, T. M. and R. W. Kiefer. 2000. Remote Sensing and Image Interpretation. 4th Ed. John Wiley and Sons, New York, NY 724 pp.

Longley, P. A., M. F. Goodchild, D. J. Maguire, and D. W. Rhind. 2005. Geographic Information Systems and Science. 2nd Ed. Wiley 515 pp.

Ma, Z. and R. L. Redmond 1995. Tau Coefficient for Accuracy Assessment of Classification of Remote Sensing Data. Photogrammetric Engineering and Remote Sensing, 61(4):435-439.

Mahalanobis, P. C. 1946. Sample Surveys of Crop Yields in India. Sankhya. 7:269-280.

McKay, R.J. and N. A. Campbell. 1982, Variable selection techniques in discriminant analysis II: Allocation, British Journal of Mathematical and Statistical Psychology, 35, 30-41.

McMahan, J. B., K. T. Weber, and J. D. Sauder. 2002. Using Remote Sensing Data in Urban Sprawl and Green Space Analyses. Intermountain Journal of Sciences 8(1):30-37.

McMahan, J. B. and K. T. Weber. 2003. Validation Alternatives for Classified Imagery. Pages 70-73 in K. T. Weber (Ed), Final Report: Wildfire Effects on Rangeland Ecosystems and Livestock Grazing in Idaho. 209pp.

Miller, H. J. 2004. Tobler's First Law and Spatial Analysis. Annals of the Association of American Geographers. 94(2):284-289.

Mundt, J.T., N. F. Glenn, K. T. Weber, T. S. Prather, L. W. Lass, J. A. Pettingill. 2005. Discrimination of hoary cress and determination of its detection limits via hyperspectral image processing and accuracy assessment techniques. Remote Sensing of Environment 96(1), 509-517.

Mundt, J. T., N. F. Glenn, K. T. Weber, and J. A. Pettingill. 2006. Assessing Detection Limits and Confidence from Classification Accuracy. Remote Sensing of the Environment. 105 (2006) 34-40.

NBII. 2006. Accuracy Assessment Procedures: Computational Issues. URL: http://biology.usgs.gov/npsveg/aa/sect5.html visited 9-Feb-2006.

Okeke, F. and A. Karnieli. 2006. Methods for fuzzy classification and accuracy assessment of historical aerial photographs for vegetation change analyses. Part I: Algorithm development. International Journal of Remote Sensing. 24(1-2): 153-176.

Ray T.W. and B. C. Murray B.C. 1998. Non-linear spectral mixing in desert vegetation. Remote Sensing of Environment, 55, 59-64.

Richards, J.A. 2005. Remote Sensing Digital Image Analysis. Springer-Verlag, New York. 360pp.

Roberts D.A., M. Gardner, R. Church, S. L. Ustin, G. J. Scheer, and R. O. Green. 1998. Mapping chaparral in the Santa Monica mountains using multiple endmember spectral mixture models. Remote Sensing of Environment, 65, 267-279.

Rouse, J. W., R. H. Haas, J. A. Schell, and D. W. Deering. 1973. Monitoring vegetation systems in the Great Plains with ERTS. Third ERTS Symposium, NASA SP-351-1, 309-317.

Sauder, J., J. B. McMahan, and K. T. Weber. 2003. Fuzzy Classification of Heterogeneous Vegetation in a Complex Arid Ecosystem. African Journal of Range and Forage Science, 20(2):126.

Savage, S. L. 2005. Vegetation Dynamics in Yellowstone's Northern Range: 1985-1999. MS Thesis, Montana State University. 139pp.

Singh, A. 1989. Review article: digital change detection techniques using remotely sensed data. International Journal of Remote Sensing, 10(6): 989-1003.

Snedecor, G. W., and W. G. Cochran. 1967. Statistical Methods. The Iowa State University Press, Ames, Iowa. 524pp.

Steele, B. M., J. C. Winne, and R. L. Redmond. 1998. Estimation and Mapping of Misclassification Probabilities for Thematic Land Cover Maps. Remote Sensing of Environment, 66 (2): 192-202.

Stehman, S. V. 1998. Selecting and Interpreting Measures of Thematic Classification Accuracy. Remote Sensing of Environment. 62:77-89.

Stehman, S. V., and R. L. Czaplewski. 1998. Design and analysis for thematic map accuracy assessment: Fundamental principles, Remote Sensing of Environment 64: 331-344.

Taylor, B. L. and T. Gerodette. 1993. The Uses of Statistical Power in Conservation Biology: the Vaquita and Northern Spotted Owl. Conservation Biology 7(3):489-500.

Titus, K., J. A. Mosher, and B. K. Williams. 1984. Chance-corrected Classification for use in Discriminant analysis: ecological applications. Am. Midl. Nat. 111:1-7.

Tobler, W. R. 1970. A computer movie simulating urban growth in the Detroit region. Economic Geography 46:234–40.

Van Niel, T. G., T. R. McVicar, and B. Datt. 2005. On the relationship between training sample size and data dimensionality: Monte Carlo analysis of broadband multi-temporal classification. Remote Sensing of Environment, 98(4) 468-480.

Verbyla, D. L. and S. H. Boles. 2000. Bias in Land Cover Change Estimates Due to Misregistration. International Journal of Remote Sensing. 21(18):3553-3560.

Weber, K. T. 2006. Challenges of Integrating Geospatial Technologies into Rangeland Research and Management. Rangeland Ecology and Management 59:38-43.

[THIS PAGE LEFT BLANK INTENTIONALLY]

Assessment of Juniper Encroachment: An Approach Using Landsat Satellite Imagery and GIS datasets

Temuulen Tsagaan Sankey, Post-doctoral Research Associate, GIS Training and Research Center, Idaho State University, 921 South 8th Avenue, Stop 8104, Pocatello, ID 83209-8104 (sankteki@isu.edu)

Matthew J. Germino, Associate Professor, Dept of Biological Sciences, Idaho State University, Pocatello, ID 83209

ABSTRACT

Juniper encroachment into otherwise treeless plant communities is one of the most pronounced environmental changes observed in rangelands of western North America in recent decades. Most studies on juniper change are conducted over small areas, although encroachment is occurring throughout regions. Whether changes in juniper cover can be assessed over large areas using long-term satellite data is an important methodological question. A fundamental challenge in using satellite imagery to determine tree abundance in rangelands is that a mix of trees, sagebrush, and herbaceous cover types can occur within a given image pixel. Our objective was to determine if spectral mixture analysis could be used to estimate changes in Rocky Mountain juniper (*Juniperus scopulorum* Sarg) and Utah juniper (*Juniperus osteosperma* [Torr.] Little) cover over 20 years and 20 000 ha in SE Idaho using Landsat imagery. We also examined the spatial patterns and variation of encroachment within our study area using GIS-based datasets of grazing use, land cover types, and topography. Juniper cover determined from 15-cm-resolution digital aerial ortho-photography was used to train and validate juniper presence/absence classification in 1985 and 2005 Landsat images. The two classified images were then compared to detect changes in juniper cover. The estimated rate of juniper encroachment over our study area was 22%-30% between 1985-2005, consistent with previous ground-based studies. Moran's *I* analysis indicated that juniper encroachment pattern was spatially random rather than clustered or uniform. Juniper encroachment was significantly greater in grazed areas ($p = 0.02$), and in particular in grazed shrubland cover type ($p = 0.06$), compared to ungrazed areas. Juniper encroachment was also greater on intermediate slopes (10%-35% slopes) compared to steeper or flatter terrain, and encroachment was somewhat less on north-facing ($p = 0.03$) and more on west-facing ($p = 0.02$) slopes compared to other aspects.

KEYWORDS: change detection, sub-pixel classification, spatial pattern, grazing, land cover

INTRODUCTION

Juniper encroachment is one of the most prominent changes occurring in the rangelands of western North America (Johnsen 1962; Blackburn and Tueller 1970; Burkhardt and Tisdale 1976; Miller and Rose 1995, 1999; Miller et al 2000; Wall et al 2001; Baker and Shinneman 2004). Juniper species are documented to have substantially increased in density and extent throughout their range in recent decades, although juniper cover fluctuated in the West during the Holocene and before the Euro-American settlement (Miller and Wigand 1994). As juniper trees mature and canopies close in encroached areas, understory herbaceous species and sagebrush cover can decrease, resulting in soil exposure and erosion (Miller et al 2000). Soil erosion and herbaceous and shrub cover decline can continue for substantial periods of time due to the longevity of junipers in the absence of fire (Waichler et al 2001). Intensive land treatments, such as prescribed burning, are now regularly performed to reduce juniper cover where the encroachment is perceived to decrease rangeland forage value or increase fire hazard.

Juniper encroachment has been attributed to climate variability and fire suppression (Miller and Wigand 1994), while variation in encroachment rates has been associated with differences in land cover types (Chamber et al 1999) and topographic positions (Miller et al 2000; Weisberg et al 2007). Interactions among these factors can lead to complex spatial patterns of encroachment, particularly when examined at small spatial scales and in the field (Weisberg et al 2007). Much of the previously documented juniper encroachment has occurred in shrub steppe communities (Miller and Wigand 1994; Weisberg et al 2007). Juniper seedlings often establish under sagebrush canopy as shrubs provide better soil moisture and protection from direct sunlight (Gottfried 1992; Miller and Rose 1995). It has been suggested that livestock grazing might promote juniper establishment by dispersing seeds, reducing competition from herbaceous forage species, and increasing shrub species that provide safe sites for juniper to establish (Gottfried 1992; Miller and Wigand 1994). However, we found no explicit statistical tests of the relationship between long-term grazing effects and increased juniper cover (Table 1).

Table 1. Non-exhaustive summary of previous studies on historical juniper expansion in sagebrush steppe of Western North America. In most cases, values were estimated from figures or tables, and converted to the common S.I. units.

Authors, year	Species of Juniper	Type of evidence	Temporal extent	Spatial extent	Estimated encroachment rate
Blackburn & Tueller 1970	*J. osteosperma*	Tree-ring/tree density	1725-1960	1.4 ha	0.3-0.6 trees/ha/yr
Burkhardt & Tisdale 1975	*J. occidentalis*	Tree-ring/tree density	1830-1970	1 040 ha	Up to 31 trees/ha/yr
Young & Evans 1981	*J. occidentalis*	Tree-ring/tree density	1600-1978	1 000 ha	Up to ~2 trees/ha/yr
Miller & Rose 1995	*J. occidentalis*	Tree-ring/tree density	1878-1990	8.8 ha over 32 km	Up to 4 trees/ha/yr
Miller & Rose 1999		Tree-ring/tree density	1840-1995	5 000 ha	N.A.
Johnson & Miller 2006	*J. occidentalis*	Tree-ring/tree density	1850-2005	N.A.; <2 500 ha	Up to 6 trees/ha/yr
Strand et al 2006		Aerial photography	1939-1998	15 ha	4.5% increase in cover/yr
Weisberg et al, 2007	*J. osteosperma*	Aerial photography	1966-1995	2 500 ha	0.4-1.1% increase in cover/yr
This study	*J. osteosperma* *J. scopularum*	Satellite imagery	1985-2005	20 000 ha	0.7-1.5% increase in cover/yr

Most evidence for juniper encroachment is provided by dendrochronological, demographic, or aerial photography studies which cover relatively small spatial extent (Table 1). However, most land use decisions and management activities are impacted by regional-scale changes and the associated regional-level policies. Assessment of juniper change over large areas is needed to guide regional policy and land use management. An important research question is whether changes in juniper cover over large areas and their relationship to grazing, resident land cover types, and topography can be assessed using moderate-resolution Landsat satellite imagery and Geographic Information Systems (GIS) datasets. Pixels in Landsat imagery are 900 m^2 (30 m x 30 m) in size and thus frequently have a mix of vegetation cover types, especially in the hilly rangelands of SE Idaho where juniper trees are dispersed amongst herbaceous and sagebrush cover types during the encroachment process. This mix of cover types within pixels poses a fundamental challenge in classifying pixels, since the spectral characteristics of the mixed pixels do not represent any single land cover type (Lillesand and Kiefer 2000). Spectral mixture analysis

techniques have been developed to allow estimates of how much of a pixel is comprised by different land cover types (Adams et al 1986; Small 2004; Xiao and Moody 2005). Spectral mixture analysis is most suited when there are a limited number of land cover types and when the spectral properties of these cover types can be assumed to be relatively constant. Spectral mixture analysis characterizes the spectral signatures in the imagery as a mix of the land cover types in each pixel, where each cover type is known as a separate "endmember" (Rencz 1999). Once "pure" endmembers (i.e., pure pixels of each cover type) are determined within imagery, endmember fractions or abundance of each cover type within each pixel can be estimated as a mixture (Rencz 1999). A mixture represents a linear combination of the endmembers, weighted by the areal coverage of each endmember in a pixel (Rencz 1999). The result is an estimate of how much of a given pixel is comprised of different cover types. Spectral unmixing of Landsat imagery has previously been used to map other tree species and to estimate tree fractions within pixels (Chen et al 2004; Small and Lu 2006), but has not been used to our knowledge for mapping juniper encroachment.

We studied juniper (*Juniperus scopulorum* Sarg and *J. osteosperma* [Torr.] Little) encroachment of the last 20 years in SE Idaho using Landsat satellite imagery and spectral mixture analysis. Our objectives were: 1) to determine if spectral mixture analysis could be used with Landsat imagery to detect and quantify changes in juniper cover over 20 years and across 20 000 ha and 2) to examine how juniper changes vary due to livestock grazing, resident land cover types, and topographic positions by combining maps of juniper change derived from Landsat imagery with GIS datasets. Juniper encroachment rates could be further complicated by issues such as distance to nearest juniper stand or dispersal limitation, and so we also determined whether juniper encroachment patterns were clustered, random, or uniform. Our choice of Landsat imagery was based on its accessibility, moderate resolution (30 m x 30 m) compared to other types of satellite data (e.g., MODIS and AVHRR), and its availability for all earth surfaces for every 16-day-period in seven spectral bands. We chose two Landsat image scenes for juniper change detection: one from August 1985 and another from August 2005. Annual seasonal drought tends to prevail in August in SE Idaho. In addition, the greenness of sagebrush communities is lowest at this time of the year following sagebrush ephemeral leaf drop and herbaceous species senescence (Bilbrough and Richards 1993; Kremer and Running 1993). We expected this time period to allow more prominent detection of evergreen juniper in the sagebrush-steppe rangeland ecosystem.

METHODS

Study Site Description

Two regions of interest across a total area of ~200 km^2 (42º53´18"N, 112º28´37"E) were selected for this study, one south of Pocatello and the other west of Pocatello (Figure 1). The western region (Region 1) included Chinese Peak and Camelback Mountain, while the southern region (Region 2) included Kinport Peak and Gibson Mountain. Both regions consist of hilly and mountainous topography ranging in elevation from 1 400 m to 1 850 m. Slope largely ranged between 0-45 degrees (in percent) in both regions, while aspect varied between 140 (southwest) and 310 (northwest) degrees in Region 1 and 280 (northwest) through north to 170 degrees (southeast) in Region 2. A majority of the area is public land managed by the Bureau of Land Management (BLM) and US Forest Service (USFS) (approximately 40% and 50%, respectively), while the rest includes private land (~10%). The soils are coarse-silty, mixed, frigid Calcic Haploxerolls (Ririe series; USDA, NRCS 1997). Average annual precipitation in Pocatello is 325 mm.

Common plant species are Rocky Mountain juniper (*Juniperus scopulorum* Sarg), Utah juniper (*Juniperus osteosperma* [Torr.] Little), big sagebrush (*Artemisia tridentata* Nutt. spp.), "three-tip" sagebrush (*Artemisia tripartita* Rydb), grey rabbitbrush (*Chrysothamnus nauseosus* [Pall.] Britt.), green rabbitbrush (*Chrysothamnus viscidoflorus* [Hook.] Nutt.), bulbous bluegrass (*Poa bulbosa* L.), thickspike wheatgrass (*Elymus lanceolatus*), needle-and-thread grass (*Stipa comata* Trin. & Rupr.), cheatgrass (*Bromus tectorum* L.), and tapertip hawksbeard (*Crepis acuminata* Nutt.) (Ratzlaff and Anderson 1995).

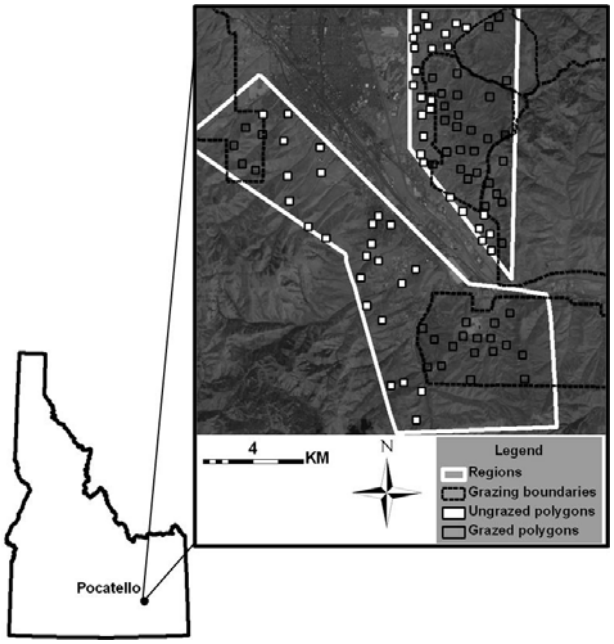

Figure 1. The study regions, grazing boundaries, and the 100 randomly generated sample polygons in the Pocatello area of southeastern Idaho.

The two regions included grazed areas dispersed throughout ungrazed areas. The grazed areas (five allotments) are managed by the BLM (Figure 1) and have been used in spring-summer seasons over the last 20 years. Our review of the BLM grazing records and discussions with BLM Range Conservationists revealed that grazing regimes in these areas have been relatively constant during the study time period. The grazed areas vary between 1 466-5 321 ha in size and 0.01-0.24 Animal Unit Months per hectare in grazing intensity.

Landsat Imagery and Juniper Classification

We used one Landsat5 Thematic Mapper satellite image subset from August 02, 1985 and one Landsat5 Thematic Mapper satellite image subset from August 13, 2005. Both images (Path 039, Row 030) were atmospherically and geometrically corrected and projected in UTM Zone 12 North, NAD 1983 projection and datum. Digital color aerial ortho-photograph with a 15-cm resolution from August 2004 (USDA National Agricultural Imagery Program) was used for training and validation of Landsat image classification. The 1985 Landsat image was co-registered to the 2005 Landsat image using 30 ground control points (root mean squared error = 0.07).

The Matched Filtering Spectral Unmixing technique was used to classify juniper in the Landsat imagery (ENVI Version 4.3, ITT Industries Inc, 2006, Boulder, CO). The Matched Filtering Spectral Unmixing approach detects a user-defined target cover type in the imagery, while suppressing the spectral signatures of other cover types. The classification training requires identification of pure pixels of the cover class of interest as well as pure pixels that do not have the cover class of interest (i.e., pixels of other cover types). In our case, the target cover type of interest was juniper. The other cover types to be suppressed largely included sagebrush and herbaceous cover as well as their mix. Using the 15-cm-resolution aerial photograph, we selected in each Landsat imagery 10 pure juniper pixels and 10 other pure pixels that clearly had no juniper, but sagebrush and herbaceous cover and their mix. The two Landsat images were trained and classified separately and fractions of juniper endmember were estimated in both images. The spectral separation of the pure pixels was successful in both Landsat images (Figure 2) and remarkably similar between the images.

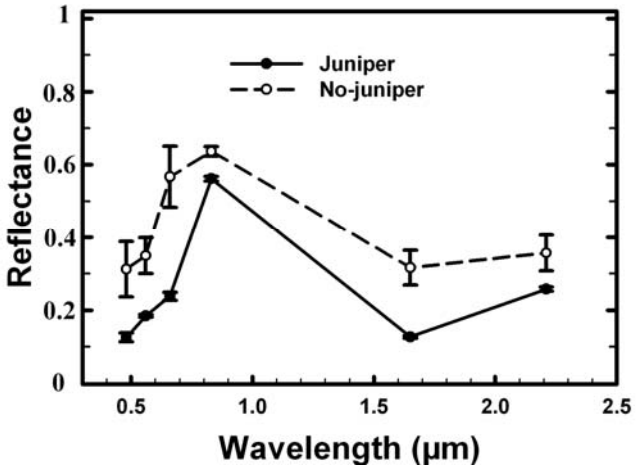

Figure 2. Mean (+/- SE) spectral reflectance of the "pure" pixels with 100% juniper cover (N = 10) and 0% juniper cover (N = 10) in the Landsat images.

Using the estimated juniper fractions in each image, juniper presence and absence was classified in each pixel to produce a binary map of juniper presence and absence for each image date. During this process, a spectral threshold was set between 0-1 to decide on juniper absence and presence and thereby optimize the classification accuracy. To determine the appropriate threshold, we assessed the accuracy of multiple classification models beginning with a nominal threshold value of 0.0 and incrementally increasing the threshold by 0.05 units until increases in threshold no longer improved accuracy. The resulting threshold value was 0.3. The accuracy of each 2005 juniper classification model was assessed with 65 randomly selected pixels (random points generated by Hawth's tools, ESRI® ArcMap™ 9.1 software (ESRI Inc, 1999-2006)) having a range of juniper cover of 0%-100% which were visually estimated in the aerial photograph in 30 m x 30 m windows to correspond with the 2005 Landsat pixels. The accuracy of each 1985 juniper classification model was assessed with 65 randomly selected pixels having either 0% or >50% cover of large juniper trees (>2 m in canopy diameter). There were no high resolution aerial photographs available for 1985, so we assumed that 30 m x 30 m windows having high values of juniper percent cover in the 2004 photographs likely had juniper presence in 1985. Similarly, windows with no juniper in 2004 nor trunk skeletons or history of juniper-excluding events between 1985-2005 were assumed to have juniper absence in 1985. Our assumptions were supported by local familiarity with this region and the slow growth rates of juniper.

Change Detection

A post-classification image differencing method (Lillesand and Kiefer 2000) was used to compare the 1985 and 2005 binary maps and to detect pixels with newly established junipers, where junipers were absent in the earlier date. This allowed us to examine the overall juniper cover increase both in the extent and density across the study area over the 20-year period. In addition, we compared the estimated abundances of juniper within each pixel between the two unmixed Landsat images using a paired *t*-test (n = 60 246) to provide additional information on pixel-level juniper density changes from 1985 to 2005. However, pixel-level juniper fraction estimates were not quantitatively assessed for classification accuracy and were, therefore, not used in further analysis. Only the juniper change map resulting from the comparison of the two binary maps was used in the statistical analysis.

GIS Datasets

We created GIS-derived independent variables of grazing, land cover types, and topography using ArcMap 9.1 software. Digital maps of fires and grazed area boundaries were acquired from the BLM (Weber and BLM Pocatello field office 2006). A thematic map of land cover types generated by the Idaho GAP Analysis project for the Pocatello area was used. This map included 15 different land cover

types in our study area (70% overall accuracy) and had a spatial resolution of 30 m and minimum mapping unit of 2 ha. We performed an independent accuracy assessment of our own within our study area and considered the accuracy of this map acceptable (75% overall accuracy). To further improve the accuracy, we combined the 15 land cover types into four classes at the next coarser level of thematic classification. For example, all shrub cover types (i.e., big sagebrush, low sagebrush, and bitterbrush) were grouped into a single cover type of shrubland. The resulting four land cover types included grassland, shrubland, riparian, and urban land (very small area of housing development outside of the city of Pocatello as the city was intentionally excluded from our study area). A USGS digital elevation model (DEM) of 26.8 m resolution was used to derive topographic aspect (in degrees) and slope (in percent).

Statistical Analyses

We examined the spatial pattern of juniper encroachment within each region using Moran's *I* to determine if juniper encroachment was clustered, random, or uniform across the landscape. Moran's *I* index was estimated using the juniper change map and Euclidian distance method with inverse distance relationship in ArcMap 9.1 software. A z-score was also estimated to determine the statistical significance of the estimated *I*. Moran's *I* values close to -1 indicates a uniform pattern, while values close to 1 indicates a clustered pattern. Moran's *I* values close to 0 indicates a random pattern (O'Sullivan and Unwin 2003).

The relationship of juniper change and landscape factors was examined using analysis of variance (ANOVA) (SPSS 14.0 for Windows, 2005). The units of replication were randomly located polygons that each had 100 pixels (a square area of 90 000 m^2). There were 100 replicate polygons, and they were distributed evenly between grazed and ungrazed areas (Figure 1), with 85 polygons in shrubland, eight in grassland, and the remaining seven in riparian and urban areas. The response variable was the number and percent of pixels in the random polygons classified as having new juniper presence in 2005 compared to the 1985 classified image. Data were square-root transformed to meet assumptions of normality. A one-way ANOVA was used to compare juniper increase in grazed and ungrazed polygons. A separate two-factor ANOVA was used to assess whether the grazing effect varied among shrubland and grassland (these were two levels of the second factor, resident land cover), with pair-wise post-hoc comparisons to examine the interactive effects of grazing and land cover types.

Multiple regression was used to assess the interactive effects of topography and grazing on juniper increase. The topographic aspect and slope associated with each pixel within each random polygon were extracted from the DEM and grouped into four categorical classes of aspect (315º-45º, 45º-135º, 135º-225º, and 225º-315º) and three categories of slope (0%-10%, 10%-35%, and >35%) within each polygon. The number of pixels showing new juniper presence from 1985 to 2005 in each polygon was modeled as a response to grazing (grazed or ungrazed), aspect (4 classes), and slope (3 classes).

RESULTS

The spectral properties associated with juniper were distinct compared to other cover types, with the most differences in spectral properties between juniper and the surrounding land cover types being particularly evident at wavelengths longer than 0.6 μM (Figure 2). The overall accuracy was 92% in the 2005 Landsat imagery and 79% in the 1985 Landsat imagery. The 2005 image classification had greater user's and producer's accuracies than the 1985 image classification (Table 2), though the spectral signatures of endmembers were remarkably similar between the two images.

Over the study period, the number of pixels with new juniper presence from 1985 to 2005 increased 29.7% in Region 1 and 21.6% in Region 2. Juniper cover per pixel increased 16.6% in Region 1 (p = 0.0001) and 14.2% in Region 2 (p = 0.0002). The estimated Moran's *I* was 0.04 with a z score of 772.3 for Region 1 (p = 0.01) and 0.03 with a z score of 1 160 for Region 2 (p = 0.03), indicating that juniper encroachment occurred in a random pattern, but not in a localized clustering or in an even distribution of trees in both regions.

Table 2. Classification accuracy of juniper presence and absence in 1985 and 2005 Landsat images.

Year of image	Class	User's accuracy	Producer's accuracy	Overall accuracy
2005	Juniper presence	91%	94%	
	Juniper absence	94%	91%	92%
1985	Juniper presence	80%	95%	
	Juniper absence	86%	62%	79%

The percentage increase between 1985-2005 in pixels of the random polygons having new juniper presence was significantly greater in grazed compared to ungrazed areas, over all land cover and topographic variation (28.2% ± 17.9 SD and 22.5% ± 13.6 SD, respectively, $F_{1,99} = 5.31$, $p = 0.02$). There was a marginally significant interaction of grazing and land cover types ($F_{2,99} = 2.8$, $p = 0.06$; Figure 3). Post-hoc comparisons indicated that ungrazed grassland had 11.1% greater juniper increase than ungrazed shrubland ($p < 0.0001$), and grazed shrubland had 9.5% greater juniper increase compared to ungrazed shrubland ($p = 0.06$) (Figure 3).

The regression model indicated grazing and topography significantly affected juniper change between 1985-2005 ($p < 0.000$ and adjusted $R^2 = 0.81$). Grazing, medium slope class (10%-35 %), and northerly and westerly aspects were significant predictor variables ($p = 0.04$; 0.001; 0.03, and 0.02, respectively). Medium slope class had 5.6% and 4.4% greater juniper increase compared to the flatter and steeper slope classes, respectively (Figure 4a). Northerly aspects had a somewhat lower rate of juniper increase than other aspects, while westerly slopes had a slightly greater rate of juniper increase (Figure 4b).

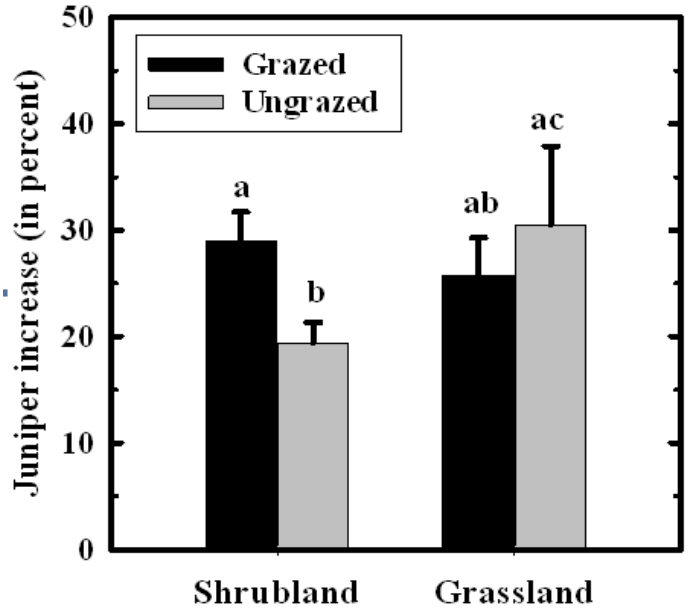

Figure 3. Mean (+/- SE) increase in the percent of pixels with new juniper presence in grazed and ungrazed shrubland and grassland cover types between 1985-2005. Letters indicate significant differences at α =0.1.

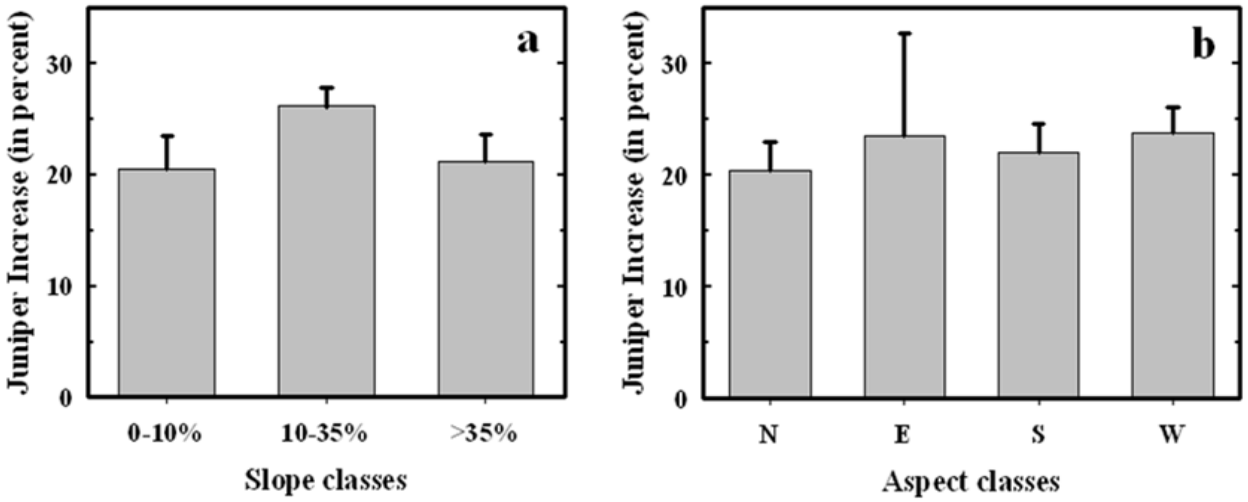

Figure 4. Mean (+/- SE) increase in the percent of pixels with new juniper presence in categorical classes of slope (panel a) and aspect (panel b).

DISCUSSION

The application of moderate-resolution Landsat imagery in classifying and detecting changes in sparsely distributed juniper cover was successful. The spectral mixture analysis allowed accurate detection of juniper presence and absence, which then generated realistic temporal change detection over the past 20 years for a large region of semi-arid rangelands. The distinct spectral characteristics of pixels that had juniper, compared to pixels without juniper, were probably due to the dark greenness and relatively high leaf area of juniper compared to the surrounding light-colored vegetation. These non-juniper cover types had less foliage and chlorophyll during the dry end-of-growing season days from which we selected our imagery.

The results of this application have important implications for the monitoring and assessment of rapidly expanding juniper woodlands which is an issue for over 24 million hectares in the western United States (Miller and Wigand 1994). Field-based approaches for detecting juniper cover changes provide highly accurate and valuable results, but they can be labor intensive, time consuming, and limited in the spatial extent they can cover. In comparison, the application of remote sensing methods can be more cost-effective and timely due to the large areal extent they cover. Digital satellite imagery also provides opportunities for more robust and comprehensive analysis of change, as the imagery can be easily integrated with other sources of digital data, such as terrain models and digital maps of grazing boundaries or land cover types. Moreover, data from satellite platforms, such as Landsat, can be acquired in retrospect to examine past changes, in this case over 20 years.

Our results indicated up to 30% increase in pixels having juniper over the past 20 years in the Pocatello area of SE Idaho. The estimated rates of increase in juniper cover in this study were in approximate agreement with the estimates of juniper increase in other areas based on different methods (Table 1). Notably, there appears to be more convergence of juniper change estimates from the large-scale studies. The estimated rate of juniper increase appeared different in our two regions, which might be due to the difference in the initial juniper cover between the two regions. Region 1 with relatively greater increase in juniper cover had greater initial juniper cover of approximately 25%. Weisberg et al. (2007) indicate that juniper expansion rate can be density-dependent and the process might be dominated by infilling. Compared to other areas, they suggest that expansion rate might be greater in areas where the initial juniper cover is >10%. Our spatial pattern analysis indicated that juniper encroachment was randomly distributed in each region, and not locally clustered or uniform. The random spatial pattern might be associated with juniper dispersal systems that are facilitated by multiple factors including gravity, birds,

frugivorous mammals, and some livestock which pass germinable seeds (Chambers et al 1999). Padien and Lajtha (1992) also found juniper encroachment patterns to be random at regional scales.
Greater juniper encroachment in grazed compared to ungrazed areas in our study was consistent with the expected, but not often explicitly tested, positive effects of grazing on juniper increase suggested by previous studies (Miller and Wigand 1994; Miller and Rose 1995, 1999). Livestock grazing can decrease the competitive effects of palatable herbaceous species on new and establishing juniper trees (Evans 1988). The reduction in competition might accelerate juniper establishment (Johnsen 1962) by making plant communities more susceptible for juniper encroachment (Miller and Wigand 1994). Our findings of marginally greater juniper encroachment in grazed shrubland compared to ungrazed shrubland are also consistent with conclusions in previous literature. Livestock grazing can increase shrub species that help facilitate juniper encroachment (Gottfried 1992), and there are several ground-based reports affirming the encroachment of juniper into shrub steppe (Miller and Wigand 1994; Miller et al 2000; Weisberg et al 2007). Shrubs provide better soil moisture and protection from direct sunlight (Gottfried 1992; Miller and Rose 1995). Litter accumulation beneath shrub canopies further improves soil moisture and temperature, and provides nutrients to the developing juniper seedlings (Evans 1988).

Our results indicated that grazing and topographic positions were important predictor variables of juniper encroachment. Indeed, this model explained much of the variability in juniper encroachment without including land cover types as a predictor variable. This might indicate that topographic heterogeneity can be a more important factor than land cover types. Little is known regarding topographic effects on juniper encroachment (Johnson and Miller 2006; Weisberg 2007). However, Johnson and Miller (2006) suggest that once a threshold is crossed in the juniper encroachment process, disturbances such as fire are no longer important and instead topography might become the important factor that explains much of the variability in juniper woodland expansion.

CONCLUSIONS

Management Implications

This study demonstrated a successful application of Landsat imagery and classification methods in detecting juniper cover increase. Juniper cover appears to be increasing in a random spatial pattern and at varying rates across the landscape due to differences in grazing use, land cover types, and topography. If further inquiry can demonstrate causality between juniper encroachment and these variables, land management can be adjusted to abate further unwanted increases in juniper. The approach described here could enable a more rapid assessment of juniper woodland changes across large areas and inform management decisions.

ACKNOWLEDGEMENTS

This study was made possible by a grant from the National Aeronautics and Space Administration Goddard Space Flight Center. ISU would also like to acknowledge the Idaho Delegation for their assistance in obtaining this grant.

LITERATURE CITED

Adams, J.B., M.O. Smith, and P.E. Johnson. 1986. Spectral mixture modeling: a new analysis of rock and soil types at the Viking Lander 1 site. *Journal of Geophysical Research* 91:8098-8112.

Baker, W.L. and D.J. Shinneman. 2004. Fire and restoration of pinon-juniper woodlands in the western United States: a review. *Forest Ecology and Management* 189:1-21

Bilbrough, C.J. and J.H. Richards. 1993. Growth of sagebrush and bitterbrush following simulated winter browsing: mechanisms of tolerance. *Ecology* 74:481-492.

Blackburn, W.H. and P.T. Tueller. 1970. Pinyon and juniper invasion in black sagebrush communities in east-central Nevada. *Ecology* 51:841-848.

Burkhardt, J.W. and E.W. Tisdale. 1976. Causes of juniper invasion in southwestern Idaho. *Ecology* 57:472-484.

Chambers, J.C., S.B. Vander Wall, and E.W. Schupp. 1999. Seed and seedling ecology of pinyon and juniper species in the pygmy woodlands of western North America. *The Botanical Review* 65:1-38.

Chen, X., L. Vierling, E. Rowell, and T. DeFelice. 2004. Using lidar and effective LAI data to evaluate IKONOS and Landsat 7 ETM+ vegetation cover estimates in a ponderosa pine forest. *Remote Sensing of Environment* 91:14-26.

Evans, R.A. 1988. Management of pinyon-juniper woodlands. United States Department of Agriculture. Forest Service. Intermountain Research Station. General Technical Report INT-249.

Gottfried, G.J. 1992. Ecology and Management of the southwestern pinyon-juniper woodlands. *In*: Ffolliott, P.F. et al. [eds.]. 1992. Ecology and Management of Oak and associated woodlands: Perspectives in the southwestern United States and northern Mexico. 27-30 April 1992; Sierra Vista, AZ: p.78-85.

Idaho GAP Analysis project vegetation coverage for the ISU GIS Center Area of Concern. *Available at:* http://giscenter.isu.edu/data. *Accessed 15 May 2006*.

Johnsen, T.N., Jr. 1962. One-seed juniper invasion of Northern Arizona grasslands. *Ecological Monographs* 32:187-207.

Johnson, D.D. and R.F. Miller. 2006. Structure and development of expanding western juniper woodlands as influenced by two topographic variables. *Forest Ecology and Management* 229:7-15.

Kremer, R.G. and S.W. Running. 1993. Community type differentiation using NOAA/AVHRR data within a sagebrush-steppe ecosystem. *Remote sensing of Environment* 46:311-318.

Lillesand, T.M. and R.W. Kiefer. 2000. Remote sensing and image interpretation. Fourth Edition. John Wiley and Sons Inc. New York. Chichester. Weinheim, Brisbane. Singapore. Toronto. 568 p.

Miller, R.F. and P.E. Wigand. 1994. Holocene changes in semiarid pinyon-juniper woodlands. *Bioscience* 44:465-473.

Miller, R.F. and J.A. Rose. 1995. Historic expansion of *Juniperus occidentalis* (western juniper) in southeastern Oregon. *Great Basin Naturalist* 55:37-45.

Miller, R.F. and J.A. Rose. 1999. Fire history and western juniper encroachment in sagebrush steppe. *Journal of Range Management* 52:550-559.

Miller, R.F., T.J. Svejcar, and J.A. Rose. 2000. Impacts of western juniper on plant community composition and structure. *Journal of Range Management* 53:574-585.

O'Sullivan, D. and D. Unwin. 2003. Geographic Information Analysis. John Wiley and Sons Inc. p.197-201.

Padien, D.J. and K. Lajtha. 1992. Plant spatial pattern and nutrient distribution in pinyon-juniper woodlands along an elevational gradient in northern New Mexico. *International Journal of Plant Sciences* 153:425-433.

Ratzlaff, T.D. and J.E. Anderson. 1995. Vegetal recovery following wildfire in seeded and unseeded sagebrush steppe. *Journal of Range Management* 48:386-391.

Rencz, A.N. 1999. Remote sensing for the earth sciences. Wiley and Sons. New York. p.251-307.

Small, C. 2004. The Landsat ETM+ spectral mixing space. *Remote Sensing of Environment* 93:1-17.

Small, C. and J.W.T. Lu. 2006. Estimation and vicarious validation of urban vegetation abundance by spectral mixture analysis. *Remote Sensing of Environment* 100:441-456.

Strand, E.K., A.M.S. Smith, S.C. Bunting, L.A. Vierling, D.B. Hann, andP.E. Gessler. 2006. Wavelet estimation of plant spatial patterns in multitemporal aerial photography. *International Journal of Remote Sensing* 27:2049-2054.

Young, J.A. and R.A. Evans. 1981. Demography and fire history of a western juniper stand. *Journal of Range Management* 34:501-505.

USDA Natural Resources Conservation Service. 1997. Soil survey geographic (SSURGO) database for St. Joe Area, Idaho. Fort Worth, Texas.

USDA National Agricultural Imagery Program Imagery. *Available at:* http://giscenter.isu.edu/data. *Accessed 15 May 2006.*

Waichler, W.S., R. Miller, and P.S. Doescher, 2001. Community Characteristics of old-growth western juniper woodlands. *Journal of Range Management* 54:518-527.

Wall, T.G., R.F. Miller, and T.J. Svejcar. 2001. Juniper encroachment into aspen in the Northwest Great Basin. *Journal of Range Management* 54:691-698.

Weber, K. and BLM Pocatello field office. 2006. The spatial database. *Available at:* http://giscenter.isu.edu/data. *Accessed 15 October 2006.*

Weisberg, P.J., E. Lingua, and R.B. Pillai. 2007. Spatial patterns of pinyon-juniper woodland expansion in central Nevada. *Journal of Range Management* 60:115-124.

Xiao, J. and A. Moody. 2005. A comparison of methods for estimating fractional green vegetation cover within a desert-to-upland transition zone in central New Mexico, USA. *Remote Sensing of Environment* 98:237-250

[THIS PAGE LEFT BLANK INTENTIONALLY]

Developing a Geospatial Search Tool Using a Relational Database Implementation of the FGDC CSDGM Model

Kit Na Goh, Idaho State University, GIS Training and Research Center, 921 S. 8th Ave., Stop 8104, Pocatello, Idaho 83209-8104

Keith Weber GISP, Idaho State University, GIS Training and Research Center, 921 S. 8th Ave., Stop 8104, Pocatello, Idaho 83209-8104 (webekeit@isu.edu)

Daniel P. Ames PhD, PE Department of Geosciences, Idaho State University, Pocatello, Idaho 83209

ABSTRACT

The GIS Training and Research Center (GIS TReC) at Idaho State University provides the public with free access to approximately 26,000 GIS datasets stored within its spatial library. As is the case with many data libraries throughout the world, the GIS TReC data library stores data in file archives (using "zip" compression) to reduce data storage requirements. However, this approach is not conducive to live web-based data queries. Rather, visitors are required to browse a massive directory of folders and sub-folders to find the needed data. In order to facilitate better discovery and delivery of geospatial data, we are developing and deploying a relational database containing geospatial metadata documentation for all datasets within the spatial library and an intelligent web interface to help website visitors more efficiently find required geospatial data. This paper describes the relational database design and the process followed to import existing XML-based metadata documents into the new fully searchable metadata database.

KEYWORDS: metadata, data discovery, public outreach

INTRODUCTION

The Idaho State University (ISU) Geographic Information System Training and Research Center (GIS TReC) is a university-wide facility administered by the Office of Research serving all ISU colleges and departments and the GIS community of southeastern Idaho and is a member of the ESRI-managed Geography Network (geographynetwork.com). The mission of the GIS TReC is to facilitate decision-making through the use and application of state-of-the-art geospatial technologies. The GIS TReC maintains over 26,000 GIS datasets within its spatial library and allows remote users to freely access both raster and vector GIS data via a simple web-based directory structure. The datasets included in this library primarily describe features within the GIS TReC Area of Concern (AOC – figure 1) including for example digital elevation model data, digital orthophoto quads, and vegetation. The library also includes data from outside the AOC such as regional, national, and world data administrative boundaries and large scale environmental data.

Figure 1. Area of Concern

The Current System

The current data delivery mechanism of the GIS TReC spatial library requires clients to browse the spatial library directory of folders and files to find the data they need and then download the data to a local desktop computer to perform GIS mapping and analysis tasks and operations. This approach, though perhaps the most simple spatial library implementation, has several drawbacks including: 1) users must know the name of the required zip file and containing folders; 2) users can not easily search the data to discover new or otherwise useful data; and 3) users must download the entire zip archive for a particular data set before they can open it and browse the contents (including the associated metadata). Figures 2 and 3 illustrate the process followed by a client using the spatial library to find geospatial data. An inherent problem with this approach is that users are not certain if the data they have chosen is correct for their application until they have downloaded, extracted, and previewed it in an application like ArcCatalog.

The existing GIS TReC geospatial library directory structure includes non-archived HTML-based metadata files stored within the same folder as the dataset it describes so that they can be indexed by Google and other search engines. This allows a user unfamiliar with the spatial library to do a Google site search (available from the GIS TReC's website) on these files to gain some idea of the available data. We recognize that the current approach is not optimal for all of these reasons,

[To Parent Directory]

Tuesday, November 28, 2006 12:42 PM	<dir>	AOC basic
Tuesday, November 28, 2006 12:42 PM	<dir>	Idaho
Tuesday, November 28, 2006 12:42 PM	<dir>	Montana
Tuesday, November 28, 2006 12:42 PM	<dir>	Nevada
Tuesday, November 28, 2006 12:42 PM	<dir>	Utah
Tuesday, November 28, 2006 12:42 PM	<dir>	Wyoming

Figure 2: Current spatial data search

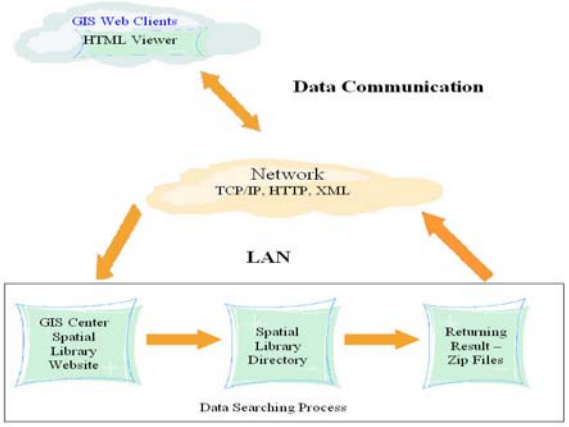

Figure 3. Schematic of how a client currently finds the data

and suspect that other geospatial librarians may have similar problems. Hence, the focus of this research is to develop a geospatial data search tool using a relational database implementation of the FGDC CSDGM model. The goal of this tool is to allow one to easily query all of the metadata describing datasets in the geospatial library through a simple, fast, and powerful search tool.

To determine the types of users of our spatial library, we generated several statistical reports using the software, Flashstats (http://www.maximized.com/). From these reports, it was determined that 26.3% of clients accessed the GIS TReC spatial data library from within the Idaho State University internet domain (isu.edu). An additional 0.43% of the clients were from local state agencies, and 2.4% of clients searched the spatial library from workstations within the GIS TReC itself. These data indicate that about 28.7% of all of our users are students, faculty members, and GIS professionals. Such users are likely to a) know what data they need from our library; and b) have the ability to easily locate it using the current directory browsing access method. However the remaining users (71.3%) who come from outside the university (e.g. from the Geography Network) and the local professional community are surely not as familiar with the GIS servers and especially the organization of the spatial library. Hence we expect that an improved search interface will better serve this large segment of the user community and indeed should expand the user base for this particular regional geospatial data library. It is very likely that other research centers and data archives are used similarly and could also benefit from the development of tools for rapidly searching and accessing geospatial metadata and raw data.

An FGDC Based Metadata Database Approach

To manage and support sophisticated geospatial data searches, we developed a relational database to act as the backbone against which the search interface executes. Our relational database design is intended to improve data discovery and delivery by including all information captured within

geospatial metadata documents. The Federal Geographic Data Committee (FGDC) geospatial metadata format was chosen for the base metadata standard for this project.

The FGDC metadata standard (FGDC 2000) describes GIS datasets using seven major sections and three supporting sections. The seven major sections are: 1) identification, 2) data quality, 3) spatial data organization, 4) spatial reference, 5) entity and attribute, 6) distribution, 7) metadata reference information. The three supporting sections are divided into 1) citation, 2) time period, 3) contact information. In addition to this information, the relational database developed for this project also contains the name and URL of the geospatial dataset, along with descriptive keywords, to better facilitate searching and download. Using a custom search interface developed with Active Server Page (ASP) technology, all geospatial metadata information for the entire library (and potentially outside the library) becomes immediately viewable without the user having to download and extract the dataset.

1.3 Anticipated Benefits

In addition to the improvement in search and query functionality for end-users, an additional benefit of this approach will be the reduction in overall disk space usage and the removal of redundant stand-alone HTML-based metadata files. We anticipate this will also help improve long-term maintenance of the archive (Figure 4).

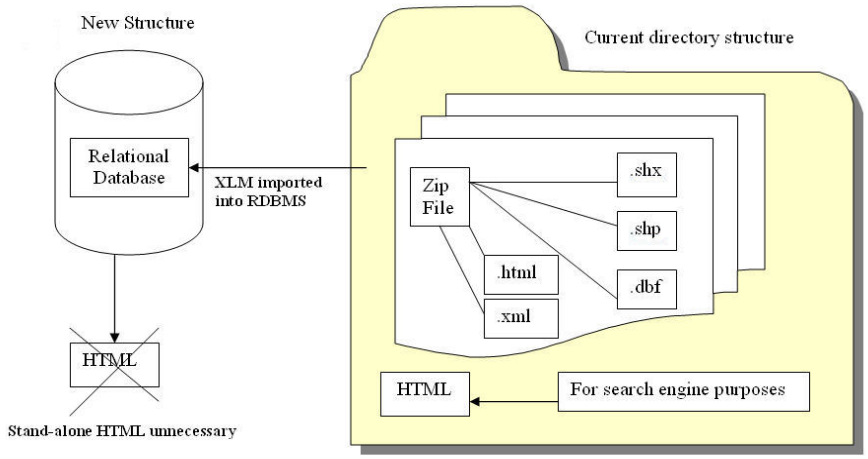

Figure 4. Reduction in redundant documentation

PROJECT DETAILS

Objectives

The objectives of this project include:

1) Improve data discovery: To improve the current search engine of the GIS TReC to help clients more efficiently find required geospatial data and understand the structure of metadata.

2) Develop a robust relational database design using UML CASE visual modeling: design a relational database (Rational Rose software was used to create the UML model) to contain the information within FGDC geospatial metadata documents (extracted from ArcXML documents). The database will include the name and the path to each geospatial dataset, along with descriptive keywords, to better facilitate searching. The database was designed following a top-down approach and normalized through third form normal. The

UML design is available at http://giscenter.isu.edu/research/techpg/nasa_tlcc/template.htm

3) Automate database population: Create an "XML Parser" to parse geospatial metadata (stored within ArcXML documents) and automatically populate the relational database described above.

4) Develop an intelligent web interface to facilitate effective use of the database: Develop an intelligent web interface (that has the capability to query the spatial data with topology keywords, such as, intersect, contain, and adjacent and view the metadata in XML style sheet before downloading) to assist clients searching for data available in the GIS TReC spatial library. This will be accomplished using ASP, HTML, and Javascript.

5) Make the entire process open to the GIS Community: Organize and documents all materials describing database design, XML parser design, and Active Server Page design to assist others in the GIS community.

Database Design Using a UML CASE Class Diagram

At the outset, a database schema or design did not exist that would support geospatial metadata documents. For this reason, the first step was a careful database design normalized to third form normal. Unified Modeling Language (UML) is a standard diagramming language used to design database schemas among other things. One software tool used to create UML models is Rational Rose (Wendy and Michael, 1999). To manage and support sophisticated searches, a relational database with tables that describe GIS datasets based on the seven major sections of the FGDC metadata standard (FGDC 2000) was created using Rational Rose. This database design includes all information captured within geospatial metadata documents, the name and file path to the geospatial dataset, along with descriptive keywords.

The advantage of using a UML model is its ability to transition into a physical database using the UML Class diagram model. Changes can be made to the model and exported using the XML (Extensible Markup Language) file (consisting of UML XMI (XML Metadata Interchange)) which facilitates transfer of UML diagrams to other software applications (such as ArcCatalog). "When a change occurs to the model, Rose can modify the code to incorporate the change" (Wendy and Michael, 1999), this helps to ensure that the model is resilient and flexible.

After exporting the XMI file from Rational Rose, a Microsoft Access relational database (though another RDBMS could just as easily be used) was created using the CASE Schema tool from ArcCatalog. The UML design is available at http://giscenter-sl.isu.edu/umlmodel/index.htm

Development of ArcXML Parser Software

To populate the relational database, all information stored in the HTML-based metadata needed to be imported. Parsing such metadata files can be quite difficult because of the variations of formatting one might encounter in different HTML files. However, when the metadata is stored within the standard ArcXML file format, the process of parsing and importing metadata becomes greatly simplified. An initial "XML File Loader" application was written using Visual Basic 2005 to perform this function and is currently undergoing update and improvement, although it is already functional.

Using the XMLTextReader function in Visual Basic 2005, the XML parser application imports ArcXML formatted metadata to the relational database. The goal of building the XML parser

software is to read an ArcXML metadata document, parse it, extract the values (fields and attributes) and write the data into the appropriate relational database tables.

A Graphical User Interface (GUI) has been designed (Figure 5) for the ArcXML parser program. The GUI includes basic functions (such as Open, Save, Add, Remove Files and Open a folder) (Figure 7) within two areas on the page: a file screen and a preview screen. The file screen displays the name of all XML files contained in the current workspace. The preview screen previews selected XML files along with their keys and values. Keys are objects that are used for selection during data retrievals.

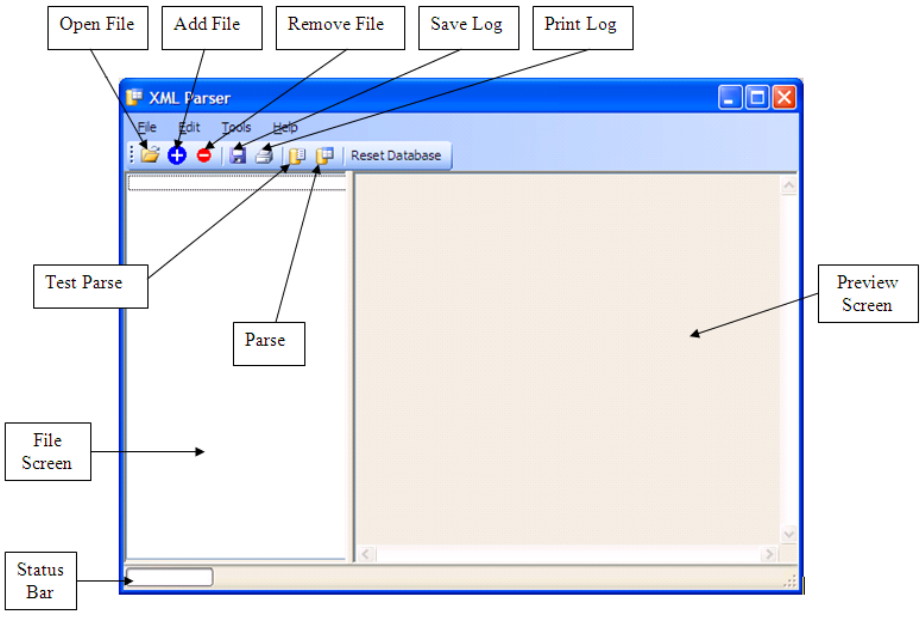

Figure 5. Screenshot of XML Parser software developed for this project.

Development of an Intelligent Web Search Interface

The GIS TReC currently offers two search options to their web clients. The first is a manual search and the second is a simple search powered by Google. The current search engines have limitations and problems which cannot fully facilitate geospatial data discovery and delivery needs, namely a connection between search HTML metadata files and download of the related dataset. Microsoft products or indexing services are also not sufficient as these do not reveal files stored within ZIP files. Because of the size of geospatial data, much of it has been bundled and compressed in ZIP format. This unfortunately, hides much of the real data from clients. In order to locate and retrieve data, an intelligent web interface was required enabling clients to choose or enter search criteria and preview the metadata (all done within the database) without having to download the dataset or try to memorize paths to the required data files.

Search engine tools are becoming common and most search through the meta-databases against meta-descriptions of their geospatial data range.

> "A natural approach is to add advanced features to search engines that allow users to express constraints or preferences in an intuitive manner, resulting in the desired information to be returned among the first results. In fact, search engines have added a variety of such features, often under a special advanced search interface, though mostly

limited to fairly simple conditions on domain, link structure, or last modifications date" (Markowetz et al, 2005).

The proposed method of data retrieval will contain features that allow clients to enter keywords or search phrases and also preferences or constraints such as, building topological relationships (intersect, contain, and adjacent) to locate the correct dataset. This feature will add more capability than the typcial geospatial data search engine (Figure 6).

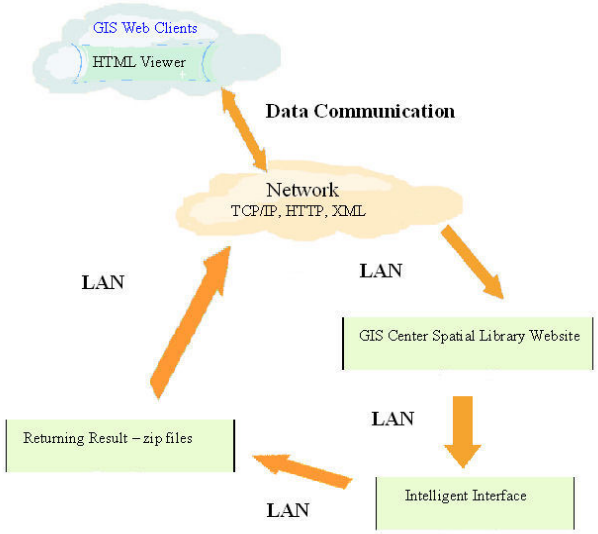

Figure 6. Schematic of new streamlined fashion of finding data

SUMMARY

To facilitate better discovery and delivery of geospatial data for GIS TReC clients, a robust relational database containing FDGC-compliant geospatial metadata was developed. To accomplish this, Rational Rose CASE software was used to create a UML class diagram of the relational database. The model was transitioned (using ArcCatalog's CASE schema tool) to a physical database currently using MS Access (though plans include a transition to IBM DB2 9.1 in the future). Currently, the relational database is being populated using ArcXML metadata documents parsed using XML Parser software developed by the author. Upon completion of this phase of the project, the database will be coupled to an intelligent web interface that searchers for data using geospatial operators.

Initially the metadata within this database will describe geospatial data within the Idaho State University GIS TReC spatial library only. However, once initial implementation is completed, the database will be opened and members of the GIS community will be able to post metadata describing geospatial data from around the world. This distributed design (potentially mirrored on other servers) where only the geospatial metadata is stored within the database (along with a URL path to the data itself) will help facilitate data discovery, sharing, and the development of the GeoWeb.

ACKNOWLEDGEMENTS:

This study was made possible by a grant from the National Aeronautics and Space Administration Goddard Space Flight Center which was made possible through efforts of the Idaho congressional delegation.

LITERATURE CITED

Boggs, M. and W. Boggs, 1999. A Tour of Rose. M*astering UML with Rational Rose (pp.34).* California: SYBEX.

Bradley, J. and A. Millspaugh, 2003. *Programming in Visual Basic .Net.* New York, NY: McGraw-Hill Higher Education.

Date, C. J. 2003. Relational Systems and Others. *An Introduction to Database Systems (8th ed.).* Addison Wesley.

ESRI, 2006. *ESRI Profile of the Content Standard for Digital Geospatial Metadata.* , March 2003. Retrieved 27 September, 2006 from http://www.esri.com/metadata/esriprof80.html

FGDC 2000. Content Standard for Digital Geospatial Metadata Workbook. Federal Geographic Data committee.

Markowetz, A., Y. Y. Chen, S. Torsten, X. Long, and B. Seeger, 2005. *Design and Implementation of a Geographic Search Engine.* Eighth International Workshop on the Web and Databases (WebDb 2005), Baltimore, Maryland, June 16-17, 2005.

Schneider, D. 2005. *An Introduction to Programming Using Visual Basic 2005, sixth edition.* Upper Saddle River, NJ: Pearson Prentice Hall.

Evaluation and Design of a Relational Database Implementation of the FGDC CSDGM Model Using Various Database Engines Along with XML Parser Design

Kit Na Goh, Idaho State University, GIS Training and Research Center, 921 S. 8th Ave., Stop 8104, Pocatello, Idaho 83209-8104

ABSTRACT

The current search methodology used for the GIS Training and Research Center's (GIS TReC) spatial library has limitations and problems which do not fully facilitate geospatial discovery and delivery. Various tools were analyzed to find a better solution by applying techniques that other researchers have used to develop a more robust and efficient search engine. The method used developed and deployed a relational database containing geospatial metadata documentation for all datasets within the spatial library and a web interface designed to efficiently query the database. This method holds great promise for helping website visitors more effectively find required geospatial data. The main purposes of this study were to: 1) develop a robust database design that is physically independent of a specific database engine and 2) populate and deploy the relational database on the Internet using a customized search application. Various Relational Database Management System (RDBMS) engines were used during the development and testing process, such as, Microsoft Structured Query Language (MS SQL) Server, Microsoft Access and International Business Machine Database 2 (IBM DB2). The database schema was developed using Unified Modeling Language Computer- aided software engineering (UML CASE) modeling. This solution is currently deployed using Microsoft Access.

KEYWORDS: IBM DB2, RDBMS, Visual Basic, Visual Studio, GIS, metadata

INTRODUCTION

To manage and support sophisticated geospatial data searches, a relational database was developed to act as the backbone against which a search interface can be executed. The relational database design was intended to improve data discovery and delivery by including all information contained within geospatial metadata documents. The Federal Geographic Data Committee (FGDC) geospatial metadata format was chosen as the base metadata standard for this project.

The FGDC metadata standard describes GIS datasets using seven major sections and three supporting sections. The seven major sections are: 1) identification, 2) data quality, 3) spatial data organization, 4) spatial reference, 5) entity and attribute, 6) distribution, and 7) metadata reference information. The three supporting sections are: 1) citation, 2) time period, and 3) contact information. In addition to this information, the relational database developed for this project also contains the name and URL of the geospatial dataset along with descriptive keywords to better facilitate searching and downloading. A customized extensible markup language (XML) Parser application was also designed to load FGDC geospatial metadata stored within XML files into a normalized relational database. This allows data from many XML files to be searched, allowing simple and complex queries to locate and find information on data to determine data availability.

In addition to improvement in search and query functionality for end-users, an additional benefit of this approach is the reduction in overall disk space usage and the removal of redundant stand-alone HyperText Markup Language (HTML)-based metadata files by importing metadata files into a relational database. The web interface will search the data based on the information in the database. It is anticipated that this will improve long-term maintenance of the archive, as shown in Figure 1.

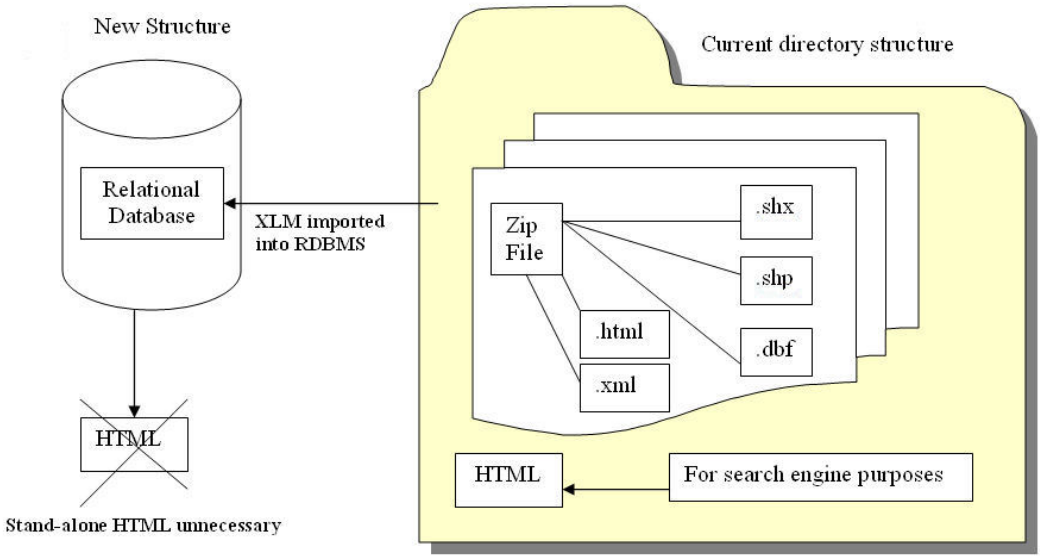

Figure 1. Reduction of HTML files improves long-term maintenance of the archive

METHODS

Database Design Using a UML CASE Class Diagram

At the outset of this project, a database schema (design) that would support geospatial metadata documents did not exist. For this reason, the first step was a careful database design normalized to third normal form. Normalization helps to remove data inconsistencies that result from data redundancies (Rob and Coronel, 2002). UML is a standard diagramming language used to design database schemas, among other things, and the software tool that was used to create UML models is Rational Rose (Boggs and Boggs, 1999). To manage and support sophisticated searches, a relational database with tables describing

GIS datasets based on the seven major sections of the FGDC metadata standard was created using Rational Rose. This database design includes the information captured within geospatial metadata documents, the name and the file path to the geospatial dataset, and descriptive keywords (Figure 2).

Based upon a careful review of both the Environmental Systems Research Institute (ESRI) profile of the content standard for digital geospatial metadata (CSDGM) and the FGDC geospatial metadata format, 50 tables representing the base metadata standard were created. These tables describe GIS datasets that include all major sections and supporting sections.

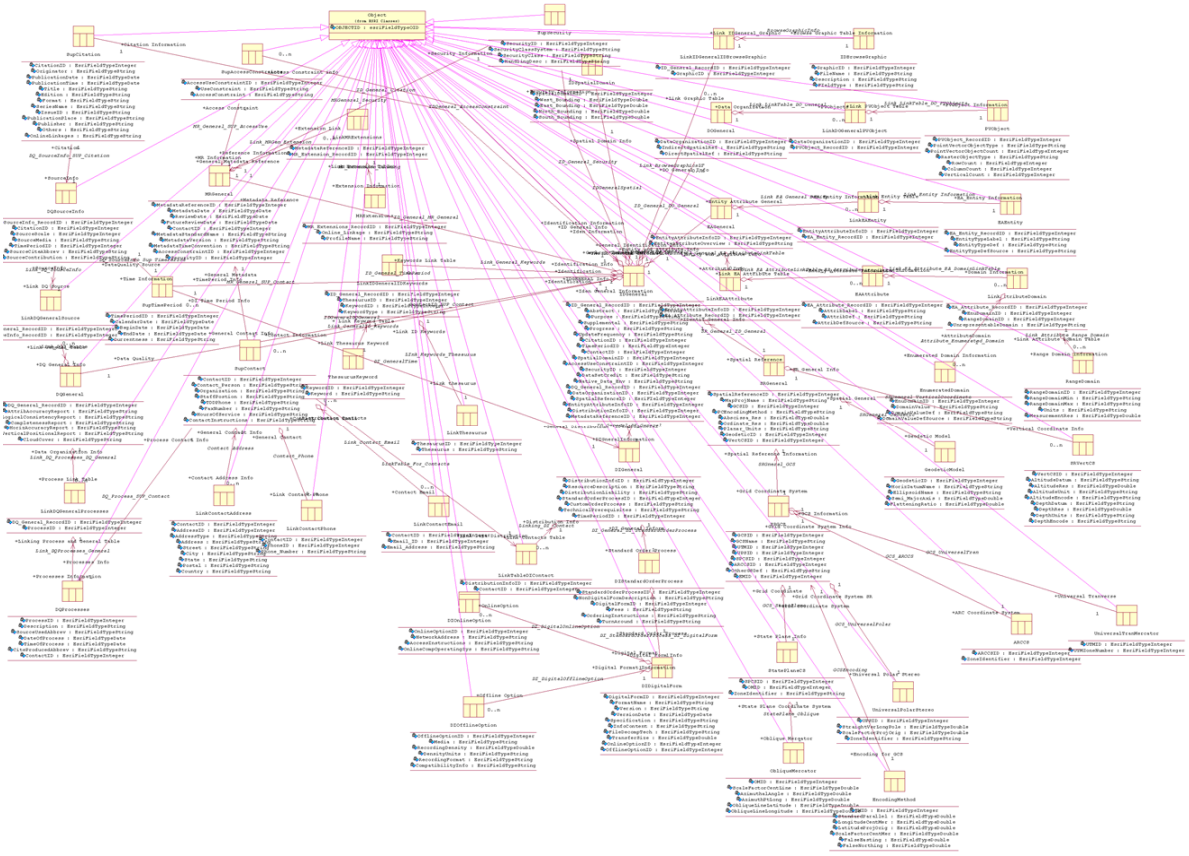

Figure 2. The UML Class Diagram for the relational database developed using Rational Rose, http://giscenter-sl.isu.edu/umlmodel/index.htm

Seven major sections are represented in the tables: identification information (***IDGeneral***), spatial reference information (***SRGeneral***), entity and attribute information (***EAGeneral***), distribution information (***DIGeneral***), data quality information (***DQGeneral***), metadata reference information (***MRGeneral***), and spatial data organization information (***DOGeneral***). The supporting sections are represented in the tables: citation information (***SupCitation***), time period information (***SupTimePeriod***) and contact information (***SupContact***).

Tables are organized into rows and columns (tuples and attributes) and some of the tables are related to other tables in the database. Using the example in Figure 3, observe that the primary key (DataOrganizationID) of the DOGeneral table uniquely identifies each row in its table. Likewise, the primary key (PVObject_RecordID) of the PVObject table is used to identify each record. LinkDOGeneralPVObject is a composite table that is used to link the tables (DOGeneral and PVObject) and thereby eliminate the possibility for redundancies. Therefore, the LinkDOGeneralPVObject table

consists of a primary key that is the combination of the foreign keys (DataOrganizationID and PVObject_RecordID).

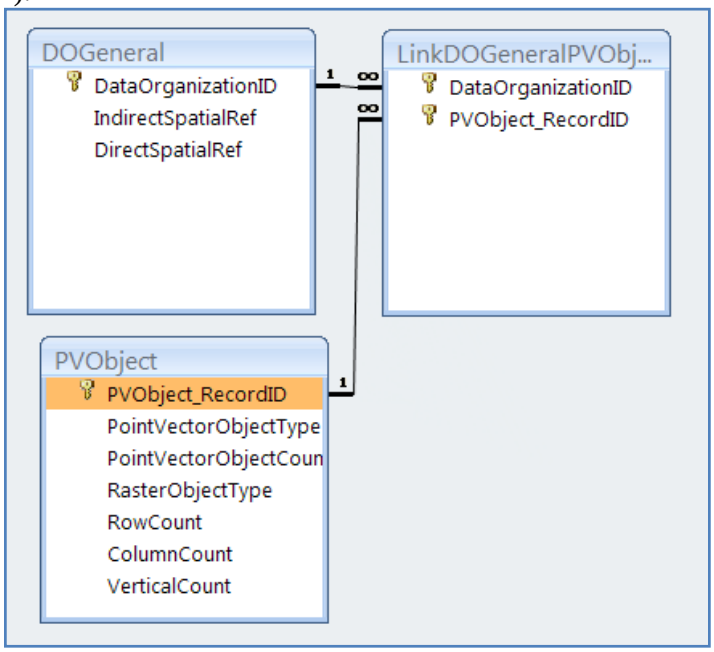

Figure 3. Sample of a relationship

After designing the database schema using the UML Class diagram model, the XML metadata interchange (XMI) file was exported from Rational Rose in order to transition into a physical database. "XMI is an Object Management Group (OMG) standard that specifies how to store a UML model in an XML file" (Perencsik et al, 2004).

The advantage of using a UML model is its ability to transition into a physical database using the UML class diagram model. Changes can be made to the model and exported using the XML file (consisting of UML XMI) that facilitates transfer of UML diagrams to other software applications (such as ArcCatalog). "When a change occurs to the model, Rose can modify the code to incorporate the change" (Boggs and Boggs, 1999), this helps to ensure that the model is resilient and flexible.

After exporting the XMI file from Rational Rose, a Microsoft Access relational database was created using the computer-aided software engineering (CASE) schema tool within ArcCatalog. "The CASE tools subsystem lets you create blueprints of the structure of the geodatabase using a graphical language – the Unified Modeling Language (UML)" (Perencsik et al, 2004). However, before running the CASE tool wizards, a semantic checker was used inside Rational Rose to make sure that the model stored in the XMI file was correctly defined and followed the set of modeling rules described by the ESRI framework. The semantic checker produces a report where it lists the errors that were found in the model. In this way, the model could be found to be free of errors before running the CASE tool wizards. The UML design is available at http://giscenter-sl.isu.edu/umlmodel/index.htm

XML Schema Testing on Various RDBMS Engines

The efficiency of using the XMI file that was exported from Rational Rose to transition into different databases (such as, MS SQL Server Express and IBM DB2) was tested.

The strategy for using the UML and CASE Schema tool from ArcCatalog to design and create the database involves using UML to define the schema and generate the XMI file. Before transitioning the

XMI file into Microsoft Access, a new personal geodatabase was first created and the CASE Schema Wizard tool was used to transition the schema into the database. Later, the same XMI file was used and transitioned into a MS SQL Server Express database by first creating a new geodatabase and repeating the process as described above. Users do not have to concern themselves with data conversion from the keyword ESRI Field Type (e.g. esriFieldTypeInteger) to standard database field types (e.g. Integer) as the CASE Schema wizard tool will perform the conversion automatically.

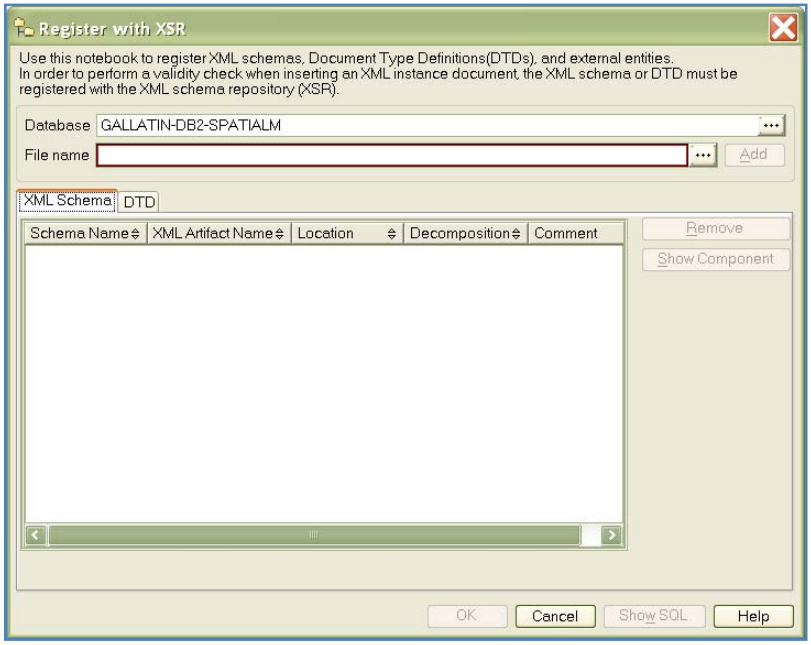

Figure 4. Register with XSR

For IBM DB2, a new database was created. Once a new database has been created, the XML Schemas, Document Type Definitions (DTD), and external entities need to be registered with the XML Schema Repository (XSR) (Figure 4). This needs to be done in order to perform a validity check when inserting the XML schema (*.XSD files). IBM DB2 allows either DTD or XSD files to be registered. In this particular instance however, the initial language used while creating the UML design was the default – "Analysis". Therefore, the UML design was saved as a Rose model (*.mdl file) that can't be registered with the XSR. If the initial language was set to XML_DTD, then the design would be saved as an *.XSD files. In this case, the file could be registered and the schema used to build the database.

Since the database design was successfully converted to each type of database in the test set, it indicates that the database design is robust and physically independent of a specific database engine. In other words, the same XMI file that encloses the UML class diagram can be transitioned into various database engines, such as Microsoft Access, MS SQL Server Express and IBM DB2.

Development of XML Parser Software

To populate the relational database, all information stored in HTML-based metadata files (approximately 30,000) needed to be imported. Parsing such metadata files can be quite difficult because of the variations of formatting one might encounter in different HTML files. Therefore, the HTML-based metadata files had to be converted to XML metadata files. There are currently only 2000 XML metadata files. This process could be done by using Microsoft Word and the U.S. Geological Survey (USGS) metadata utility "cns" to produce a well-formatted text file, which was then imported into ArcCatalog via the "import metadata tool". With the metadata stored within the standard ArcXML file format, the

process of parsing and importing metadata became greatly simplified. An "XML Parser" application was written using Visual Basic 2005 to perform this function.

Using the XMLTextReader function in Visual Basic 2005, the XML Parser application could import ArcXML formatted metadata to the relational database. The goal of building the XML Parser software was to read an ArcXML metadata document, parse it, extract the values (fields and attributes), and write the data to the appropriate relational database tables.

A graphical user interface (GUI) was designed (Figure 5) for the XML Parser program. The GUI includes basic functions (such as Open, Save, Add, Remove Files, and Open a folder) within two areas on the page: a file screen and a preview screen. The file screen displays the name of all XML files contained in the current workspace. The preview screen previews selected XML files along with their keys and values. Keys are attributes that are used for selection during data retrievals.

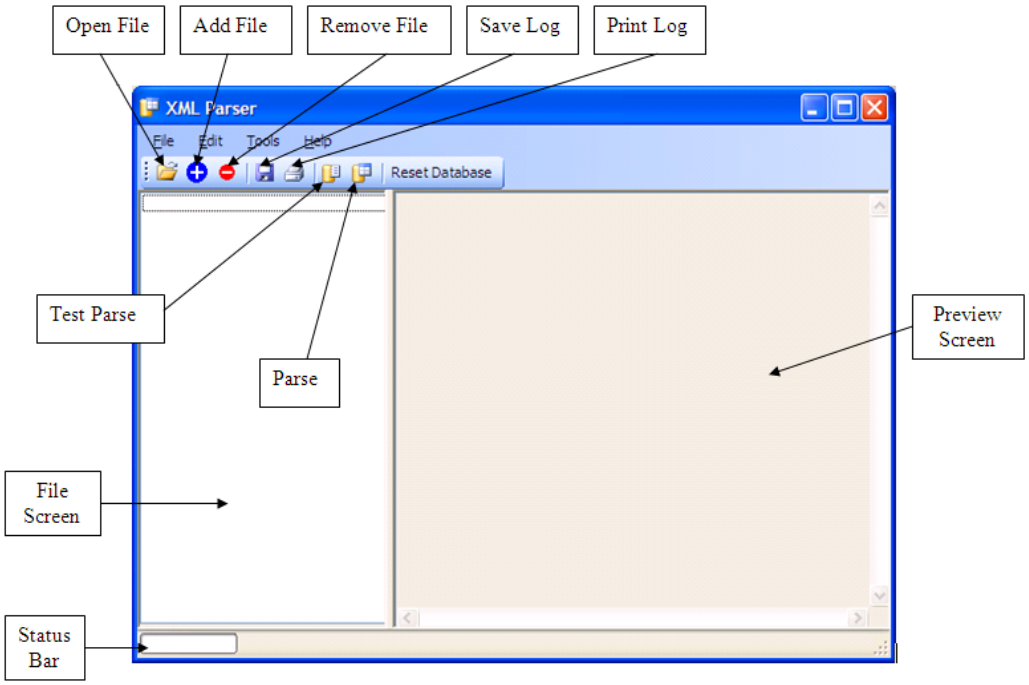

Figure 5. Screen of XMLParser software

Exploring XML Parser

Hash tables were used to store values inside the XML tags. "A hash table is a fixed-length array of pointers to link lists of nodes; each node contains a string and a pointer to the next node" (Zobel et al, 2001). These values were then inserted into the database (MetadataSpatialGDB.mdb) using the SQL SELECT statement. Active Data Object (ADO) connections were created that executed the SQL commands and inserted the values into the database.

After selecting a set of XML files for parsing, the user can parse them to the database directly by clicking the parse button  . "The numeric conversion functions examine the value stored in the argument and attempt to convert it to a number in a process called *parsing*, which means to pick apart, character by character, and convert to another format" (Bradley and Millspaugh, 2003). In this case, parsing means the process of extracting the values stored inside the XML tags. The XML Parser application will parse all files in the file index list.

When the parse button  is activated (the parse button click event), the *ReadMetaID* and *ReadOnlineLink* sub procedures are called to retrieve the MetaID (a Globally Unique Identifier (GUID)) and Online Linkages, which store the locations of the files using a Universal Resource Locator (URL). The *FieldExists* sub procedure is then called, and uses these same two attributes to determine if the XML file has already been parsed and its data already exists in the relational database. These two attributes were used instead of the GUID because if the ArcXML metadata files were created using a template (as is often done with automed software like NPS metadata tools), all ArcXML files will have the same GUID as the template. Therefore, the user would not be able to store the files. To avoid this situation and allow the use of automated software, two alternative unique attributes were used to identify the XML files and allow numerous XML files with the same GUID -- but different online linkages -- to be stored within the database.

If the record does not exist in the database, then the *ParseTheFile* sub procedure is invoked. If the record does exist, the *File Exists* message is displayed requiring the user to choose to either "update the record" or "cancel" the parse process. If the user chooses to "update", the *DeleteRecord* sub procedure is first called to delete the particular record(s) and it then inserts the updated records by calling the *ParseTheFile* sub procedure.

Inside the *ParseTheFile* sub procedure, the Select CASE function allows the parser to compare the XML tags against multiple criteria. "Select CASE is able to determine the choices by the value of selector and take appropriate actions (Schneider, 2005). "Each of the possible actions is preceded by a clause of the form ***Case valueList,*** where *valueList* itemizes the values of the selector for which the action should be taken" (Schneider, 2005). If the XML tags match one of the criteria, all the information within the tag is extracted and the values are inserted into a hash table. The tag name and the values within the tag are stored as keys and key values inside the hash table (Figure 6). There are eight CASE selections, which include the seven major sections of FGDC geospatial metadata and ESRI header information.

The sample code shown in Figure 6 shows that the XML text reader function reads the node trees and if the child element of the parent node matches the Select case criteria, such as "spref", then ReadSubTree method is used to create a boundary around that specific element. Therefore, the application can work with the information inside the "spref" element instead of the whole XML document. Next, the variable "NameValue" reads the whole string including the XML tag within the element. For example, <semiaxis Sync="TRUE"> 6378206.400000 </semiaxis> will be read into the "NameValue" (Figure 7). In this case, "semiaxis" will be stored as a key and the value within "semiaxis" (6378206.400000) will be the value for its key and added to the hash table called "spref" that was declared at the beginning of the program code, thereby identifying spatial reference information group. However, if there is any XML tag that is repeated, it will be caught in the Try…Catch statement since the hash table does not allow duplicate keys. Under the Catch statement, the count will be incremented and added as a suffix after the key's name to avoid duplication.

Seven text files were created representing the list of possible attributes included within the identification, data quality, spatial data organization (Figure 8), spatial reference, entity and attribute, distribution, and metadata reference information major section.

```
'parse the file
While (Reader.Read)
Select Case nodeName
   Case "spref"
        subReader = Reader.ReadSubtree
        Dim Name As String
        Dim NameValue As String = ""
        Dim Count As Integer = 1
        Dim Value As String = ""

        ' unicode for quote characters
        Const DoubleQuote As Char = ChrW(39)

        While (subReader.Read)
           If subReader.NodeType = XmlNodeType.Text Then
           'Add the keys and values inside the spref Hash Table
           Try
             NameValue = subReader.ReadString
             If NameValue.Contains("'") Then
                Value = Replace(NameValue, "'", DoubleQuote & "'")
                NameValue = Value
             End If
              spref.Add(subReader.Name, NameValue)
              'If the same key exists, then add count number to
make a new key
             Catch
                  Name = subReader.Name & Count
                  spref.Add(Name, NameValue)
                  Count += 1
             End Try
          End If
        End While
    End Select
End While
```

Figure 6. Sample Code showing Case Selection

```
<geodetic>
  <horizdn Sync="TRUE">North American Datum of 1927</horizdn>
  <ellips Sync="TRUE">Clarke 1866</ellips>
  <semiaxis Sync="TRUE">6378206.400000</semiaxis>
  <denflat Sync="TRUE">294.978698</denflat>
</geodetic>
```

Figure 7. Sample XML tag

Abstract	browset	cntper	edition	northbc	publish	sername
accconst	bottombc	cntpos	enddate	onlink	pubplace	southbc
address	caldate	cnttdd	geoform	origin	pubtime	state
address	city	cntvoice	hours	othercit	purpose	supplinf
addrtype	cntemail	country	issue	place	rightbc	theme

Figure 8. A list of attributes that may be found in the spatial data organization information major section

After parsing the file, the *InsertInfo* sub procedure (Figure 9) is called to compare the attribute names inside the appropriate text file with the keys inside the hash table. If the attributes contained in the text files are not found in the hash table, then the attribute names are added to the hash table with an empty string value. This is done to eliminate an element not found error while performing the SQL INSERT statement later on.

```
Sub InsertInfo(ByVal FileName As String, ByRef HashName As
Hashtable)
   Dim sr As IO.StreamReader = IO.File.OpenText(FileName)
   Dim De As DictionaryEntry
   Dim HashCount As Integer = HashName.Keys.Count
   Dim Counting As Integer = 0
   Dim FoundValue As Boolean
   Dim valtofind As String
   Do While sr.Peek <> -1
       valtofind = sr.ReadLine
       FoundValue = False
       For Each De In HashName
           If CStr(De.Key) = valtofind Then
               FoundValue = True
               Counting = 0
               Exit For
           Else
               Counting += 1
               'Debug.Print(CStr(De.Key))
               Continue For
           End If
       Next De
       If FoundValue = False Then
           HashName.Add(valtofind, "")
           Counting = 0
       End If
   Loop
   sr.Close()
End Sub
```

Figure 9. The InsertInfo Procedure

The *InsertDatabase* sub procedure is then called to insert the records into the MetadataSpatialGDB.mdb database. The data is inserted according to the seven major sections.

Insert Records into the Database

There are three main steps for inserting records into the database: 1) insert data to individual tables (Figure 10), 2) retrieve the primary key generated for each record (Figure 11), and 3) insert the primary keys into the link tables that have one-to-one, one-to-many, and many-to-many relationship (Figure 12).

```
CommandQuery = "INSERT INTO DQGeneral" _
& " (AttribAccuracyReport, LogicalConsistencyReport,
CompletenessReport, HorizAccuracyReport,
VerticalPositionalReport, CloudCover) " _
& " VALUES ('" & Dataqual.Item("attraccr").ToString & "', " & "'"
& Dataqual.Item("logic").ToString & "', " & "'" &
Dataqual.Item("complete").ToString _
& "', " & "'" & Dataqual.Item("horizpar").ToString & "', " & "'"
& Dataqual.Item("vertaccr").ToString & "', " & "'" &
Dataqual.Item("cloud").ToString & "')"
strSQL.CommandText = CommandQuery
strSQL.Connection = connection
strSQL.ExecuteNonQuery()
```

Figure 10. Step 1 – Insert relevant information into the individual tables

```
'Get the primary key generated
CommandQuery = "SELECT Max(DQ_General_RecordID) FROM DQGeneral;"
strSQL.CommandText = CommandQuery
strSQL.Connection = connection
reader = strSQL.ExecuteReader
strSQL.Dispose()
'Return the primary key that generated
If reader.Read() Then
  DQGeneralRecordID = Convert.ToInt32(reader(0))
End If
```

Figure 11. Step 2 - Retrieve the Primary key generated from each record

```
'Insert all the values stored in the array
If dataqualprocessid.Count > 0 Then
  For I = 0 To dataqualprocessid.Count - 1
CommandQuery = "INSERT INTO LinkDQGeneralProcesses" _ & "
(DQ_General_RecordID, ProcessID) " _ & " VALUES ('" &
DQGeneralRecordID & "', " & "'" &
dataqualprocessid.Item(I).ToString & "')"
   strSQL.CommandText = CommandQuery
   strSQL.Connection = connection
   strSQL.ExecuteNonQuery()
  Next
End If
```

Figure 12. Step 3 - Insert the primary keys into the link tables

The record is inserted by calling the sub procedures accordingly: spatial reference information (*SR_General*), data quality information (*DQ_General*), entity and attribute information (*EA_General*), metadata reference information (*MR_General*), distribution information (*DI_General*), data spatial data organization information (*DO_General*) and identification information (*ID_General*). The XML Parser will retrieve all the primary keys for each major section before inserting data into the Identification information table.

The XML Parser will then continue the parsing operation until completion of the last file in the list, at which point a message will be displayed indicating the results of file loading. The message “Complete Inserting to Database” is shown when all files have been successfully inserted into the database.

Efficiency Testing of XML Parser
Based on the response time that I set, I assumed if the XML Parser software was able to load one metadata file with all tags of data represented in less than 30 seconds then the software is considered as efficient. Testing the system was done by loading 100 XML files at once and inserting the files into the database in less than 2 minutes. The system met the performance requirements (<30 seconds per file).

Currently there are approximately 2000 XML metadata files stored in the relational database (MetadataSpatialGDB.mdb). When the rest of the GIS Center HTML-based metadata files are converted to XML metadata files, they will be inserted into the database for metadata files search.

RESULTS AND DISCUSSION

To better facilitate discovery and delivery of geospatial data for GIS TReC clients, a robust relational database containing FGDC-compliant geospatial metadata was developed and deployed. This database design is physically independent of a specific database engine and was tested by transitioning the schema into different physical databases (Microsoft Access, MS SQL Server Express, and IBM DB2). However, before running the CASE Schema tool, the semantic checker was used to make sure the model stored in the XMI file was correctly defined according to the ESRI framework.

After transitioning the schema into a database, the geodatabase rules were removed since the relational database only consists of tables and not feature classes or feature datasets. This represents a benefit for database developers as it shows that it is possible to transfer a database design to another database without manual recreation.

Each database has its own advantages. If the user only wants to store a small amount of data, then the class diagram model should be transitioned into a Microsoft Access personal geodatabase. However, if the user requires larger storage spaces to accommodate more data (>2GB), then a SQL Server Express or IBM DB2 are recommended.

The custom built XML Parser loads metadata stored within ArcXML files into a Microsoft Access database. There were three components in the parser software: the graphical user interface component, the XML parsing component, and the insert records component. The GUI component initializes the program and allows the users to select XML files to insert into the database and displays the results of the file loadings. The XML parsing component extracts the values inside the XML tags of the XML metadata files and stores them as keys and keys values in the hash tables. The insert records component writes the data into the appropriate table(s).

All code for the UML class diagram model and the executable for the XML Parser software are freely available under the L-GPL open source license and can be downloaded here: http://giscenter.isu.edu/research/techpg/nasa_tlcc/results.htm. Users can download the files, deploy the solution, and populate their own database

ACKNOWLEDGEMENTS

This study was made possible by a grant from the National Aeronautics and Space Administration Goddard Space Flight Center which was made possible through efforts of the Idaho congressional delegation.

LITERATURE CITED

Boggs, M. and W. Boggs 1999. A Tour of Rose. M*astering UML with Rational Rose (pp.34).* California: SYBEX.

Bradley, J. and A. Millspaugh 2003. *Programming in Visual Basic .Net.* New York, NY: McGraw-Hill Higher Education.

Perencsik, A., E. Idolyantes, B. Booth, and J. Andrade 2004. *ArcGIS 9: Introduction to CASE Tools.* Retrieved December 6th, 2007 from http://support.esri.com/index.cfm?fa=knowledgebase.documentation.viewDoc&PID=43&MetaID=658

Rob, P. and C. Coronel 2002. Normalization of Database Tables. *Database Systems Design, Implementation, & Management (5th ed.).* Boston, Massachusetts: Course Technology.

Schneider, D. 2005. *An Introduction to Programming Using Visual Basic 2005, sixth edition.* Upper Saddle River, NJ: Pearson Prentice Hall.

Zobel, J., S. Heinz, and E. H. Williams 2001. *In-memory Hash Tables for Accumulating Text Vocabularies.* Retrieved March 30th, 2007 from http://goanna.cs.rmit.edu.au/~jz/fulltext/ipl01.pdf

Testing Usability of an Active Server Page-based Geospatial Search Engine Tool

Kit Na Goh, Idaho State University, GIS Training and Research Center, 921 S. 8th Ave., Stop 8104, Pocatello, Idaho 83209-8104

ABSTRACT
Using Active Server Page technology, an intelligent web interface was created having the capability to 1) query spatial data against various keywords or search phrases and 2) allow users to view the metadata without first downloading the entire dataset. The web interface was built to facilitate rapid data discovery and download. The efficacy of the interface was tested by comparing it with 1) Idaho State University's GIS Center existing search engine, 2) the search capabilities found on USGS's Earth Resource Observation and Science data center website, and 3) the search capabilities of Inside Idaho's data center website. The efficiency of each interface was evaluated using a survey-based approach with both quantitative and qualitative metrics. The goal of this paper was to assess the newly developed web interface to facilitate its effective use and evaluate its efficiency. This paper includes a description of the applicable research, the web application development, and a summary of the survey results.

KEYWORDS: ASP, metadata, GIS

INTRODUCTION

The GIS Training and Research Center (GIS TReC) currently offers two search options to their web clients: a manual search and a simple search powered by Google. This approach has limitations which limit geospatial data discovery and delivery needs. Because of the size of geospatial data, most of the nearly 30,000 geo-spatial datasets stored at the GIS TReC's spatial library have been bundled and compressed in ZIP format. This unfortunately, hides much of the data from clients and even server-based indexing services are not sufficiently robust to reveal files stored within Zip files. To maintain the advantages of file bundling and compression, yet allow clients the ability to easily locate and retrieve data, an intelligent web interface was required enabling clients to enter search criteria and preview the metadata (all done within the database) without having to first download the dataset or try to memorize the server path to manually retrieve the required dataset.

Search engine tools are becoming common and most search through the meta-databases against meta descriptions of their geospatial data range.

> "A natural approach is to add advanced features to search engines that allow users to express constraints or preferences in an intuitive manner, resulting in the desired information to be returned among the first results. In fact, search engines have added a variety of such features, often under a special advanced search interface, though mostly limited to fairly simple conditions on domain, link structure, or last modifications date" (Markowetz et al, 2005).

The method of data retrieval will contain features that allow clients to enter keywords or search phrases and also permit the clients to preview the metadata in XML stylesheet before downloading the files. This will help the clients to locate the correct dataset. This feature will add more capability than typical geospatial data search engine (Figure 1).

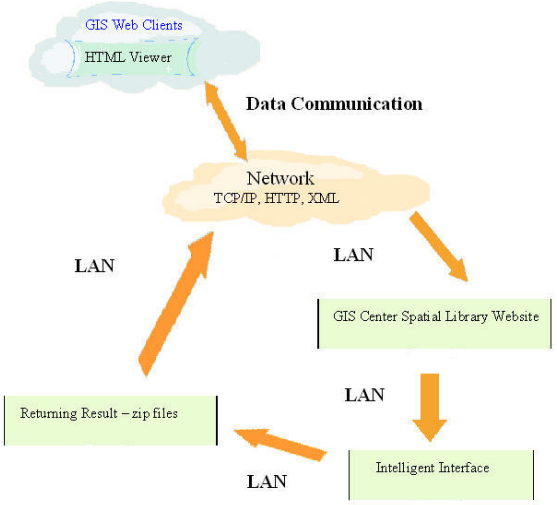

Figure 1. Schematic of new data discovery concept.

MATERIALS AND METHODS

Development of Intelligent web interface

The two technologies used to develop the intelligent web interface were Active Server Pages (ASP) and ActiveX Data Objects (ADO). "Active Server Pages (ASP) can intelligently interact with the user at the front end and with servers and datastores at the back end. ActiveX Data Objects (ADO) allows easy, powerful and robust control of technologies that access datastores" (Kauffman et al, 1999). ASP and ADO work together by reflecting current state of the database on the website without modifying scripting codes (Kauffman et al, 1999).

In addition, simple JavaScript codes were placed within the HTML and ASP files to capture and pass the input elements between the various WebPages. Compared to the common gateway interface (CGI), JavaScript can be inserted between codes and called within the webpage; However, CGI differs in that its process is started when the Web server receives a CGI-enabled URL request but there is no sequence of interaction among the browser and server (Thiemann, 2002). There are other server-scripting languages that are already existed, such as, PHP, CGI, Perl and etc. However, I chose to use ASP with JavaScript embedded because it is commonly-used scripting language and most browsers support ASP codes.

Three HyperText Markup Language (HTML) and two ASP pages (SearchResult.asp and XML.asp) were embedded with JavaScript codes and used to develop the Geospatial Search Engine tool (Figure 2). The HTML files (Result.htm, KeywordSearch.htm, and Other.htm) were designed to display a simple graphical user interface that allows clients to enter keywords or search phrases subsequently locate the matching dataset(s).

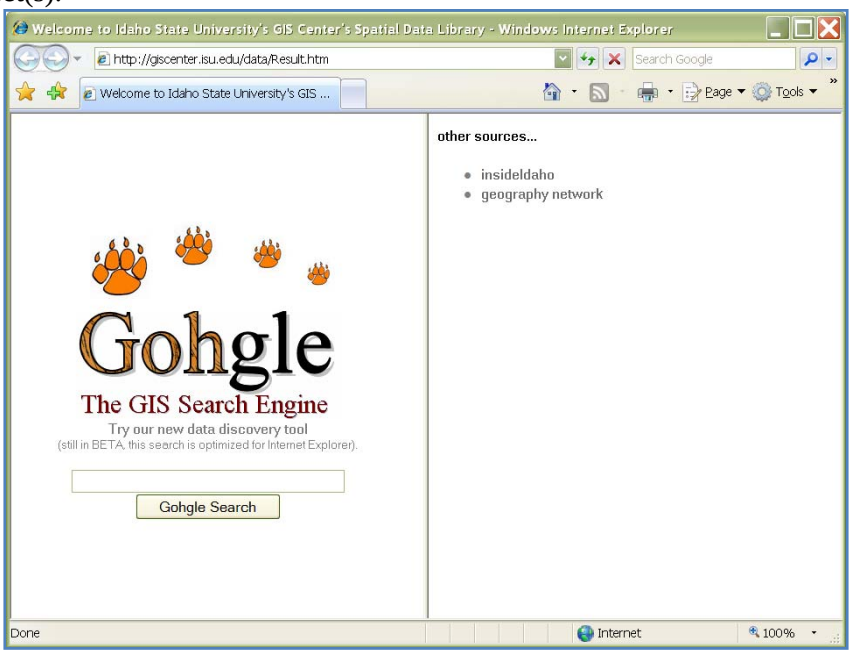

Figure 2. The simple interface of the geospatial search tool

When the clients enter a keyword or search phrase inside the input textbox and click the "Goghle Search" button, JavaScript code is called to capture the input element. If the input element contains an empty string, an alert is shown requesting proper input from the clients. If the input element is not null, the input element parameter (txtKeyword) is passed to *SearchResult.asp* page (Figure 3).

```
function submitkeywords()
{
        var urlToOpen = "";
        var KeywordValue = "";
        KeywordValue = document.getElementById("txtKeyword").value.toLowerCase();
        if (KeywordValue=="")
          {alert("Please enter a keyword or phrase to search the data!")
           }
        else
           {
        parent.right.location.reload("Other.htm");
        urlToOpen = "searchresult.asp?txtKeyword=" + KeywordValue;
        window.open(urlToOpen, "_self");
        document.getElementById("txtKeyword").focus();
          }
}//end of submitKeywords()
</script>
```

Figure 3. Javascript captures the input element and passes the element to SearchResult.asp page

Next, the ASP will connect to the database (using ADO) and retrieve the description (Abstract, Purpose, Data Type and URL link) of the file(s) that match the input element provided by the client through built-on-the-fly Structural Query Language (SQL) (Figure 4) expressions. The result is shown on the left areas of the webpage (Figure 5).

```
dim keyword
keyword=Replace(Request.queryString("txtKeyword"),"'", "''")
set conn=Server.CreateObject("ADODB.Connection")
conn.Provider="Microsoft.Jet.OLEDB.4.0"
conn.Open(server.mappath("Database/MetadataSpatialGDB.mdb"))
set rs=Server.CreateObject("ADODB.Recordset")
sql="SELECT distinct IDGeneral.Abstract,
IDGeneral.ID_General_RecordID,IDGeneral.Purpose,
SupCitation.OnlineLinkages, DOGeneral.DirectSpatialRef "
sql=sql & "FROM IDGeneral, SupCitation, DOGeneral,
LinkIDGeneralIDKeywords, ThesaurusKeyword "
sql=sql & "WHERE ((LCASE(IDGeneral.Abstract) LIKE '%" & keyword & "%')"
sql=sql & " OR (LCASE(ThesaurusKeyword.keyword) LIKE '%" & keyword &
"%')"
sql=sql & " OR (LCASE(SupCitation.OnlineLinkages) LIKE '%" & keyword &
"%'))"
sql=sql & " AND
ThesaurusKeyword.KeywordID=LinkIDGeneralIDKeywords.KeywordID AND
IDGeneral.DataOrganizationID=DOGeneral.DataOrganizationID "
sql=sql & "AND
LinkIDGeneralIDKeywords.ID_General_RecordID=IDGeneral.ID_General_Record
ID AND IDGeneral.CitationID=SupCitation.CitationID"
rs.Open sql, conn
```

Figure 4. The ADO connection is made to retrieve the description of files that match the input element.

When the client clicks a "Details and Download" link, the ID number and the URL link of the selected file are passed to the *XML.asp* page as these two unique attributes are used to identify individual metadata records stored within the database. A preview of the metadatae that selected by the clients is then generated on the right side of the webpage using JavaScript (Figure 6) and SQL (Figure 7). If the client then decides to download the file, they would click the "Download Data" button above the metadata preview (Figure 5).

Figure 1. Search Results with XML previews and download available

```
<script language="javascript">
function submitkeywords()
{
      var idx = document.URL.indexOf('&');
      var link = document.URL.substring(idx+8,document.URL.length);
      var urlToOpen = "";
      urlToOpen = link;
      window.open(urlToOpen, "_self");
}//end of submitKeywords()
</script>
```

Figure 6. Algorithm used to extract the ID number of the selected file when the user clicks the "Download Data" button.

```
<!--Print ARC coordinate system information -->
<%sub ARCSS()
set conn=Server.CreateObject("ADODB.Connection")
conn.Provider="Microsoft.Jet.OLEDB.4.0"
conn.Open(server.mappath("Database/MetadataSpatialGDB.mdb"))
set rs=Server.CreateObject("ADODB.Recordset")
rs.open rs5, conn
If Not rs.EOF Then%>
  <%if rs.Fields("ZoneIdentifier") <> 0 Then%>
     <%response.write("   <b>ARC Coordinate System: " & "</b><br>")%>
     <%response.write("    ARC System Zone Identifier: " & rs.Fields("ZoneIdentifier") & "<br>")%>
  <%end if%>
<%end if%>
<%rs.close
set rs=Nothing
conn.close%>
<%end sub%>
```

Figure 7. Example of displaying the information of the selected file for metadata preview.

Once the database and web interface were developed and deployed an assessment was made to determine its efficiency. This determination was made using a survey-based approach.

Survey Analysis

Questionnaires were created which helped determine whether the new database-driven web interface is better (i.e., easier to use and more efficient) than 1) the GIS TReC existing search tool (Browse folders), 2) USGS' Earth Resource Observation and Science (EROS) data center website (http://edc.usgs.gov/) and 3) the Inside Idaho data center website (http://insideidaho.org/asp/geodata.asp). The EROS and Inside Idaho data center search engines were chosen because 1) both are well known and popular data clearinghouse-type sites within the GIS field and 2) both data centers store some of the same data as ISU's GIS TReC. The efficiency of these interfaces was quantitatively evaluated based on the speed each could find and retrieve data and qualitatively evaluated based upon the respondents' ratings for ease of use, user-friendliness, clear navigation and web interface design.

The questionnaires were given to 35 Geographic Information Science (GIS) students who were currently taking GIS- related classes at Idaho State University. Their self-identified knowledge levels ranged from beginners (14 students), intermediates (13 students) and professionals (9 students). The different levels of knowledge groups were used to allow better understanding of the usefulness of each search engine tools. The responses from the questionnaires were collected and entered into Microsoft Excel to evaluate the effectiveness of the tools.

According to survey results, 74% of those surveyed believed that the new interface (Gohgle) is the easiest tool to locate data (Figure 8) and 91% of the respondents were able to find their required data using the Gohgle search engine tool. It is noted that 64% of beginners thought Gohgle was equally as easy to find data as the Inside Idaho search tool (Figure 9). In addition, 40% of the respondents agreed that the overall ease of use of Gohgle was good.

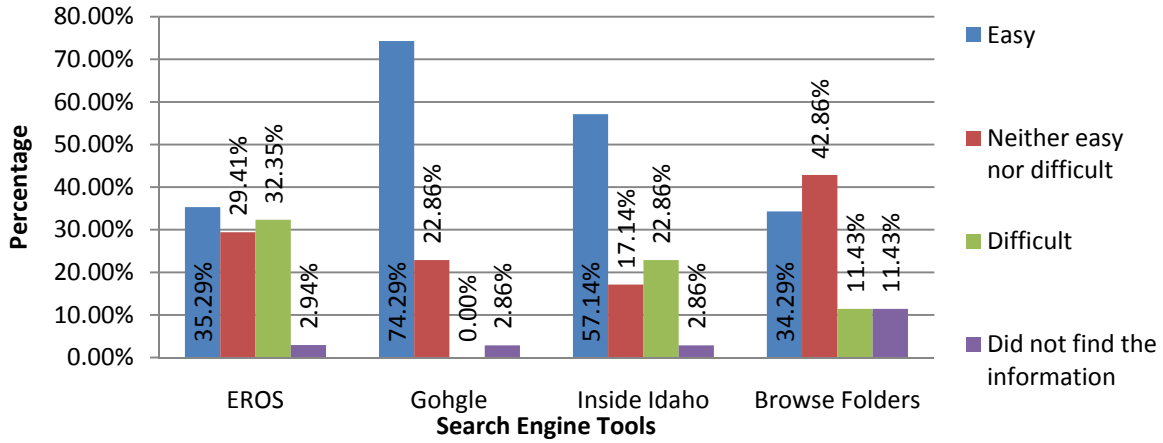

Figure 8. Difficulty level for all respondents to locate data

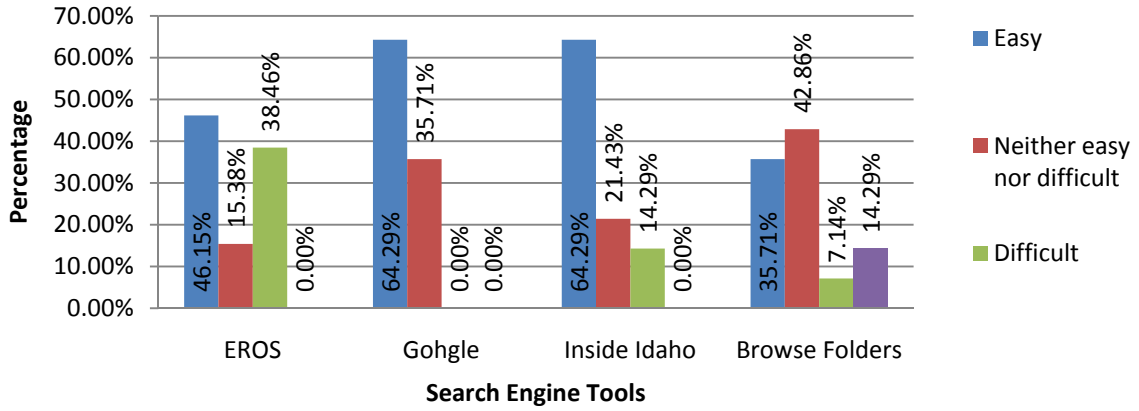

Figure 9. Difficulty level for beginner users to locate data

The efficacy of the Gohgle interface was the highest compared to the other search tools. Nearly 82% of respondents were able to locate and retrieve data in less than 5 minutes with the longest search and retrieve session lasting 10 minutes. The average time for Gohgle user's to search, return and download data was 7.8 minutes, while GIS TReC folder browsing required 9.4 minutes to complete the same process. In comparison, 11.4 minutes was required for Inside Idaho search tool users and 13.4 minutes was required for users of the USGS EROS data center search tool (Table 1).

To evaluate the qualitative aspects of the search tool (i.e., user-friendliness, clear navigation, self-explanatory use, and the "look and feel" of Gohgle) the survey responses were studied. For self-explanatory aspect, the users will know what they need to do with the interface without further instructions. Clear navigation means the interface is easy to browse and search for data. In addition, user-friendliness explains if the interface is common looking and whether the users like the design of the interface. The analysis suggests that the majority of respondents felt the Gohgle interface provided fairly

clear navigation (23% of the respondents rated average, 51% respondents rated above average and 23% rated good navigation). Nearly 83% of respondents were satisfied with the self-explanatory nature of Gohgle and 86% of respondents liked the look and feel of Gohgle. This suggests that the Gohgle web interface is user-friendly to the GIS TReC's clients.

Table 1. The length of time for each tool to search, retrieve and download data

	EROS	Gohgle	Inside Idaho	Browse Folders
<5 minutes	55.88%	81.82%	64.71%	62.50%
5-10 minutes	20.59%	18.18%	20.59%	34.38%
10-20 minutes	17.65%	0.00%	5.88%	0.00%
>20 minutes	5.88%	0.00%	8.82%	3.13%
Mean time	13.4min	7.8min	11.4min	9.4min

While survey results illustrate that Gohgle had the highest satisfaction among beginners (57%), intermediate users (85%), and professional users (88%), 50% of beginner users preferred the Inside Idaho search tool, but overall (Figure 10). In comparison, both intermediate (69%) and professional (75%) users preferred using the Gohgle search tool (Figure 11).

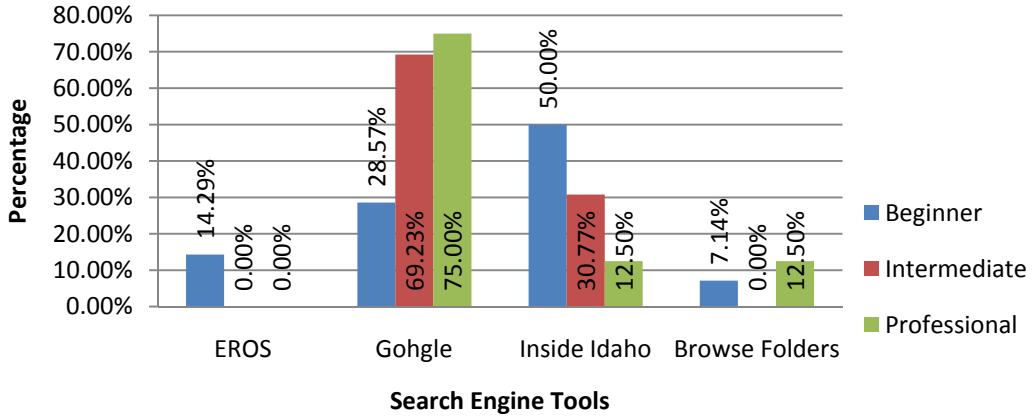

Figure 10. Respondent's search tool preferences organized by user category.

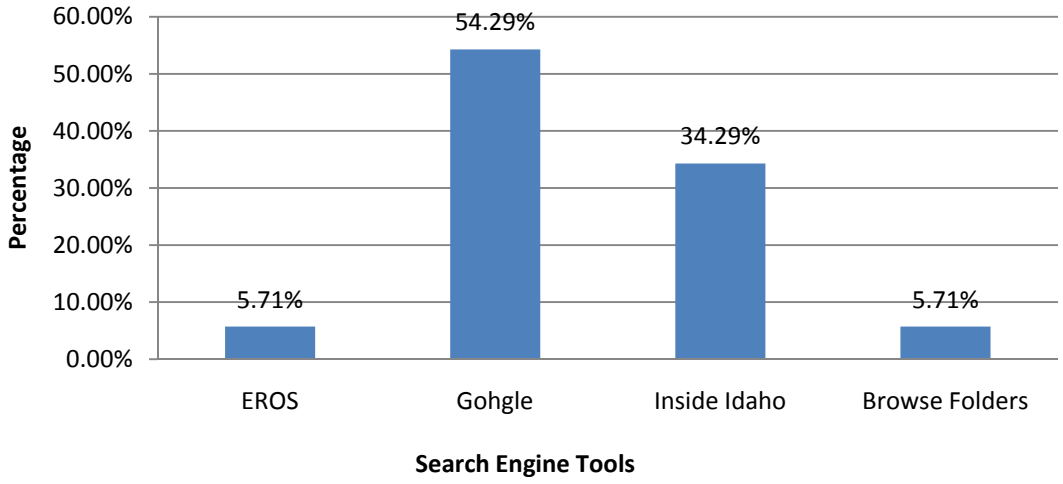

Figure 11. Respondent's search tool preferences.

RESULTS AND DISCUSSION

The survey data indicates that the majority of respondents agree that Gohgle is efficient, user-friendly and easy to use. It also suggests that the respondents were highly satisfied with Gohgle's functionalities; however, some results are different than expected, in that the simple Gohgle interface was not preferred by the beginner user group as this web interface was created to specifically support novice users and students. The tool was developed to be informative and easy to navigate for all the clients. Nevertheless, the analysis (Figure 10) suggested that the beginners preferred using Inside Idaho search tool than Gohgle search tool. In contrast, both intermediate and professional users favored Gohgle while more specialized - EROS data center search interface was rated the least favorite search tool among the tools tested.

Based upon the written comments from the respondents (4 students), they tended to like the default data description information and metadata preview of Gohgle as this saved search time. The Gohgle design was considered very standardized in appearance and easy to follow. However, beginners felt that the descriptive information on the page was not clear enough and they were hoping for thumbnail images of the data. Both of these are good suggestion for further improvement of Gohgle. The descriptive information of the files were retrieved from the database (MetadataSpatialGDB.mdb) and displayed to the clients. The information could be improved by metadata librarian and re-import into the database. The thumbnails of the data were not provided since thumbnails were not created for the metadata and this could be added in the future. In addition, the beginners chose to favor to Inside Idaho, it could also be due to they were more familiar with Inside Idaho tool for their class assignment. However, Gohgle search engine tool is a new tool that they were not used to. People have more tendencies to like the tools that they are more familiar with.

For the Inside Idaho data center website, the respondents expressed that they used this website more often and were more familiar with its contents. It is also predicted that the students (from Idaho State University) were mostly given the class assignments based on the data inside the Idaho.

The USGS EROS data center website was the least favorite search engine tool overall because the respondents found the website to be "clunky" and not well documented. Users did not like the fact that they needed to open up a map window to figure out the layers, perform location searches, or browse a File Transfer Program (FTP) directory structure if a map name was known before hand. This method was difficult for both beginner and intermediate users that weren't familiar with the data. Similarly, these users indicated that the existing GIS TReC search tool (Browse with folders) and USGS EROS tool were alike since the existing GIS TReC website is using web-browsing enabled file folder structure. As a result, the USGS EROS data center and the existing GIS TReC search engine were the least favorite tools among the users.

The database-driven search engine tool (Gohgle) was built to reduce the time and energy required to locate and download geospatial data and better ensure the correct data is downloaded to the users. The survey comparing Gohgle with three other search tools helped to determine that Gohgle had reached its expected outcome. The responses from the survey also brought to light Gohgle's perceived weaknesses which provide an opportunity for future enhancements to the tool. The final results suggest the tool did perform its required tasks and has the potential to be improved in the future.

ACKNOWLEDGEMENTS

This study was made possible by a grant from the National Aeronautics and Space Administration Goddard Space Flight Center which was made possible through efforts of the Idaho congressional delegation.

LITERATURE CITED

Kauffman, J., K. Spencer, and W. Thearon 1999. Beginning ASP Databases. New York, NY: Apress. Pp12.

Markowetz, A., Y. Y. Chen, S., Torsten, X. Long, and B. Seeger June, 2005. Design and Implementation of a Geographic Search Engine. Eighth International Workshop on the Web and Databases (WebDb 2005), Baltimore, Maryland, June 16-17, 2005.

Thiemann, P. 2002. WASH/CGI: Server-Side Web Scripting with Sessions and Typed, Compositional Forms. S.Krishnamurthi, C.R Ramakrishnan (Eds): PADL 2002, LNCS 2257, pp.192-208, 2002. Springer-Verlag Berlin Heidelberg.

[THIS PAGE LEFT BLANK INTENTIONALLY]

Contribution of Deep Soil Water to Invasion of Sagebrush Steppe by *Euphorbia esula* Following Fire

Matthew J Germino, Department of Biological Sciences, Idaho State University, Pocatello ID 83209-8007, germmatt@isu.edu, 208-282-3285

Jonathan L Horton, Biology Department, University of North Carolina, Asheville NC 27109

Steven S Seefeldt, Research Agronomist, USDA-ARS, SubArctic Agricultural Research Unit, University of Alaska Fairbanks, Fairbanks, Alaska 99775

Judson P Hill, Biology Department, Idaho State University, Pocatello ID 83209

ABSTRACT

A long-standing hypothesis for the invasive success of exotic species following disturbance is that disturbances promote invasions by increasing resource availability to the selective advantage of invasive species. Consistent with this hypothesis, efficiency of resource use is predicted to be less in invasive compared to native species. Furthermore, differences in soil resource use could lead to greater depletion of soil resources beneath invasive species, which, in turn, could be reflected in lower physiological performance of native species occurring in proximity to invaders. We examined relationships of water potentials in soils and plants, and photosynthetic gas exchange properties of *Euphorbia esula*, a forb from Eurasia, sagebrush (*Artemisia tridentata ssp. vaseyana*), and dominant native forbs (*Eriogonum heracleoides*) and grasses (*Pseudoregneria spicata*), in sagebrush steppe of Western N. America that had or had not been burned and/or invaded. Depth of water uptake was determined for all plants by comparing stable isotopes of water in stem and soils. Following snowmelt in early spring, soils were near field capacity to several m depth in all sites. As the growth season proceeded into dry summer conditions, soil water potentials decreased more in unburned compared to burned soils, particularly at depths below the main rooting zone of grasses (shallower than about 50 cm). Within burned areas, depletion of soil water at depths between about 75 and 125 cm was greater where *E. esula* occurred compared to where only native herbs occurred. Isotopic analyses revealed that *E. esula* and *A. tridentata* likely acquired water from similar depths in soils, which were consistently deeper than for native herbs and especially grasses. Predawn water potentials were similarly high (>-0.5 MPa) among species in treatments in early season, but became low in native herbs in later summer (<-1.5 MPa) in burned and invaded plots (<-2.5 MPa). In contrast, *A. tridentata* and especially *E. esula* maintained water potentials above -1.5 MPa in late summer. However, *E. esula* did not have any greater photosynthesis or photosynthetic water use efficiency than the other species. These correlations are consistent with the hypothesis that *E. esula* relies on access to relatively abundant sources of soil water below the typical rooting zone of grasses to sustain photosynthesis in this semiarid site. Fire appears to disrupt partitioning of soil water in the native community by selectively disfavoring sagebrush, thereby making deeper water more available in deep soils and providing a key resource for photosynthesis in *E. esula*.

KEYWORDS: Fire, soil water, sagebrush, stable isotopes, Euphorbia esula, photosynthesis.

INTRODUCTION

Ecological disturbance is a commonly cited factor contributing to invasion of plant communities by non-indigenous species. By disrupting resource partitioning among native plants, disturbances are thought to increase resources in ways that selectively favor exotic invaders. However, few studies have provided direct evidence that exotic plants selectively benefit from resources made available by disturbance. Such evidence would point to the potential importance of vacant niches to success of exotic plants, compared to other eminent hypotheses for success of invasive species.

Sagebrush steppe rangelands in the Great Basin cold desert of western North America are unusually vulnerable to invasion by exotic herbaceous species. Factors affecting the success of exotic annual grasses are well known in these ecosystems (eg. Chambers et al. 2007), but less is known about factors enhancing the success of the large number of species of exotic forbs that can be even more noxious problems in rangeland ecosystems (Pyke 1999). Many species in this suite of exotic forbs are tap-rooted and more persistent during water-limited periods of late summer than are native herbs, indicating a possible role for soil water to their success. Species in this suite of forbs, such as leafy spurge (*Euphorbia esula*) and thistles, knapweeds, tumbleweeds (Whitson 2002), have persisted for decades following colonizing phases of succession after disturbance (e.g. Selleck et al. 1962, Kulmatistki 2006). A greater understanding of factors promoting persistence of exotic forbs should lead to control strategies that are more effective than current emphases on eradication with chemicals or introduced insects.

In sagebrush steppe, soil water available for plant growth results mainly from winter snow and early spring rain, when soil throughout the rooting profile of plant communities reaches water-holding capacity (Smith et al. 1997). By the mid to late growth season, partitioning of soil water uptake among plant species contributes to nearly complete utilization of extractable water in soils, at least in undisturbed, native sagebrush steppe communities (Anderson et al. 1987). Following disturbances such as fire, sites in sagebrush steppe tend to be dominated for decades by herbaceous cover, while sagebrush slowly reestablishes (Harniss and Murray 1973). The paucity of shrubs or other deep-rooted species led to less depletion of water from soils deeper than about 50 cm on a recently burned site (Link et al. 1992).

The objective of our study was to determine how changes in soil water resulting from fire might affect the water relations and corresponding photosynthesis of *E. esula*. We hypothesized that 1) water availability in soils would be greater in burned compared to unburned sites, particularly in deeper soils but except where *E. esula* had become abundant, 2) *E. esula* in burned areas would utilize soil water from similar depths as the dominant species of unburned areas (*Artemisia tridentata*), 3) *E. esula* and *A. tridentata* would utilize water from deeper and wetter soils than native herbs after midsummer, and would correspondingly have greater water status at predawn, 4) that *E. esula* would not exhibit greater photosynthesis or photosynthetic water use efficiency during seasonal drought compared to native species, which would otherwise indicate more efficient use of soil water as a mechanism contributing to its success in these desert sites, and 5) that *E. esula* would exhibit lower water potentials and greater water-related limitations to photosynthesis in the rare circumstances in which it is found adjacent to sagebrush.

METHODS

Water potentials and isotopic compositions of plants and soil were measured to determine water availability, water status, and depth of plant water uptake. Photosynthetic CO_2 and H_2O exchange of leaves was also measured as an indicator of water use that could affect plant water balance, and carbon gain that could indicate possible advantages that might result from differences in water relations. Sampling occurred twice, during June 25-30 and August 10-14. All samples for isotopic determination of depth of water uptake were collected on the same day, and all plant samples were collected within about 1 hr during late afternoon.

The experimental design consisted of a 2 x 2 factorial arrangement of twelve plots (n=3 per treatment) that differed in two factors: disturbance history (burned in 1999 or unburned in previous 70 years) and invasion by *E. esula* (invaded or not invaded). Soil water and depth of water uptake could not be measured on the three plots that were unburned and un-invaded. Plots were each about 1 m in diameter, and were separated by 20-100 m. Twelve plots were established for each of the two sampling efforts, to avoid resampling plots in August that had been disturbed during the previous sampling.

Site and species descriptions

All data were collected at the US Sheep Experimental Station (USSES; 44°14'44" N Latitude, 112°12'47" W. Longitude; 1650 m a.s.l.) near Dubois ID, USA, where most precipitation comes as winter snow and spring rain, and soils progressively dry during summer months. The dominant shrub in this community is mountain big sagebrush, *Artemisia tridentata* ssp. *vaseyana* Nutt. Other, less abundant shrubs are *Chrysothamnus viscidiflorus* Nutt., *Tetradymia canescens* DC. and *Purshia tridentata* (Pursh) DC. Perennial bunchgrasses such as *Pseudoregneria spicata* (Pursh) A. Löve, *Agropyron dastychium* (Hook.) Scribn., *Festuca idahoensis* Elmer and *Poa sandbergii* Vasey were common, as were perennial forbs such as *Eriogonum heracleoides* Nutt., *Cordylanthus ramosus* Nutt., *Achillea millefolium* L., *Erigeron corymbosus* Nutt., and *Lupinus* species. Soils are fine, loamy, mixed, frigid Calcic Argixerolls derived from wind blown loess or residuum (Natural Resources Conservation Service 1995). Total annual precipitation averaged 297 mm over the last 78 years, with 131 mm accumulating from May through August (Western Regional Climate Center, Desert Research Institute, Reno NV). Annual precipitation during our study period of January through September was 190 mm, respectively, compared to 240 mm for mean precipitation over these months over the previous 80 years. There has been grazing (21.3 sheep days/ha) on the site from 1968-2002.

Water uptake, water status, and leaf physiology were measured for the exotic forb leafy spurge (*Euphorbia esula*) and the following native species: bluebunch wheatgrass (*P. spicata*), Wyeth's or parsley-flowered buckwheat (a perennial forb, *E. heracleoides*), and sagebrush (*A t. vaseyana*). These species were the dominant cover of their respective functional groups in each of the plots, as assessed by estimating plant cover to the nearest 5% (1% below 5%) in four replicate sampling frames (0.5 m^2) positioned adjacent to the central soil cover in each replicate plot (Table 1). *Euphorbia esula* was scarce (<~3% of cover) in plots that were unburned and thus had abundant sagebrush, but was 2-fold more abundant than grasses and 5-fold more abundant than native forbs in the portions of burned areas it had invaded (Table 1). *E. esula* was present only in very small abundances at this site prior to the 1999 fire, and was the only exotic species present during our sampling.

Table 1. Mean percent cover (±1 SE) of bare soil, *Euphorbia esula*, and all species of grasses, forbs, and shrubs, in plots having different combinations of fire and invasion history (n = 3 plots; 4 sampling frames averaged per plot).

	Burned, invaded	Unburned, uninvaded	Burned, uninvaded
Grass	14.0 ± 4.3	10.8 ± 0.4	35.4 ± 7.0
Forb	4.5 ± 3.5	16.5 ± 3.1	11.9 ± 2.7
Shrub	0.6 ± 0.4	38.6 ± 3.9	1.5 ± 0.6
E. esula	26.7 ± 2.5	0	0
Bare ground	55.4 ± 8.1	35.8 ± 2.6	50.7 ± 6.1

Euphorbia esula is a rhizomatous perennial herb native to Eurasia that commonly can have abundant root mass at 2.4 m deep in soil, and maximum rooting depths are between 4.6 to 9 m (Raju et al. 1963, Raju 1985). Proliferation of *E. esula* after fire occurs through seedling establishment and resprouting. The shrub *A. tridentata* is among the deepest-rooted native species in sagebrush steppe, with rooting depths

commonly reaching 2 m or frequently deeper (Richards and Caldwell 1987, Welch and Jacobson 1988). *Artemisia tridentata* has both evergreen and deciduous leaves that collectively enhance water relations and carbon gain as soil water availability decreases during summer. *A. tridentata* reproduces only by seed. The native *P. spicata* is a perennial grass that can reproduce through tillers, and resprouts vigorously after fire. Root depths of *P. spicata* are commonly deeper than other, co-occurring grasses (< 0.5 m), but the maximum rooting depth of *P. spicata* (1.4 m) is much less than that of *E. esula* and *A. t. vaseyana* (Cline et al. 1977, Canadell et al. 1996).

Isotopic determination of depth of water uptake
In each plot, we extracted 1 soil core from the soil surface to bedrock (lava) using a tractor-mounted hydraulic corer (2.5 cm diameter, Giddings Inc, Ft. Collins, CO). Cores were extracted, divided into 5-10 cm increments that were sealed in thick plastic bags and stored in a cooler on ice, within a 10-minute period. Each increment samples was frozen at the end of the day, and later thawed, mixed, and separated into fractions to be used for isotopic analysis or measurement of water potential and content. Water potential and content were measured immediately, and soils for isotopic analysis were repackaged in sealed glass vials and frozen until analysis.

Two samples of non-photosynthetic tissue were collected per species from around each core, and were bulked to form each replicate for plant isotopic analysis. Woody stem was sampled from sagebrush, non-photosynthetic culms were sampled in the grass, tissue near the root stem interface was sampled from *E. esula*, and woody fibrous tillers from litter were sampled for the native forb. Samples were stored in glass vials and sealed with parafilm and then frozen until extraction of water for isotopic analysis.

Water was extracted from soil and plant samples using cryogenic vacuum distillation (Ehleringer and Osmond 1989), and analyzed for stable isotopes of hydrogen and oxygen by the Stable Isotope Ratio Facility for Environmental Research at the University of Utah. The ratio of deuterium to hydrogen and ^{18}O to ^{16}O in each sample was expressed relative to Standard Mean Ocean Water (SMOW) as follows:

$$\delta_{sample} = ((Ratio_{sample}/Ratio_{standard})-1)*1000$$

where R_{sample} is the ratio of the heavy to light isotope in the sample and $R_{stnadard}$ is the ratio of heavy to light isotopes in SMOW.

Mean isotopic ratios were calculated for each soil depth and plant species across treatments and sampling times (n = 3 for each treatment * sampling period). Plots were made of soil water potential (*see below*) and isotopic ratio as a function of soil depth. Plant isotopic values were compared to these graphs to determine the potential depths of water uptake.

Determination of water potential
Soil water potentials were determined for each increment of soil cores in the laboratory, using a temperature-controlled, WP4-T dewpoint hygrometer (Decagon, WA). Plant water potentials were determined at predawn and midday, on excised stems or grass blades, using a field-portable pressure chamber (Model 1000, PMS Instrument Co., Corvallis, Oregon, USA).

Photosynthetic gas exchange
Photosynthetic gas exchange was measured under clear sky conditions, using a portable photosynthesis instrument equipped with an artificial light source and a CO_2 controller (model 6400, LiCOR, NE). Light levels during measurement were 1000 μmol m^{-2} s^{-1} (400-700 nm), which was sufficient to saturate photosynthesis in all species, and [CO_2] was controlled at 370 μl l^{-1}. Humidity and temperature during measurement were maintained within about10-15% of ambient levels. Photosynthesis and stomatal conductance were reported on a projected leaf area basis. Leaf areas were determined using digital

photography with objects of known size in the field-of-view, and image processing software (ImageJ, National Institute for Health) to calculate areas.

RESULTS

Soil water availability

During the June sampling, soil water was generally above typical minimum levels (-1.5 MPa) for plant uptake, at nearly all depths and in all plots (Figure 1). Soil water potentials during this period were greatest in plots in the unburned, uninvaded areas that had intact vegetation communities. Soil water potentials decreased considerably from the June to August sampling dates, and only soils deeper than about 75-125 cm had water potentials above about -3 MPa by August. In August, water potentials in soils at approximately 50-150 cm depths were several times greater in burned compared to unburned plots, except where *E. esula* was abundant (Figure 1).

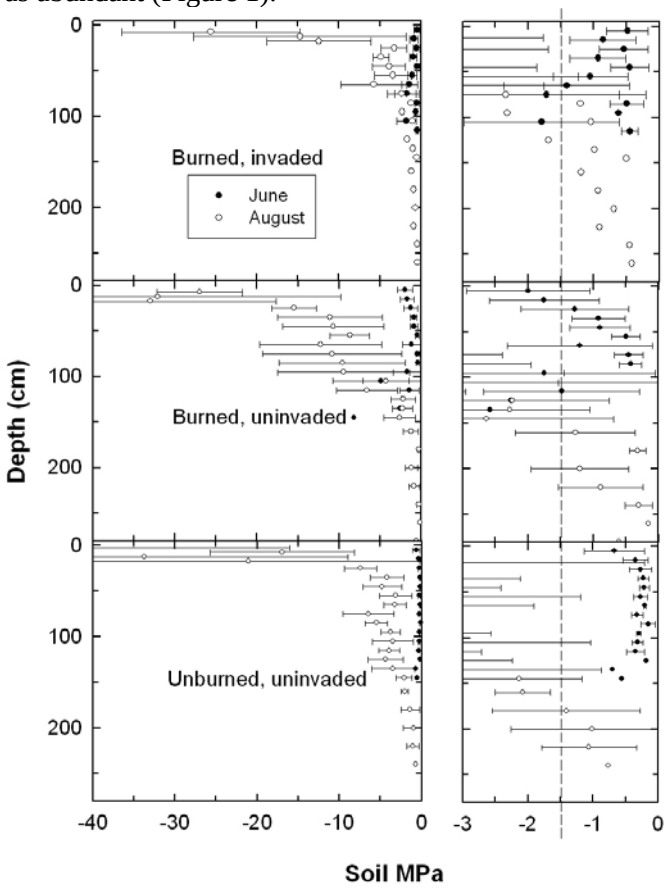

Figure 1. Soil water potential of soil in each treatment. Panels on the right are an expanded view of the plant-relevant values of soil water potential. The vertical dashed line shows the nominal value for permanent wilting point for crops (-1.5 MPa).

Isotopic evidence for depth of water uptake

In all plots, soils located between the surface and approximately 25 cm depth consistently had greater δD and $\delta^{18}O$ values than soils located deeper than ~25 cm (Figures 2-3). Below these depths, there were no consistent trends in isotopic ratios in soil water that could indicate depth of water uptake in plants. Despite the lack of inconsistent trends in isotopic ratios in soil, both δD and $\delta^{18}O$ were always greatest in the native grass (*P. spicata*), less in the native forb (*E. heracleoides*), and least in sagebrush (*A. tridentata*) and *E. esula*. No differences in δD and $\delta^{18}O$ were detected between *A. tridentata* and *E. esula*.

δD and $\delta^{18}O$ decreased in plants relative to maximum δD and $\delta^{18}O$ in soils at 0-25 cm depths (Figures 2-3), from June to August, due to both seasonal decreases in δD and $\delta^{18}O$ in plants and increases in δD and $\delta^{18}O$ in soils. Slightly greater δD and $\delta^{18}O$ in grasses than any soil values in June could be due sampling artifacts, such as accidental inclusion of transpiration-affected water in plant samples, or from possible plant uptake of water from the top few cm of soils. There were likely gradients of δD and $\delta^{18}O$ within each 10 cm increment of bulk soil we analyzed, and it is likely that such gradients would have been most pronounced in the shallowest soil depths, in which δD and $\delta^{18}O$ would were likely greater at a 1 cm than at 10 cm depth, for example (Figures 2-3).

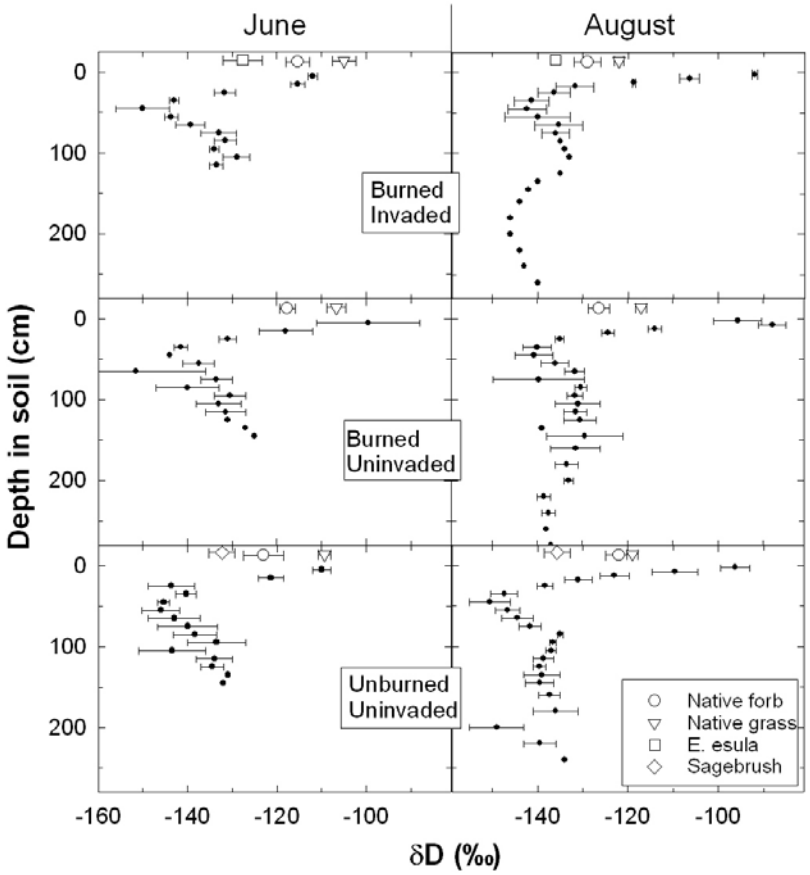

Figure 2. D/H in each treatment. Dark symbols show values in soil, and open symbols above the 0 cm depth in soil show the different plant species sampled.

Soil water uptake in *E. esula* and *A. tridentata* in August appeared possible from two depths in soil, at approximately 25 and 100 cm depths, based on comparisons of plant and soil δD and $\delta^{18}O$ (Figure 2, and top panel only of Fig. 3). Assuming that plants can only extract water from soils that have water potentials than the plants, these species were likely extracting soil water from the deeper depths (Figs. 1,4). Isotopic ratios of *P. spicata* and *E. heracleoides* were similar to ratios of soil water only in the dry soils from about 15-25 cm depth.

Plant water status

Predawn plant water potentials decreased by nearly three fold or more from June to August (Figure 4). The native grass *P. spicata* tended to have lower water potentials than the forb, and sagebrush and *E. esula* tended to have greater water potentials than the native herbs at predawn. The native grass and forb both had higher water potentials in plots that did not have *E. esula*, compared to plots that did have *E.*

esula. Daily decreases in water status from predawn to midday were greater in sagebush and *E. esula* than in the native herbs (Figures 4-5).

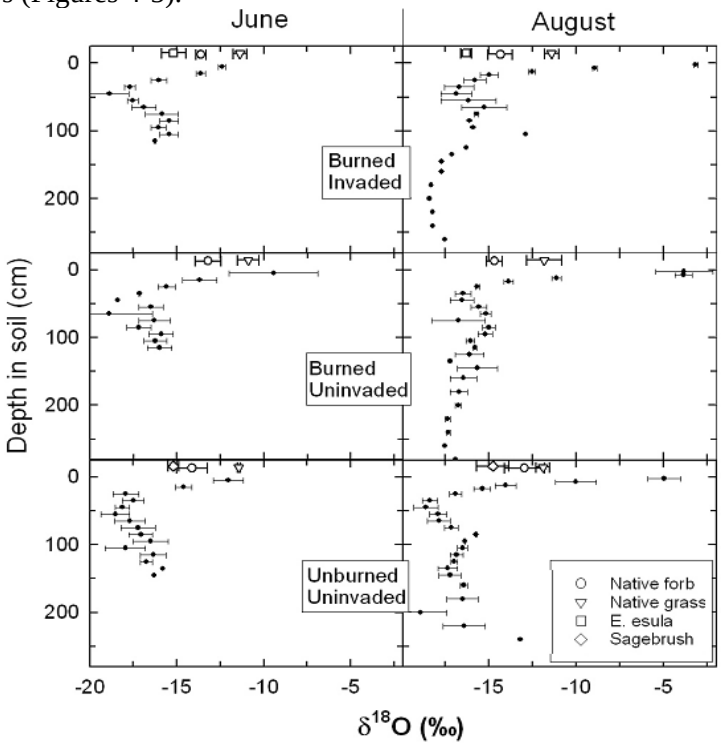

Figure 3. $^{18}O/^{16}O$ in each treatment Dark symbols show values in soil, and open symbols above the 0 cm depth in soil show the different plant species sampled.

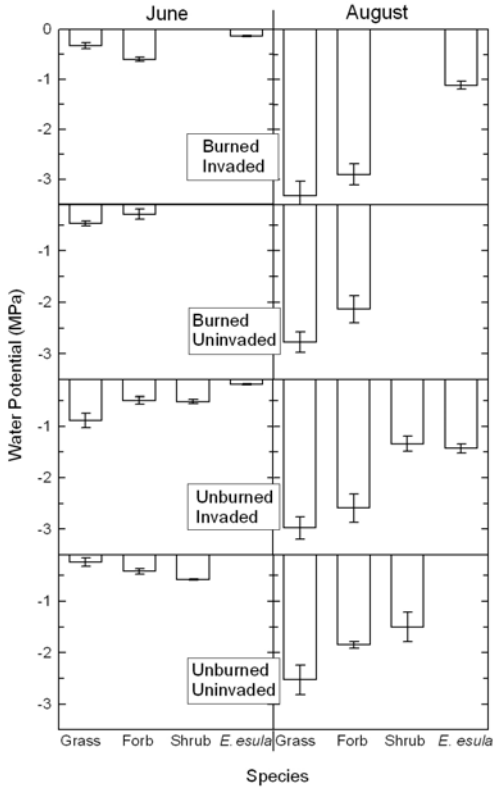

Figure 4. Predawn water potentials of the species sampled in each treatment.

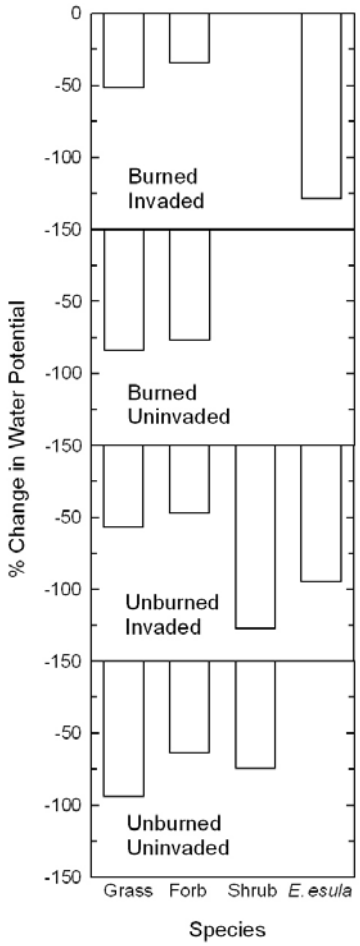

Figure 5. Percent change in water potentials from predawn to midday, in August.

Photosynthetic gas exchange

Leaf-level photosynthesis decreased 96% from June to August in *E. esula*, compared to decreases of 70% in sagebrush, 78% in the native forb, and 92% in the native grass (Table 2). Photosynthesis in *E. esula* was similar to or significantly less than in any native species, during both sampling periods. In the unburned plots, photosynthesis was least of all species in *E. esula*, with the native forb and sagebrush having nearly 5-fold greater photosynthesis. In burned plots during June, photosynthesis was 30% greater in the native forb compared to *E. esula*, but by August the forb had 5-fold greater photosynthesis. Photosynthesis was similar in *E. esula* and the native grass in the burned plots. Stomatal conductances in *E. esula* were similar or greater than in the native grass, but less than in the other native species. Water-use efficiency was similar or less in *E. esula* than in adjacent native species, except in unburned plots where photosynthesis was exceptionally low.

Comparisons of photosynthesis in native plants among plots that did or did not have *E. esula* did not indicate any negative effects of *E. esula* on photosynthesis or conductance in neighboring native species (Table 2). However, water-use efficiency was 77% greater in native species in plots with *E. esula* (3.22 μmol/mol) compared to plots that had no *E. esula* (1.82 μmol/mol; Paired T = 2.06, P = 0.05, using means for each species x treatment as replicates).

Table 2. Photosynthesis (μmol CO_2 m^{-2} s^{-1}), stomatal conductance (mol H_2O m^{-2} s^{-1}), and water-use efficiency (WUE, photosynthesis/evapotranspiration, mol/mmol) among the species in each treatment type.

	Period	Species	Photosynthesis (μmol m^{-2} s^{-1})	Conductance (mol m^{-2} s^{-1})	WUE (μmol/mmol)
Burned, invaded	June	Native forb	17.0 ±2.6	0.406 ±0.069	1.3 ±0.1
		Native grass	11.0 ±1.3	0.158 ±0.015	1.8 ±0.3
		E. esula	12.8 ±2.7	0.260 ±0.064	1.6 ±0.1
	August	Native forb	3.6 ±0.7	0.053 ±0.017	1.8 ±0.3
		Native grass	0.9 ±0.2	0.003 ±0.003	4.2 ±0.8
		E. esula	0.6 ±0.3	0.003 ±0.003	1.4 ±4.8
Unburned, uninvaded	June	Native forb	20.3 ±1.5	0.421 ±0.029	1.0 ±0.1
		Native grass	10.0 ±1.3	0.203 ±0.036	0.9 ±0.1
		Sagebrush	13.2 ±1.9	0.376 ±0.041	0.9 ±0.1
	August	Native forb	4.5 ±1.8	0.080 ±0.045	1.6 ±0.3
		Native grass	0.9 ±0.3	0.008 ±0.005	2.2 ±0.6
		Sagebrush	3.9 ±1.4	0.078 ±0.048	1.4 ±0.3
Burned, uninvaded	August	Native forb	2.9 ±1.6	0.045 ±0.033	0.6 ±1.0
		Native grass	0.9 ±0.5	0.005 ±0.003	3.3 ±1.2
Unburned, invaded	August	Native forb	5.3 ±1.6	0.078 ±0.028	1.6 ±0.6
		Native grass	1.1 ±0.1	0.003 ±0.003	6.2 ±2.9
		Sagebrush	4.9 ±2.1	0.070 ±0.047	2.3 ±0.4
		E. esula	0.8 ±0.1	0.003 ±0.003	5.3 ±7.7

DISCUSSION

Whether interspecific difference in soil resource contribute to invasions of semiarid communities is a critical question not only for understanding community stability, but also for land management practices that affect soil resources through altering species compositions and abundances. For example, sheep grazing has affected the relative abundance of forbs within the herbaceous component of the mountain sagebrush communities we examined (Seefeldt et al. 2007). Prescribed burning practices, aside from promoting invasive, exotic species, are perceived as have little impact on the composition of herbaceous communities. One potentially important exception has been that prescribed fires have selected against *Cordylanthus racemosus*, one of the few late-season native forbs that presumably persists on deeper soil water reserves and has been promoted by domestic grazing activities (Seefeldt and McCoy 2001; Seefeldt et al. 2007).

Euphorbia esula dominated burned areas but was scarce in the undisturbed sagebrush steppe we evaluated, and correspondingly tended to have lower photosynthesis than native species despite having greater or equal water potentials than the natives (Tables 1-2, Figure 4). Moreover, *E. esula* tended to have lower photosynthetic water use efficiency, and exhibited no greater ability to photosynthesize under its low midday water potentials than native species (Table 2, Figure 5). Depth of water uptake was similar in *E. esula* and sagebrush, and both acquired water from deeper soils than the native forb and especially grass. Water availability was greater in deep soils, especially in burned areas in which sagebrush was absent. Correspondingly, both sagebrush and *E. esula* tended to have greater water status at predawn, compared to the native herbs. *E. esula* had lower predawn water potential in unburned areas having sagebrush compared to burned plots, and greater water-use efficiency. These differences point to greater water stress for *E. esula* in the rare cases in which we observed it near sagebrush. Interestingly, water potentials of native herbs were lower when herbs occurred near *E. esula*, which could also indicate belowground interactions in shallower soils. These findings suggest a greater reliance on soil water availability in *E. esula* than native herbs that recolonize burn sites. *E. esula* needs the deep soil water

used by sagebrush, and increases in deep soil water that result from the temporary loss of sagebrush appear to be a mechanism contributing to the persistence of *E. esula* on the sites we examined.

Differences in water source have been demonstrated for exotic forbs and native shrub-steppe species (Kulmatiski et al. 2007), and were the basis of surmising a "tap-root advantage" for the exotics. However, use of a water source does not alone indicate the importance of the water source to a plant. Here, we demonstrate that leafy spurge appears to have a marginal photosynthesis and water status in cold desert. In the absence of conservative water use abilities, use of more abundant supplies of water available beneath the rooting zone of native herbs is likely critical for its persistence in cold desert. Restoration of abandoned dry farms and stabilization of burn areas often focuses on promoting grass cover, which should render sites vulnerable to infestation of leafy spurge. Efforts to prevent or restore infestations of leafy spurge could benefit from promotion of native forbs and especially shrubs like sagebrush. Deep-rooted perennials that persist though seasonal drought are clearly better poised to preempt the soil resources required by leafy spurge.

ACKNOWLEDGEMENTS
This study was made possible by a grant from the National Aeronautics and Space Administration Goddard Space Flight Center which was made possible through efforts of the Idaho congressional delegation.

LITERATURE CITED

Anderson J. E., Shumar M.L., Toft N.L., Nowak R. S. 1987. Control of the soil water balance by sagebrush and three perennial grasses in a cold-desert environment. Arid Soils Research and Rehabilitation 1:229-244.

Canadell, J., Jackson, R. B.; Ehleringer, J. R.; [and others]. 1996. Maximum rooting depth of vegetation types at the global scale. Oecologia. 108(4): 583-595. [27670]

Chambers J. C., Roundy B.A., Blank R.B., Meyer S.E., Wittaker A. 2007. What makes Great Basin sagebrush ecosystems invasible by *Bromus tectorum*? Ecological Monographs 77:117-145.

Cline, J. F.; Uresk, D. W.; Rickard, W. H. 1977. Comparison of soil water used by a sagebrush-bunchgrass and a cheatgrass community. Journal of Range Management. 30(3): 199-210

Ehleringer, J.R. and C.B. Osmond. 1989. Stable Isotopes. pp. 281-300 *in* Pearcy, R.W., J.R. Ehleringer, H.A. Mooney, and P.W. Rundel (eds). Plant Physiological Ecology. Chapman & Hall, London.

Kulmatiski, A. 2006. Exotic plants establish persistent communities. Plant Ecology 187:261-275.

Kulmatiski, A. Beard K.H., Stark, J.M. 2006. Exotic plant communities shift water-use timing in a shrub-steppe ecosystem. Plant Soil 288:271-284

Harniss R.O., Murray R.B.. 1973. 30 years of vegetal change following burning of sagebrush grass range. Journal of Range Management 26:322-325

Hill J.P., Germino M.J., Wraith J.M., Olson B.E., Swan M.B. 2006. Advantages in water relations contribute to greater photosynthesis in *Centaurea maculosa* compare with established grasses. International Journal of Plant Sciences 167: 269-277.

Link S, Gee G.W., Thiede M.E., Beedlow P.A. 1990. Response of a shrub-steppe ecosystem to fire: soil water and vegetational change. Arid Soils Research and Rehabilitation 4: 163-172.

Pyke D.A. 1999. Invasive exotic plants in sagebrush ecosystems of the Intermountain west. Pages 43-45 in PG Entwistle et al. (eds) Proceedings: sagebrush steppe ecosystems symposium. Publication BLM/ID/PT-001001+1150. Bureau of Land Management, Boise ID.

Seefeldt, S.S. Germino, M.J. DiCristina, K. 2007. Prescribned fires in *Artemisia tridentata* ssp. *vaseyana* steppe have minor and transient effects on herb cover and composition. Applied Vegetation Science 10: 249-256

Selleck, G. W.; Coupland, R. T.; Frankton, C. 1962. Leafy spurge in Saskatchewan. Ecological Monographs. 32(1): 1-29.

Smith S.D., Monson R.K., Anderson J.E. 1997. Physiological Ecology of North American Desert Plants. Springer NY.

Raju, M. V. S. 1985. Morphology and anatomy of leafy spurge. In: Watson, Alan K., ed. Leafy spurge. Monograph Series No. 3. Champaign, IL: Weed Science Society of America: 26-41.

Raju, M. V. S.; Steeves, T. A.; Coupland, R. T. 1963. Developmental studies on *Euphorbia esula* L.: morphology of the root system. Canadian Journal of Botany. 41: 579-588.

Richards, J. H.; Caldwell, M. M. 1987. Hydraulic lift: substantial nocturnal water transport between soil layers by *Artemisia tridentata*. Oecologia. 73(4): 486-489.

Welch, B. L., Jacobson, T. L. C. 1988. Root growth of *Artemisia tridentata*. Journal of Range Management. 41(4): 332-334.

[THIS PAGE LEFT BLANK INTENTIONALLY]

Fire Effects on Wind Erosion in Sagebrush Steppe Rangelands of the Snake River Plain

Joel B. Sankey, 921 S. 8th Ave Stop 8072, Department of Geosciences, Idaho State University, Pocatello, ID, 83209-8072. sankjoel@isu.edu. Tel.: 208-220-6571.

Matthew J. Germino, 921 S 8th Ave, Stop 8007, Department of Biological Sciences, Idaho State University, Pocatello, ID 83209-8007. germmatt@isu.edu. Tel.: 208-282-3285; fax: 208-282-4570.

Nancy F. Glenn, 322 E. Front St., Suite 240, Department of Geosciences, Idaho State University- Boise, Boise, ID 83702. glennanc@isu.edu. Tel.: 208-345-1994

ABSTRACT

Wind erosion of soil is an appreciable but unstudied event following fires in cold desert. We examined aeolian transport of sediment for one year following fire in semiarid shrub steppe of southern Idaho. Sediment collectors were used to determine horizontal mass transport of soil ($\int_{height=0}^{2m} mass * area^{-1} * time^{-1}$) and saltation sensors and anemometers were used to determine saltation activity (# seconds saltation is detected per 300 seconds) and threshold wind speed in an unburned control site and an area burned in August. Horizontal mass transport (per 30 d periods) was negligible in the unburned area, but in the burned area was 5.40 kg m^{-1} in October and decreased to 2.80 kg m^{-1} in November and 0.32 kg m^{-1} in December. Mean threshold wind speeds were between 10.0 and 10.6 m s^{-1} at the burned site during fall. A lack of saltation precluded determination of thresholds thereafter at the burned site and for the entire course of the study at the unburned site. Differences in sediment flux and saltation activity at burned and unburned sites became much less pronounced following the emergence of herbaceous vegetation in the spring. Our results indicate that the burned shrub steppe was prone to aeolian sediment transport in the first months following summer wildfire and became less so by early winter, through spring and summer.

KEYWORDS: Aeolian sediment transport, wind erosion, wildfire, sediment flux, saltation

INTRODUCTION

Aeolian sediment transport is a fundamental geomorphic process that has wide-ranging environmental implications for human and environmental health (Whicker et al., 2006), ecological functioning at multiple spatial and temporal scales (Okin et al., 2006), local and global biogeochemical cycling (Okin at al., 2004; Reynolds et al., 2001; Chadwick et al., 1999), and contaminant transport (Whicker et al., 2004). Aeolian sediment transport is a function of the wind's ability (impeded by vegetation and terrain) to entrain soil particles, and the soil's susceptibility to this entrainment (Okin et al., 2006; Bagnold, 1941). Field-based research on aeolian transport in non-agricultural systems has largely focused on cropland and arid landscapes, however semiarid landscapes, and shrublands in particular, exhibit considerable annual fluxes of wind-transported sediment (Breshears et al., 2003). Wind erosion can be especially significant following fire, as shown for prairie and warm desert in the southern United States. Transport via wind can exceed that by water in semiarid shrublands (Vermeire at al., 2005; Whicker et al., 2002; Zobeck et al., 1989).

Increased wind erosion has been reported immediately following fall or spring prescribed fires in areas also affected by grazing (Vermeire et al., 2005), and at various intervals following summer wildfire (Whicker et al., 2002; Zobeck et al., 1989). Whether wind erosion persists through plant re-colonization of burned areas, particularly in more northerly regions in which plant reestablishment is delay during cold winters, is not well known. Moreover, the previous studies of fire effects on wind erosion have all occurred on sandy soils, which were probably impacted by a previous history of soil erosion. We examined the course of wind erosion as it related to changes in plant abundance and hydroclimatology following a fire in cold desert sagebrush-steppe occurring on fine-textured loess soils, which appeared to otherwise have not been affected by recent fire and aeolian losses of soil. This vast habitat type (10 M ha) is uniquely characterized by warm, dry summers, and cold, snowy winters, and spring snowmelt provides the bulk of the annual plant available water at the time of green-up (Smith et al. 1997). Fire frequencies and area burned per year have increased substantially in the recent decade in sagebrush steppe, becoming nearly 500 ha in some years (eg. 2007 Murphy complex fire in Western North America). Fire typically occurs in summer, and charred soils frequently remain un-vegetated until re-sprouting of grasses, as well as some forbs and occasionally shrubs, occurs in the subsequent spring and summer (Harniss 1970). Herb cover, especially grasses, dominate vegetation cover for decades following fire, while species such as sagebrush slowly recover to pre-fire levels. Seeding and planting are commonly used in attempt to bolster cover in the first years after fire (US DOI, BLM), which implies the assumption that natural plant recovery is not adequate to stabilize soil.

Simultaneous observations of saltation activity, the fraction of time in which saltating particles can be detected, and critical aeolian threshold (hereafter "threshold", the minimum windspeed required for saltation) were useful for distinguishing erodibility of geomorphic surfaces with expectedly different susceptibility to erosion by wind (Stout, 2007). We expected that simultaneous observations of saltation activity and critical aeolian threshold in conjunction with sediment flux measurements would similarly be useful for describing differences between the wind erosion potential of burned and unburned rangelands. Saltation activity, threshold, and actual rates of horizontal sediment transport can be determined from simultaneous micrometeorological measurements of wind and other boundary layer atmospheric characteristics, passive sediment sampling systems for measurement of horizontal and vertical sediment mass flux, and direct measurements of soil loss and deposition at the soil surface (Vermeire et al., 2005; Whicker et al., 2002; Zobeck et al., 1989). We used these approaches to determine the following for a burned and unburned control area: 1) differences in wind erosion potential, and 2) the longevity of these differences, in burned vs. unburned semiarid cold desert shrub steppe. We hypothesized that: (i) wind erosion potential would be significantly greater at burned compared to unburned sites during fall, and (ii) significant differences in wind erosion potential between burned and unburned sites would not be detectable following the spring emergence of herbaceous vegetation.

MATERIALS AND METHODS

Study Sites

The study sites are located in the southern portion of the Eastern Snake River Plain, near Aberdeen, Idaho. The area is located in a zone of 200 mm to 280 mm of mean annual precipitation and 7 to 13 degrees C mean annual temperature (NCSS Web Soil Survey). This portion of the Snake River Plain is characterized by near surface winds that trend generally throughout the year from SW to NE (Clawson et al., 1989). On average, the frequency of high wind events is greatest in spring and summer, with fall being calmer, and winter the calmest season (Clawson et al., 1989).

The rangeland vegetation includes Wyoming big sagebrush (*Artemisia tridentata ssp. wyomingensis* Rydb.) and the less abundant shrubs "three-tip" sagebrush (*Artemisia tripartita* Rydb.) and green rabbitbrush (*Chrysothamnus viscidoflorus* [Hook.] Nutt.), bluebunch wheatgrass (*Agropyron spicatum* Pursh.), prairie junegrass (*Koeleria macrantha* Ledeb.), and sandberg bluegrass (*Poa secunda* J. Presl) (NCSS Web Soil Survey). Soils at the study sites have developed from silty loess overlying basalt bedrock (NCSS Web Soil Survey). Depth to bedrock ranges from 20 to 150 cm, and surficial soil textures are silt loam in deeper loess-derived soils and a stony loam in some locations where either fractured bedrock is nearer the surface or small, intermittently active alluvial channels cross the sites (NCSS Web Soil Survey). Soils at the sites are rated with a Wind Erodibility Index value of 1.9×10^5 kg ha^{-1} $year^{-1}$ soil loss, and have a Wind Erodibility Group rating of 4, which is intermediate to values for all USA soils (NRCS Web Soil Survey).

Site Characterization

Sampling was initiated in September, 2006 at a large fire on the Eastern Snake River Plain (Crystal Fire, approximately 80,000 ha, August, 2006). Two study sites in the burn and one study location in the neighboring unburned area were selected, at the easternmost extent of the fire. Sampling intensity was greater at one of the burn sites (hereafter referred to as the primary burn site), compared to the other burn site. Each site was delineated as a 100-m radius circle, and there was at least 300 m between the study sites and the edge of the burn area. Four transects radiating out from the center of the circle in the cardinal directions were used for the characterization of vegetation composition at each site. Percent cover of shrubs, herbaceous plants, and bare ground was measured along each transect using the line intercept method, in which cover beneath all lengths of transects was recorded and reported as a fraction of total cover. Height of individual shrubs along each transect were measured.

Micrometeorological data collection

At the outset of the study the average shrub, herbaceous vegetation, and bare ground cover, as well as shrub height means and standard deviations, were calculated from the eight transects for the two burned sites and from the four unburned site transects. Micrometeorological and saltation monitoring equipment was installed at the center of the unburned site and the primary burned site in the last week of September, 2006. Sensors included two anemometers (Model 014A, MetOne Instruments Inc., Grants Pass, OR, USA) mounted at the top of and below the unburned vegetation canopy (110 and 40 cm), a SENSIT® piezoelectric sensor (Sensit Company, Portland, ND, USA) mounted at 5 cm above the ground surface that records impacts from saltating soil particles, and temperature and relative humidity sensors (Model HMP50L, Vaisala Group, Vantaa, Finland) mounted at 5 cm above ground. The mean, standard deviation, and maximum wind velocity, the number of seconds with particle impacts, and average relative humidity and temperature were recorded at 5-minute intervals, at a 1-second scan rate using dataloggers (model CR10, Campbell Scientific Inc., Logan, UT, USA). Data collection was suspended in mid-January due to winter access problems. Data were simultaneously collected at the burned and unburned sites during approximately 105 days during this period of the study (fall/winter).

The micrometeorological and saltation monitoring equipment was reinstalled following the spring emergence of herbaceous vegetation on May 16, 2007 and data were collected until August 11, 2007. Vegetation cover was resampled on the unburned and primary burn site at the end of this 2007 period.

Data were collected simultaneously at the two sites for 85 days during this period of the study (spring/summer).

Aeolian sediment collectors

Big Springs Number Eight (BSNE®) (Custom Products, Big Spring, TX, USA) omnidirectional passive sediment collectors mounted at 5, 10, 20, 55, and 100 cm height were installed at the center of all three sites. Two additional sediment collector towers with collectors at 5, 10, and 20 cm height were installed at each site approximately 20 meters laterally from the site center, with one tower on either side of the axis of prevailing wind direction.

The aeolian sediment collectors were installed on September 28th at all three sites. Collections were made on October 30, November 30, and January 18, during fall/winter. The collectors remained in the field at all three sites after January 18th and were emptied once on May 14, 2007. Sediment collectors were then emptied on June 10th, July 21st, and August 17th, during spring/summer.

When the collectors were emptied, the sediment was placed in airtight bags, dried for 16 hours at 110 degrees C and weighed to 0.000 g precision. Sediment mass was averaged at each height, over each sampling interval, for the burned and the unburned sites, respectively. This resulted in potential sample sizes of n = 6 and n = 3 at heights of 5, 10, and 20 cm for the combined burned sites and the unburned site, respectively, and n = 2 and n = 1 at 55 and 100 cm for the combined burned sites and the unburned site, respectively. These are potential sample sizes because there were 9 instances on January 18th, and 6 on May 14th when a collector at a specific height could not be reliably sampled due to water or ice in the collector.

Data Analysis

The root mean squared difference (RMSD) of mean wind speeds between the burned and unburned sites was determined for each anemometer height using the mean wind speeds of simultaneous 5-minute intervals. This provided an average difference between the burned and unburned sites in mean wind speed at heights corresponding to the top and beneath the plant canopy height of the unburned site, for both fall/winter and spring/summer.

The proportion of each five-minute period during which impacts were recorded by the saltation sensor, termed saltation activity, was calculated by dividing the number of seconds with particle impacts by 300 seconds. Following Stout (2004), saltation activity is related to the minimum wind speed required to entrain saltating soil particles, termed the critical aeolian threshold, by the following equation:

$$\gamma = \Phi \frac{\overline{\mu} - \mu_t}{\sigma}$$

where γ is saltation activity, μ_t is the critical aeolian threshold wind speed of the higher anemometer in units of m s^{-1}, $\overline{\mu}$ is the mean wind speed of the higher anemometer in units of m s^{-1}, σ is the standard deviation of wind speed for the higher anemometer in units of m s^{-1}, and Φ is the normal distribution function. The critical aeolian threshold in wind speed units of m s^{-1} was determined by solving the previous equation for critical aeolian threshold (μ_t) (Stout, 2004).

Rain drops and splash can be falsely recorded as saltating sediment by the Sensit, so saltation activity and critical aeolian threshold were not reported on days in which rain was measured at the nearby USDA Aberdeen weather station. Critical aeolian threshold was determined for saltation activity values between 0.02 and 0.98, (Stout, 2004).

Aeolian sediment horizontal mass flux was calculated for each sediment sampling interval and height as:

$$mass * area^{-1} * time^{-1}$$

where mass is kg of sediment, area is size of the opening on the BSNE© sampler (0.0002 m^2 at heights 5 and 10cm, and 0.001 m^2 at 20, 55, and 100 cm), and time is the sampling interval in days. Sediment flux was normalized to a 30-day rate for each sampling interval (i.e. kg m^{-2} $30d^{-1}$), and plotted as a function of sample height. A power model was fit to this plot and integrated over 200 cm to calculate a sediment mass transport value of the form (VanDonk et al., 2003):

$$\int_{height=0}^{2m} mass * area^{-1} * time^{-1}$$

with units of kg m^{-1}. This resulted in 30-day sediment mass flux and sediment mass transport estimates over each sampling interval for the combined burned sites, and for the unburned site.

RESULTS

Fall/Winter

The unburned site had greater shrub and herbaceous vegetation cover than the burned sites, during fall/winter following wildfire (Table 1). The burned sites had more exposed bare soil. Shrub mean height and standard deviation were 2 to 3 times greater for the unburned site relative to the burned site. Mean wind speed at the top of (110 cm) and below (40 cm) the unburned vegetation canopy was noticeably smaller at the unburned compared to burned site for almost all periods of time during fall/winter (Figure 1). The mean difference between the burned and unburned sites for measured wind speeds at these heights was 1.79 and 1.55 m s^{-1}, respectively.

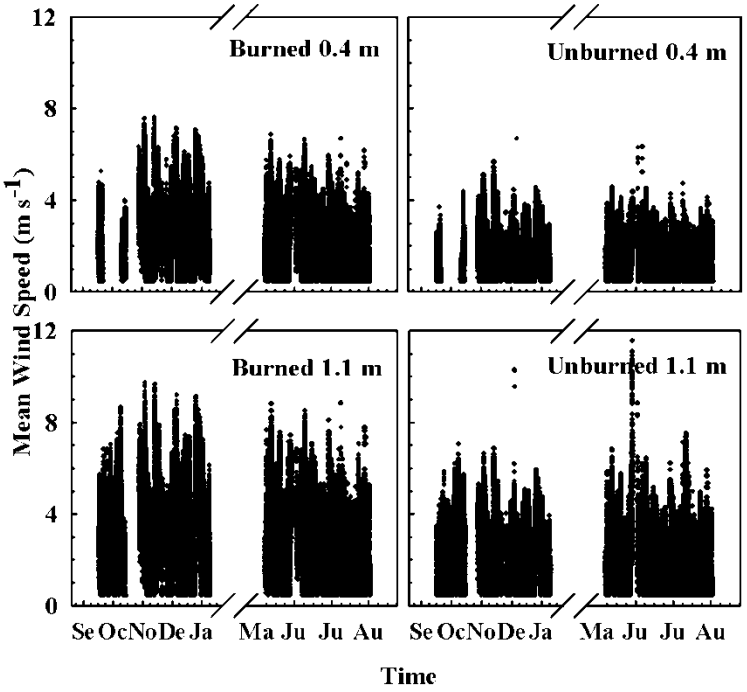

Figure 1. Mean wind speed measured below (40 cm above ground) the unburned vegetation canopy (upper panel), and at the top (110 cm above ground) of the unburned vegetation canopy (lower panel) at unburned and burned sites.

Saltation activity was more frequently detected, and greater in magnitude when detected, at the burned compared to unburned site over the course of fall/winter (Figure 2). Saltation was detected during less than 2% of the time, indicating an episodic nature of erosion events (Table 2). The fraction of time during which saltation was detected at the burned site was an order of magnitude greater relative to the unburned site.

Substantial differences were detected for saltation activity during the few periods in which both sites simultaneously achieved saltation activities greater than 0.02. There were only 39, 5-minute periods during which saltation activity was simultaneously determined for the burned and unburned sites in fall/winter. The mean saltation activity was 0.35 ± 0.04 SE in the burned sites, indicating 35% of 5-minute periods had saltation, compared to 0.05 ± 0.00 in the unburned sites.

Table 1. Mean (standard error) ground cover of sampling sites

		Ground Cover		
Period	Site	shrub %	herbaceous %	bare %
Fall 2006	Unburned (4 transects)	35 (2)	40 (3)	25 (4)
	Burned (8 transects)	6 (1)	3 (1)	91 (9)
Spring 2007	Unburned (4 transects)	40 (2)	54 (2)	6 (1)
	Burned (4 transects)	6 (1)	45 (9)	59 (6)

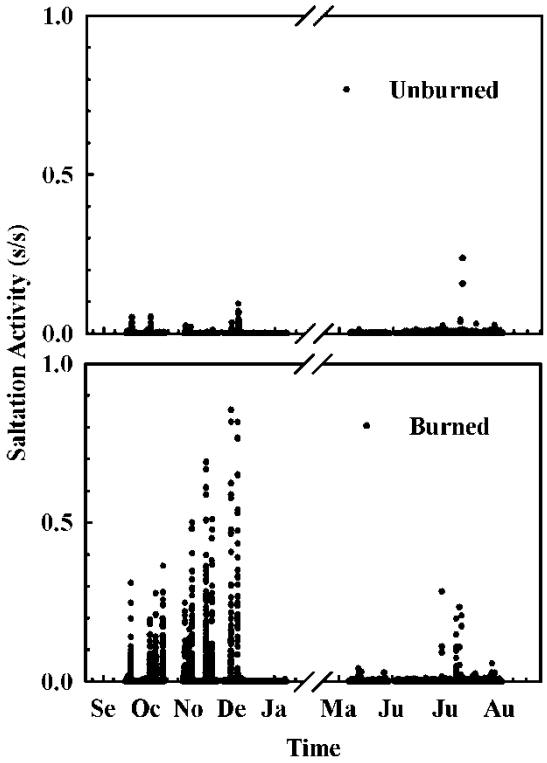

Figure 2. Saltation activity detected at unburned (upper panel) and burned (lower panel) sites. Saltation activity is unitless and is calculated as the number of seconds in a 300 second period during which particle counts were recorded.

Table 2. Fall, 2006 and Spring, 2007 saltation particle count results

Period	Site	Saltation Detected (minutes)	Fraction of Study Period (%)
Fall 2006	Unburned	220	0.1
	Burned	2825	1.9
Spr 2007	Unburned	35	0.0
	Burned	155	0.1

Reliable estimates of threshold wind speed could not be made for the unburned site because of the absence of sustained saltation events at this site (Figure 4). There were five days with sustained saltation events when threshold wind speeds could be determined at the burned site. Mean threshold wind speeds for these days were between of 9.15 and 10.62 m s^{-1} [October 19 (mean = 10.02 m s^{-1}, s.d. = 0.30 m s^{-1}, n

= 23), October 20 (mean = 10.10 m s^{-1}, s.d. = 0.32 m s^{-1}, n = 17), November 8 (mean = 9.15 m s^{-1}, s.d. = 0.71 m s^{-1}, n = 21), November 13 (mean = 10.62 m s^{-1}, s.d. = 0.63 m s^{-1}, n = 40), November 23 (mean = 10.12 m s^{-1}, s.d. = 0.54 m s^{-1}, n = 94).

Burned site horizontal sediment flux appeared comparable at most heights for the first two sampling intervals of fall/winter, and was substantially smaller in December and the first half of January (Figure 3). There was never a detectable quantity of sediment at any heights at the unburned site during fall/winter. The integrated power functions fit to burned site sediment flux measurements yielded sediment mass transport values of 5.40, 2.80, and 0.32 kg m^{-1} for the three fall/winter sampling intervals from the end of September through mid-January.

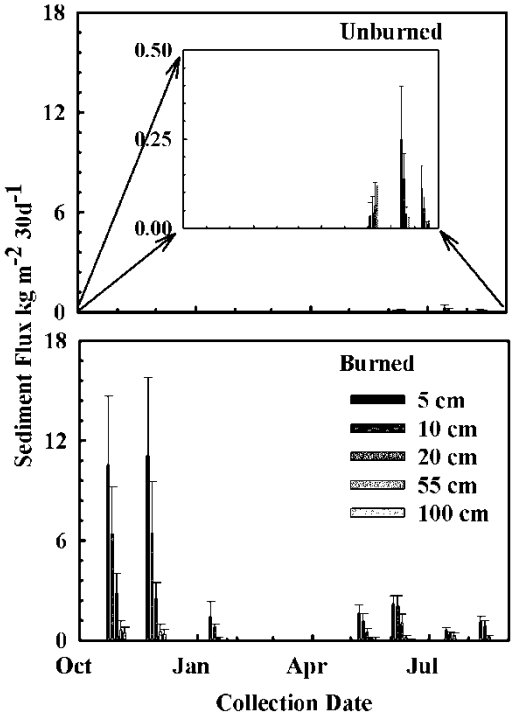

Figure 3. Mean horizontal sediment mass flux at unburned (upper panel) and burned (lower panel) sites. The unburned and burned sites were sampled at the same intervals and missing values for the unburned site represent periods when no measurable amount of sediment accumulated in the collector.

Spring/Summer

After the emergence of herbaceous vegetation in the spring, large differences persisted between the amount of exposed bare soil and shrub cover at the unburned site and primary burned site, though the sites were more comparable in terms of herbaceous vegetation cover (Table 1). The mean difference between wind speeds at the burned and unburned sites was not as great for either anemometer height during spring/summer (RMSD = 1.15 m s^{-1} [110 cm] and 0.92 m s^{-1} [40 cm]) compared to fall/winter. Saltation activity was never greater than 0.30 during spring/summer at either the burned or unburned sites (Figure 2). Saltating particles were detected during less than 0.1% of the study period during spring/summer at both sites (Table 2). There were only 2, 5-minute periods during which saltation activity was simultaneously determined at the burned and unburned sites in spring/summer. Reliable estimates of threshold wind speeds could not be determined for spring/summer at either site, due to the scarcity and very short duration of saltation events.

Detectable quantities of sediment did accumulate in the unburned site collectors during spring/summer, in contrast to fall/winter. Sediment flux, however, was lower at all collector heights at the unburned site

compared to the burned sites during this time period (Figure 4). Mean flux values did not fit power functions with high correlation for the June 10 and August 17 collection dates at the unburned site and were therefore not integrated to estimate sediment mass transport values. Unburned site mean flux values for the July 21 collection date fit a power function with a moderate correlation ($R^2 = 0.7$) and resulted in a mass transport value of 0.08 kg m^{-1}. Burned site mean flux values did fit power functions with high correlation ($R^2 \geq 0.9$) and resulted in mass transport values of 0.46, 0.83, 0.21, and 0.47 kg m^{-1} for the four spring/summer sampling dates (May – August).

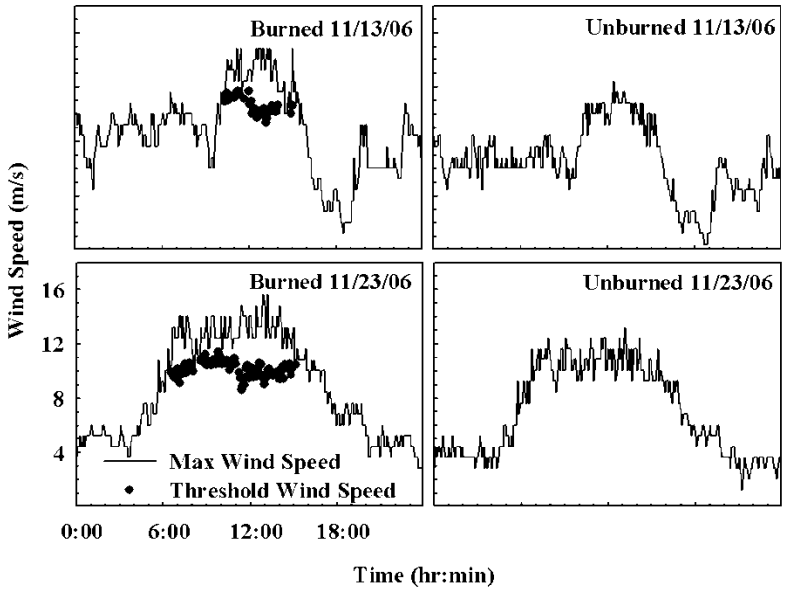

Figure 4. Examples of maximum wind speed and aeolian critical threshold determined for unburned and burned sites on November 11th and 23rd, 2006. Maximum wind speed and threshold wind speed data are determined for 5 minute periods.

DISCUSSION AND CONCLUSIONS

The combination of greater vegetation cover, shrub height, and variability in shrub height at the unburned site would be expected to result in fundamentally different wind-height relationships at burned and unburned sites (Hagen and Armbrust, 1994; Driese and Reiners, 1997; Campbell and Norman, 1998; Lancaster and Baass, 1998). We predicted our data to reflect this primarily through observed differences in wind speed at the two measurement heights, because our sites were not instrumented with enough anemometers to determine wind profiles and derivative measures (i.e., zero plane displacement, aerodynamic roughness, and friction velocity). Simultaneous wind speed measurements were lower on average at the unburned site, suggesting greater wind attenuation within the unburned plant canopy relative to the burned site. They show greater differences between burned and unburned wind speeds in fall/winter relative to spring/summer, as well.

These observations corresponded with substantial differences in the magnitude and frequency of saltation activity at burned and unburned sites during fall/winter. They also corresponded with the observed greater similarity between sites in spring/summer, when there was a smaller difference between the fraction of the time that saltation was detected at the burned and unburned sites (Table 2). Overall, the frequency of saltation events was low at both sites compared to more erodible landscapes such as sand dunes or playas (Stout, 2004, 2007). These results appear to corroborate findings of previous studies of wind erosion in burned and unburned semiarid rangelands; highlighting the episodic nature of wind erosion in these environments (Vermeire, 2005; Whicker, 2002). Whereas these previous studies of post-fire erosion occurred on sandy soils, our study occurred on finer textured soils in which appreciable

erosion has likely not occurred for decades and probably centuries, and so our sites were presumably more prone to erosive losses.

Our saltation activity and sediment flux data for fall/winter show more near-ground sediment transport at the burned compared to unburned sites, providing indirect evidence of the relative erodibility of the burned and unburned soil surfaces (Whicker et al., 2002). The determination of critical aeolian threshold wind speeds provides another measure of erodibility for an aeolian surface, with a higher measured threshold suggesting a lower erodibility and vice versa. Differences amongst the mean threshold values observed during erosion events in October and November provide evidence of temporal variability in erodibility within the burned shrubland. Due to the lack of sustained erosion events at the unburned site, threshold could not be used as a means to compare the relative erodibility of unburned and burned sites. Whicker et al. (2002) suggest fire can result in differences in erodibility at burned and unburned locations due to both the direct effects of burning on the soil surface and to vegetation differences. Our findings appear to indicate that fire increased the potential for wind erosion by temporarily excluding the boundary layer protection provided by the vegetation to the soil surface. Experiments using portable wind tunnels or experimental modification of vegetation would help explain whether the difference in wind erosion potential between burned and unburned sites in our environment is due additionally to direct effects of fire on the erodibility of the soil surface.

We observed a great deal of within-site variability in sediment flux, though this is not evident in our presented results due to the averaging of sediment catch from all collectors within a site. Figure 5 shows a photo taken on June 10, 2007 of a blowout that formed in the preceding fall/winter, post-fire, at the secondary burned site adjacent to a sediment collector. This blowout persisted throughout the spring/summer study period and the nearby collector had consistently higher sediment fluxes than many of the other burned site collectors. Spatial variability in wind erosion within burned sites was described in one previous study (Whicker et al., 2002).

Figure 5. Photo taken on 06/10/07 showing herbaceous vegetation surrounding a blowout that developed in fall, post-fire (note sediment collector in background).

Our sediment flux data provide insight into the longevity of erosion potential differences between the burned and unburned sites post-fire. The sediment mass transport values determined for fall/winter show a decrease in aeolian sediment transport during this time period. The values for the last sampling interval in fall/winter and throughout spring/summer are considerably smaller than those for the first two sampling intervals post-fire. The bulk of wind erosion at our sites, therefore, occurred during the initial months following fire. This is similar to the results of a two-year study of post-prescribed fire wind

erosion that reported more aeolian sediment transport at burned relative to unburned sites during the first 5 months following burning (Vermeire et al., 2005). Their study environment was a shrubland in a more humid climate than ours, and erosion of the greatest magnitude occurred at their sites during the dormant season of December through April; several of the months when the ground at our environment would typically be covered by snow. The magnitude and frequency of sediment transport became much more similar at our burned and unburned sites following the emergence of herbaceous vegetation in late spring, though horizontal sediment flux appeared to remain slightly greater at the burned site. This is also comparable to findings of the post-prescribed burn study (Vermeire et al., 2005), in which the researchers suggested that observed differences in spring and summer erosion between the two years of their study might be dependent on interannual variations in climate of the dormant season and resultant degree of vegetation growth in the spring. Both burned and unburned pastures in the Vermeire et al. (2005) study were subjected to grazing disturbance during spring and summer, however.

Our findings suggest that erosion increased following burning, similar to findings of two previous studies specific to wind erosion following wildfire (Whicker et al., 2002; Zobeck et al., 1989). The scope of our findings in this regard is limited by the lack of spatial replication, with only paired comparisons possible between a single burned site and single unburned site throughout the course of the study period. This degree of replication is comparable to previous studies of post-wildfire wind erosion (Whicker et al., 2002; Zobeck et al., 1989), however, and to studies of wind erosion in semiarid shrublands in general (Breshears et al., 2003), and highlights the challenges of instrumenting such study sites to monitor aeolian transport. We present our work as a case study, and hypothesize that greater variability in the frequency and magnitude of erosion events might be expected amongst and within burned and unburned areas, could more sites be instrumented for a spatially explicit characterization of post-wildfire aeolian transport during future research.

In contrast to previous studies (Whicker et al., 2002; Zobeck et al., 1989), our study additionally examined the longevity of increased erosion following wildfire. Our study also took place in cold desert shrub steppe versus warm desert shrubland and prairie of previous studies, highlighting fundamental differences in the potential timing of fire and erosion due primarily to hydroclimatology at our sites versus those previously studied. In our study, the potential for wind erosion initially increased following a wildfire initiated by lightning in an August thunderstorm, decreased throughout the fall and early winter, then remained similarly low through the following late spring and summer, and appeared to be only slightly greater in the burned shrub steppe one year after the wildfire. Future research that examines the relative roles of vegetation removal and burning effects on soil erodibility, with greater spatial and temporal replication, would help land managers determine the degree to which seeding and other restoration efforts which are widely implemented following fires in this region are necessary to stabilize the soil surface following fire in cold desert shrub-steppe.

ACKNOWLEDGMENTS

Funding was provided by the US DOD, NASA Goddard Space Flight Center, and Inland Northwest Research Alliance. Jesse Shaffer assisted in initial instrumentation configuration, and Teki Sankey assisted in field sampling. ISU would also like to acknowledge the Idaho Delegation for their assistance in obtaining this grant.

LITERATURE CITED

Bagnold, R. A., 1941. The Physics of Blown Sand and Desert Dunes. Methuen, New York.

Breshears, D.D., Whicker, J.J., Johansen, M.P., and Pinder, J.E., 2003. Wind and water erosion and transport in semi-arid shrubland, grassland and forest ecosystems: quantifying dominance of horizontal wind driven transport. Earth Surface Processes and Landforms 28, 189-1209.

Campbell, G.S., Norman, J.M., 1998. An introduction to environmental biophysics. Springer Science + Business Media Inc., New York, NY, USA.

Chadwick, O.A., Derry, L.A., Vitousek, P.M. Huebert, B.J., Hedin, L.O., 1999. Changing sources of nutrients during four million years of ecosystem development. Nature 397, 491-497.

Clawson, K.L, Start, G.E., Ricks, N.R. (eds.), 1989. Climatography of the Idaho National Engineering Laboratory, 2nd Edition, DOE/ID-12118. U. S. Department of Commerce, National Oceanic and Atmospheric Administration, Environmental Research Laboratories, Air Resources Laboratory, Field Research Division, Idaho Falls, ID, USA.

Driese, K.L., Reiners, W.A., 1997. Aerodynamic roughness parameters for semi-arid natural shrub communities of Wyoming, USA. Agricultural and Forest Meteorology 88, 1-14.

Hagen, L.J., Armbrust, D.V., 1994. Plant canopy effects on wind erosion saltation. Transactions of the ASAE 37, 461-465

Lancaster, N., Baas, A., 1998. Influence of vegetation cover on sand transport by wind: field studies at Owens Lake, California. Earth Surface Processes and Landforms 23, 69-82.

NCSS Web Soil Survey. http://websoilsurvey.nrcs.usda.gov/app/.

Okin, G.S., Gillete, D.A., Herrick, J.E., 2006. Multi-scale controls on and consequences of aeolian processes in landscape change in arid and semi-arid environments. Journal of Arid Environments 65, 253-275.

Okin, G.S., Gillete, D.A., 2004. Modeling wind erosion and dust emission on vegetated surfaces, In *Spatial Modeling of the Terrestrial Environment*., edited by R. Kelly and N.A. Drake, pp. 137-156, John Wiley, N.J.

Okin, G.S., Mahowald, N., Chadwick, O.A., Artaxo, P., 2004. Impact of desert dust of phosphorous in terrestrial ecosystems. Global Biogeochemical Cycles 18.

Reynolds, J.F., Belnap, J., Reheis, M., Lamothe, P., Luiszer, F., 2001. Eolian dust in Colorado Plateau soils: nutrient inputs and recent change in source. Proceedings of the National Academy of Sciences 98, 7123-7127.

Stout, J.E., 2004. A method for establishing the critical threshold for aeolian transport in the field. Earth Surface Processes and Landforms 29, 1195-1207.

Stout, J.E., 2007. Simultaneous observations of the critical threshold of two surfaces. Geomorphology 85, 3-16.

USGS. http://geomaps.wr.usgs.gov/parks/province/basinrage.html

Vermeire, L.T., Wester, D.B., Mitchell, R.B., Fuhlendorf, S.D., 2005. Fire and grazing effects on wind erosion, soil water content, and soil temperature. Journal of Environmental Quality 34, 1559-1565.

Whicker, F.W., Hinton, T.G., MacDonell, M.M., Pinder, J.E., Habegger, L.J., 2004. Avoiding destructive remediation at DOE sites. Science 303, 1615-1616.

Whicker, J.J., Pinder, J.E., Breshears, D.D., 2006. Increased wind erosion from forest wildfire: implications for contaminant-related risks. Journal of Environmental Quality 35, 468-478.

Whicker, J.J., Breshears, D.D., Wasiolek, P.T., Kirchner, T.B., Tavani, R.A., Schoep, D.A., Rodgers, J.C., 2002. Temporal and spatial variation of episodic wind erosion in unburned and burned semiarid shrubland. Journal of Environmental Quality 31, 599-612.

Zobeck, T.M., Fryrear, D.W., Pettit, R.D., 1989. Management effects on wind-eroded sediment and plant nutrients. Journal of Soil and Water Conservation 44, 160-163.